The University Of Sheffield.

Crosstalk between Cancer cells and Fibroblasts:

Role of tumour-associated fibroblasts in the tumour microenvironment of the oropharynx

A thesis submitted in partial fulfilment of the requirements for the degree of Doctor of Philosophy by

Naeima Bader Hendawi

The University of Sheffield

Faculty of Medicine, Dentistry and Health

School of Clinical Dentistry

March 2021

Abstract

Introduction: High risk-human papillomavirus (HR-HPV) is a well-established aetiological factor in a subset of oropharyngeal squamous cell carcinoma (OPSCC) that shows distinct biological and clinical behaviour when compared to HPV-negative OPSCC. HPV-positive OPSCC patients have improved responses to oncological treatment and better overall survival in comparison to HPV-negative OPSCC patients. The role of the tumour microenvironment (TME) in tumour cell promotion and metastasis has been studied intensively in the last decades, and it is thought to play a crucial role in HPV-negative OPSCC progression. In oral squamous cell carcinoma (OSCC), cancer-associated fibroblasts (CAFs) phenotypes have been characterised thoroughly in our lab and we have reported, with others, the critical function of CAFs in OSCC progression. CAF phenotypes and their role in OPSCC, and the influence of HPV on this, have not been investigated before.

Objective: To investigate the presence and clinical significance of CAFs in OPSCC and explore novel candidates in tumour-fibroblast crosstalk.

Results: A retrospective cohort of primary OPSCC presented in tissue microarrays (n=143) was subjected to HPV 16 and 18 RNAScope assay and p16 IHC to determine the prevalence of HPV-associated OPSCC. α-SMA IHC was performed for CAF detection. Although α-SMA expression was observed in both OPSCC subtypes ($p>0.05$), it provided further survival stratification in the HPV-positive group (n= 87) with significant prognostic value for the poor prognosis (Log-Rank $p=0.02$).

To investigate the functional role of CAFs in HPV-positive and HPV-negative OPSCC TME, we had first to establish a strong framework of understanding in OPSCC fibroblast phenotypes. Using 3 normal tonsillar fibroblasts cultures (NTFs), myofibroblastic and senescent *in vitro* models were established and characterised; moreover, two OPSCC-derived CAF cultures, originating from HPV-positive tumours, were established and characterised. The comparison between OPSCC CAFs models and previous data from previously established models derived from oral fibroblasts revealed no differences in the developed phenotypes in responses to TGF-β1 and H_2O_2 stimuli (which in oral fibroblasts induce myofibroblast differentiation and senescence, respectively), suggesting that the biological differences in OPSCC subtypes are mainly attributed to cancer cells and their capacity to modulate the underlying microenvironment.

With the purpose to test this hypothesis, cytokine expression profiling was performed on *in vitro* co-culture 2D models to identify novel candidates in the crosstalk between OPSCC tumour cells and fibroblasts. Osteopontin (OPN) was identified among other factors as a novel secreted factor, particularly with HPV-negative OPSCC cell line (SCC89), but not with HPV-positive cell line (SCC2). Using interactive co-culture 2D models provided further validation regarding OPN expression and revealed an upregulation in IL-6 in the associated fibroblasts in the co-cultured model.

The preliminary investigation of OPN effect on NTFs showed a potential alteration in NTF phenotype. Targeting CD44v6 attenuated the production of Interleukin-6 (IL-6) in recombinant OPN-induced NTFs. However, blocking of CD44v6 on NTF before the incubation with OPSCC cell line conditioned media revealed a variable degree of IL-6 reduction. The initial assessment of OPN effect on OPSCC cell lines demonstrated activation of CD44 receptor in response to recombinant OPN treatment that was more evident in HPV-negative cell lines.

Assessment of OPN expression on the study cohort was limited to IHC; this indicated OPN as an independent prognostic biomarker in OPSCC associated positively with favourable survival at univariate and multivariate regression models (HR= 0.37; 95% CI: 0.17-0.79, p-value = 0.01) and (HR= 0.44; 95% CI: 0.20-0.93, p-value = 0.03) respectively.

Conclusion: The isolation and characterisation of OPSCC fibroblasts described provide novel insights into the role of CAFs in OPSCC mediated by OPSCC cancer cell:CAF crosstalk. Moreover, it is proposed that α-SMA has the potential as a prognostic biomarker for HPV-positive OPSCC stratification. The positive correlation between OPN overexpression and survival warrants further investigations.

Acknowledgement

First and foremost, I would like to express my sincere gratitude to my supervisor Professor Keith Hunter for his endless support, encouragement and guidance during my Master and PhD studies. I have learnt so much from his extensive knowledge, dedication and wisdom, for that I cannot thank him enough.

I would like to thank my second supervisor, Professor Daniel Lambert for his valuable contribution and advice throughout this journey. I have been lucky to have a supervisor who cared so much about my work. Also, I must say thanks to Dr Robert Bolt for his supervision in the tissue culture lab work during the first year.

A big thank you to all the technical staff who helped me along these four years; Brenka, Jason and Kirsty and do not miss Hayley and David for their advice in TMAs construction. Special thanks to my colleagues in Hunter's group; Sven, Hannah and Cony for their assistance whenever I needed it, and to the other fabulous people on the third floor Esra, Mariem, Asma, Basma, Karima and Antia. My lovely friends Hajer and Alaa, I must acknowledge you here for your endless help, support and kind words. Our friendship is one of the best things that I achieved during my study abroad.

Thanks, must be shown to Ministry of Education - Libya and the University of Benghazi, for funding my postgraduate's studies.

My beloved, no words would suffice to express my deep gratitude for the unconditional love, support, and inspiration. I must say conducting research and raising kids is not an easy task, but without your assistance, this would not have been achievable. I appreciate your new excellent skills in cooking, home-schooling, and kids caring besides doing your job. I just can say I love you!

And not to miss my co-author, my baby, Ibrahim who collaborated the lab work for 9 months during the third year, joined online supervisory meetings and added his fine touches on the keyboard during my writing up. Hodayfa and Rahaf your frequent tiny cards which filled with warm wishes and a lot of kisses were meant a lot to me. I love you all xxx.

My parents and brothers although I spent these years away from you, that was to meet your dreams and inspirations to be fully proud of your daughter. I owe it all to you.

.

Publications

Hendawi, N., Niklander, S., Allsobrook, O., Khurram, S., Bolt, R., Doorbar, J., Speight, P. and Hunter, K., 2020. Human papillomavirus (HPV) can establish productive infection in dysplastic oral mucosa, but HPV status is poorly predicted by histological features and p16 expression. *Histopathology*, 76(4), pp.592-602.

Al-Sahaf, S., **Hendawi, N.**, Ollington, B., Bolt, R., Ottewell, P., Hunter, K. and Murdoch, C., 2021. Increased Abundance of Tumour-Associated Neutrophils in HPV-Negative Compared to HPV-Positive Oropharyngeal Squamous Cell Carcinoma Is Mediated by IL-1R Signalling. *Frontiers in Oral Health*, 2.

Disclaimer

The entirety of the laboratory work and clinical data analysis presented in this thesis, unless otherwise stated, is that of the author. The author has been responsible entirely for writing up and drafting. A thesis editor has not been used.

Table of content

List of Tables

Chapter 1

Chapter 2

Chapter 3

Chapter 5

Chapter 7

List of Figures

Chapter 1

Chapter 2

Chapter 3

Chapter 5

Chapter 6

Chapter 7

Chapter 9

Abbreviations

AJCC	American Joint Committee on Cancer.
AUC	Area Under Curve
BCA	Bicinchoninic Acid assay
CAFs	Cancer-Associated Fibroblasts
CAP	College of American Pathologists
CCL2	C-C motif ligand 2
CK	Cytokeratin
COL11A1	Collagen 11-α1
dH2O	Distilled Water
DMEM	Dulbecco's Modified Eagle's Media
DMSO	Dimethyl Sulphoxide
E	Early genes
ECM	Extracellular Matrix
ELISA	Enzyme-Linked Immunoassay
EMT	Epithelial to Mesenchymal transition
EndMT	Endothelial to Mesenchymal Transition
EVs	Extracellular vesicles
FAP	Fibroblast Activation Protein
FBS	Fetal bovine serum
FFPE	Formalin-Fixed and Paraffin-Embedded material
FSP	Fibroblast-specific protein
GM-CSF	Granulocyte-Macrophage Colony Stimulating Factor
GS-OSCC	Genetic Stable-Oral squamous cell carcinoma
GU-OSCC	Genetic Unstable- Oral squamous cell carcinoma
H-score	Histo-score
H2O2	Hydrogen Peroxide
HDMEC	Human Dermal Microvascular Endothelial Cells
HLA-DR	Human Leukocyte Antigen–DR
HNSCC	Head and Neck Squamous Cell Carcinoma
HPV	Human papillomavirus
HR	Hazard Ratio
hr-HPV	high-risk Human papillomavirus
IHC	Immunohistochemistry
IL	Interleukin

iOPN	Intracellular Osteopontin
ISH	In Situ Hybridization
KLK	Kallikrein
L	Late genes
LCR	Long Control Region
M	Media
MAPK	Mitogen-Activated Protein Kinase
MDM	Monocyte-Derived Macrophage
NC	Negative Control
NICE	National Institute for Health and Care Excellence
NOFs	Normal Oral Fibroblasts
NOK	Normal oral keratinocyte
NTFs	Normal Tonsillar Fibroblasts
OP	Oropharynx
OPN	Osteopontin
OPSCC	Oropharyngeal Squamous Cell Carcinoma
OSCC	Oral squamous cell carcinoma
PBS	Phosphate-buffered saline
PCR	Polymerase Chain Reaction
PIS	Premature Induced Senescence
pRb	Retinoblastoma protein
PVDF	Polyvinylidene difluoride
Ref	Reference
RIPA	Radioimmunoprecipitation Assay Buffer
ROC curve	Receiver Operating Characteristic curve
ROS	Reactive Oxygen Species
RT	Room Temperature
SA-β-gal	Senescence-Associated β-galactosidase Staining Assay
SASP	Senescence-Associated Secretory Phenotype
SCC	squamous Cell Carcinoma
scRNA-seq	Single-cell RNA Sequencing
sOPN	Secretory OPN
TE	Trypsin/ Ethylenediaminetetraacetic acid
TGF-β1	Transforming growth factor beta 1
TME	Tumour Microenvironment

UICC	Union for International Cancer Control
URR	Upstream Regulatory Region
α-SMA	alpha-smooth muscle actin
β2M	beta 2 microglobulin

Chapter 1: Literature Review

1. Literature Review

1.1 Oropharyngeal squamous cell carcinoma

The oropharynx (OP) is the middle part of the pharynx that extends from the mobile soft palate superiorly to the upper border of the epiglottis inferiorly. Anteriorly, it is bordered by the base of the tongue and laterally by the tonsillar pillars with palatine tonsils and lateral pharyngeal walls. The back wall of the pharynx represents the posterior boundary of the oropharynx (Logan, 2016) (Figure 1.1). Oropharyngeal squamous cell carcinoma (OPSCC) is one of the head and neck cancers (HNC) that has been studied intensively in the literature, coinciding with marked increases in incidence over the last three decades. The traditional HNC risk factors (tobacco use and alcohol drinking), in addition to HPV oncogenic infection, are considered the main risk factors for OPSCC development. Diversity in risk factor distribution among countries, besides the demographic disparities, reflect the discrepancies in OPSCC trends worldwide, making the understanding of OPSCC epidemiology a complex issue. However, generally, HPV-positive OPSCC displays distinct clinical and molecular profiles from its HPV-negative counterpart, in addition to superior prognosis. This advantage offers the possibility of reducing treatment intensity in HPV-positive OPSCC populations to improve patients' quality of life while maintaining a favourable clinical outcome.

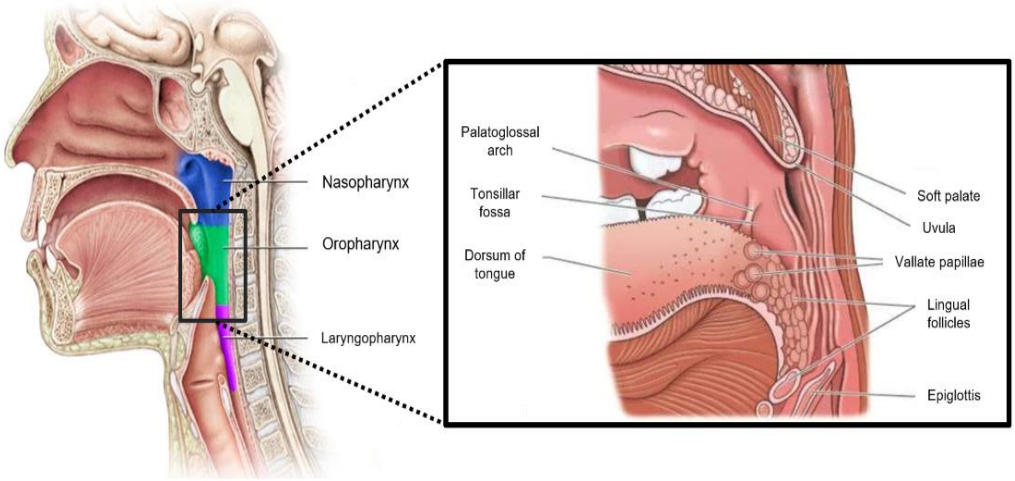

Figure 1.1: The anatomy of the oropharynx. Parts of the pharynx (l*eft*). A detailed illustration of the oropharynx (*Right*). The illustration is modified from (Oropharynx: Introduction, 2021) and (Parts of the throat (pharynx), 2021).

1.1.1 OPSCC Risk factors

Tobacco and alcohol consumption are known as the traditional primary causes for the development of HNC and they are responsible for approximately 80% of upper aero-digestive tract cancers (Schiffman, Clifford and Buonaguro, 2009). Cigarette smoking is a common form of tobacco consumption. It comprises a complex mixture of more than 500 carcinogenic and mutagenic substances, including polycyclic aromatic hydrocarbons, N-nitrosamines, formaldehyde, and a variety of free radicals (Schlotzhauer and Chortyk, 1987; Zhang *et al.*, 2003). The synchronised consumption of alcohol and tobacco further potentiates the risk of cancer developing (Kreimer *et al.*, 2005), however, the mechanism of pathogenicity of alcohol in the development of cancer is still unclear.

In the literature, the presence of a significant proportion of OPSCC patients who are non-smokers and non-drinkers suggests different aetiological factors. Since the 1970s, when the aetiological role of HR-HPV was initially proposed, a large number of reports have offered supportive evidence regarding the significant association between OPSCC and HPV oncogenic infection. In 2009, the International Agency for Research on Cancer (IARC) acknowledged HPV 16 as a causative agent in OPSCC (Bouvard *et al.*, 2009), then the categories of HPV-positive or HPV-negative tumours were formally introduced in the World Health Organization 2017 classification of HNC (El-Naggar *et al*., 2017).

HPV-associated OPSCC is described as a sexually acquired disease, with a most likely genital-oral route of infection (D'Souza *et al.*, 2007a; Heck *et al.*, 2010; Gillison *et al.*, 2015). High-risk HPV genotypes have been detected in OPSCC, mainly HPV 16 genotypes, that were reported at a higher percentage of detection in HPV-positive OPSCC (>85%) (Kreimer *et al.*, 2005; Schache *et al.*, 2011; Craig *et al.*, 2020; Zamani *et al.*, 2020). Changes in sexual behaviour were believed to be the primary risk factors in developing HPV-positive OPSCC (Rettig, Kiess and Fakhry, 2014). Earlier age at sexual debut, a higher number of lifetime oral and genital sexual partners (greater than 8-10), women with HPV-positive cervical lesions and their partners and an increase in oral sex practices (>6-4 oral sexual partners), all these are considered risk factors in developing HPV-OPSCC (D'Souza *et al.*, 2007a; Heck *et al.*, 2010; Selcuk, 2016).

1.1.2 Epidemiology

OPSCC has been highly debated over the last two decades. In 2018, the epidemiological data presented 140,000 new cases of OPSCC in addition to 50,000 deaths worldwide. The burden attributed to HPV-associated OPSCC was estimated to be a third of all OPSCC cases (42,000 cases) (Bray, Ferlay and Soerjomataram, 2018; Martel *et al.*, 2020). However, this proportion may not portray the realistic picture of HPV driven OPSCC incidence in the epidemic areas. There is a great discrepancy in the distribution of HPV-related OPSCC around the world, with a high increase in incidence being most observed in North America, Europe, and Australia (Martel *et al.*, 2017). The alarming increase in OPSCC in epidemic countries was believed to be linked to an HPV oncogenic infection that was reported as being responsible for around 70% of all OPSCC. However, due to the inconsistency in HPV detection methods between the reports, the range in this percentage was between 18% and 65%, as presented in a recent systematic review assessing HPV prevalence in Europe (Stjernstrøm *et al.*, 2019).

Although the early evidence from western countries showed an evident increase in HPV-associated OPSCC compared to non-HPV OPSCC in the period between 1988-2011 (Schache *et al.*, 2011; Gillison *et al.*, 2015; Schache *et al.*, 2016), the following data in the period between 2002-2015 showed a levelling out of HPV incidence that was accompanied by a comparable increase in non-HPV related OPSCC, suggesting the possible contribution of another aetiological factor to the growing OPSCC incidence (Schache *et al.*, 2016). This observation was based on the largest nationwide study (n=1710) recruited from 11 centres around the UK (Schache *et al.*, 2016). However, in a recent comparable large population-based study (n= 2169) from Eastern Denmark that covered a consecutive 18-year span (2000-2017), there was an increase in OPSCC incidence per 100,000 from 1.8 in 2000 to 5.1 in 2017, with a trend break around 2008. Intriguingly, oncogenic HPV infection was the main contributor to the total OPSCC figure. The incidence of HPV-positive OPSCC was increased by 3-fold compared with a 2-fold increase in HPV-negative OPSCC (Zamani *et al.*, 2020). It is worth mentioning here that in 2020, Denmark recorded the highest OPSCC incidence in Europe according to the European Cancer Information System (2021).

The promising effect of the HR-HPV vaccination programme could potentially prevent HPV-related cancer; however, changes in the incidence due to the vaccination are not expected to be observed until after 2060 (Gillison *et al.*, 2015).

1.1.3 OPSCC Patient profile

HPV-positive HNSCC possesses unique demographic characteristics with features that are distinct from the classic population of HNC patients. HPV-positive OPSCC patients tend to be overwhelmingly male, mostly Caucasian, within the middle age group (less than 60 years) (Gillison *et al.*, 2015; Schache *et al.*, 2016; Zamani *et al.*, 2020; Sheth *et al.*, 2021). However, recent studies reported an expansion of the age group up to more than 70 years (Zumsteg et al., 2016, Melina et al., 2018, Rettig et al., 2018 a, Rettig et al., 2018 b). The favourable prognosis is a characteristic in HPV-positive OPSCC white patients, whereas evidence has suggested that racial disparities have a lower survival effect (Schrank *et al.*, 2012; Sheth *et al.*, 2021)

In the USA, compared to HPV-negative OPSCC patients, HPV-positive OPSCC patients are unlikely to have a history of tobacco and alcohol. In the majority of OPSCC, HPV-positive OPSCC consists of about 30% non-smokers, while in the HPV-negative group, the percentage of non-smokers is less than 5% (Hong *et al.*, 2013). The site distribution of HPV-positive OPSCC shows it is more common in tonsil and base of tongue subsites and less common in the soft palate and uvula (Bishop, 2015). This association between the virus and these anatomical subsites is unexplained but may be related to the anatomical structure of the tonsillar mucosa including deep invagination and a reticulated epithelium structure, which might offer virus capture and maintenance sites and promote its access to basal cells (Chu *et al.*, 2013).

Histologically, HPV-positive OPSCC displays a distinct pattern from conventional OPSCC. In HPV-unrelated lesions, the origin of tumour epithelium is the lining epithelium and often shows squamous differentiation in the form of squamous pearls (keratinization) and abundance of keratinizing cytoplasm attributing for the “pink” appearance of the tumour at low-power. Unlike conventional OPSCC, HPV-positive OPSCC arises from the specialised lympho-epithelium of the tonsillar crypts and the tumour lacking keratin formation. The general appearance of HPV-related OPSCC is characteristically “blue”, which might be attributed to the high nuclear-cytoplasmic ratios, and numerous tumour-associated lymphocytes (Bishop, 2015). Initially, HPV-positive OPSCC was described as “a non-keratinized, poorly differentiated basaloid tumour” (Gillison et al., 2000); however, after further histopathological analysis, these terms have been modified and used more specifically. Although most HPV-positive OPSCCs demonstrate some basaloid features, they usually are not aggressive tumours. Using the “basaloid” term may not precisely reflect that fact; furthermore, most HPV related OPSCCs do not exhibit the basaloid SCC criteria that were set out initially by Wain *et al.* (1986). According to

the classical SCC grading system, most HPV-positive OPSCCs have been graded as poorly differentiated, and that description might be attributed to the origin of the tumour cells which resemble the tonsillar crypt epithelium rather than tumour behaviour; particularly, this subtype of OPSCC possesses a better prognosis and response to the treatment (Bishop, 2015). From this point, some authors have suggested to regard HPV-positive OPSCC as well-differentiated (Westra, 2012), whereas others have agreed not to assign a histologic grade to HPVSCC (Lewis, Chernock and Chernock, 2014). In the 4th edition of the WHO head and neck tumour classification, the histologic grading of HPV-positive OPSCCs has been discouraged until appropriate histologic correlates are established (El-Naggar *et al*., 2017).

HPV-positive OPSCC patients usually present with small primary tumours that are associated with more advanced nodal disease (O'Sullivan *et al.*, 2012). Nodal disease may be present as a cystic lesion as a consequence of tumour necrosis, which is sometimes misdiagnosed clinically and histologically as a branchial cleft cyst, especially if the primary tumour is asymptomatic (Corey and Hudgins, 2012; Pickard *et al.*, 2012). Compared with HPV-negative OPSCC at the same advanced tumour stage, HPV patients demonstrate better clinical outcomes. Based on these features, HPV-positive OPSCC has been categorised as a separate entity from non-HPV related OPSCC, with a distinct staging system, in the last TNM edition of the American Joint Commission on Cancer (AJCC/UICC 8).

HPV-related OPSCCs have been reported with an unusual pattern and timing of metastases. HPV-OPSCC has a higher tendency to disseminate to distant sites rather than the head and neck region. Secondary non-keratinized SCC has been reported in bones such as vertebrae, humerus and multiple organs such as skin, lung, liver, pancreas (Mü *et al.*, 2012). Additionally, in HPV-positive patients, these metastases might appear after 2 years from the initial treatment, whereas patients with HPV-negative OPSCC typically presented with metastases within 2 years (O'Sullivan *et al.*, 2013).

1.1.4 De-escalation of therapy in HPV-positive OPSCC

Currently, strategies in OPSCC management are determined by conclusive decisions in multidisciplinary meetings depending on presented data regarding the histopathological features, tumour stage, general patient health, and fitness. At the early stage, surgery or radiotherapy are the available options, however, in more advanced stage disease with

lymph node metastases, surgery combined with postoperative radiotherapy or chemoradiotherapy are the treatment options. Cytotoxic chemotherapy and targeted drugs such as Methotrexate, 5-fluorouracil, Bleomycin, Cisplatin, Cetuximab, and Nivolumab have been used accompanied by radiotherapy. Unfortunately, despite different treatment modalities and approaches, the five-year survival rate for HNSCC has not shown an improvement over the past few decades. At the same time, the majority of patients who are completely cured still suffer from late side-effects resulting in non-cancer morbidity and even mortality in a small proportion.

The emergence of an HPV-associated OPSCC subtype with better survival rates has encouraged clinicians to explore modifying non-surgical therapy according to the viral status with the aim to decrease acute and long-term treatment morbidity and mortality, and at the same time maintain survival (Sturgis and Ang, 2011). This would involve de-intensification of treatment protocols using less invasive surgical procedures, such as organ preservation by transoral robotic surgery or transoral laser microsurgery; also, de-intensifying radiation therapy dosage and using targeted molecular agents or immunotherapy as an alternative for chemotherapy (Budu *et al.*, 2019). However, Initial clinical trials investigating this concept have not proven successful (Mehanna *et al*., 2018).

1.2 Human papillomavirus

Human papillomaviruses belong to the Papillomaviridae family which are characterised by a non-enveloped DNA genome and high affinity to the cutaneous and mucocutaneous epithelium (Burk *et al.*, 2011). HPV subtypes can cause a wide range of diseases from benign lesions such as benign condylomas to invasive tumours involving different organs. However, HPV's affinity to mucosal squamous epithelia varies depending on the histological features of different body organs; for instance, the squamocolumnar junction zone in the cervix has shown to be a highly susceptible location for HPV infection (Herfs *et al.*, 2012).

1.2.1 HPV Structure

The virus genome size is approximately 8 kb, while the size of the virion (infective form) is around ~55 nm in diameter (Zheng and Baker, 2006). All papillomaviruses consist of a circular double-stranded, non-enveloped DNA genome which is divided into three major regions separated by two polyadenylation sites. The "Early region" occupies over 50% of the virus genome and encodes six genes including E1, E2, E4, E5, E6 and E7. This part is responsible for virus replication and cellular transformation. The "Late region" encodes the L1 and L2 capsid proteins which are responsible for virion self-assembly and release. The third region is the "Upstream Regulatory Region" (URR), also known as "Long Control Region" (LCR), which includes transcription factor-binding sites and controls gene expression (Danos, Katinka and Yaniv, 1982; Zheng and Baker, 2006) (Figure 1.2).

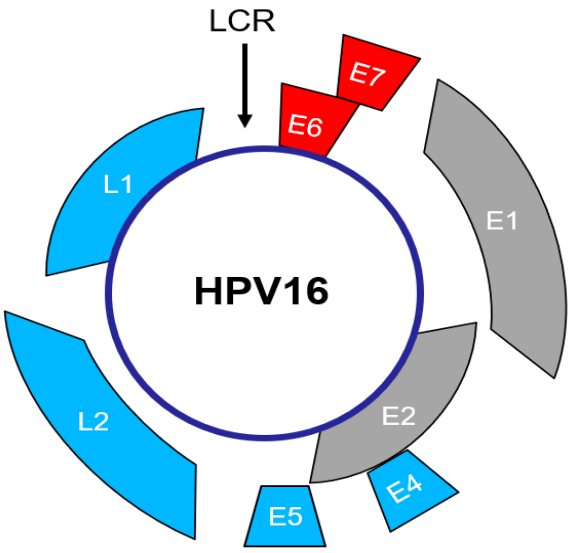

Figure 1.2: HPV16 genome organisation. Illustration showing the position of the three major regions of the HPV genome: (E) early genes, (L) late genes, and (LCR) long control region. The illustration was created using PowerPoint software, adapted from Berg and Archambault (2010).

1.2.2 HPV Classification

The HPV genotype classification scheme has proven its efficiency in different applications such as in basic research, clinical evaluation, epidemiological studies and vaccine generation (Bzhalava, Eklund and Dillner, 2015). The given number in the HPV genotype name is dependent on the nucleotide sequence in the open reading frame (PRF) which encodes the capsid protein L1. According to the similarity within the L1 part of the genome, HPV has been categorised into major five genera: α-papillomavirus, β-papillomavirus, γ-papillomavirus, mu-papillomavirus, and nu-papillomavirus among the 65 genotypes under the α-papillomavirus category, a limited set of viruses are linked to precursor and cancer development (Bernard *et al.*, 2010).

According to epidemiological data on cervical cancer aetiology, HPV has been classified based on the oncogenic capability into two groups: high risk and low-risk. However, in head and neck squamous cell carcinoma (HNSCC), an HPV low-risk group also was detected. HPV 11 and HPV 6 were reported in association with squamous cell carcinoma (SCC) of the larynx and giant condyloma acuminatum (D'Souza *et al.*, 2007; Osei-Sarfo *et al.*, 2013).

HPV-16 is the most common type associated with SCC in the cervical and head and neck region. Over 80% of OPSCC is associated with HPV-16, while this percentage is lower in cervical cancer (60%) (Gillison *et al.*, 2008; Sanjose *et al.*, 2010). HPV-16 genotype was correlated with a better prognosis compared to HPV-18 in cervical cancer and OPSCC (Kónya *et al.*, 1995; Thibaudeau *et al.*, 2013; Mazul *et al.*, 2016).

Besides the heterogeneity in virus virulence among HPV genotypes, lineages and sub-lineages originated from the same genotypes exhibit distinct phenotypic profiles. Differences between lineages were observed in their ability to induce the tumour; for instance, HPV 31 A and B lineages have a higher risk than lineage C in developing cervical intraepithelial neoplasia grades 2 and 3 (Xi *et al.*, 2014). Moreover, some lineages appeared with characteristic geographic dispersion, with HPV58 sub-lineage A3 being highly detected in East Asia compared to other HPV58 variants and associated with 7-9 fold higher in cervical cancer development (Chan *et al.*, 2011). These data suggest further investigations on HPV genomes and variants classification that might provide a new basis for the preventative/therapeutic interventions of HPV infection and epidemiology studies.

1.2.3 Pathogenesis of HPV related cancer

The full mechanism of HPV gene regulation within the differentiated keratinocyte is still unclear. According to the observations in cervical cancer, there is a general agreement that the non-structural proteins which include E1, E2, E4, E5, E6 and E7 are expressed in the basal cell layer and intermediately differentiated keratinocytes, whereas the two-structural viral capsid proteins that include L1 and L2 are expressed at more superficial layers in keratinocytes undergoing terminal differentiation (Longworth and Laimins, 2004). Thus, HPV oncoprotein expression is proportional to their function during the virus life cycle: E1 and E2 contribute to HPV DNA replication and the regulation of the process of early transcription; E5 increases the proliferative capacity of keratinocytes; E6 and E7 maintain the differentiating keratinocyte in a state that allows viral genome amplification and consequent late gene expression; and E4 associates with cytokeratin filament collapse and virion assembly (Zaravinos, 2014) (Figure 1.3).

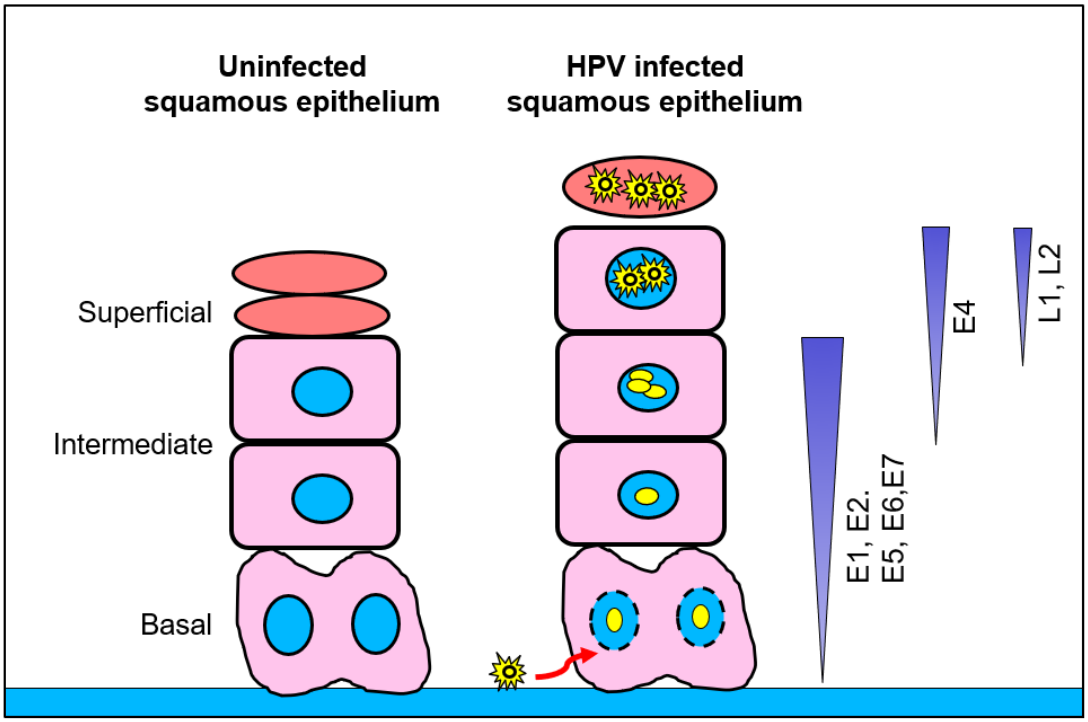

Figure 1.3: The HPV productive life cycle. Uninfected epithelium (left) and HPV infected epithelium (right). The HPV life cycle is dependent on epithelial differentiation and coincident with virus protein expression. Expression of HPV proteins within the stratified epithelium is correlated with their function in infection establishment and virion production. The infection starts by virion penetrating the basal layer and is maintained at low copy numbers until cells start to differentiate to increase the expression of early proteins (E1, E2). By entering the differentiating cells into the active cell cycle, the viral genome starts to amplify, making a high copy number coincident with E6/E7 expression. At higher layers, L1, L2 and E4 start to be expressed at a high level to enable virion assembly and egress. Finally, on reaching the superficial layers of epithelium, virion particles are released. The illustration was created using PowerPoint software, adapted from Mac and Moody (2020).

E6 and E7, which are known as HPV viral oncogenes, are characterised by their pleiotropic functions in overlapped pathways, resulting eventually in cell immortalisation, genetic instability alongside virion production (Yim and Park, 2005). E6 protein acts on p53 protein through ubiquitin ligase E6-associated protein (E6AP), leading to p53 ubiquitin changes and proteasomal degradation of p53 (Huibregtse, Scheffner and Howley, 1991). p53 is known as the “guardian of the genome” due to its regulatory effect on cell cycle arresting and apoptosis formation as a response to cellular stress or DNA damage, while loss of p53 check-point leads to uncontrolled cell cycle progression (Huibregtse, Scheffner and Howley, 1991).

Similarly, E7 protein elicits its action through Rb/E2F inactivation which results in cell cycle promotion and reciprocal p16 overexpression. p16 protein is a cell cycle inhibitor that controls the G1-S phase transition of the cell cycle by inhibiting phosphorylation of retinoblastoma protein (pRb)/E2F complex leading to E2F release and subsequently cell cycle activation (Bova *et al.*, 2001). This pathway is regulated by E2F re-binding to Rb. E7-pRb/E2F complex interaction results in an independent release of E2F which results in loss of the p16 feedback loop (Figure 1.4). The high affinity of E6 and E7 protein to bind p53 and Rb is a feature of high-risk HPV rather than low-risk genotypes (Jones and Münger, 1996), however, the correlation between p16 pattern of expression in OPSCC and low-risk HPVs has not been studied thoroughly yet.

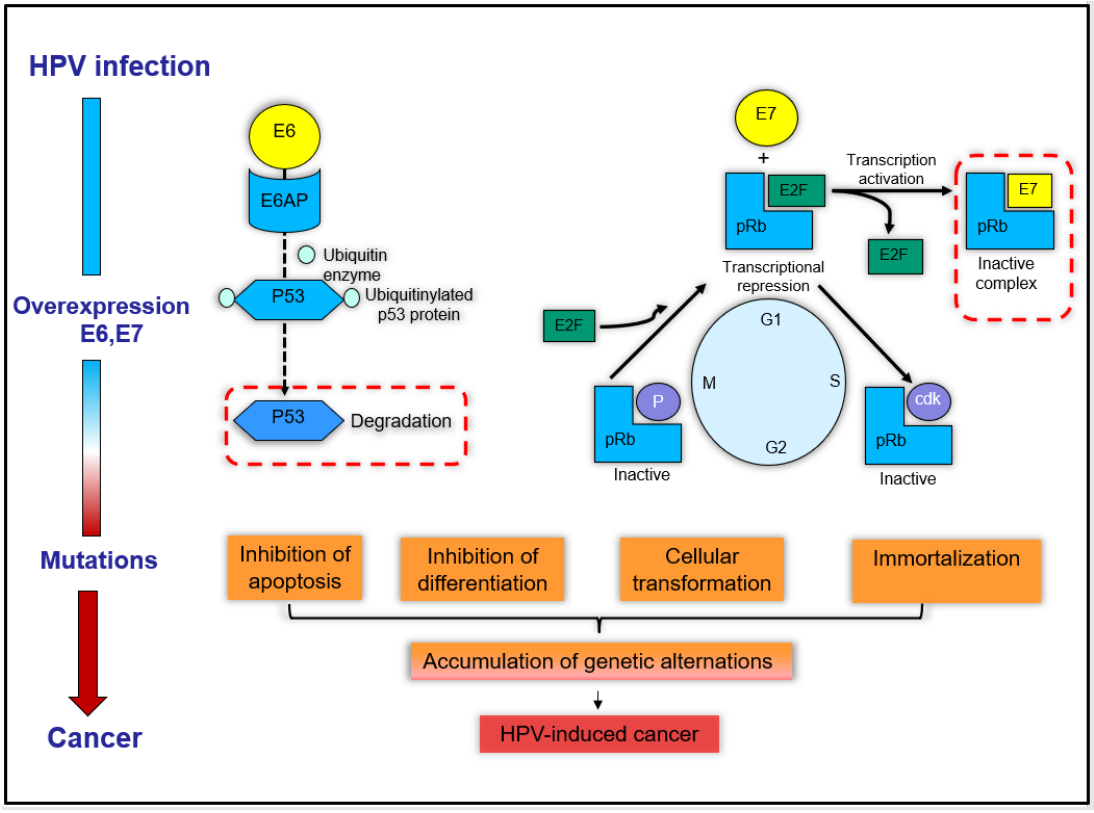

Figure 1.4: Dysregulation of cell cycle proteins mediated by HPV oncoproteins. E6 and E7 viral oncogenes target P53 and pRb, respectively, and cause irreversible degradation and inactivation. The abrogation of cell cycle regulators (p53 and pRb) leads eventually to genetic instability which contributes to the development of cancer. The illustration was created using PowerPoint software, adapted from Yim and Park (2005) and Mirghani *et al.* (2014).

The pathogenesis of HPV-associated cervical lesions is well documented in the literature, whereas in OPSCC, the precise mechanism of HPV pathogenesis still is unclear. Although there is some evidence suggesting the same mechanism in OPSCC, including detection of E6 and E7 oncogenes within the tumour, p16 biomarker overexpression, and lack of p53 somatic mutations (El-Naggar & Westra 2012; Mork *et al*. 2001), the comparison of HPV pathogenesis between cervical cancer and OPSCC reflects discrepancies in several aspects that might suggest a different unexplained mechanism in OPSCC. Cervical cancer is developed over a sequential progression process from low premalignant phase to high-grade intraepithelial neoplasias. However, in OPSCC, the vast majority of lesions present primarily at an advanced neoplastic stage and the concept of *in situ* carcinoma or precancerous has not been identified in OPSCC, which may be due to the histological nature of lymphoid tissue (Westra, 2012). Moreover, *in vitro* observations reported a transition from HPV-genome as extrachromosomal episomes into a genome integrated form in higher grade dysplastic epithelium. This feature is a characteristic of cervical lesions, while it is found to be less frequent in OPSCC. Non-integrated HPV episomes are the predominant form in OPSCC (Pett *et al.*, 2004; Gao *et al.*, 2014; Olthof *et al.*, 2014; Morgan, Dinardo and Windle, 2017). HPV productive mechanism through the stratified squamous epithelium is understood and documented in the cervical and oral mucosa (Griffin *et al.*, 2015; Hendawi *et al.*, 2020), however, it is not known if the virus establishes a productive infection in the 'unsorted' keratinocytes of the tonsil crypt.

1.2.4 Methods of HPV detection

The basic clinical requirement of HPV testing is the detection of HPV-relevant infection within the lesion. Identification of HR-HPV E6/E7 mRNA is strong evidence of transcriptionally active infection (Smeets *et al.*, 2007). E6/E7 mRNA (qRT-PCR) for HR-HPV has been suggested as a gold standard test in fresh-frozen tissue (Gillison *et al*. 2000), however, in practice, implementation of this technique in routine clinical settings is challenging; the test sensitivity depends mainly on the integrity of RNA in a fresh tissue sample that could deteriorate during the fixation process in FFPE material (Schache *et al.*, 2011). Different strategies have been investigated concerning HPV detection in HNSCC, including HPV DNA, HPV RNA, HPV oncoproteins, HPV-related cellular proteins, and HPV antibodies. Meanwhile, the target is to achieve a reliable, accurate method that can be applied with less cost in the clinical setting (Westra, 2014).

1.2.4.1 p16 IHC - The surrogate biomarker

Klussmann *et al.* (2003) were the first to suggest p16 IHC expression as a surrogate for HPV infection. Years later, Lassen *et al.* (2009) correlated p16 IHC expression with the survival in OPSCC as part of the Danish Head and Neck Cancer Group (DAHANCA) 5 Trial. Overexpression of p16 IHC has been used widely in clinical settings as a surrogate biomarker for HPV associated lesions in cervical and head and neck lesions. p16 abundance in tissue is believed to be attributed to cell cycle protein dysregulation mediated by E7 expression (McLaughlin-Drubin, Crum and Münger, 2011). Due to its acceptable sensitivity, high prognostic value and cost-effectiveness, p16 has been utilised by the majority as a first-line test for HPV in OPSCC. In 2017, the eighth edition of the staging manual of AJCC proposed p16 as the key test for OPSCC stratification into p16-positive and p16-negative OPSCC sub-entities. The classification was based on compelling evidence supporting p16 as highly predictive. In the same year, the College of American Pathologists (CAP) issued the recent update on HPV detection guidelines that recommended p16 IHC testing in OPSCC, with emphasis on using >70% p16 tissue positivity as a threshold. Adding a specific test is also suggested in areas with low HPV prevalence (Lewis, 2020).

These guidelines were accompanied by ongoing evidence highlighting the shortcomings of p16 regarding specificity and emphasising the necessity of adopting algorithm-based two-test protocols in HPV testing (Schache *et al.*, 2011). Although p16 is considered a strong independent prognostic biomarker in OPSCC, it has low specificity (82%) against the gold standard test. False-positive p16 expression has been detected in the normal structure of pharyngeal mucosa and in various tumours independent of HPV which might be due to other mechanisms involved in pRb inactivation such as gene deletions, point mutations or epigenetic modifications (Witkiewicz *et al.*, 2011). p16's relatively low specificity is responsible for a percentage of non-HPV related patients (5%-20%) who demonstrated worse outcomes compared to the HPV-negative group. Another pitfall in considering p16 IHC for testing is the ambiguity regarding the positivity threshold of the test; >70% tissue strong positivity is generally defined as the cut-off and that was stressed within CAP guidelines, however, partial staining of 50–70% revealed a number of HPV-related cases using other HPV tests (Carpén *et al.*, 2018).

1.2.4.2 Two-step Algorithms

With the purpose to enhance the low specificity of p16 IHC, an HPV-specific test was suggested to be included, establishing two step-wise algorithms. Smeets *et al*. (2007) were the first to propose and test this concept. p16 IHC and (Gp)5+/6+ Polymerisation chain reaction (PCR) algorithm revealed superior performance with 100% sensitivity and specificity compared with the gold standard test, however, it is worth mentioning that the PCR primers were designed to cover the HPV16 genotype only, and the analysis was limited to 48 cases of HNSCC. In a larger cohort of OPSCC (n=108), Schache *et al*. (2011) reported acceptable diagnostic and prognostic performance for p16 IHC / DNA qPCR algorithm compared with the reference test (97% sensitivity and 94% specificity, overall survival p=0.002). The qRT-PCR primers in this study cover HPV 16, 18 and 33 genotypes. p16 IHC / HR HPV in situ hybridization (ISH) combination displayed relatively low specificity that affected the prognostic performance of the algorithm (p=0.02). DNA ISH covers 12 genotypes of high-risk HPV.

Schache *et al*., among others, emphasised that HPV DNA PCR or HPV DNA ISH should not be used alone. Although the PCR technique is known for its high sensitivity in simplifying detection of low copy numbers of viruses, the risks of contamination and detection of latent or transit HPV infection increase the false positive risk (Robinson *et al*. 2012; Venuti and Paolini 2012; Westra, 2014). DNA ISH is preferable to qRT-PCR since it is applicable for formalin-fixed and paraffin-embedded material (FFPE). It provides clinical significance as it permits direct visualisation of HPV DNA signals within the section (Moutasim, Robinson, and Thavaraj 2015). However, DNA ISH is considered less sensitive for low copy number infection. Increasing the number of signal amplification steps improved DNA ISH sensitivity, although that was on account of background clarity (Huang *et al*., 1998). Advances in using automated systems have made DNA ISH a convenient procedure for sample processing in most pathology laboratories. In the UK, currently, HPV DNA ISH is the second line test for all p16-positive OPSCCs to confirm HPV status and is recommended by the National Institute for Health and Care Excellence (NICE, 2021).

1.2.4.3 RNAScope assay

HPV RNA testing has been demonstrated as a more reliable approach. Detecting the transcriptionally active mRNA within the tumour relieves any doubt regarding the viral contamination or thoughts of transient non-related infection (Mirghani *et al.*, 2016; Plebani *et al.*, 2018). Nevertheless, the standing challenge is the feasibility of implementing this approach in FFPE tissue material. While RNA PCR offers excellent sensitivity, the technical hurdles were enough to exclude the test from clinical settings (Amin *et al.*, 2017).

In the last decade, the investments of Advanced Cell Diagnostics (ACDbio, CA, USA) in RNA-ISH introduced RNAScope assay as a promising alternative in FFPE material. The technique is based on a unique "Z-shaped" complementary probe to E6 and E7 mRNA nucleotides that offers superior advantages; the lower arm of the probe provides high sensitivity and mRNA identification, and the upper arm amplifies the signals specifically within a clear background which makes results interpretation an easy forward step. Visualisation of in-situ E6/E7 mRNA chromogenic signals definite evidence on the viral involvement in lesions development.

RNAScope diagnostic performance against the reference test (E6 E7 mRNA qRT-PCR) was evaluated firstly by Schache *et al*. (2013), followed by Mirghani *et al*. (2015). The test revealed high sensitivity (97% and 93%) and specificity (93% and 94%, respectively) with respect to the difference in HPV probes number between the two studies (7 and 18, respectively). Although RNAScope demonstrated excellent prognostic performance, an unproven issue remains in the literature regarding whether it is superior to p16 or at least at an equivalent level. A few studies reported a comparison between RNAScope and p16 prognostic values (Ukpo *et al*., 2011, Schache *et al*. 2013, Craig *et al*., 2020). At univariate analysis, RNAScope displayed an equivalent prognostic value to p16, although in multivariate analysis the comparison between them was ambiguous. While p16 showed a stronger prognostic value in the Upko *et al*. report, p16's strength was reported as equivalent in the Craig *et al*. report with respect to the difference in HPV probes (Table 1.1).

Different methods have been suggested recently to enhance p16's diagnostic performance, such as using digital droplet PCR (Marques *et al.*, 2021) and combining p16 IHC with p53 assessment (p16/p53 IHC) (Benzerdjeb *et al.*, 2021). Utilising digital imaging for the detection of HPV histological features in the H&E sections also was proposed as a promising approach in HPV-detection (Klein *et al.*, 2021).

Table 1.1: List of studies concerning RNAscope diagnostic and prognostic performance in OPSCC.

Authors	Sensitivity	Specificity	Reference test	Number of cases	RISH/P16 discordant cases	Number of HPV probe	Predictive value compered by p16
Ukpo et al., 2011	98%	90%	p16	196	2.6%	7	P16 appeared stronger only in multivariant analysis (DSS).
Bishop et al., 2012	88%	97%	p16	77	17%	7	-
Schache et al., 2013	97%	93%	qRT-PCR	79	-	7	RNAscope showed better correlation than p16 in OS &DSS using Kaplan-Meier.
Mirghani et al., 2015	93%	94%	qRT-PCR	50	10%	18	-
Rooper et al., 2016	92%	100%	p16	82		18	-
Mendez-Pena et al., 2017	100%	87%	DNA PCR	58	22.8%	2	-
Randen-Brady et al., 2019	93%	92%	p16	357	5%	18	-
Craig et al., 2020	89%	100%	p16	221	11%	18	Equal values at Kaplan-Meier. Comparable performance at multivariant analysis OS (HR,P16= 0.31. RISH= 0.26).
Suresh et al., 2021	100%	100%	p16	122	-	18	-

1.3 Tumour microenvironment

Although the components of the TME may vary depending on the type and location of the tumour, thus making each tumour unique, TME generally comprises two major components (Gkretsi *et al.*, 2015). First, the extracellular matrix (ECM) consists of a basement membrane and an interstitial matrix that contains and maintains various soluble molecules including chemokines, matrix metalloproteinases, protease inhibitors, and growth factors, among others. The significance of ECM in tumours is presented in the anchorage and facilitating cancer cells migration (Alphonso and Alahari, 2009). The second important component in TME is the cellular part. Various cell types are integrated into ECM and present significant participation in tumorigenicity. Fibroblasts are the main cellular component, in addition to other cell types such as cells of the immune system, pericytes, endothelial cells, adipocytes and mesenchymal stem cells. Communication between tumour cells and surrounding stroma is constantly maintained through a complex and dynamic network of factors including cytokines, chemokines, exosomes, growth factors, among others, that contribute to tumour progression and survival (Joyce and Pollard, 2009) (Figure 1.5).

Fibroblasts are a heterogeneous population of spindle-shaped cells of mesenchymal origin that are characterised by varying degrees of contractility, ranging from quiescent fibroblast at homoeostasis to myofibroblast in acute inflammation and wound healing (McAnulty, 2007). In tumour stroma, the associated fibroblasts showed active phenotype properties similar to the myofibroblast but are known as cancer-associated fibroblasts (CAFs).

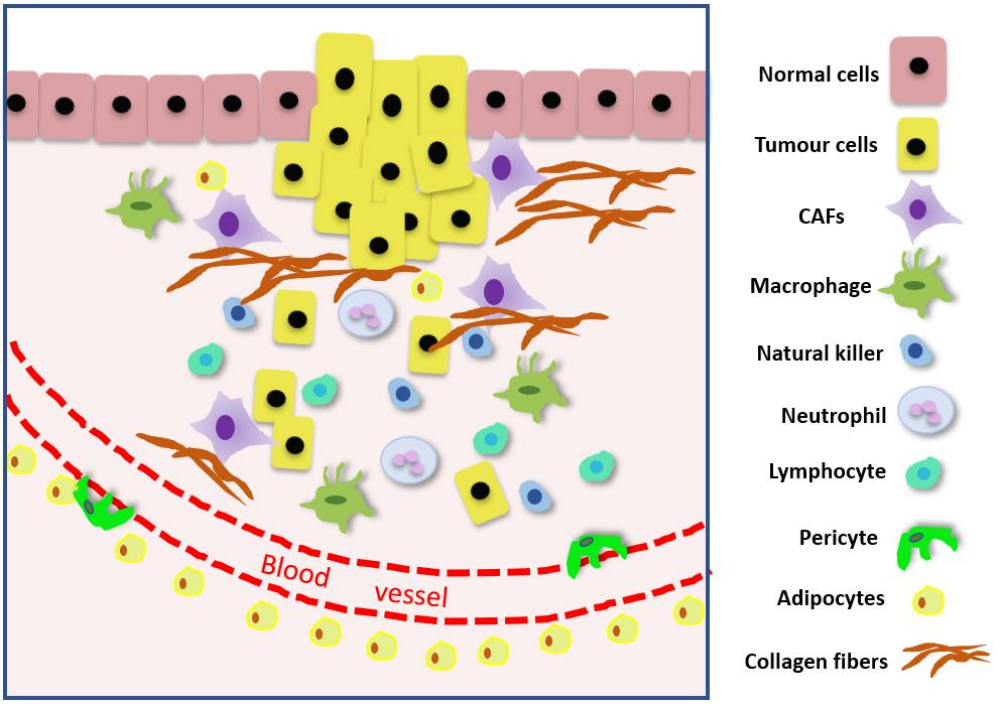

Figure 1.5: Tumour microenvironment components. The diagram illustrates the wide variety of cells within TME. The illustration was created using PowerPoint software, adapted from Foster *et al.* (2018).

1.3.1 Quiescent fibroblasts

Quiescent fibroblasts or resting fibroblasts are non-dividing, low metabolic fibroblasts that are scattered within the stromal tissue as single cells (Kristensen and Petersen, 1988). They are located proximal to the basement membrane, but without direct contact to the epithelial compartment or the basement membrane (Tschumperlin, 2013). They perform a crucial function in defining the differentiation status of the overlying epithelium through the production of signalling factors, and the secretion and organisation of matrix proteins, such as collagen and elastin at the minimum rate (Kalluri, 2016).

In general, they are defined as fibroblasts that do not express activated fibroblasts markers such as α-smooth muscle actin (α-SMA) and fibroblast activation protein (FAP) while expressing tissue mesenchymal markers including vimentin, Cluster of Differentiation (CD39), and fibroblast specific protein-1 (FSP-1) (Kalluri, 2016; Agorku *et al*., 2019). However, there is a lack of data concerning the quiescent fibroblasts in the literature, which may be attributed to the inability to achieve fibroblast cultures with definite 'resting' status *in vitro*. Culturing fibroblasts in plastic flasks reminiscent of a

stiffened, fibrotic ECM can at least induce partial fibroblast phenotype (proto-myofibroblast) activation (F. Liu *et al.*, 2015).

1.3.2 Myofibroblasts

Myofibroblasts have a specialised phenotype that is generated during wound healing and in different fibro-contractive diseases (Serini and Gabbiani, 1999). It is a hybrid differentiated type that displays combined features between fibroblast and smooth muscle cells; they are able to produce intense matrix consisting of extracellular matrix proteins, proteases, growth factors, and cytokines resembling fibroblast, besides their ability to form well-developed microfilament (Gabbiani, Ryan and Majno, 1971; Frangogiannis, Michael and Entman, 2000). The key function of the myofibroblasts in active stroma is demonstrated in the enhanced collagen formation and production of ECM modulators and growth factors (Madar, Goldstein and Rotter, 2013). However, myofibroblasts are not simply limited to this function; they also communicate with other cell types via a plethora of secreted factors (Arina *et al.*, 2016). In wound healing, fibroblasts are involved as a part of a dynamic process with other cell types including platelets, epithelial, endothelial, and immune cells to re-establish the normal tissue homoeostatic status and architecture. This process is mediated via a continuous sequence of signals including growth factors and cytokines.

1.3.3 Cancer-associated fibroblasts

These are among the most fundamental components of TME. In general, they are described as fibroblasts located within or approximate to the tumour (Kanzaki and Pietras, 2020). Fibroblasts within the TME acquire an active phenotype similar to the myofibroblasts in wound healing and acute inflammation and are known as CAFs. However, they have the ability to secrete vital factors contributing to tumour cells proliferation, differentiation, and migration. This might explain the correlation between the abundant presence of myofibroblasts and local disease recurrence and poor prognosis (Powell *et al*., 1999; Lewis *et al*., 2004; De Wever *et al*., 2008).

1.3.3.1 Original heterogeneity of CAFs

During tumour growth, the number of CAFs increases within the tumour stroma. Normal resident fibroblasts are considered the most immediate pool of cells to be recruited at tumour sites (Ishii, Ochiai and Neri, 2016). However, although laboratory studies support the idea that the initial functional role of fibroblasts is to suppress the early lesions (Özdemir *et al.*, 2014; Rhim *et al.*, 2014), validation of this hypothesis on tissue is not feasible due to the difficulty of longitudinal sampling of the same lesion (Sahai *et al.*, 2020). Other local sources from non-fibroblastic lineage have also been described as possible progenitors of CAFs, including adipocytes, pericytes, smooth muscle cells, epithelial cells, and endothelial cells (Alt *et al.*, 2010; Dulauroy *et al.*, 2012; Fischer *et al.*, 2015). Bone-marrow derived mesenchymal stem cells also have been reported as a source of CAFs in various tumour types (Jung *et al.*, 2013; Zhu *et al.*, 2014) (Figure 1.6).

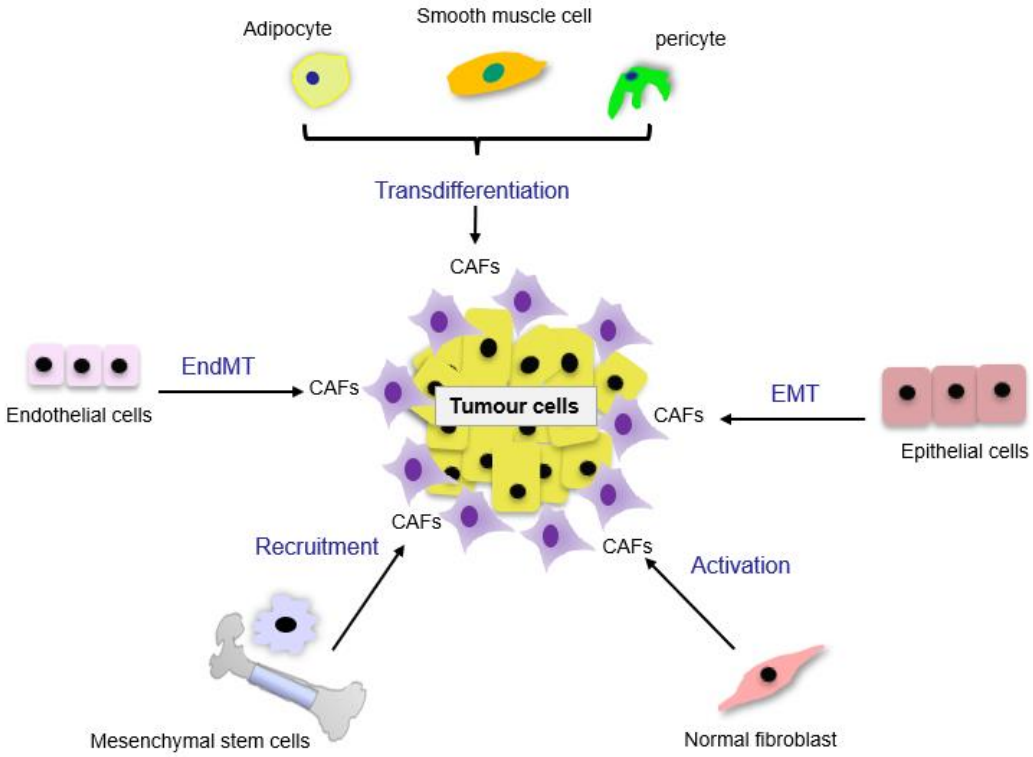

Figure 1.6.: CAF sources in the TME. CAFs are derived from different cell populations. CAF precursors undergo a series of molecular events that lead eventually to phenotype transformation. Epithelial cells undergo Epithelial to Mesenchymal transition (EMT), and Endothelial cells are transformed through Endothelial to Mesenchymal transition (EndMT). Normal resident fibroblasts become CAFs through the activation pathway and mesenchymal stem cells through the recruitment and activation process. Other cells like pericytes, adipocytes and smooth muscle cells undergo a transdifferentiation mechanism. The illustration was created using PowerPoint software, adapted from Liu *et al.* (2019).

1.3.3.2 CAFs generation in TME

Compelling evidence has demonstrated that fibroblast activation is a critical step in tumour growth and progression. Reciprocal epithelial-mesenchymal interaction has been described as a fundamental process that modulates fibroblasts phenotype to myofibroblast phenotype which in turn modulates cancer cells progression. This interaction occurs through the direct cell to cell interaction in addition to the effect of secretions in the form of cytokines, exosomes, growth factors or through secretion of ECM molecules (Mukaratirwa *et al.*, 2005; Powell *et al.*, 2005; Camussi *et al.*, 2010; Wang, Su and Amoah, 2020).

Tumour cell and fibroblast interactions have been investigated in OSCC using *in vitro* and *in vivo* models (Lewis *et al.*, 2004; Vered *et al.*, 2007; Kellermann *et al*., 2008). The evidence revealed further validation of tumour cells' ability to induce differentiation in normal fibroblasts through the TGF-β1 pathway, also demonstrating the effect of a significant increase in tumour cell growth and invasion into a Matrigel matrix when they were treated with myofibroblast conditioned media (Lewis *et al.*, 2004). Using experimental animal models also provides evidence indicating the role of malignant epithelial cells in presence of myofibroblasts in oral cancer patients compared to the hyperplastic and dysplastic epithelium (Vered *et al.*, 2007). TGF-β is the main cytokine inducing the myofibroblastic phenotype that is tightly regulated by integrins (Löhr *et al.*, 2001; Hassona *et al.*, 2013; Khan and Marshall, 2016). Its action is mediated through a signalling pathway via interaction with an intracellular receptor-regulated effector (SMAD2 / SMAD3) and (SMAD4) (Massagué, 2012). Once fibroblasts are activated, they form stress fibers (proto-myofibroblasts) which generate mechanical tension in the extracellular matrix resulting in uncontrolled TGF-β1 activation (Wipff *et al.*, 2007). Further production of TGF-β1 leads to myofibroblast trans-differentiation that, consequently, increases the stromal stiffness (Khan and Marshall, 2016).

Reports from our lab described successfully establishing a myofibroblastic CAF model derived from normal oral fibroblasts (NOFs) using TGF-β1 and highlighted the significance of miRNA upregulation in CAF transdifferentiation (Abidin, 2017; Melling *et al.*, 2018). Moreover, the functional role of oral-derived CAFs in bone invasion was studied thoroughly (Elmusrati *et al.*, 2017; Elmusrati, 2020). However, the response of normal tonsillar fibroblasts (NTFs) to TGF- β1 induction has not been investigated yet.

Other factors that promote CAF activation include inflammatory modulators that can promote CAF activation, such as interleukin-1 through NF-κB signal transducer (Erez *et al.*, 2009; Mughees *et al.*, 2021). Changes in ECM physical properties are also capable of triggering CAFs (Avery *et al.*, 2018). Additionally, genomic stresses can provoke alteration in the fibroblast phenotype. Double-stranded DNA breaks can induce TGFβ family activity and upregulate IL-6 production (Fordyce *et al.*, 2012). In some conditions, these factors transdifferentiate fibroblasts into senescent CAF phenotypes (Demaria *et al.*, 2017). Tumour-derived Osteopontin was linked to fibroblasts activation in HNC (Qin *et al*., 2018). The functions which it plays in promoting a tumour-permissive TME are yet to be fully elicited in OPSCC. Osteopontin (OPN) shall be discussed in detail in the next section 1.4.

1.3.3.3 Phenotypic heterogeneity of CAFs

The diversity of CAFs' origin is believed to be reflected in the heterogeneity of CAF biomarkers and functionality in TME (Kidd *et al.*, 2012; Prime *et al.*, 2017). Mounting evidence based on the molecular analysis and single-cell RNA-sequencing data described CAFs as a heterogeneous population of cells, with different biomarkers expression and functions. In a recent RNA-sequence analysis on HNSCC (n=18), fibroblasts were categorised into 4 populations: resting fibroblasts, myofibroblasts, CAF1, and CAF2. While CAF1 expressed mesenchymal biomarkers and ECM proteins, CAF2 subtype expressed immediate-early response genes such as *JUN*, *FOS*, besides ligands and receptors such as Keratinocyte growth factor 7 (FGF7) and, TGF-β receptor (Puram et al., 2018). Similar reports on CAFs RNA-sequencing emphasise the concept of CAFs' heterogeneity in other tumours including non-small cell lung cancer (Lambrechts *et al.*, 2018), colorectal carcinoma (Li *et al.*, 2017), and breast cancer (Bartoschek *et al.*, 2018). However, despite the wide variety between CAFs subtypes among distinct cancer types, CAFs were shown to share similar gene signatures and molecular functions. In recent work on CAFs RNA-sequencing from three different tumours (HNSCC, lung cancer and melanoma), six pan-CAF subtypes were observed including normal fibroblasts, proliferative CAF like fibroblasts, myofibroblasts, two inflammatory fibroblasts and desmoplastic fibroblasts. CAF phenotypes analysis has identified the prognostic utility of signature genes for these CAF subsets, providing new insights into how cancers residing in specific tissue types may benefit from CAF subtype targeted therapy (Galbo, Zang and Zheng, 2021).

α-SMA expression is a widely accepted biomarker for CAF detection, although its expression has been observed also in pericytes, endothelial cells in addition to muscle fibers (Hinz *et al.*, 2007; Eyden *et al.*, 2009). Moreover, CAFs with no α-SMA expression have also been reported (Mellone *et al.*, 2016; Patel *et al.*, 2018). *In vitro*, CAF culture isolation is performed by excluding contamination by other lineages such as epithelial cells, endothelial cells, and macrophages; in addition to confirming fibroblasts' identity using a number of biomarkers (Table 1.2). Asporin (Maris *et al.*, 2015) and collagen 11-α1 (COL11A1) (Galván *et al.*, 2014) were reported as markers that expressed specifically with CAFs *in vitro* in studies on breast tumour and colon adenocarcinoma, respectively; nevertheless, further validation is required to assess the clinical significance as a prognostic biomarker in tissue.

Table 1.2: Examples of CAFs markers. The table is modified from Gascard and Tlsty (2016).

Marker	Fibroblasts specific	Expression change in CAF Vs. fibroblast
α-SMA	No	Gain
FAP	No	Gain
PDGFR-α/β	No	None
FSP-1	No	Gain
Vimentin	No	Gain
Neuron glial antigen	No	Gain
Desmin	No	Gain
Podoplanin	No	Gain
Asporin	Yes	Gain
Col11A1	Yes	Gain
MFAP5	Yes	Gain
CD36	No	Loss
Caveolin	No	Loss

CAF subtype heterogeneity was also evident based on the traditional molecular biomarker expression. In pancreatic ductal adenocarcinoma, CAF populations have been categorised according to α-SMA expression into α-SMA^{high} and α-SMA^{low}. The latter population has shown to be more tumour-promoting by producing chemokines and cytokines, while the former demonstrated high capability in ECM deposition (Öhlund *et*

al., 2017). Moreover, based on analysing the expression of fibroblast markers including αSMA, FAP, FSP1, PDGFRβ, caveolin1 and β1/CD29, Givel *et al.* (2018) identified four subsets of CAFs in ovarian cancer with distinct functional roles. The role of $CAFs^{\alpha\text{-}SMA}$ was described as enhancing tumour proliferation, immunosuppression, besides impeding drug delivery, while $CAFs^{FSP1}$ and $CAFs^{FAP}$ were linked to tumour metastasis and immune evasion (Han, Liu and Yin, 2020). To the best of our knowledge, CAFs have not previously been extracted and assessed from OPSCC. We highlight this aspect as a gap in the literature that warrants further investigation. Identification of CAFs subtypes and their functional role in OPSCC may reveal a target therapeutic approach.

1.3.3.4 Clinical significance of CAF detection in tissue

Although myofibroblasts shared similar features in inflammation/repair and tumours, there is a crucial difference in the established reactive stroma. In the former, the functional role of myofibroblasts is constitutively activated and then terminated when the tissue has repaired, either by a reversion to a normal phenotype or undergoing apoptosis (Desmouliere *et al.*, 1995; Shiga *et al.*, 2015). However, CAFs in tumour stroma undergo irreversible activation via signalling pathways mediated by many tumour-derived factors and autocrine loops (Augsten, 2014; Costa, Scholer-Dahirel and Mechta-Grigoriou, 2014); therefore, the tumour stroma fails to abate the fibrotic response, which leads to further matrix deposition and disorganisation and tissue desmoplasia. The abundance of CAFs in tumours is described to be strongly associated with a worse prognosis in distinct tumour types (Galbo, Zang and Zheng, 2021). In desmoplastic tumours such as breast and pancreatic cancers, CAFs form up to 80% of the tumour mass; conversely, a low percentage has been found in kidney and brain tumours (Öhlund, Elyada and Tuveson, 2014; Gascard and Tlsty, 2016). CAFs were observed in approximately 60% of OSCC (Kellermann *et al.*, 2008). Tumours with a high percentage of CAFs (>50%) within the stroma are correlated with poor survival (Gascard and Tlsty, 2016). That is thought to be attributed to the generated mechanical forces which in turn activate further CAFs' precursors. Moreover, the dense desmoplastic tumour creates hypoxia within the tissue that has its drawback effects on treatment response, and angiogenesis promotion (Semenza, 2000; Jain, Martin and Stylianopoulos, 2014).

In OSCC, Kellermann et al. (2007) reported the first evidence for the importance of myofibroblasts' presence as a prognostic factor in OSCC patients' mortality. Among 72 samples of invasive tumour front in tongue SCC, 71% showed a high abundance of

myofibroblasts. This high proportion also demonstrated a significant correlation with lymph node stage and shorter overall survival. The same correlation also was reported in a larger OSCC cohort study by Marsh *et al*. (2011) where α-SMA IHC expression demonstrated the highest hazard ratio (HR) = 3.06 (95% CI 1.65–5.66) among the other significant prognostic features (surgical margins, metastatic disease, and pattern of invasion). In a recent meta-analysis that investigated CAF expression in OSCC tissue, high levels of CAF revealed a strong correlation with poor prognosis, disease-specific survival (DFS) HR = 3.32 (95% CI: 2.09-5.26, p < .00001) and overall survival (OS) (HR: 2.16, 95% CI: 1.60-2.92, p < .00001) (Dourado *et al.*, 2018). Furthermore, in the majority of included studies in the previously mentioned meta-analysis, high CAF detection was associated with advanced clinical parameters such as advanced disease stage, high tumour grade, recurrence, and extranodal metastatic spread. However, there is no consistency among the reports in defining the CAF detection threshold in the tissue; while the majority look for the amount/percentage of CAF within the stroma (Kellermann *et al.*, 2007, 2008; Marsh *et al.*, 2011), others consider the α-SMA intensity as another significant criterion in the scoring scheme (Oguejiofor, 2016).

In OPSCC, the presence of CAFs and their clinical significance has not been investigated thoroughly. It is thought that CAF distribution in HNSCC is correlated with the anatomical sites; while tumours localised to palatine tonsils present more often with α-SMA positive-CAFs, on the other hand, oral cavity, pharyngeal wall, and soft palate are more likely to demonstrate α-SMA-negative CAFs (Valach *et al.*, 2012). Concerning HPV-positive OPSCC, CAFs were reported as being a common feature associated with HPV-driven tumours (Rahrotaban *et al.*, 2019). The limited available data on CAFs' clinical significance in OPSCC tissue revealed no correlation with overall survival (Oguejiofor, 2016). However, reports from our lab demonstrated a difference in normal fibroblasts' early response to conditioned media from HPV-negative OPSCC cell lines, but not from HPV-positive cell lines (Bolt *et al.*, 2018; Peacock *et al.*, 2018; Al-Sahaf *et al.*, 2019), which may indicate a difference in stroma reactivity in OPSCC subtypes. From the above, α-SMA positive-CAFs' abundance among OPSCC subtypes is an interesting area within the literature that requires further investigations in terms of its relation to the survival, nature of the behaviour, and anatomical site. These findings might suggest α-SMA biomarker as an independent effective predictor for OPSCC mortality.

1.3.4 Senescent CAFs

Senescence is another feature of CAFs within the solid tumour stroma. Senescent CAFs characteristically demonstrate the status of proliferation arrest associated with the active production of a plethora of pro-inflammatory mediators including cytokines, chemokines, in addition to metabolites, growth factors and other factors. Collectively, active CAFs secretome called the senescence-associated secretory phenotype (SASP), is known for its established role in creating a permissive TME that supports tumour cells' proliferation and spread (Coppé *et al.*, 2008, 2010).

The senescent CAFs phenotype is developed as a consequence of persistent DNA damage that might be caused by internal insults including oxidative stress (Campisi and Fagagna, 2007), or external inducers such as cigarette smoke, irradiation, and chemotherapy (e.g., Cisplatin) (Coppé *et al.*, 2008). CXCL1 also demonstrated the ability to induce senescence in normal oral fibroblasts through an autocrine mechanism (Kim *et al.*, 2018). The senescent CAFs phenotype exhibits several changes in gene expression, the majority of which are related to permanent growth arrest (p53/p21 or/and p16/pRb pathways). It is also characterised by the secretion of more active secretome (SASP) (Campisi and Fagagna 2007; Hassona *et al*. 2013; Laberge *et al.*, 2015) that generates pro-inflammatory and pro-metastatic factors, providing supportive media for further tumour progression (Kabir *et al*., 2016; Prime *et al*. 2017). Mellone *et al*. (2012) have introduced a successful *in vitro* induction model of oral fibroblast senescence, which has been performed by exposing the fibroblasts to DNA damaging agents (H_2O_2 and Cisplatin). The senescent fibroblasts conditioned media analysis demonstrated more active SASP compared to the control, besides the ability to promote cancer cells proliferation and invasion.

To date, the molecular mechanisms underlying SASP generation remain poorly understood. The role of COX-2/miRNA-335/PTEN signalling cascade has been demonstrated from our lab as a novel modulator for the inflammasome in senescent fibroblasts in HNSCC (Kabir *et al*., 2016); moreover, in senescent skin fibroblasts miRNA-146a/b has been demonstrated as a supportive factor in excessive IL-6 and IL-8 secretion via IL-1α depending on the manner of skin fibroblasts senescence (Bhaumik *et al.*, 2009). The senescence-associated β-galactosidase (SA-βgal) is the most specific senescent cell marker (Dimri *et al.*, 1995). It is thought to be derived from lysosomal biogenesis, a mechanism which frequently occurs in senescent cells (Lee *et al.*, 2006); however, SA-βgal expression could be induced by cellular stress in prolonged

confluence culture (Campisi and Fagagna, 2007). Lack of DNA replication markers including proliferating cell nuclear antigen (PCNA) and Ki-67 are suggested as other senescence markers; nevertheless, they cannot distinguish between quiescent and senescent cells (Campisi and Fagagna, 2007). p16 expression is utilised by some authors to identify the senescent cells as it is considered an important regulator in this process (Krishnamurthy *et al.*, 2004). It is worth mentioning here that not all senescent cells engage the p16-pRb pathway, and the possibility of other pathways has been suggested (Shelton *et al.*, 1999; Olsen *et al.*, 2002), which might explain the lack of p16 expression in some senescent cells (Beausejour *et al.*, 2003).

The clinical significance of senescent CAFs is presented in high inflammatory secretome (SASP) that has been implicated in transcriptional regulatory mechanisms (Krtolica, Parrinello, Lockett, P. Y. Desprez, *et al.*, 2001). Although there is an overlap between the senescent CAF and myofibroblastic CAF secretome, as represented in a high amount of IL-6 production (Mellone *et al.*, 2016), the non-proliferative status of senescent CAFs suggests less effect in developing desmoplastic tumours (Parrinello *et al.*, 2005). The exact identity of myofibroblastic CAFs and senescent CAFs phenotypes is controversial; while some authors consider them as stages in a unified pathway, as they share common functions and are mediated by similar signalling pathways (Prime *et al*., 2017), there is another view which considers CAFs as a “dynamic state” in the fibroblast lifecycle that is present in the tumour vicinity and promotes its progression (Madar, Goldstein and Rotter, 2013). To date, the biological behaviour of these phenotypes and their impacts on OPSCC have not yet been investigated.

1.4 Osteopontin (OPN)

OPN is a phosphorylated glycoprotein that was first identified in 1979 as a secreted phosphoprotein in mamillary transformed cell lines (Senger, Wirth and Hynes, 1979). In 1985, OPN was detected in osteoblasts (Franzen and Heinegard, 1985). Osteopontin is a combined word of “osteo = bone” and “pontin = binding”, which typically describes its function in linking bone cells to the bone extracellular matrix. OPN is also known as Bone Sialoprotein 1 (BSP1) and Early T-lymphocyte Activation 1 (ETA1) protein. At present, OPN has been included as a member of the Small Integrin-Binding Ligand N-linked Glycoprotein (SIBLING) family, as they share several structural and functional properties (Fisher *et al.*, 2001). OPN is predominantly expressed in osteoclasts, osteoblasts, in addition to its expression in skeletal smooth muscle cells, neural cells, endothelial cells and immune cells. OPN was established as a protumorigenic and premetastatic factor in malignant cells in various cancer types including oral cancer, breast cancer, kidney cancer, pulmonary cancer, colon cancer and hepatic carcinoma (Senger, Wirth and Hynes, 1979; O’Brien *et al.*, 1994; Malyankar *et al.*, 1997; Abdel-Hafiz *et al.*, 2018; Assidi *et al.*, 2019; Maleš *et al.*, 2021).

OPN is a pleiotropic factor that involves several physiologic and pathologic processes such as bone remodelling, wound healing, immunity regulation, and cancer progression. The multifunctionality of OPN is attributed to the presence of different isoforms and variants that undergo further posttranslational modifications such as phosphorylation, sulfation, glycosylation, and proteolytic cleavage (Qin, Baba, and Butler, 2004). Despite OPN’s heterogeneity, it is assessed and reported by the majority as a standard molecule (OPN), although a few studies reported a distinction in biological function between OPN variants.

1.4.1 The molecular structure of OPN

OPN is encoded by the human gene secreted phosphoprotein 1 which is located on chromosome 4, locus 4q13.22. OPN gene carries seven exons which are responsible for OPN isoforms generation (Young *et al.*, 1990). SPP1 gene undergoes alternative splicing that results in the formation of five transcript variants encoding five different isoforms for OPN protein (Figure 1.7). OPN-a is the full-length isoform of OPN gene that is translated to full protein amino acid sequence (314 AA) (Christensen, Petersen and Sørensen, 2008). It is considered as the canonical reference sequence for OPN, while

the rest of the isoforms, OPN-b and OPN-c, were compared against OPN-a sequence; however, much is still unknown regarding OPN-d and OPN-e isoforms and whether they are translated to protein or not (Moorman *et al.*, 2020). OPN isoforms all share the feature of being secreted forms of OPN (sOPN) that are produced and delivered extracellularly (Castello *et al.*, 2017) (Table 1.3). According to the limited available reports, sOPN isoforms appear to be tumour specific with different biological effects. OPN-a is highly expressed in pulmonary tumours and papillary thyroid carcinoma and acts as a bone metastatic factor and invasion modulator, respectively (Ferreira *et al.*, 2016; Hao *et al.*, 2017). OPN-c was detected in prostate tumour and its expression was correlated with the degrees of cell transformation from benign to an invasive tumour (Tilli *et al.*, 2012). In breast tumours, OPN-c overexpression was correlated with tumour grade and worse outcome, suggesting a prognostic role for OPN biomarker (Mirza *et al.*, 2008), while in ovarian cancer it gained further clinical significance through its association with platinum-resistant therapy that suggested OPN as a prognostic and predictive tool in ovarian cancer (Dion *et al.*, 2020).

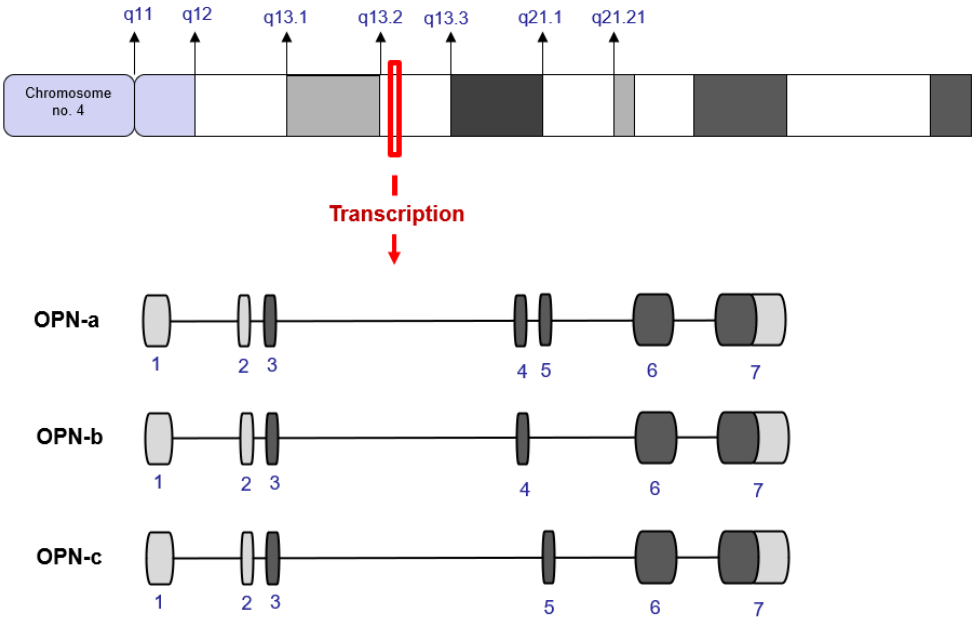

Figure 1.7: Human OPN gene and OPN isoform transcripts. SPP1 locus (red rectangle) on chromosome 4. SPP1 genes have seven exons that encode three alternative spliced isoforms, OPN-a. OPN-b and OPN-c. The illustration was created using PowerPoint software, adapted from Lamort *et al.* (2019).

Table 1.3: The molecular structure of sOPN isoforms.

Type	Isoform	Exons	AA differences	Putative differences
sOPN	OPN-a	2-7	Full length	Full length protein.
	OPN-b	2-7 (5 missing)	AA 59-72 missing	Less phosphorylated domains.
	OPN-c	2-7 (4 missing)	AA 31-57 missing	Less phosphorylated domains. Lack trans-glutamination signal.
	OPN-d	Lacks two alternate exons	AA 95-116 missing	-
	OPN-e	2-7 (1 extra)	AA 59-72 missing	-

*sOPN, secreted OPN, AA= Amino acid.

1.4.2 Secreted OPN and Intracellular OPN

Although OPN has been studied intensively and identified as an extracellular protein, few reports have precisely differentiated between the OPN isoforms. Otherwise, unless specifically noted, previous studies have been concerned with the sOPN form. The intracellular form of OPN (iOPN) was identified initially by Zohar *et al.* (1997) in rat calvarial cells. Years later, Shinohara *et al*. (2008) described iOPN as an alternative translation for OPN mRNA that demonstrated a distinct biological function in dendritic cells. iOPN was described as a short non-secreted form of OPN that is lacking the signal sequence due to the initiation of OPN mRNA translation from the downstream noncanonical start codon. This leads to the missing of the first 16 AAs which acts as a membrane localisation signal peptide (Shinohara *et al.*, 2008) (Figure 1.8). Further work from the same group indicated that iOPN and sOPN may differentially control the nature of immune responses (Inoue and Shinohara, 2011). At the cellular level, iOPN is thought to be accumulated in the peri-membranous zone, retained inside the nuclear zone, and distributed in the cytoplasm, whereas sOPN is localised at the perinuclear zone (Castello *et al.*, 2017). Expression of OPN form (sOPN and iOPN) has been shown to depend on the cell type, which suggests that cell-type-specific factors might regulate the alternative translation of OPN transcript (Cantor and Shinohara, 2009).

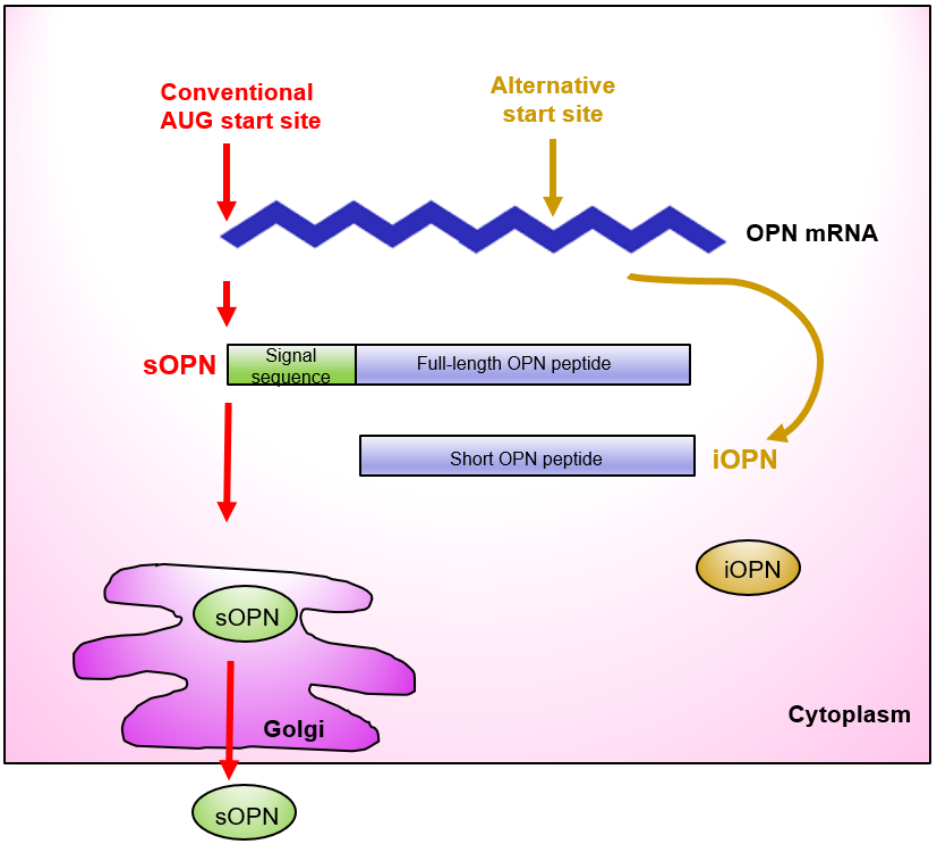

Figure 1.8: OPN mRNA translation. OPN mRNA has two translation sites: the canonical AUG translation initiation site (left) and an alternative translation initiation site (right). Translation from the canonical initiation site results in the formation of the full length of OPN peptides (sOPN), including a signal sequence that is targeted to secretory vesicles. Translation from the alternative initiation site leads to a short peptide (iOPN) that lacks a signal sequence and accumulates intracellularly. The illustration was created using PowerPoint software, adapted from Cantor and Shinohara (2009).

The differences between iOPN and sOPN were described in a few reports concerning the biological effects of OPN on immunity. Innate immune cells such as dendritic cells and macrophages appeared to have more iOPN stored in the cytoplasm than the produced OPN (sOPN), while the lymphocytes produced a higher proportion of sOPN compared by iOPN (more than 50-fold) (Shinohara *et al.*, 2008). Immune cells-derived sOPN has shown to be implicated in adaptive immunity by promoting immune cell proliferation, migration, and cytokine production (Clemente *et al.*, 2016), whereas iOPN acts as an adaptor molecule in signalling pathways downstream of innate immune receptors (Inoue and Shinohara, 2011), in addition to its crucial role in the natural killer cells (NK) expansion and survival (Leavenworth *et al.*, 2015). These observations suggested different functional roles for iOPN and sOPN in the innate and adaptive responses, respectively (Cantor and Shinohara, 2009).

1.4.3 Expression regulatory factors and signal mediators

OPN expression is regulated by several transcription factors such as Myb proto-oncogene protein (c-Myb) (Schultz et al., 2009) and Erythroblast transformation-specific -related gene (ERG) (Flajollet *et al.*, 2011). Moreover, a number of potential regulatory sequences have been described in SPP1 promoter such as vitamin-D-responsive (VDR)-like motifs (nucleotides −1892 to −1878 and −698 to −684), and an Ets-1 motif (nucleotides −47 to −39) (Safran, Butler and Farach-Carson, 1998; Tang et al., 2008). Mechanical stress and inflammatory mediators such as TNFα, IL-6, TGFβ and IL-17a also were reported as an inducer for OPN (Liu *et al.*, 2015).

CD44 and integrin receptors are the binding partners of OPN. CD44 is a surface glycoprotein expressed in a wide variety of cells including malignant epithelial cells and CAFs (Kinugasa, Matsui and Takakura, 2014; Ludwig *et al.*, 2019). OPN/CD44 interaction mediates cell-matrix or cell-cell interactions. It plays functional activities in the regulation of invasion, angiogenesis, and metastasis (Senbanjo and Chellaiah, 2017), in addition to cellular adhesion, lymphocyte activation, chemotaxis of macrophages (Schimizu *et al.*, 1989; Zhu *et al.*, 2004). Three integrin-binding domains were identified for OPN isoforms: RGD domain, OPN-R domain, and N-terminal thrombin cleavage fragment (Wai and Kuo, 2008). Each domain is associated with specific integrin isoforms as illustrated in Figure 1.9 OPN/integrin interaction contributes to the activation of several signal transduction pathways such as STAT-3, ERK1/2, PI3K/Akt/mTOR and NF-κB that are involved in immune cell regulation, cell adhesion, tumour metastasis and survival (Behera *et al.*, 2010; Zou *et al.*, 2013; Zhang *et al.*, 2014).

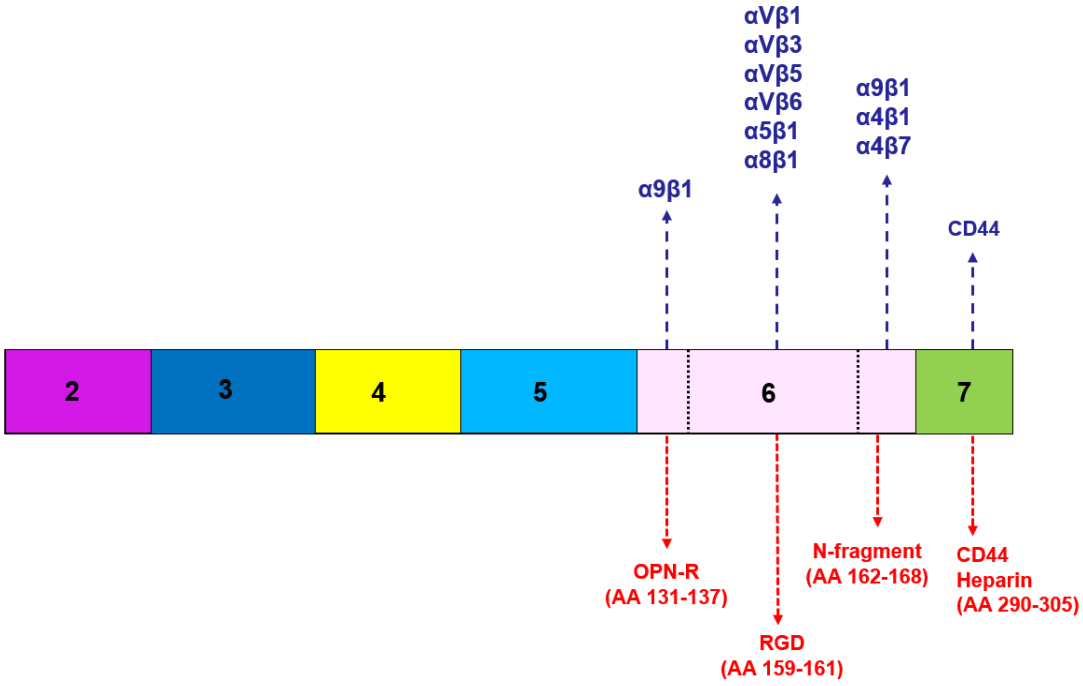

Figure 1.9: Human OPN protein. A translated full-length OPN isoform (OPN-a). The receptor-interacting domains are illustrated in red. The respective receptors are illustrated in blue. The illustration was created using PowerPoint, adapted, and modified from Mooreman *et al*. (2020).

1.4.4 OPN in Cancer

As has been mentioned above, OPN overexpression has been detected in several tumour types. Its expression has been linked to the aggressiveness of the tumour and worse clinical outcomes and that might be attributed to its active participation in several oncogenic pathways such as PI3K/Akt/mTOR and JAK2/STAT3 signalling pathways (Guertin and Sabatini, 2007; Behera *et al.*, 2010). In HNSCC, OPN overexpression was linked to tumour progression, metastasis, and cancer therapy resistance (cetuximab and cisplatin) (Luo *et al.*, 2015; Liu *et al.*, 2020). Compelling evidence indicated that high OPN plasma level is correlated positively with neck lymph nodes (Maleš *et al.*, 2021). Comparisons between metastatic nasopharyngeal carcinoma and its non-metastasised counterpart showed a discrepancy in plasma OPN level, the level being higher in the former (Hui *et al.*, 2008); moreover, a high OPN level was associated with lymph node metastasis (Celetti *et al.*, 2005; Wong *et al.*, 2005). In laryngeal squamous cell carcinoma, OPN demonstrated a pro-invasive effect *in vitro* and its expression was correlated with the lymph nodes' involvement and low survival (Celetti *et al.*, 2005). In OSCC, overexpression of OPN in tissue and body fluids was associated with advanced

tumour stage, high lymph nodes status, therapy resistance and development of recurrence (Table 1.4). Based on this evidence, OPN was suggested as a prognostic and predictive biomarker in OSCC. Notably, these observations were built on OPN overexpression in tumour cells only within the tissue, however, the Avirović *et al*. (2013) study revealed a difference in the clinical significance of OPN expression in cancer cells and tumour stroma; only high tumour-OPN IHC expression was correlated positively with advanced clinical parameters and outcome, while that was not evident with stroma-OPN expression. The study finding suggests that tumour-derived OPN may have a different function compared with stromal OPN and probably only the tumour derivation has independent prognostic value in OSCC (Avirović *et al.*, 2013).

In OPSCC, the clinical significance of OPN expression has not been assessed until now. Small numbers of OPSCC patients have been included in a few studies investigating OPN's effect in HNSCC (Overgaard *et al.*, 2005; Maleš *et al.*, 2021). Meanwhile, OPN assessment in OPSCC tissues requires a comprehensive evaluation for OPN expression in tumour cells and stroma independently, owing to the pro-inflammatory nature of OPN.

Table 1.4: Main features and findings of studies investigating OPN expression in OSCC.

Study	Sample & method	Number of cases	Association with clinical parameters	Correlation with survival
(Ogbureke *et al.*, 2007)	FFPE. IHC	87	No correlation with the clinical parameters	-
(Chien *et al.*, 2009)	Plasma. ELISA	94	High OPN plasma level associated positively with advanced tumour stage ($p<0.001$), and positive nodal status ($p< 0.001$).	-
	FFPE. IHC	256	High OPN IHC expression also associated positively with advanced tumour stage ($p<0.001$), positive nodal status ($p< 0.001$), and advanced TNM stage ($p < 0.001$).	Five-year overall survival rates correlated significantly with positive osteopontin immunostaining ($p<0.001$).
(Chiu *et al.*, 2010)	FFPE. IHC	58	High OPN IHC expression associated positively with advanced tumour stage ($p<0.02$) and positive nodal status ($p< 0.02$).	-

(Continue)

Study	Sample & method	Number of cases	Association with clinical parameters	Correlation with survival
(Ogbureke *et al.*, 2012)	FFPE. IHC	20	OPN overexpression was proposed as a predictive biomarker for OSCC recurrence.	
(Avirović *et al.*, 2013)	FFPE. IHC	86	High tumour-OPN IHC expression associated positively with positive nodal status ($p < 0.045$) and higher TNM stage ($p=0.03$). High stromal-OPN IHC was not significantly associated with clinical parameters.	High tumour-OPN IHC expression correlated with poor clinical outcome ($p = 0.02$). In multivariate analysis, tumour-OPN emerged as an independent prognostic biomarker ($p = 0.04$). High stromal-OPN IHC was not correlated with patients' outcome.
(Routray, Kheur and Kheur, 2013)	FFPE, IHC	40	OPN overexpression was associated with tumour invasion.	-

Continue…

Study	Sample & method	Number of cases	Association with clinical parameters	Correlation with survival
(Luo *et al*., 2015)	FFPE. IHC	21	Positive expression of OPN predicts a poor response and survival in patients with locally advanced stage IV OSCC treated with cisplatin-based induction chemotherapy followed by concurrent chemoradiotherapy	-
(Chakraborty *et al*., 2018)	FFPE. IHC Saliva. ELISA	146	OPN overexpression in tongue cancer compared with the control. OPN was suggested for clinical implication as an early diagnostic biomarker	-
(Lakshmi *et al*., 2019)	FFPE. IHC	30	No significant association with tumour stage or lymph node status.	-

*FFPE= formalin-fixed paraffin-embedded. IHC= immunohistochemistry. ELISA= Enzyme linked immunoassay.

1.4.4.1 Effect of tumour-derived OPN on TME

Tumour-derived OPN has a supportive role for tumour cells by contributing to establishing an active microenvironment and promoting metastasis. Tumour-derived OPN has shown the ability to underpin CAFs' presence in TME and to do that by reprogramming normal resident fibroblasts as reported in breast cancer. OPN-derived CAFs demonstrated mimics of molecular and functional profiles similar to the myofibroblastic CAF phenotype (Sharon *et al.*, 2015; Prasanna *et al.*, 2021). Mesenchymal stem cells are considered one of the alternative sources of CAFs in TME. Tumour-derived OPN was described as a mediator for mesenchymal stem cells' transformation into CAFs in breast cancer. This process was demonstrated by OPN-integrin interaction, which in turn activated the transcription factor myeloid-zinc finger 1 (MZF1). The latter has been found to have a promoting effect on TGF-β1 production (Weber *et al.*, 2015). Inhibition of OPN-integrin binding using aptamer abolished the MSC-CAF transformation process (Weber *et al.*, 2015).

Further evidence for the supportive role of OPN in metastasis is presented in the ability of the systemic sOPN to instigate indolent disseminated tumour cells to form a premetastatic niche. This function was supported by the ability of sOPN to activate and mobilise bone marrow-derived cells into distant metastatic cells, which subsequently results in the outgrowth of the distant metastases (McAllister *et al.*, 2008). The growing evidence supports the hypothesis that tumour-derived sOPN and iOPN have a complementary role in the tumour metastasis process. sOPN promotes EMT in the primary non-invasive tumour to establish early metastatic dissemination (Thiery, 2002; Thiery *et al.*, 2009). On the other hand, iOPN function appeared at later stages of metastasis by inducing MET in the disseminated cancer cells to facilitate metastatic colonisation (Zohar *et al.*, 2000; Junaid *et al.*, 2007; Jia *et al.*, 2016).

OPN enhances tumour progression through the recruitment of macrophages and suppression of T cell response. Tumour-derived OPN showed the ability to attract macrophages to a tumour site by promoting chemotaxis. The presence of a high number of tumour-associated macrophages was linked to tumour stage and poor disease outcome (Qian and Pollard, 2010). The functional role of the macrophage in TME was implicated in tumour formation and progression (Liguori *et al.*, 2011; Shih *et al.*, 2014); moreover, OPN had an immunosuppressive influence on macrophages by inducing M2 polarisation and regulating Programmed death-ligand 1 (PD-L1) expression, which further contributes to cancer immunosuppression. OPN also appears to act as an

immune checkpoint that inhibits T cell activity in the tumour environment (Klement *et al*., 2018).

1.4.4.2 Effect of stromal-derived OPN on tumour cells

OPN was also detected in cells within TME with a distinct biological effect on tumour cells. iOPN expression in NK cells demonstrated anti-tumour function through its ability in NK activation and inhibition of apoptosis. This process maintains NK activity by reaching the full maturation and lytic function. This observation was evident *in vivo* using Rag−/− γC−/− mice co-injected with melanoma cells and NK cells expressing iOPN only. Compared with the control that had been co-injected with tumour cells and NK lacking iOPN, the former had a significant increase in NK number and less metastatic dissemination (Leavenworth *et al.*, 2015). In keeping with this report, Danzaki *et al.* (2016) described the functional role of stromal-derived OPN in enhancing NK infiltration *in vivo* using a transgenic adenocarcinoma of mouse prostate model. However, antitumorigenic functions of OPN appeared to give a tumour-specific response. Using B16 melanoma tumours, OPN did not show OPN-mediated cell recruitment (Danzaki *et al.*, 2016).

To the contrary, OPN produced by senescent fibroblasts showed tumour-supportive effects. Accumulating evidence in the literature supports the fact that senescent fibroblasts have an important role in tumour development/formation in ageing tissues (Krtolica, Parrinello, Lockett, P. Desprez, *et al.*, 2001; Krtolica and Campisi, 2002). OPN driven by senescent fibroblasts has been shown as a necessary factor of preneoplastic cell growth *in vitro* and *in vivo*. Targeting OPN also blocked the senescent fibroblasts' ability to promote keratinocytes' growth (Pazolli *et al.*, 2009).

From the above, the functional effects of OPN indicate its importance as a mediator in tumour-stroma interaction. Tumour-derived or stromal-derived OPN was reported with a supportive function in tumour cells' progression and metastasis. However, some evidence revealed a suppressive role of OPN tumour progression; particularly, an *in vivo* model for SCC in OPN-deficient mice showed development in tumour growth and higher metastatic dissemination (Crawford, Matrisian and Liaw, 1998). Moreover, OPN deficient macrophages displayed improper anti-tumour activity (Bourassa, Monaghan and Rittling, 2004) which indicates OPN either inhibits or promotes leukocyte functions. This may indicate a presence of balance between the OPN effect on the tumour that determines whether the overall effect of the immune response will be tumour promoting or tumour inhibiting (Terabe and Berzofsky, 2007).

1.5 Hypothesis and aims

Hypothesis:

The poor clinical outcomes of HPV-negative OPSCC are believed to be attributed to the activated underlying microenvironment. Tumour microenvironment plays a crucial role in tumour growth and behaviour. Previous research from our lab demonstrated a remarkable response of normal fibroblast to HPV-negative OPSCC cell lines conditioned media, but not with HPV-positive counterpart.

These observations inspire us to test this hypothesis: that the abundance and activity of CAFs correlate with poor clinical outcomes in OPSCC owing to their ability to modulate cancer cell behaviour, and that will differ between HPV-negative and HPV-positive tumours.

Research aim:

To investigate the presence and clinical significance of CAFs in OPSCC and explore novel candidates in tumour-fibroblasts crosstalk.

Specific aims:

- To determine the status of biologically relevant HPV infection in an established OPSCC cohort. Explore α-SMA expression in OPSCC subtypes and assess its prognostic value.

- To establish *in vitro* models of myofibroblastic-CAF and senescent-CAF models using NTFs, and isolate and characterise OPSCC CAF primary cultures.

- To explore the secretome mediated crosstalk between tonsil derived fibroblasts and HPV-positive and HPV-negative OPSCC subtypes and provide further investigations on novel candidates identified by cytokine profiling.

Chapter 2: Materials and Methods

2.1. Cell Culture

2.1.1 Cell lines

Two OPSCC HPV negative cell lines (UPCI:SCC 089 and UPCI:SCC 072) and two HPV16 positive cell lines (Hypopharynx UD:SCC 2 and UPCI:SCC 090) were kindly provided by Dr Suzanne Gollin (University of Pittsburgh) following the university guidelines for the material transfer agreement. Table 2.1 summarises the relevant information linked to each cell line, as reported in the literature (Virgilio *et al.*, 1996; Camille, 2004; Ferris *et al.*, 2005; White *et al.*, 2007; Wald *et al.*, 2011). HPV status of the provided cell lines was confirmed by the HPV Cytology Screening Unit (Royal Hallamshire Hospital) (Appendix A.1).

Cell lines are a commonly used tool in the investigation of response to treatment and assessment of the drivers of carcinogenesis. However, they do not have the complexity of the tissues, thus there is limitation as to how representative they are. When considering cell lines as a potential model of HPV- positive OPSCC, there is a necessary reliance on cell lines that are indeed reported to be HPV-positive, yet they do not necessarily derive from the same anatomical subsite of the head and neck. The majority of *in vitro* studies on HPV-positive HNSCC cell lines use a limited number of established cell lines that are commercially available (Greaney-Davies et al., 2020). These cell lines have disparate aetiologies: they have been isolated from both oral and oropharyngeal anatomical subsites and from individuals with a history of cigarette and alcohol use, yet they still represent the most readily available model for the study of HPV-positive HNC, OP or otherwise. Complexity of experiments in this thesis leads to the decision to use one cell line from each entities, but then to validate in another pair of HPV-positive and HPV-negative cells lines. Conclusions based solely on a single cell culture of each type are preliminary, unless were validated using other cell lines.

Table 2.1: Summary of used cell lines relevant information.

Cell line	Nature	P53 status	11q13	Age	Gender	Smoker	Drinker
UPCI:SCC 089	New primary	-	Amplified	58	M	Y	Y
UPCI:SCC 072	New primary	Mut 179	Amplified	61	F	y	y
UPCI:SCC090	Recurrence	Wild type	Not	46	M	Y	Y
UD-SCC2	-	Wild type	Not	-	M	Y	Y

Cells were cultured using basal media consisting of Dulbecco's modified Eagle's media (DMEM) (Gibco, Life Technology), supplemented with 10% Foetal bovine serum (FBS) (Sigma-Aldrich, UK) owing to its high content of embryonic growth promoting factors which support cells growth. 2mM L-Glutamine also was added as an alternative energy source for rapidly dividing cells. 50 IU/50 µg ml-1 Penicillin-Streptomycin (Sigma-Aldrich, UK) also was added to control bacterial contamination. Cells were maintained in the incubator with 5–7% CO_2 - the recommended CO_2 tension concentration to obtain the appropriate pH level of the media.

2.1.2 Normal tonsillar fibroblasts

Human primary normal tonsillar fibroblasts (NTF322, NTF6 and NTF10) were provided by Dr Helen Colley, University of Sheffield (IRAS number 09/H1308/66). Table 2.2 summarised the relevant information. Cells were cultured using the same mentioned cell lines' growth media unless otherwise stated when the serum is omitted from the growth media recipe, to obtain a precise evaluation of cellular function and more consistent performance.

Table 2.2: Summary of clinical information related to normal tonsil fibroblasts.

Primary culture	Gender	Age (Y)	Site
NTF6	Female	29	Tonsil
NTF10	Female	19	Tonsil
NTF322	Female	21	Tonsil

2.1.3 Tonsillar cancer-associated fibroblasts

Human primary tonsillar cancer-associated fibroblasts (CAF1 and CAF2) were isolated from biopsies taken during a tonsillectomy surgical procedure, (as part of initial cancer treatment), at the Royal Hallamshire Hospital, Sheffield Teaching Hospitals NHS Foundation Trust with informed consent: IRAS 13/NS/0120. Both CAF1 and CAF2 were isolated from HPV-positive tumours. Table 2.3 summaries the available relevant information.

Table 2.3: Summary of clinical information of tumour from which cancer fibroblasts were isolated.

Primary culture	Gender	Age (Y)	Site	Stage	p16-status
CAF1	Male	61	L. Tonsil	T2N1	Positive
CAF2	Male	80	R. Tonsil	T2 N3b	Positive

2.1.3.1 **CAF isolation:**

We followed a common method in cell isolation from primary tissue utilising the enzymatic disaggregation effect of collagenase. Fragments of human tonsil tissue were received in transport media (DMEM supplemented with 100 IU/ml penicillin, 100 µg/ml

streptomycin and 0.625 µg/ml amphotericin B). CAFs were isolated from the tissue by fine mincing of the tissue in a 9 cm dish in the transport media, then all the tissue pieces were transferred to a 15 ml falcon tube and centrifuged at 1400 rpm for 10 mins. The supernatant was pipetted carefully, and tissue resuspended in growth media followed by spinning at 1400 rpm for 10 mins. The supernatant was then discarded, and the precipitated tissue was washed with PBS followed by a further spin and elimination of the supernatant. 3 ml of 0.5% (w/v) collagenase (Sigma Aldrich, UK) was added to the precipitated tissue in a 15 ml falcon tube and incubated overnight at 37°C. The next day, the tube was centrifuged at 1400 rpm for 10 mins, and the supernatant was pipetted carefully, while the precipitated tissue was resuspended in growth media. The mixture was transferred to a T25cm^2 flask and incubated for 7 days at 37°C in a humidified incubator with 5% CO_2 and the media was replaced carefully every 2 days. Seeding stock and working stock were generated (section 2.1.5). Cells were expanded as needed (section 2.1.6).

2.1.4 Routine maintenance of cells

OPSCC cancer cell lines' working passages were up to 15 passages starting from the earliest available passage. Primary tonsillar fibroblasts were cultured up to passage 7. Growth media change was undertaken every 2 days for OPSCC cell lines and every 5 days for primary tonsillar fibroblast cultures. Cells were cultured in T75cm^2 flasks up to approximately 70% confluence. At this time point, cells were still actively dividing (Log phase). Late log phase is the appropriate time to passage cells, before reaching Plateau (Stationary) Phase, where cell growth slows down due to overcrowding and cellular stress (Figure 2.1).

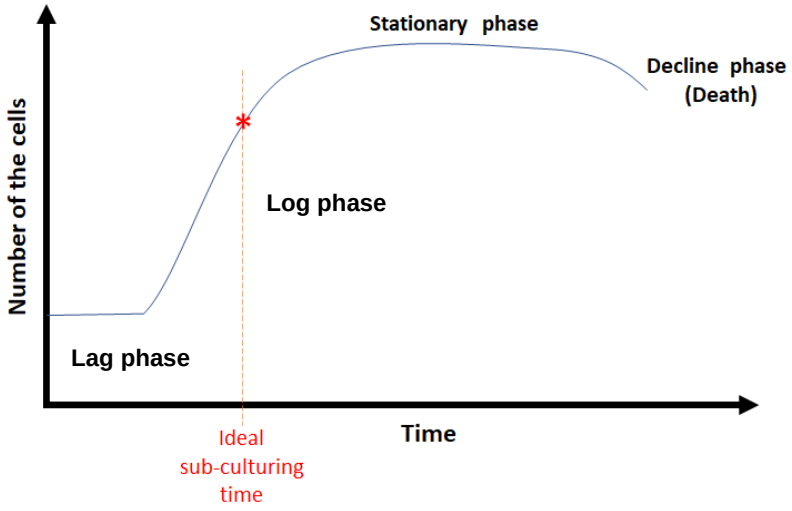

Figure 2.1: Growth phases of cultured cells. The semi-logarithmic plot shows the cell density versus the time spent in culture. Lag phase, the first phase of growth after cell accommodation in the new culture. The log phase, the period when the cells proliferate exponentially and consume the nutrients in the growth medium. Stationary phase, the stage where cells' proliferation is greatly reduced or ceases entirely. Decline phase, a reduction in the number of viable cells death as a natural progression of the cellular cycle. The late Lag phase is the ideal sub-culturing time.

To detach the adherent cells from the flask/plate for the sub-culturing step, (TE) Trypsin/ Ethylenediaminetetraacetic acid (EDTA) (Sigma-Aldrich, UK) was used. Cells were washed twice with PBS and incubated with 3 ml of TE for 5 minutes at 37ºC. TE was then neutralized using 10% v/v serum-containing media followed by centrifuging at 1000 rpm for 5 minutes. The supernatant was discarded, and the cell pellet was re-suspended in growth media and seeded at the desired concentration.

Mycoplasma test was performed routinely by the Core facility service using Mycoplasma Detection Kit (Cat. No. 13100-01, Southern biotech). The kit incorporates polymerase chain reaction (PCR) to amplify the conserved 16S ribosomal RNA coding region within the Mycoplasma genome.

2.1.5 Cell freezing

A cryoprotectant is added to the freezing medium to avoid the risk of ice crystal formation which can cause cellular damage during the freezing process. Dimethyl sulphoxide (DMSO) was selected for the best osmotic features upon the cell suspension thawing.

For stock preparation, cells were resuspended in 100% FBS and placed in well-labelled cryotubes (Greiner Bio-one, UK) at density 1 $x10^6$ cells for cell lines and 15 $x10^4$ cells for fibroblasts in 1 ml FBS. 10% DMSO diluted in FBS (Sigma-Aldrich, UK) was added to the cryotubes then placed in a cryo-cooler (Mr Frosty) filled with isopropanol to allow slow freezing of the cells. The cryo-cooler was stored immediately at - 80ºC for 24 h, then cryotubes were moved into liquid nitrogen for longer storage.

2.1.6 Cell resurrection

After retrieving the cryotube from the liquid nitrogen, it was thawed by hand for a few minutes. Cell suspension was added to 10 ml of pre-warmed media in a 15 ml falcon tube then centrifuged at 1000 rpm for 5 minutes. The supernatant was discarded, and the cell pellet was re-suspended in 10 ml of growth media and seeded in a T75 cm^2 flask at the required concentration. The flask kept at 37ºC in a humidified incubator with 5% CO_2. The next day, cells were checked and incubated with fresh growth media.

2.1.7 Counting Cells

The haemocytometer and cover-slip (Baxter Scientific) were cleaned with alcohol and left to dry at RT. 10 µl of 0.4% trypan blue dye (Life Technologies, UK) was added to 10 µl cell suspension and mixed by pipetting up and down. Trypan Blue dye was added to identify the percentage of viable cells present in the cell suspension. The mixture was incubated for not more than 1 min at room temperature (RT), to avoid false-positive results in counting of non-vital cells. The coverslip was fixed in position on the haemocytometer, and 10 µl of the trypan blue/cell mixture was pipetted at the slide notch. Cell counting was undertaken using an inverted microscope at 10X objective (Figure 2.2).

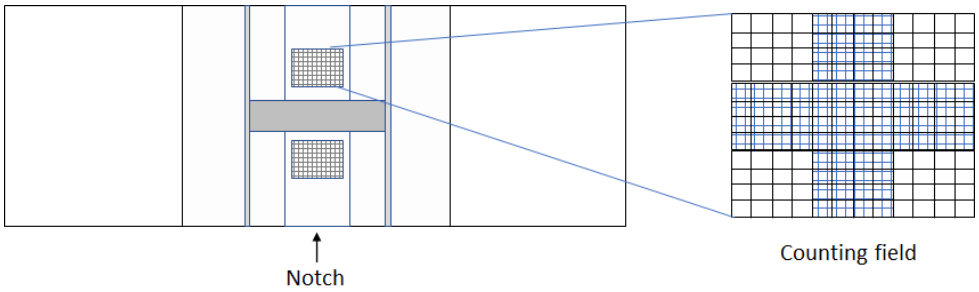

Figure 2.2: Haemocytometer slide.

Cells were counted (blue-stained and unstained cells) in all large squares at the corners of the haemocytometer and the average was obtained by dividing the total cells number by 4. Final cell count estimation = the average X suspension dilution factor X 10^4.

The proportion of viable cells was determined by dividing the number of unstained cells by the number of total cells then multiplying by 100. Culture viability of more than 90% is considered appropriate to continue the culturing work.

2.1.8 Fibroblast stimulation using rh-TGF-β1

To characterise the response of NTFs to TGF-β1 stimulation and establish active myofibroblastic phenotype, cells were incubated with rh-TGF-β1, the master cytokine in fibroblast differentiation and the activation of cancer stroma (Postlethwaite *et al.*, 1987; Caja *et al.*, 2018).

The activation protocol is based on previous work from our lab on oral fibroblasts (Melling *et al.*, 2018). NTF322, NTF10, and NTF6, cells were incubated with TGF-β1 (R&D Systems, USA) at 24 h or 48 h or 72 h, at a concentration of 5 ng/ml. Cells were plated into 6-well plate (Greiner Bio-one, UK) at a density of 1.5 x 10^5 per well with 2 ml of growth media and incubated overnight at 37°C in a humidified incubator with 5% CO_2. The next day, the media was aspirated, and cells were washed with PBS x2 and serum-starved overnight using DMEM serum-free media. On the third day, 1 ml of DMEM serum-free medium containing 5 ng/ml rh-TGF-β1 was added to each well. The experimental control wells were incubated with 1 ml serum-free medium. Plates were incubated for 24 h, 48 h or 72 h in a humidified incubator. At the end of the experiment, cells were pelleted for downstream RNA/protein analysis and the media was aspirated,

centrifuged, and the supernatant was stored at -20°C. The experiment was performed in three biological repeats.

2.1.9 Tonsillar fibroblast stimulation using rh-OPN

To explore the correlation between OPN and IL6 expression in OPSCC tumour cells/ fibroblasts crosstalk, NTF322, NTF10 and CAF2 were incubated with 180 ng/ml rh-OPN (R&D Systems, USA) for 48 h then IL-6 expression/production was assessed. The activation protocol is based on previous work (Bramwell *et al.*, 2006; Weber *et al.*, 2015).

Fibroblasts were cultured in a T75 cm^2 flask in growth media up to 70% confluence. Cells were washed with PBS x3 and serum-starved overnight. On the third day, cells were incubated with 10 ml of serum-free medium containing 180 ng/ml of rh-OPN for 48h at 37°C in a humidified incubator with 5% CO_2. The experimental control was incubated with 10 ml serum-free media only in the same conditions. At the end of the experiment, the media were aspirated, centrifuged, and stored at -20°C for IL-6 ELISA analysis. Cells were harvested and counted to normalise ELISA analysis results then cells were collected for further IL-6 gene evaluation. The experiment was performed in triplicate.

2.1.10 Collagen gel contraction assay

Myofibroblastic phenotype is characterised by the capability to form potent actin stress fibres through a well-developed contractile apparatus. Collagen gel contraction assay is commonly used in the field of mechanobiology to investigate cell-induced contraction of extracellular in wound healing and inflammation. We utilised this technique as a parameter to quantify the degree of NTF contractility by measuring the reduction in NTF gel diameter after TGF-β1 or OPN treatment.

Following the protocol of the collagen gel contraction kit (Cell Bio-Lab Inc, CBA-201), NTFs were harvested and resuspended in growth medium at 2 x 10^4 cells/ml. A collagen lattice was prepared by mixing 2 parts of cell suspension and 8 parts of cold collagen gel working solution. From this mixture, 0.5 mL was pipetted in a well in a 24-well plate and incubated for an hour at 37ºC. After collagen polymerization, 1.0 ml of growth medium was added on the top of the collagen gel lattice and the plate incubated for 24 h at 37ºC in a humidified incubator with 5% CO^2. The next day, the cells were serum-starved for a

further 24 h, then were treated with 5 ng/ml TGF-β1 or 180 ng/ml OPN before releasing the stressed gel matrix from the plate using a sterile spatula. The gels were then incubated for 72 h in the TGF-β1 stimulation experiment or 48 h in the OPN stimulation experiment. Photographs of the gel disc were taken at 24 h, 48 h and 72 h. The contractility of the gels was then calculated by measuring the distance between the collage disc border and the plate well using ImageJ. The experiment was performed in triplicate.

2.1.11 Fibroblast senescence induction

Senescence typically occurs in response to damaging stimuli, such as DNA damage (DNA damage-induced senescence), oxidative stress or replicative exhaustion. Cells were treated with Hydrogen peroxide (H_2O_2) which provokes oxidative stress-induced premature senescence. This experimental protocol is based on previous similar work on oral fibroblasts (Kabir *et al.*, 2016) using the optimal dose of H_2O_2 (500 µM) that caused a gradual reduction in the rate of cell proliferation overtime points with minimum cytotoxicity.

Early-passage NTF322, NTF6 and NTF10 cells were grown in 75cm^2 flasks up to 70% confluence. Cells were then washed with PBS x2 and incubated with 500µM of H_2O_2 (Sigma-Aldrich, UK) in serum-free media for 2h at 37°C in a humidified incubator with 5% CO_2. The negative control cells were incubated with serum-free media alone for 2h, at the same incubation conditions. After that, cells were washed with PBS x3 and incubated with growth media for 15 days. Cells were split on day 8. At the end of the experiment, the media were collected, centrifuged at 3000 rpm for 5 min and stored at -20°C. Cells were counted and the culture viability percentage was recorded. 4 x 10^4 cells were seeded in a 12-well plate, prepared for Senescence-Associated β-galactosidase Assay (SA-β-gal) staining (section 2.1.12). The rest of the suspension was centrifuged, and the formed pellet was collected and stored at -80°C for further analysis. The experiment was performed in triplicate.

2.1.12 Senescence-Associated β-galactosidase Staining Assay

The SA-β-gal assay is a cytochemical assay used for the detection of senescent cells based on an increased level of lysosomal β-galactosidase activity. Under normal conditions, the lysosomal β-galactosidase activity can be detected at pH4 using the chromogenic stain 5-bromo-4-chloro-3-indolyl-β-d-galactopyranoside (X gal). In

senescent cells, the lysosomes produce a high level of β-galactosidase that can be detected at pH 6 (Kurz *et al.*, 2000).

SA-β-gal activity was assessed using a Senescence Detection Kit (ab65351; Abcam, Cambridge, UK) following the manufacturer's instructions. 40,000 cells were seeded in 12 well-plates and left to adhere overnight. The next day, cells were washed twice with PBS and incubated with 500 µL fixative reagent for 20 min at RT, followed by a wash with PBS x2. 500µL of total solution mixture (Table 2.4) was added to each well, then the plate was kept overnight in the incubator after wrapping with aluminium foil and sealed in a plastic bag to prevent pH changes during the incubation. The next day, SA-βgal staining was observed at 20X magnification using an inverted microscope (Olympus; CKX41). The percentage of stained cells was calculated using ImageJ 1.45s software.

Table 2.4: SA-β-gal stain recipe per well.

Component	Volume
X-gal solution	25 µl
Staining solution	470 µl
Staining supplement	5 µl

2.1.13 Cell growth kinetics of CAFs

To assess and compare the proliferation rate of the CAFs cultures, CAF1 and CAF2 were seeded at a density of 5,000 cell/ml in a 6 well-plate with 2ml growth media. At two-day intervals, cells from one well of the 6 well-plate were detached and counted giving the total count/mL of cells. The experiment was repeated 3 times allowing calculation of mean and standard deviation. A graph was plotted of cells per ml at each time point, namely 1, 2, 3, 4, 5, and 6 days. The experiment was performed in triplicate.

2.1.14 Cancer cell line induction with IL-6

To test the ability of IL-6 to induce OPN production in OPSCC cells, the OPSCC cell lines were incubated with rIL-6 (Catalogue 200-06, Peprotech, UK) for 48h. We started with a dose of 15ng/ml rIL-6, as this has been shown to be sufficient for induction in previously

reported optimising work on the tumour cells (Chen *et al*., 2018). SCC89, SCC72 and SCC2 were cultured in a T75cm^2 flask in growth media up to 70% confluence. Cells were washed with PBS x3 and serum-starved overnight. Next day, cells were incubated with serum-free media supplemented with 15ng/ml of rh-IL6 (PeproTech, USA. Catalogue 200-06) for 48h at 37°C in a humidified incubator with 5% CO_2. The experimental control was incubated with 10 ml serum-free media only in the same conditions. Thp-1 monocytes were included as a positive control (Uchibori *et al*., 2017). Thp-1 cells were provided kindly by Dr Emilia Barker. At the end of the experiment, the media was aspirated, centrifuged, and stored at -20°C for OPN ELISA analysis. Cells were harvested and counted to normalise ELISA analysis results then cells were collected for further OPN gene evaluation. The experiment was performed in triplicate.

2.1.15 CD44v6 blocking in NTFs

NTF322 and NTF10 were cultured in T75 cm^2 flask with growth media up to ~70% confluence. Cells were incubated for 1h with serum-free media supplemented with 5µg/ml of CD44var (v6) Monoclonal Antibody (VFF-18) supplied by eBioscience™ (Catalogue: BMS125). The experimental control was incubated with serum-free media only. 6.5 ml of cell lines conditioned media (SCC89, SCC72 and SCC2) (prepared in section 2.1.1) was thawed in the water bath and supplemented with 1.5ml of fresh growth media. After 1 h of CD44 blocking, rOPN or cell line CM was added to NTFs and incubated for 24 h at 37°C in a humidified incubator with CO_2. The next day, media were collected, centrifuged, and stored at -20°C immediately. Fibroblasts were harvested, counted and collected as a pellet for further gene analysis.

2.2 Protein analysis

2.2.1 Cytokine analysis

Cell-cell communication between tumour cells and cells in the microenvironment plays an important role in cancer initiation, promotion, and progression (Lorusso and Rüegg, 2008). CAFs have functional or regulatory roles in HNSCC carcinogenesis and malignancy such as metastasis, proliferation, and angiogenesis through the cytokine signals facilitating autocrine and paracrine interactions between tumour cells and cells in the microenvironment (Orimo and Weinberg, 2006).

To understand the nature of this communication in OPSCC and investigate differences between HPV positive and HPV negative subtypes, an *in vitro* co-culture system was used in which these cellular interactions in OPSCC can be examined. Different approaches to the study of cell-cell communication in co-culture systems have been used in the literature depending on the hypothesis of interest (Bogdanowicz and Lu, 2013) (Table 2.5). The objectives of this study were to identify secreted cytokines in tumour/fibroblast cells crosstalk and explore the source of these secretory cytokines.

For cytokine screening, we collected fibroblast conditioned media after incubation with the relevant OPSCC cell line media for 24 h, then subjected these media to cytokine array analysis. To validate the array findings and explore the source of the cytokine production, we used an indirect co-culture system (Transwell) taking advantage of cell culture separation with a porous membrane which permitted fluid movement between the co-cultivated cell populations while they were kept separated. In these experiments, all collected media was stored at −20°C in small aliquots to avoid a freeze-thaw cycle. Most of the cytokines are stable for up to three freeze-thaw cycles (Thavasu *et al.*, 1992).

Table. 2.5: Comparison between co-culture methods.

Culture method	Advantages	Limitations	Reference
Conditioned media	• Easy to perform. • Allowing for identification of soluble factors and detecting their effects in co-culture media.	• Nutrient deficiency issue in the culture. • Difficulty in reproducing the optimal concentrations and temporal distribution of the secreted factors.	(Antonelli et al., 1989)
Direct co-culture (mixed monolayer)	• Maximises local heterotypic interactions. • Control the relative levels of heterotypic and homotypic communication by altering the seeding densities of each cell type. • Can be modified by adding temporary barrier between two cultures to monitor cell migration.	• Several factors should be considered during results' Interpretation: a possible dilution effect due to mixed culture, metabolic differences between cell types and the relative contribution of each cell population to any observed effects. • Separation of the two populations is a complicated procedure.	(Wang et al., 2007, Proffen et al., 2013)
Indirect co-culture (Transwell type)	• Ideal for studying paracrine interaction. • Ability to identify effects of co-culture on individual populations. • A continuous effect can be monitored. • Provided more reproducible and reliable in vitro results.	• Observation of both culture cells with time-lapse microscopy at the same time is impossible. • Communication only via soluble factors, no true physical contact as would occur under *in vivo* conditions.	(Renaud and Martinolj, 2016)

2.2.1.1 Collection of cell line conditioned media for fibroblast activation

HPV negative cell lines (SCC89) and HPV positive cell lines (SCC2) were cultured in T75 cm^2 flasks using growth media (section 2.1) until ~85% confluency. Cells were washed twice in PBS, then incubated for 24h in 7 ml of growth media. The next day, the (conditioned) media was collected and centrifuged for 5 minutes at 3,000 rpm. 6.5 ml of

the supernatant was aspirated carefully and stored immediately at -20°C. Cells were trypsinised and counted to record the number of cells that contributed to each ml of conditioned media, 3 ±1 million cell/ml was the target.

2.2.1.2 Fibroblast stimulation with cell line conditioned media – Passive coculture

NTF322, NTF10, CAF1 or CAF2 cells were cultured in T75 cm^2 flasks with growth media up to ~70% confluence (as fibroblasts will be incubated for a further 48 h, enough space is required between cells to avoid cellular stress). Conditioned media (section 2.1.1) from the HPV negative cell line (SCC89) and HPV positive cell line (SCC2) were thawed in the water bath. Fibroblasts were washed three times with PBS, then 6.5 ml of HPV positive or HPV negative cell line conditioned media was added to fibroblasts and incubated for 24 h at 37°C in a humidified incubator with CO_2. The experimental control cells were incubated with fresh growth media and incubated at the same condition. The next day, media were collected (Media1), centrifuged, and immediately stored at -20°C. Fibroblasts were washed with PBS x3 and incubated with 6.5 ml of fresh serum-free media for a further 24 h. After that, media were collected (Media2), centrifuged, and stored at -20°C immediately. Fibroblasts were harvested and counted to allow for normalisation of the ELISA results (Figure 2.3).

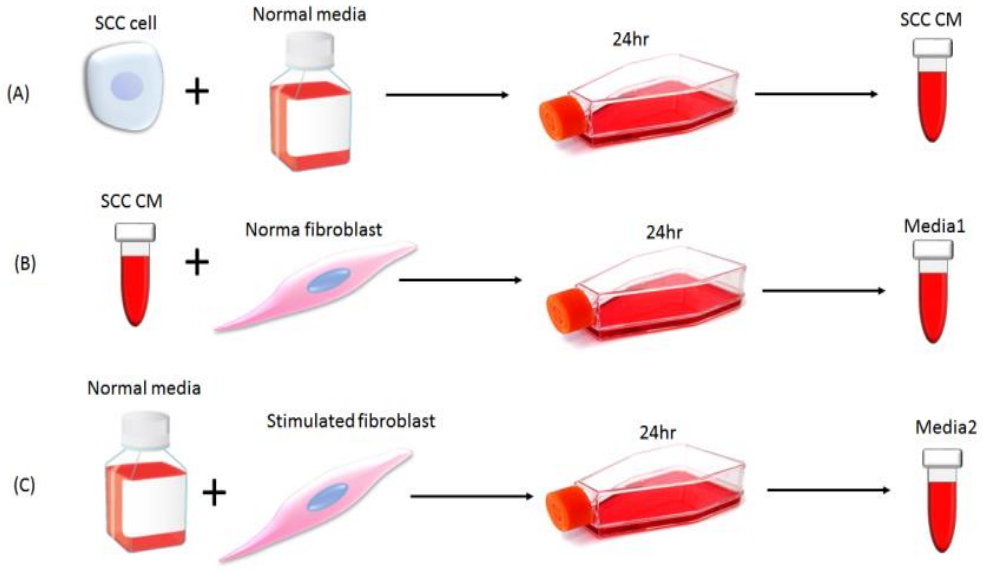

Figure 2.3: Illustration for conditioned media procedure. A. cell line conditioned media collection. B. Stimulation of fibroblast by cell line media and collection of the stimulated fibroblasts media. C. incubation of fibroblast with normal media to get media2.

2.2.1.3 Cytokine arrays

Multiplex arrays are an antibody-pair-based assay for screening and comparing expression levels of up to hundreds of cytokines in a single assay. By comparing cytokine arrays with other methods for cytokine screening, such as Mass Spectrometry and Cytometric Bead Array, cytokine arrays are simpler, use standard lab equipment, and are relatively cost-effective. However, a cytokine array is a semi-quantitative method that requires further quantitative analysis using for example an ELISA assay for validation.

The technology is based on the specific binding ability between captured antibody spotted in duplicate on nitrocellulose membranes and target cytokine that can be applied in different forms such as cell culture supernatant, cell lysate, serum, or plasma samples. Detection and visualisation of cytokine-capture antibody complex are obtained by incubating the membrane with streptavidin-Horseradish Peroxidase and chemiluminescent detection reagents. The signals are presented in the semi-quantitative form in proportion to the amount of cytokine bound.

The Proteome Profiler Human XL Oncology Array kit (Catalogue number ARY026) was purchased from R&D Systems, Inc., Minneapolis, US. The arrays are designed to provide a relative expression of 84 human cancer-related proteins (Figure 2.4) the full names of included factors are listed in Appendix A.2. The protocol was followed according to the manufacturer's instructions throughout the experimentation. Developed films were then scanned at high resolution and analysed using Image Studio software (Version 5.2; LI-COR, Inc, USA). Densitometry data were then normalised to the positive control spot (reference spots).

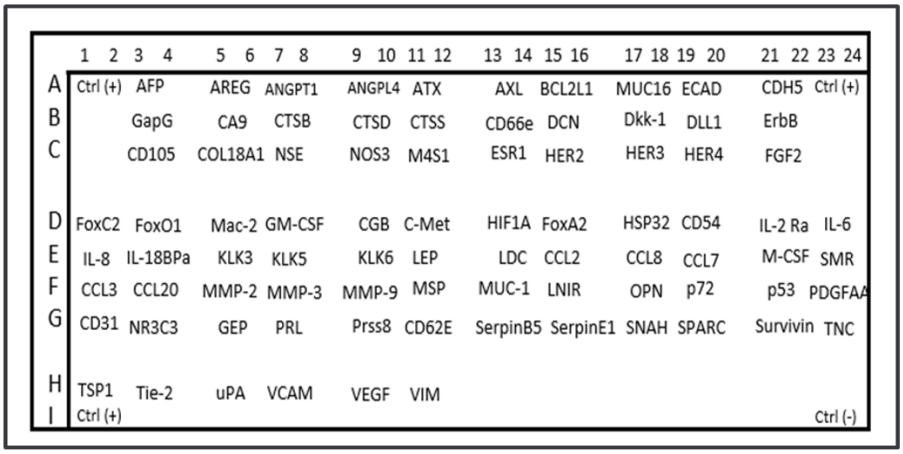

Figure 2.4: The Proteome Profiler Human XL Oncology Array map (Catalogue number ARY026, R&D Systems, UK).

2.2.1.4 Indirect interactive co-culture (Transwell)

In this experiment, we followed a modified protocol of the transwell co-culture method, based on a previous report (Aiuti *et al.*, 1998). $3x10^5$ Cancer cells were seeded in 1.5ml of growth media on cell culture inserts (Life Sciences, USA) containing a 0.45µm plastic membrane filter and placed on a 6-well plate filled with 2.6 ml of growth media. Cells were allowed to adhere overnight at 37°C in a humidified incubator with 5% CO_2. The filters were conditioned before cell seeding to enhance the cellular adhesion by preincubation for a minimum of 1 hr at 37°C. 50,000 cells of NTF 3, NTF 10, CAF1 or CAF2 were plated in 6-well plate in 2 ml growth media and incubated for 24 h The experimental controls were plated in the same way with omitting the fibroblasts or cancer cells. The next day, the media change was undertaken, 1.5 ml fresh growth media was added to the inserts and 2.6 fresh growth media was added to the fibroblasts in 6-well plate, then the cell culture inserts were inserted into the wells carefully to avoid air bubble formation (Figure 2.5). The co-culture system was maintained for 48 h at 37°C in a humidified incubator with 5% CO_2. At the end of the experiment, the media were aspirated and centrifuged at 3000 rpm for 5 min and stored immediately at 20°C. Cancer cells and fibroblasts were detached from the culture system, counted and stored separately as pellets at -80°C.

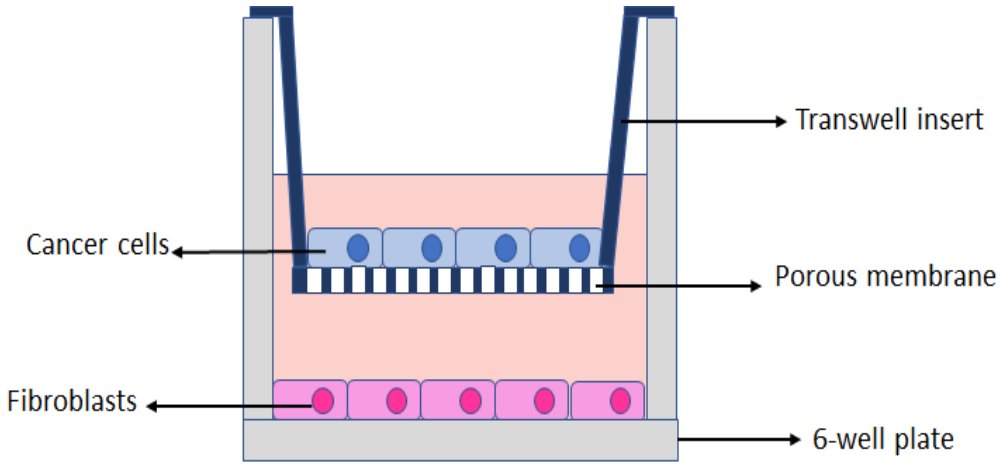

Figure 2.5: Illustration of transwell co-culture model.

2.2.2 ELISA analysis

The indirect ELISA detection method was utilised in this study where the captured antigen (the target) has been coated on a plate surface and then complexed with an antibody that is linked to a reporter enzyme (horseradish peroxidase). Detection of cytokine-captured antibody complex is achieved by measuring the activity of the reporter enzyme via incubation with the appropriate substrate to produce measurable signals.

Secreted IL-6, and CCL2 were quantified using the BD OptEIA™ sets for human IL-6 and CCL2 detection (BD Biosciences, San Jose, US). OPN was quantified using the DuoSet Elisa set (R&D Systems, Minneapolis, US). For IL-6 and CCL2 analysis, conditioned media was diluted 1:100, whereas in OPN conditioned media was used without dilution. The calculated values were adjusted to the respective dilution factors. Delta Soft Microplate Analysis Software (MTX Lab system, USA) was used for ELISA data analysis. The corrected wavelength was used to plot the standard curve in (Log-Log) regression. The standard curve equation was used to determine the target protein concentration (pg/ml). The concentration of secreted target protein was normalised according to the cell number at 10,000 cell/ml.

2.2.3 SDS-PAGE

SDS-PAGE was used to separate and identify target proteins. The protein mixture is separated on a polyacrylamide gel matrix based on molecular weight. The negatively charged proteins migrate depending on their size down the gel towards the positively charged electrode when a voltage is applied. However, this technique provides a semi-quantitative result compared to other relative protein levels.

2.2.3.1 Protein extraction and quantification:

Radioimmunoprecipitation assay buffer (RIPA buffer, Sigma-Aldrich, UK) was used to lyse cells and solubilise proteins. One tablet of complete mini-EDTA free protease inhibitor cocktail and one tablet of phosphatase inhibitors were added to 10 ml RIPA to ensure protein stability. The cell pellet was removed from - 80 °C storage and kept in an ice box. 150-300 ml lysis buffer was added to the cell pellet and gently pipetted up and down to mix thoroughly and kept in the ice for 30 min followed by cooling centrifugation for 20 min at 13,300 rpm to avoid protein denaturing. The supernatant (soluble protein) was then aspirated and stored at -20°C, and the formed pellet was discarded. Protein

was quantified using the bicinchoninic acid assay (BCA) (Fisher-Scientific, UK) following the manufacturer's protocol. A POLAR-star Galaxy spectrophotometer was used for plate reading.

2.2.3.2 Separation by size

The percentage of acrylamide gel to use was determined according to the target protein molecular weight. Table 2.6. illustrates the recipe of used Acrylamide gel to make 1.5 mm gel thickness.

Table 2.6: acrylamide gels' recipe

Resolving gel					
Gel %	Acrylamide (ml)	Lower Tris (ml)	H2O (ml)	TEMED (µl)	APS 10% (µl)
12	1.2	2.5	6.1	5	350
15	1.9	2.5	5.4	5	350
Stacking gel					
	Acrylamide (ml)	Upper Tris (ml)	H2O (ml)	TEMED (µl)	APS 10% (µl)
	1	2.1	4.7	17	100

Total protein lysate (20-30 µg) was mixed with 5x SDS lysis buffer (1:5) then heated for 5 min at 95°C in a heat block. This step aimed to denature the higher-order structure, which ensures that the negative charge of amino acids is not neutralized, enabling the protein to move in an electric field. The gel was placed into the XCell SureLock Mini Cell electrophoresis system (Invitrogen Ltd, UK) following the manufacturer's instructions and filled with 1x SDS running buffer. A pre-stained protein ladder (Ez run protein ladder) and the protein samples were loaded into gel wells then the gel was run for 60 min, at 100 V.

2.2.3.3 Transfer to a solid support

Protein in the gel was transferred into nitrocellulose membrane or polyvinylidene difluoride (PVDF) membrane using the Trans-Blot® TurboTM Transfer System (Bio-Rad, UK). PVDF offers a higher protein binding capacity which allows it to detect lowly expressed proteins at a cost of higher background noise. More attention is required during the washing steps to minimise the dark background. Membrane was then stained with a Ponceau solution (Sigma- Aldrich, UK) to check for even protein transfer followed by washing dH_2O.

2.2.3.4 Marking the target protein

The immunodetection step started by membrane blocking with 5% (w/v) milk (Marvel, UK) in TBS-T (Tris-buffered saline 10mM, containing 0.5% Tween (v/v)) for 1 hour at room temperature. The membrane was then incubated overnight at 4°C on a rocking platform with the primary antibody at the recommended concentration (Table 2.7) in 5% TBS-T milk.

Table 2.7: List of used primary antibodies in immunoblotting.

Primary antibody	Working concentration	Catalogue No – Supplier
Anti-α-SMA	1:1000	A5228 - Sigma-Aldrich, UK
Anti-p16	1:1000	108349 – Abcam, Cambridge, UK
Anti-p21	1:1000	MAB1047 – R&D Systems, US
Anti-phosphorylated p38	1:1000	Ab4822 – Abcam, UK
Anti p38	1:500	Ab27986 – Abcam, UK
Anti-CD44	1:1000	15675-1-AP – Proteintech, UK
Anti-β-actin	1:3000	A1978 – Sigma-Aldrich, UK

The next day, the membrane was washed x3 for 5 min with TBS-T and then was incubated with the secondary antibody (Table 2.8) in 5% TBS-T milk for 1hr at room temperature on a rocking platform.

Table 2.8: List of used secondary antibodies in immunoblotting.

Secondary antibody	Work concentration	Catalogue No – Supplier
Anti-mouse	1: 5000	GTX22166701 - Genetex, US
Anti-rabbit	1:3000	7074S - Cell Signalling, UK

The membrane was then washed twice for 10 min with TBS-T and once with TBS for 5 min. Membrane was developed with enhanced chemiluminescence (ECL), Pierce ECL western blotting substrate (Thermo-Fisher, USA), according to the manufacturer's instructions, then the membrane was scanned with a digital scan. Image Studio Software (LI-COR Biosciences, US) was used for densitometry analysis of the bands and the intensity of each band was expressed normalized to the corresponding internal control (β-actin). When needed, membranes were stripped of bound antibodies using 10 ml of stripping buffer (Sigma-Aldrich, UK) for 30 minutes at room temperature on a rocking platform and then washed with TBS.

2.2.4 Immunofluorescence staining

Immunofluorescence staining was performed to detect and localise the antigens in cellular contexts (α-SMA, FAP-α, FSP-1), also, to determine the activation states of CD44 in OPN-treated OPSCC cell lines.

8-well slide chamber (Starstedt, GER) was used to culture the cells for immunofluorescence analysis. 20,000 cells were seeded in each chamber with 800 µL of growth media. Chambers were covered with a lid and incubated for 24 h at 37°C in a humidified incubator with 5% CO_2. After treatment with TGF-β1 or OPN, cells were fixed using the recommended reagent according to the manufacturer's instructions (Table 2.10). This was followed by another incubation with the permeabilisation reagent if needed (Table 2.11). After that, cells were blocked by the appropriate blocking (Table 2.9) on a shaker for 15 mins. 200 µL of the diluted primary antibody was added, including

in the experiment negative control and incubated for 1.5h. Cells were then washed twice with PBS and incubated with the secondary antibody for 1h (if a non-conjugated antibody). The antibody control chamber was incubated with 200 µL of secondary antibody only. After that, the chambers were washed x3 with PBS and mounted with a coverslip containing a drop of Prolong diamond antifade mountant (DAPI, thermo fisher P36966). The slide was placed in a slide box at 4°C for 24h. Images have been taken used Ziess Axioplan 2 fluorescence light microscope (Carl Zeiss, UK), staining intensity has been quantified using Image J software quantifying the green colour only in fields with equal cells number.

Table 2.9: Summary of the essential information for the used antibodies in immunofluorescent staining.

Protocol	α-SMA	FAP-α,	FSP-1	CD44
Fixation	100% Methanol for 15 min	4 % formaldehyde for 10 minutes	100% Methanol for 15 min	100% Methanol for 15 min
Permeabilization	4mM Sodium deoxycholate for 15 min	0.1 % TX-100/PBS for 15–20 minutes	Not required.	4mM Sodium deoxycholate for 15 min
Blocking and incubation time	Blocking Buffer (2.5% BSA in PBS) 15 min	5 % normal goat serum/PBS. 15 min	10% goat serum in PBS. 15 min	10% goat serum in PBS. 15 min
Primary antibody and incubation time	1:100, 1.5h Mouse monoclonal (clone 1A4, F3777, Sigma Aldrich, UK).	1:100, 1.5h RT Rabbit monoclonal (66562, cell signalling technology).	1:100, 1.5 h RT Rabbit monoclonal (13018, cell signalling technology).	1:200, 1.5 h RT Rabbit polyclonal. (1567-1-AP, Proteintech, UK)
Secondary antibody and incubation time	Not required	1:1000, goat anti rabbit. 1h at 37°C	1:1000, goat anti rabbit. 1h at 37°C	1:1000, goat anti rabbit. 1h at 37°C

2.3 Molecular analysis

2.3.1 RNA extraction and reverse transcription

Total RNA was extracted using the Isolate II RNA Mini Kit (Bioline, UK) following the manufacturer's instructions. RNA was quantified using a Nanodrop spectrophotometer. The purity of extracted RNA was determined by 260/280 ratio. 400ng of extracted RNA was reverse transcribed using a High-Capacity cDNA reverse transcription Kit (Applied Biosystems, USA) following manufacturer´s protocol using Peltier Thermal cycler (MJ Research, UK). The thermal cycler was set to run at 25°C for 10 min, followed by 2 h at 37°C, and finally at 85°C for 5 min. cDNA was then stored at -20˚C.

2.3.2 Quantitative PCR (qRT-PCR)

Gene expression was quantified by a Rotor-gene qRT- PCR cycler (Qiagen, UK) using SYBR green chemistry or TaqMan chemistry. The quantification result was calculated using delta CT values normalized to the cellular reference gene beta2-microglobulin (β2m). All reactions were performed in a total volume of 10 µl, loading 500-120 ng of cDNA. The standard thermal cycle consisted of 95ºC for 10 sec, 60ºC for 15 sec and 72 ºC for 20 sec. Table 2.10 outlines the probes used in this project.

Table 2.10: List of the used qRT-PCR primers and probes in the study

SYBR Green primers		
Name	Sequence	Supplier
α-SMA	F: 5'GAAGAAGAGGACAGCACTG3' R: 5'TCCCATTCCCACCATCAC3'	Sigma-Aldrich, UK
FSP-1	F: 5'-TGTAATTGTGTCCACCTTCC-3 R: 5'-GCTCATCACCTTCTGGAATG-3	Sigma-Aldrich, UK
Cytokeratin 6	F-GTCCTCAGGCCCCTCTCTGG R-CCCCTGGCAATTTTCTGCAA	Sigma-Aldrich, UK

Table 2.10 B: List of the used qRT-PCR probe in the study

TaqMan chemistry probe		
Name	Hs number	Supplier
HAL-DR	00219575	Thermo Fisher scientific, UK
CD31	01065279	Thermo Fisher scientific, UK
FAP-α	00159849	Thermo Fisher scientific, UK
PDGFRα	00183486	Thermo Fisher scientific, UK
IL-6	00985639	Thermo Fisher scientific, UK
CDKN1A (P21)	00355782	Thermo Fisher scientific, UK
CDKN2A (P16)	00923894	Thermo Fisher scientific, UK
SPP1 (OPN)	00960942	Thermo Fisher scientific, UK
β2m	4325797	Thermo Fisher scientific, UK

N.B: SSP1 TaqMan probe is designed to cover the five isoforms of secretory-type OPN (sOPN).

2.4 Tissue microarrays

We constructed TMAs to validate the expression of some of the HNSCC biomarkers on OPSCC tissue samples. The TMA technique has been used widely in cancer research in clinical outcome analysis, and validation of tumour biomarkers. It allows high-throughput molecular profiling to the tissue sections (Hoos and Cordon-Cardo, 2001), and provides rapid visualisation and analysis of molecular targets in hundreds/thousands of tissue samples at a time, either the DNA, RNA or protein level. The speed of molecular analyses is increased by more than 100-fold when compared with conventional techniques (Kallioniemi *et al.*, 2001). Additionally, the simultaneous processing of tissue material in arrays provides high reproducibility as well as the reliability of the score interpretation (Radhakrishnan *et al*., 2007). The validation of TMAs results has been assessed and compared previously with the whole section results, no significant differences between the two methods have been observed (Hoos and Cordon-Cardo, 2001). The major limitation is the small tissue volume may not be representative of the entire sample. To overcome this point, 3 cores from each sample were selected purposely including stroma and tumour cells, so they were similar and representative of the tumour in areas of interest in the main diagnostic slide. TMA construction can be a time-consuming method especially in the preparatory step of marking the tissue area, however, this time is worth using multiple replicates in array construction as this will be time and effort efficient at the staining assessment stage.

Two retrospective pre-treated primary cohorts of OPSCC patients have been employed in this project: Cohort of 96 cases associated with all relevant clinical information was shared kindly by Dr Hisham Mehanna - University of Birmingham. The material formed part of the PREDICTR-OPC study cohort. The clinical material was provided as 10 unstained TMA slides. A material transfer between the two universities was approved under the project ethical number 12/Lo/2018.

Cohort of 72 cases associated with all relevant clinical information, original diagnostic biopsy blocks, and respective slides were retrieved from Sheffield Teaching Hospitals pathology reporting database in the period between 2002-2012 (also authorised under IRAS ethics 12/Lo/2018).

2.4.1 Array design and construction:

Relevant haematoxylin-stained tissue sections of the corresponding FFPE donor blocks were histologically reviewed by KDH & NBH. Tumour representative areas (including epithelium and stroma) subsequently were marked, using a microscope mounted biomarker. By counting the number of marked cores, the TMA maps were designed (Appendix A.4):

3 TMAs blocks were designed to cover all cohort cases; each recipient TMA block was designed to include 70 cores. Triplicate 1.0 mm cores from each donor block were included in the TMA design (whenever possible). Controls cores account for 28.5% of TMA cores in each TMAs block, including controls in the same OPSCC slide which helps in ensuring the specificity and sensitivity of used biomarkers. Controls were located at template borders to minimise the risk of losing OPSCC cores. Positive control tissues include lymph node (LN), submandibular salivary gland (Sub SG), tonsillar tissue, granulation tissue, and normal mucosa (N moucsa). Additionally, 3 orientation cores were added to the template to allow easy slide orientation. TMAs were constructed manually with high precision and according to the manufacturer's instructions (Parsons and Grabsch, 2009) using MTA-1 Beecher manual instrument (Sun Prairie, USA). Blocks were then incubated at 37° C for 30 minutes in an upside-down position facing a glass slide for block tempering and to get all cores at the same horizontal level. Sequential FFPE sections (4µm thickness) were cut from TMAs blocks and placed on coated super-adhesive slides (Thermo Fisher Scientific). Slides dried at RT for 24 h and then stored in a slides box at 4 °C. Slide baking was postponed until 1 hr before the staining procedure. Slide baking was done by incubation in the lab oven at 50°C for one hour, then drying at RT for 30 min.

2.4.2 RNAScope assay

RNAScope is a novel nucleic acid *in situ* hybridization (ISH) technology that provides high specificity detection for single-RNA molecules within the context of complex tissue microenvironments. The principle of this technology relies on a unique probe design that provides simultaneous signal amplification and suppresses background noise. RNAScope is quite similar to IHC in terms of tissue deparaffinization, rehydration, blocking endogenous peroxidase activity, and antigen retrieval, however, the target in IHC is to detect and amplify the interested protein signals, whereas in RNAScope the target is mRNA molecules within the intact cell. In this study, we utilised this technique

to detect HPV-16, HPV-18 and IL-6 mRNA using hybridisation targeting probes followed by several highly specific amplification steps using HybEZ oven (Advanced Cell Diagnostics (ACD), CA, USA).

RNAScope assay reagents

The assay was provided by Advanced Cell Diagnostics (ACD), CA, USA. Reagents in ISH and their preparation are listed in (Table 2.11).

Table 2.11: Materials used in RNAScope assay

Reagent	Volume and preparation	Source
Xylene	300 ml x 2	Fisher Scientific, UK
Ethanol 100%	300 ml x 2	Fisher Scientific, UK
Pre-treat 1	750µl for each TMAs slide	Ref. 320037, ACD
Pre-treat 2	70 ml, 630 ml dH_2O Boiling at 92-104 °C	Ref. 310020, ACD
Pre-treat 3	750µl for each TMAs slide	Ref. 320037, ACD
Hybridise probes: **Negative control (Bacterial gene Dap B)** **Positive control (Housekeeping gene PPIB)** **HPV-16 /18** **IL-6**	750µl for each TMAs slide	ACD Ref.310043 Ref.313901 Ref.311121
Washing buffer	60 ml wash buffer, 2.94L dH_2O	Ref.310091, ACD

RNAScope protocol

The humidity tray was loaded with fresh wet humidifying paper and inserted in place into the HybEZ oven (Advanced Cell Diagnostics, USA). The oven was warmed to 40°C for 30 minutes in advance. Deparaffinization and rehydration of the slides were performed by immersing the sections twice in Xylene, for 5 minutes followed by 2 immersions in fresh 100% Ethanol for 1 minute, then a hydrophobic barrier was drawn around each section with IMMEDGE hydrophobic barrier pen, to ensure proper coverage to the whole TMAs cores, slides were placed on absorbent paper and allowed to dry for 5 minutes at RT. Pre-treat 1 was added to cover the whole cores and incubated for 10 minutes at RT followed by brief washing in dH_2O. Slides were then submerged carefully, using plastic forceps, in boiling 'pre-treat 2' for 15 minutes, and left to cool down in dH_2O. Pre-treat 3 was added to the slides and incubated in the HybEZ oven at 40°C, for 30 minutes, followed by two washes in dH_2O. The hybridisation probe was pre-warmed in an incubator at 37°C, to dissolve any precipitations before use. The target hybrids probe was added and incubated for 2 hours in the HybEZ oven at 40°C, followed by two washes in wash buffer for 2 minutes. According to the manufacturer's instructions, sequential signal amplification steps were carried out using RNAScope 2.5 HD Detection Reagents BROWN (Table 2.12). Signal Detection was obtained by incubating the slides for 10 minutes with DAB Mixture (1:1 Brown-A & Brown-B, amplification kit) then slides were immersed in a water bath to stop the colour reaction. Counterstaining was performed using Leica ST4020 Stainer, and the glass coverslips were mounted using DPX mounting media.

Table 2.12: Amplification Protocol for RNAScope technique.

Reagent	Incubation time	Temperature
Amplification 1	30 minutes	40°C, HybEZ oven
Amplification 2	15 minutes	40°C, HybEZ oven
Amplification 3	30 minutes	40°C, HybEZ oven
Amplification 4	15 minutes	40°C, HybEZ oven
Amplification 5	30 minutes	RT
Amplification 6	15 minutes	RT

2.4.2.1 RNAScope scoring criteria

All the stained slides were scored independently by KDH and NH, then the final scores were recorded with an agreement between the two parties. For each case, all relevant cores were analysed and the highest score among the cores was selected. Scoring criteria in HPV-16 RNAScope assay was according to the manufacturer's instructions. We considered score (0) as a negative result whereas scores (1-4) as positive HPV results (Table 2.13).

Table 2.13: HPV RNAScope scoring criteria

score	Description
0	No staining or less than 1 dot every 10 cells at 40X magnification.
1	1-3 dots/cell visible at 20-40X magnification.
2	4-10 dots/cell. Very few dot clusters visible at 20-40X magnification.
3	>10 dots/cells. Less than 10% positive has dot clusters visible at 20X.
4	>10 dots/cell. More than 10% positive cells have dot clusters visible at 20X.

IL-6 RNAScope scoring criteria:

The expression of IL-6 signals has been evaluated and scored for OPSCC stroma according to modified scoring scheme from Yu *et al.*, (2015) work in their scoring scheme, IL-6 expression has been classified to 4 levels according to the number of positive cells: 0, no cells. 1, areas with 5-10 positive cells per 20x field. 2, areas with 11-25 positive cells per 20x field. 3, areas with 26-50 positive cells per 20x. 4, areas of more than 50 positive cells per 20x field.

We grouped those 4 levels into 2 groups: group 1 “Low IL-6” (≥26 positive cells) and group 2 “High IL-6” (≤25 positive cells).

2.4.3 Immunohistochemistry analysis (IHC)

A standard two-step IHC staining procedure was followed to detect the expression of p16, α-SMA, and OPN biomarkers using the streptavidin-biotin-peroxidase complex. Primary antibodies, the appropriate secondary antibody, blocking serum and control are summarised in Table 2.14.

Table 2.14: Summary of the essential information in IHC procedure.

Primary antibody	Antigen retrieval method	Working concentration	Secondary antibody	Blocking serum	Antibody positive control
Anti-p16	P16 IHC staining has been carried out by the Royal Hallamshire Hospital laboratory using E6H4 (CINTECH) p16 clone				
Anti-α-SMA mouse, monoclonal antibody (Sigma Aldrich, UK)	HIER, 0.01M pH 6 citrate buffer microwaved for 10 min	1:100	Anti-mouse (Vectastain ABC kit)	Normal horse serum (Sigma Aldrich, UK)	Submandibular salivary tissue section
Anti-OPN rabbit polyclonal antibody, (Proteintech, UK)	HIER, 0.01M pH 6 citrate buffer microwaved for 10 min	1:50 1:200	Anti-rabbit (Vectastain ABC kit)	Normal goat serum (Sigma Aldrich, UK)	Placenta tissue section

* Heat-induced epitope retrieval

IHC reagents

IHC reagents in IHC analysis and their preparations are listed in (Table 2.15)

Table 2.15: IHC reagents.

Reagent	Concentration	Volume & preparation	Supplier
Xylene	-	300ml x 2	Fisher Scientific, UK
Ethanol	100%	300ml x 2	Fisher Scientific, UK
Hydrogen Peroxide	3%	30ml H_2O_2 270ml methanol	Fisher Scientific, UK
Sodium citrate buffer	0.01M	1.180g Sodium citrate 400ml dH_2O	Fisher Scientific, UK
avidin-biotin complex (ABC)	-	2 drops from reagent A & B in 5ml dH_2O	Vectastain ABC Kit (PK- 6102, CA, USA)
DAB Peroxidase Substrate	-	2 drops buffer, 4 drops DAB 2 drop H_2O_2, 5ml H_2O	SK-4100, Burlingame USA
PBS	-	42.5g NaCl 5.8g K_2HPO_4 1.25g KH_2PO_4 5L H_2O	Sigma-Aldrich Fisher Bioreagents Sigma Life Science

IHC Protocol

Tissue deparaffinization and rehydration was performed by immersing the sections twice in Xylene for 5 minutes each followed by another immersion in absolute Ethanol, twice for 5 minutes in each. The endogenous peroxidase activity was quenched using 3% methanolic hydrogen peroxide for 20 minutes to minimise background staining, followed by a brief wash in PBS. Antigen retrieval was conducted according to the recommendation of the manufacturer of the relevant primary antibody (Table1.2). A hydrophobic barrier was drawn around each slide using IMMEDGE TM hydrophobic barrier pen to ensure proper coverage of the whole TMA cores. 100% normal serum was used as a blocking serum to prevent the non-specific staining, slides were incubated for 30 minutes at RT in humidity. After that, the blocking serum was discarded, and slides

were further incubated with a sufficient volume of primary antibody diluted in serum in a humidity chamber overnight at 4°C. The next morning, slides were washed 2X with PBS for 5 minutes, followed by incubation with the secondary antibody for 30 minutes at RT (The secondary antibody is conjugated to biotin which has a strong affinity to ABC solution, the latter works as an amplifier to the antigen signals and aids in antigens visualisation). After the incubation, the slides were washed x2 with PBS for 5 minutes each and covered with ABC solution for a further 30 minutes at RT, followed by x2 wash in PBS, for 5 minutes. DAB Peroxidase Substrate was used for colour development for 8-10 minutes then slides immersed immediately in dH_2O to stop the colour reaction. Haematoxylin counterstaining was performed using an automated linear staining machine (Shandon). Glass coverslips were mounted with DPX mountant (Thermo Fisher Scientific).

2.4.3.1 IHC scoring criteria

All biomarkers have been scored semi-quantitatively by KH and NH, then the final score was agreed by the two parties. The highest score among the 3 TMA cores was chosen:

p16 IHC biomarker:

TMAs slides were scored using Histo-score (H-score). H-score is the sum of individual stain intensity level seen in the field giving more relative weight to higher-intensity staining in each tumour core. For each core, the staining intensity (0, 1+, 2+, or 3+) is determined then the percentage of cells at each staining intensity level is recorded, then H-score is calculated using the following formula: [1 × (% cells 1+) + 2 × (% cells 2+) + 3 × (% cells 3+)]. H-score results range from 0 to 300.

α-SMA biomarker:

α-SMA immunopositivity was scored to “Low” and “High” based on positive staining amount, followed by Kellermann *et al*., (2008) criteria. “Low” indicated a patchy/focal expression less than 50% of the stroma, while High referred to a diffuse expression throughout the tumour, more than 50% of the stroma.

OPN biomarker:

The expression of OPN was scored in tumour cells only. OPN IHC score was based on the assessment of OPN stain intensity in the tumour cells: (0=absence, 1=weak, 2=moderate, 3=strong) multiply by the score of stained percentage of epithelium thickness (0=<5%, 1=<25%, 2=<50%, 3=<75, 4=75-100%). The scoring scale range from 0-12.

The extent of the OPN staining (E) within tumour cells (percentage of positive cells concerning the total number of epithelial cells) was scored from 0-4, 0 = 0% positive cells, 1 ≤ 25% positive cells, 2 = 26%–50% positive cells, 3 ≥ 50% positive cell, 4 100% positive cells. OPN final score is corresponding to the yield of (I * E), with the maximum score being 12.

2.4.4 Imaging

All histological images for H&E, ISH, and IHC slides were obtained using Cell-D^ software 2.8 (soft imaging solutions GmbH, Munster, Germany).

Chapter 3: TMA-based clinical validation of molecular biomarkers in OPSCC

3.1. Introduction

High-risk HPV infection is a well-established risk factor for developing OPSCC, in addition to traditional OPSCC risk factors, including tobacco use and alcohol consumption. However, HPV-driven OPSCC is a distinct entity with a characteristic molecular and clinical profile. The differences between both OPSCC subtypes are evident in the clinical epidemiological figures which report an alarming increase in the incidence of HPV-associated OPSCC over the last few decades. OPSCC incidence was expected to increase further in England by 239% in the period between 2011 to 2025, at that time point, OPSCC would compose 35% of all HNC (Louie, Mehanna and Sasieni, 2015). The differences in OPSCC subtypes are also demonstrated in the clinical patient profile. HPV-positive patients tend to be male, younger in age, with no history of chronic smoking and drinking habits. Most importantly, HPV-positive OPSCCs display better clinical outcome than their non-HPV related counterparts regardless of the treatment modalities (Lindquist *et al*., 2007, Lassen *et al*., 2009, Ang *et al*., 2010). Based on these clinical differences, there was a key change regarding HPV-positive OPSCC in the 8th edition of the UICC TNM classification (Union for International Cancer Control), which considers HPV-associated OPSCC a separate entity, based on p16 expression.

In this context, determining HPV status in OPSCC has become a mandatory requirement in routine practice, based on p16 IHC as a first-line test. Although this technique is considered sensitive, cost-effective, and feasible to apply, it is subject to the limitations of IHC evaluation, with a lack of standardised scoring criteria and an agreement on a definite single threshold. Intense nuclear and cytoplasmic expression in >70% of tumour cells has been adopted by the majority; however, others demonstrated >50% positivity threshold with better specificity. An H-score based scheme was also proposed for p16 scoring which still awaits extensive clinical validation (Jordan *et al*., 2012).

Given the superior prognosis of HPV-driven OPSCC, currently, there is wide interest in treatment de-escalation programmes, seeking to reduce treatment morbidity whilst maintaining favourable survival features. Several ongoing trials are considering de-intensifying chemotherapy or radiotherapy and/or applying targeted therapy or immunotherapy as alternative approaches (Howard *et al*., 2018, Beaty *et al*., 2019, Jones *et al*., 2020). However, the criteria of patient selection based on HPV-status only could be too simplistic, raising the concern of establishing additional adequate parameters for HPV-positive OPSCC stratification based on molecular biomarkers.

The crucial role of tumour microenvironment (TME) in cancer progression is a promising approach in cancer research generally. CAFs are the most prominent TME component in solid tumours which have been suggested to have profound influences on tumour behaviour. CAFs have shown the capability to enhance tumour growth, local invasion and metastasis and were, characteristically, known by the expression of α-SMA (Attieh and Vignjevic, 2016, LeBleu and Kalluri, 2018). Given the established functional features of CAFs, they have become increasingly accepted as prognostic biomarker. CAFs have been correlated with poor clinical outcome in several tumours (Chen *et al*., 2017, Cong *et al*., 2020, Zhan *et al*., 2020). In OSCC, Marsh *et al*. (2011) linked the high presence of CAFs in OSCC stroma with worse prognosis compared to OSCC with fewer CAFs detected, introducing α-SMA IHC as an independent and effective mortality predictor. Although well-established for OSCC, CAFs' prognostic role in OPSCC has not been investigated thoroughly in the literature. In previous work from our lab, Bolt *et al*. (2018) reported a significant difference in HPV-positive and HPV-negative OPSCC cell lines' interaction with stromal fibroblasts in 2D and 3D models. HPV-negative cell lines showed the ability to promote normal fibroblast production of a supportive secretome able to enhance cancer cell migration and invasion. These interesting observations underpin the need for further investigation and clinical validation on fibroblasts' function in OPSCC tissue.

3.2. Aims

- Determine the status of biologically relevant HPV infection in an established OPSCC cohort and compare its demographic characteristics with non-HPV related OPSCC.

- Determine the p16 H-score threshold in OPSCC and evaluate its diagnostic and prognostic performance in OPSCC.

- Explore and compare α-SMA presence in OPSCC subtypes and assess its prognostic value.

3.3. Experimental approach and statistical analysis

- The main study cohort was established from two small cohorts: Cohort 1 was collected from cases treated between 1996-2004 in Birmingham and Oxford, as part of the Predictr study. Cohort 2 was collected from cases treated between 2002-2012 at Sheffield Teaching Hospitals NHS Trust.

- Tissue microarrays were constructed, then subjected to RNAScope assay to detect HPV 16/18 mRNAs. The whole cohort was divided into two sub-groups according to HPV status. Demographic features were compared using contingency table chi-square tests, age mean compared using *t*-test (two-tailed).

- Overall survival information only was obtained for the whole cohort of cases. Kaplan-Meier method was used to analyse survival based on the predictor groups. The survival curves were compared using Log-Rank test. Estimated overall survival time was expressed as mean with 95% CI. Five-year survival rate was selected as an endpoint in the survival analysis, which is consistent with more commonly cited statistics in HNSCC.

- p16 IHC staining was performed using the E6H4 antibody clone and assessed using H-score. The p16 positivity threshold was determined using ROC curve. The curve was plotted against p16 sensitivity and 1-specificity in HPV detection using RNAScope as the reference assay. The prognostic performance of p16 biomarker was assessed using Kaplan-Meier method and Log-Rank test.

- α-SMA biomarker expression was assessed by performing IHC staining for the whole cohort. α-SMA expression distribution between OPSCC subtypes was assessed using contingency table chi-square tests. The prognostic value of α-SMA biomarker was evaluated and compared in OPSCC subtypes using Kaplan-Meier method and Log-Rank test.

- An unadjusted Cox regression model (Univariate) was established to evaluate the hazard ratio (HR) for each predictor separately.

- All statistical analyses were performed using SPSS (versions 23-26). p-value<0.05 was considered significant. HR>1 indicated a positive correlation with the hazard (Mortality).

3.4 Results

3.4.1. Establishing the study cohort

In this study, two retrospective pre-treated primary cohorts of OPSCC patients were employed. Cohort 1 consisted of 96 cases treated in the period between 1996-2005 which were kindly shared by Professor Hisham Mehanna, University of Birmingham. These cases were originally part of the cohort for the Predictr-OPC study. The cohort was provided in 10 unstained slides associated with relevant clinical information, HPV 16/18 RNA ISH score and p16 H-score. However, 13 cases were excluded due to unavailable RNA ISH score (n=5) and missing survival-related information (n=8). The second cohort, "Cohort 2", included 72 cases associated with all relevant clinical information, original diagnostic biopsy blocks and respective slides that were retrieved from the Sheffield Teaching Hospitals pathology reporting database, in the period between 2002-2012. During the histological examination and core selection, 12 cases were excluded due to insufficient tumour tissue availability (n=8) and insufficient survival information (n=4) (Figure 3.1).

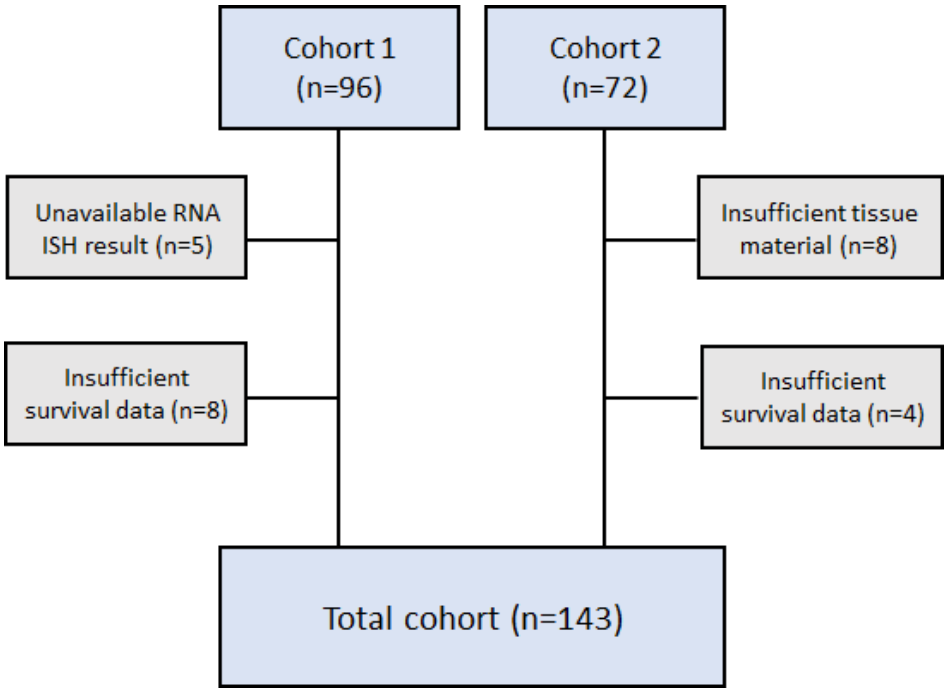

Figure 3.1: Flow-chart illustrating the establishment of the study cohort.

3.4.2. HPV-positive OPSCC prevalence and cohort characterisation

RNAScope assay for HPV 16/18 was the utilised method for detecting HPV-driven OPSCC in the study cohort. In Cohort 1 the assay result was provided in terms of “positive” or “negative”. To identify HPV-associated OPSCC in “Cohort 2”, TMAs slides were subjected to HPV 16/18 RNAScope assay (Advanced Cell Diagnostics, CA, USA). The assay was conducted and scored according to the manufacturer’s instructions (Refer to section 2.4.21 for the detailed score information). The full range of RNAScope scores (1-4) was observed in Cohort 2. RNAScope negative case was identified by the complete lack of mRNA signals (Figure 3.2).

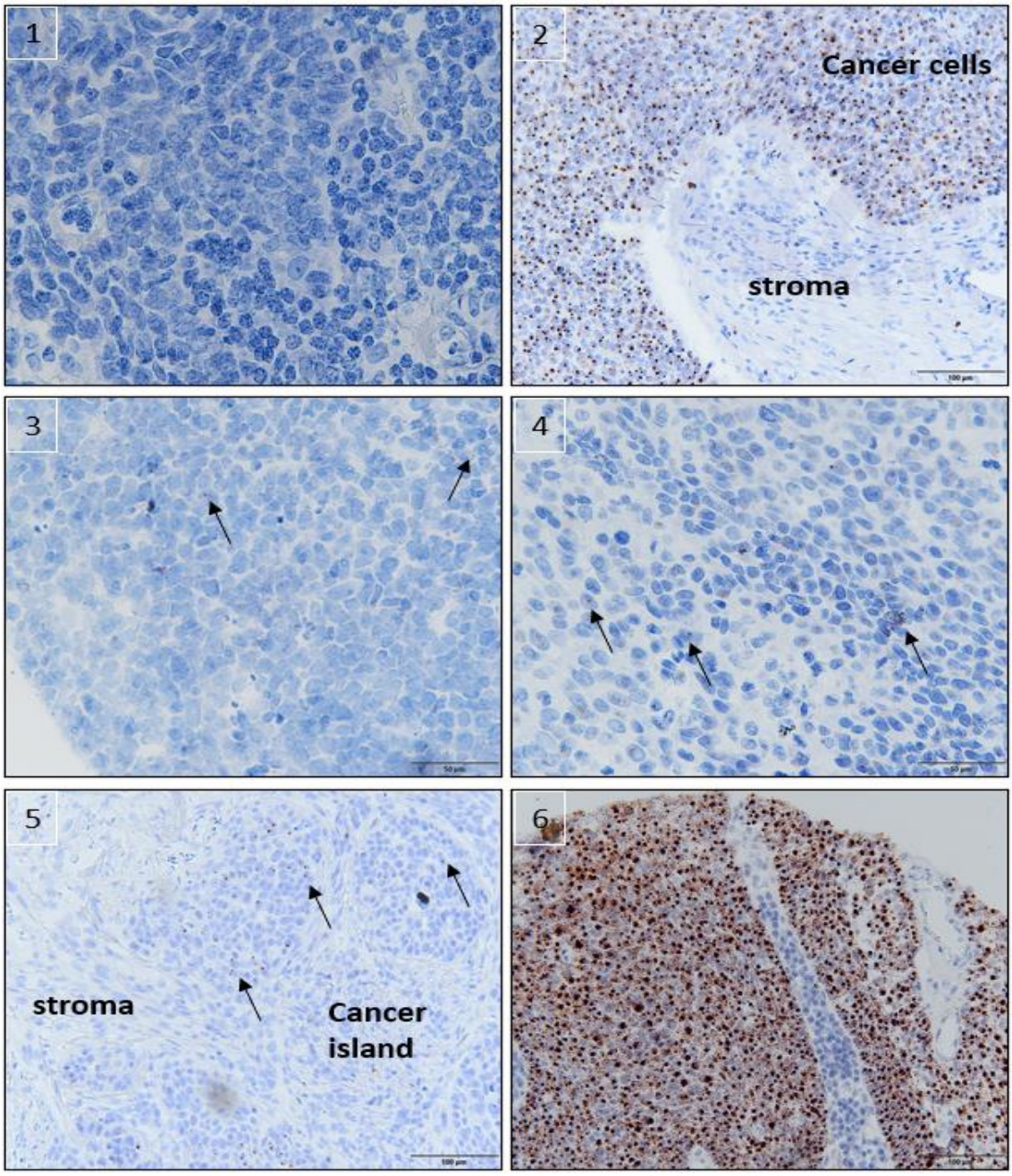

Figure 3.2: HPV16/18 mRNA expression in OPSCC cohort 2 using RNAScope assay. **1**, The assay negative control, using bacterial gene DapB on OPSCC tissue section. **2**, HPV16 & 18 RNA-ISH positive controls, using known positive OPSCC case positive for HPV-DNA ISH, dark dots of stained HR-HPV RNA can be seen within the epithelial cells and nuclei (arrow). **3**, RNAScope score 1 (40X magnification), 1-3 dots of stained HPV RNA can be seen per epithelial cell (arrow). **4**, RNAScope score 2 (40X magnification), more than 3 dots per cell, also very few dot clusters are visible (arrow). **5**, RNAScope score 3 (20X magnification), HPV RNA of more than 10 dots/cells and less than 10% of the field has positive dot clusters. **6**, RNAScope score 4, (20X magnification), HPV RNA stains clusters in more than 10% of the field's cells.

3.4.2.1 HPV-positive Prevalence

The HPV 16/18 prevalence across the whole study cohort was 60.8% (87/143), while 39.2% (56/143) of the cohort was HPV 16/18 negative. Since the main study cohort consisted of two cohorts collected from different periods, we had to look at HPV 16/18 prevalence separately in each small cohort for the comparison. The HPV-associated OPSCC percentage was 57.8% (48/83) in “Cohort 1” and 65% (39/60) in “Cohort 2”.

3.4.2.2 Cohort characterisation based on HPV status

According to HPV status, the study cohort was divided into two sub-groups, HPV-positive and HPV-negative. Descriptive comparisons for demographic and clinicopathologic variables are summarised in (Table 3.1). Patients' age distribution between the HPV-positive and negative groups was comparable based on Chi-square comparison between age groups ($p=0.71$). The mean ages of the HPV-positive and negative groups were nearly identical: 56.1 years in the HPV-positive and 56.9 in the counterpart group ($p=0.91$), however, there was a little shift in HPV-negative group median toward the older age group (55 and 57.5, respectively). No gender predilection was observed in HPV-OPSCC. Although the study cohort included a higher percentage of “Males” than “Females”, HPV-OPSCC distribution was comparable between both genders ($p=0.65$).

Smoking information was obtained in 129 cases, categorised, generally, into “Never”, “Former” and “Current”. In the HPV positive group, the percentage of non-smokers was 48.7% (38/78), while this percentage was lower in the HPV negative group: 13.7% (7/51). On the contrary, the current smoker subgroup of the HPV-negative group recorded a higher value than the HPV-positive group (56.8% and 25.6%, respectively). Statistically, smoking status categories revealed a significant difference between the two groups ($p<0.001$). In this study, TNM staging information was available according to the previous staging scheme (TNM7). Data represent the status at the time of diagnosis. We did not observe evident differences in T and N grades distribution between OPSCC entities ($p=0.07$). OPSCC cohort cases were distributed between stage III and stage VI, no earlier stages were detected. HPV-positive cases showed a higher percentage of stage VI than HPV-negative cases: 65.5% (57/87) and 46.4% (26/56), respectively. The difference in TNM staging between the two groups was statistically significant ($p<0.02$).

Treatment modalities records were obtained in 73 cases. All cases received surgical resection for the primary tumour. Adjuvant radiotherapy was afforded for all the cases except 6 cases who, sadly, died a few months following the diagnostic date. Chemoradiotherapy was provided for 23.91% (11/46) of the HPV group, while 7.4% (2/27) of the non-HPV group received the treatment.

Among the HPV group, 10.3% (9/87) developed recurrent disease, while the rest of the group remained disease-free at the last time seen. The non-HPV related group suffered a high percentage of tumour recurrence: 25% (14/56).

Overall survival (OS) was only available for the study cohort, disease specific survival (DSS) may reflect evident differences between OPSCC subtypes rather than21 OS.
Based on comparing the percentage of deaths in each group over 5 years of follow up, the HPV-positive group showed a lower figure of 15.9%, while this percentage was higher in the counterpart HPV negative group (38.2%). The prognostic value of HPV infection in OPSCC will be analysed in detail in the next sections using Kaplan-Meier method.

Table 3.1: OPSCC Cohort characterisation based on HPV-status

Characterisation	HPV-positive (%)	HPV-negative (%)	Total (%)	*P*-value
No. of cases	87 (60.8)	56 (39.2)	143 (100)	-
Age at diagnosis: ≤45 46-55 56-65 ≥66 Mean (yrs.) Median (yrs.)	 9 (10) 31 (35.6) 33 (37.9) 14 (16.1) 56.1 55	 6 (10.7) 15 (26.7) 24 (42.8) 11 (19.6) 56.9 57.5	 15 (10.6) 46 (32) 57 (39.3) 25 (18) 	 0.71 0.91
Gender: Men Women	 64 (62.1) 21 (56.8)	 39 (37.9) 16 (43.2)	 103 (100) 37 (100)	0.65
Smoking: Never Former Current Total	 38 (48.8) 20 (25.6) 20 (25.6) 78 (100)	 7 (13.8) 15 (29.4) 29 (56.8) 51 (100)	 45 (34.8) 35 (27.3) 49 (37.9) 129 (100)	 <0.001
T grade: T1/T2 T3/T4 Total	 56 (65.1) 30 (34.2) 86 (100)	 27 (50) 27 (50) 54 (100)	 83 (59.2) 57 (40.7) 140 (100)	0.07
N grade: N0/N2a Nb-N3 Total	 35 (44.8) 43 (55.2) 78 (100)	 17 (30.9) 38 (69.1) 55 (100)	 52 (39.1) 81 (60.9) 133 (100)	0.07
TNM Staging: (7th) III IV Total	 30 (34.4) 57 (65.5) 87 (100)	 30 (53.5) 26(46.4) 56 (100)	 60 (41.9) 83 (58.1) 143 (100)	0.02
Treatment: Radiotherapy Chemoradiotherapy N/A Total	 34 (73.91) 11 (23.91) 1 (2.17) 46 (100)	 20 (74.07) 2 (7.40) 5 (18.51) 27 (100)	 6 (8.21) 54 (73.97) 13 (17.80) 73 (100)	-
Recurrence Total	9 (10.3) 87 (100)	14 (25) 56 (100)	23 (16) 143 (100)	-
Clinical outcome: Death (OS) Alive Total	 14 (15.9) 74 (84.1) 88 (100)	 21 (38.2) 35 (61.8) 55 (100)	 35 (24.4) 109 (75.6) 143 (100)	0.002

3.4.3. Prognostic potential of HPV-driven OPSCC

The 5-year survival rate for the HPV-positive group was favourable compared with the HPV-negative group (Figure 3.3). The survival percentage for the HPV-positive cases was higher than in the counterpart group (84.1% against 62.5%). Log-rank statistical test revealed a significant difference between both OPSCC curves (p= 0.002) (Table 3.2).

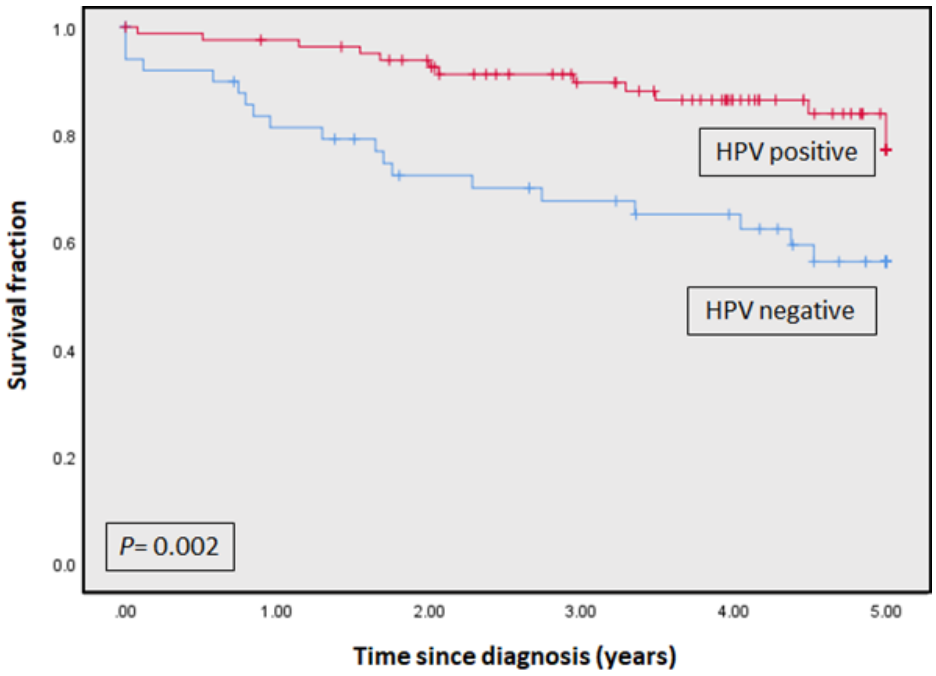

Figure 3.3: Better overall survival rate in HPV 16/18 positive group than HPV-negative group. The survival curve at 5-years follow-up concerning overall survival using Kaplan-Meier method. The red curve represents the HPV-OPSCC group (n=87) and the blue curve represents the non-HPV OPSCC group (n=54). Each drop-step in the curve illustrates a case of death. Each vertical line (Hash lines) on the curve indicates censored data. The HPV-positive group demonstrated a favourable prognosis with high survival fraction (0.84). Log-rank p= 0.002.

Table 3.2: Summary of Kaplan-Meier method for OPSCC based on HPV status

	HPV-positive group	HPV-negative group	Log-rank *p* value
5 Year Survival (%)	84.1	62.5	0.002
Estimated survival time (Yrs) (mean, 95% CI)	4.56 (4.3-4.8)	3.63 (3.1-4.1)	

3.4.4. Influence of smoking on OPSCC survival

In OPSCC cohort characterisation, the smoking status at diagnosis revealed a significant difference between HPV-positive and HPV negative groups, although these data lack accuracy in the definitions of “Former” and “Current " in terms of the number of packs and years since quitting the smoking habit. Here, we evaluated the effect of smoking status on OPSCC survival in both HPV groups based on smoking data at the time of diagnosis; smoking status during the treatment and follow-up periods was not documented. In the HPV-positive group, analysis of the obtained survival information for 78 cases revealed no significant impact of smoking on HPV-positive group survival. The estimated survival time for “Never” and “Current” was 4.7 years and 4.6 years, respectively, while for “Former” it was 4.2 years, (p=0.48) (Figure 3.4).

On the contrary, smoking habit seems to have had a significant negative impact on the survival of the HPV-negative group (n=51) based on smoking status: the “Never” group (n=7) showed a favourable clinical outcome over the 5 years, with a survival fraction of 1, followed by former smoker patients (n=15), with a survival fraction of 0.86. The current smoker group (n=29) demonstrated the worst survival among the three categories, with a 0.37 survival fraction. Log-Rank (p=0.001) (Figure 3.5).

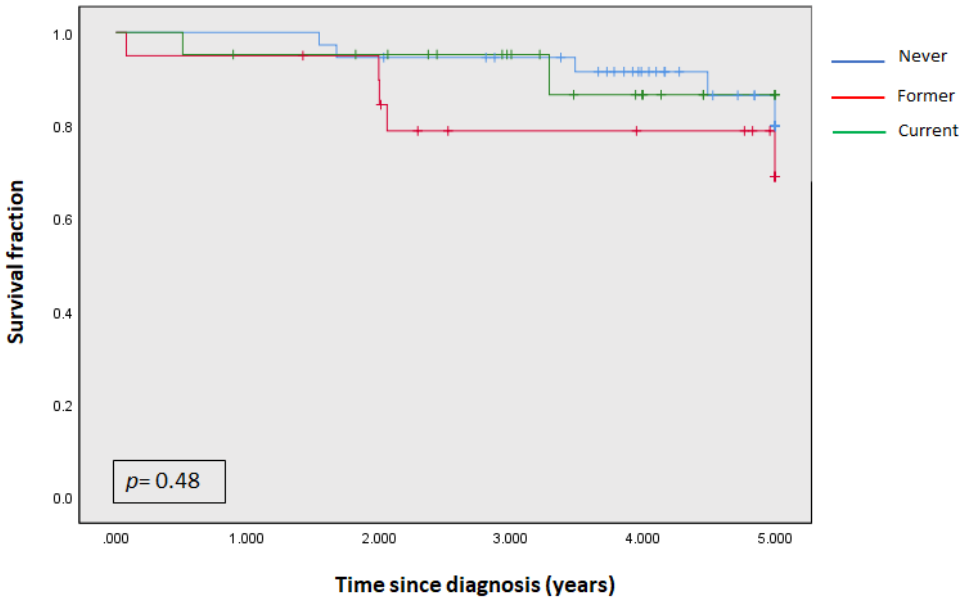

Figure 3.4: 5-years overall survival rates in HPV-positive OPSCC cohort based on "smoking status at diagnosis". Kaplan-Meier analysis for HPV-positive group (n=78) revealed no significant differences in the survival based on smoking status at diagnosis. Each drop-step in the curve illustrates a case of death. Each vertical line (Hash lines) on the curve indicates censored data Log-Rank p= 0.48.

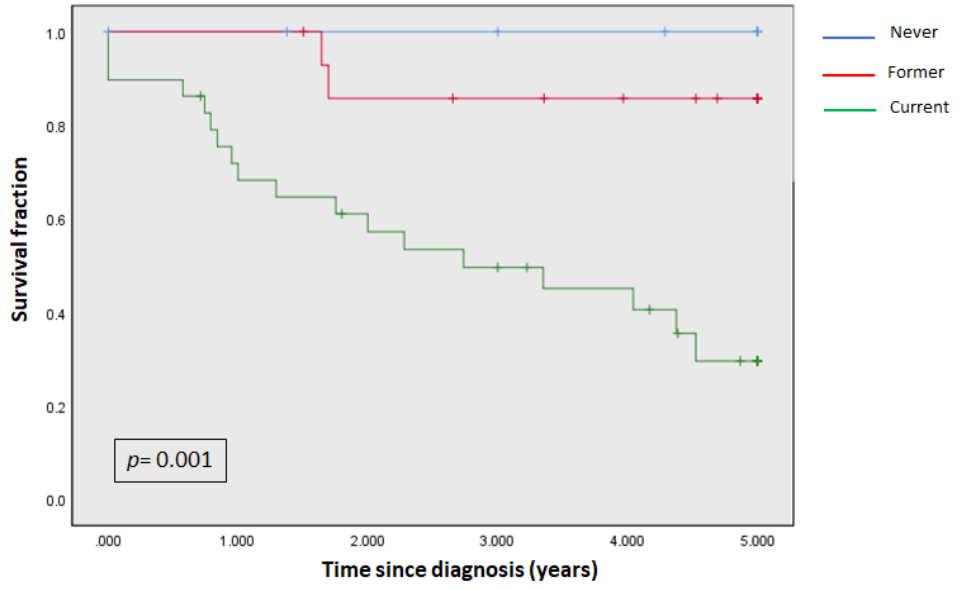

Figure 3.5: 5-years overall survival rates in HPV-negative OPSCC cohort based on "smoking status at diagnosis". Kaplan-Meier analysis for HPV-negative group (n=51) revealed significant differences in survival based on smoking status at diagnosis. "Current" smoking group

showed the worst survival. Each drop-step in the curve illustrates a case of death. Each vertical line (Hash lines) on the curve indicates censored data Log-Rank p= 0.001.

3.4.5. p16 expression in OPSCC

In the study cohort, we evaluated the diagnostic and prognostic performance of the surrogate biomarker p16. The cohort 1 TMAs were provided with p16 expression information as H-score values. Cohort 2 was subjected to an anti-p16 monoclonal antibody (clone E6H4) and the staining was scored using H-score. Examples of p16 positivity are shown in relation to the commonly used thresholds: (1) diffuse strong staining in the nucleus and cytoplasm in >70% of tumour cells in the tissue. (2) diffuse strong staining in the nucleus and cytoplasm in >50% of cells in the tissue (Figure 3.6).

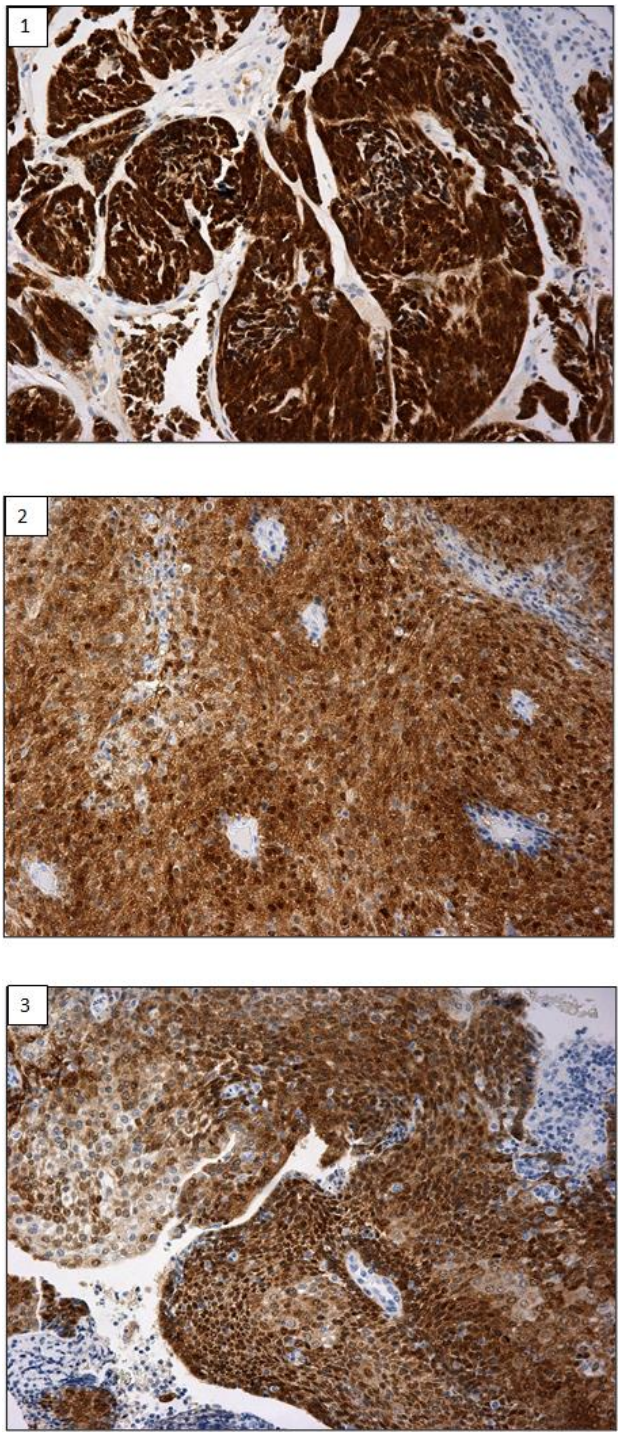

Figure 3.6: Examples of different p16 expression thresholds in OPSCC. 1, strong cytoplasmic and nuclear p16 expression in >70% of the tumour. **2**, an example of p16 intensity cut-off at >50%, with strong p16 expression in tumour cells. **3**, varying patterns of p16 staining and intensity can be interpreted using the H-score formula. All images are presented in 20X magnification.

3.4.5.1. p16 expression distribution in relation to OPSCC subtypes

p16 expression analysis was undertaken by evaluating H-score distribution among OPSCC sub-cohorts (Figure 3.7). Among the HPV-positive cases, 70.9% (61/87) demonstrated high H-score value ranges of 200-300. The lowest value among this group was “100” (n=1). In contrast, 27.5% (14/52) of the HPV-negative group showed expressions of 200-300, whilst the lowest value was “0”, seen in 58.8% (30/52) of the HPV-negative group. The difference in H-score means between the two groups was statistically significant (p<0.001) using *t*-test.

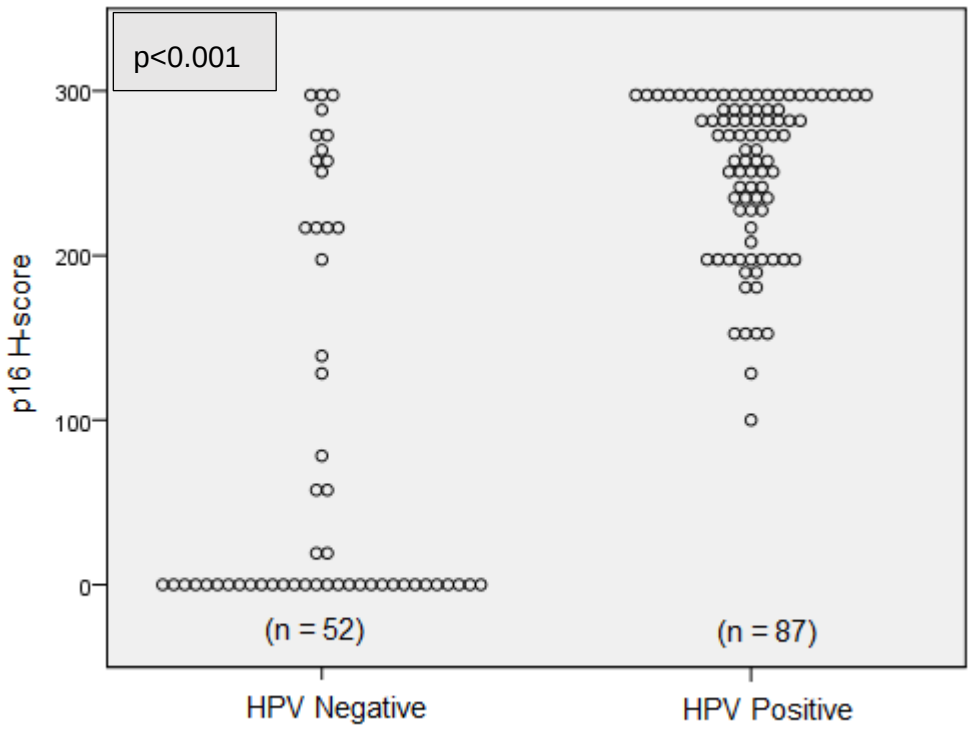

Figure 3.7: p16 expression distribution in OPSCC cohort sub-groups. HPV-negative group (n=52) and HPV-positive group (n=87) illustrated contrasting patterns in p16 expression according to H-score values. HPV-positive cases were associated with higher H-scores, while the lowest expression occurred in HPV-negative cases (p<0.001).

3.4.5.2. Diagnostic H-score threshold determination using ROC curve

To assess p16 diagnostic and prognostic values in OPSCC, we first had to determine the H-score cut-off point for p16 positivity. ROC curve was selected to achieve the diagnostic cut-off point of p16 in HPV detection using RNAScope as a reference test. The curve was plotted between two axes of p16 sensitivity and 1-specificity values in HPV detection (Figure 3.8).

Area under the curve (AUC= 0.87) displayed a good diagnostic performance of p16 in HPV 16/18 genotypes detection with a value close to “0.9” which indicated an excellent performance. ROC analysis presented a list of suggested diagnostic thresholds with the corresponding sensitivity and specificity (Appendix A.5). A threshold H-score of 144.5 was selected for the highest sensitivity (97.7%) accompanied by acceptable specificity (72%) among the suggested thresholds.

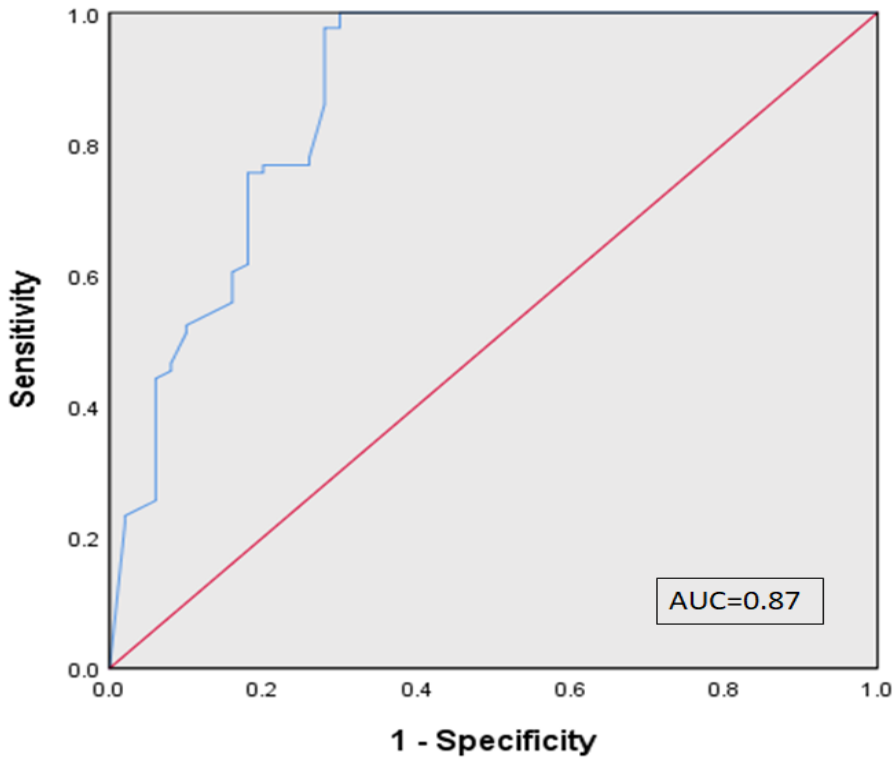

Figure 3.8: Diagnostic p16 H-score threshold determination using ROC curve. The curve plotted against p16 sensitivity and 1-specificity in HPV detection using RNAScope as a reference test. (AUC=0.87) indicated a good p16 diagnostic performance.

3.4.5.3. p16 prognostic value in OPSCC cohort

Based on the ROC curve, H-score of 144.5 was selected as a cut-off point for p16 IHC expression positivity. In order to investigate the prognostic value of p16 expression in the OPSCC cohort, Kaplan-Meier method was conducted to establish the survival curves for OPSCC p16-positive and negative groups and Log-Rank tests assessed the significance between the curves (Figure 3.9). Over 5 years of follow up, 84.7% of the p16-positive group exhibited a better outcome with an estimated longer survival time (4.5 years; 95%CI: 4.3-4.8), while 52.6% of p16-negative survived with shorter survival time estimation (3.3 years; 95%CI: 2.6-3.9). The difference between the two groups was statistically significant (p<0.001) (Table 3.3).

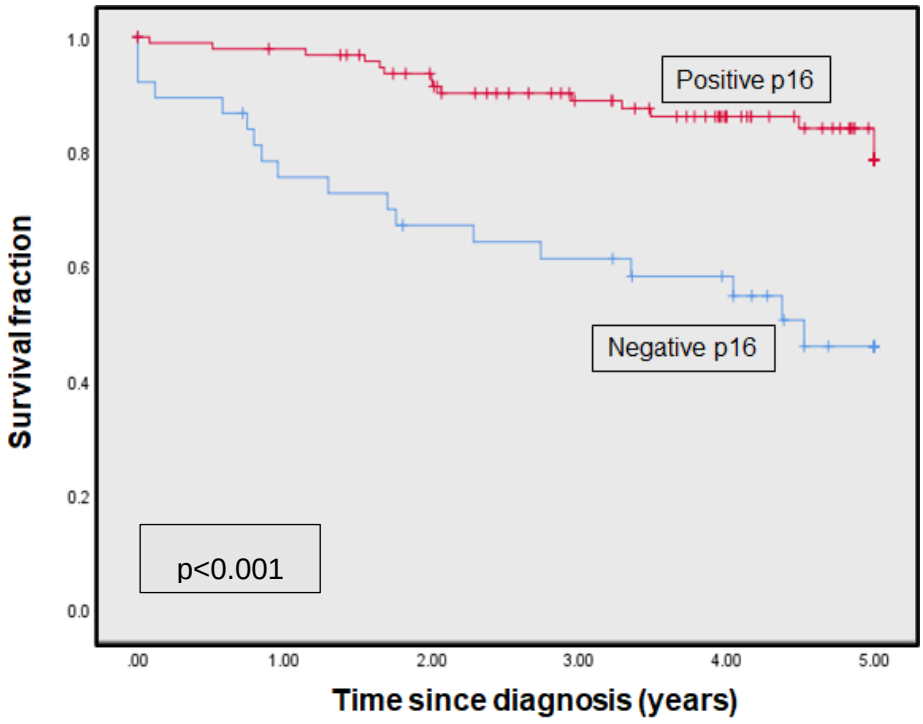

Figure 3.9: Better overall survival rate in p16-positive group than p16-negative group. The survival curve at 5-years follow-up concerning overall survival using Kaplan-Meier method. The red curve represents the p16-positive group, and the blue curve represents the p16-negative group.). Each drop-step in the curve illustrates a case of death. Each vertical line (Hash lines) on the curve indicates censored data. The p16-positive group demonstrated a favourable prognosis with high survival fraction. Log-rank p< 0.001.

Table 3.3: Summary of Kaplan-Meier method for OPSCC based on p16 expression

	p16-positive group	p16-negative group	Log-rank *p* value
5-Year Survival (%)	84.7	52.6	0.000
Estimated survival time (Yrs) (mean, 95% CI)	4.56 (4.3-4.8)	3.32 (2.6-3.9)	

3.4.5.4. Cohort stratification according to HPV status and p16 expression

p16 is considered the first-line test in routine clinical practice for detection of HPV-driven OPSCC. Due to p16 low specificity, specific HPV testing is highly recommended as a second-line test using either HPV-DNA ISH or PCR which were validated clinically. In this study, we investigated the performance of p16 against RNAScope and assessed the percentage of discordant cases. By matching HPV status with p16 expression, the OPSCC cohort was stratified into four classes. Among the cases, 60.4% (84/139) exhibited a p16 positive result in tumour areas harbouring HPV 16/18 RNAScope signals (class III). Meanwhile, 26% (36/137) of cases were negative for HPV 16/18 and p16 expression (class I). Discordant results were observed in 10.8% of cases, which displayed p16 positivity, but no HPV 16/18 mRNA was detected (class II). This class represents the p16 false positive percentage, whereas there was a p16 false negative percentage in 1.4% of cases. Only 2 cases were positive for HPV16/18 but lacked overexpression of p16 (class IV). (Figure 3.10).

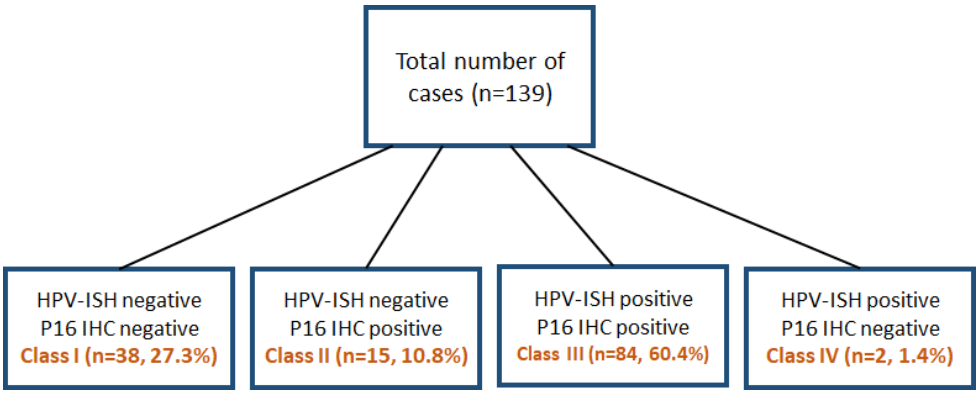

Figure 3.10: OPSCC cohort stratification according to HPV 16/18 status and p16 overexpression.

Due to the small number of discordant cases in this study, the survival comparison between the stratified classes was not feasible. However, a highly significant correlation was found between the expression of p16 and the presence of HPV 16/18 ($p<0.001$). Survival curves illustrated that “Class I” had the worst outcome among all OPSCC classes, achieving the lowest survival fraction (Figure 3.11).

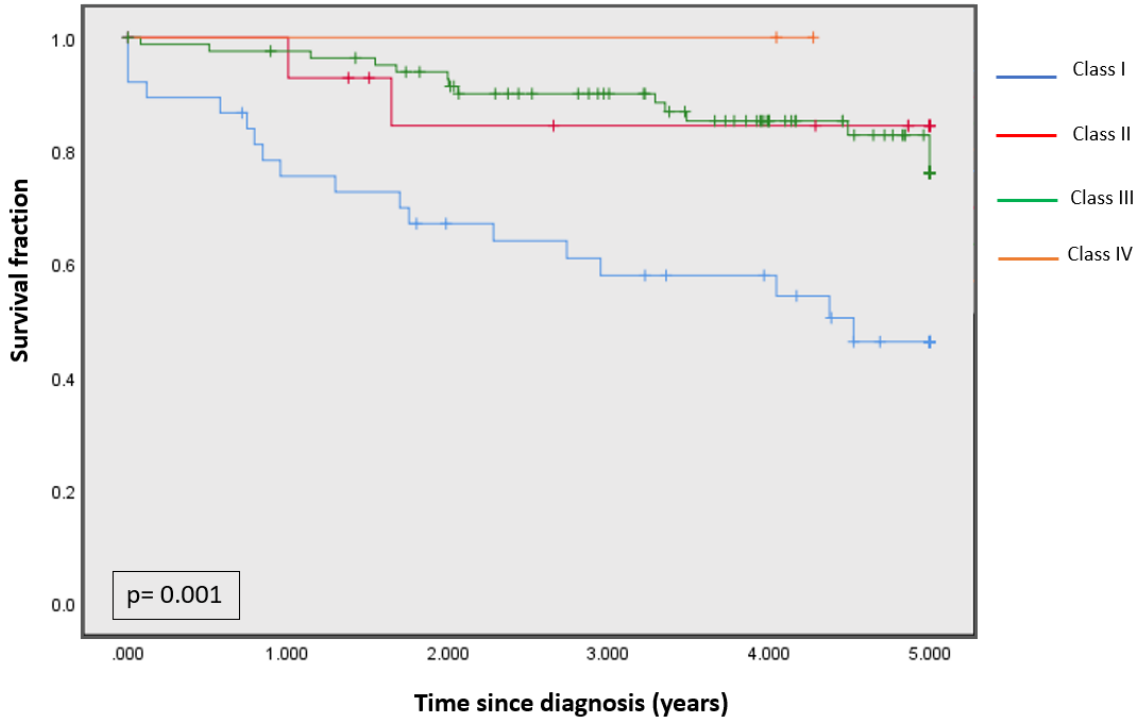

Figure 3.11: Overall survival curves for OPSCC cohort based on p16 and HPV 16/18 expression using Kaplan-Meier method. OPSCC cohort stratified into 4 classes based on p16/HPV expression. Class I (HPV and p16 negative) showed a lower survival fraction compared to Class III (HPV and p16 positive). Each drop-step in the curve illustrates a case of death. Each vertical line (Hash lines) on the curve indicates censored data. Log-rank p= 0.001.

3.4.6. α-SMA expression in OPSCC

To explore the presence of CAFs in the OPSCC microenvironment and investigate their prognostic value, TMA slides were subjected to IHC using an anti-α-SMA monoclonal antibody (1:100, Sigma Aldrich, UK). The submandibular salivary gland tissue section was included as a positive control. Antibody-negative control was obtained by omitting the primary antibody incubation step on the submandibular salivary gland section. CAFs were identified by positive α-SMA staining and were distinguished from other inflammatory and endothelial cells-stained cells by their morphology and pattern of organisation. CAFs appeared as long and spindle-shaped with an elongated nucleus. Typically, in larger amounts, CAFs were arranged in long arrays patterns (Figure 3.12). α-SMA immunopositivity was scored to “Low” and “High” based on positive staining amount. Following Kellermann *et al.* (2008) criteria, “Low” indicated a patchy/focal expression of less than 50% of the stroma, while High referred to a diffuse expression throughout the tumour, affecting more than 50% of the stroma.

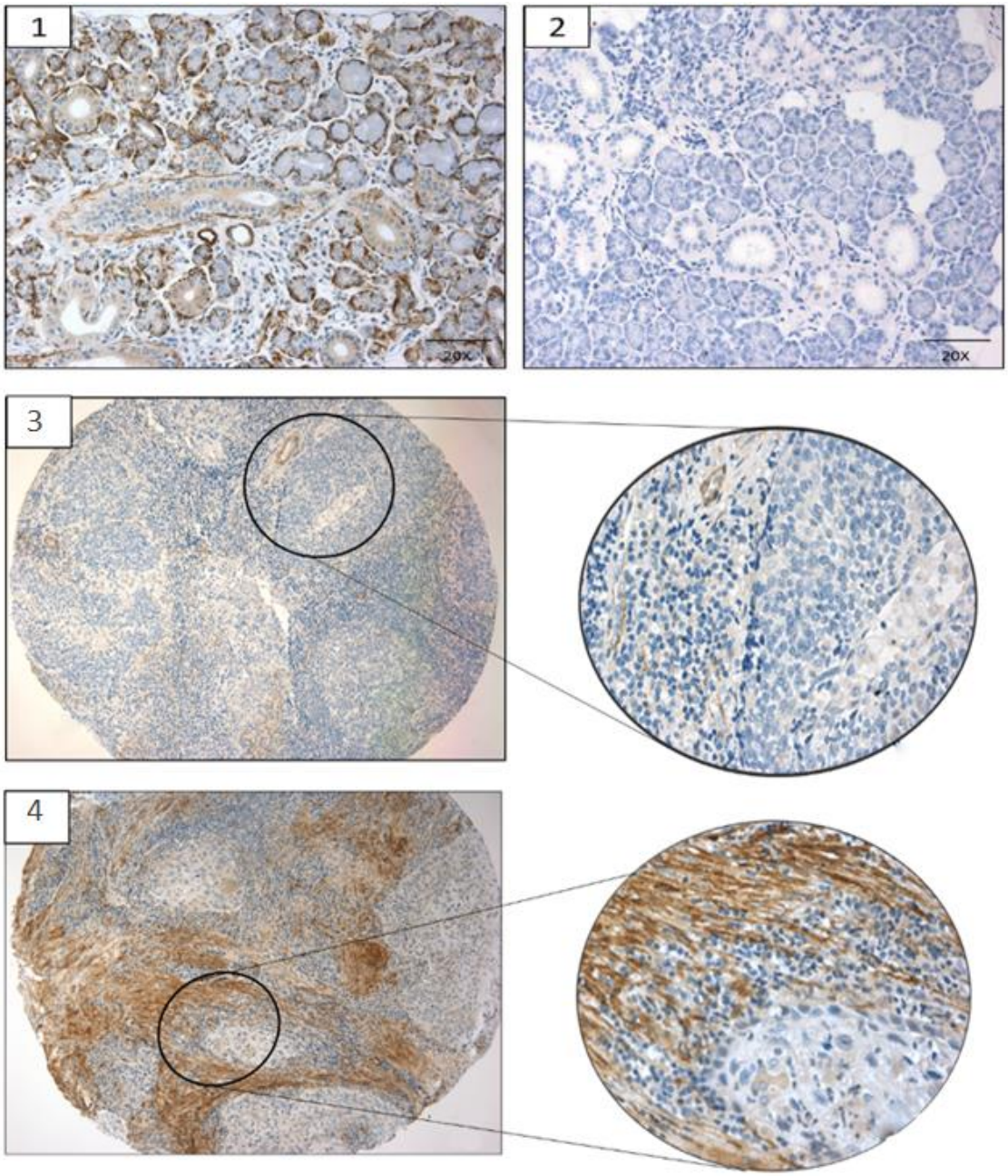

Figure 3.12. α-SMA IHC expression in OPSCC. Anti α-SMA monoclonal antibody (1:100) was used for IHC staining. **1**, positive control, submandibular salivary gland (myoepithelial-like cells) shows strong α-SMA positivity. **2**, α-SMA negative control, the omission of α-SMA antibody in submandibular gland serves as antibody negative control. **3**, Low α-SMA expression. **4**, High α-SMA expression. Images presented at 20X & 40X magnifications.

3.4.6.1. α-SMA expression distribution in relation to OPSCC subtypes

α-SMA expression was observed in both OPSCC entities in a comparable pattern. Within HPV-negative tissue, 46% expressed a high amount of α-SMA, while in HPV-positive tissue the percentage was 54.1%. Statistically, no significant difference was observed in α-SMA distribution between OPSCC subtypes (Chi-square p=0.36) (Figure 3.13).

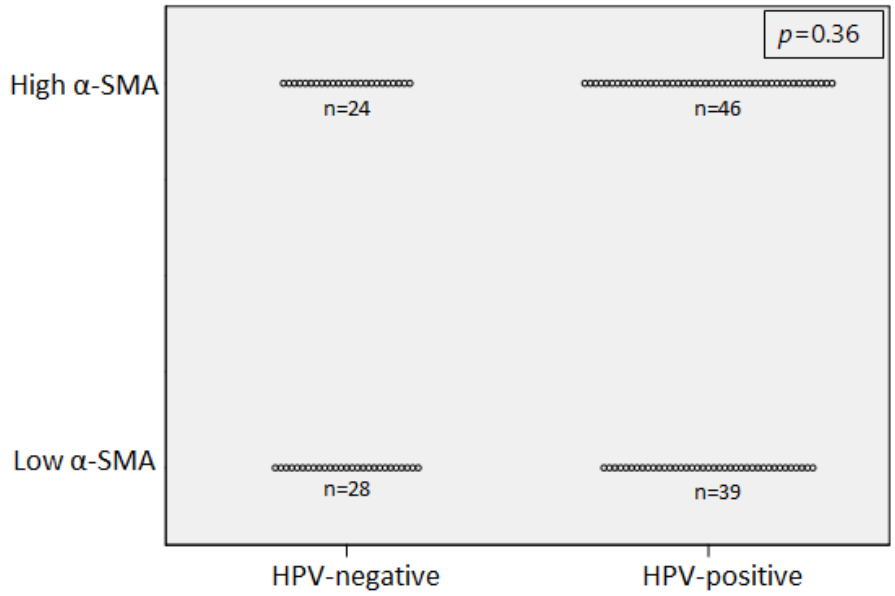

Figure: 3.13: α-SMA expression distribution in OPSCC cohort sub-groups. HPV-negative group (n=52) and HPV-positive group (n=87) displayed comparable patterns in α-SMA IHC. Chi-square test (p=0.36).

3.4.6.2. α-SMA prognostic value in OPSCC

The prognostic value of α-SMA was evaluated firstly in total for the whole OPSCC cohort and then for the sub-cohorts, based on HPV-status. Kaplan-Meier method revealed better survival time in the “Low” α-SMA OPSCC group (4.4 years; 95% CI: 4-4.7) compared to the “High” α-SMA OPSCC group (4 years; 95% CI: 3.7-4.4). However, the Log-Rank comparison between both α-SMA survival curves was non-significant (p=0.12), indicating a weak correlation between α-SMA biomarker and OPSCC survival.

On the contrary, in the HPV-positive sub-cohort, α-SMA expression revealed a significant prognostic value which further stratified survival in the HPV-positive group. “Low” α-SMA HPV-positive patients demonstrated a favourable clinical outcome compared to “High” α-SMA HPV-positive, (4.8 years; 95% CI:4.6-5) and (4.3 years; 95% CI:3.9-4.7), respectively, (p=0.02). In the HPV-negative group, both α-SMA survival curves showed an overlapped pattern throughout the 5 years of follow up, suggesting a weak prognostic value of α-SMA in HPV-negative cases (p=0.77) (Table 3.4) (Figures 3.14-16).

Table 3.4: Summary of Kaplan-Meier method for assessing α-SMA biomarker prognostic value in OPSCC cohort and HPV-subgroups.

HPV status	α-SMA expression	Overall survival (years)	95% Confidence interval	*P*-value
Whole cohort	Low	4.4	(4-4.7)	0.12
	High	4.0	(3.7-4.4)	
HPV-positive sub-cohort	Low	4.8	(4.6-5)	0.02
	High	4.3	(3.9-4.7)	
HPV-negative sub-cohort	Low	3.7	(3-4.4)	0.77
	High	3.6	(2.9-4.3)	

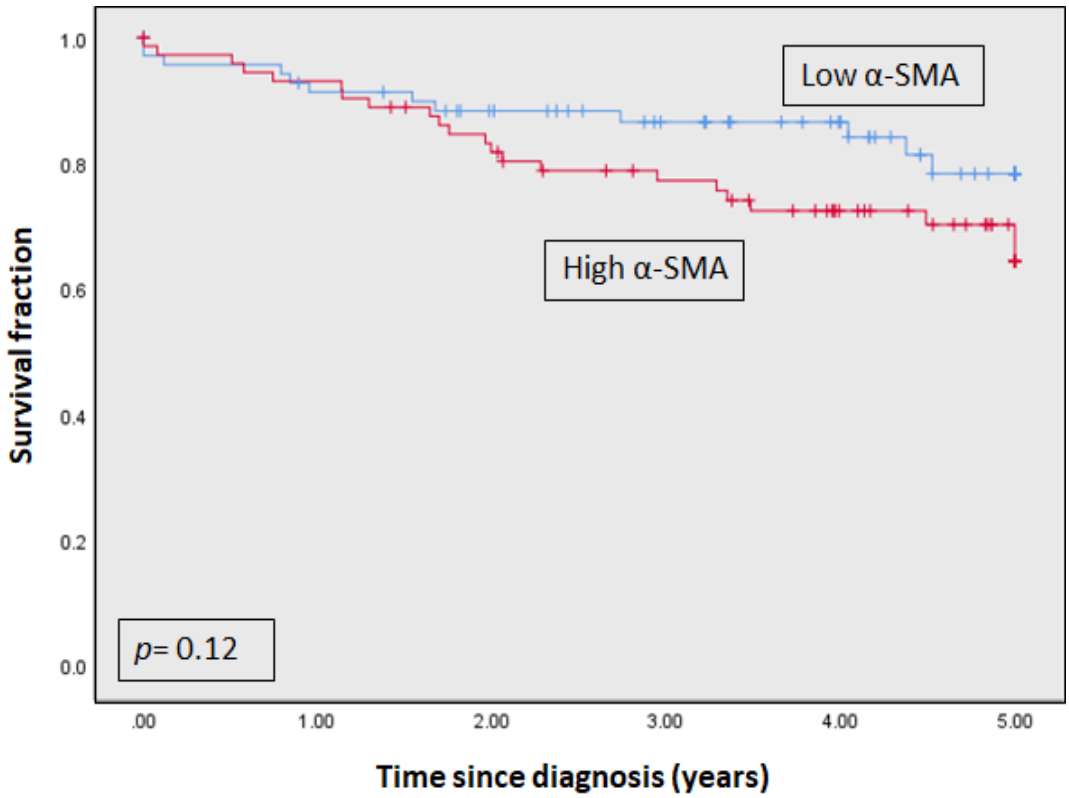

Figure 3.14: 5-years overall survival rates in OPSCC cohort based on α-SMA expression. Kaplan-Meier analysis for α-SMA expression in OPSCC cohort (n=137). Log-Rank p= 0.12. α-SMA low expression cases showed better survival, although that was not significant. The blue curve represents the α-SMA-negative group, and the red curve represents the α-SMA-positive group). Each drop-step in the curve illustrates a case of death. Each vertical line (Hash lines) on the curve indicates censored data.

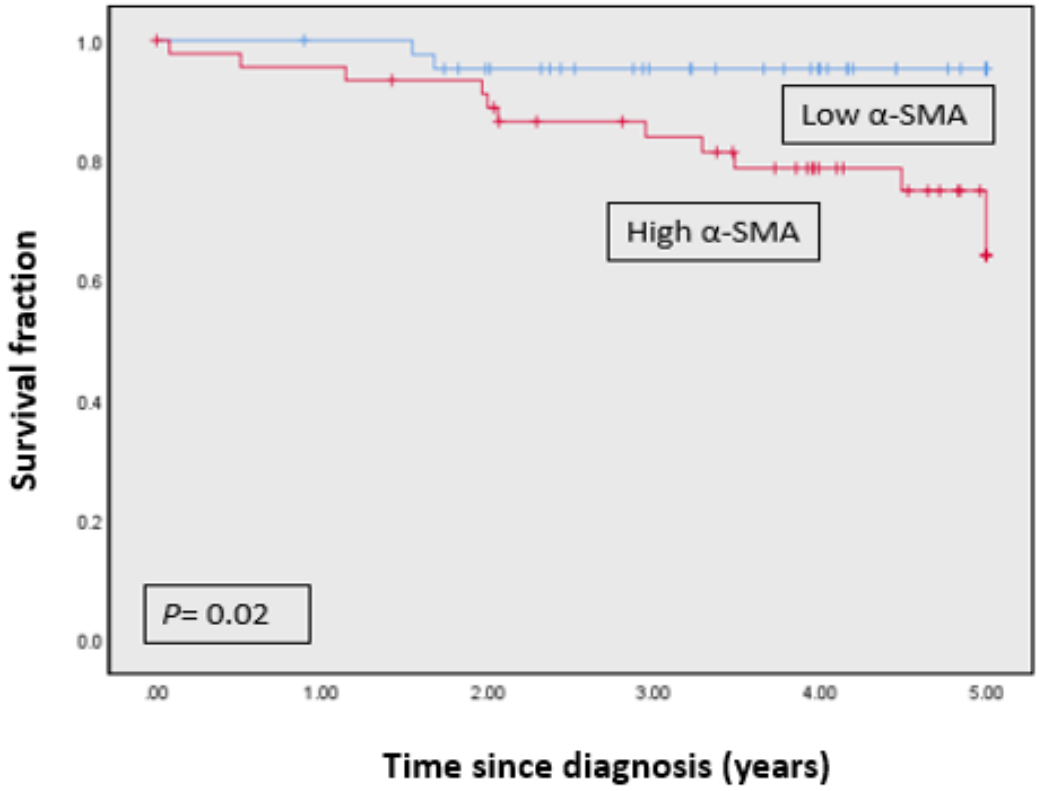

Figure 3.15: 5-years overall survival rates in HPV-positive OPSCC group based on α-SMA expression. Kaplan-Meier analysis for α-SMA expression HPV-positive group (n=85). Log-Rank p= 0.02. Low α-SMA expression significantly predicted better survival among the HPV-positive OPSCC group. The blue curve represents the α-SMA-negative group, and the red curve represents the α-SMA-positive group. Each drop-step in the curve illustrates a case of death. Each vertical line (Hash lines) on the curve indicates censored data.

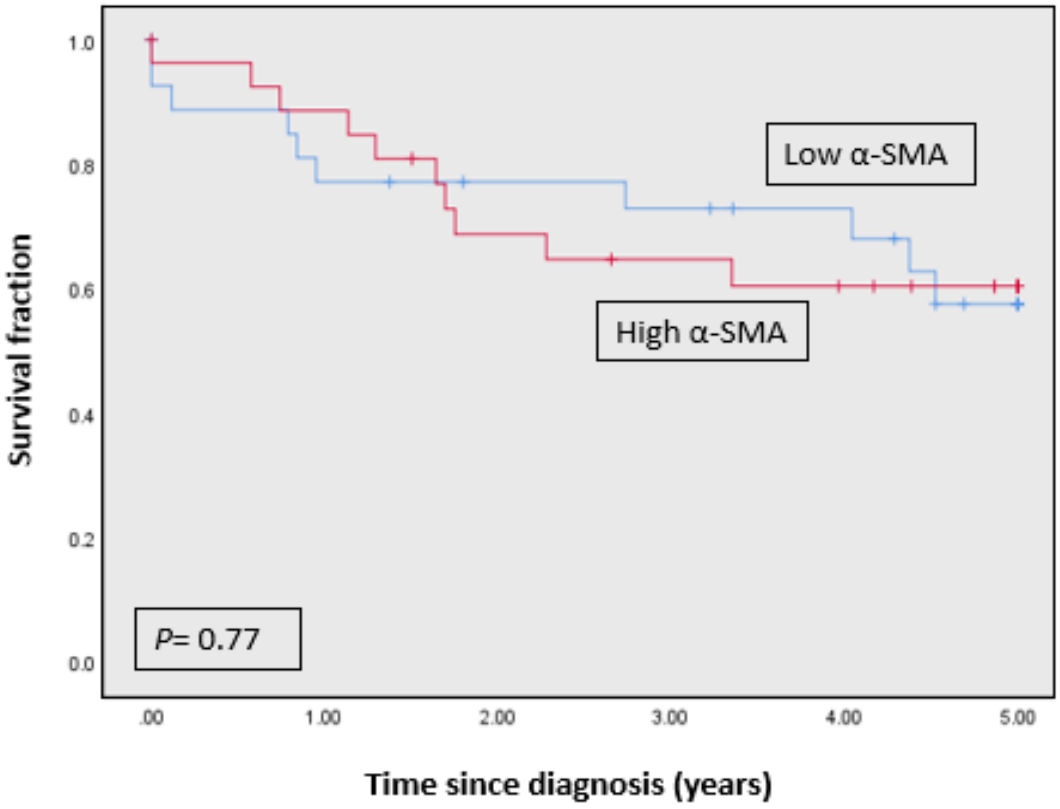

Figure 3.16: 5-years overall survival rates in HPV-negative OPSCC group based on α-SMA expression. Kaplan-Meier analysis for α-SMA expression HPV-negative group (n=52). Log-Rank p= 0.77. No significant prognostic value was identified for α-SMA biomarker in HPV-negative OPSCC. The blue curve represents the α-SMA-negative group, and the red curve represents the α-SMA-positive group). Each drop-step in the curve illustrates a case of death. Each vertical line (Hash lines) on the curve indicates censored data.

3.4.7. Cox regression model

In the previous survival assessments, the Kaplan-Meier method was used with the null hypothesis: “there is no difference between the two populations’ survival curves”. This analysis examined the association of favourable outcomes with the presence and/or pattern of putative prognostic biomarkers. Looking at the other side of the coin, we aimed to measure the hazard of predictors in OPSCC mortality. Cox regression model (proportional hazards regression) was selected to provide further prognostic value for the cohort mortality “Hazard ratio, HR”. The model was established at the “Univariate” level to assess HR for each biomarker separately. A simultaneous “Multivariate” comparison of all the predictors’ strength will be presented and discussed in chapter 7.

3.4.7.1. Unadjusted regression Model (Univariate)

In the univariate model, HR is based on a single predictor where other predictors hold constant during the analysis, “unadjusted to other predictors’ effect”. In this model, HR reflects the hazard proportion based on a comparison between the predictor’s positive and negative groups and their strength in outcome prediction in OPSCC. If the HR is greater than 1, that is an indicator for a positive associated with the hazard and low survival prediction. If the HR is less than 1, then the predictor is associated with favourable survival, not the hazard, and in cases where it is equal to 1, that means the predictor does not affect the survival (Table 3.5) (Figure 3.17).

HPV 16/18-negative status (RNAScope) was significantly associated with increased hazard compared to the HPV 16/18-positive counterpart (p=0.005). The mortality in the HPV-negative group was 2.68 higher compared to the negative group at any particular time (HR: 2.68, 95%CI: 1.35-5.31). On the other hand, HPV 16/18 positivity status exhibited a protective feature with HR=0.37 (95% CI; 0.18-0.73).

Absence of p16 overexpression showed a relatively strong association with poor outcome (HR: 3.88, 95%CI: 1.95-7.72), while its positivity was linked to favourable survival with low HR: 0.25 (95% CI: 0.12-0.51). The difference in HR between the two groups was statistically significant (p<0.001).

α -SMA low expression showed an association with better survival in OPSCC cohort in total (HR: 0.60, 95%CI: 0.29-1.22); however, that was not statistically significant when compared with α-SMA positive group (HR: 1.65, 95%CI: 0.81-3.37) (p= 0.16).

Table 3.5: Summary of Univariate regression model for OPSCC covariates.

Covariate	Un-adjusted Model (Univariate)	
	HR (95% CI)	*P*-value
HPV16 & 18 (RNAscope) Negative Positive	 2.68 (1.35-5.31) 0.37 (0.18-0.73)	0.005
p16 (IHC expression) Negative Positive	 3.88 (1.95-7.72) 0.25 (0.12-0.51)	<0.001
α–SMA (IHC expression) Low High	 0.60 (0.29-1.22) 1.65 (0.81-3.37)	0.167

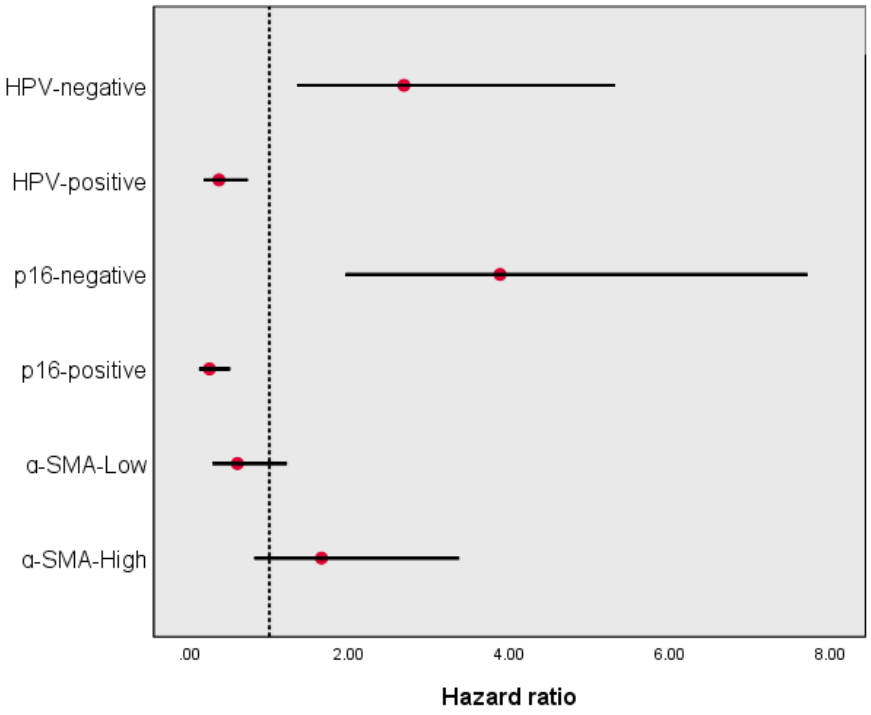

Figure 3.17: Forest plot illustrating the strength of study covariates. A Univariate model was established to obtain the hazard ratio values for each factor separately. HR (Red dot) presented with 95% CI upper and lower values. The dotted line represents the strength cut-off of HR (1). HR before the line indicates a weak correlation with the hazard and *vice versa*.

3.5. Discussion

In this chapter, we presented our investigation of a retrospective cohort of primary pre-treated OPSCC consisting of 143 FFPE tissue samples presented in tissue microarrays. HPV 16/18 mRNA ISH prevalence was 60.8% using RNAScope assay. The HPV-positive group demonstrated a better survival rate than the counterpart (Log-Rank p= 0.002) with low HR in the univariate model HR=0.37 (95% CI: 0.18-0.73). Available smoking data revealed a significant difference between two OPSCC subtypes (p<0.001); the HPV-negative group presented with a high percentage of “current" smokers who demonstrated the worst survival fraction in OPSCC. p16 IHC H-score distribution showed a clear difference between OPSCC groups (p<0.001). Using ROC curve, H-score threshold “144.5” was selected for best diagnostic performance. p16 positivity provided a protective feature with superior survival for the positive group HR = 0.25 (95% CI: 0.12-0.51) based on H-score threshold 144.5. Although High α-SMA IHC expression was observed in both OPSCC subtypes, it provided further survival stratification in the HPV-positive group, with significant potential prognostic value (Log-Rank p=0.02).

3.5.1. HPV prevalence

Currently, there is compelling evidence that HR-HPV is the primary cause of the increased incidence of OPSCC around the world. HPV 16/18, which was described originally as the main risk factor for cervical cancer, has been detected in a significant proportion of OPSCC, with an alarming increase in incidence recently. However, reporting HPV data within the literature requires caution considering several factors, including sociosexual diversity among the nations, the period in which the study was conducted and, most importantly, the robustness of HPV testing methods.

The reported range of HPV-driven OPSCC worldwide is wide: 25%-74%, considering the scarce data from South America, Africa, and Asia (Gillison *et al*., 2000, Evans *et al*., 2013, Würdemann *et al*., 2013, Franceschi, 2017, Dickstein *et al*., 2020). In this study, using RNAScope assay for HPV 16/18, HPV prevalence was 60.8% (87/143), while 39.2% (56/143) of OPSCC was non-HPV 16/18 related. To compare the prevalence with studies located within the same time frame, we had to look at HPV 16/18 prevalence among the two small cohorts comprising the main study cohort because they were collected from different periods. Cohort 1 consisted of cases collected between 1996-2005 (Oxford and Birmingham), and Cohort 2 of cases collected between 2002-2012

(Sheffield Teaching Hospitals). HPV 16/18 prevalence in these small cohorts was 57.8% (48/83) and 65% (39/60), respectively. Although the latest cohort showed higher HPV prevalence, we cannot consider that an increase in incidence occurred over the years because the two cohorts originated from different regions, without available previous data for the comparison. Generally, data from Europe demonstrates a significant steady increase in HPV-OPSCC incidence over the same time frame. In the period between (1995-1999) and (2000-2004), HPV incidence increased from 35.6% (95% CI: 26.5%-44.7%) to 42.4% (95% CI: 35.6%-49.1%), and by 2015, it had risen to 49.5% (95% CI:36.4%-62.6%) (Stein *et al*., 2015).

In the first UK nationwide study evaluating HPV prevalence between (2002-2011), 1710 OPSCC cases were collected from 11 recruiting centres around the UK. The Sheffield and Birmingham centres did not take part in the study. The average percentage of HPV-associated OPSCC identified across the centres was 51.8%. Among the 11 centres, Liverpool and London recorded the highest percentages (67.5% and 65.2%, respectively) and the lowest percentage was seen in Belfast (35.7%). The study is based on tier-wise diagnostic algorithms (p16 IHC, HPV DNA-ISH and/or PCR) for HPV detection. HPV DNA ISH probes covered 12 HPV genotypes, while PCR primers were used for the most common 24 genotypes. Among the tested HPV genotypes, the HPV 16/18 percentage was 93.5% (95% CI, 91.5–95.1) (Schache *et al*., 2016).

3.5.2. HPV Patient profile

According to the above-mentioned study, Schache and team found the majority of HPV cases are located in younger age groups, whilst the HPV percentage is decreased in the older age groups (37.2% of ≥75 years vs 69.2% in age ≤ 45). The mean age for HPV-positive OPSCC was 57.4 years which was statistically younger than among the HPV-negative counterpart (61.4 years) ($p<0.001$). Here, in this study, we did not observe a significant difference in age between the HPV-positive and HPV-negative groups ($p>0.05$). The incidence of OPSCC in relation to patient age showed a bell shape pattern, regardless of HPV-status, which started with a few cases at an early age ≤ 45, peaked between ages 46 and 65, then declined around ≥66, which indicates that all the OPSCC cases can be considered as falling within middle-aged groups. This disagreement in age distribution might be attributed to the relatively small size of our cohort.

Over the last decades, HPV-positive OPSCC has been known as a disease affecting the middle-aged groups (45–64 years old), in particular, whilst non-HPV related OPSCC was linked to the elderly with a long history of tobacco and alcohol consumption. Recently, a few studies reported an evolving epidemiologic landscape of HPV-OPSCC population, with a significant shift in the age range spectrum toward older year groups (Zumsteg *et al*., 2016, Melina *et al*., 2018, Rettig *et al*., 2018 a, Rettig *et al*., 2018 b). Melina *et al*. (2018) reported a significant increase in age median in the study population (n=239) from 53 years to 58 years, (p=.01), based on a timeline ranging from 1995-2013. However, the study population comprised a wide variety of ethnic groups, which might indicate the effect of diversity in sociosexual conditions among the study cohort. Another report, from the Westra group, presented the same significant shift in the mean age of the study cohort (n=1068), from 51.6 years to 58.5 years in cases collected between 2002 and 2017 (Rettig *et al*., 2018 b). However, the determination of HPV-status was dependent solely on p16 IHC overexpression which was observed in 89.3% (954/1068) of the study cohort. The high HPV percentage in their study raises a concern regarding p16 low specificity. The p16 false positive percentage has been reported to be between 5% and 20% in the literature; this fraction could be a reason behind the age range extension in this report.

Much work is required to understand the evolving clinical profile for HPV-OPSCC patients and its clinical implications. The available clinical data demonstrated a concerningly high hazard ratio in the older HPV group compared to the younger age group ($p<0.001$) (Rettig *et al*., 2018 a), although HPV detection methods in this report were not stated clearly. The elderly group is the ideal age group for potentially gaining benefit from de-intensification protocols. Establishing a rigorous clinical trial incorporating the HPV-elderly group might reveal significant implications in the optimisation of de-intensification protocols.

In this study, gender distribution among the HPV-positive and negative groups was similar ($p>0.05$), although the study incorporated more men than women (M:F ratio 2.8:1). In the literature, there is no marked dominant effect of HPV infection linked with a specific gender. HPV-associated OPSCC has a varied distribution between both genders around the world. While the United States demonstrates a strong male predilection (Gillison *et al*., 2015), other reports across Europe showed the opposite trend, with greater increasing incidence in women than men (Evans *et al*., 2013, Henneman *et al*., 2015, Würdemann *et al*., 2017, Mirghani *et al*., 2019). Interpretation of

gender distribution across the geographic regions reflects the diversity in sociosexual behaviour among these populations (Gillison *et al*., 2015).

3.5.3. Prognostic potential of RNAScope

The prognostic value of RNAScope has been reported by a small number of studies in the literature (Ukpo *et al*., 2011, Schache *et al*., 2013, Craig *et al*., 2020). Although it demonstrated a strong correlation with survival, further clinical validation is still needed to prove its performance against p16 IHC. In this study, the HPV positive group showed a clear improvement in overall survival time compared to the non-HPV group over the 5 years of follow up. Log-Rank test detected this significance between the survival curves of both HPV groups (p=0.002), whilst the univariate regression model displayed a lower hazard ratio with HPV-positive status than in the negative counterpart (p=0.005).

Comparing RNAScope prognostic performance with p16, the latter showed more significant value in prognosis prediction (Log-Rank p<0.001) compared to HPV-curve values. Moreover, its prediction strength in the hazard ratio analysis presents a significant and superior factor in univariate analysis (p<0.001). According to the available limited data in the literature, RNAScope and p16 demonstrated equal prognostic value using the Kaplan-Meier method. However, based on an adjusted regression analysis, Ukpo *et al*. reported a stronger prognostic value in patient outcome stratification with p16 than RNAScope using 7 hybridization HR-HPV probes, over a follow-up period of 14 years (Ukpo *et al*., 2011). On the other hand, Craig *et al*. reported a comparable prognostic value between RNAScope and p16 (HR=0.26 and 0.31 respectively) using 18 HR-HPV probes, over 5 years of follow-up (Craig *et al*., 2020). No multivariate analysis was reported in Schache *et al*. (2013).

From the above, RNAScope showed a strong correlation with survival rate. Compared to p16, RNAScope showed an equivalent performance in univariate analysis; however, in the case of multivariate analysis, there was disagreement between the reports, the difference in HPV probes number possibly being a reason. Additionally, we should be aware of other prognostic influences that might have an impact on the multivariate comparison. In our study, the number of HPV probes used is a clear limitation. The RNAScope prognostic value could be minimised by linking cohort cases' survival with the expression of two HPV genotypes only. Full validation of RNAScope prognostic strength clinically could end the era of diagnostic algorithms in clinical practice, especially

after the success of automated RNAScope validation (Anderson *et al*., 2016). Using a single test approach could minimise the risk of false-positive and false-negative results in the two-test approach. Besides, it would minimise the issues in test result interpretation due to the unique probe design that amplifies the signals specifically within a noise-free background. However, the financial implications of such a test are a challenge to be considered.

3.5.4. Influence of smoking on OPSCC survival

Due to the retrospective nature of sample and data collection, data concerning smoking and alcohol intake could not be reliably obtained. Smoking history was available in 129 cases but with poor definition of the status in terms of date, pack number per year and history of smoking quitting. Based on smoking status, cases were put in three categories: Never, Former and Current. The distribution of cases in these categories revealed highly significant differences between the HPV-positive and negative groups ($p<0.001$). The HPV-positive cohort showed a higher percentage of “Never” versus the HPV-negative cohort which had a higher number with “Current” status. These findings suggest modifying the aetiological role of risk factors in OPSCC development. Notably, a small proportion in the study cohort was identified as “Never smoked” and “HPV-negative patient” (n=7). These cases could be attributed to other HR-HPV genotypes rather than HPV 16/18 or linked to heavy drinking of alcohol.

Our data regarding the effect of smoking on survival needs to be interpreted with caution; firstly, we analysed the effect of “smoking status at diagnosis”, and this might have changed during the treatment and follow up periods. Most importantly, our data is based on overall survival analysis rather than disease-specific survival, which may not be the most appropriate parameter for outcome comparison. Tobacco use has general health complications, including cardiovascular and lung disease, besides the development of other malignancies (Roden *et al*., 2020). In our study, smoking status appeared to have no evident impact on the survival rate in the HPV-positive group ($p=0.48$); meanwhile, the HPV-negative group showed a significant sub-stratification in survival based on smoking status ($p=0.001$).

Smoking has a significant negative impact on patient survival, regardless of HPV-status (Ang *et al*., 2010, Gillison *et al*., 2012, Chen *et al*., 2020). Smoking status at diagnosis and during treatment has been shown to be associated with treatment response, and increased risk of developing second primary tumours (Browman *et al*., 1993, Fountzilas *et al*., 1997, Khuri *et al*., 2006). Although HPV-infection is the main aetiological factor in

HPV-positive OPSCC development, the available evidence suggests that tobacco smoking might have an impact on HPV-associated OPSCC behaviour and treatment response (Hafkamp *et al*., 2008, Kumar *et al*., 2007), possibly because of an increased risk for both local recurrence and distant metastases (Maxwell *et al*., 2010). However, in our analysis, as many retrospective studies, smoking habits did not demonstrate an evident influence on HPV-associated OPSCC outcomes (Yin *et al*., 2018, Hawkins *et al*., 2019, Roden *et al*., 2020).

3.5.5. p16 expression in OPSCC

p16 expression distribution based on H-score values revealed a highly significant difference between HPV-positive and negative OPSCC ($p<0.001$). A completely negative p16 value (H-score = 0) was detected in 58.8% of the HPV negative group, whereas none of the HPV-positive group showed complete p16 negativity. p16 expression reflects the pathogenesis of HPV oncoprotein E6 and E7 in deregulated cell cycle-associated proteins (p16, pRB, cyclin D1 and p53) (Wiest *et al*., 2002). However, by other less well-described mechanisms, p16 overexpression has been reported in a significant minority of non-HPV driven OPSCC (15-30%) (Sedghizadeh *et al*., 2016). This could in part be attributed to the normal structure of oropharyngeal mucosa. Reticulated epithelium lines the oropharyngeal crypt and can show a weak patchy pattern of p16 expression in the absence of HPV infection (Robinson *et al*., 2012, Moutasim *et al*., 2015).

RNAScope assay was the selected approach in this study to detect the transcriptionally active E6 and E7 mRNA in FFPE tissue. Compared to “the gold standard test” in the fresh frozen tissue samples (E6 & E7 RT-PCR), RNAScope showed excellent sensitivity and superior specificity in FFPE tissue (Geo *et al*., 2013, Schache *et al*., 2013). Moreover, it revealed a promising diagnostic performance, higher than DNA-ISH and PCR, when compared to p16 IHC. In a study of 357 cases, comparing p16 expression with HPV available tests, RNAScope displayed the highest sensitivity (93.4%) and specificity (92.4%) over DNA-ISH (86.3% and 95.3%) and DNA PCR (83.5 and 89.1) (Randén-Brady *et al*., 2019). Similarly, Craig *et al*. (2020) introduced RNA-ISH using RNAScope technique as a superior test over DNA-ISH and PCR with 95% sensitivity and 100% specificity compared to p16. However, it is worth mentioning that in both previously mentioned studies, DNA-ISH probes covered 12 HPV genotypes only, whereas RNAScope probes covered 18 genotypes. In this study, we aimed to determine

the p16 H-score cut-off in OPSCC by utilising RNAScope super performance in FFPE tissue.

p16 immunoreactivity cut-off is a controversial issue in the literature. CAP and AJCC 8th guidelines, in addition to the majority of authors, considered >70% of cells expressing p16 (H-score approx. 210) as the diagnostic threshold of p16, whilst many authors introduced a >50% positivity cut off (H-score approx. 150) as a reproducible and high specificity threshold (Singhi and Westra, 2010, Amin *et al*., 2017, Shelton *et al*., 2017, Fakary *et al*., 2018). In this study, we investigated the performance of a p16 H-score scheme in OPSCC. H-score was obtained by identifying the proportions of each stain's intensity levels (0, 1+, 2+, or 3+) and then calculated according to the H-score formula (Hirsch *et al*., 2003, John, Liu and Tsao, 2009). Using ROC curve, 144.5 was selected as an acceptable H-score threshold with 97.7% sensitivity and 72% specificity (AUC=0.87). The percentage of p16 false-positive cases was 10.8% of p16+/HPV- discordant cases. In the literature, 3-23% is the reported range of p16+/HPV- disagreement using DNA-ISH (Weinberger *et al*., 2006, Smeets *et al*., 2007).

Jordan *et al*. (2012) investigated the previous diagnostic performance of p16 H-score on OPSCC compared to qRT-PCR E6/E7 mRNA findings on material extracted from FFPE (n=240). A threshold score of 60 was suggested as a cut-off point for H-score with 91.56% (85.93%-95.07%) sensitivity and 90.41% (80.70%-95.69%) specificity. However, the calculation method relied on the cross product of the intensity score (0 to 3) and the percent of tumour staining at the highest intensity only. No further survival correlation was provided in Jordan's study. In our study, based on the H-score threshold (144.5), p16 demonstrated a strong prognostic factor in OPSCC (Log-Rank $p<0.001$). The prognostic strength for the hazard ratio is significant and superior in the univariate comparison ($p<0.001$).

Concerning the prognostic significance of p16, UICC and AJCC accepted p16 IHC as a single test for HPV status determination in OPSCC in the 8th edition of the TNM classification of malignant tumours (Amin *et al*., 2017). However, one of the foremost shortcomings of using p16 IHC alone is the low specificity, which is responsible for a proportion of false-positive cases with poorer survival comparable to HPV-negative OPSCC, as we have found. It is possible that p16+/HPV- OPSCC represents an HPV-unrelated subtype, not fully biologically characterised, which would not benefit from de-intensification protocols (Albers, Qian, Kaufmann and Coordes, 2017). Consequently, mounting evidence has emphasised the significance of double positivity for p16 and an

HPV specific test (DNA ISH) in demonstrating improved diagnostic accuracy and prognostic value (Mena *et al*., 2018, Ragin *et al*., 2018, Craig *et al*., 2019, Craig *et al*., 2020). In our cohort, stratifying the cases based on p16/HPV results revealed a small percentage of discordant cases. We were not able to compare their clinical outcome due to the small size of classes II and IV.

3.5.6. α-SMA IHC expression in OPSCCs

α-SMA immunoreactivity in FFPE tissue is commonly used for detection of active CAF within tumour stroma, and its overexpression is considered indicative of an active tumour microenvironment (Ostman and Augsten, 2009, Marsh *et al*., 2011, Meng *et al*., 2011). CAFs are capable of inducing profound influences on tumour cell growth, behaviour and the response to treatment (Madar, Goldstein and Rotter, 2013, Akrish *et al*., 2016). In many solid tumours, CAF detection is linked to poorer survival; the presence of a myofibroblastic stroma has been reported to be associated with local recurrence and metastasis in tongue carcinomas (Kellermann *et al*., 2007). Additionally, it demonstrated a strong and independent prognostic factor in OSCC regardless of TNM staging (Marsh *et al*., 2011). From this aspect, the presence of CAFs within a tumour is becoming accepted as a predictor of clinical outcome, suggesting the value of further investigations.

Here, we explored the presence of CAFs in OPSCC stroma in terms of α-SMA expression distribution among two OPSCC subtypes and its correlation with the clinical outcomes. We observed a comparable distribution of α-SMA expression in OPSCC subtypes. Among the HPV-positive group, 60.4% showed α-SMA-high percentage whilst 47% of HPV-negative showed a high-α-SMA percentage; however, no statistically significant difference was detected (p=0.78).

CAFs activation is a result of a reciprocal interaction between cancer cells and surrounding stroma, mediated by paracrine signals including cytokines, metabolites, and exosomes (Kalluri and Zeisberg, 2006, Cirri and Chiarugi, 2011, Peacock *et al*., 2018, Fiori *et al*., 2019). Undertaking *in vitro* characterisation of extracellular vesicles (EVs) using HPV-positive and HPV negative cell lines, Peacock *et al*. (2018) reported an increase in EV production by HPV-negative cell lines compared to HPV-positive, with overlapping miRNA content. Interestingly, stimulating normal oral fibroblasts cultures (n=3) with extracted EVs from both HPV cell lines revealed variable upregulation of α-

SMA expression, regardless of HPV status. One high-responder NOF culture showed marked α-SMA expression with HPV-negative cell line (SCC89 and SCC72), whilst two other NOF cultures induced α-SMA upregulation using EVs from HPV-positive cell lines (SCC90 and SCC2) (Peacock, 2018).

To the best of our knowledge, a robust assessment of the presence of CAFs in OPSCC tissue has been limited to two published works. Rahrotaban and colleagues reported a comparison in α-SMA expression "intensity" and α-SMA amount "Percentage" in a relativity small cohort of OPSCC (n=44). Only α-SMA expression percentage showed a significant result with a higher correlation with HPV-positive group (n=23) than HPV-negative group (n=21) (p=0.02), and no further survival information was provided. HPV status determination in the study was based on Nested Polymerase Chain Reaction for common HPV genotypes (n=16) (Rahrotaban *et al*., 2019). In the second report, Oguejiofor *et al*. (2016) assessed α-SMA IHC expression in a larger OPSCC cohort (n=139) and correlated the expression with the clinical outcomes. Their α-SMA scoring scheme was based on the sum of "Intensity X Percentage" which was to some extent different from our score criteria of "Percentage only". In their study, α-SMA expression was significantly higher in the HPV-positive group (n=74/139) than the HPV-negative counterpart. Using a univariate regression model, higher α-SMA expression was not associated with the clinical outcome in the whole cohort, HPV-positive only, or in HPV-negative only groups. This observation disagreed with our finding in the HPV-positive group. We detected a significant association between α-SMA survival curves in the HPV-positive cohort (Log-Rank p=0.01) indicating better overall survival in the HPV+/Low α-SMA subgroup, whereas in the HPV-negative group, no correlation was found between α-SMA and overall survival (p>0.05).

According to our observations, the prognostic value of α-SMA is related to the HPV-status of OPSCC, and it suggests that CAFs derived from HPV-negative OPSCC may have a greater capability for supporting the tumour than CAFs from HPV-positive OPSCC stroma. This assumption proposes a crucial role of OPC cancer cells in CAF phenotype differentiation. Originally, CAFs were established from several cell types within the tumour microenvironment which undergo phenotypic transdifferentiation in response to educating signals from tumour cells. This interaction between tumour cells and CAFs appears to have additional characteristic features based on the genetic stability of cancer cells which is reflected in CAFs' phenotype and behaviour (Hassona *et al*., 2013, Bolt 2015).

Further investigations are required to identify the interaction discrepancy between OPSCC subtypes and CAFs. α-SMA expression in HPV-positive tumours might be utilised as a potential prognostic tool for HPV-OPSCC stratification in de-intensifying treatment. Also, it might provide an opportunity to develop individualised treatment strategies.

3.6. **Limitations**

This study is limited by the nature of retrospective research; thus, it has variation in patients' management protocols, follow-up duration, lack of detailed information regarding the risk factors (sociosexual history, tobacco/drink use) and causes of patient censored data, which might reflect unperceived selection biases. The relatively small sample size must be considered during result interpretation, although the survival data and p16 performance were consistent with the vast majority of published work.

Our research is TMA-based, which means each case was represented by a 1 mm tissue section in the TMAs slide. TMAs might raise concern in terms of case representativeness; however, the cores, ranging in number between 3 and 6, were selected thoroughly. The most compelling evidence suggests that small-sized cores have been proven as totally functional for HPV mRNA and p16 performance (Ukpo *et al*., 2011, Ma and Lewis, 2012).

The survival information was limited to overall OS that might not reflect the nature of the disease. HPV-negative patients are typically have increased co-morbidities and therefore are more liable to death from "other" causes rather than OPSCC.

We are also aware that the RNAScope probes were limited to HPV16 and HPV18 only. Other high-risk HPV genotypes could be associated with some HPV-negative cases; however, low percentages would be expected as HPV16 is responsible for more than 90% of OPSCC cases.

3.7. **Summary of main findings and clinical implications**

This chapter investigated the diagnostic and prognostic performance of p16 H-score against RNAScope assay for the first time. We derived a p16 H-score cut-off of 144.5 as

a promising diagnostic and prognostic tool that demonstrated high sensitivity and acceptable low specificity compared to HPV 16/18 mRNA, in addition to the prognostic performance. This finding underpins the requirement for clinical validation of H-score performance that might be adopted as a tool addressing the partial stain dilemma between >70% and >50% positivity thresholds. We also identified a significant cohort of p16+/HPV- cases which reinforces the need for an HPV specific test, in addition to p16, for diagnosis.

Our findings on α-SMA provided a novel insight into the role of CAFs in HPV-positive OPSCC suggesting the pivotal role of tumour microenvironment in OPSCC outcomes discrepancy. Clinically, these findings urge a further study of the α-SMA biomarker and clinical validation to assess its prognostic strength in HPV-positive OPSCC. The findings might provide a stratification within HPV-positive OPSCC for the best benefit of de-intensifying protocols. Moreover, the proposed crucial influences of CAFs in the HPV-OPSCC tumour microenvironment suggest introducing HPV-positive OPSCC as an option in the emerging potential immunotherapy strategies targeting the tumour.

Chapter 4: Characterisation of OPSCC-derived cancer-associated fibroblasts

4.1 Introduction

Fibroblasts are the dominant cell type within the tumour microenvironment (TME) of many tumour types. In the TME, fibroblasts are continuously exposed to varied chemical and physical stimuli that contribute to phenotype transdifferentiation known commonly as cancer-associated fibroblasts (CAFs). Compelling evidence based on single-cell RNA sequencing (scRNA-seq) (Puram *et al.*, 2018), in addition to previous *in vitro* and *in vivo* observations, emphasised the concept of CAF heterogeneity. CAFs are a group of a highly heterogeneous population. The wide discrepancy between CAF subtypes is demonstrated in the protein expression profile, besides the capacity of CAFs to promote or inhibit the tumours.

Active myofibroblastic CAFs and senescent CAFs are the most common phenotypes which have been studied intensively in the literature concerning OSCC. They exhibit distinct signatures, which, to some extent, is evident in the transcriptional profiles and activation pathways, however, the clinical implications of both phenotypes are still not well established (Biffi and Tuveson, 2021). The role of fibroblasts in the development of oral squamous cell carcinoma is well documented and has been extensively studied in our lab; normal oral fibroblasts (NOFs) were prompted to differentiate into a myofibroblastic phenotype and senescent phenotype. Both phenotypes were well characterised, and their molecular profile was thoroughly studied (Melling, 2015; Kabir *et al.*, 2016; Abidin, 2017). In the previous chapter, HPV-positive OPSCC with myofibroblastic stroma demonstrated clinical poorer outcomes than HPV-positive OPSCC with a lower myofibroblast content, however, there is no established background related to OPSCC-derived fibroblasts. The present chapter focuses on the characterisation of the two most common phenotypes in OPSCC fibroblasts and compares them to what we have seen in NOFs. A better understanding of OPSCC fibroblast behaviour and modulation provides a solid framework for exploring initial events in cancer cell crosstalk in HPV positive and negative OPSCC microenvironment.

4.2 Aims

- To establish *in vitro* models of myofibroblastic-CAF and senescent-CAF models using NTFs

- To isolate and characterise OPSCC CAF primary cultures.

4.3 Experimental approach and Statistical analysis

- Myofibroblastic phenotype was induced in NTF322, NTF6 and NTF10 using TGF-β1 and the cell transdifferentiation was assessed by evaluating *de novo* expression of α-SMA at transcript and protein level using qRT-PCR, western blot, and immunofluorescence assay. Further validation was performed using the collagen gel contraction assay to observe the generated contractile force in the TGF-β1 induced phenotype. Also, the secretory profile was assessed using IL6 ELISA analysis.

- Premature induced senescence (PIS) was induced in NTF322, NTF6 and NTF10 using DNA damaging agent (H_2O_2). Phenotype induction was assessed by many investigations including defining SA-βgal activity, analysis of the upregulation of CDK inhibitors including CDKN2A (p16) and CDKN1A (p21) using western blot, monitoring the proliferative capacity and quantifying IL-6 production.

- For CAF extraction, an enzymatic digestion protocol was followed to isolate CAFs from fragments of tonsillar carcinoma specimens using Collagenase-I.

- Purification of CAFs' primary culture was assessed by the analysis of CK6, HDL-AL and CD31 mRNA expression to exclude keratinocyte, immune cell and endothelial cells contamination, respectively.

- CAFs' identity was examined by analysing a panel of CAF biomarkers including FSP-1, PDGFRα, FAP-α, and α-SMA using qRT-PCR and immunofluorescence staining.

- Statistically, detection of non-normality is less likely among the data due to small sample numbers, however, Shapiro-Wilk test was used to check the normality due to its high sensitivity. For the comparison between two normally distributed samples' mean, two-tailed unpaired *t*-test was used. In multiple data sets, one-way analysis of variance (ANOVA) was used.

- Data were presented graphically illustrating the mean with error bars demonstrating the standard deviation (SD). The probability of similar random result detection (p-value) was considered significant if ($p<0.05$). "N" followed by a number denotes the biological repeats, while "n" denotes the technical repeats. Data were analysed using Graph-pad prism versions 7-9.

4.4 Results

4.4.1 Establish myofibroblastic-CAF model derived from OPSCC fibroblasts.

TGF-β1 has been used widely in the literature in inducing myofibroblast phenotype. To establish reactive myofibroblastic phenotypes from NTF322, NTF6 and NTF10 cell cultures, cells were treated with 5 ng/ml of TGF-β1 for 24h, 48h, and 72h, following the previous protocol on oral fibroblast activation (Melling, 2015, Abidin, 2017). At present, the detection of α-SMA microfilaments is the commonly accepted method for the recognition of differentiated myofibroblasts. Phenotype transdifferentiation was confirmed and validated by assessing α-SMA expression at gene and protein levels. The contraction ability of developed actin microfilaments was observed using collagen gel contraction assay. Moreover, changes in the secretory profile of NTFs were investigated using IL-6 ELISA analysis.

4.4.1.1 TGF-β1 upregulates α-SMA gene expression in NTFs

For α-SMA gene analysis, NTF322, NTF6, and NTF10 were harvested, and total RNA was extracted and quantified. cDNA was constructed in 20µl volume using 400 ng of total RNA. α-SMA gene expression was quantified using delta CT values normalised to β2m. NTFs showed varied levels of α-SMA gene upregulation at different time points, with the highest expression level observed at 48 h in NTF322 and NTF6. NTF322 expressed the highest level of α-SMA, (16 ± 4.2) fold at 48 h, whereas the gene expression levels at 24 h and 72 h were less, (4.5 ± 3.2 and 14 ± 1.4) fold, respectively. NTF 6 showed a similar pattern in α-SMA gene response at different time points; the initial lower expression was after the first 24 h, (8.6 ± 1.9) fold, followed by remarkable elevation at 48 h of (38.5 ± 2.12) fold. After 72 h, NTF6 showed a decrease of (23.5 ± 9.1) fold. NTF 10 showed the highest upregulation of α-SMA in the first 24h, of (14.2 ± 6.6) fold, then there was a steady decrease at 48h and 72h of (13.5 ± 3.5 and 10.2 ± 1.09) fold, respectively (mean ± SD), compared to the untreated counterparts (Figure 4.1).

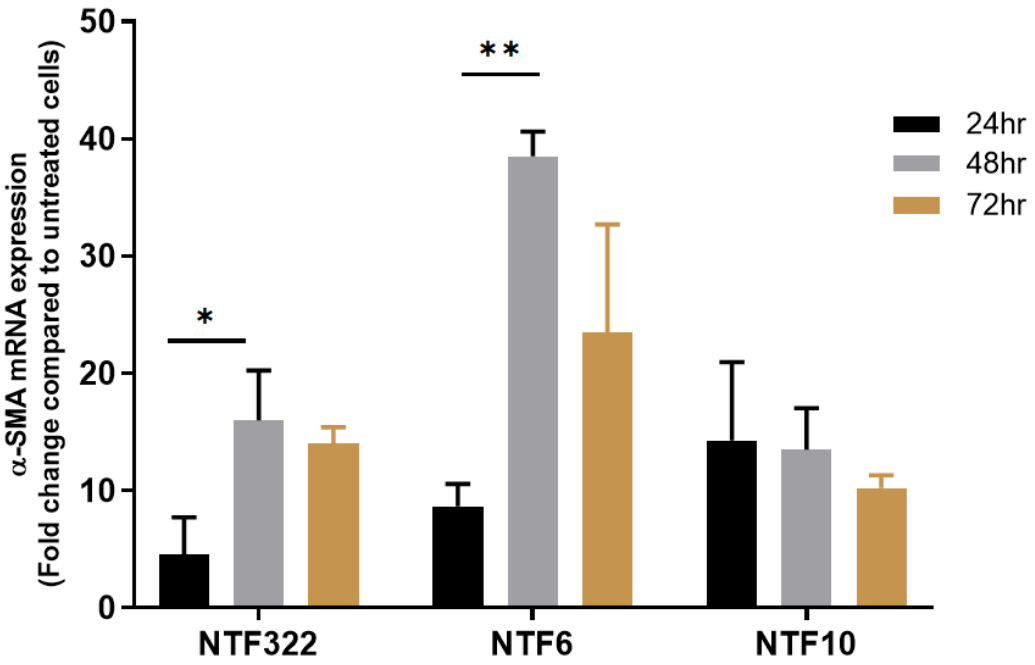

Figure 4.1: α-SMA mRNA expression in TGF-β1-stimulated NTFs. NTF 322, NTF 6, and NTF 10 were treated with 5 ng/ml TGF-β1 for 24 h, 48 h, and 72 h after being starved for the serum for 24 h. α-SMA expressions were variable between NTFs, with significant upregulation seen at 48h in NTF322 and NTF6. Each bar on the figure represents the mean of relative α-SMA expression levels normalised to β2m. Statistical analysis was performed using Student's *t*-test, and statistical significance is shown on the figure by *p<0.05. Error bars = SD for (N=3, n=3).

4.4.1.2 TGF-β1 enhances α-SMA protein abundance in NTFs

Anti-α-SMA monoclonal antibody was used for α-SMA detection whereas Anti-β-actin monoclonal antibody was used to normalise α-SMA expression. α-SMA protein abundances were recognised as a single band at ~42 kDa. The intensity of α-SMA protein expression was greater after TGF-β1 stimulation compared to the untreated cells, following a time-dependent response pattern. The effect of TGF-β1 stimulation on NTF 10 revealed comparable expressions of α-SMA protein with control at different time points, with higher protein expression seen after 72 h. NTF322 and NTF6 showed a similar response to TGF-β1 stimulation, with remarkable protein abundance after the first 48h (Figure 4.2).

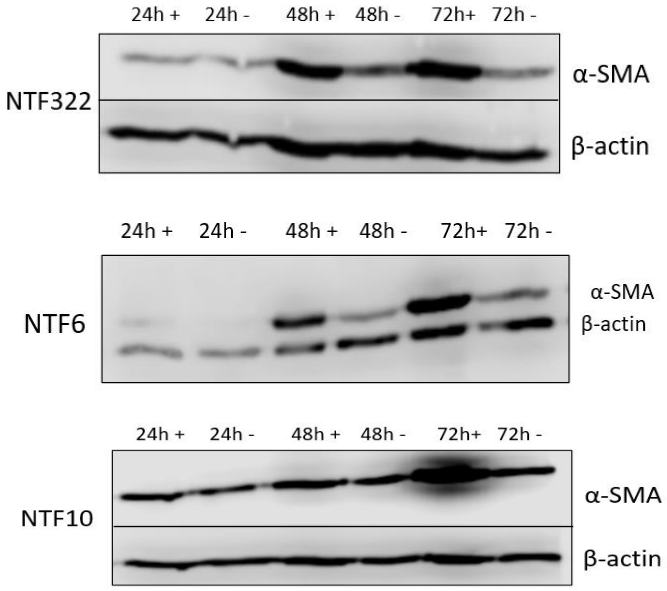

Figure 4.2: α-SMA protein expression in NTFs following TGF-β1 treatment. NTF 322, NTF 6, and NTF 10 were treated with 5 ng/ml TGF-β1 for 24 h (24h+), 48 h (48h+), and 72 h (72h+) after being starved for the serum for 24h. negative control were incubated with serum free media only (24h-), (48h-) and (72h-). Total protein lysates (20 µg) were separated on a 15% SDS-PAGE gel and transferred to a nitrocellulose membrane for immunodetection. After membrane blocking using 5% (v:w) milk. A monoclonal α-SMA antibody (1:1000) was used to detect α-SMA protein and Anti-β-actin monoclonal antibody (1:3000) was used as a loading control after membrane stripping as in NTF322 and NTF10. NTF6 membrane was blotted by both antibodies at the same time.

4.4.1.3 TGF-β1 enhances contraction of NTFs

Collagen gel contraction assay was performed to assess the generated contractile force of NTFs after TGF-β1 stimulation. An *in vitro* three-dimensional contraction model of NTFs was constructed as described in section 2.1.10. Cells were incubated under mechanical tension conditions by leaving the lattices attached to the culture well. After 48h, the collagen lattice was completely detached with a sterile spatula and incubated for 24 h, 48 h or 72 h with TGF-β1. At each time point, the lattices were photographed, and NTFs' contractility was recorded by measuring the distance between the lattice disc and the well using Fiji-ImageJ (Figure 4.3). TGF-β1 significantly promoted the contraction ability of NTFs with time-dependent responses compared to their untreated counterparts. NTF322 showed a significant decrease in lattice disc at 48 h (2.6 ± 0.5mm)

and 72 h (3.6 ± 0.5mm) compared to the contraction in the first 24 h (2 ± 1mm; $p<0.05$). NTF6 demonstrated a marked gel contraction of (4 ± 0) mm (mean + SD) that was statistically significant at 48h and 72h ($p<0.01$). NTF10 exhibited the highest lattice contraction of 5 ± 0 mm (mean + SD) which peaked at 72 h. The difference between lattice contraction at 72 h and 24 h was significant ($p<0.001$). These findings represent the acquired mechanical property in NTFs following TGF-β1 stimulation, confirming the success in myofibroblastic model establishment.

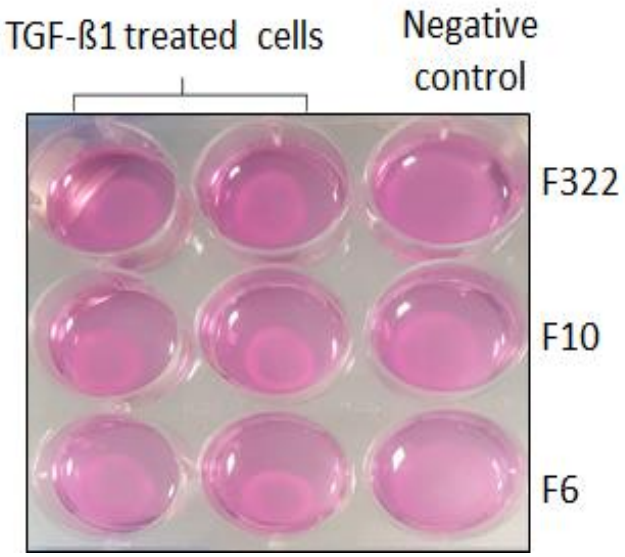

(A)

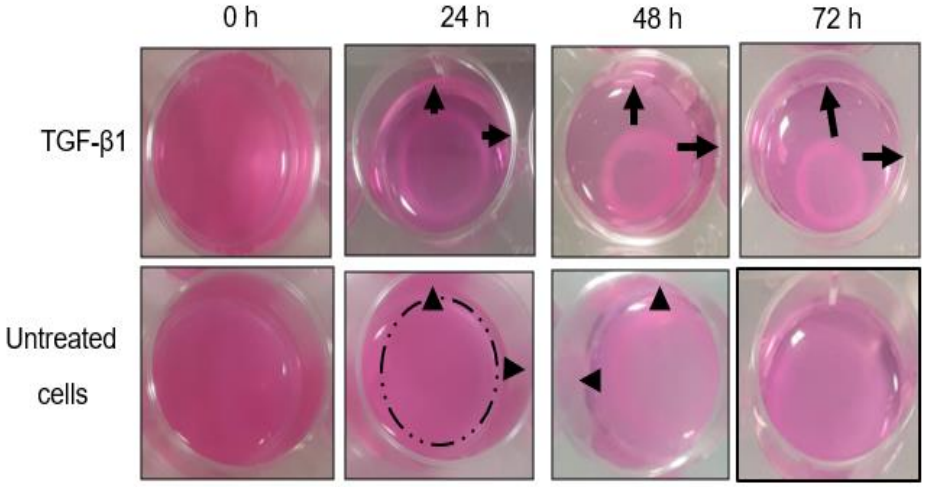

(B)

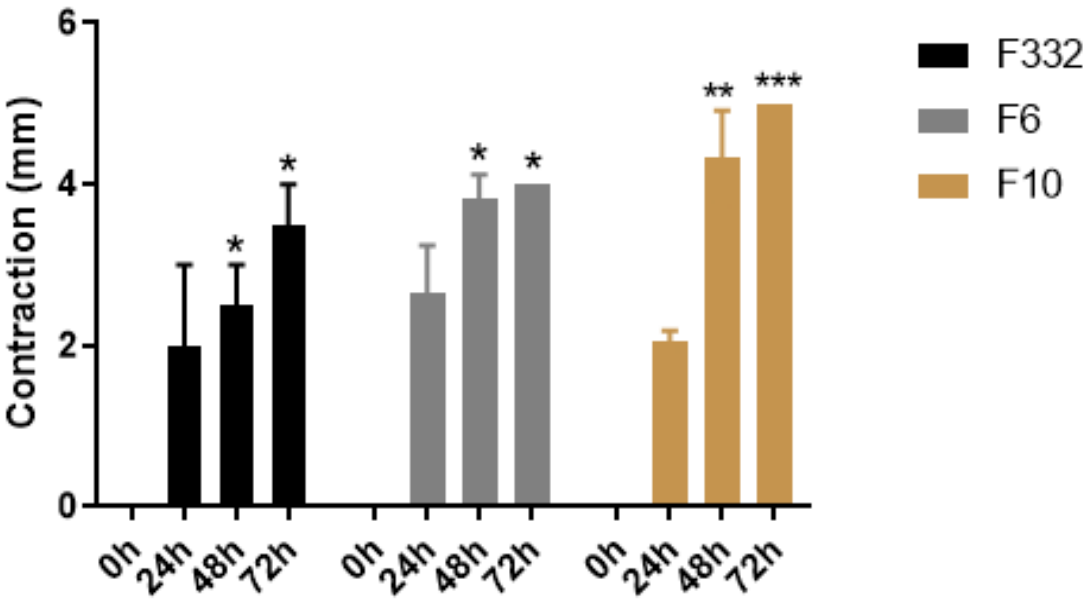

(C)

Figure 4.3: Matrix contraction ability of stimulated NTFs varies between different cultures. NTF322, NTF6, and NTF10 (2 x 10^4 cells) were seeded in 0.5 ml of collagen lattice solution in a 24-well plate and left in the incubator for an hour at 37ºC. 1.0 ml of growth media was added on the top of the collagen gel lattice and the plate was incubated for 24 h. The next day, the cells were serum-starved for a further 24 h, then were treated with 5 ng/ml TGF-β1 before releasing the stressed gel matrix from the plate using a sterile spatula. The gels were then incubated for 72 h in the TGF-β1 stimulation experiment. Photographs of the gel disc were taken at 24 h, 48 h, and 72 h. TGF-β1 provoked actin fibre formation in NTFs that generated apparent mechanical stress across the collagen matrix. **(A)** Image of detached lattices after 72 h of TGF-β1 dose in NTF322, NTF6 and NTF10. **(B)** Gel contraction over time in NTF10. The black arrows illustrate the distances between the gel and the well border. The black dot line represent the gel disc. **(C)** Quantification of gel disc contraction used ImageJ. Relative lattice contraction (mm) was obtained by measuring the distance between the gel and the well border. Error bars= SD of three repeatS.

4.4.1.4 TGF-β1 induces stress fiber formation in NTFs

Immunofluorescence assay was performed to visualise α-SMA fibre formation within the cells after being incubated with TGF-β1 for 48 h. NTF322, NTF6, and NTF10 were incubated with primary FITC-conjugated α-SMA antibody (1:100) for 1.5h. The intensity of FITC expression (green) for each NTF culture was quantified using Image J by including the same number of cells in the observed field (Figure 4.4). TGF-β1 treatment provoked α-SMA stress fibre formation in NTFs compared to untreated cells which demonstrated little or no detectable auto-fluorescence. TGF-β1-treated NTFs showed the typical spindle shape with strong green staining of α-SMA myofilaments along the cell axes, whereas central nuclei-stained blue with DAPI stain. NTF322 and NTF10 demonstrated statistically significant increases in FITC expression compared to the untreated cells with an approximate 3-fold and 3.7-fold, respectively, whereas NTF6 showed a faint FITC stain that was a 2 fold change compared with the control.

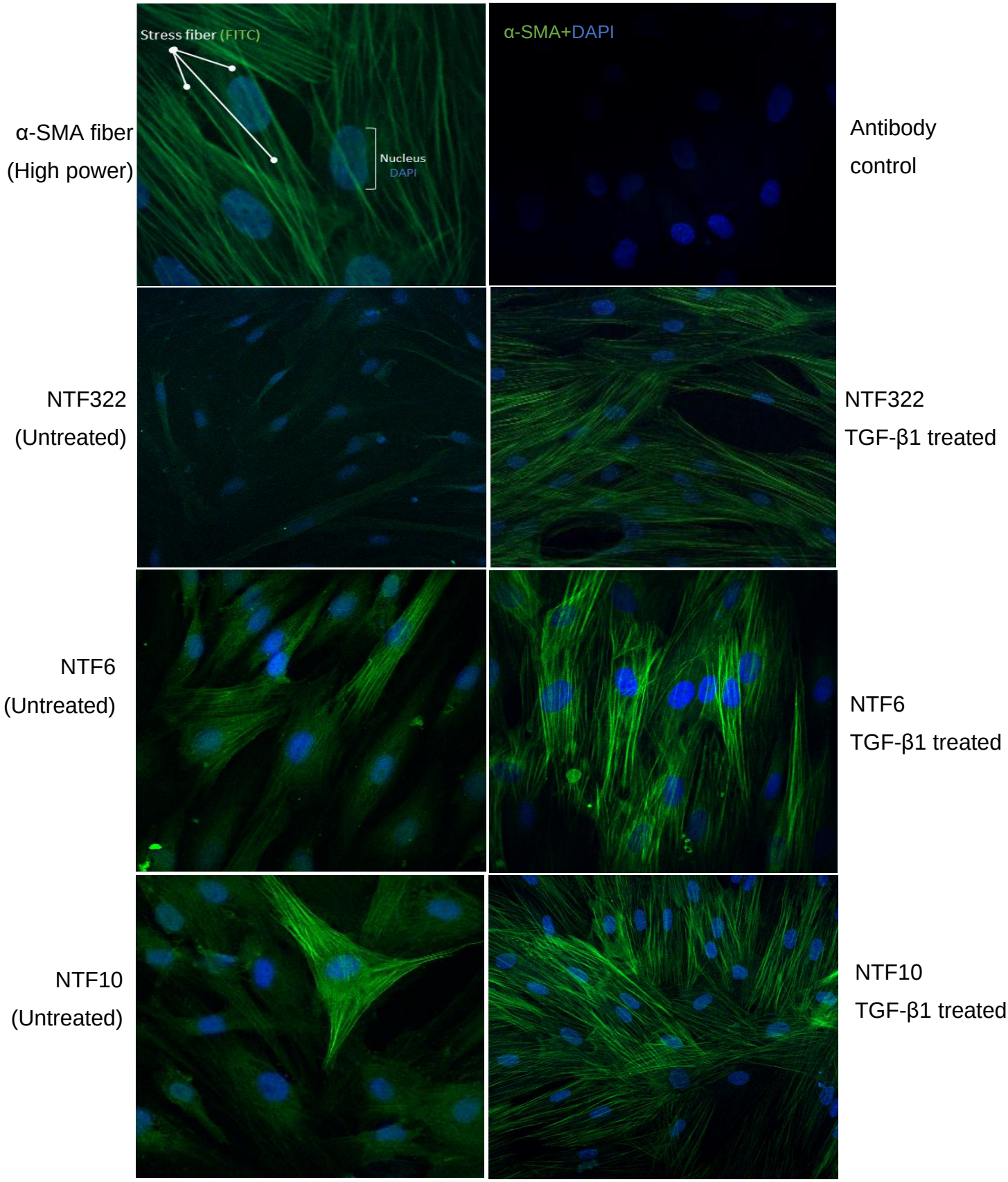
Stress fiber (FITC)
Nucleus
DAPI
α-SMA+DAPI
α-SMA fiber
(High power)
Antibody
control
NTF322
(Untreated)
NTF322
TGF-β1 treated
NTF6
(Untreated)
NTF6
TGF-β1 treated
NTF10
(Untreated)
NTF10
TGF-β1 treated

(A)

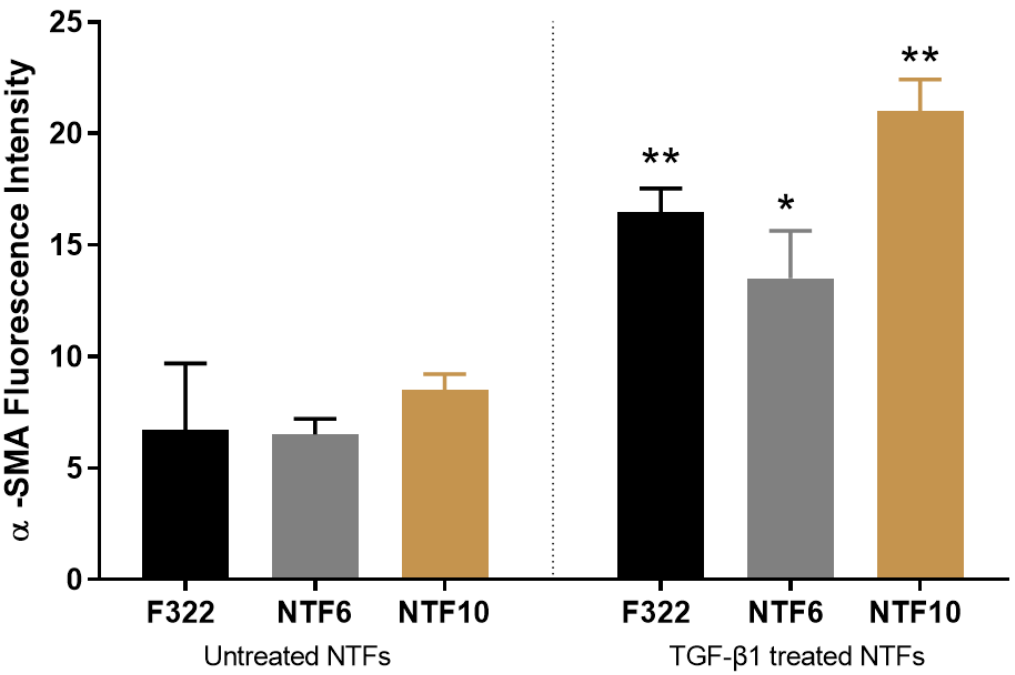

(B)

Figure 4.4: α-SMA fibre formation in NTFs in response to TGF-β1 stimulation. **(A)** Representative photomicrographs demonstrated α-SMA basal and induced expression in OPSCC NTFs. Top panel represent SMA expression (high power) in NTF6. NTF322, NTF6, and NTF10. Cells were stimulated with 5ng/ml TGF-β1 for 48 h then stained with Anti-α-SMA FITC-conjugated antibody (1:100). The slide was then mounted on a microscope coverslip using a DAPI containing mounting medium. High-power image clarifying α-SMA structure within the cell. (Magnification 60x). Fluorescent images were taken using a Zeiss 880 Airy-Scan confocal microscope (Carl Zeiss) at 40x magnification. **(B)** Quantification for detected α-SMA fibres by image quantification was performed using Fiji-ImageJ. The negative control for each cell line was processed. Statistical analysis was performed using Student's *t*-test, and statistical significance is shown on the figure by *p<0.05. Error bars = SD for (N=3, n=3).

4.4.1.5 Potential alteration in NTFs' secretory profile upon TGF-β1 stimulation

We performed IL-6 ELISA analysis to evaluate the changes in the secretory profile of stimulated NTF322, NTF6 and NTF10 following TGF-β1 incubation for 24h, 48h and 72h. NTF322 revealed a time-dependent increase in IL-6 production in both treated and untreated cells that peaked at 72 h (2.5 ± 1.4 pg/ml and 2.8 ± 0.8 pg/ml, respectively). By comparison to its counterpart, NTF322 showed no statistically significant difference.

NTF6 and NTF10 showed the highest amount of IL-6 at 48h (6.9 ± 1.2 pg/ml and 4.7 ± 0.05 pg/ml, respectively). NTF6 demonstrated a significant elevation in IL-6 when compared to controls at 48 h and 72 h time points ($p<0.05$), while NTF10 displayed a significant difference in IL6 expression at 48 h only ($p<0.05$). Variation in IL-6 amount production indicated the heterogeneity among NTFs cultures in response to TGF-β1 stimulation.

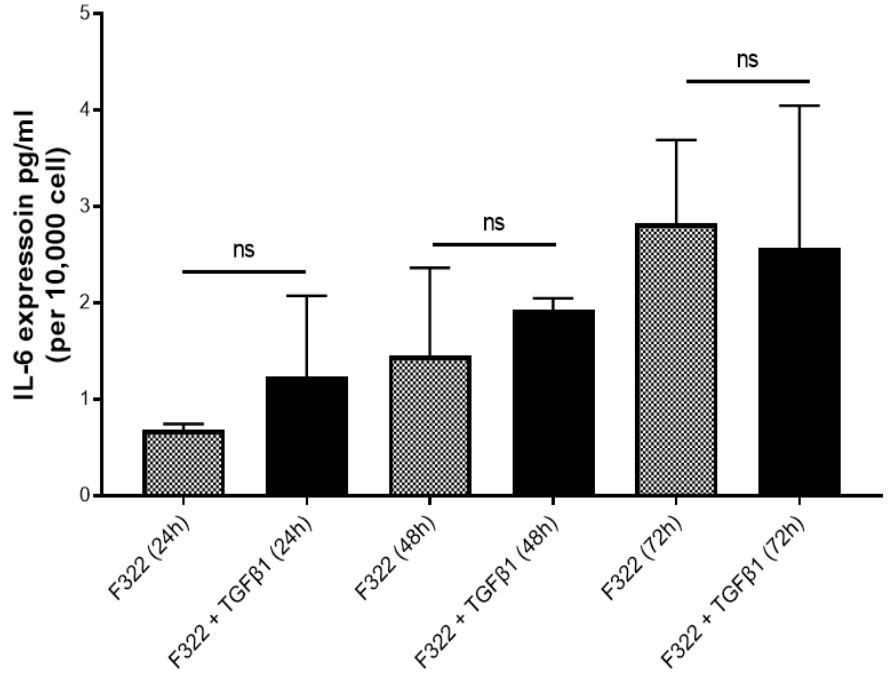
IL-6 expressoin pg/ml
(per 10,000 cell)
5
4
3
2
1
0
ns
ns
ns
F322 (24h)
F322 + TGFβ1 (24h)
F322 (48h)
F322 + TGFβ1 (48h)
F322 (72h)
F322 + TGFβ1 (72h)

(A)

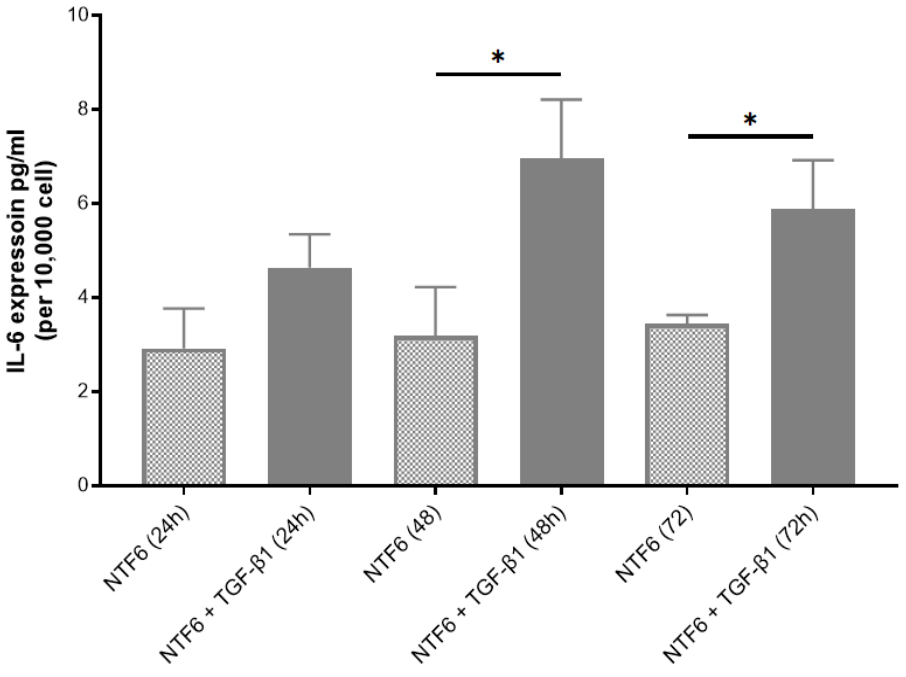
IL-6 expressoin pg/ml
(per 10,000 cell)
10
8
6
4
2
0
*
*
NTF6 (24h)
NTF6 + TGF-β1 (24h)
NTF6 (48)
NTF6 + TGF-β1 (48h)
NTF6 (72)
NTF6 + TGF-β1 (72h)

(B)

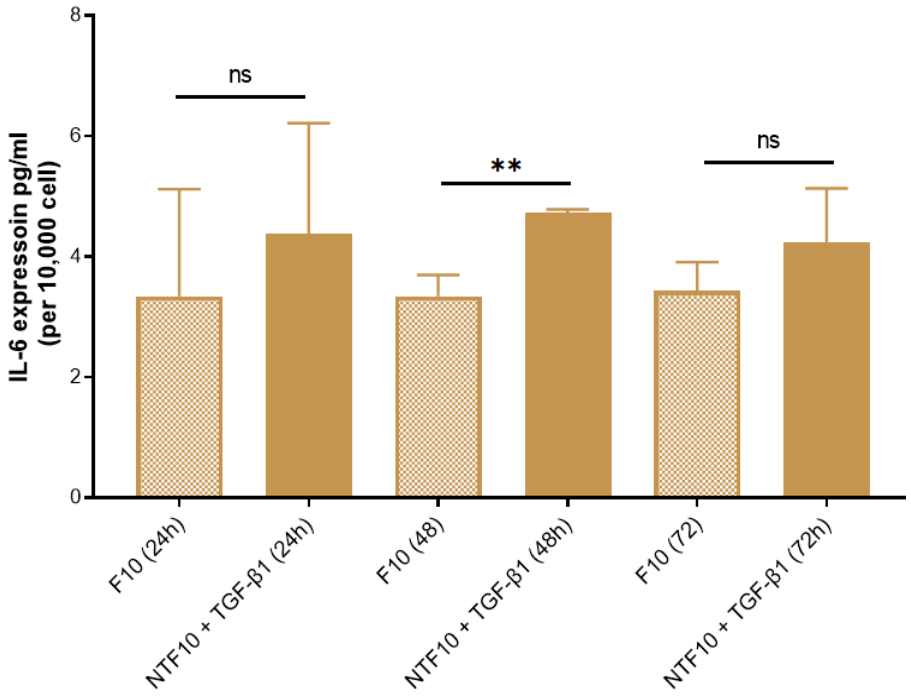

(C)

Figure 4.5: Variation in IL-6 upregulation in NTFs following TGF-β1 stimulation. NTF 322, NTF 6, and NTF 10 were treated with 5 ng/ml TGF-β1 for 24 h, 48 h, and 72 h after being starved for the serum for 24 h. The media was collected and subjected to IL6 ELISA analysis. Untreated cells were included as a negative control. **(A)** IL-6 ELISA analysis for NTF322. **(B)** IL-6 ELISA analysis for NTF6. **(C)** IL-6 ELISA analysis for NTF10. Y-axis denotes standardised IL-6 concentration in pg/ml. Dot bars denote the untreated fibroblasts. IL-6 concentrations were optimised according to a fibroblast density of 10,000 cells. Statistical analysis was performed using Student's *t*-test, and statistical significance is shown on the figure by *p<0.05. Error bars = SD for (N=3, n=3).

4.4.2 Establishment of a senescent-CAF model using NTFs

Fibroblasts within the tumour microenvironment undergo phenotypic changes as a result of cellular stress and ageing which affect the growth and proliferation of the cells. Senescent fibroblasts adopt a specific phenotypic state which is characterised by growth arresting and metabolic active secretome. These cellular alterations are evident by an upregulation in CDK inhibitors and changes in the expression profile that is known by the senescence-associated secretory phenotype (SASP). IL-6 is considered a canonical inflammatory factor among SASP (Naugler and Karin, 2008). An increase in β-gal enzyme activity also is considered a hallmark of senescence.

In this section, we started by determining the senescence status of NTF322, NTF6 and NTF10 at the basal level, followed by premature senescence induction using DNA damaging agent (H_2O_2) and following the previously optimised protocol from our lab in NOFs (Kabir *et al.*, 2016). NTFs were incubated with a single sublethal dose of H_2O_2 (500mM) for 2 h, then maintained for 14 days with subculture at day 8. During this time, cells were incubated with normal growth media. On the last day, SA-β-gal assay was used to determine the percentage of the induced senescent cells. Trypan blue stain was used to ensure cells' vitality at the end of the experiment.

Notably, compared with untreated NTFs under the light microscope, H_2O_2-treated cultures demonstrated an alteration in cell morphology (Figure 4.6). NTF322 treated cells showed a larger, bulbous appearance with dark, prominent cytoplasm. NTF6-treated cells appeared more flattened with poorly defined edges and NTF10 cells displayed more heterogenicity in shape with more granular cytoplasm. Trypan blue percentages were negligible in treated NTFs cultures, indicating cell vitality upon H_2O_2 treatment. NTF322 (5% ± 0.5), NTF6 (3% ± 1) and NTF10 (6.3%± 0.5) (mean ± SD).

4.4.2.1 SA-β-gal positivity in PIS

At basal levels, NTFs showed low percentages of SA-β-gal stained cells. NTF322: 2.3% ± 0.21, NTF6: 3.2% ± 0.14 and NTF10: 3.7% ± 0.14 (mean ± SD). Following H_2O_2 treatment, the percentage of SA-β-gal positivity increased dramatically in all NTFs cultures. NTF322 (59% ± 4.2) (p<0.01), NTF6 (65.6 ± 3.7) (p<0.001), and NTF10 (73 ± 1.4) (p<0.001) (Figure 4.6).

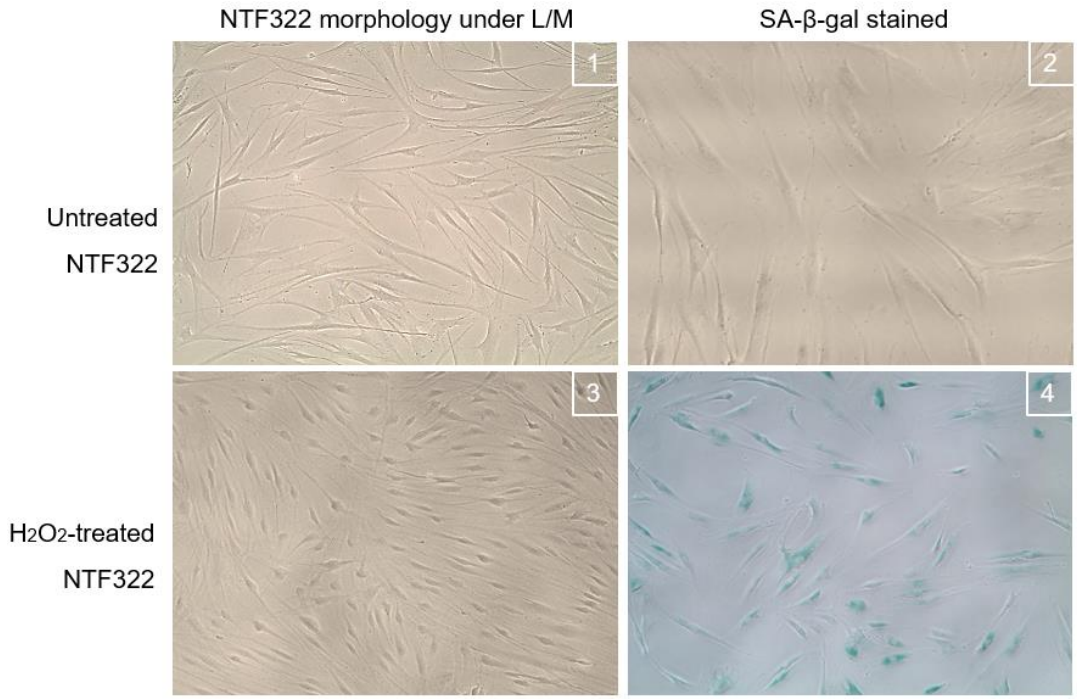
NTF322 morphology under L/M
SA-β-gal stained
Untreated
NTF322
H2O2-treated
NTF322
1
2
3
4

(A)

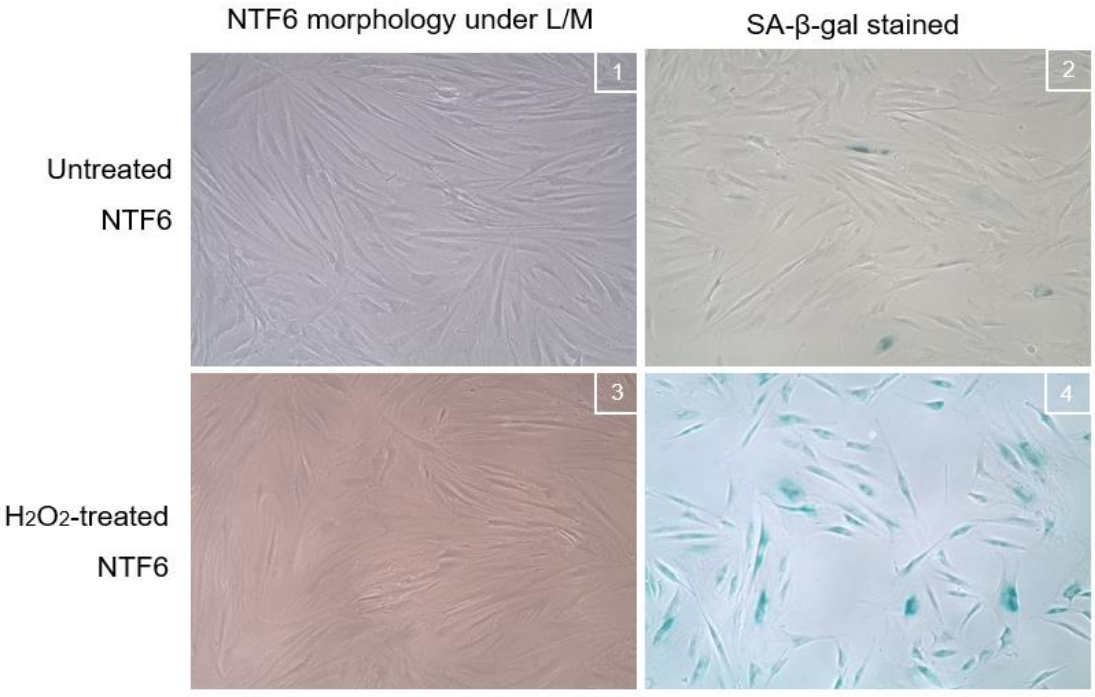
NTF6 morphology under L/M
SA-β-gal stained
Untreated
NTF6
H2O2-treated
NTF6
1
2
3
4

(B)

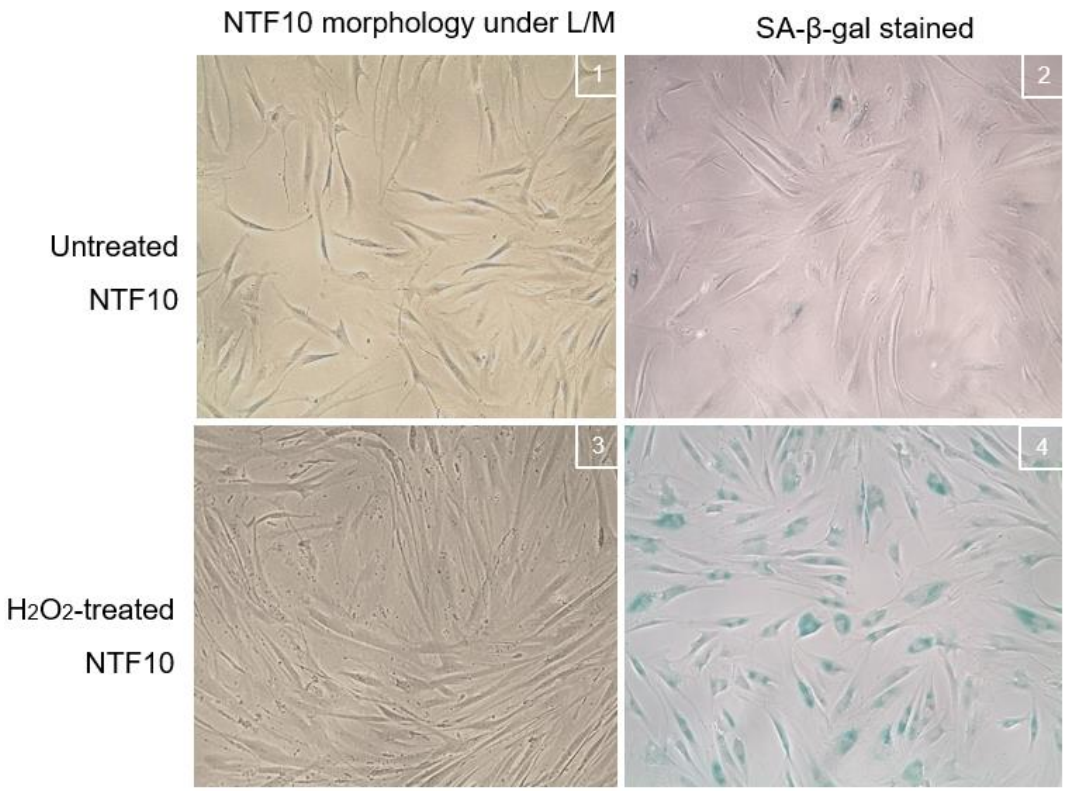
NTF10 morphology under L/M
SA-β-gal stained
Untreated NTF10
H2O2-treated NTF10
1
2
3
4

(C)

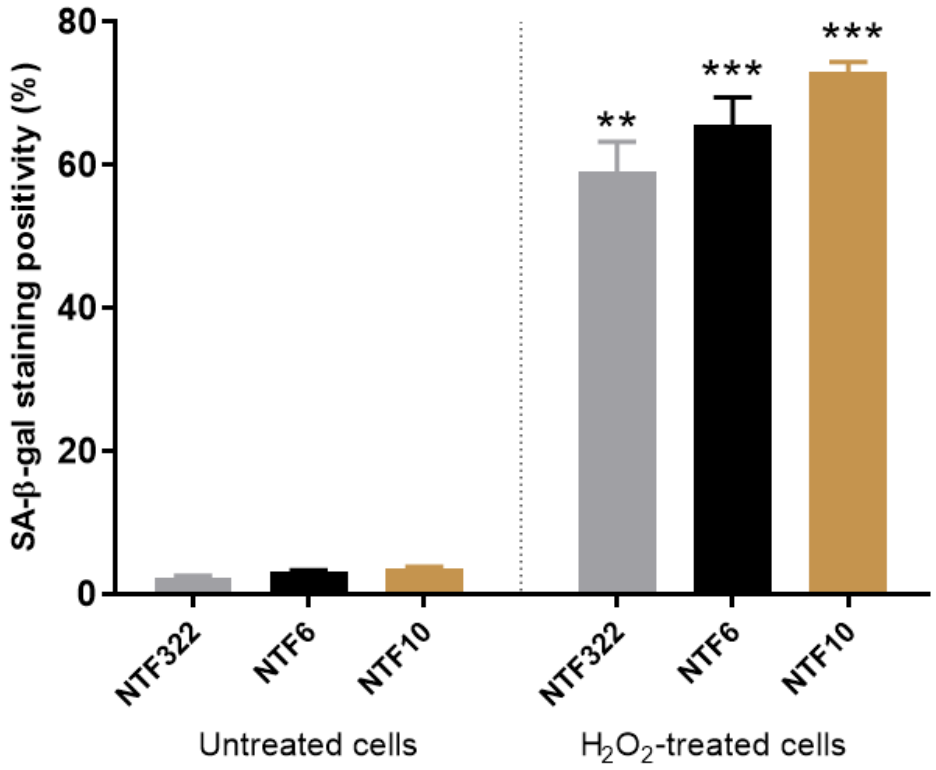

(D)

Figure 4.6: Senescence status in NTFs. Images representing SA-β-gal stain at basal level and after H_2O_2 treatment in **(A)** NTF322, **(B)** NTF6, **(C)** NTF10 cells. Image **1**, illustration for cell morphology at normal conditions. Image **2**, SA-β-gal stain at normal conditions. Image **3**, cell morphology upon H_2O_2 treatment. Image **4**, SA-β-gal stain upon H_2O_2 treatment. Magnifications 10x and 20x. **(D)** Quantification of SA-β-gal stain. The proportion of stained cells (blue precipitate) in 3 random fields (magnification 20x and 40x). Statistical analysis was performed using Student's *t*-test, and statistical significance is shown on the figure by **p<0.01, ***p<0.001. Error bars = SD for (N=3, n=3).

4.4.2.2 Overexpression of CDK inhibitors in PIS

p16 and p21 overexpression have been utilised widely as biomarkers in the detection of senescent cells *in vitro* and *in vivo* (Kabir *et al.*, 2016; Prieto, Graves and Baker, 2020). Their expression is linked to activation of growth arrest mediated by pRB and p53, the major tumour-suppressor pathways. H_2O_2-treated NTFs demonstrated marked upregulation in p16 and p21 (Figure 4.7).

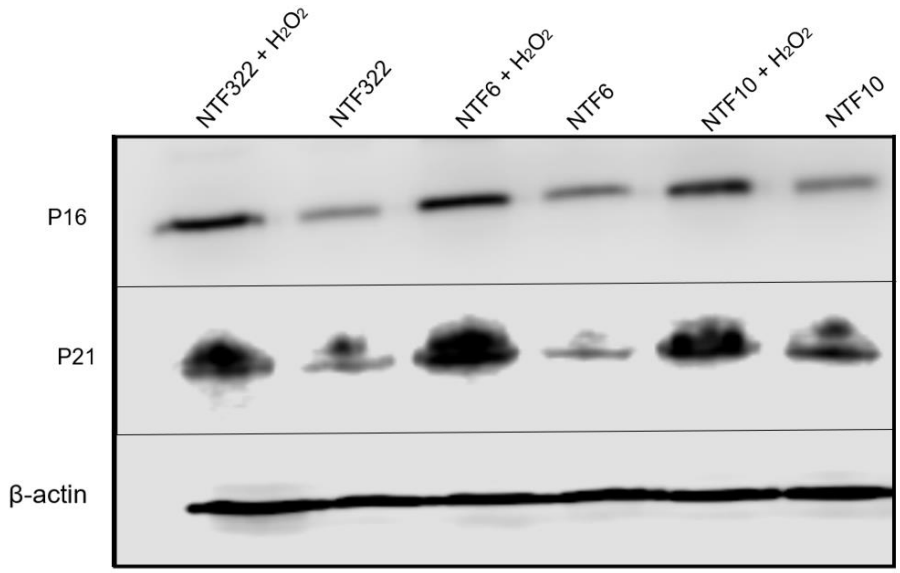

Figure 4.7: Western blot analysis of p21 and p16. NTF322, NTF6 and NTF10 were treated with a single dose of 500mM H_2O_2 for 2 h, then the culture was maintained for 14 days. Protein expression of 20 µg of whole cell lysate per lane using anti-p21 antibody or anti-p16 antibody. H_2O_2 treated NTFs expressed marked levels of p16 and p21.

4.4.2.3 Upregulation of IL-6 secretion in PIS

The most prominent cytokine of the SASP is IL-6, which has been associated with induced senescence in DNA damaging and oncogenic stress conditions. We quantified IL-6 expression in NTFs at basal level and after H_2O_2 induction using ELISA analysis (Figure 4.8). All H_2O_2-treated NTFs showed an upregulation in IL-6 production. NTF6 and NTF10 showed a significant increase compared to controls (23.4 ± 1.1 and 17.7 ± 1.3 respectively: $p<0.01$). However, NTF322 showed insignificant elevation statistically (5.1 ± 1.4: $p>0.05$).

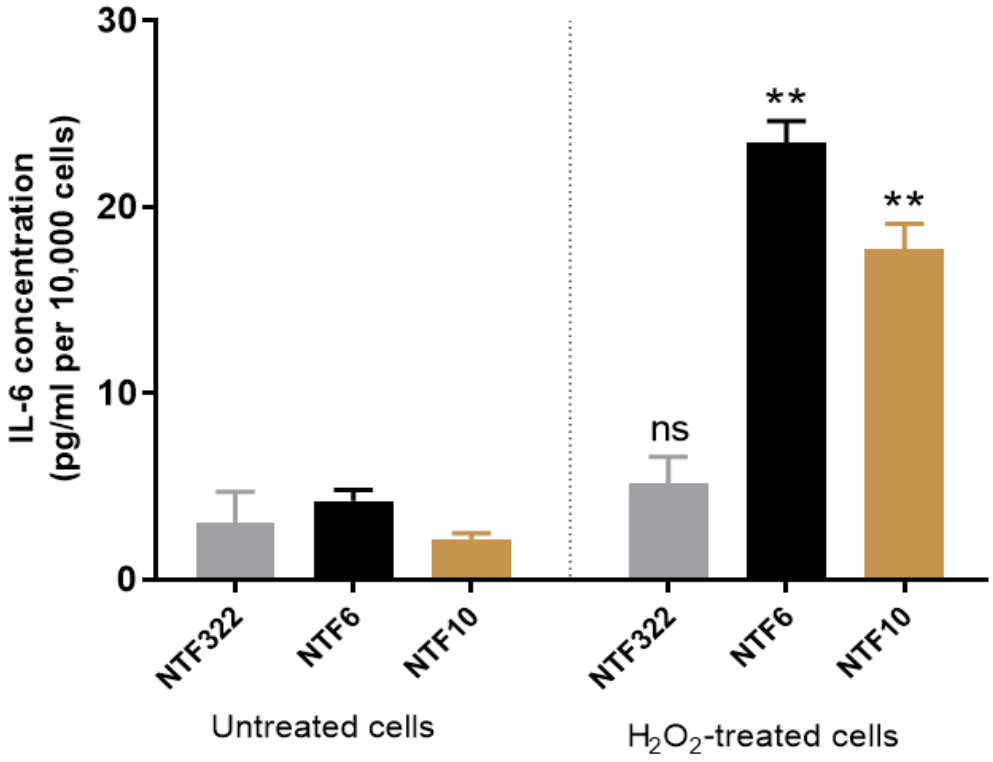

Figure 4.8: Upregulation in IL6 production in NTFs following H_2O_2 exposure. NTF322, NTF6 and NTF10 were treated with a single dose of 500mM H_2O_2 for 2 h, then the culture was maintained for 14 days. The media was collected and subjected to IL6 ELISA analysis. Untreated cells were included for the comparison. All treated NTFs showed an increase in IL-6 production. Samples number (n=6), Y-axis denotes standardised IL-6 concentration in Pg per ml. IL-6 concentrations were optimised according to fibroblasts density at 10,000 cells. Statistical analysis was performed using Student's *t*-test, and statistical significance is shown on the figure by **p<0.01, ***p<0.001. Error bars = SD for (N=3, n=3).

4.4.3 Establishment of primary OPSCC CAF cultures

To isolate stromal CAFs in the microenvironment of OPSCC, fragments of tonsillar tissue from tonsil HPV-positive carcinomas were subjected to collagenase I digestion. After 1 week of the isolation procedure, CAF1 and CAF2 were seen outgrowing and remained attached to the culture plate. After establishing seeding and working stock of isolated CAFs, cultures were characterised according to their morphology, gene signature, and secretory profile. We tried to isolate further CAFs from fragments of the posterior third of the tongue tissue, however, the sample was small in size with little stromal portion.

4.4.3.1 Microscopic appearance of OPSCC CAFs

Under the light microscope, CAF1 showed a mixture of long, spindle-shaped and flat irregular cells which varied in size. We noticed CAF1 tended to grow separately in random patterns, whereas CAF2 appeared more crowded and overlapped with larger volume and irregular morphology. At higher power examination, most CAF1 cells had a granular cytoplasm and enlarged nuclei with more than nucleolus. These microscopic features are distinct from NTFs which were included in this study. NTFs tend to have a smaller uniform appearance and form characteristic parallel arrays at the confluence (Figure 4.9).

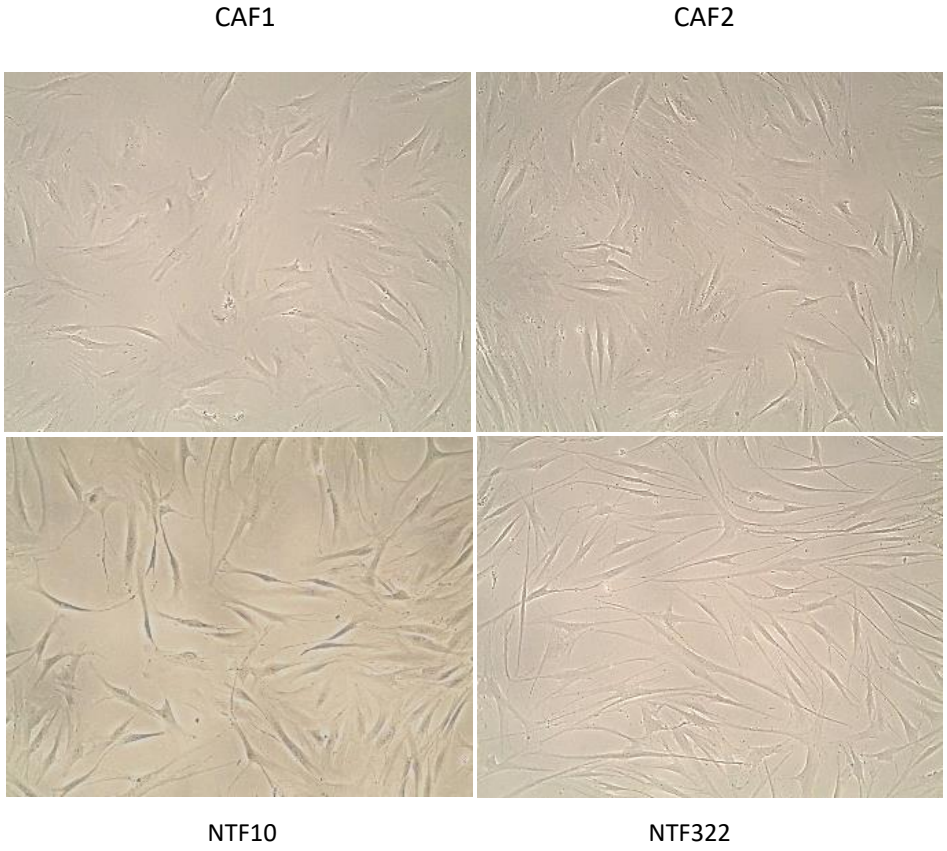

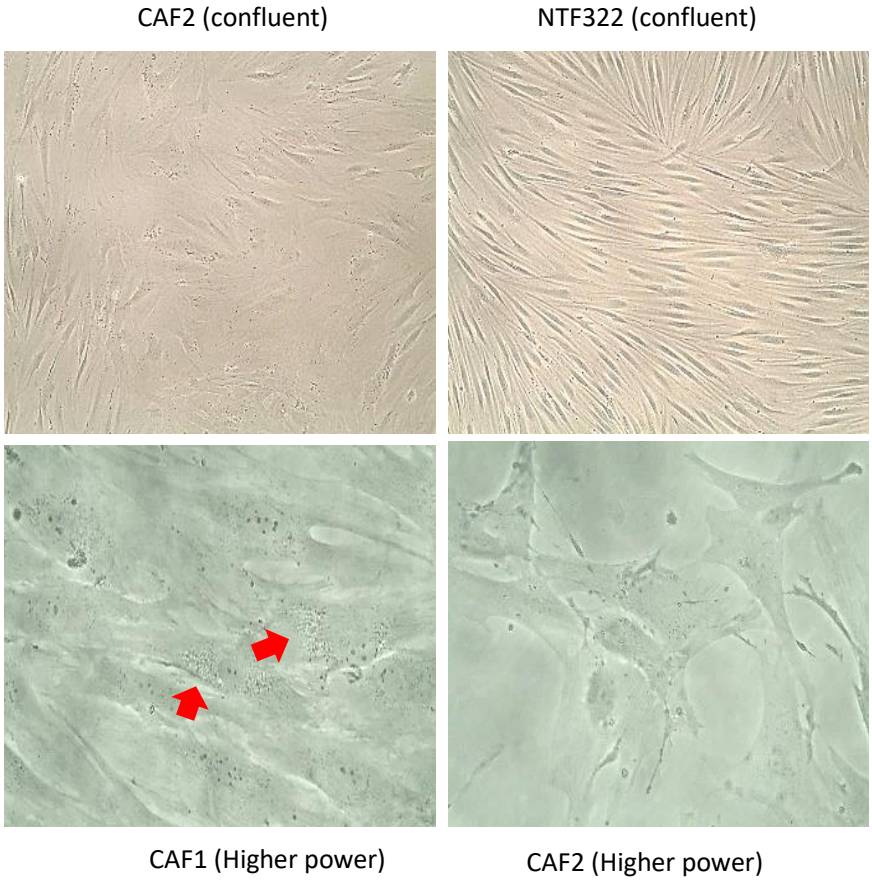

Figure 4.9: Microscopic appearance for OPSCC CAFs and NTFs. Arrows demonstrate the vacuolated cytoplasm. Representative photos were taken with an Olympus BX51 optical microscope at 10X and 40X magnifications.

4.4.3.2 Primary CAF culture purification

Purification of isolated CAFs cultures was confirmed by excluding other cell contamination. CAF1 and CAF2 were harvested, and total RNA was extracted and quantified. cDNA was constructed at volume 20 µl using 400ng RNA. qRT-PCR analysis was carried out for the target genes utilising β2m, the housekeeping gene, for result normalisation. NTF6 was included for the comparison.

Epithelial cells were excluded by assessing the gene expression of Cytokeratin 6 (CK6). It is one of the epithelial cell biomarkers. Keratins are dense networks of intermediate filament proteins distributed throughout the cytoplasm of epithelial cells. Normal oral keratinocyte 8 (NOK8) was included as a positive control for the CK6 expression. qRT-PCR analysis revealed marked expression of CK6 in NOK8 (2.89 ± 0.25), while CAF1 and CAF2 showed a minimal amount of CK6 expression (0.02 ± 0.03) and (0.10 ± 0.004)

(mean± SD), respectively. The difference was statistically significant (p<0.001), indicating high CAF cultures purity without epithelial cell contamination (Figure 4.10).

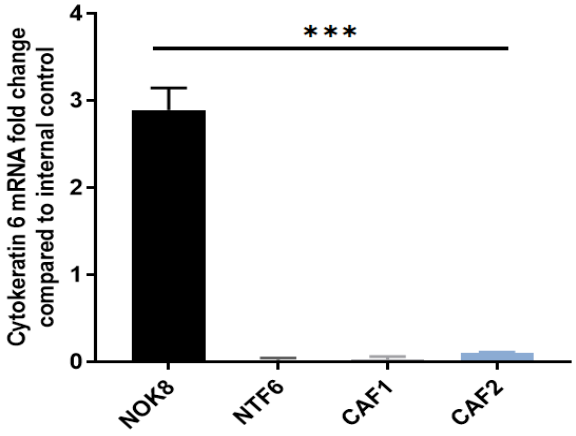

Figure 4.10: OPSCC CAFs clear of epithelial cell contamination. CAF1 and CAF2 were collected, and total RNA was extracted and quantified. qRT-PCR was performed with the constructed cDNA to amplify the CK6 gene. β2m was utilised for result normalisation. NOK8 represents the positive control and NTF6 represents the negative control. CAFs culture exhibited negligible expression of CK6 suggesting cultural purity. Statistical significance is shown on the figure by ***p<0.001, using one-way ANOVA. Error bars = SD of (N=2, n=3).

Immune cell contamination was excluded by assessing the gene expressions of HLA-DR (Human leukocyte antigen–DR isotype). HLA-DR is a cell surface receptor that presents at the human leukocyte which is expressed at high levels on professional antigen-presenting cells, and T lymphocytes in some autoimmune diseases (Viallard *et al.*, 2001). Monocyte-derived macrophage (MDM) was included as a positive control. MDM demonstrated relatively high gene expression (0.07 ± 0.01) compared to CAF1, CAF2, and NTF6 that showed no expression of HLA-DR. (0.000 ± 0.000) (mean± SD) (Figure 4.11).

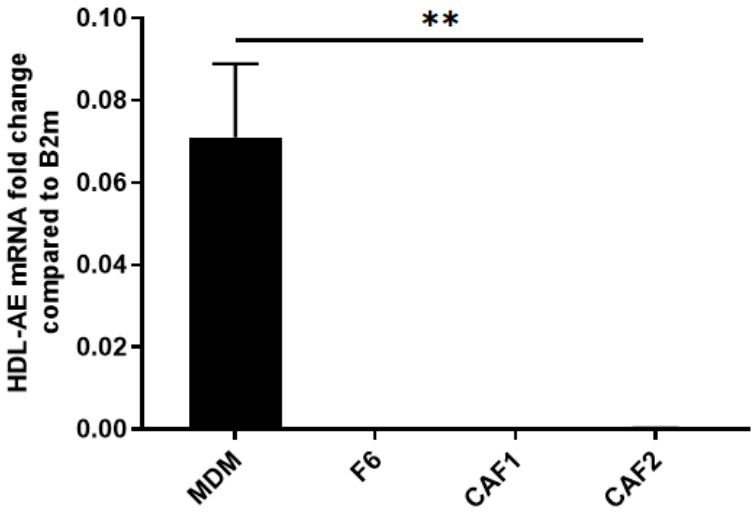

Figure 4.11: OPSCC CAFs clear of immune cell contamination. CAF1 and CAF2 were collected, and total RNA was extracted and quantified. qRT-PCR was performed with the constructed cDNA to amplify the HLA-DR gene. β2m was utilised for result normalisation. MDM represents positive control. CAFs culture exhibited a negligible expression of HLA-DR. Statistical significance is shown on the figure by ***p<0.001, using one-way ANOVA. Error bars = SD of (N=2, n=3).

Endothelial cells contamination was excluded by assessing CD31 expression which is known as (Platelet endothelial cell adhesion molecule, PECAM-1). It is found at endothelial cell intercellular junctions, also detected on the surface of platelets, macrophages and lymphocytes (van Mourik *et al.*, 1985). Human Dermal Microvascular Endothelial Cells (HDMEC) was included as a positive control. HDMEC demonstrated relatively high gene expression (0.6 ± 0.12) compared to CAF1, CAF2, and NTF6 that showed no expression of CD31. (0.000 ± 0.000) (mean± SD) (Figure 4.12).

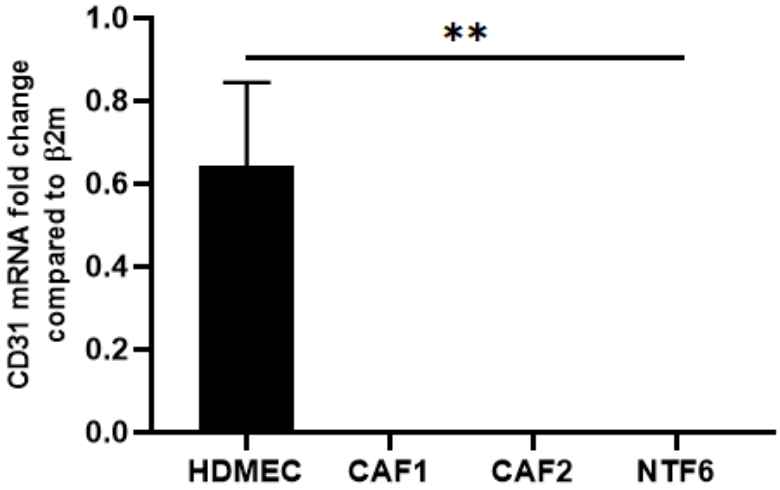

Figure 4.12: OPSCC CAFs clear of endothelial cell contamination. CAF1 and CAF2 were collected, and total RNA was extracted and quantified. qRT-PCR was performed with the constructed cDNA to amplify the CD31 gene. β2m was utilised for result normalisation. HDMEC represents positive control. CAFs culture exhibited a negligible expression of HDMEC. Statistical significance is shown on the figure by ***p<0.001, using one-way ANOVA. Error bars = SD of (N=2, n=3).

4.4.3.3 CAF biomarker expression

CAF cultures were further explored for molecular characterisation to confirm the reactive nature of the CAFs and confirm their identity. A panel of biomarkers including α-SMA, FSP-1, FAP-α, and PDGFRα were assessed at gene and protein levels.

4.4.3.3.1 α-SMA expression in OPSCC CAFs

The basal level of expression in CAF1 and CAF2 was investigated using qRT-PCR and immunofluorescence assay. CAF2 showed a higher expression α-SMA gene (2.1 ± 0.5 fold) compared to CAF1 (0.4 ± 0.04) fold (mean± SD) (Figure 4.5). This pattern of expression was consistent with what we observed in α-SMA immunofluorescence assessment. The tested cells revealed a heterogeneous expression pattern of α-SMA stain, CAF2 displayed brighter green discrete fibers along the cell axes, whereas that was hardly detected in CAF1 using the same cell number in the examined field (Figure 4.13).

To generate an *in vitro* model of myofibroblastic CAF phenotype, α-SMA expression was induced further in CAFs using a single dose of TGF-β1 (5 ng/ml), following the previously optimised protocol from our lab (Abidin, 2017; Melling *et al.*, 2018). Cells were serum-starved then incubated with TGF-β1 for 48 h. TGF-β1 treatment resulted in a significant increase in α-SMA expression in all treated cells compared with their untreated counterpart (p<0.05). CAF1 showed a significant increase in α-SMA transcript expression of 4.5 ± 0.4 fold compared to β2m. CAF2 demonstrated a dramatic response to TGF-β1 that elevated α-SMA expression to 34.7 ± 12 fold compared to β2m (Figure 4.5). α-SMA staining was also evident and well-formed as cytoskeletal fibres were seen throughout the whole treated cell (Figure 4.14).

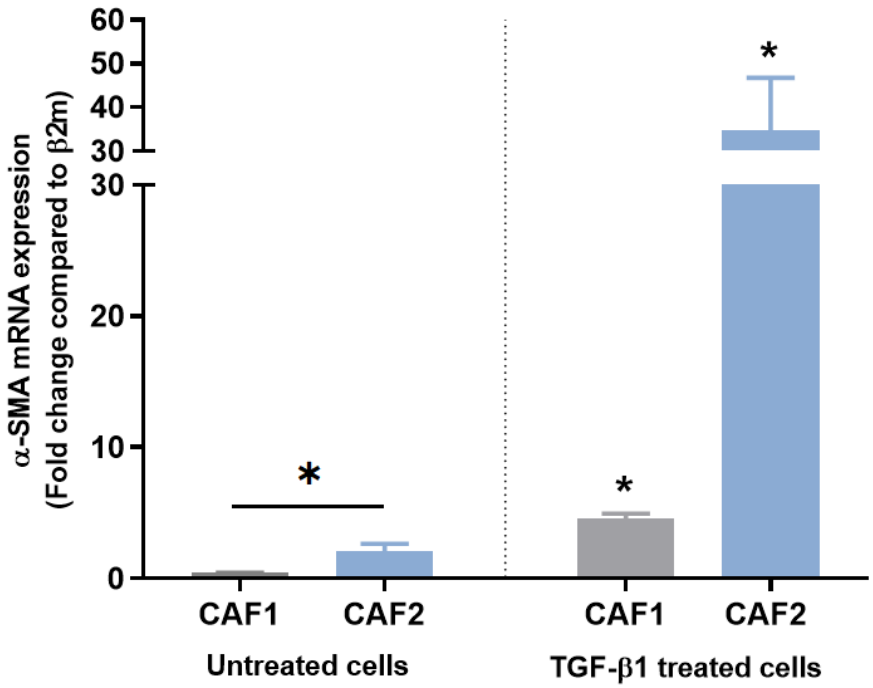

Figure 4.13: α-SMA mRNA expression in OPSCC CAFs following TGFβ1 treatment. Assessment of basal αSMA mRNA (untreated cells) revealed significant expression in CAF2 compared CAF1. CAFs (250,000 cells/ well) were seeded in 6 well plates, starved for serum (24 h), then treated with TGFβ1 (5 ng/ml) for 24h. A significant upregulation in αSMA mRNA was seen in all tested cells (*=p<0.05), with the most striking increase in CAF2. Error bars= SD (N=3, n=3). Student's *t*-test and one-way ANOVA were used for the statistical comparison.

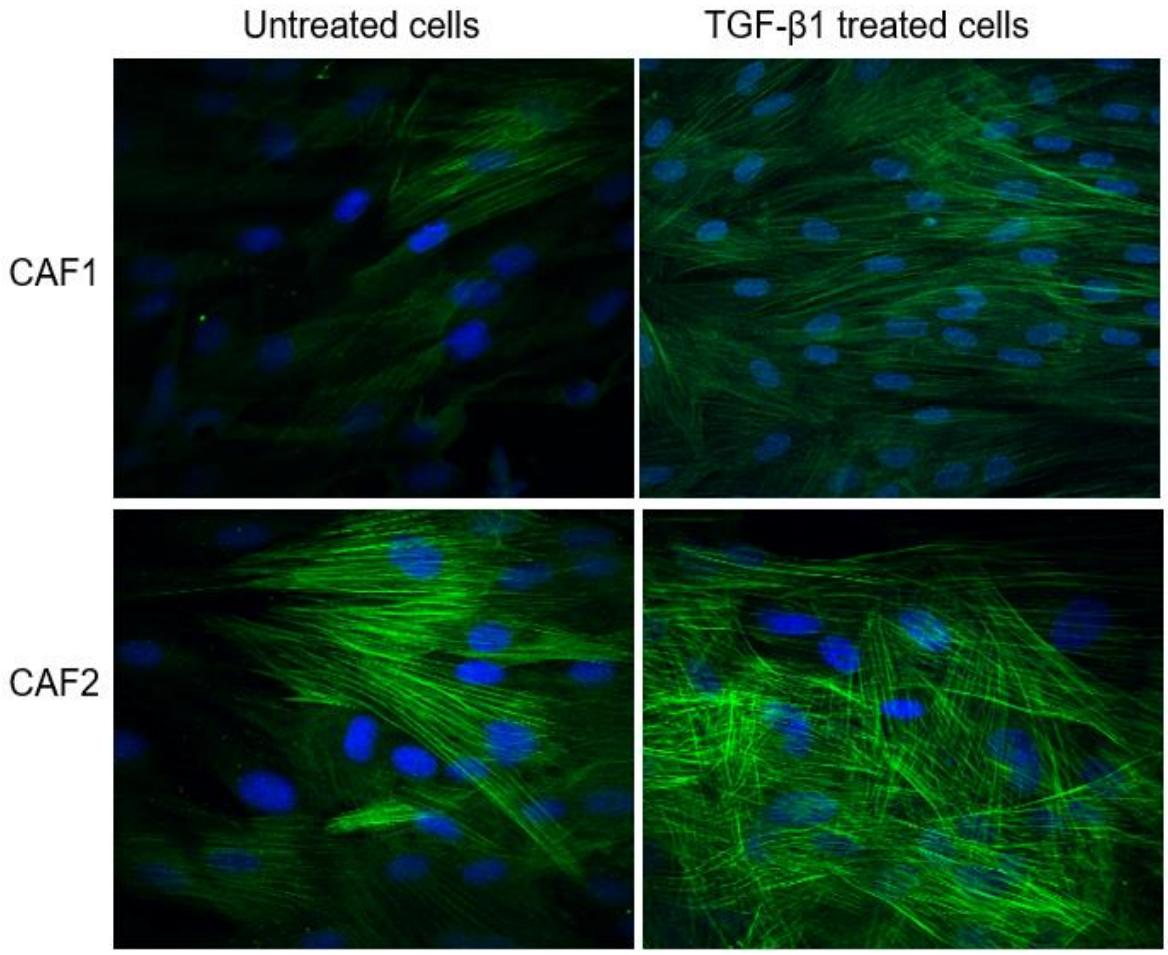

(A)

(B)

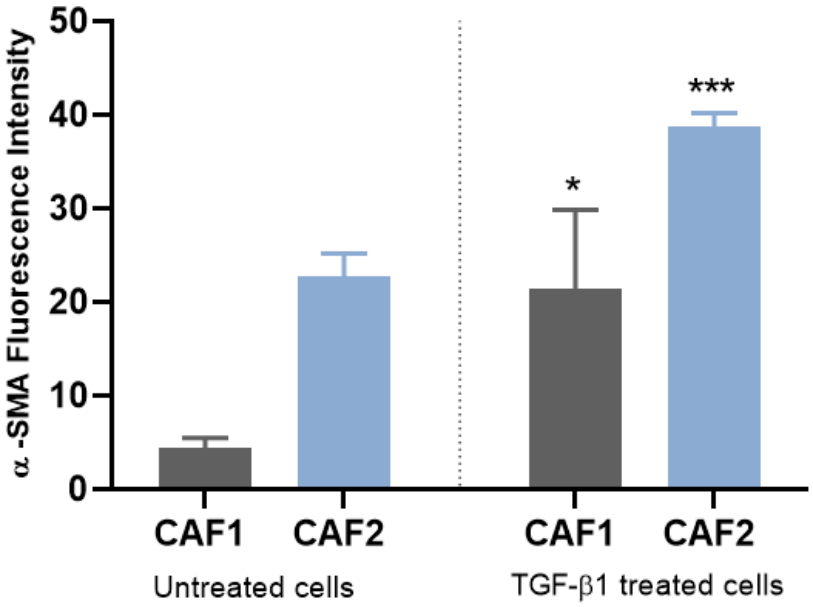

Figure 4.14: α-SMA immunofluorescence expression in OPSCC CAFs. **(A)** Immunofluorescent representative photomicrographs demonstrated α-SMA basal and induced expression in OPSCC CAFs. Cell induction was performed by TGF-β1 (5 ng/ml) incubation (48 h). CAF2 displayed evident basal α-SMA expression. Images were taken using a confocal microscope (Zeiss 880 Airy Scan). Magnification (40X). **(B)** Quantification for detected α-SMA fibers by image quantification was performed using Fiji-ImageJ. Error bar= SD (N=3, n=3).

4.4.3.3.2 FAP-α biomarker expression in OPSCC CAFs

FAP-α (Fibroblast Activation Protein Alpha) is a transmembrane glycoprotein that is expressed by reactive stromal fibroblasts during an injury response, fibrosis and certain types of tumours including 90% epithelial cancers (Servais and Erez, 2013; Berdiel-Acer *et al*., 2014; Kalluri, 2016). In this study, CAF1 and CAF2 showed the highest expression of FAP-α mRNA normalised to β2m, (0.50 ± 0.09) and (0.42 ± 0.04), respectively, while NTF6 expressed the lowest value (0.26 ± 0.09) (mean ± SD) (Figure 4.15 A). This difference was statistically significant compared with CAF1 and with all tested cells ($p<0.05$). FAP-α immunofluorescence staining was observed in all tested cells in a relatively homogenous pattern using a fluorescent-labelled antibody (Figure 4.15 B).

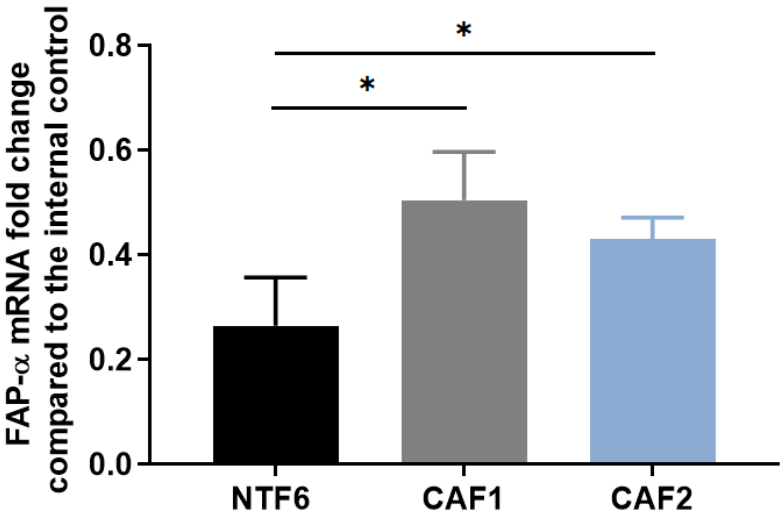

(A)

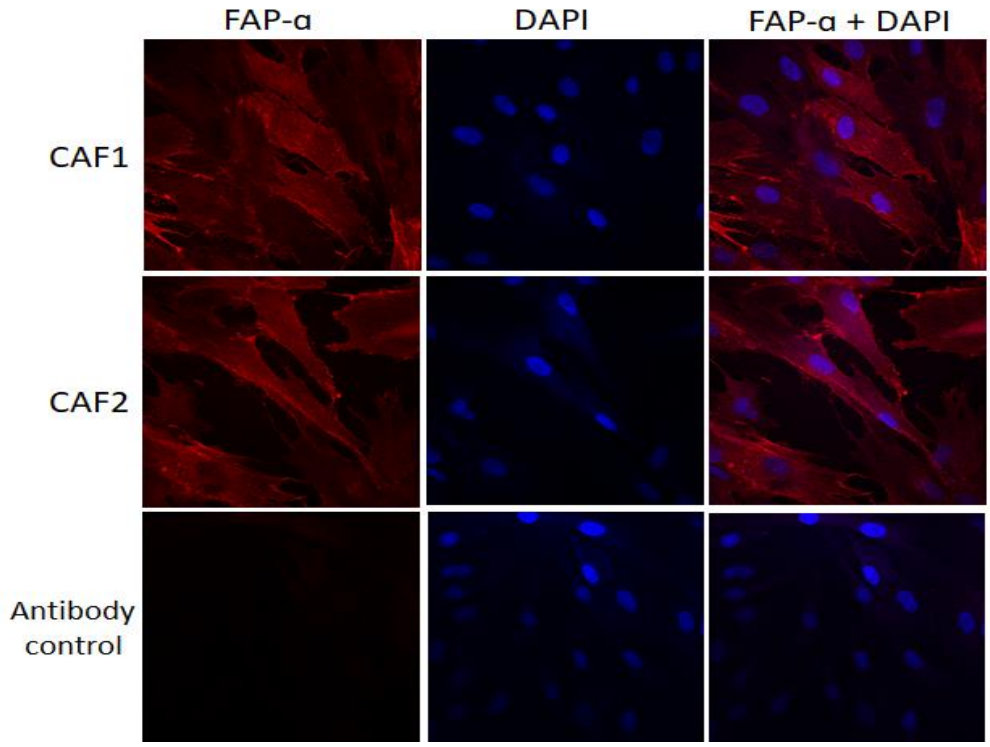

(B)

Figure 4.15: FAP-α expression in OPSCC CAFs. **(A)**, FAP-α mRNA expression in CAF1, CAF2, and NTF6. Error bars= SD (N=2, n=3). CAF1 and CA2 showed significant FAP-α expression compared to NTF6 (*p<0.05). Student's *t*-test and one-way ANOVA were used for the statistical comparison. **(B)**, Immunofluorescence staining of FAP-α, all tested cells exhibited evident homogenous FAP-α protein using (1:100) anti-FAP-α monoclonal antibody. Images were taken using a confocal microscope (Zeiss 880 airy Scan). Magnification (x40).

4.4.3.3.3 PDGFRα biomarker expression in OPSCC CAFs

PDGFRα (platelet-derived growth factor receptor A or α) is a tyrosine-protein kinase that acts as a transmembrane protein receptor and is involved in the regulation of embryonic development, cell proliferation, and chemotaxis (Gotlib and Cools, 2008). It is expressed more widely over the larger fibroblast population than more specific biomarkers such as α-SMA. In this study, CAF2 demonstrated the highest expression of PDGFR1 mRNA (~0.22 fold). CAF1 and NTF6 showed relative expression of 0.13±0.12 fold and 0.12± 0.04 fold, respectively. None of these differences was statistically significant. (Figure 4.16 A). Immunofluorescent staining showed a punctate pattern within the cell cytoplasm, however, as the nuclei also showed antibody positivity there is most likely significant non-specific staining (Figure 4.16 B).

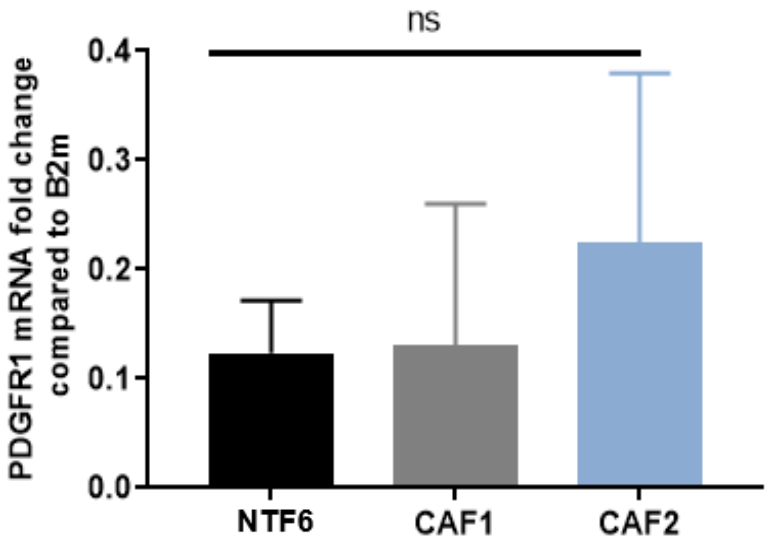

(A)

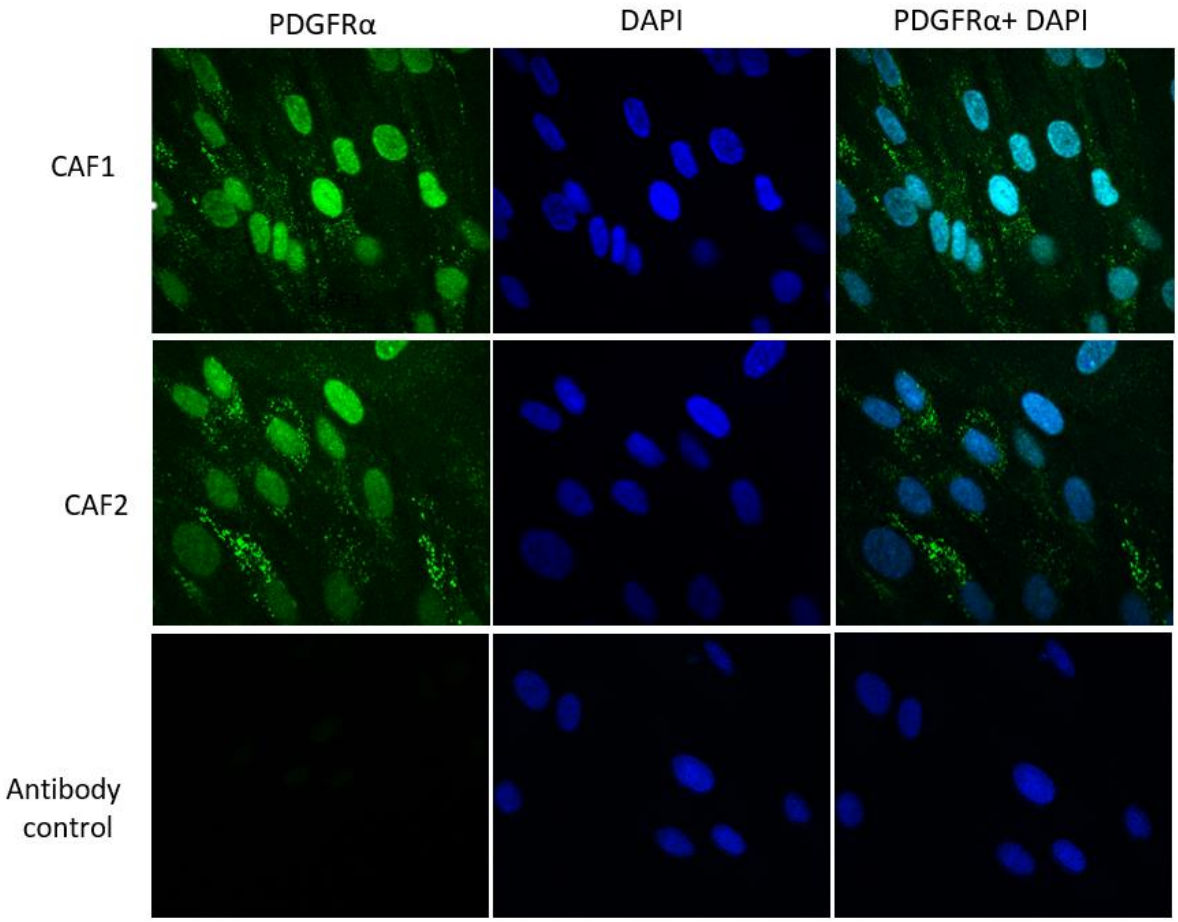

(B)

Figure 4.16: PDGFRA expression in OPSCC CAFs. (A), PDGFRA mRNA expression in CAF1, CAF2, and NTF6. All tested cells showed a comparable level of expression. Student's *t*-test and one-way ANOVA were used for the statistical comparison. Error bars= SD (N=2, n=3). **(B)**, Immunofluorescence staining of PDGFRA. CAF1 and CAF2 showed stained granular structures within their cytoplasm, however, this is most likely a non-specific reaction. Images were taken using a confocal microscope (Zeiss 880 airy Scan). Magnification (x40).

4.4.3.3.4 FSP-1 biomarker expression in OPSCC CAFs

FSP-1 protein, (Fibroblast-specific protein 1) also called S100A4, is a calcium-binding protein localised in the cytoplasm and nucleus of a wide variety of cell types including CAFs. It is involved in cell differentiation and cell cycle progression (Cajone and Sherbet, 1999). In the tumour microenvironment, FSP-1 derived-CAFs are linked to cancer cell invasion and metastasis, and they are considered an important factor in promoting cancer cell growth (Grum-Schwensen *et al.*, 2005; Park, Jung and Koo, 2016). In this study, there was a trend towards higher FSP-1 mRNA levels in CAF1 and CAF2 (0.08 ± 0.06 and 0.09 ± 0.02 fold respectively when compared to β2m), while NTF6 showed the lowest expression (0.04 ± 0.01) (mean ± SD) (Figure 4.17, A). However, there was no statistically significant difference between the tested cells following student's *t*-test and one-way ANOVA test. The immunofluorescent analysis shows widespread expression throughout the cytoplasm and nucleus, with little on the cell membrane, which would be the predicted localisation. Again, it is likely that this pattern of expression is non-specific (Figure 4.17, B), but this could not be improved despite many optimisations.

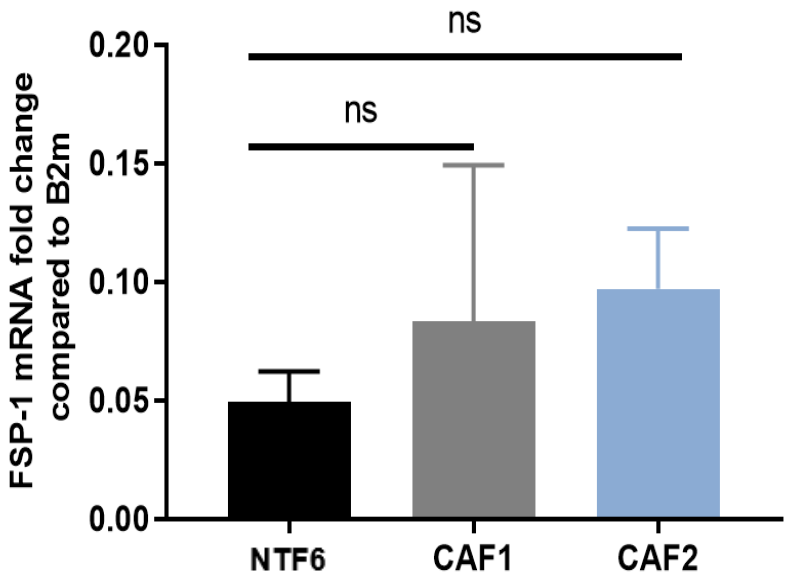

(A)

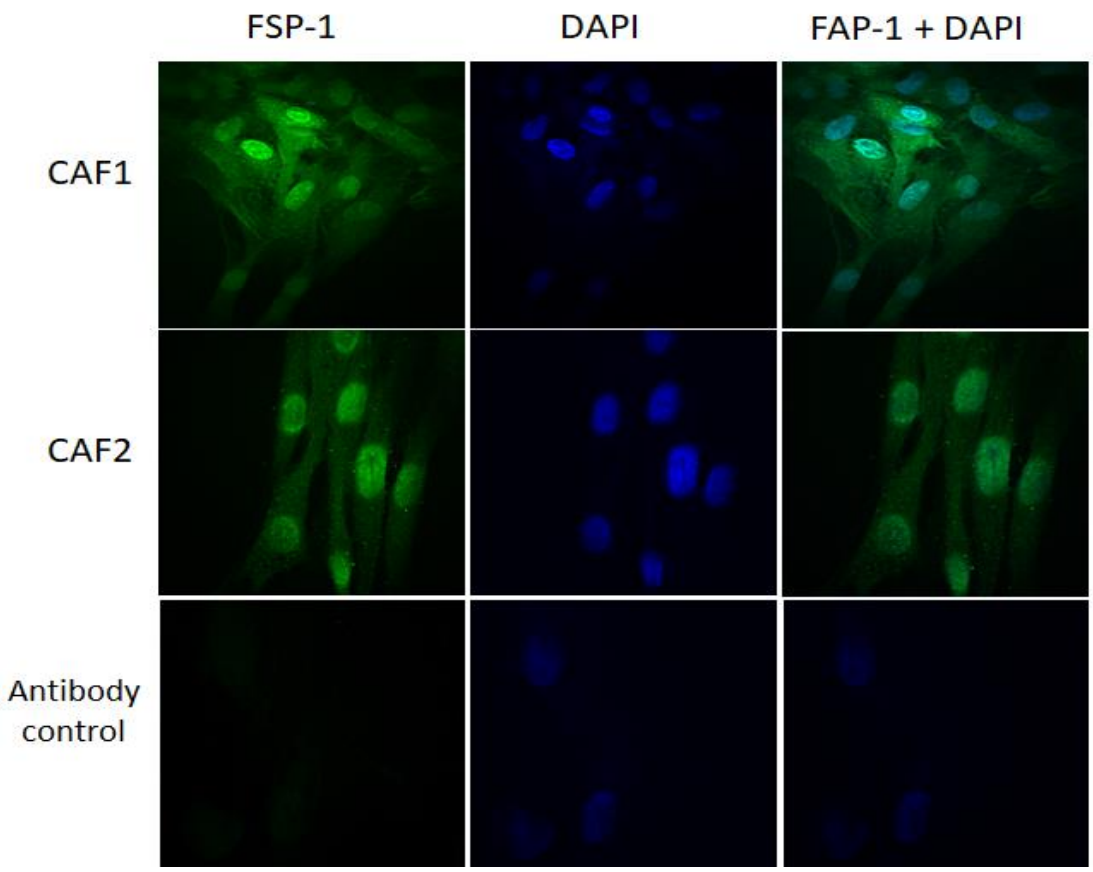

(B)

Figure 4.17: FSP-1 expression in OPSCC CAFs. (A), FSP-1 mRNA expression in CAF1, CAF2, and NTF6. Error bars= SD (N=2, n=3). CAF1 and CA2 showed higher FSP-1 expression compared to NTF6. Student's *t*-test and one-way ANOVA were used for the statistical comparison. **(B)**, Immunofluorescence staining of FSP-1. All tested cells exhibit evident homogenous FAP-α protein cytoplasmic and nuclear expression using (1:100) anti-FSP-1 monoclonal antibody. Images were taken using a confocal microscope (Zeiss 880 airy Scan). Magnification (x40).

4.4.4 Evaluation of senescence in OPSCC CAFs

The heterogeneity in senescence among CAFs populations has been reported in OSCC-derived CAFs (Patel *et al.*, 2018). Herein, we evaluated the senescence status of isolated CAFs by assessing senescence features. CAF primary cultures showed a variable percentage of SA-β-gal positivity. CAF1 populations exhibited (39% ± 1.4) of SA-β-gal stained cells, while only 0.5% ± 0.3 of CAF2 cells stained (Figure 4.18).

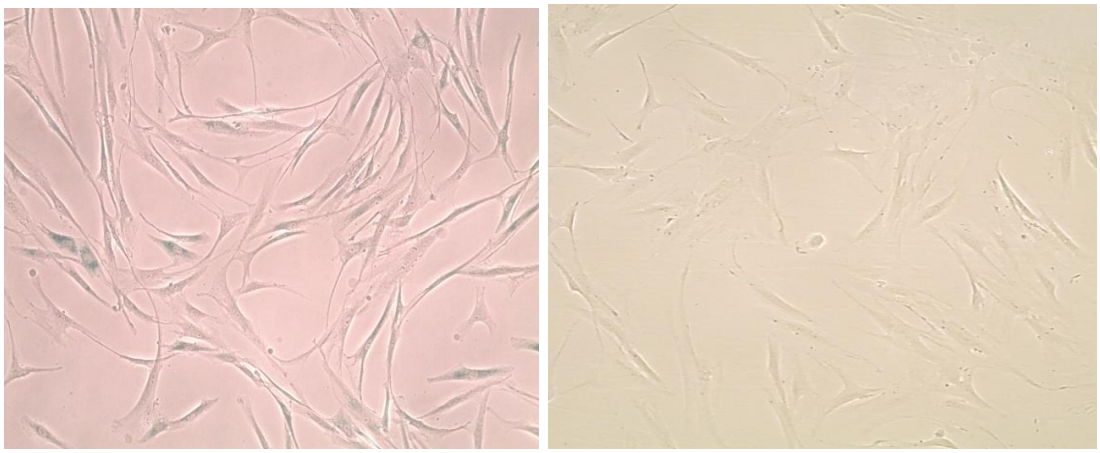

CAF1 CAF2

(A)

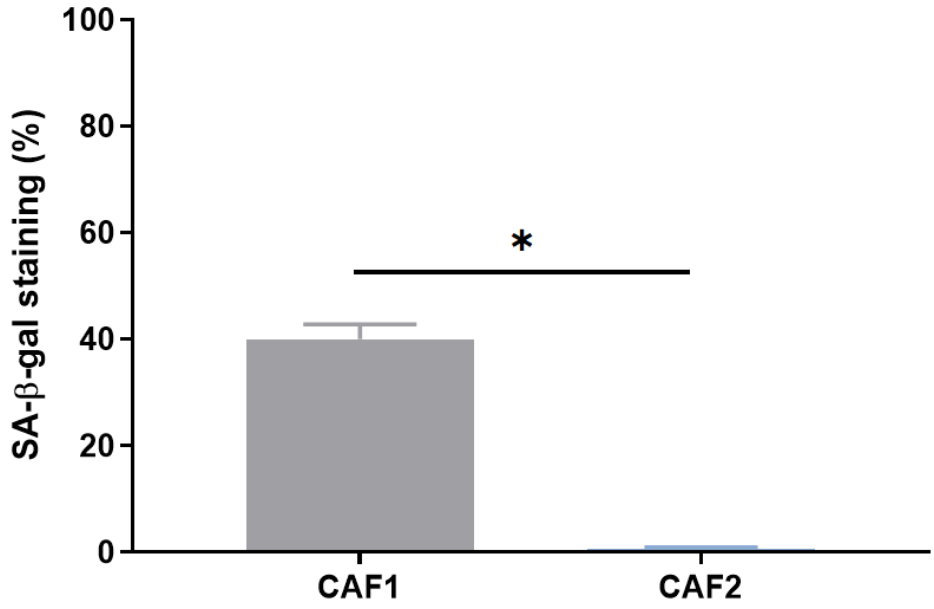

(B)

Figure 4.18: Senescence status in OPSCC CAFs. (A) Images representing SA-β-gal stain in CAFs at the basal level (magnification x20). Cells were seeded into a 12 well plate at a density of 10,000 cells/well. Next day, cells were washed with PBS, fixed, and stained with X-gal staining solution for 24 h. **(B)** Quantification of SA-β-Gal stain. The number of stained cells (blue precipitate) in 3 random fields (magnification x20). CAF1 showed the highest percentage of senescence. Error bar = SD of (N=3, n=3). Student's *t*-test used for the comparison. *p<0.05.

.

4.4.4.1 Growth kinetic of OPSCC CAFs

To assess the proliferation ability, cells were seeded at a density of 5,000 cell/ml in 6 well-plate with 2ml growth media. Every 2 days, cells from one well of the 6 well-plate were detached and counted. By monitoring cells' duplication rate over 12 days, CAFs and NTF6 showed a doubling in culture density on day 4, after being adapted to new cultures. Differences in proliferation rates between cultures were observed clearly at day 12, however, this difference was not statistically significant (p> 0.05) (Figure 4.19).

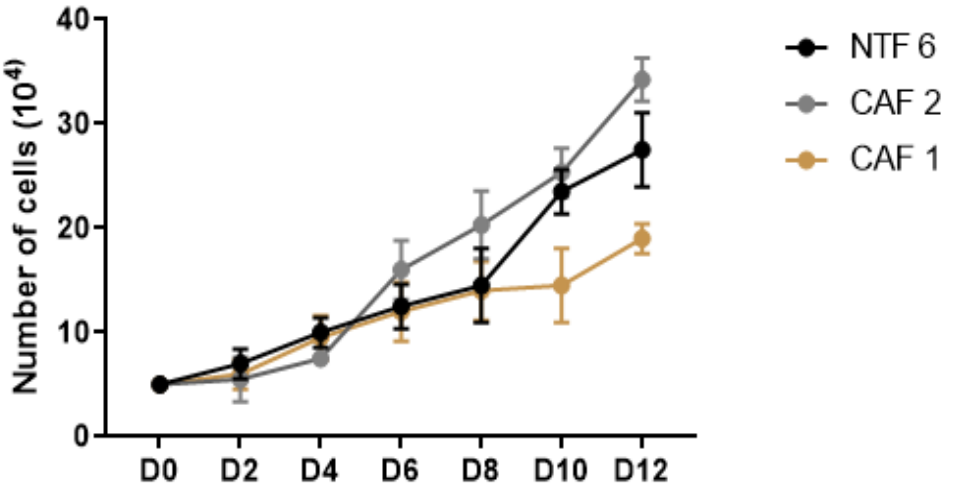

Figure 4.19: Growth kinetics of OPSCC CAFs. 5,000 cells of CAF1, CAF2, and NTF6 were plated into 6-well plates and incubated with the growth media. Cell counting was performed at two-day time intervals. CAF1 showed the slowest proliferation rate. Each line on the figure represents the mean of the relative cell number. Error bar = SD of three independent experiments.

4.4.4.2 IL-6 secretory profile in OPSCC-derived CAFs

The IL-6 ELISA assay was used to assess the basal secretory level of IL-6 in CAF1 and CAF2 (Figure 4.20). Both CAF1 and CAF2 produced higher concentrations of IL6 compared to NTF6 (p<0.01). CAF2 showed the highest value with (103.5 ± 19), however, that was not statistically significant compared with CAF1 (77.5 ± 10.6) (p>0.05).

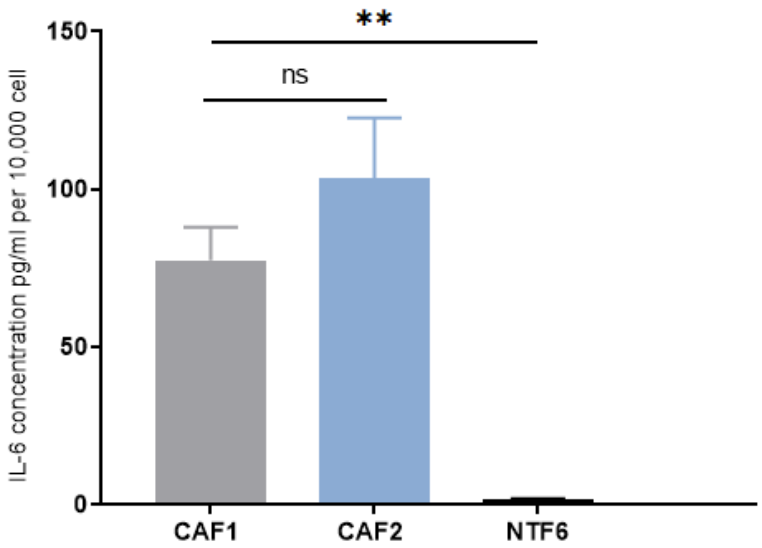

,

Figure 4.20: IL6 production in OPSCC CAFs. CAF1 and CAF2 showed significantly higher IL-6 concentration than NTF6. Samples number (n=3), Y-axis denotes standardised IL-6 concentration in pg per ml. IL-6 concentrations were optimised according to fibroblasts density at 10,000 cells. Student's *t*-test and one-way ANOVA were used for the statistical comparison. Data represent the mean of (N=3, n=3). Error bars= SD. **p<0.01.

4.5 Discussion

The purpose of this work at the beginning of our research was to establish a strong framework of understanding in OPSCC fibroblast phenotypes, as that has not been done before. Exploring the similarity or diversity of OPSCC fibroblast from OSCC fibroblasts is an essential step in investigating the role of the OPSCC TME in HPV-positive and HPV-negative OPSCC subtypes.

In this chapter, we established *in vitro* models of the myofibroblastic-CAF phenotype and senescent-CAF phenotype derived from NTFs. The myofibroblastic phenotype was generated using a single dose of TGF- β1 (5 ng/mL) and confirmed by assessment of de novo α-SMA gene and protein expressions. Premature induced senescent phenotype was induced using hydrogen peroxide (500 µM) and assessed by evaluating SA-β-gal activity and confirmed by assessment of p21, p16, and IL-6 expressions. The heterogeneity in fibroblasts' responses was an evident feature in both models.

Furthermore, we established primary CAFs cultures isolated from HPV+ tonsillar carcinomas. The molecular assessment of CAF cultures including CK6, HLA-DR and CD31 revealed the purity of other cell lineage contamination, while expression of FSP-1 and PDGFR confirmed the fibroblast identity. Most importantly, significant FAP-α expression in CAF1 and CAF2 in relation to NTF6 indicated CAFs' active status. Heterogeneity was evident in CAFs cultures too; CAF1 exhibited the senescent-CAF like feature by demonstrating a high ratio of SA-β-gal precipitation (39% ± 1.4) compared to CAF2's low SA-β-gal percentage (0.5% ± 0.3). Another evident difference was observed in α-SMA upregulation on comparison of CAF1 and CAF2. The latter showed significant overexpression of α-SMA that was sensitive to further stimulation following a single dose of TGF-β1.

4.5.1 Established CAF myofibroblastic phenotype in OPSCC

We established an activated tonsil myofibroblastic model derived from NTFs, following the previous protocol in our lab in NOFs activation. Cells were stimulated with 5 ng/ml TGF-β1 at different time points, then the activation status was evaluated by analysing α-SMA expression. NTFs phenotype differentiation was validated by assessing the alterations in cells' mechanical and secretory properties. The results showed a remarkable upregulation of de novo α-SMA at gene and protein levels after TGF-β1

stimulation which mostly peaked at 48h, with a corresponding increase in cytoskeletal fibers formation. Stimulated NTFs were also able to generate enough contractile force to shrink the stressed collagen lattice using collagen gel contraction assay. This activation was associated with slightly increased IL-6 production in NTF10 and NTF6 compared with untreated counterparts.

TGF-β1 has been shown to promote fibroblast differentiation to myofibroblast phenotype *in vivo* and *vitro* (Desmouliere *et al.*, 1993; Vaughan, Howard and Tomasek, 2000; Mellone *et al.*, 2016). However, it is believed that TGF-β1 requires mechanical stress alongside to enhance cell differentiation. The mechanical stress promotes the differentiation into proto-myofibroblasts which are characterised by fibronexus adhesion complexes, fibronectin production and stress fiber formation (Tomasek *et al.*, 2002). In presence of TGF-β1, proto-myofibroblasts become able to differentiate into a myofibroblastic phenotype that can exert contractile force on ECM, the feature that defines the contraction phase in wound healing process (Hinz *et al.*, 2001). This description was observed clearly using the collagen gel contraction assay. NTFs were placed under a mechanical tension in the attached collagen lattice with the presence of TGF-β1. Once the collagen pad was released, the transformed myofibroblasts generated a contractile force in the collagen pad which reduced the disc diameter.

In comparison with NOFs, our findings are in keeping with previous reports from our lab (Abidin, 2017; Melling *et al.*, 2018). 5ng/ml of TGF-β1 was sufficient to upregulate α-SMA expression in a time-dependent manner that peaked at 48h. This pattern of expression was also reported by Evans *et al*. (2003) and Zhang *et al.* (2005). The 48h time-duration may reflect the length of the negative feedback loop mediated by Smad7, the inhibitory regulator (Kavsak *et al.*, 2000). In human peritoneal mesothelial cells, Smad2/3 (TGF-β1 receptors) was phosphorylated and upregulated 15 min after the stimulation with 5ng/ml of TGF-β1. The Smad2/3 phosphorylation level is increased, allowing translocation into the nucleus where it provokes target genes transcription (Zhang *et al.*, 2005). As a feedback circuit, Smad7 is upregulated simultaneously with Smad 2/3 activation, acting on TGF- degradation. Smad7 was observed reaching a remarkable level after 24h of TGF-β1 stimulation and peaked at 48h.

Similar to NOFs, not all the tested NTFs cultures responded equally to TGF-β1. α-SMA showed variable levels of expression at gene and protein levels. This observation also was consistent with Chaudhri *et al*. (2013), supporting the previous data that α-SMA expression is diverse per cell. Cell-to-cell variation is described among the tissues in

terms of gene expression profile, morphology, and function, which might reflect the variations in response between NTFs cultures (Yuan *et al.*, 2017). Fibroblast passage and TGF-β1 freshness also were considered factors (Chen and Thibeault, 2012a).

4.5.2 Establishment of an NTF senescent phenotype

Senescence can occur as a result of exposure to a variety of intracellular and extracellular stimuli, including DNA damage, telomere shortening, oncogenic stress, and Reactive Oxygen Species (ROS). Senescence status is characterised by cellular proliferation arrest accompanied by a range of morphologic, molecular, and behavioural changes that have been tentatively adopted as hallmarks for senescence. Here, in this section, we established and characterised a model of PIS in NTFs using Hydrogen peroxide which has been widely used to provoke persistent DNA damage response in a variety of cell types (Frippiat *et al*., 2001, 2002).

To date, there is no specific biomarker for senescent cell detection, as there are many non-specific cellular changes that occur as a response to cellular stress. In practice, observing three signs collectively was recommended for senescence detection *in vivo* and *in vitro* (Sharpless and Sherr, 2015; Fafián-Labora and O'Loghlen, 2020). Lysosomal biogenesis enhancement is one hallmark of senescence. It results in the upregulation of lysosome number and content that can be observed clearly in the cell cytoplasm. Increase in the activity of the lysosomal enzyme SA-β-gal is utilised widely as a surrogate biomarker for senescence. In the earliest passage of tested NTFs, SA-β-gal percentages were negatable, however, following H_2O_2 treatment NTFs demonstrated a significant amount of accumulated β-galactosidase in their cytoplasm. The exact mechanism behind this phenomenon is still obscure; a recent report linked GLB1, the SA-β-gal enzyme coding gene, with the NOTCH1 pathway. NOTCH signalling has been reported to promote a type of cellular senescence (NOTCH-induced senescence) with characteristic SASP components (Kagawa *et al.*, 2015; Hoare *et al.*, 2016).

Having mentioned above that none of the senescence biomarkers is specific, high lysosomal activity and accumulation of SA-β-gal also have been identified in non-senescence cells. The stressed culturing condition was described as a reason in β-galactosidase accumulation. Figure 4.21 shows an example of SA-β-gal stain overexpression in an early passage culture of NTF6 after having been grown to over-confluence.

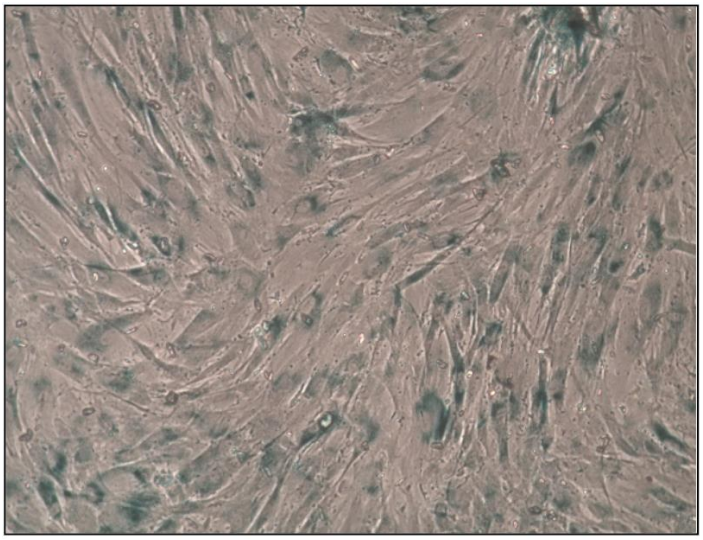

Figure 4.21: Confluent NTF6 culture demonstrates high SA-β-gal positivity. Early passage culture of NTF6 was grown to confluence with the media changed every 5 days. SA-β-gal assessment revealed a high proportion of SA-β-gal staining cells. (Magnification x10).

Morphological alterations and growth arrest are the observed features in senescent cells (Chandrasekhar, Sorrentino and Millis, 1983). An increase in cell size has been linked to the activation of mTOR pathway that integrates various stress signals (Lloyd, 2013). mTOR was found to be activated in response to premature senescence stimuli (Blagosklonny, 2012), in addition to normal ageing as a response to growth factors decline (Loffredo *et al.*, 2013). Moreover, alterations in the cellular shape of the senescent cells were reported as a consequence of cytoskeletal microfilaments rearrangement; particularly, the production of vimentin is promoted by ATF6/NF-kB signalling pathway during senescence (Druelle *et al.*, 2016).

Morphological features have been observed more clearly in CAF1 and CAF2 cultures in early passages, although CAF2 demonstrated low SA-β-gal positivity and exhibited evident active myofibroblastic phenotype profile by expressing FAP-α and α-SMA. Changes in normal fibroblast morphology upon the activation and α-SMA upregulation were monitored thoroughly in Desai et al.'s work (Desai, Hsia and Schwarzbauer, 2014) which indicated morphological changes are not a specific hallmark for the senescent cell.

Stable cell cycle arrest is another characteristic feature in senescent cells. It is mediated by activation of cell cycle proteins Rb and p53 and results in the engagement of various cyclin-dependent kinase inhibitors including CDKN2A, CDKN2B, and/or CDKN1A which encoding p16, p15, and/or p21 proteins, respectively. However, they are not senescence specific biomarkers, they were also detected in non-dividing somatic cells (Fafián-Labora and O'Loghlen, 2020). Both p16 and p21 over expressions were observed clearly at gene and protein level in H_2O_2-treated NTFs in this study.

Although senescent cells are arrested cells, they are metabolically hyperactive compared to cells under normal conditions (James *et al.*, 2015). They are known for their ability to produce a plethora of factors called collectively SASP which is considered the 'soul' of senescence. SASP contents are not constant, they vary according to fibroblast cell and culturing conditions (Coppé *et al.*, 2008). However, IL6 is considered a core cytokine secreted by senescent cells in both ageing and induced senescence. Quantification of IL6 production was our tool to assess the SASP secretory profile; we observed a significant IL6 overproduction in H_2O_2-induced NTFs compared by the control. This observation is in parallel with many other studies which have utilised IL-6 overexpression as a senescence biomarker (Acosta et al., 2008; Bhaumik et al., 2009).

Collectively, NTFs demonstrated CAFs senescence-phenotype like features following the treatment of DNA damaging agent. The senescent status induction was confirmed by observing the senescence hallmark features simultaneously, including SA-β-gal high positivity, p16/p21 over-expression, and IL-6 overproduction.

4.5.3 CAFs isolation and characterisation

In HNSCC, the most common approach in CAFs isolation is the explant technique with or without further enzymatic digestion (Custódio, Biddle and Tavassoli, 2020). This technique allows fibroblasts only to outgrow rather than another cell lineage. Other methods, including flow cytometry and differential trypsinization, also were utilised in CAF isolation (Johansson *et al.*, 2012; Li *et al.*, 2014). The lack of specific biomarkers for CAFs poses a challenge while considering a purified CAF culture. CAFs can originate from different sources and that might explain the variety of biomarker expression which is shared with the other cells from the same origin (Orimo and Weinberg, 2007; Cirri and Chiarugi, 2012; Shiga *et al.*, 2015). The anatomical position and morphological

appearance were considered by many authors as characteristic features for CAFs identification (Liu *et al.*, 2006; Potdar and Chaudhary, 2017). In this study, cells were isolated from fragments from tonsillar carcinoma using the enzymatic digestion method. Under the light microscope, CAFs revealed a distinctive morphology compared with NTFs. CAFs appeared flat, larger with variable shapes, and contained dark vacuolated cytoplasm. Notably, in high-density culture, CAFs crowd together in a disorderly manner, lacking the characteristic regular array pattern that specifies NTFs at confluency.

However, in practice, CAF isolation is based on a consensus of other lineage exclusion combined with mesenchymal biomarker positivity (Xing, 2010; Ishii, Ochiai and Neri, 2016). Lack of expression for epithelial, leukocyte, and endothelial biomarkers is the preferred approach to exclude CAFs culture contamination and confirm cultural homogeneity (Potdar and Chaudhary, 2017). The negativity of CK6, HLA-DR, and CD31 biomarkers confirmed CAF purification in this study; meanwhile, confirming CAFs' identity is a more challenging process.

A number of the cell surface, extracellular, and intracellular proteins have been utilised to identify CAFs; nevertheless, to date, there is no specific biomarker for CAFs (Biffi and Tuveson, 2021). The positivity of mesenchymal biomarkers such as FSP-1, vimentin, and fibronectin provides sufficient evidence for CAFs' identity (Sugimoto *et al.*, 2006). However, we should be aware these biomarkers are not specific for CAFs, they are also expressed by other cell types sharing the mesenchymal origin, including adipocytes, chondrocytes, and osteocytes (Ishii, Ochiai and Neri, 2016). Herein, both CAF1 and CAF2 showed a transcript positive for FSP-1 and PDGFRα biomarkers and their expressions were comparable to NTF6. Both biomarkers have been used collectively in *vitro* and in *vivo* studies for CAFs identification (Tomasek *et al.*, 2002; Dangi-Garimella *et al.*, 2011, 2013). Although FSP-1 is considered a specific biomarker for both normal and activated fibroblasts (Strutz *et al.*, 1995), confirmation of another lineage contamination is still recommended. PDGRFs are general, stable biomarkers for fibroblasts at different environmental conditions (Madsen *et al.*, 2015). However, they lack specificity for CAF detection, indicating an overall fibroblast population present in the tumour (Gascard and Tlsty, 2016).

α-SMA and FAP-α expression/overlapping expression were used widely for activated fibroblast identification in wound healing, fibrosis, and tumours (Park *et al.*, 1999; Serini and Gabbiani, 1999; Tchou *et al.*, 2013; Kilvaer *et al.*, 2015). However, recent accumulating evidence using scRNA-seq technique and multicolour flow cytometry

(Costa *et al.*, 2018; Jackson *et al.*, 2020) raised concerns regarding the specificity of some classic-CAFs; for instance, α-SMA expression was reported in other lineages such as pericyte, while its expression was lacking in other CAFs subtypes (Alarcon-Martinez *et al.*, 2018; Bartoschek *et al.*, 2018; Costa *et al.*, 2018). FAP-α protein expression was also reported in several types of cells other than CAFs, including immune cells and certain cancer cells (Kikuchi *et al.*, 2006; Österreicher *et al.*, 2011).

From the above, CAFs identification based on a combination of morphological appearance and a biomarker definition is a reliable practical approach. Following this method, we achieved pure primary CAF cultures of OPSCC. Although we observed a molecular heterogeneity in CAFs that originated from the same OPSCC subtype, similarities of CAFs signatures across different malignancies were reported recently using scRNA-seq (Salgueiredo-Giudice *et al.*, 2011; Puram *et al.*, 2018; Davidson *et al.*, 2020). Analysing the shared features in fibroblast from different tumour types may reveal a new promising therapeutic approach.

4.5.4 OPSCC CAF phenotypes

The reasons behind CAFs' phenotypic heterogeneity have been studied intensively in the literature. Extracellular matrix composition and elasticity were reported as main factors directing CAFs phenotypic heterogeneity in the presence of TGF-β1 signalling (Chen and Thibeault, 2012b). In the Avery et al. study, fibroblast activation status was assessed on substrata of defined stiffness and composition. Low-stiffness ECM with high-fibronectin content was sufficient to drive FAP^{Hi} - $\alpha\text{-}SMA^{low}$ active phenotype development; meanwhile, high-collagen I in stiff ECM enhanced FAP^{low}- $\alpha\text{-}SMA^{Hi}$ myofibroblastic phenotype formation. Interestingly, each subtype of these activated fibroblasts has its gene expression signature which indicates distinct functionality *in vitro*. FAP^{Hi} activated fibroblasts displayed an ECM synthetic and proteolytic gene profiling property, whilst $\alpha\text{-}SMA^{Hi}$ reactive fibroblast showed a contractile and proliferative gene signature (Avery *et al.*, 2018).

Heterogeneity of CAFs subtypes was also correlated to the spatial distribution of the CAFs in tumour tissue specimens. In pancreatic ductal adenocarcinoma, CAFs population that showed upregulation of myofibroblasts biomarkers, such as α-SMA, was found to be located adjacent to cancer cells, while CAFs population with inflammatory secretion profile, such as IL-6, was located farther away, surrounded by dense stroma

(Biffi *et al.*, 2019). Types of tumour and variation among patients were also proposed as factors regulating CAFs' phenotypic diversity (Bozõky *et al.*, 2013).

In human cancer, two CAF phenotypes have been reported consistently in the literature, the myofibroblastic and non-myofibroblastic. Both phenotypes were described with characteristic features and linked to specific roles in TME. In this study, characterisation of CAFs phenotypes revealed heterogeneity among CAFs cultures that was evident in α-SMA expression levels and SA-β-gal stain positivity. CAF2 demonstrated active myofibroblast-like features by showing low SA-β-gal stain and expressing relatively high levels of α-SMA and FAP-α biomarkers. Interestingly, it exhibited a significant overexpression of α-SMA upon TGF-β1 induction compared with NTF6. A similar observation was reported by Kojima *et al.* (2010) suggesting a greater individual variation of α-SMA expression in CAFs than normal fibroblasts. Across various cancer types, the myofibroblastic CAF-phenotype is characterised by ECM signature; it becomes involved in tumour progression by generating an increasing tension in the stroma and promoting tumour cell invasion and metastasis (Levental, K. Yu, 2010; Lu, Weaver and Werb, 2012). Clinically, the significance of SMA-positive CAF in the tumour's stroma was linked with the poor survival rates.

CAF1 showed a senescent phenotype by displaying a significant uptake of SA-β-gal stain (39% ± 1.4). However, senescent fibroblasts commonly co-express a high level of α-SMA. Interestingly, CAF1 showed low α-SMA basal level, and also showed the lowest value in gene upregulation in response to TGF-β1 compared with CAF2 and NTF6. This observation was consistent with Mellone and team's findings in HNSCC-derived CAFs; they reported a weaker correlation between co-expression of SMA and SA-β-gal in 6 strains of CAFs (r2=0.32) compared to 6 normal fibroblast cultures (r2=0.82). This inconsistency of co-expression was linked to the greater heterogeneity in CAFs population (Mellone *et al*., 2016).

Generally, non-myofibroblastic CAFs share senescent fibroblast features. Senescence is considered a highly productive inflammatory phenotype sharing similar transcriptional profiles and signalling pathway activation, including interleukin, NF-kB and NOTCH pathways (Kuilman *et al.*, 2008; Chien *et al.*, 2011; Hoare *et al.*, 2016). This difference in secretory profile supports our observations in the CAFs established models, as IL-6 production was higher in the PIS model than the myofibroblastic model.

Moreover, non-myofibroblastic CAFs display a lower proliferation rate compared to myofibroblastic CAFs (Biffi *et al.*, 2019). CAF1 had a low proliferation rate compared to CAF2, particularly at higher passages, although statistically, this difference was not significant. Functionally, in the tumour stroma, non-myofibroblastic CAFs secrete inflammatory SASP-like products and their pro-tumorigenic effects have been described (Krtolica *et al.*, 2001). However, much work is required to understand the effects of inflammatory CAF-secreted factors on tumorigenicity (Biffi and Tuveson, 2021).

4.6 **Limitations**

We are aware although *in vitro* monolayer 2D cultures of fibroblasts can be useful to investigate some biological aspects of CAF, however, it has been reported that the transcriptome of CAFs cultured *in vitro* does not recapitulate the heterogeneity of CAFs *in vivo* (Puram *et al.*, 2018). Other approaches, such as a short-term co-cultures that retain all cell populations found in tumours, of liquid-air interface models (Neal *et al*., 2019) and multi-cell-type three-dimensional bio-printed tissues (Langer *et al*., 2019) are being implemented and optimised.

According to the CAFs isolation protocol (Enzymatic digestion approach), a heterogeneous population of CAFs was isolated. Theoretically, CAFs were isolated and characterised in a population of different subtypes from the single tumour. Among this isolated population, CAFs might display heterogeneity in the phenotypes and that might explain the percentage of the senescent population in CAF1 culture. Single-cell resolution techniques including laser microdissection, pressure catapulting and fluorescence-activated cell sorting provide the advantage of isolating a pure cell population for molecular comparisons.

4.7 **Summary of main findings and clinical implications**

Using NTFs, myofibroblastic and senescent models were established and characterised. The comparison between these models and previously established models derived from oral fibroblasts revealed no differences in the developed phenotypes in responses to TGF-β1 and H_2O_2 stimuli although they were extracted from different anatomical locations. This observation indicates that the biological differences in OPSCC subtypes

are mainly attributed to cancer cells and their capacity in modulation the underlying microenvironment.

Two OPSCC-derived CAF cultures, originating from HPV-driven tumours, were established and characterised. To the best of knowledge, this is the first time CAFs were extracted from HPV-associated OPSCC. Establishment of OPSCC-CAFs cultures provides the opportunity for further investigations *in vitro* to understand OPSCC tumour cells and CAF crosstalk.

Recognition of CAF characteristics in different phenotypes provides a framework for better understating of CAFs' role in OPSCC. Moreover, it highlights the need to consider multiple parameters for the analysis of CAF activation.

Chapter 5: Cytokine array analysis of tumour cells and fibroblast crosstalk

5.1 Introduction

“No tumour is an island, entire of itself; every tumour is a piece of a continent.” This quote is a paraphrase of the famous quote written by the English poet John Donne (Custódio, Biddle and Tavassoli, 2020). It summarises the available knowledge on epithelial solid tumour development and progression as dysfunctional tissues as a whole rather than an accumulation of a critical number of mutations in tumour cells (Hanahan and Weinberg, 2011). Efforts to develop cancer therapies have mainly been concerned with the malignant cell component, although non-malignant cells in the underlying tumour microenvironment (TME) substantially contribute to the progression of the tumour and cancer therapy resistance. In the last decade, there has been an increasing focus on the non-malignant mesenchymal components within the TME intending to understand the biology of complex interactions with the neighbouring malignant cells.

The TME consists of several cell types which encompass fibroblasts, in addition to other immune cells, pericytes, endothelial cells, adipocytes, mesenchymal cells, in addition to the extracellular matrix. These normal residents in the tumour stroma have the capability to be stimulated by tumour cells and differentiate into more tumour-supportive phenotypes, especially, those demonstrating a cellular senescence-status (Lawrence *et al.*, 2015). Induction of an activated CAF phenotype and the potentiation of tumour cell behaviour involves crosstalk between the TME and cancer cells. The cytokines TGF-β1, TNF-a and IL-1α/β have been reported as epithelial cancer-derived factors in CAF activation. CAFs, in turn, secrete several factors includes TNF-a, IL-1α/β, CCL7, Collagen 1, Activin A, , SDF-1, MMPS, IL-33, PGE2, HGF, and PDGF which have been implicated in tumour invasion, metastasis and resistance to cancer therapy (Leef and, Thomas, 2013; Togo *et al*., 2013; Sun *et al*., 2012).

However, little is known about the role of the tumour microenvironment in HPV-positive and HPV-negative OPSCC subtypes. Much is unclear regarding the specific pathways of stromal activation and if this has a pivotal role in tumour cells modulation, regardless of HPV status. Previous work from our lab demonstrated evident differences between OPSCC subtypes in term of stroma modulation (Bolt *et al*., 2018; Peacock *et al*., 2018). Conditioned media-derived from HPV-negative cell lines (SCC89 & SCC72) and HPV-positive cell lines (SCC90 & SCC2) were subjected to cytokine analysis previously in our lab using Raybiotech C2000 Human Cytokine Arrays (Raybio-technology, Norcross, USA, cat number: AAH-CYT-2000). (Appendix A.3) (Bolt, 2016). HPV-negative cell lines produced higher amounts of cytokines than the HPV-positive cells. nevertheless, further

work is required to understand the early events in tumour-stroma activation and identify novel candidates facilitating the cellular crosstalk.

5.2 Aims

- To explore the secretome mediated crosstalk between tonsil derived fibroblasts and HPV-positive and HPV-negative OPSCC subtypes.

5.3 Experimental approach and statistical analysis

- Modelling of tumour-stroma interaction was established by incubating OPSCC fibroblasts for 24h with conditioned media collected from HPV-positive SCC (SCC2) or HPV-negative OPSCC cell lines (SCC89) (M1). This incubation was followed by another 24h incubation with serum-free media (M2) (Figure 5.1). Media collected from these interactions was subjected to cytokine multiplex array technique to screen a wide panel of cytokines that may play a role in the activated microenvironment.

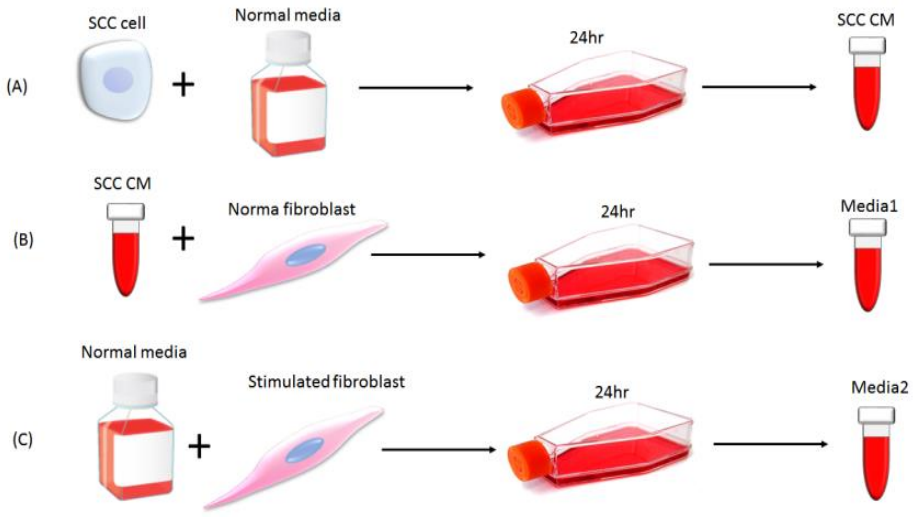

Figure 5.1: Illustration for conditioned media procedure. **A,** cell line conditioned media collection. **B**, Stimulation of fibroblast by cell line media and collection of the stimulated fibroblasts media (M1). **C,** incubation of fibroblast with normal media to get media2

- An interactive co-culture model consisting of HPV-positive OPSCC or HPV-negative OPSCC cell lines and OPSCC fibroblasts was performed using culturing

inserts (pores size= 0.4 µm) to validate the array results and identify which cell was contributing particular cytokines to the secretome (Figure 5.2).

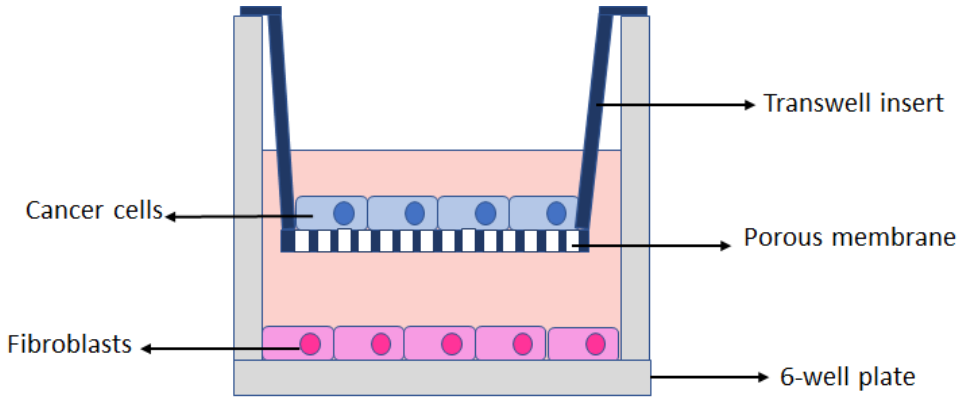

Figure 5.2: Illustration of transwell co-culture model.

- Statistically, detection of non-normality is less likely among the data due to small sample numbers, however, Shapiro-Wilk test was used to check the normality due to its high sensitivity. For the comparison between two normally distributed samples' mean, two-tailed unpaired *t*-test was used. In multiple data sets, one-way analysis of variance (ANOVA) was used.

- Data were presented graphically illustrating the mean with error bars demonstrating the standard deviation (SD). The probability of similar random result detection (p-value) was considered significant if ($p<0.05$). "N" followed by a number denotes the biological repeats, while "n" denotes the technical repeats. Data were analysed using Graph-pad prism versions 7-9.

5.4 Results

5.4.1 Cytokine analysis of OPSCC fibroblasts media following stimulation with OPSCC cell lines media

5.4.1.1 CAF1

From the previous observations in chapter 4, CAF1 demonstrated senescent-like features by displaying a high percentage of SA-gal and low proliferation rate. The basal secretory profile of CAF1 cells was determined by incubating the cells with normal growth media (Figure 5.3) or serum-free media (Figure 5.4). Noted from visual inspection and densitometry analysis, MMP2 was the only factor was detected under both conditions.

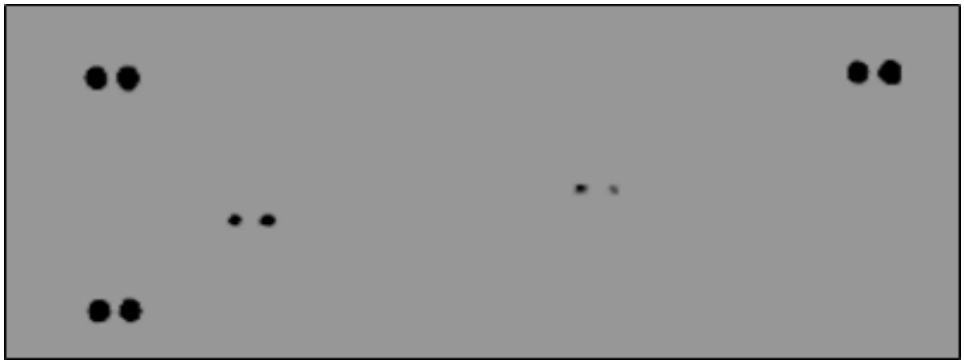

(A)

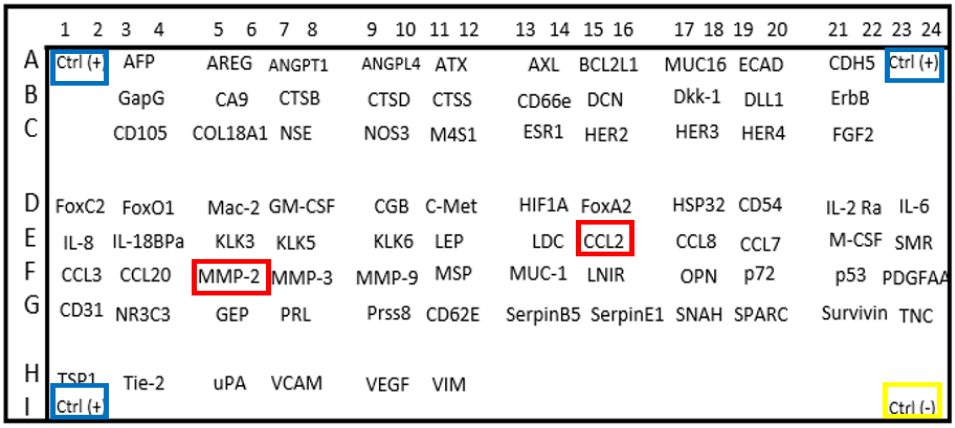

(B)

Figure 5.3 A & B: Cytokine Array analysis of CAF1 conditioned normal growth media (M1). **(A)** Representative image of the developed CAF1-M1 cytokine membrane. **(B)** The array map. The blue and yellow boxes in the array map denote the positive and negative array controls, respectively. Red box denotes factors present in CAF1-M1 conditioned media. Only CCL2 and MMP2 were detected.

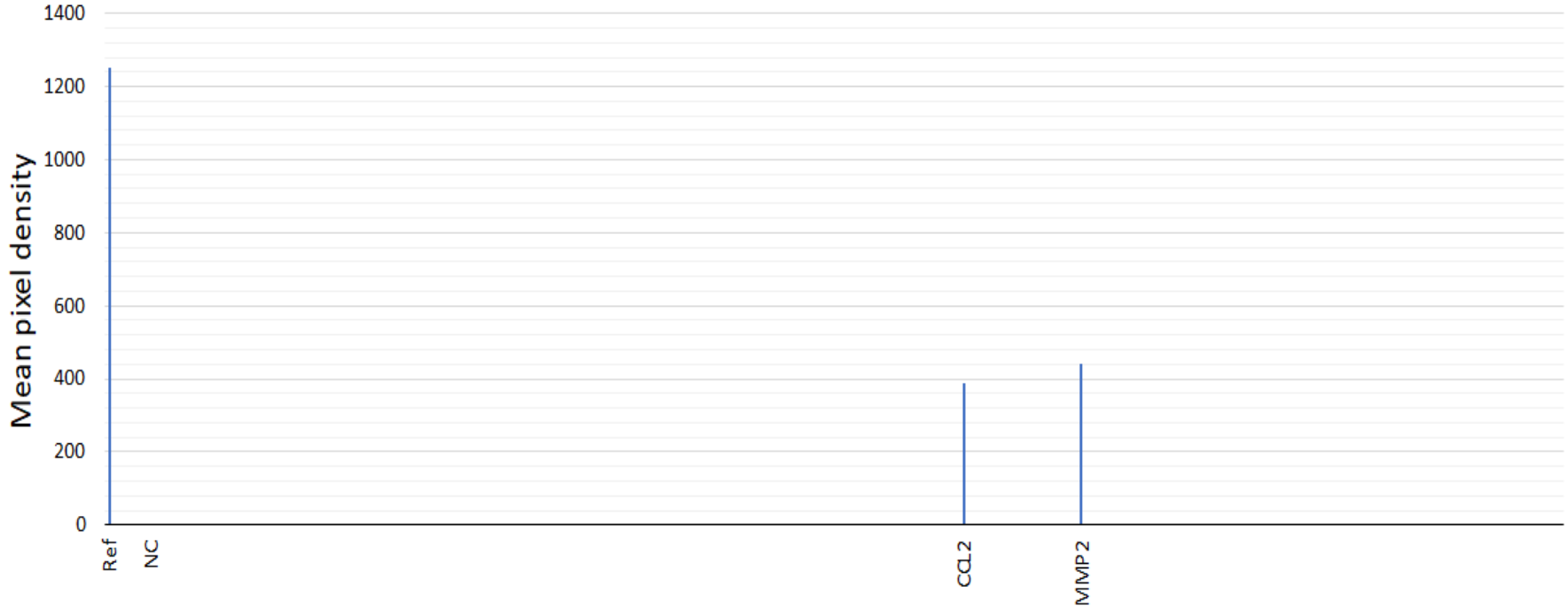

(C)

Figure 5.3 C: Cytokine Array analysis of CAF1 conditioned normal growth media (M1). **(C)** Densitometry analysis of factors detected in CAF1-M1 conditioned media. Bars represent the mean of densitometry values of each array's duplicate repeat spot. (Ref) denotes a positive control value that is used as a reference for result optimisation between the membranes. (NC) denotes array negative control spots. CCL2 and MMP2 showed expression relative to the reference bar.

(A)

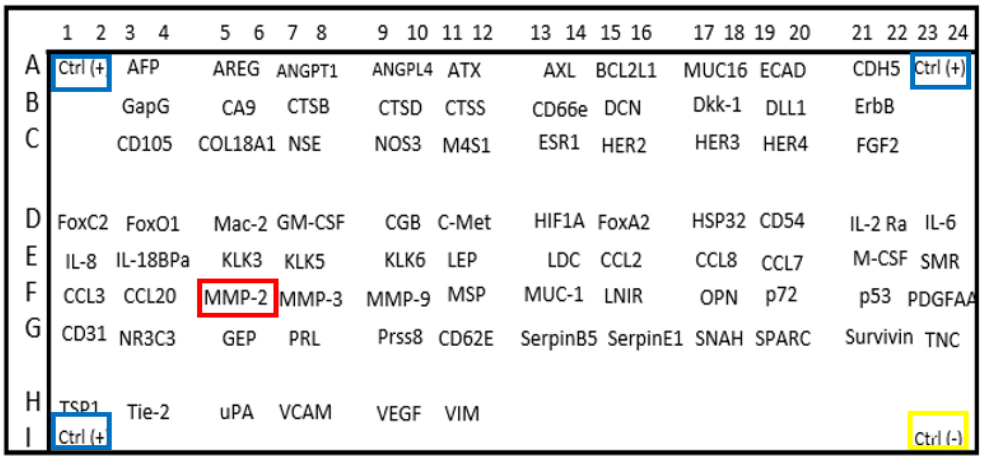

(B)

Figure 5.4 A & B: Cytokine Array analysis of CAF1 serum-free conditioned media (M2). **(A)** Representative image of the developed CAF1-M2 cytokine membrane. **(B)** The array map (*Right*). The blue and yellow boxes in the array map denote the positive and negative array controls, respectively. Red box denotes factors present in CAF1-M2 conditioned media. Only MMP2 showed expression on the array membrane.

(C)

Figure 5.4 C: Cytokine Array analysis of CAF1 serum-free conditioned media (M2). (C) Densitometry analysis of factors detected in CAF1-M2 conditioned media. Bars represent the mean of densitometry values of each array's duplicate repeat spot. (Ref) denotes a positive control value that is used as a reference for result optimisation between the membranes. (NC) denotes array negative control spots. MMP2 showed a modest expression compared to the reference bar.

Incubation of CAF1 with HPV-negative OPSCC cell line conditioned media (SCC89) demonstrated production of a larger number of cytokines with variable uptake densities, including CSTD, GM-CSF, IL-6, IL-8, KLK6, CCL2, MMP2, MMP3, OPN, GEP, SPARC and VEGF (Figure 5.5). Incubation of CAF1 with serum-free media following SCC89 media stimulation revealed upregulation in CAF1 secretory profile includes CTSB, IL-6, IL-8, CCL2, MMP2, MMP3, GEP, SER, and SPARC (Figure 5.6).

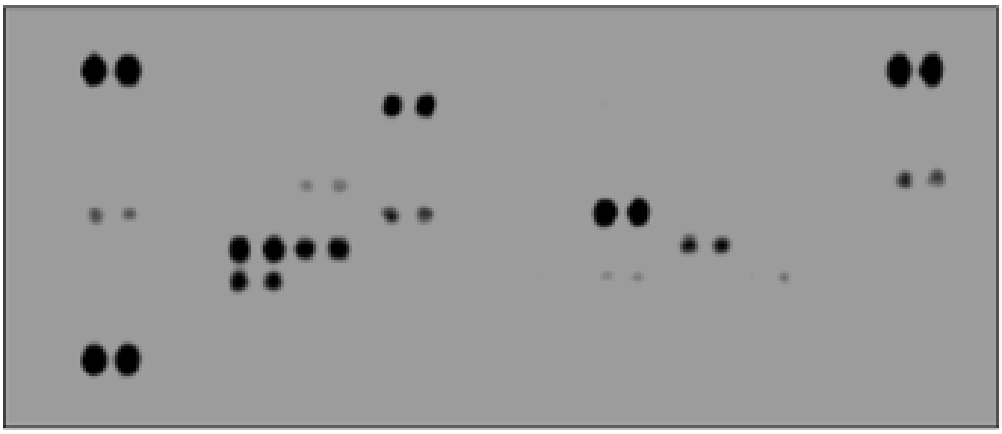

(A)

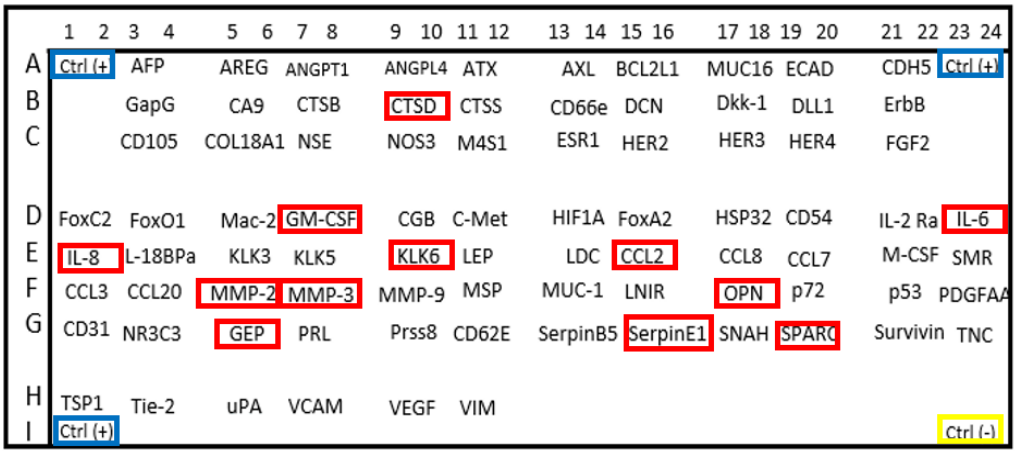

(B)

Figure 5.5 A & B: Cytokine Array analysis of conditioned media taken following CAF1 stimulation with SCC89 CM (M1). **(A)** Representative image of the developed cytokine membrane for CAF1 media after SCC89 CM treatment **(B)** The array map. The blue and yellow boxes in the array map denote the positive and negative array controls, respectively. The red box denotes factors present in CAF1-SCC89-M1 conditioned media. Numerous cytokines showed densitometry uptakes, with CSTD, CCL2, MMP2 and MMP3 displaying strong intense spots compared to other factors.

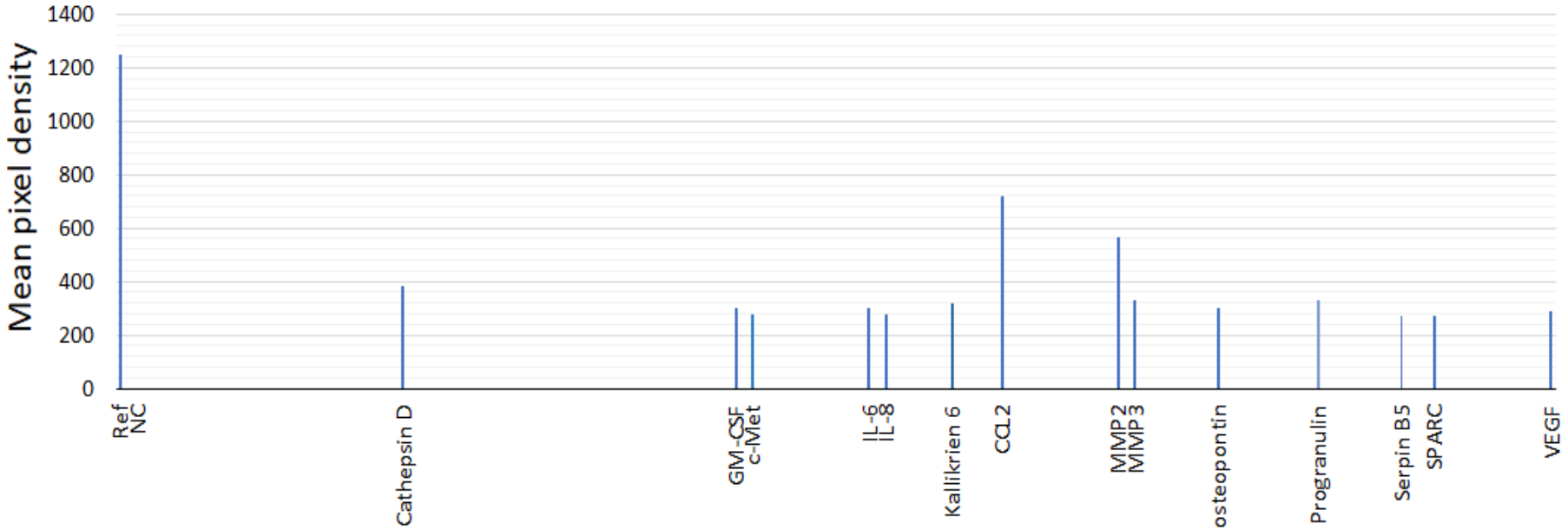

(C)

Figure 5.5 C: Cytokine Array analysis of conditioned media taken following CAF1 stimulation with SCC89 CM (M1). **(C)** Densitometry analysis of factors detected in CAF1-SCC89-M1 conditioned media. Bars represent the mean densitometry values of each duplicate repeat spot. (Ref) denotes a positive control value that is used as a reference for result optimisation between the membranes. (NC) denotes array negative control spots. Analysis reveals varying levels of cytokine expression in SCC89-CAF M1. CCL2 and MMP2 showed the highest level of expression compared to other cytokines and compared by other factors in CAF1 M1.

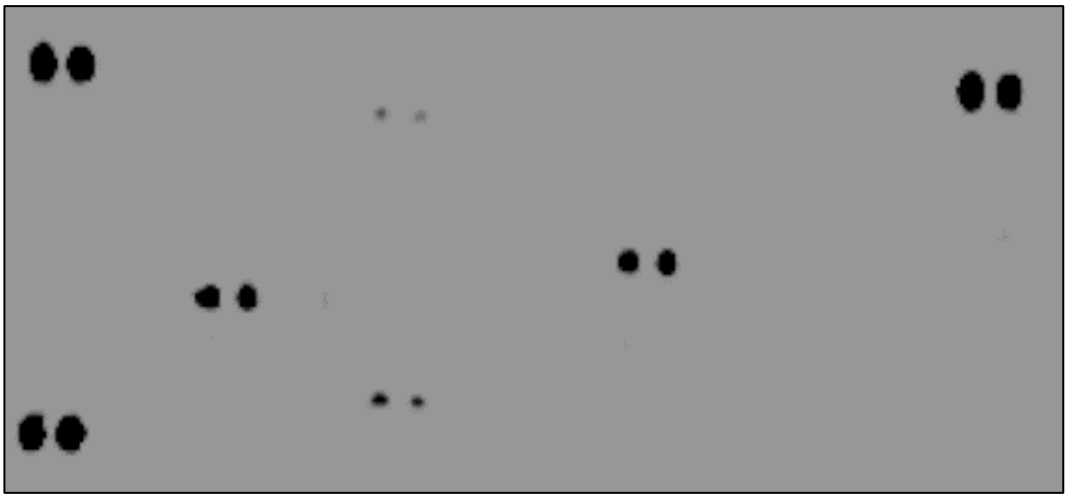

(A)

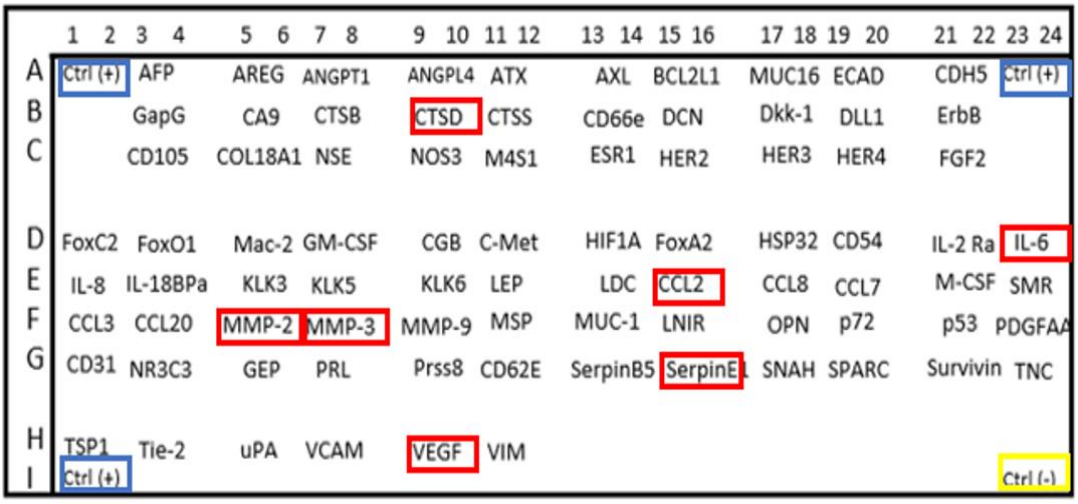

(B)

Figure 5.6 A&B: Cytokine Array analysis of CAF1 serum-free conditioned media following SCC89 CM stimulation (M2). (A) Representative image of the developed cytokine membrane for CAF1 serum-free media following SCC89 CM treatment. **(B)** The array map. The blue and yellow boxes in the array map denote the positive and negative array controls, respectively. The red box denotes factors present in CAF1-SCC89-M2 conditioned media. Relatively fewer cytokines are expressed compared to SCC89-CAF1 M1. The CCL2, MMP2 and MMP3 spots showed the highest intensity compared to other factors.

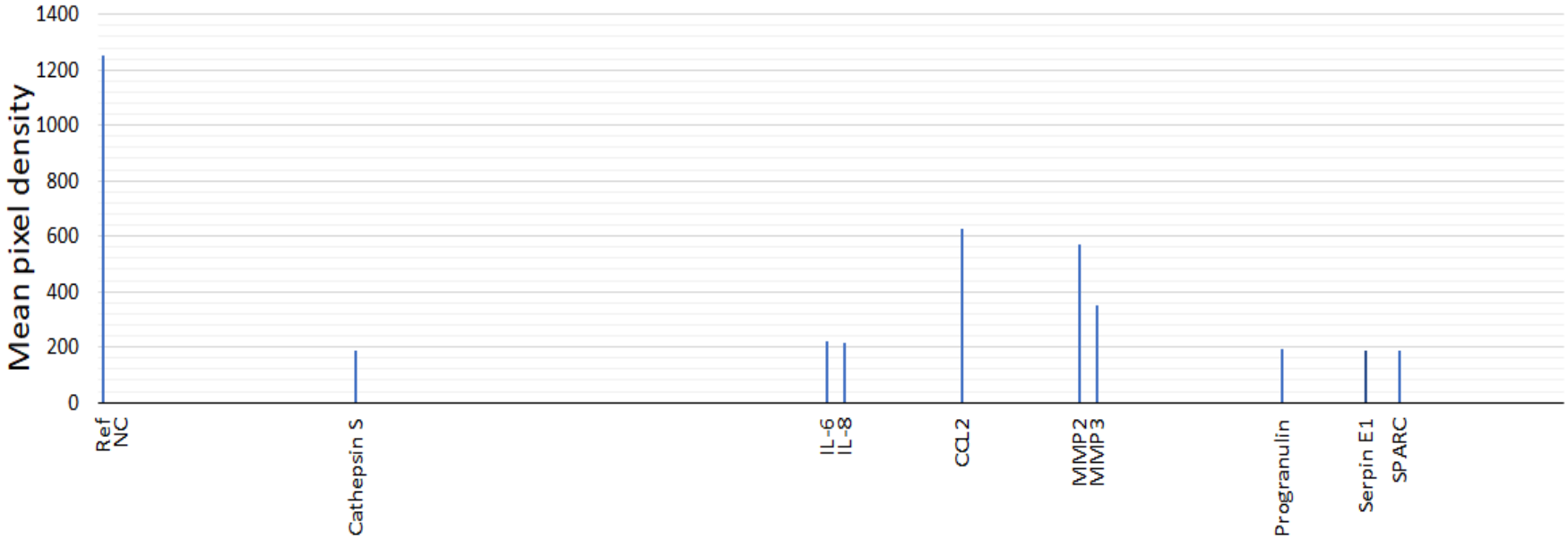

(C)

Figure 5.6 C: Cytokine Array analysis of CAF1 serum-free conditioned media following SCC89 CM stimulation (M2). (C) Densitometry analysis of CAF1-SCC89-M2 conditioned media. Bars represent the mean of densitometry values of each array's duplicate repeat spot. (Ref) denotes a positive control value that is used as a reference for values normalisation. (NC) denotes array negative control spots. A number of cytokines showed expression with fewer expression values compared to M1 conditioned medium.

The HPV-positive SCC2 cell line conditioned media induced less cytokine secretion from CAF1, namely, CSTD, IL-6, CCL2, MMP2, MMP3, SerpinE and VEGF (Figure 5.7). Also, fewer cytokines were detected in CAF1-M2 following SCC2 conditioned media stimulation including MMP2, MMP3, SerpinE and SPARC (Figure 5.8).

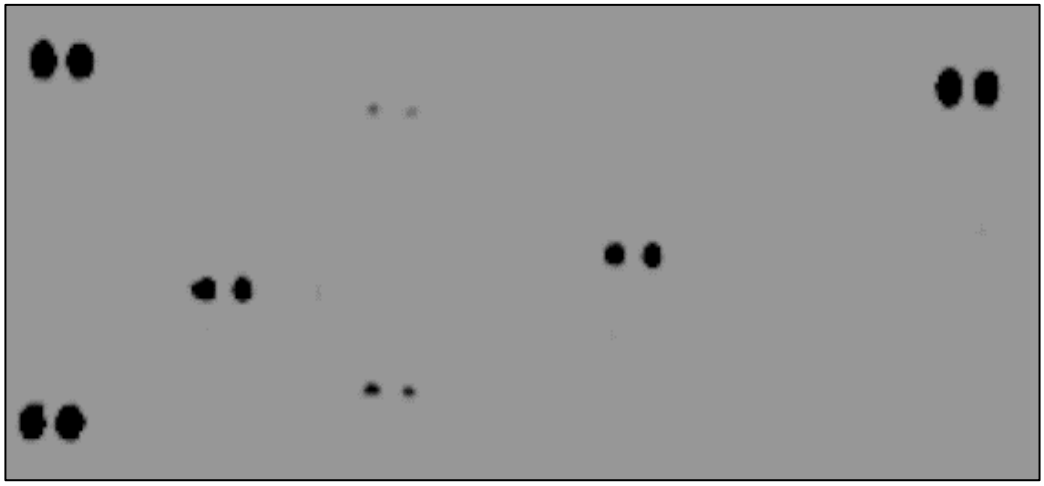

(A)

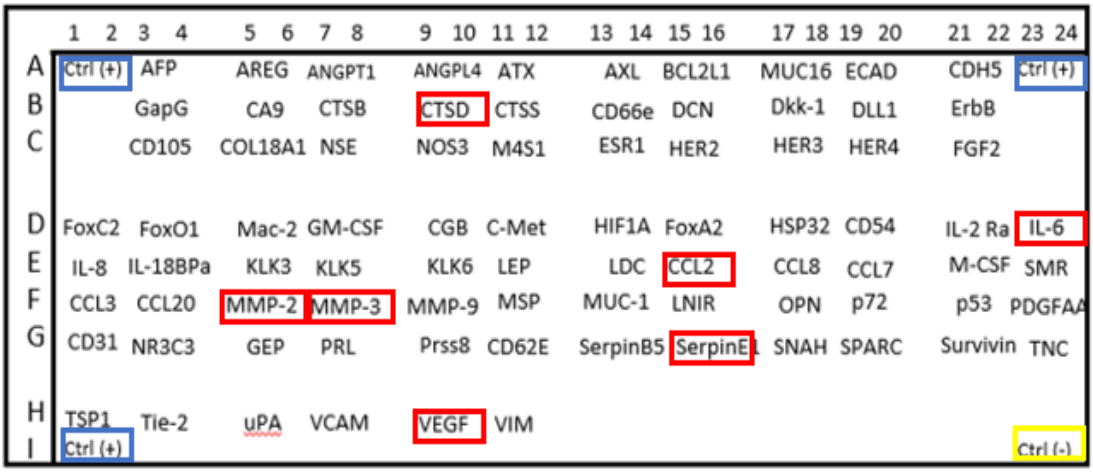

(B)

Figure 5.7 A & B: Cytokine Array analysis of conditioned media taken following CAF1 stimulation with SCC2 CM (M1). (A) Representative photo for developed cytokine membrane for CAF1 media after SCC2 CM treatment. **(B)** The array map. The blue and yellow boxes in the array map denote the positive and negative array controls, respectively. The red box denotes factors present in CAF1-SCC2-M1 conditioned media. A relatively low number of cytokines uptakes. MMP2 and CCL2 displayed more intense spots.

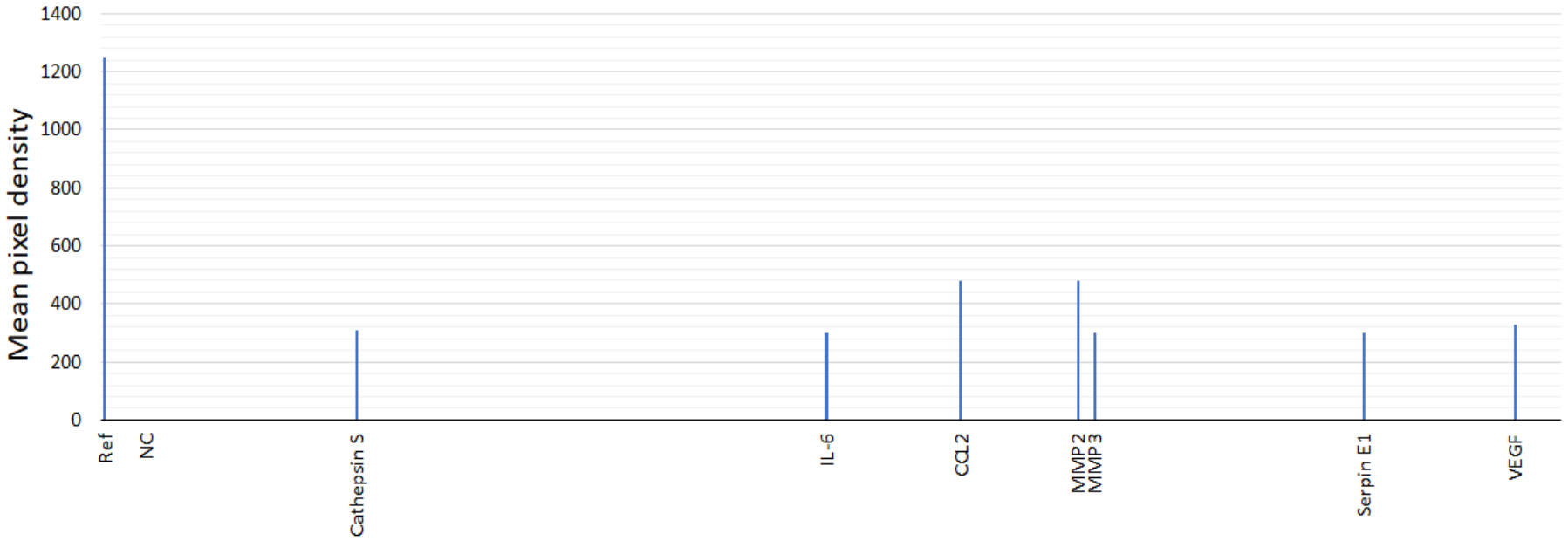

(C)

Figure 5.7 C: Cytokine Array analysis of conditioned media taken following CAF1 stimulation with SCC2 CM (M1). (C) Densitometry analysis of CAF1-SCC2-M1 conditioned media. Bars represent the mean of densitometry values of each array's duplicate repeat spot. (Ref) denotes a positive control value that is used as a reference for values normalisation. (NC) denotes array negative control spots. Fewer cytokines were identified in SCC2-CAF1 M1 compared to SCC89 CM. CCL2 and MMP2 showed a slight elevation upon SCC2 CM culture.

(A)

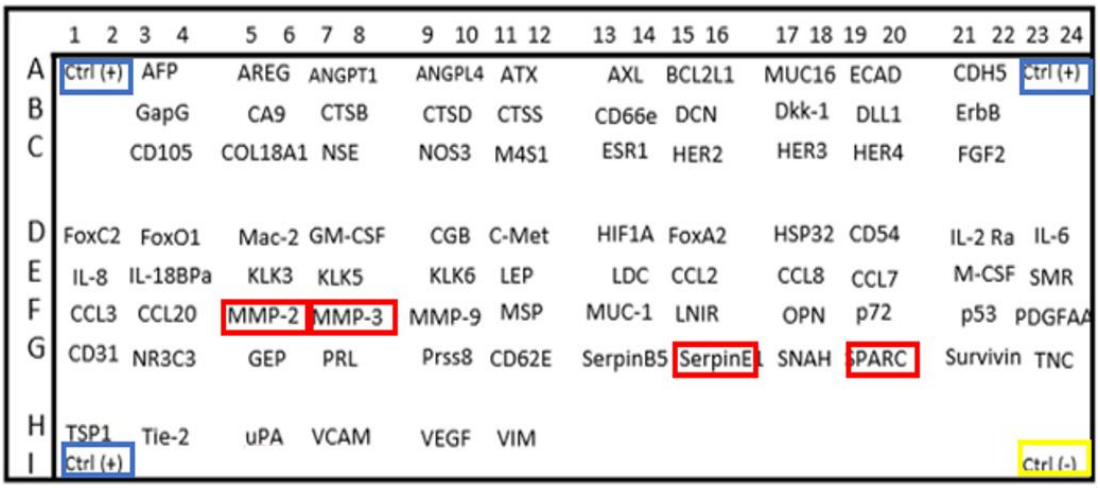

(B)

Figure 5.8 A & B: Cytokine Array analysis of CAF1 serum-free conditioned media following SCC2 CM stimulation (M2). **(A)** Representative image of the developed cytokine membrane for CAF1 serum-free media following SCC2 CM treatment. **(B)** The array map. The blue and yellow boxes in the array map denote the positive and negative array controls, respectively. The red box denotes factors present in CAF1-SCC2-M2 conditioned media. A reduced number of cytokines were expressed, with weak signals.

(C)

Figure 5.8 C: Cytokine Array analysis of CAF1 serum-free conditioned media following SCC2 CM stimulation (M2 (C) Densitometry analysis of CAF1-SCC2-M2 conditioned media. Bars represent the mean of densitometry values of each array's duplicate repeat spot. (Ref) denotes a positive control value that is used as a reference for values normalisation. (NC) denotes array negative control spots. Slight elevation of MMP2 is noted followed by MMP3, Serpin E1 and SPARC.

5.4.1.2 CAF2

In characterisation work in chapter 4, CAF2 showed myofibroblastic phenotype features by expression high level of α-SMA and low SA-β-gal percentage. The basal secretory profile of CAF2 cytokine was determined by incubating the cells with normal growth media (Figure 5.9) or serum-free media (Figure 5.10). MMP2 and SPARC were only the detectable factors by CAF2.

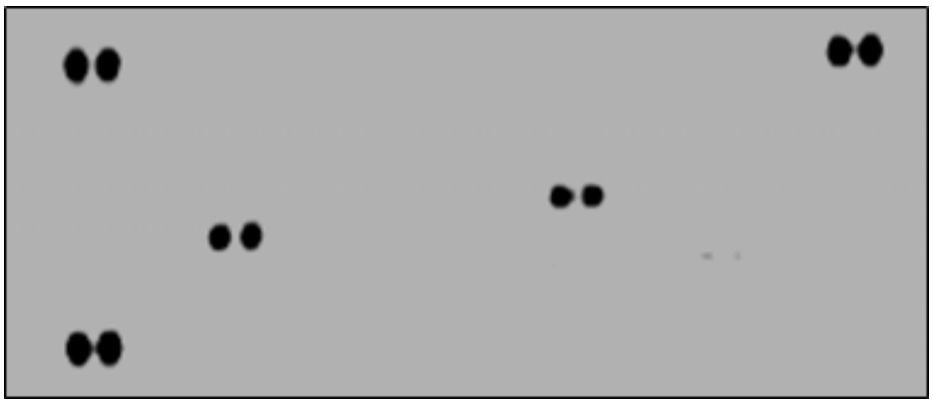

(A)

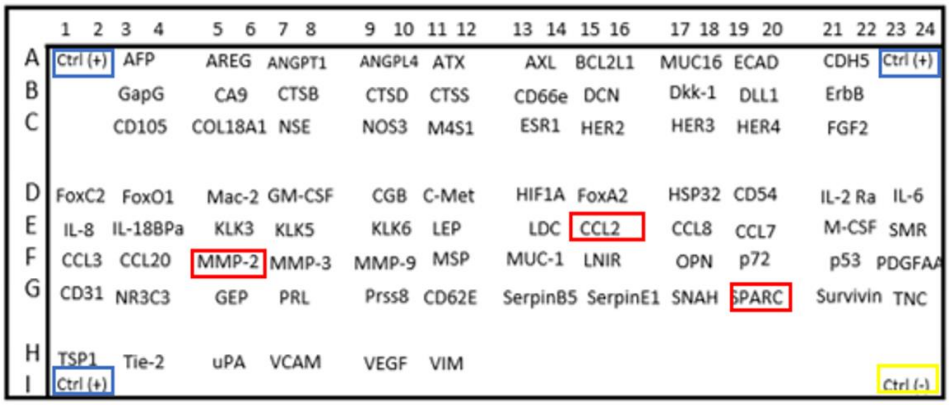

(B)

Figure 5.9 A & B: Cytokine Array analysis of CAF2 conditioned media (M1). **(A)** Representative image of the CAF2-M1 developed cytokine membrane. **(B)** The array map. The blue and yellow boxes in the array map denote the positive and negative array controls, respectively. Red box denotes factors present in CAF2-M1 conditioned media. The large dark spots relate to CCL2 and MMP2. Weak expression of SPARC was detected.

(C)

Figure 5.9 C: Cytokine Array analysis of CAF2 conditioned media (M1). **(C)** Densitometry analysis of factors detected in CAF2-M1 conditioned media. Bars represent the mean of densitometry values of each array's duplicate repeat spot. (Ref) denotes a positive control value that is used as a reference for result optimisation between the membranes. (NC) denotes array negative control spots. MMP2, CCL2 and SPARC were the detected factors in CAF2 M1.

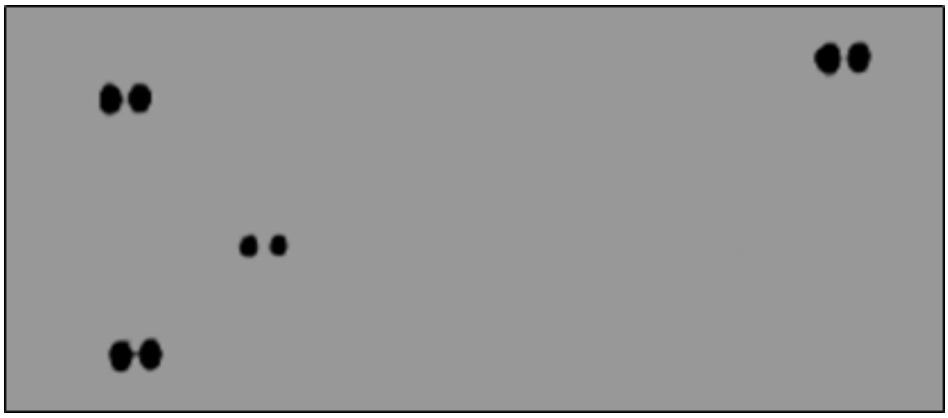

(A)

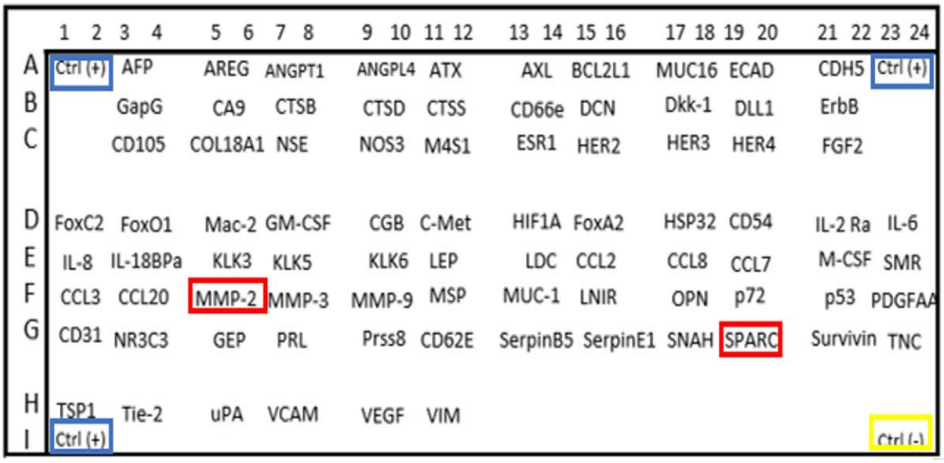

(B)

Figure 5.10 A & B: Cytokine Array analysis of CAF2 serum-free conditioned media (M2). **(A)** Representative photo for CAF2-M2 developed cytokine membrane. **(B)** The array map. The blue and yellow boxes in the array map denote the positive and negative array controls, respectively. Red box denotes factors present in CAF2-M2 conditioned media. Evident expression of MMP2 spots is observed. Hints of SPARC expression was detected using densitometry analysis.

(C)

Figure 5.10 C: Cytokine Array analysis of CAF2 serum-free conditioned media (M2). **(C)** Densitometry analysis of factors detected in CAF2-M2 conditioned media. Bars represent the mean of densitometry values of each array's duplicate repeat spot. (Ref) denotes a positive control value that is used as a reference for result optimisation between the membranes. (NC) denotes array negative control spots. The basal CAF2 secretome consists of MMP2 and low levels of SPARC.

The cytokine expression profile of CAF2 culture stimulated with SCC89 conditioned media demonstrated a relatively high number of cytokines with variable densities, namely, CSTD, GM-CSF, C-Met, IL-6, IL-8, KLK6, CCL2, MMP2, MMP3, OPN, GEP, SerpinE, SPARC and VEGF (Figure 5.11). The range of cytokines identified in CAF2 culture is reduced after replacing the SCC89 conditioned media with serum-free media and includes IL-6, IL-8, CCL2, MMP2, MMP3, and SPARC (Figure 5.12).

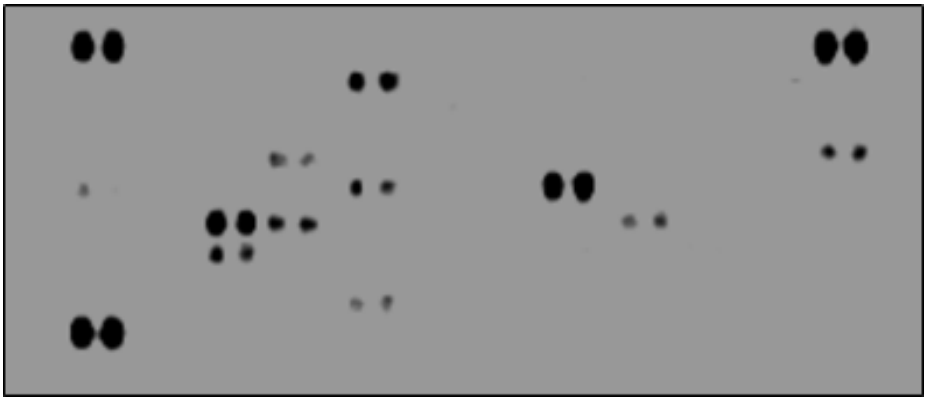

(A)

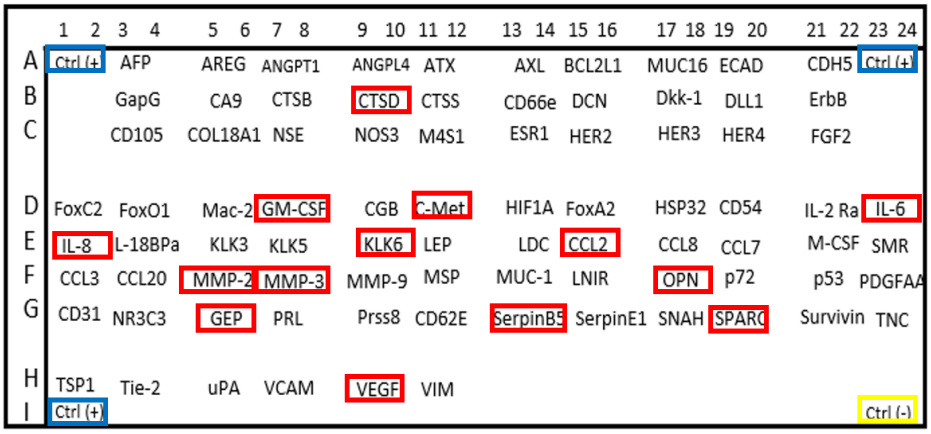

(B)

Figure 5.11 A & B: Cytokine Array analysis of conditioned media taken following CAF2 stimulation with SCC89 CM (M1). **(A)** Representative photo for developed cytokine membrane for CAF2 media after SCC89 CM treatment. **(B)** The array map. The blue and yellow boxes in the array map denote the positive and negative array controls, respectively. The red box denotes factors present in CAF2-SCC89-M1 conditioned media. Many cytokines were expressed with varied intensity. CCL2, MMP2 and CSTD were the larger dark spots.

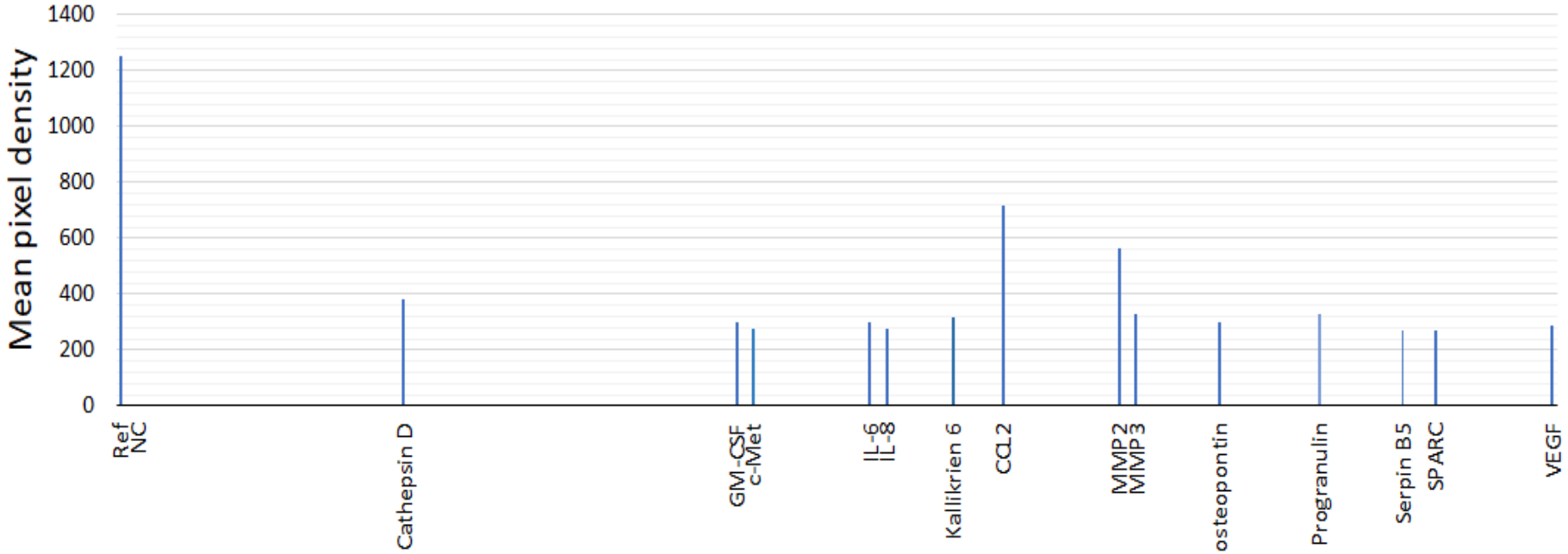

(C)

Figure 5.11 C: Cytokine Array analysis of conditioned media taken following CAF2 stimulation with SCC89 CM (M1). **(C)** Densitometry analysis of factors detected in CAF2-SCC89-M1 conditioned media. Bars represent the mean of densitometry values of each array's duplicate repeat spot. (Ref) denotes a positive control value that is used as a reference for result optimisation between the membranes. (NC) denotes array negative control spots A wide variety of cytokines were detected, comparable to SCC89-CAF1 M1 densitometry analysis (Figure 5.3 C).

.

(A)

	1	2	3	4	5	6	7	8	9	10	11	12	13	14	15	16	17	18	19	20	21	22	23	24
A	Ctrl (+)		AFP		AREG		ANGPT1		ANGPL4		ATX		AXL		BCL2L1		MUC16		ECAD		CDH5		Ctrl (+)	
B			GapG		CA9		CTSB		CTSD		CTSS		CD66e		DCN		Dkk-1		DLL1		ErbB			
C			CD105		COL18A1		NSE		NOS3		M4S1		ESR1		HER2		HER3		HER4		FGF2			
D	FoxC2		FoxO1		Mac-2		GM-CSF		CGB		C-Met		HIF1A		FoxA2		HSP32		CD54		IL-2 Ra		IL-6	
E	IL-8		IL-18BPa		KLK3		KLK5		KLK6		LEP		LDC		CCL2		CCL8		CCL7		M-CSF		SMR	
F	CCL3		CCL20		MMP-2		MMP-3		MMP-9		MSP		MUC-1		LNIR		OPN		p72		p53		PDGFAA	
G	CD31		NR3C3		GEP		PRL		Prss8		CD62E		SerpinB5		SerpinE1		SNAH		SPARC		Survivin		TNC	
H	TSP1		Tie-2		uPA		VCAM		VEGF		VIM													
I	Ctrl (+)																						Ctrl (-)	

(B)

Figure 5.12 A & B: Cytokine Array analysis of CAF2 serum-free conditioned media following SCC89 CM stimulation (M2). **(A)** Representative image of the developed cytokine membrane for CAF2 serum-free media following SCC89 CM treatment. **(B)** The array map. The blue and yellow boxes in the array map denote the positive and negative array controls, respectively. The red box denotes factors present in CAF"-SCC89-M2 conditioned media. A reduced number of cytokines were detected, varying in intensity compared to M1.

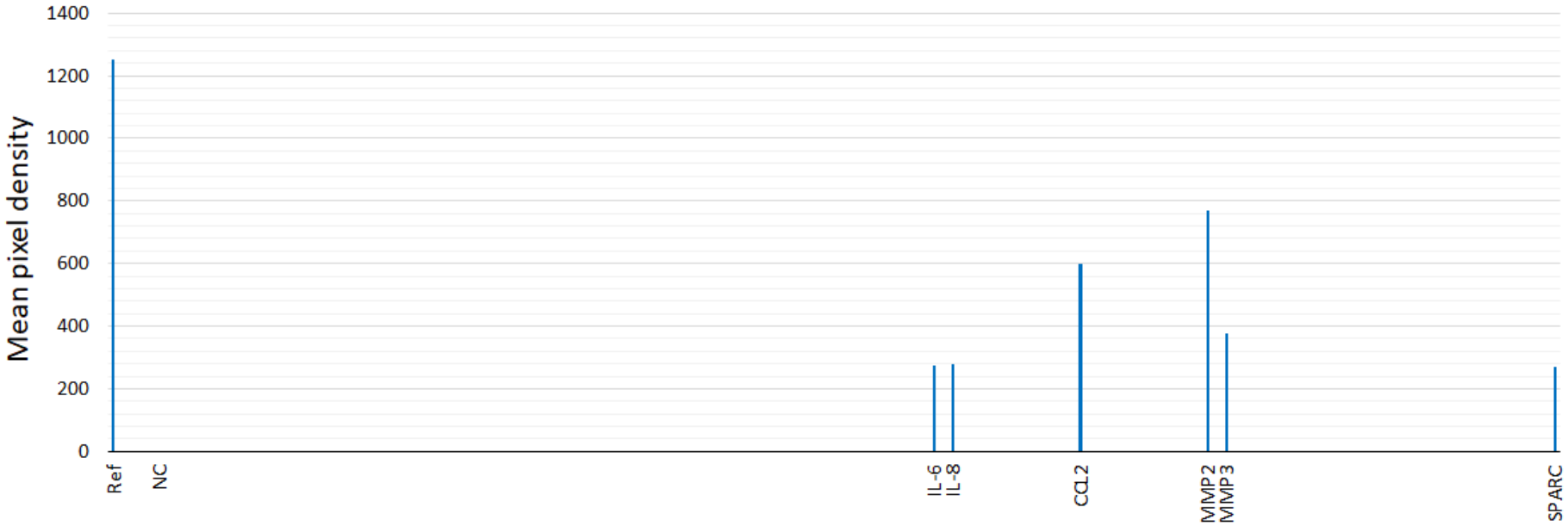

(C)

Figure 5.12 C: Cytokine Array analysis of CAF2 serum-free conditioned media following SCC89 CM stimulation (M2). (C) Densitometry analysis of CAF2-SCC89-M2 conditioned media. Bars represent the mean of densitometry values of each array's duplicate repeat spot. (Ref) denotes a positive control value that is used as a reference for values normalisation. (NC) denotes array negative control spots. MMP2, CCL2 showed the highest expression. IL6 and IL8 were expressed at a comparable level to SCC89-CAF2 M1.

Similar to our observation in CAF1 stimulation, the SCC2 cell line conditioned media induced less cytokine secretion from CAF2 cells during the stimulation time (CAF2-M1), namely CSTD, IL-6, CCL2, MMP2, MMP3, SPARC and VEGF (Figure 5.13). Also, fewer cytokines were noted in CAF2-M2 following SCC2 conditioned media stimulation, including MMP2, MMP3, CCL2 and SPARC (Figure 5.14).

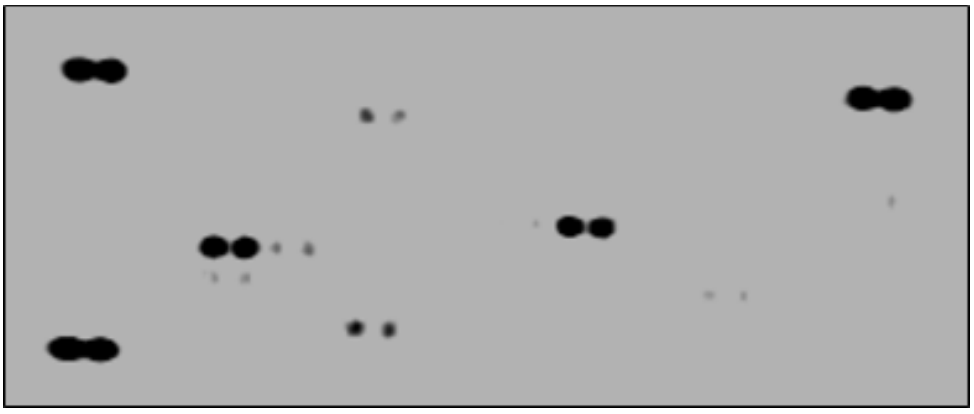

(A)

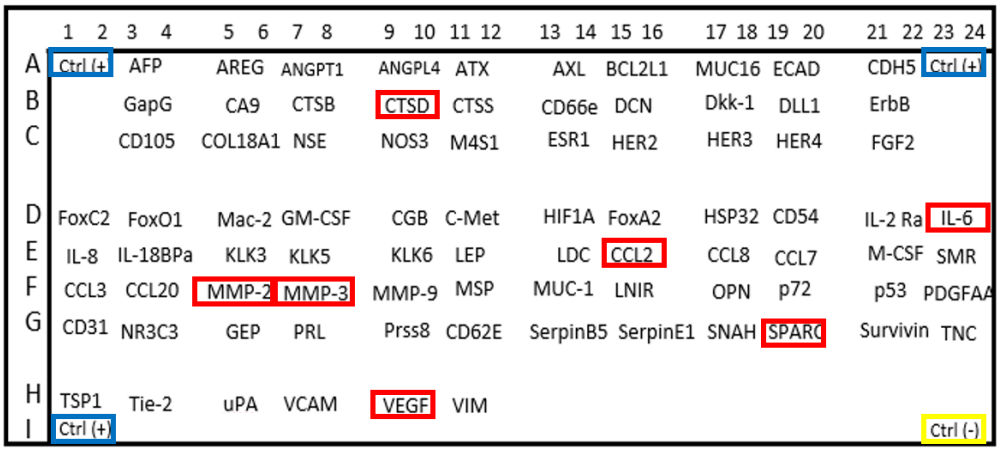

(B)

Figure 5.13 A & B: Cytokine Array analysis of conditioned media taken following CAF2 stimulation with SCC2 CM (M1). **(A)** Representative image of the developed cytokine membrane for CAF2 media after SCC2 CM treatment. **(B)** The array map. The blue and yellow boxes in the array map denote the positive and negative array controls, respectively. The red box denotes factors present in CAF2-SCC2-M1 conditioned media. Only CCL2 and MMP2 showed strong intense spots. Other cytokines present with weak spot intensity.

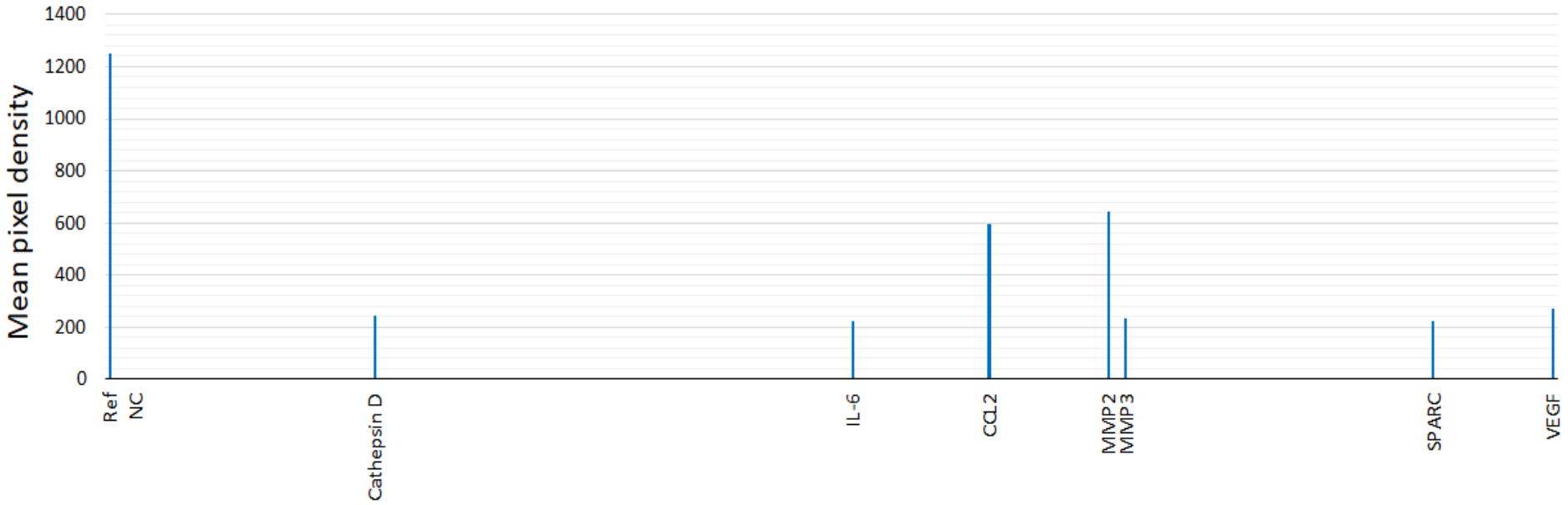

(C)

Figure 5.13 C: Cytokine Array analysis of conditioned media taken following CAF2 stimulation with SCC2 CM (M1) (C) Densitometry analysis of CAF2-SCC2-M1 conditioned media. Bars represent the mean of densitometry values of each array's duplicate repeat spot. (Ref) denotes a positive control value that is used as a reference for values normalisation. (NC) denotes array negative control spots. Compared with basal secretion, CCL2 and MMP2 showed upregulation in production, however, a slight elevation was noticed in other upregulated cytokines.

(A)

	1	2	3	4	5	6	7	8	9	10	11	12	13	14	15	16	17	18	19	20	21	22	23	24
A	Ctrl (+)		AFP		AREG		ANGPT1		ANGPL4		ATX		AXL		BCL2L1		MUC16		ECAD		CDH5		Ctrl (+)	
B			GapG		CA9		CTSB		CTSD		CTSS		CD66e		DCN		Dkk-1		DLL1		ErbB			
C			CD105		COL18A1		NSE		NOS3		M4S1		ESR1		HER2		HER3		HER4		FGF2			
D	FoxC2		FoxO1		Mac-2		GM-CSF		CGB		C-Met		HIF1A		FoxA2		HSP32		CD54		IL-2 Ra		IL-6	
E	IL-8		IL-18BPa		KLK3		KLK5		KLK6		LEP		LDC		CCL2		CCL8		CCL7		M-CSF		SMR	
F	CCL3		CCL20		MMP-2		MMP-3		MMP-9		MSP		MUC-1		LNIR		OPN		p72		p53		PDGFAA	
G	CD31		NR3C3		GEP		PRL		Prss8		CD62E		SerpinB5		SerpinE1		SNAH		SPARC		Survivin		TNC	
H	TSP1		Tie-2		uPA		VCAM		VEGF		VIM													
I	Ctrl (+)																						Ctrl (-)	

(B)

Figure 5.14 A & B: Cytokine Array analysis of CAF2 serum-free conditioned media following SCC2 CM stimulation (M2). **(A)** Representative image of the developed cytokine membrane for CAF2 serum-free media following SCC2 CM treatment. **(B)** The array map. The blue and yellow boxes in the array map denote the positive and negative array controls, respectively. The red box denotes factors present in CAF2-SCC2-M2 conditioned media. MMP2 was the most prominent spot followed by CCL2 and SPARC. A weak signal was detected in the MMP3 location.

(C)

Figure 5.14 C: Cytokine Array analysis of CAF2 serum-free conditioned media following SCC2 CM stimulation (M2). **(C)** Densitometry analysis of CAF2-SCC2-M2 conditioned media. Bars represent the mean of densitometry values of each array's duplicate repeat spot. (Ref) denotes a positive control value that is used as a reference for values normalisation. (NC) denotes array negative control spots. 4 cytokines only were upregulated upon CAF2 stimulation with SCC2.

5.4.1.3 NTF322

NTF322 conditioned media revealed a number of upregulated cytokines including, IL6, CCL2, MMP2, SerpinE, SPARC and VEGF (Figure 5.15) However, NTF322 serum-free media exhibited a relatively higher basal secretory profile which consists of MMP3, SerpinE, SPARC and low levels of DCN (Figure 5.16).

(A)

	1	2	3	4	5	6	7	8	9	10	11	12	13	14	15	16	17	18	19	20	21	22	23	24
A	Ctrl (+)		AFP		AREG		ANGPT1		ANGPL4		ATX		AXL		BCL2L1		MUC16		ECAD		CDH5		Ctrl (+)	
B			GapG		CA9		CTSB		CTSD		CTSS		CD66e		DCN		Dkk-1		DLL1		ErbB			
C			CD105		COL18A1		NSE		NOS3		M4S1		ESR1		HER2		HER3		HER4		FGF2			
D	FoxC2		FoxO1		Mac-2		GM-CSF		CGB		C-Met		HIF1A		FoxA2		HSP32		CD54		IL-2 Ra		IL-6	
E	IL-8		IL-18BPa		KLK3		KLK5		KLK6		LEP		LDC		CCL2		CCL8		CCL7		M-CSF		SMR	
F	CCL3		CCL20		MMP-2		MMP-3		MMP-9		MSP		MUC-1		LNIR		OPN		p72		p53		PDGFAA	
G	CD31		NR3C3		GEP		PRL		Prss8		CD62E		SerpinB3		SerpinE1		SNAH		SPARC		Survivin		TNC	
H	TSP1		Tie-2		uPA		VCAM		VEGF		VIM													
I	Ctrl (+)																						Ctrl (-)	

(B)

Figure 5.15 A & B: Cytokine Array analysis of NTF322 conditioned media (M1). **(A)** Representative image of the NTF322-M1 developed cytokine membrane. **(B)** The array map. The blue and yellow boxes in the array map denote the positive and negative array controls, respectively. Red boxes denote factors present in NTF322-M1 conditioned media.

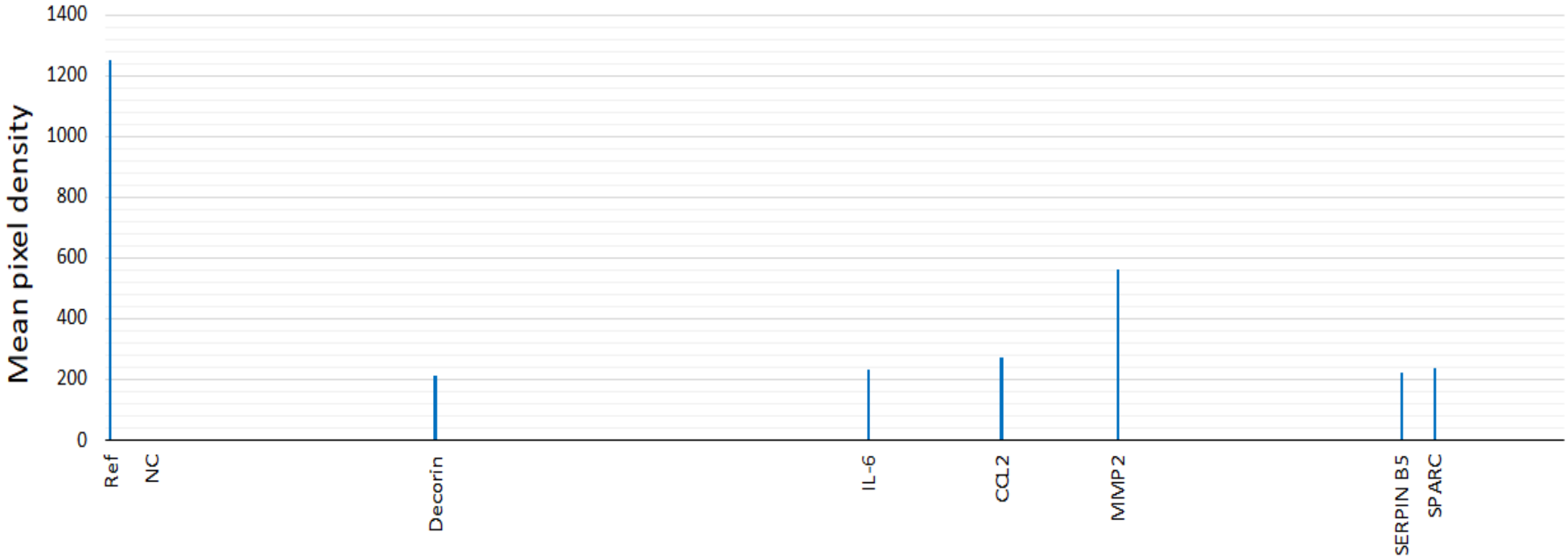

(C)

Figure 5.15 C: Cytokine Array analysis of NTF322 conditioned media (M1). (C) Densitometry analysis of NTF322-M1 conditioned media. Bars represent the mean of densitometry values of each array's duplicate repeat spot. (Ref) denotes a positive control value that is used as a reference for values normalisation. (NC) denotes array negative control spots. MMP2 is the factor identified at the highest level in NTF322-M1.

(A)

	1	2	3	4	5	6	7	8	9	10	11	12	13	14	15	16	17	18	19	20	21	22	23	24
A	Ctrl (+)		AFP		AREG		ANGPT1		ANGPL4		ATX		AXL		BCL2L1		MUC16		ECAD		CDH5		Ctrl (+)	
B			GapG		CA9		CTSB		CTSD		CTSS		CD66e		DCN		Dkk-1		DLL1		ErbB			
C			CD105		COL18A1		NSE		NOS3		M4S1		ESR1		HER2		HER3		HER4		FGF2			
D	FoxC2		FoxO1		Mac-2		GM-CSF		CGB		C-Met		HIF1A		FoxA2		HSP32		CD54		IL-2 Ra		IL-6	
E	IL-8		IL-18BPa		KLK3		KLK5		KLK6		LEP		LDC		CCL2		CCL8		CCL7		M-CSF		SMR	
F	CCL3		CCL20		MMP-2		MMP-3		MMP-9		MSP		MUC-1		LNIR		OPN		p72		p53		PDGFAA	
G	CD31		NR3C3		GEP		PRL		Prss8		CD62E		SerpinB5		SerpinE1		SNAH		SPARC		Survivin		TNC	
H	TSP1		Tie-2		uPA		VCAM		VEGF		VIM													
I	Ctrl (+)																						Ctrl (-)	

(B)

Figure 5.16 A & B: Cytokine Array analysis of NTF322 serum-free conditioned media (M2). **(A)** Representative image of the NTF322-M2 developed cytokine membrane (**B)** The array map. The blue and yellow boxes in the array map denote the positive and negative array controls, respectively. Red boxes denote factors present in NTF322-M2 conditioned media. Only MMP2 spots showed strong expression, other cytokines expressed weak signals.

(C)

Figure 5.16 C: Cytokine Array analysis of NTF322 serum-free conditioned media (M2. (C) Densitometry analysis of NTF322-M2 conditioned media. Bars represent the mean of densitometry values of each array duplicate repeat spot. (Ref) denotes a positive control value that is used as a reference for values normalisation. (NC) denotes array negative control spots.

Incubation of NTF322 with SCC89 cell line media resulted in the production of a number of cytokines, seen with variable uptake density on the array, including CSTD, GM-CSF, IL-6, IL-8, KLK6, CCL2, MMP2, MMP3, OPN, GEP, SPARC and VEGF (Figure 5.17). Incubation of NTF322 with serum-free media following SCC89 conditioned media stimulation revealed upregulation in NTF322 secretory profile represented by CTSB, DCN, IL-6, IL-8, CCL2, MMP2, MMP3, GEP, and SPARC (Figure 5.18).

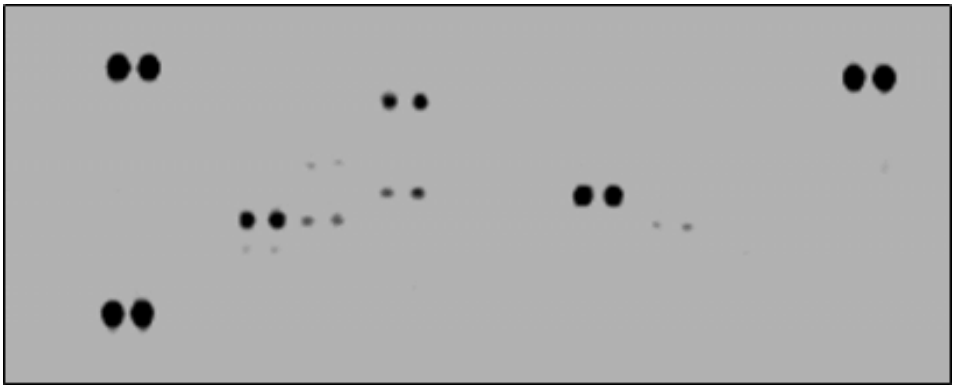

(A)

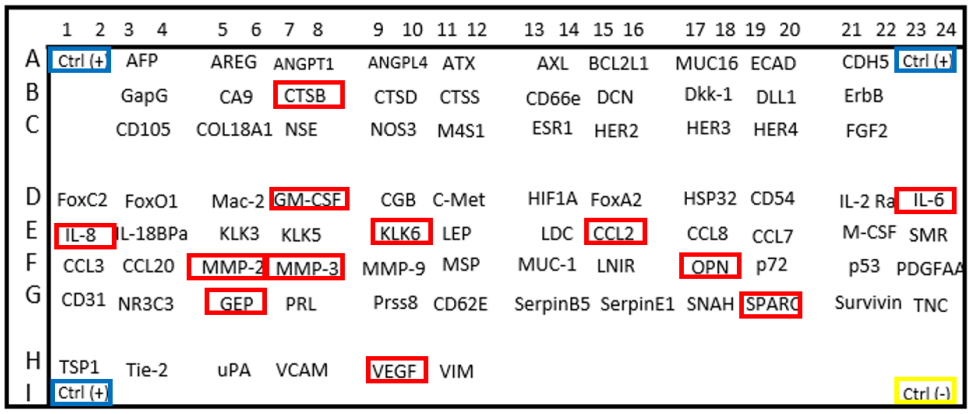

(B)

Figure 5.17 A & B: Cytokine Array analysis of conditioned media taken following NTF322 stimulation with SCC89 CM (M1). **(A)** Representative image of the developed cytokine membrane for NTF322 media after SCC89 CM treatment **(B)** The array map. The blue and yellow boxes in the array map denote the positive and negative array controls, respectively. The red box denotes factors present in NTF322-SCC89-M1 conditioned media. A number of duplicated spots expressed at different size and intensity.

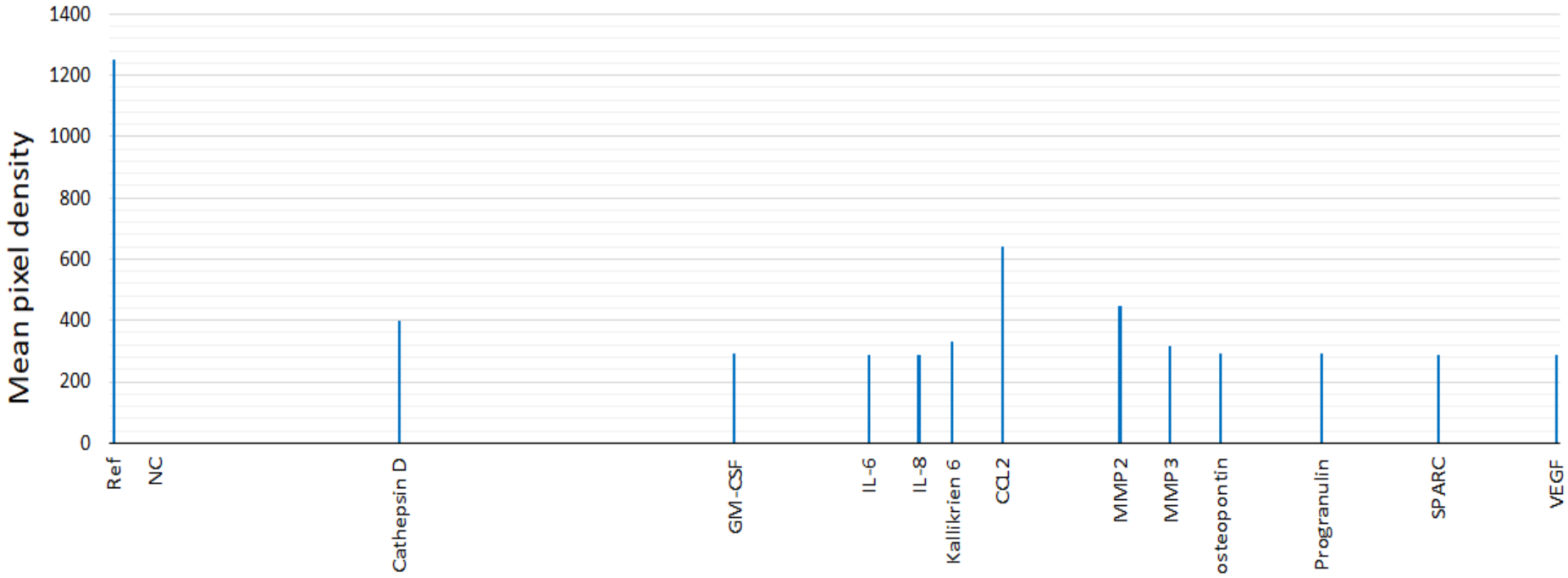

(C)

Figure 5.17 C: Cytokine Array analysis of conditioned media taken following NTF322 stimulation with SCC89 CM (M1). **(C)** Densitometry analysis of NTF322-SCC89-M1 conditioned media. Bars represent the mean of densitometry values of each array's duplicate repeat spot. (Ref) denotes a positive control value that is used as a reference for values normalisation. (NC) denotes array negative control spots. CCL2, MMP2 and CSTD were the highest secreted factors.

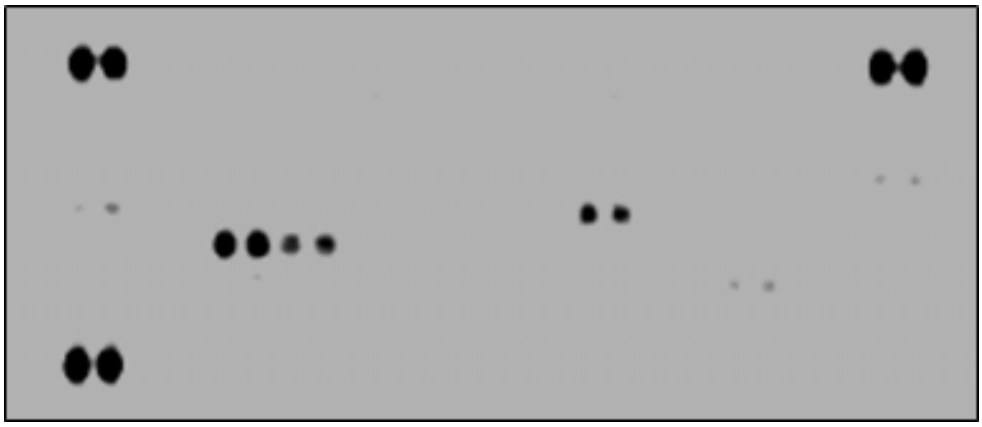

(A)

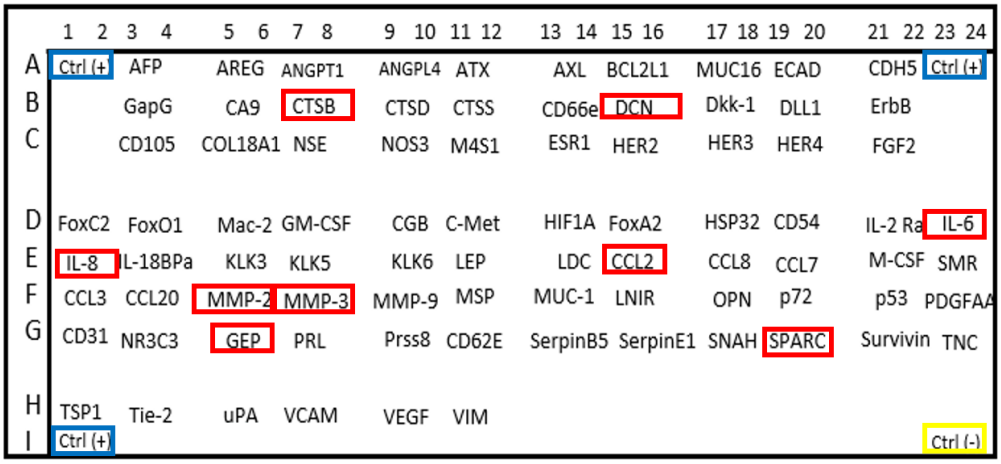

(B)

Figure 5.18 A & B: Cytokine Array analysis of NTF322 serum-free conditioned media following SCC89 CM stimulation (M2). **(A)** Representative image of the developed cytokine membrane for NTF322 serum-free media following SCC89 CM treatment **(B)** The array map. The blue and yellow boxes in the array map denote the positive and negative array controls, respectively. The red boxes denote factors present in NTF322-SCC89-M2 conditioned media. A lesser number of cytokines is expressed compared to M1.

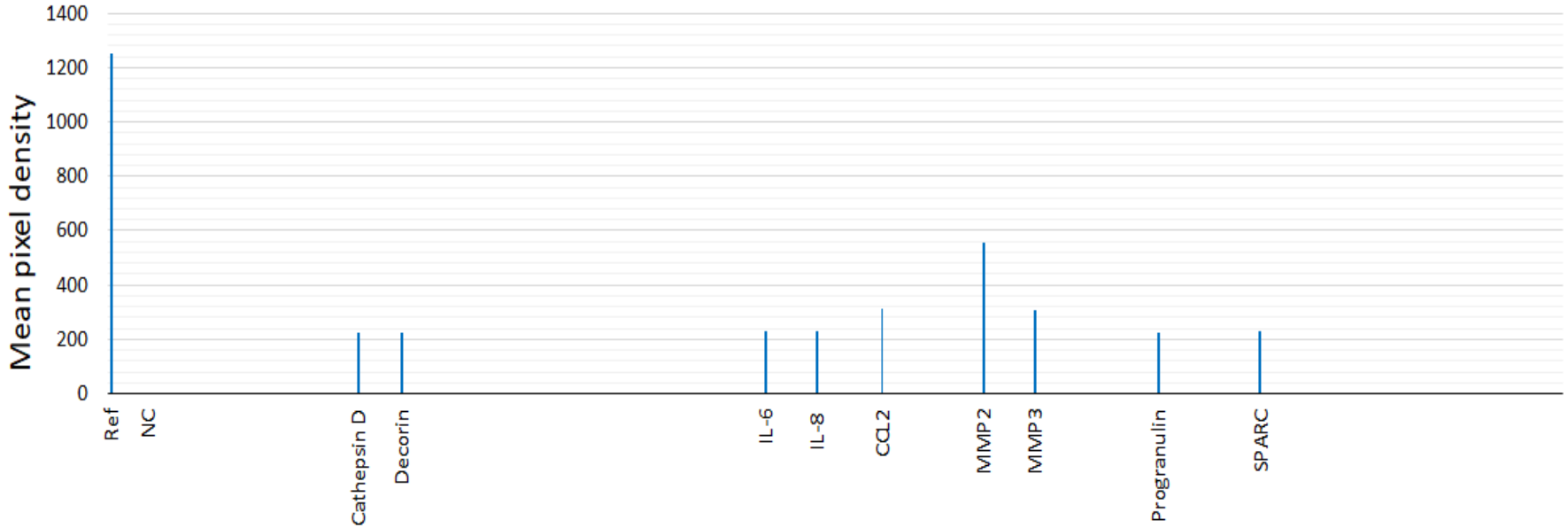

(C)

Figure 5.18: Cytokine Array analysis of NTF322 serum-free conditioned media following SCC89 CM stimulation (M2). **(C)** Densitometry analysis of NTF322-SCC89-M2 conditioned media. Bars represent the mean of densitometry values of each array's duplicate repeat spot. (Ref) denotes a positive control value that is used as a reference for values normalisation. (NC) denotes array negative control spots.

Cytokine analysis of SCC2 cell line conditioned media and NTF322 culture revealed a smaller range cytokine secretion including CSTD, DKK1, IL-6, IL-8, LDC, CCL2, MMP2, GEP SerpinE and VEGF when compared to SCC89-NTF322 (Figure 5.19). Also, fewer cytokines were noted in NTF322-M2 following SCC2 conditioned media stimulation including DCN, MMP2, SerpinE and SPARC (Figure 5.20).

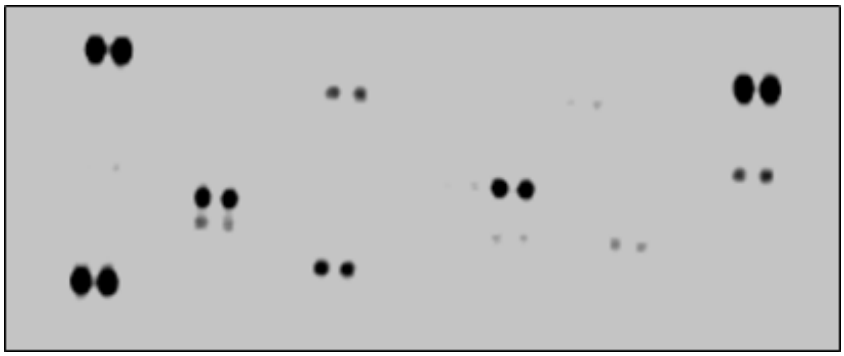

(A)

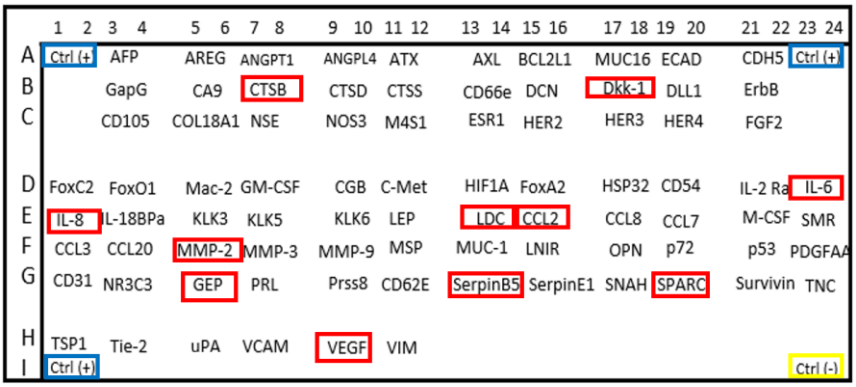

(B)

Figure 5.19 A & B: Cytokine Array analysis of conditioned media taken following NTF322 stimulation with SCC2 CM (M1). **(A)** Representative image of the developed cytokine membrane for NTF322 media after SCC2 CM treatment **(B)** The array map. The blue and yellow boxes in the array map denote the positive and negative array controls, respectively. The red boxes denote factors present in NTF322-SCC2-M1 conditioned media. A larger number of factors are expressed. IL6 and VEGF are the most prominent spots following CCL2, MMP2 and CTSB.

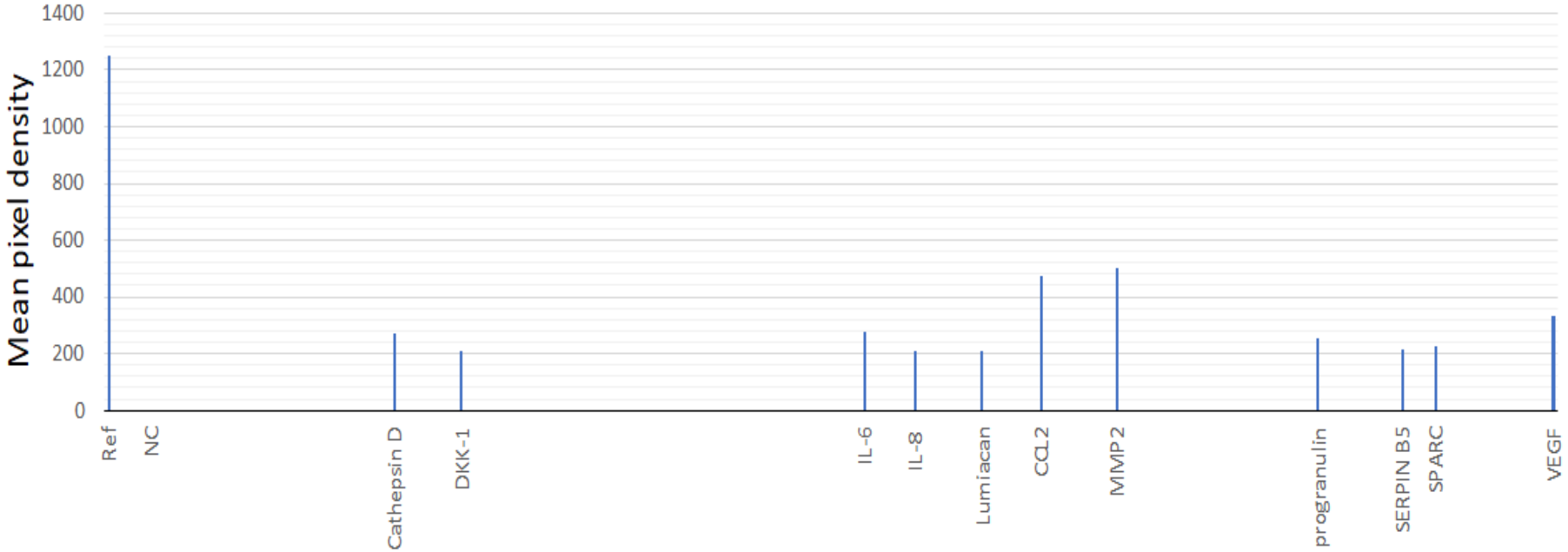

(C)

Figure 5.19 C: Cytokine Array analysis of conditioned media taken following NTF322 stimulation with SCC2 CM (M1). **(C)** Densitometry analysis of NTF322-SCC2-M1 conditioned media. Bars represent the mean of densitometry values of each array's duplicate repeat spot. (Ref) denotes a positive control value that is used as a reference for values normalisation. (NC) denotes array negative control spots.

(A)

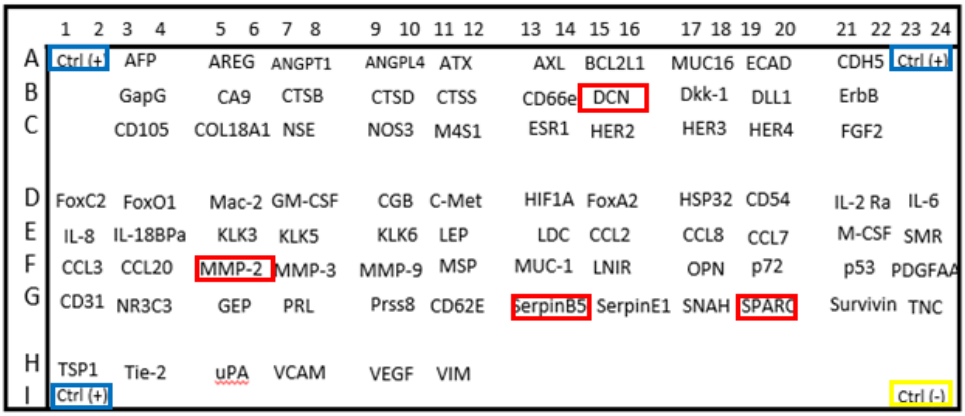

(B)

Figure 5.20 A & B: Cytokine Array analysis of NTF322 serum-free conditioned media following SCC2 CM stimulation (M2). **(A)** Representative image of the developed cytokine membrane for NTF322 serum-free media following SCC2 CM treatment. **(B)** The array map. The blue and yellow boxes in the array map denote the positive and negative array controls, respectively. The red box denotes factors present in NTF322-SCC2-M2 conditioned media. Less factors expressed compared by M1.

(C)

Figure 5.20 C: Cytokine Array analysis of NTF322 serum-free conditioned media following SCC2 CM stimulation (M2). **(C)** Densitometry analysis of NTF322-SCC2-M2 conditioned media. Bars represent the mean of densitometry values of each array's duplicate repeat spot. (Ref) denotes a positive control value that is used as a reference for values normalisation. (NC) denotes array negative control spots. MMP2 is the prominent cytokine following SCC2 media stimulation.

5.4.2 A summary of cytokine array analysis

Data presented in the previous cytokine arrays analysis is summarised in the following tables. Tables 5.1- 5.3 summarise cytokines production in response to M1 in all tested OPSCC fibroblasts. Tables 5.4-5.6 summarise cytokines production in OPSCC fibroblasts response to M2.

Table 5.1: Summary of cytokines produced in M1: CAF1 incubated with SCC89 or SCC2 conditioned media.

Factors detected in all cell lines CM incubated with CAF1	Factors more elevated in SCC89-CAF1 CM	Factors more elevated in SCC2-CAF1 CM
Cathepsin D	Decorin	VEGF
IL-6	IL-8	
CCL2	GM-CSF	
MMP3	Osteopontin	
Serpin E1	Progranulin	
	Kallikrein 6	
	Serpin B5	
	SPARC	

Table 5.2: Summary of cytokines upregulated in CAF2 during incubation with SCC89 or SCC2 conditioned media (M1).

Factors detected in all cell lines CM incubated with CAF2	Factors more elevated in SCC89-CAF2 CM	Factors more elevated in SCC2-CAF2 CM
Cathepsin D	GM-CSF	
IL-6	Kallikrein 6	
IL8	Osteopontin	
CCL2	Ep-CAM	
Progranulin	C-Met	
MMP3		
VEGF		

Table 5.3: Summary of cytokines produced during the incubation of NTF322 with SCC89 or SCC2 conditioned media (M1).

Factors detected in all cell lines CM incubated with NTF322	Factors more elevated in SCC89-NTF322 CM	Factors more elevated in SCC2-NTF322 CM
Cathepsin D	GM-CSF	DKK-1
IL-6	MMP3	Lumiacan
IL-8	Osteopontin	
CCL2	Kallikrein 6	
Progranulin		
VEGF		

Table 5.4: Summary of cytokines produced in CAF1 serum-free media following a period of SCC89 or SCC2 conditioned media stimulation (M2).

Basal Secretion of CAF1	Elevated in All Stimulated CAF1 SFM	More Elevated in SCC89-CAF2 SFM	More Elevated in SCC2- CAF2 SFM
MMP-2	MMP3	Cathepsin D	
	Serpin E1	IL-6	
	SPRAC	IL-8	
		CCL2	
		Decorin	
		Progranulin	

Table 5.5: Summary of cytokines produced in CAF2 serum-free media following a period of SCC89 or SCC2 conditioned media stimulation (M2).

Basal Secretion of CAF2	Elevated in All Stimulated CAF2 SFM	More Elevated in SCC89-CAF2 SFM	More Elevated in SCC2- CAF2 SFM
MMP-2	CCL2	IL-6	
SPARC	MMP3	IL-8	

Table 5.6: Summary of cytokines produced in NTF322 serum-free media following a period of SCC89 or SCC2 conditioned media stimulation (M2).

Basal Secretion of NTF322	Elevated in All Stimulated NTF322 SFM	More Elevated in SCC89-NTF322 SFM	More Elevated in SCC2- NTF322 SFM
Decorin		Cathepsin D	
MMP-2		IL-6	
SPARC		IL-8	
Serpin B5		CCL2	
		MMP3	
		Progranulin	
		VEGF	

From the above previous tables, we can conclude that M1 contained more cytokines compared to M2. The former consists of a mixture of cancer cell line conditioned media plus fibroblast media under the activation condition, while the latter represents fibroblasts media only after short incubation with OPSCC cell lines media. Moreover, all stimulated OPSCC fibroblasts stimulated secretion of a wide range of cytokines produced in response to SCC89, but much less so in response to SCC2. This remarkable difference was also evident when comparing the relevant M1 and M2 analyses.

OPN, KLK6 and GM-CSF were detected exclusively in SCC89 M1, and they were not observed in SCC2 M1. Furthermore, IL-6 and IL-8 were secreted exclusively from fibroblasts upon SCC89 conditioned media incubation (M2), and they were not expressed in response to SCC2 CM. Other factors, including CCL2 and MMP3, were secreted in response to both OPSCC cell lines incubation.

MMP2 was the detectable factor in CAF1 and CAF2 basal secretome that was upregulated during activation with cell line CM. However, stimulated CAF1 showed a wider range of cytokines produced in response to both cell lines stimulation compared to CAF2. Notably, NTF322 produces a wider range of cytokines at M2 than CAFs and showed relatively high cytokine production in reaction to SCC89 only.

5.4.3 OPN basal level in OPSCC

OPN expression was assessed in additional OPSCC cell lines, SCC90 (HPV-positive cell line) and SCC72 (HPV-negative cell line). Firstly, we investigated OPN basal expression in all OPSCCs used in this study. qRT-PCR analysis showed differences in OPN expression between the four cell lines. SCC89 and SCC72 (HPV-negative) displayed higher values of OPN mRNA expression (relative to β2m). This difference was statistically significant compared to the HPV-positive cell lines SCC90 and SCC2 ($p<0.05$) (Figure 5.21).

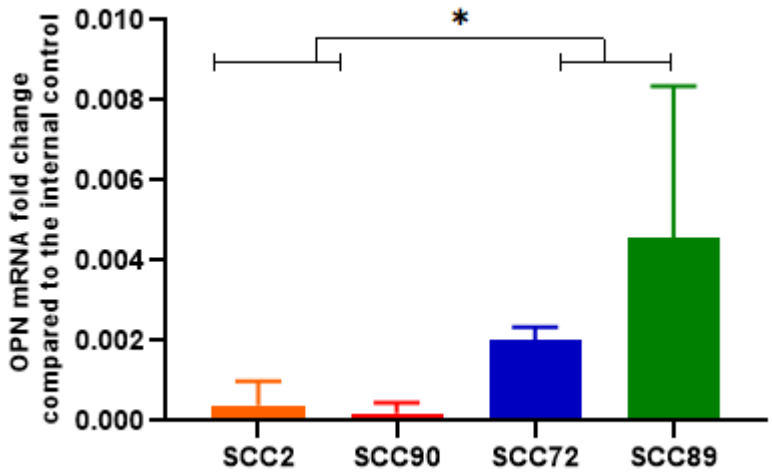

Figure 5.21: High basal level of OPN mRNA in HPV-negative cell lines compared HPV-positive cell lines. The cells pellets were collected, and RNA extraction was performed. cDNA was constructed at volume 20µl using 400ng of the RNA. OPN mRNA expression was analysed using the qRT-PCR technique. OPN fold change compared to β2m. Data represent the mean of (N=3,n=3). Error bars= SD. Statistical analysis was determined using two-tailed Student *t*-test with $*p < 0.05$.

5.4.4 Interactive co-culture validation for arrays findings

The interactive approach was selected to validate the cytokine array findings and explore the molecular changes in the co-cultured cells. NTF10 were added to the interactive co-culture experiment for further results validation.

Transwell inserts (pore size 0.4 µm) were utilised in the co-culture model bringing the advantages of fluid movement and secretion transportation between two cultures through the pores in the membrane without direct physical contact. Cultivation in a separate compartment provides the feasibility of analysing the two cell types used in the experiment without adding additional steps for sorting the cells. To do so, $3x10^5$ cancer cells were grown in growth media on cell culture inserts then co-cultured for 48h with 50,000 cells of NTF3, NTF10, CAF1 or CAF2 plated in a 6-well plate. (NTF10 was added for further result validation). ELISA analysis was performed to detect and quantify the secreted cytokines in the co-culture media. Since the numbers of two cell populations were approximate in all models, target concentration was not subjected to cell number optimisation. qRT-PCR analysis was performed to identify the source of secretion in the co-culture model, also to provide an accurate comparison in target expression levels in monoculture and co-culture models.

In the cytokine array analysis, OPN was produced in all M1s related to SCC89 only, not SCC2. Corresponding to this observation, IL-6 also was secreted particularly from SCC89-induced fibroblasts only. OPN and IL6 have been described in a few studies as candidates in a reciprocal communication loop between the tumour cells and CAFs in OSCC (Qin *et al.*, 2018). Expression of OPN and IL6 in tumours have been associated with tumour cell migration, poor therapeutic response, and poorer clinical outcomes (Chen *et al.*, 2013). CAF-derived IL6 enhances cancer cell metastasis and growth via induction of cancer-derived OPN transcription. Both candidates were suggested as prognostic biomarkers in a number of human tumours including OSCC, however, their expression patterns have not been investigated in OPSCC as yet. Thus, OPN and IL6 were selected for further molecular investigations in this research.

5.4.4.1 Osteopontin

ELISA analysis

To confirm the association between OPN and OPSCC subtypes, OPN ELISA analysis was used for media collected from OPSCC co-cultures. SCC89-fibroblast co-cultures demonstrated a higher level of OPN production while the majority of SCC2-fibroblast co-cultures failed to produce a detectable amount of OPN using DuoSet ELISA set (sensitivity range 4000-62.5 pg/ml). The differences between co-cultured SCC89s were not statistically significant using One-way ANOVA ($p>0.05$). Figure 5.22 and Table 5.7 illustrate OPN expression values in the co-culture models.

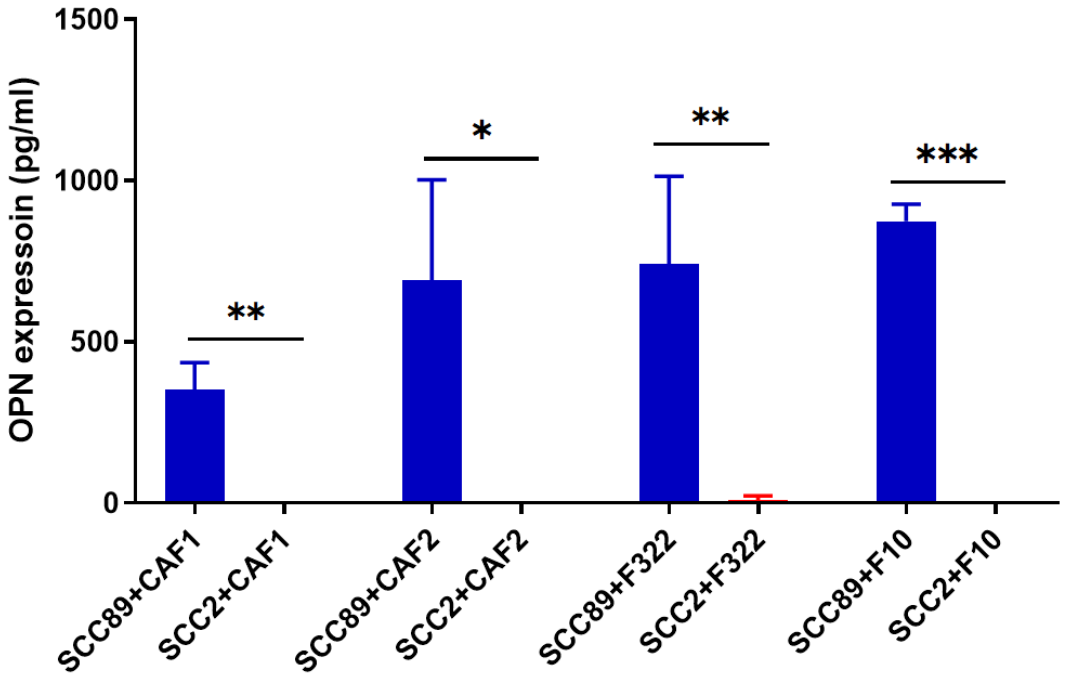

Figure 5.22: Higher levels of OPN protein secretion in SCC89-fibroblast co-cultures than in SCC2-fibroblast co-cultures. SCC89 or SCC2 ($3x10^5$ cells) were co-cultured with OPSCC fibroblasts (CAF1, CAF2, NTF322, NTF10) (50,000 cells) using transwell insert (0.45 µm) for 48h. The collected media was subjected to OPN ELISA analysis. Samples number (n=8), Y-axis denotes standardised OPN concentration in Pg per ml. Blue bars denote SCC89 co-cultures. Red bars denote SCC2 co-cultures. Only SCC89 co-cultures showed apparent OPN expression. Error bars= SD. Data represent the mean of (N=3, n=3) in the attached table. Statistical analysis was determined using two-tailed Student *t*-test with $*p < 0.05$, $**p < 0.01$, $***p < 0.001$.

Table 5.7: Summary of OPN ELISA findings in SCC89 & SCC2 co-culture models

Co-culture model = (OPN mean ± SD) (Pg/ml)	Co-culture model = (OPN mean ± SD) (Pg/ml)	p value
SCC89-CAF1 = (352.6 ± 83)	SCC2-CAF1 = (0.0 ± 0.0)	< 0.01
SCC89-CAF2 = (690 ± 312.6)	SCC2-CAF2 = (0.0 ± 0.0)	< 0.05
SCC89-NTF322 = (741.6 ± 272.5)	SCC2-NTF322 = (8.2 ± 14.2)	< 0.01
SCC89-NTF10 = (874.5 ± 52.3)	SCC2-NTF10 = (0.0 ± 0.0)	< 0.001

mRNA analysis (qRT-PCR)

To identify the source of OPN secretion, qRT-PCR analysis was performed on RNA extracted from the co-cultured cells. β2m was selected as an internal reference gene to compare target expression in both populations as it showed a similar level of expression: mean of β2m ct value in fibroblasts was 16.69 ± 0.39, while in the cancer cell lines this was 16.8 ± 0.99. OPN qRT-PCR findings were as follows (Figure 5.23): SCC89 cells in different co-culture models were the main source of OPN production. Moreover, Among the co-cultured SCC89s, SCC89-CAF1 displayed the highest production of OPN while SCC89-NTF10 showed the lowest value. The differences between co-cultured SCC89s were statistically significant using one-way ANOVA test ($p<0.05$). Comparing OPN expression between SCC89 and SCC2 in co-culture models revealed statistically significant differences. (Table 5.8).

Table 5.8: Summary of OPN mRNA expression in SCC89s & SCC2s upon interactive co-culturing for 48h.

(OPN mean ± SD) Fold change in relation to β2m	(OPN mean ± SD) Fold change in relation to β2m	p-value
SCC89 (CAF1) = (0.025 ± 0.004)	SCC2 (CAF1) = (0.0002 ± 0.0001)	< 0.01
SCC89 (CAF2) = (0.015 ± 0.004)	SCC2 (CAF2) = (0.0001 ± 0.000)	< 0.05
SCC89 (NTF322) = (0.017 ± 0.001)	SCC2 (NTF322) = (0.0001± 0.000)	< 0.01
SCC89 (NTF10) = (0.007 ± 0.001)	SCC2 (NTF10) = (0.000 ± 0.000)	< 0.01

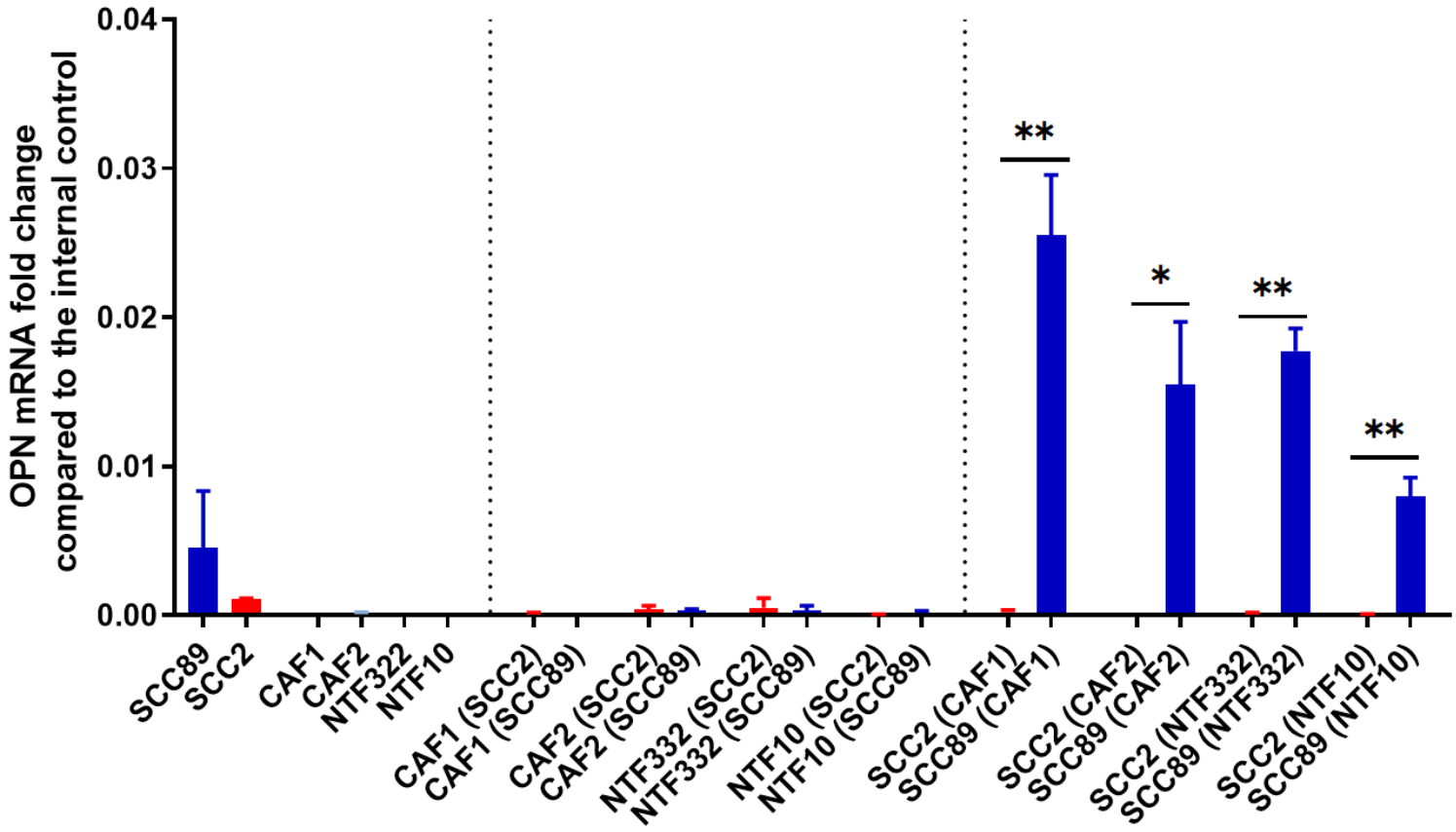

Figure 5.23: Higher OPN mRNA upregulation in SCC89 than SCC2 from different fibroblasts co-culture models. SCC89 or SCC2 ($3x10^5$ cells) were co-cultured with OPSCC fibroblasts (CAF1, CAF2, NTF322, NTF10) (50,000 cells) using transwell insert (0.45 µm) for 48h. The cells pellets were collected, and RNA extraction was performed. cDNA was constructed at volume 20µl using 500ng of the RNA. OPN mRNA expression was analysed using the qRT-PCR technique. Untreated cells were included for comparison. Blue bars denote HPV-negative co-cultures (SCC89). Red bars denote HPV-positive co-cultures (SCC2). Co-cultured SCC89s showed higher OPN mRNA expression compared to Co-cultured SCC2s. OPN fold change compared to β2m. Data represent the mean of (N=3, n=3) except co-cultured cancer cells (N=2.n=3). Error bars= SD. Statistical analysis was determined using two-tailed Student *t*-test with *$p < 0.05$ and **$p < 0.01$.

5.4.4.2 Interleukin -6

ELISA analysis

IL6 ELISA analysis provided further validation to arrays' findings and demonstrated a difference between the co-culture models. SCC89 co-cultures showed higher IL6 expression than SCC2 co-cultures and these differences presented statistically significant values (Table 5.9). Assessing the differences between SCC89 co-cultures, one-way ANOVA test revealed a significant difference ($p<0.01$) that also was observed between SCC2s co-cultures ($p<0.001$) (Figure 5.24).

Table 5.9: summary of OPN ELISA findings in SCC89 & SCC2 co-culture models

Co-culture model = (IL-6 mean ± SD) (Pg/ml)	Co-culture model = (IL-6 mean ± SD) (Pg/ml)	p value
SCC89-CAF1 = (824.3 ± 75.2)	SCC2-CAF1 = (357.4 ± 35.9)	<0.001
SCC89-CAF2 = (752.3 ± 425.7)	SCC2-CAF2 = (270.4 ± 16.5)	ns
SCC89-NTF322 = (1276.8 ± 383)	SCC2-NTF322 = (178.8 ± 20.3)	< 0.01
SCC89-NTF10 = (2277.7 ± 1166)	SCC2-NTF10 = (439 ± 77.5)	<0.05

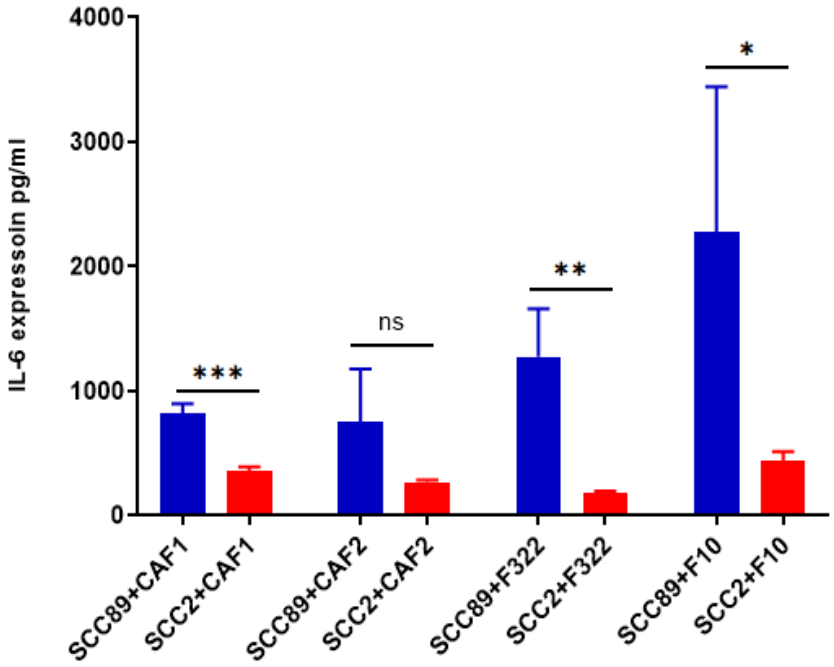

Figure 5.24: Higher levels of IL-6 protein with SCC89-fibroblast co-cultures than SCC2-fibroblast cocultures. SCC89 or SCC2 ($3x10^5$ cells) were co-cultured with OPSCC fibroblasts (CAF1, CAF2, NTF322, NTF10) (50,000 cells) using transwell inserts (0.45 µm) for 48h. The collected media was subjected to IL-6 ELISA analysis. Samples number (n=8), Y-axis denotes standardised IL-6 concentration in pg per ml. Blue bars denote SCC89 co-cultures. Red bars denote SCC2 co-cultures. SCC89 co-cultures showed higher IL-6 expression. Data represent the mean of (N=3, n=3). Error bars = SD. Statistical analysis was determined using two-tailed Student *t*-test with *p<0.05, $^{**}p < 0.01$ and ***p< 0.0001.

mRNA analysis (qRT-PCR)

IL-6 qRT-PCR analysis demonstrated that fibroblasts were the main source for IL-6 production in the co-culture models. A specific association between IL6 mRNA expression and SCC89-fibroblast cultures was evident that showed significant differences statistically when compared with SCC2-fibroblast cultures. (Table 5.10) & (Figure 5.25).

Table 5.10: Summary of IL-6 mRNA expression in SCC89s & SCC2s upon interactive co-culturing for 48h.

(IL-6 mean ± SD) Fold change in relation to β2m	(IL-6 mean ± SD) Fold change in relation to β2m	p-value
CAF1 (SCC89) = (0.25 ± 0.07)	CAF1 (SCC2) = (0.013 ± 0.013)	< 0.05
CAF2 (SCC89) = (0.08 ± 0.01)	CAF2 (SCC2) = (0.005 ± 0.004)	< 0.01
NTF322 (SCC89) = (0.22 ± 0.03)	NTF322 (SCC2) = (0.005 ± 0.005)	< 0.001
NTF10 (SCC89) = (0.12 ± 0.00)	NTF10 (SCC2) = (0.011 ± 0.000)	< 0.001

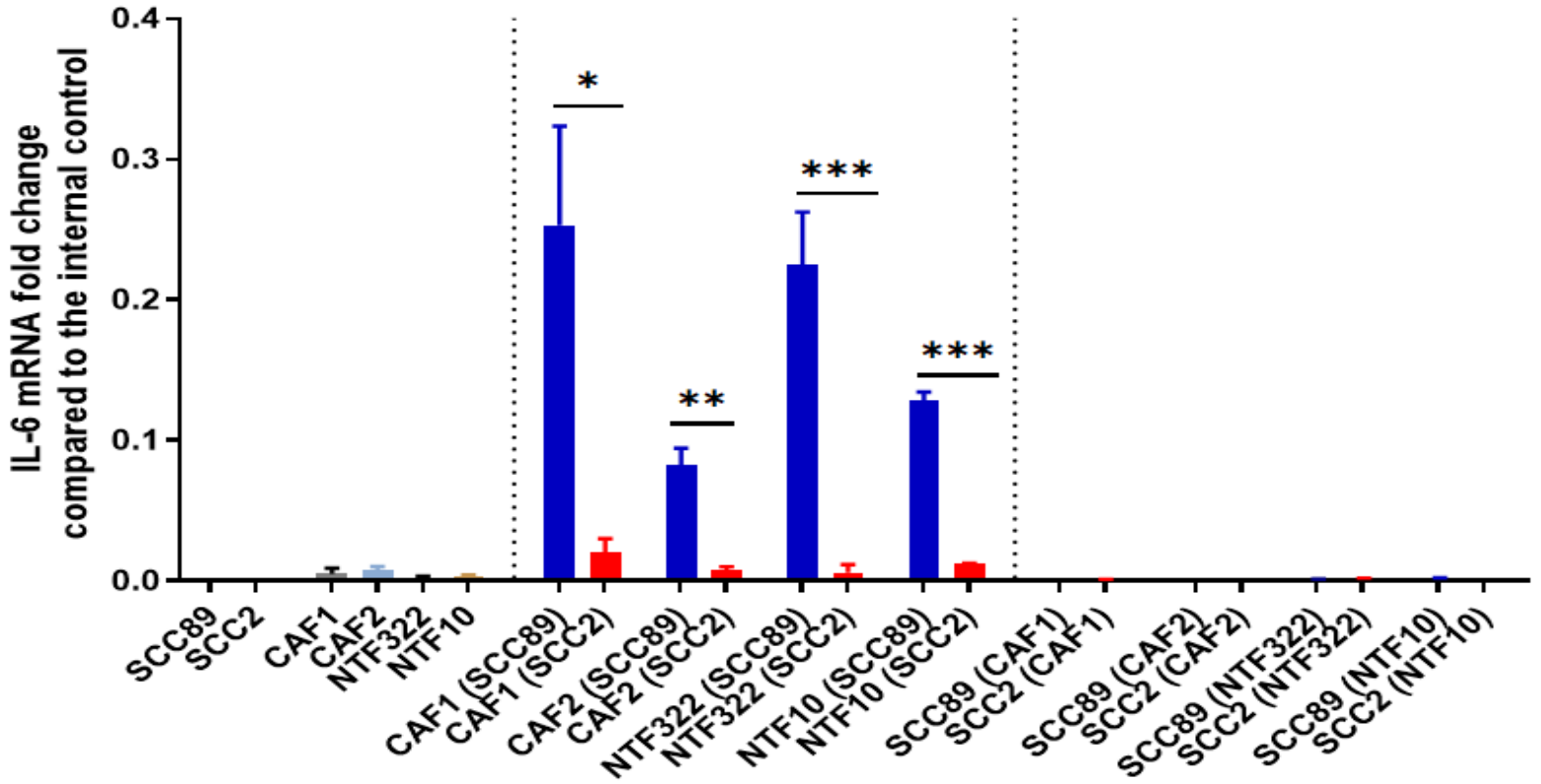

Figure 5.25: Higher IL-6 mRNA upregulation in SCC89 than SCC2 from different fibroblasts co-culture models. SCC89 or SCC2 ($3x10^5$ cells) were co-cultured with OPSCC fibroblasts (CAF1, CAF2, NTF322, NTF10; 50,000 cells) using transwell insert (0.45 µm) for 48h. The cell pellets were collected, and RNA extraction was performed. cDNA was constructed using 500ng RNA and IL-6 mRNA expression was analysed using qRT-PCR. Untreated cells were included for comparison. Blue bars denote HPV-negative's co-cultures (SCC89). Red bars denote HPV-positive's co-cultures (SCC2). Co-cultured SCC89s showed higher IL-6 mRNA expression compared to Co-cultured SCC2s. IL-6 fold change compared to β2m. Data represent the mean of (N=3,n=3), except co-cultured cancer cells (N=2,n=3). Error bars= SD. Statistical analysis was determined using two-tailed Student *t*-test with $*p < 0.05$ and $**p < 0.01$.

5.5 Discussion

The purpose of this chapter is to identify novel candidates in the crosstalk between tumour cells and fibroblasts in the OPSCC subtypes. Our aim was based on the accumulating evidence on the pivotal role of CAFs in tumour development and progression and how that might relate to the distinct clinical courses of both OPSCC entities.

Previous work from our research group demonstrated, for the first time, that HPV-negative OPSCC cell lines, not HPV-positive, have a greater capacity to promote the secretion of pro-invasive secretome that includes HGF and IL-6 from normal oral fibroblasts. The effect of these factors was studied thoroughly using a 3D-model and further validated by using Foretinib, the clinically available c-MET inhibitor (Bolt *et al.*, 2018). Here, in this chapter, we identified further potential mediators of the initial crosstalk between fibroblasts and HPV-negative cell lines using cytokine expression profiling. We detected GM-CSF, OPN, and KLK6 as factors expressed exclusively with HPV-negative cell line co-cultures. Moreover, cytokine analysis of stimulated fibroblasts media demonstrated an alteration in their secretory profile to a more pro-inflammatory secretome that was characterised by IL6 and IL8 production. ELISA analysis on media from interactive co-culture provided validation for the previous findings, while further gene analysis of co-cultured cells revealed their sources of production.

5.5.1 Cytokines expressed exclusively in HPV-negative cell line (M1)

Many *in vitro* investigations demonstrated different approaches in normal fibroblasts activation, including co-culturing models with the cancer cells (Li, Zhou and Gao, 2018; Kim *et al.*, 2019), incubation with tumour-derived microvesicles (Peacock *et al.*, 2018; Jiang *et al.*, 2019), and using activation and senescence inducers (Kabir *et al.*, 2016; Kim *et al.*, 2018; Melling *et al.*, 2018; Wei *et al.*, 2019). Upon co-culturing, activated fibroblasts demonstrated a group of changes including cell morphology (Kim *et al.*, 2019), ECM proteins (Kaukonen *et al.*, 2016), and miRNAs expression (Shen *et al.*, 2017). In this study, the initial events in fibroblasts activation were observed through the passively co-cultured model by incubating the fibroblasts with cell line conditioned media for 24hr. We observed significant differences in cytokine production between HPV-positive and

HPV-negative OPSCC co-cultures as an early response. Densitometry analysis, the array analysis of HPV-negative cell line media with the included fibroblasts (SCC89-M1), exhibited expression of a plethora of cytokines, many of which are known for their association with the cellular senescence and ageing, namely, OPN, GM-CSF and KLK6 which were detected exclusively in all HPV-negative co-culture media.

OPN: is a pleiotropic phosphorylated glycoprotein that possesses numerous functions that have been involved in bone remodelling, inflammation and wound healing. In human cancers, OPN is considered a critical mediator of stromal-epithelial interactions both *in vitro* and *in vivo* (Pazolli *et al.*, 2009). Overexpression of OPN has been reported for 34 different types of human cancer implicated in invasion, angiogenesis and metastasis processes. Whole-genome transcriptional profiling for senescent fibroblasts identified OPN as one of the most highly elevated transcripts compared to the normal fibroblasts (Pazolli *et al.*, 2009). OPN will be discussed in detail in Chapters 6 and 7.

GM-CSF: The granulocyte-macrophage colony-stimulating factor (GM-CSF) is an essential regulator of granulopoiesis and neutrophil functions. It is produced by macrophages, fibroblasts and epithelial cells, playing an important role in inflammatory responses in autoimmune disease (Tlsty, 2001; Lotfi *et al.*, 2019). In human tumours, GM-CSF is considered one of the core features of the SASP besides IL-6, IL-8, GRO-α, MCP-1 (Coppé *et al.*, 2008). In HNSCC, high expression of GM-CSF significantly correlated with invasion and poor prognosis (Ninck *et al.*, 2003).

KLK6: Kallikrein is a subgroup of serine proteases. Kallikrein 6 (KLK6) is known to be an age-related protease expressed at high levels in the central nervous system and its level in the body fluids increases with age (Bayani and Diamandis, 2011). Dysregulation in KLK6 expression is a common feature in human tumours. It shows proteolytic properties in the degradation of ECM proteins *in vitro* (Ghosh *et al.*, 2004). KLK6 also is implicated in tissue remodelling and promotes tumour progression via facilitating migration and invasion processes (Borgoño and Diamandis, 2004). Although KLK6 overexpression was linked with worse clinical outcomes in ovarian and colorectal cancers (Shan *et al.*, 2007; Inoue *et al.*, 2010), in other carcinomas it has been found to be downregulated, such as in renal cell carcinoma and salivary gland tumours (Petraki *et al.*, 2005; Darling *et al.*, 2006).

5.5.2 Effects of OPSCC cells basal secretion in the results of M1 analyses

Understanding of the molecular and genetic changes associated with OPSCC subtypes might explain differences in M1 contents between SCC89 and SCC2. Over the last few decades, the genetic profile of OSCC has been well established (Kim and Califano, 2004; Hunter, Parkinson and Harrison, 2005). Master genetic changes in OSCC include changes at chromosomes 3p (telomerase repressor) (Cuthbert *et al.*, 1999), 9p (INK4A locus) (Sharpless and Depinho, 1999) and 17p (p53) (Baker *et al.*, 1989). These locations are essential checkpoints in cellular senescence and the cell cycle. In HPV positive HNSCC, the only occasional chromosomal loss has been detected, with these features outlined above impaired or bypassed by HPV oncogene expression. However, in HPV-negative HNSCC, gross deletions of whole or large parts of chromosomal arms are an early essential process for tumour formation (Braakhuis *et al.*, 2004). Based on this understanding, oral dysplastic lesions and OSCC have been categorised according to their genome stability, related to the number of copy gene alterations, including loss of heterozygosity TP53 and CDKN2A. The genetically unstable subtype of OSCC (GU-OSCC) is characterised by several genetic mutations and senescent status (Loughran *et al.*, 1997; Weber *et al.*, 1998; Pickering *et al.*, 2014), while genetically stable OSCC (GS-OSCC) has fewer genetic alterations/mutations and retains wild type p53 (Agrawal *et al.*, 2011; Stransky *et al.*, 2011; Pickering *et al.*, 2014). HR-HPV-associated SCC is considered a genetically stable tumour, harbouring less genetic mutation and loss of heterozygosity on chromosome 3p and retaining active p53 and pRb pathways (Braakhuis *et al.*, 2004; Parkinson, James and Prime, 2016).

It is believed that the genetic stability status exerts remarkable impacts on the evolving microenvironment. Signalling pathways via Ras, p53, p21, and p16 generates a high level of Reactive Oxygen Species (ROS), which are considered potentially critical factors for the induction and maintenance of cellular senescence (Lawless *et al.*, 2012). CAF senescence is a characteristic early event in GU-OSCC which is thought to be a consequence of the exposure to tumour-derived ROS, besides the effects of chemicals toxins in tobacco cigarettes (Coppé *et al*., 2008; Salem, Sotgia and Lisanti, 2013; Hassona *et al*., 2014).

In distinction, GS-OSCC demonstrates an intact senescence programme owing to relatively low levels of ROS production (Parkinson, James and Prime, 2016), additionally, to the low production of the inflammatory-mediator (IL-1β) within tumour-derived

secretome. IL-1 is a master regulator in senescence, allowing spread from cell to cell in TME via a paracrine pathway (Costea *et al.*, 2013). It is considered the key to establishing an inflammatory TME (Wu *et al.*, 2016). In published work from our lab, HPV-negative OPSCC cell lines (SCC89 and SCC72) expressed a remarkable level of IL-1β production which, in turn, promoted significant upregulation of a broad spectrum of CXC, CX3CL and CCL chemokines from NTF6, while that was not evident in HPV-positive OPC cells (SCC90 and SCC2) (Al-Sahaf *et al.*, 2019). This work was in agreement with our array findings to some extent. It provided a further explanation of the M1 differences between OPSCC subtypes.

The senescent status of CAFs in CAFs-derived from GU-OSCC and GS-OSCC was evaluated by a limited number of studies (Lim *et al.*, 2011; Hassona *et al.*, 2013, 2014). They reported a higher percentage of SA-b-gal positivity, besides an upregulation in pro-inflammatory proteins by fibroblasts from GU-OSCC compared to GS-OSCC CAFs. Functional analysis of the secretome derived from GU-OSCC-CAFs revealed pro-tumorigenic roles promoting keratinocyte invasion *in vitro* (Krtolica *et al.*, 2001; Pazolli *et al.*, 2009; Hassona *et al.*, 2013). In our lab, the concept of genetic stability in OSCC has been evaluated in OPSCC based on OPSCC subtypes aetiology. Normal fibroblasts were incubated for 13 days fed by HPV-negative cell lines media (SCC89 and SCC72) or HPV-positive cell lines media (SCC90 and SCC2). Fibroblasts showed senescence features by significantly upregulating SA-β-gal percentage with HPV-negative cell lines, while only a few scant traces of SA-β-gal were observed with HPV-positive cell lines.

To sum up, OPSCC demonstrated two distinct genetic profiles based on HPV-status. These differences are also reflected in the underlying TME activation that was evident in the transitory early response seen in the difference in M1 cytokines production when comparing SCC89 and SCC2.

5.5.3 Pro-inflammatory signature of activated OPSCC fibroblasts (M2)

After 24h of cell line media incubation, fibroblasts were incubated for a further 24h with serum-free media to observe the acquired (late) alternation in fibroblast phenotype and secretome. Omitting serum from the growth media provides consistent reproducible results and avoids contamination by other interfering factors which may be present within

the exogenous serum. M2 contained fewer cytokines compared to M1. It represents the fibroblast's initial response to OPSCC cell lines stimulation and that might explain the differences in M2 between SCC89 and SCC2 stimulated fibroblasts. Fibroblasts that had been incubated with SCC89 cell line media released a relatively larger number of cytokines including IL-6 and IL-8 which were completely absent in SCC2-related fibroblast M2. IL-6 and IL-8 are closely collaborating pro-inflammatory chemokines. Both factors participate in the control of essential hallmarks of tumour development and progression, including migration, proliferation, survival, senescence, and differentiation (Jayatilaka *et al*., 2017; Njainday *et al*., 2018). Although we observed their upregulation in response to SCC89 specifically, other reports consider IL6 overexpression is a non-specific cellular mechanism that occurs as a part of the adaption process into altered or new environmental conditions (Son *et al.*, 2015; Kim *et al.*, 2018).

The heterogeneity in fibroblasts was evident in culture reaction with OPSCC cell line media. Although both CAF1 and CAF2 are derived from the same OPSCC subtype and exhibited a comparable basal secretome, stimulated CAF1 showed higher numbers of cytokines in response to SCC89 and SCC2 cell lines. This observation might be ascribed to the senescent status of CAF1 culture and its high producible capability in SASP release. According to our finding in chapter 4, CAF1 showed a non-myofibroblastic CAF like feature which is more known for the highly productive inflammatory profile than the myofibroblastic counterpart.

We did not detect an established active secretome in CAFs at a basal level. Similar observations were also reported in the Erez *et al.* (2009) study, where CAFs derived from mouse cervical tumours (HPV16 transgenic mouse model) did not express the inflammatory gene signature compared to CAFs from mammary adenocarcinomas in a similar model. This observation might be attributed to the origin of the included CAFs, since both CAF1 and CAF2 were extracted from HPV-positive OPSCC, which, it is surmised, carries fewer genetic mutations background and less ability to stimulate normal fibroblasts as we discussed above. Moreover, the anatomical position also was proposed as a reason behind genome-wide heterogeneity in 47 normal fibroblasts strains across the human body. Tissue-specific expressions exhibited consistent and distinct gene expression profiles depending on their anatomical positional (Rinn *et al.*, 2006). Furthermore, an evident desmoplastic stroma response was identified in specific types of tumours including mammary and pancreatic ductal adenocarcinoma (Erez *et al.*, 2009). However, further investigations are required, associated with the presence of

CAFs derived from HPV-negative OPSCC, for molecular comparisons and better understanding.

NTF322 demonstrated an active reaction in response to SCC89 cell lines media that was comparable to the CAF1 and CAF2, however, NTF322 did not show cytokines upregulation upon SCC2 cell line incubation (M2). This observation is in keeping with the finding by Bolt *et al*. (2018) using NOFs. The upregulated NTF322 secretory profile following SCC89 incubation indicated acquisition of CAF phenotype to some extent. CXCL1 was reported by Kim *et al.* (2018) as a key regulator in NOF activation via an autocrine pathway. In their study, 3 NOFs cultures were co-cultured with the OSCC cell line (YD-10B) at different time points. NOFs showed transformation into a senescent CAFs-like phenotype by demonstrating a significant SA-β-gal positivity at 48h ($p<0.05$). This alternation in NOF phenotype was associated with significant upregulation of CXCL1 in co-cultured NOFs, rather than in NOFs in monoculture. Incubation of NOFs with a CXCL1-neutralising antibody revealed a significant decrease in SA-β-gal percentage ($p<0.05$). In our lab, CXCL1 was overexpressed in activated NTF6 following HPV-negative cell lines media incubation (SCC89 and SCC72) compared to NTF6 in monoculture. Interestingly, HPV-positive cell lines (SCC90 and SCC2) failed to induce CXCL1 expression in co-cultured NTF6 (Al-Sahaf *et al.*, 2019). From the above, NTF322 demonstrated a CAF-like secretome in reaction to SCC89 cell line media, but not to SCC2. Further investigations are required to understand the underlying signalling pathways in NTFs activation.

5.5.4 Candidates in interactive co-culture models

The indirect interactive model was established to validate the cytokines array findings in M1 and M2. Although the co-culturing conditions were different from conditioned media co-culture models in terms of incubation time and the active nature of communication between cells, it provided consistent validated results and additional insight into the cell origin of the particular cytokines. ELISA analysis showed a significant upregulation in OPN and IL-6 in the SCC89 interactive models exclusively, these findings consistent with M1 and M2 observations. Direct comparisons between OPN and IL6 levels in mono-cultures and co-cultures were not valid due to the difference in cell population number that was implicated in cytokines production. OPN has been reported to be produced from different sources in the TME including senescent CAFs and tumour cells. Alternatively,

we utilised the extracted mRNA from the co-cultured cells to explore the source of production. OPN qRT-PCR analysis revealed that co-cultured SCC89 was the main source of OPN in SCC89 co-culture models. On the other hand, IL6 mRNA qRT-PCR analysis revealed that activated fibroblasts were the main source of IL-6 production in SCC89 co-culture models and its overexpression was driven by SCC89 incubation. Mono-culture fibroblasts showed a significantly low level of IL-6. These results were consistent with the Qin *et al.* (2018) observations. Qin and team showed that CAF-derived IL-6-mediated expression of OPN. They studied the effect of αvβ3 blockade (an integrin, and an OPN receptor) on IL-6 production. Functional analysis of IL-6 and OPN in OPSCC will be discussed in detail in Chapter 7.

Quantifications of the transcriptome and secretome response of OPSCC fibroblasts upon the interactive model also revealed heterogeneity between co-cultured fibroblasts (CAF1, CAF2, NTF322 and NTF10). NTF322 and CAF2 responses to the co-culture models demonstrated a comparable pattern, which was different from CAF1. CAF1 showed unrelated patterns in protein and mRNA expressions in the interactive model, where OPN and IL-6 ELISA analysis demonstrated the highest expression with SCC89-CAF1 co-culture; conversely, qRT-PCR analysis presented the lowest values. This discrepancy between protein/gene expression might be related to the phenotypic status of CAF1. According to the characterisation work in chapter 4, CAF1 exhibited a senescent phenotype feature by displaying a high percentage of SA-β-gal positivity. The senescent condition was reported with an influence on a post-transcriptional modification which might lead to inconsistency in protein/gene levels of expression (Lai *et al.*, 2019).

5.6 Limitations

It is worth mentioning that the indirect co-culture models used (passive co-culture and interactive coculture) are still rather simple and are likely not completely representative of cell interactions. True physical contact between the two populations in presence of signals from other cell types in the tumour microenvironment may reveal different or additional findings.

The multiplex cytokines array was conducted for only one repeat, due to the kit's high expense, nevertheless, analysis of a single repeat mandated the use of another technique to validate the results, as we have done. Cytokine array demonstrated

high-quality results. All the membranes' backgrounds were clear from contamination and produced a consistent densitometry reading throughout the whole membrane. It exhibited reproducible results, as became obvious through monitoring the expression and intensity of basal secretory profile for each culture, also by comparing the densitometry reading for the duplicate repeat spots within a single array membrane. As a technical limitation, a multiplex array presents a semi-quantitative result that is recommended to be followed by ELISA for target quantification as we have done. We further acknowledge the fact that our observations are built on a limited number of OPSCC cell lines. Moreover, CAF cultures were both HPV positive tumour derived. Use of the CAFs from an HPV-negative tumour will be essential for better understanding and comparison.

5.7 Summary of the main findings and clinical implications

In this chapter, we reported for the first time a number of cytokines secreted particularly with HPV-negative OPSCC cell line, namely OPN, KLK6 and GM-CSF, in addition to other cytokines produced under all conditions.

Molecular analysis of interactive co-culture models identified the source of OPN and IL6 production. At the basal level, more OPN was produced by HPV-negative cell lines than HPV-positive cell lines. Upon 48h of interactive co-culturing, only HPV-negative cell lines demonstrated significantly higher levels IL-6 overexpression indicated active crosstalk between cancer cells and fibroblasts

These findings underpin the need for a better understanding of the role of TME in OPSCC development and progression. Further investigations of OPN and IL6 crosstalk might introduce promising prognostic and diagnostic indicators as well as potential cancer therapeutic targets in OPSCC.

Chapter 6: Functional analysis of candidates identified by cytokine arrays: OPN and IL-6

6.1. **Introduction**

In the study cohort, we observed that CAFs are a common feature of the stroma in OPSCC, regardless of HPV status, however, it provided a potential clinical significance in the HPV-positive group. Despite the compelling evidence for a tumour-supportive role of CAFs, the detailed molecular mechanisms behind CAFs transition in OPSCC are largely unclear. Cytokine array profiling identified OPN as a factor expressed in one of the OPSCC cell lines which corresponded to an elevation of IL-6 production in fibroblasts in co-cultured models. These findings suggest crosstalk between OPSCC cancer cells and fibroblasts may be mediated by OPN and IL-6. OPN is highly expressed in healing wounds and fibrotic lesions in addition to its involvement in myofibroblast differentiation (Lenga *et al*., 2008). However, few reports have evaluated its role in CAF functionality.

The involvement of tumour-derived OPN in CAF phenotype development was described in breast tumour, where OPN has been shown as a sufficient factor in fibroblasts activation (Sharon *et al.*, 2015, Prasanna *et al.*, 2021). In HNSCC, CAF-derived IL-6 was identified as the major upstream molecule that triggers the induction of tumour-derived OPN which enhances tumour cell growth, migration, and invasion (Qin *et al.*, 2018). In addition to its secretion by tumour cells, OPN was expressed by the senescent CAFs, that mediated signalling events impacting neoplastic progression in preneoplastic immortalized keratinocytes (HaCaT) (Pazolli *et al.*, 2009) (Figure 6.1).

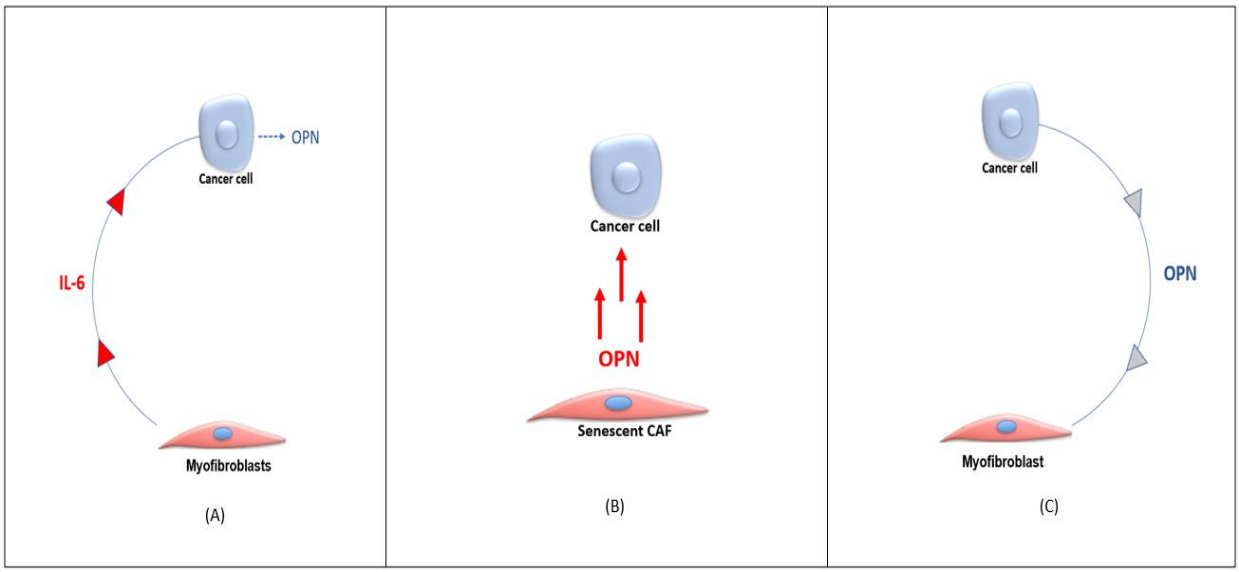

Figure 6.1: Conceptual model of cancer cell and fibroblast crosstalk mediated by OPN and IL-6. As it has been described in different human tumours, OPN and IL-6 showed functional effects on cancer cells and fibroblast. **(A),** CAF-derived IL-6 has been shown as major inducers for tumour-derived OPN that enhance tumour cell proliferation and invasion *in vitro.* **(B),** senescent dermal fibroblasts have been described as a promoter for pre-neoplastic cells transformation using immortalized keratinocytes cell line (HaCaT). **(C)**, In breast tumour, tumour-derived OPN was introduced as a crucial factor for normal fibroblasts reprogramming into myofibroblastic CAFs phenotype.

In this chapter, we aimed to identify the role of OPN and IL6 as novel mediators of interactions between CAFs and OPSCC tumour cells. We sought to explore the functional effect of OPN on fibroblast differentiation based on our observation in fibroblast phenotypic characterisation in chapter 4. Moreover, we aimed to identify if OPN induces IL-6 production in fibroblasts. We also aimed to test if IL-6 is sufficient for tumour-derived OPN production.

In addition to its impact on TME components, OPN also has a well-established role in tumour behaviour in terms of promoting migration and invasion of the tumour cells. Here, we planned to explore the downstream pathways of OPN interaction with OPSCC cell lines, to establish a molecular understanding of OPN mechanism in OPSCC modulation.

However, due to time restrictions affected by pandemic national lockdown, parts of this work have not been conducted completely and further validation will be required at some points.

6.2. **Aims**

- To investigate the effects of OPN on OPSCC fibroblast phenotype.

- To assess if OPN directly stimulates IL-6 production in OPN-induced fibroblasts by targeting CD44v6, one of OPN receptors.

- To investigate CD44-dependent MAPK activation in OPSCC cancer cells mediated by OPN.

- To identify if tumour-derived OPN production in OPSCC cells is driven by IL-6.

6.3. **Experimental approach and statistical analysis**

- OPSCC fibroblasts were treated with recombinant OPN (rOPN), followed by the assessment of resultant phenotype; the contraction ability of OPN-induced fibroblasts was assessed using collagen contraction gel. Senescent status was assessed using the SA-β-gal assay.

- The effect of OPN on IL-6 production was assessed in rOPN-induced fibroblasts using IL-6 qRT-PCR and ELISA analysis. The effect of CD44V6 blocking antibody was evaluated by monitoring IL-6 production upon rOPN-induction. Next, to test if OPN was responsible for IL-6 production, OPSCC fibroblasts were incubated with OPSCC conditioned media after 1 hr of CD44v6 blocking. However, due to time restrictions, only NTF322 was assessed in this experiment.

- OPSCC cancer cells were treated with rOPN, and CD44 expression was assessed using immunofluorescence staining and western blot. Alterations in p38 MAPK phosphorylation were assessed using western blot.

- The effect of IL6 on tumour-derived OPN production was tested by incubating OPSCC cell lines with recombinant IL6 (rIL-6). OPN qRT-PCR and ELISA analysis were used to evaluate OPN expression.

- Statistically, detection of non-normality is less likely among the data due to small sample numbers, however, Shapiro-Wilk test was used to check the normality due to its high sensitivity. For the comparison between two normally distributed samples' mean, two-tailed unpaired *t*-test was used. In multiple data sets, one-way analysis of variance (ANOVA) was used.

- Data were presented graphically illustrating the mean with error bars demonstrating the standard deviation (SD). The probability of similar random result detection (p-value) was considered significant if ($p<0.05$). "N" followed by a number denotes the biological repeats, while "n" denotes the technical repeats. Data were analysed using Graph-pad prism versions 7-9.

6.4. **Results**

6.4.1 OPN induces alteration in NTFs morphology

Under the light microscope, NTF322 and NTF10 displayed alterations in cell morphology following 48h incubation with a single dose of 180 ng/ml of rOPN. This dose was determined thoroughly in an optimising study reported by Weber *et al.*, (2015). Moreover, the 180ng/ml dose has worked well in other studies (Driver *et al.*, 2015; Che *et al.*, 2018). NTF322 showed darker cytoplasm and a larger cell body. NTF10 appeared more flattened with long anastomosing processes (Figure 6.2).

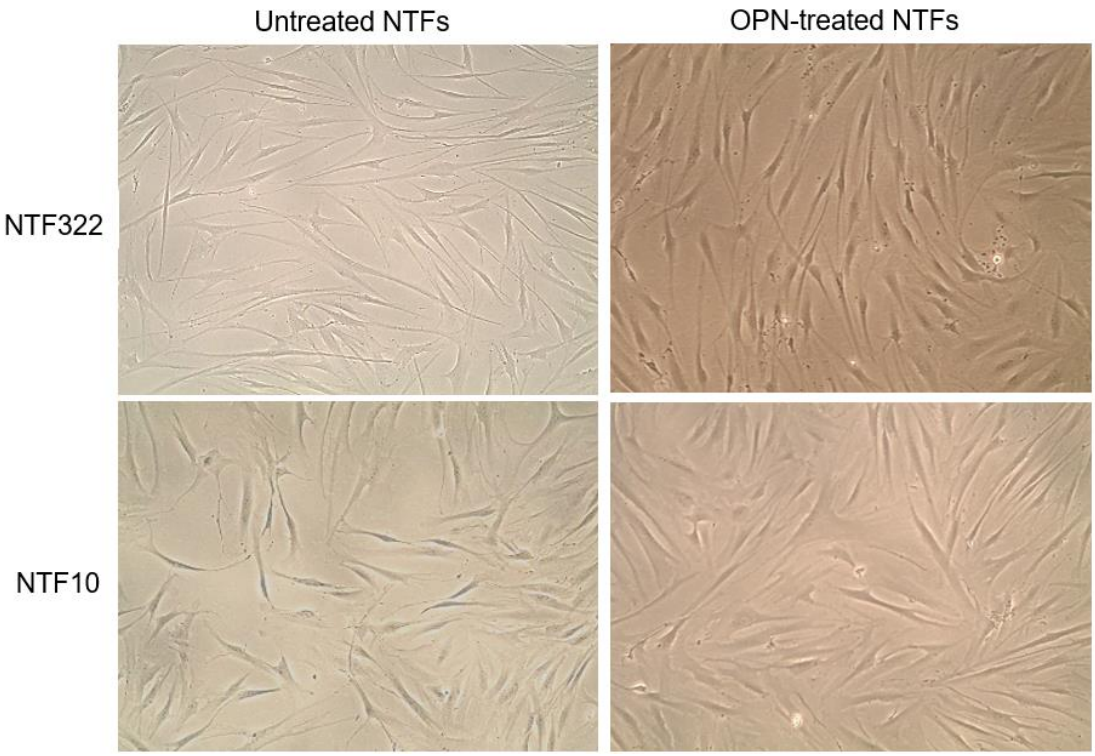

Figure 6.2: Alterations in NTFs morphology following rOPN induction. NTF322 and NTF10 were incubated with 180ng/ml of rOPN for 48h. Under the light microscope, both cultures displayed morphological changes. Images were taken with an Olympus BX51 optical microscope at 10X magnifications.

6.4.2 OPN potentially enhances the contraction in OPSCC fibroblasts.

The collagen gel contraction assay was performed to assess the contractility of OPSCC fibroblasts. According to our observations in chapter 4, an active myofibroblastic like CAF showed a significant contractile ability compared to the control. An *in vitro* three-dimensional contraction model of NTF322, NTF10 and CAF2 were constructed as described in section 2.1.10. Cells were incubated under mechanical tension conditions by leaving the lattices attached to the culture well. After 48h, the collagen lattice was completely detached with a sterile spatula and incubated for a further 48h with the addition (or absence) of 180 ng/ml OPN. At the end of the experiment, NTFs contractility was recorded by measuring the distance between the lattice disc and the well using Fiji-ImageJ (Figure 6.3).

Untreated cells showed different capacity in gel contraction. The CAF2 lattice disc was the smallest, followed by NTF10 then NTF322 ($p<0.001$). OPN enhanced the contraction ability of OPSCC fibroblasts to some extent compared to their untreated. CAF2 showed a significant decrease in lattice disc size (4.6 ± 0.1mm) compared by the control (3.2 ± 0.2mm) ($p<0.001$). NTF10 demonstrated a degree of gel contraction of 1.8 ± 0.6mm ($p<0.05$). However, NTF322 showed a negligible amount of contraction (0.13 + 0.1) (mean + SD) compared to the control that showed 0 contraction ($p=0.05$). However, compared to the myofibroblastic model in chapter 4, this is considered a slight increase in the acquired mechanical properties in NTFs following OPN induction (please refer to figure 4.3 for the comparison).

Notably, untreated CAF2 showed high capability for collagen disc contraction, which suggested an active myofibroblastic phenotype. This observation is in agreement with our findings in chapter 4 regarding CAF2 phenotypic characterisation.

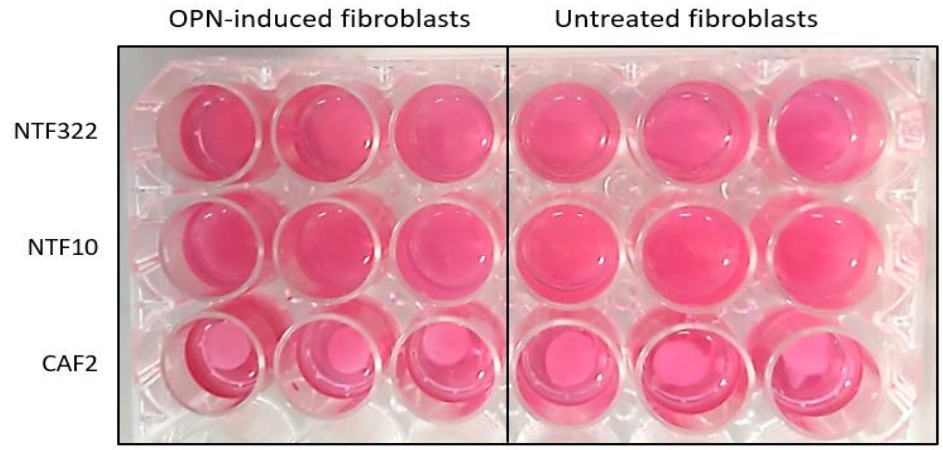

(A)

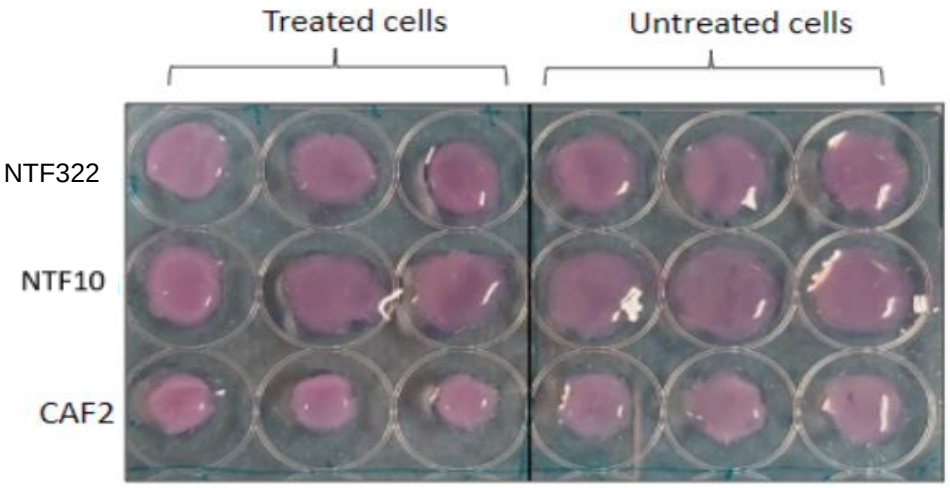

(B)

Figure 6.3: Matrix contraction ability of stimulated NTFs varies between different cultures. **(A)** Image of detached lattices for NTF322, NTF10 and CAF2 floating in the growth media. **(B)** Image of the gel disc for NTF322, NTF10 and CAF2. NTF322, NTF10, and CAF2 (2 x 10^4 cells) were seeded in 0.5 ml of collagen lattice solution in a 24-well plate and left in the incubator for an hour at 37ºC. 1.0 ml of growth media was added on the top of the collagen gel lattice and the plate was incubated for 24h. The next day, the cells were serum-starved for a further 24h, then were treated with 180 ng/ml OPN before releasing the stressed gel matrix from the plate using a sterile spatula. The gels were then incubated for 48h in the OPN stimulation experiment. OPN provoked a slight degree of mechanical stress across the collagen matrix.

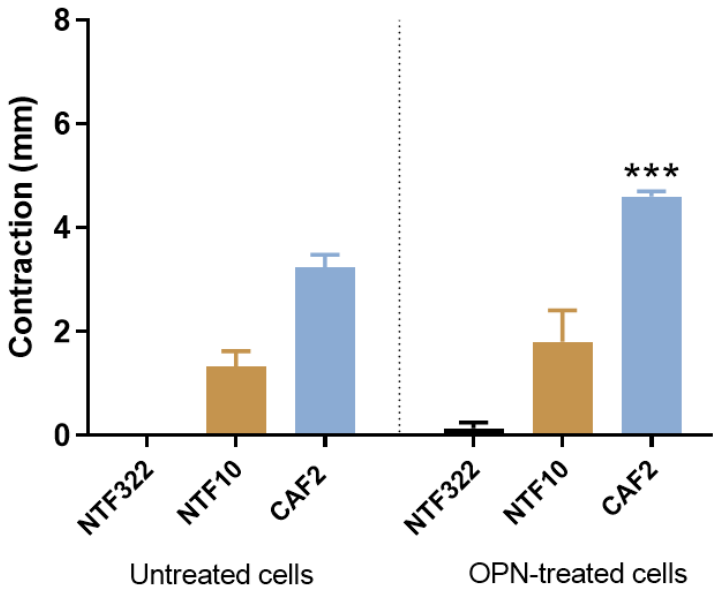

Figure 6.3 C: Matrix contraction ability of stimulated NTFs varies between different cultures. Quantification of gel disc contraction used ImageJ. Relative lattice contraction (mm) was obtained by measuring the distance between the gel and the well border. Statistical analysis was performed using Student's *t*-test to compare between the treated culture and its counterparts. One-way ANOVA was used to compare the difference between the untreated cultures or treated cultures. Statistical significance is shown on the figure by *p<0.05, ****p*<0.001. Data represent the mean of (N=3, n=3). Error bars= SD.

6.4.3 Senescence assessment in rOPN-treated fibroblasts

In a characterisation process for the evolving OPN-induced fibroblast phenotype, SA-β-gal assay was performed to evaluate the senescence status of OPSCC fibroblasts following OPN induction. Senescence analysis was performed for NTFs 322 and NTF10 only (Figure 6.4). No evident increase in SA-β-gal positivity percentage was detected in the induced cells ($p>0.05$).

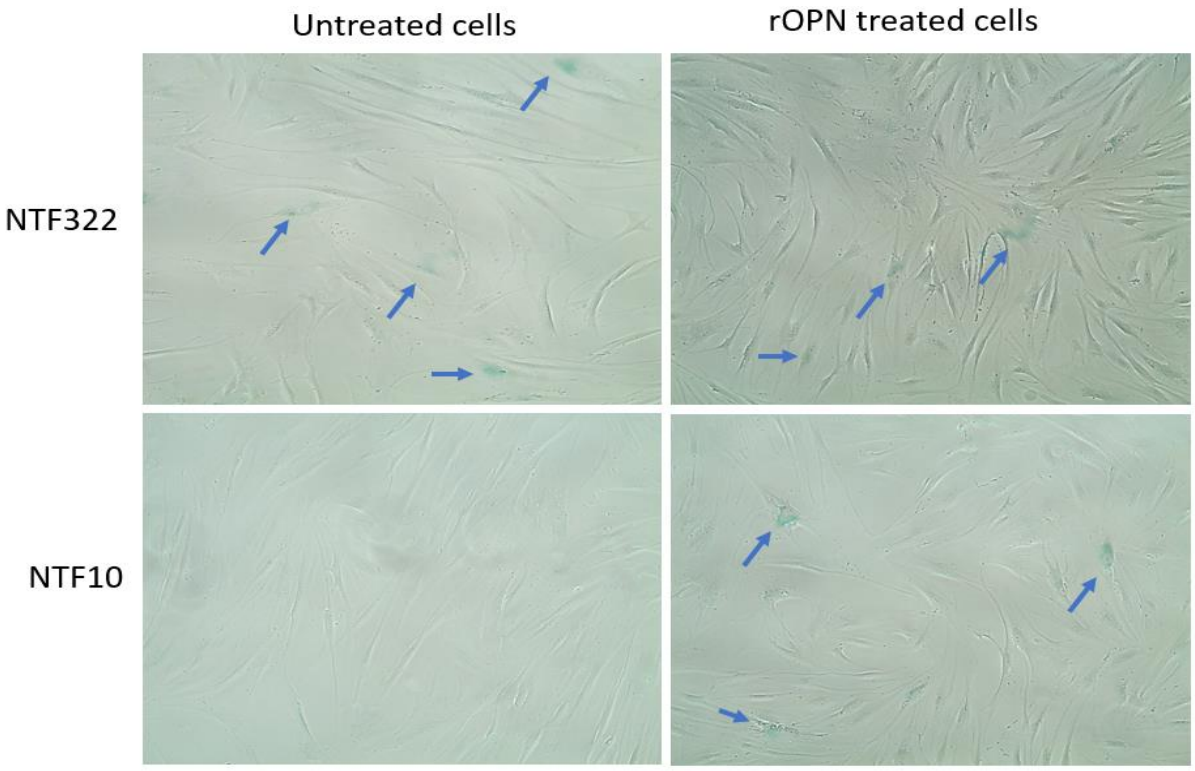

(A)

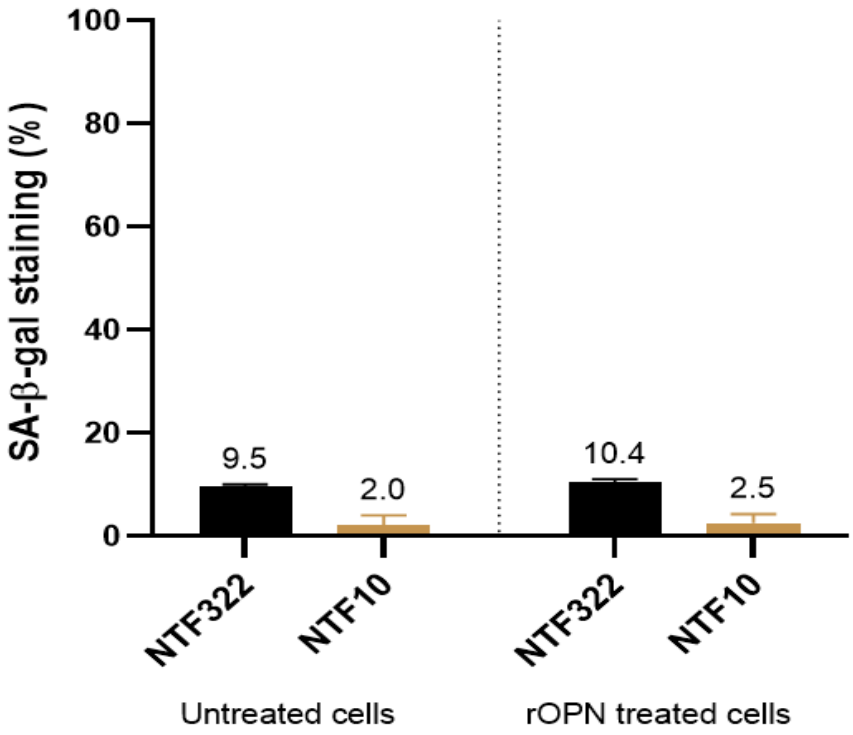

(B)

Figure 6.4: Senescence status in OPN-induced NTFs. (A) Images representing SA-β-gal stain at basal level and after OPN treatment in NTF322 and NTF10. Images were taken with an Olympus BX51 optical microscope at 10X magnifications. **(B)** Quantification of SA-β-gal stain. The proportion of stained cells (blue precipitate) in 3 random fields at magnification 20x. Statistical analysis was performed using Student's *t-test*. Error bars = SD for (N=3, n=3).

6.4.4 OPN induces a slight increase in IL-6 production in OPSCC fibroblasts

Next, we assessed the level of IL-6 production to identify mediators of the phenotypic change, but also to test the hypothesis of a reciprocal tumour-stroma loop in OPSCC mediated by OPN and IL-6 (Qin *et al.*, 2018). Alteration in IL-6 production was assessed at the transcript and secretory levels. NTF10 and CAF2 showed a slight increase in IL-6 transcript following rOPN treatment, however, statistically, it revealed a significant difference ($p<0.05$ and $p<0.01$). NTF322 showed a minimum upregulation in IL-6 mRNA expression with no statistically significant value. The fold change compared to β2m was (0.08 ± 0.00) (mean ± SD) (Figure 6.5). This marginal increase in IL-6 production upon rOPN induction may indicate an alteration in OPSCC fibroblast phenotypes, however, further validation includes the assessment of α-SMA and FAP expressions is required to confirm the evolving phenotype.

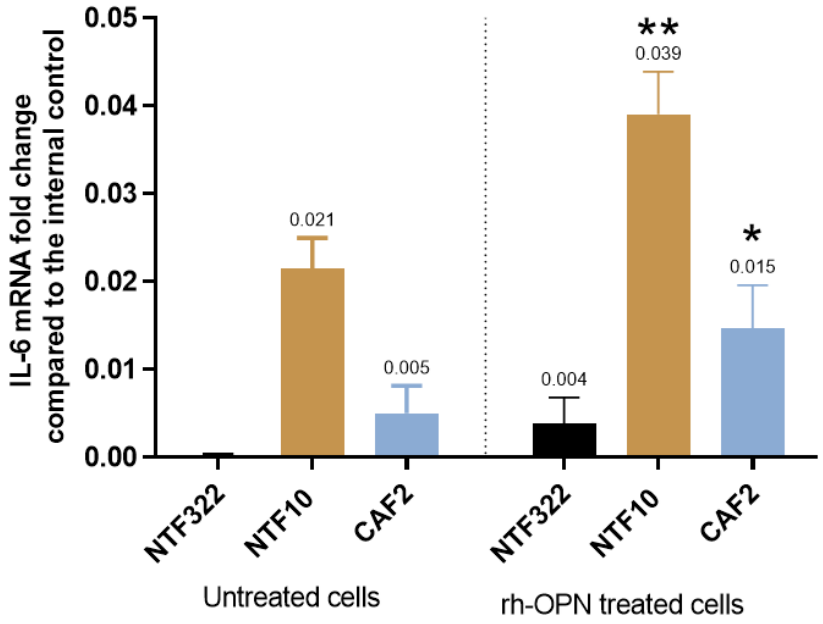

Figure 6.5: IL-6 upregulation following rOPN treatment. OPSCC Fibroblasts were cultured in T75 cm^2 flasks in growth media up to 70% confluency then treated with 180ng/ml rOPN for 48h. The cell pellet was collected, and cDNA was constructed using 120 ng/ml of total RNA. qRT-PCR was used to analyse IL-6 expression, normalised to β2m. NTF10 and CAF2 expressed slightly increased IL-6 transcript levels compared to the untreated counterparts ($p<0.01$). Statistical analysis was performed using Student's *t*-test, and statistical significance is shown on the figure by *$p<0.05$. Error bars = SD for (N=3, n=3).

IL-6 ELISA analysis revealed an increase in IL-6 concentration in OPSCC fibroblasts media following rOPN treatment. NTF10 showed relatively high increases compared to the control and other included fibroblasts cultures (137 ± 3.72 pg/ml; $p<0.001$). NTF322 showed a slight increase in IL-6 production that was statistically significant (12.5 ± 2.1 pg/ml; $p<0.05$). CAF2 showed a marginal increase that was comparable to the untreated counterpart ($p>0.05$) (Figure 6.6).

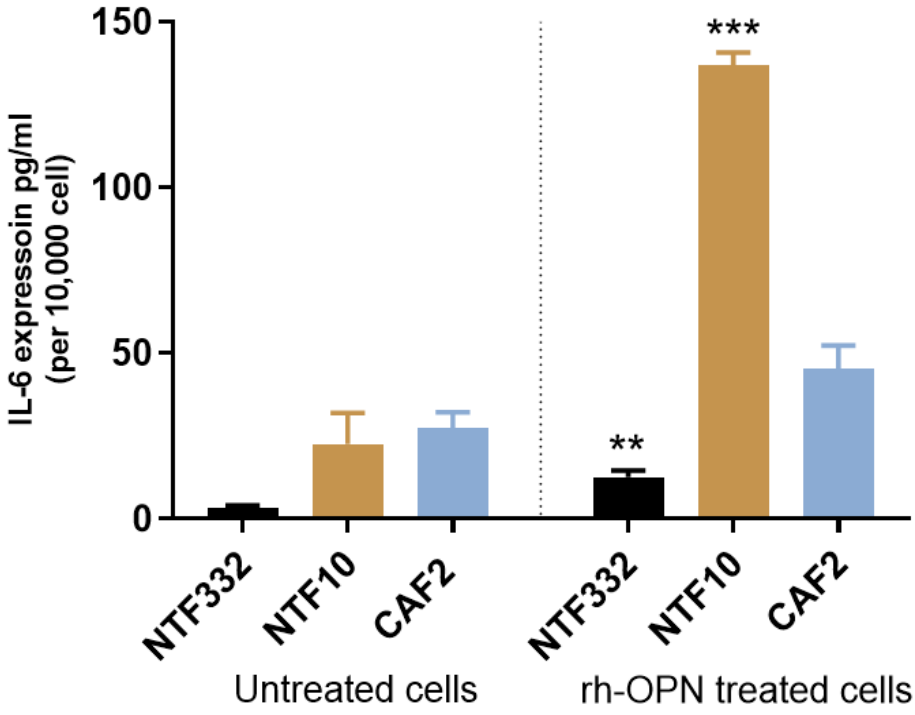

Figure 6.6: Increase in IL6 production in NTFs following OPN treatment. NTF322, NTF10 and CAF2 were treated with a single dose of 180ng/ml OPN for 48h. The media was collected and subjected to IL6 ELISA analysis. Untreated cells were included for the comparison. All treated NTFs showed an increase in IL6 production. Samples number (n=6), Y-axis denotes standardised IL-6 concentration in pg/ml. IL-6 concentrations were optimised according to fibroblasts density at 10,000 cells. Statistical analysis was performed using Student's *t*-test, and statistical significance is shown on the figure by $^{**}p<0.01$, $^{***}p<0.001$. Data represent the mean of (N=3, n=3). Error bars= SD.

6.4.5 Targeting of CD44v6 potentially reduces IL-6 production in rOPN stimulated fibroblasts

At the cellular level, OPN has two cell surface binding sites; the N-terminal region of OPN binds to integrins, whereas C-terminal region interacts with CD44 (Weber *et al.*, 1996; Rangaswami, Bulbule and Kundu, 2006). CD44 is a family of plasma membrane glycoproteins encoded by a single gene on chromosome 11. It is composed of at least 20 exons, 10 of them are expressed simultaneously giving the standard form CD44s, while the rest are variant exons that are subjected to alternative splicing, generating many isoforms (Screaton *et al.*, 1992). CD44 variants have been found to be associated with advanced H&N cancer: CD44v6 is an oncogenic variant that is strongly expressed by more than 95% of HNSCC (Heider *et al.*, 2004). Its expression is largely restricted to advanced-stage of tumours and is more associated with metastatic cancers (Rail and Rustgi, 1995). In the Sharon *et al.*, (2015) study, the ability of secreted OPN to activate mammary fibroblasts relied upon the receptors CD44 and αVβ3 integrin, moreover, targeting OPN binding sites using blocking antibodies inhibited fibroblast activation *in vitro* and remarkably attenuated tumour growth and fibroblast activation *in vivo*.

In OPSCC, we tested the effect of blocking CD44v6 on IL-6 production, cells were incubated with 5µg/ml of CD44var (v6) monoclonal antibody (VFF-18) (eBioscience™, UK). It has a blocking property (inhibiting antibody) by prohibiting further molecular binding without reacting with the ligand-binding site. It has been used in Phase I clinical trial targeting immunoconjugate bivatuzumab mertansine in HNSCC (Riechelmann *et al.*, 2008). Also, has been shown to work effectively *in vitro* in many reports at the same concentration (5µg/ml). (Afify, Purnell and Nguyen, 2009; Gutjahr *et al.*, 2018; Khan *et al.*, 2021).

Incubation of NTF10 with CD44v6 blocking antibody for 1 h before rOPN induction revealed a significant reduction in the IL-6 mRNA fold change ($p<0.05$). This effect was less evident with NTF322. However, the latter has low baseline IL-6 transcripts and showed a slight, but insignificant, elevation in IL-6 following rOPN induction. Blocking with CD44v6 antibody resulted in a marginal decrease in IL-6 in rOPN-induced NTF322 ($p>0.05$) (Figure 6.7). Quantification of secreted IL-6 demonstrated a clearer difference between the NTFs' cultures. rOPN-treated NTF10 showed a significant reduction in IL-6 release following CD44v6 blocking (137.0 ± 3.7 to 60.8 ± 15.3; $p<0.05$), while rOPN-treated NTF322 showed minimal IL-6 reduction upon CD44v6 blocking ($p>0.05$) (Figure 6.8).

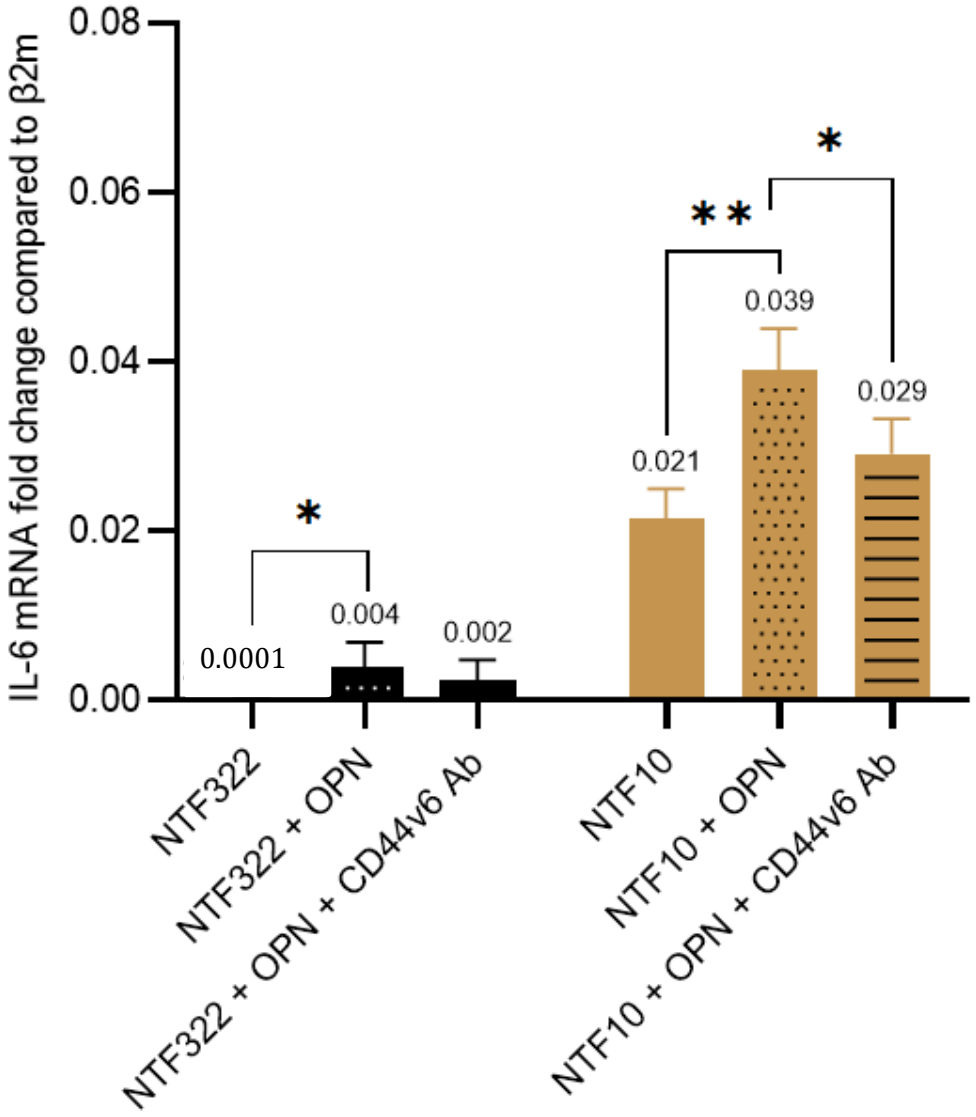

Figure 6.7: Variable reduction in IL-6 expression following CD44v6 blocking in rOPN treated fibroblasts. NTF322 and NTF10 were grown up to 70% confluence in T75 flasks. Cells were cultured with 5µl/ml of anti-CD44v6 AB for 1 h, followed by incubation with 180 ng/ml of rOPN for 24 h. Untreated counterparts were incubated with serum-free media only without blocking antibody. Cells were collected, and RNA extracted. cDNA was constructed using 400ng of total RNA. qRT-PCR was used to assess IL-6 transcript expression normalised to β2m. Only NTF10 showed a response to rOPN induction and CD44v6 antibody blocking ($p<0.05$) and ($p<0.01$) using Student's *t*-test. Data represent the mean of (N=3, n=3). Error bars= SD.

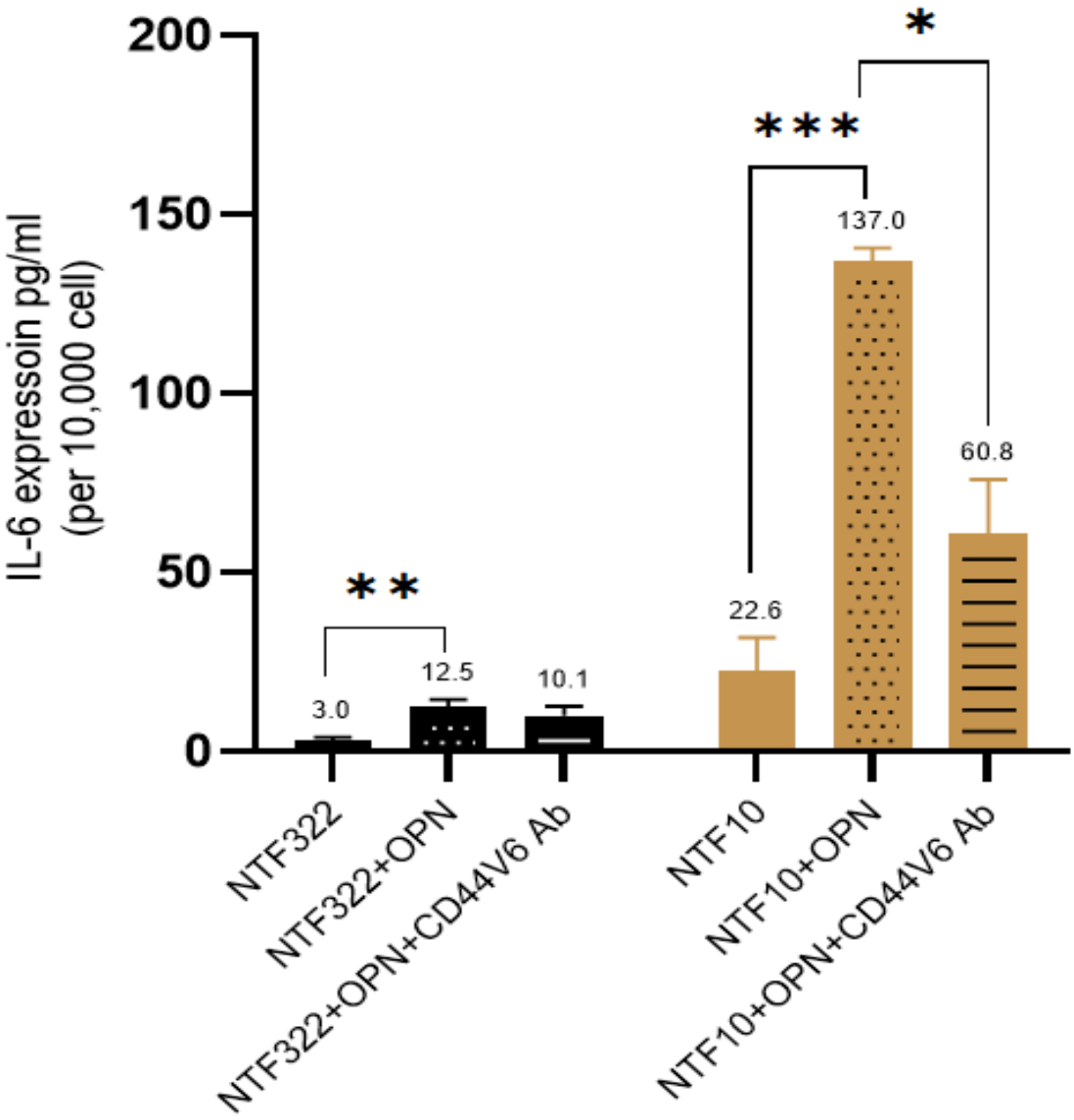

Figure 6.8: Variation in IL-6 protein secretion following CD44v6 blocking in rOPN treated NTFs. NTF 322 and NTF 10 were cultured up to 70% confluence in T75 flask. Cells were incubated with 5 µl/ml of anti-CD44v6 AB for 1 h, followed by incubation with 180 ng/ml of rOPN for 24 h. Untreated counterparts were incubated with serum-free media only without blocking antibody. The media was collected and subjected to IL6 ELISA analysis. Untreated cells were included as a negative control. Y-axis denotes standardised IL-6 concentration in pg/ml. IL-6 concentrations were optimised according to a fibroblast density of 10,000 cells. Statistical analysis was performed using Student's *t*-test, and statistical significance is shown on the figure by *p<0.05. **p<0.01 and p<0.001. Error bars = SD for (N=3, n=3).

6.4.6 Targeting CD44v6 potentially reduces IL-6 production in NTF322 following OPSCC CM stimulation

Following evaluating CD44v6 antibody efficiency on IL-6 reduction in NTFs. We tested our hypothesis that OPN is necessary for inducing IL-6 in NTFs. However, due to the time and lab restriction upon the epidemic, only NTF322 was tested in the CD44v6 blocking experiment. Although NTF10 was more responsive than NTF322 on rOPN treatment, we assumed that might reflect clearly on the CD44v6 blocking step.

NTF322 culture was incubated with anti-CD44v6 antibody for 1h before incubation with OPSCC cell line conditioned media (CM) for 24 h. SCC2, SCC89 and SCC72 CM were prepared as described in section 2.1.1. Untreated cells were incubated with serum-free media before cell line media stimulation. At the end of the experiment, cells and media were collected for IL-6 analysis.

OPSCC cell lines conditioned media induced high variable concentrations of IL-6 from NTF322 at the transcript and secretory levels. SCC89 and SCC72 CM promoted NTF322 to overexpress IL-6 transcript at a higher fold change than in SCC2 ($p<0.01$ one-way ANOVA) (Figure 6.9). ELISA analysis also showed the same pattern in NTF322 response to different OPSCC cell line CM stimulation ($p<0.01$). NTF322 responded to cell lines CM incubation by a high upregulation in IL-6 production levels (Figure 6.10).

CD44v6 blocking also revealed different effects on IL-6 reduction in NTF322 culture-stimulated with OPSCC cell lines CM. NTF322 induced with SCC2 CM showed a reduction in IL-6 transcript fold from (0.009 ± 0.01 to 0.003 ± 0.004 fold) compared to β2m. This reduction was accompanied by a decrease in IL-6 release on ELISA analysis (155.8 ±118 to 93.6 ± 71.8 pg/ml). However, that was not a statistically significant difference ($p>0.05$).

The CD44v6 antibody blocking effect was evident the most with SCC89-CM-induced NTF322 cells. It was able to significantly reduce the IL-6 upregulation at the gene and protein level ($p<0.05$). On contrary, CD44v6 antibody failed to show a blocking effect in SCC72-induced NTF322 that showed a comparable IL-6 level to the control ($p>0.05$).

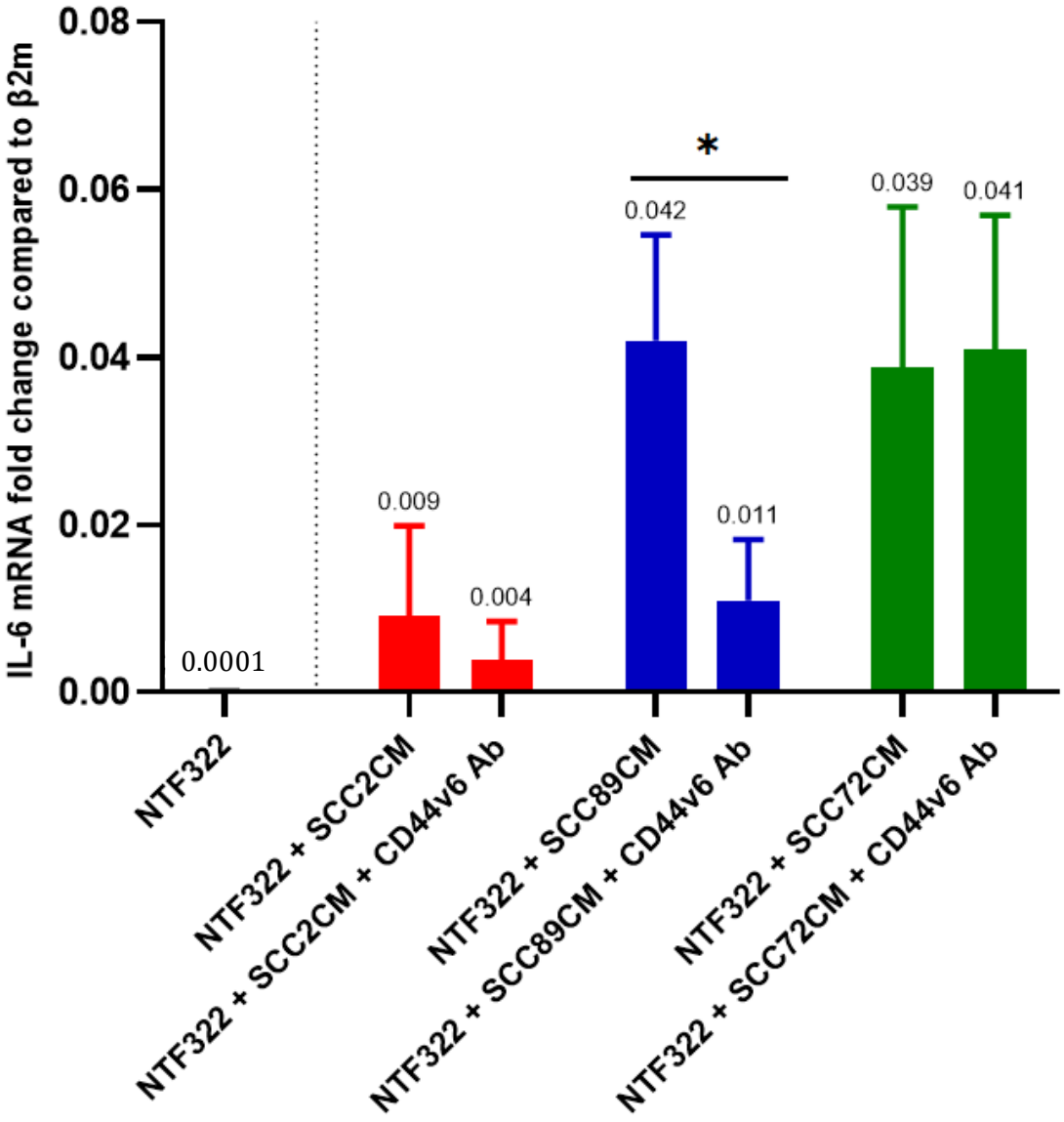

Figure 6.9: Variable reduction in IL-6 expression following CD44v6 blocking in cell lines treated fibroblasts. NTF322 and NTF10 were grown up to 70% confluence in T75 flasks. Cells were cultured with 5 µl/ml of anti-CD44v6 AB for 1h, followed by incubation with SCC2, SCC89 or SCC72 CM for 24h. Untreated counterparts were incubated with serum-free media only without blocking antibody. Cells were collected, and RNA extracted. cDNA was constructed using 120 ng of total RNA. qRT-PCR was used to assess IL-6 transcript expression normalised to β2m. Anti-CD44v6 AB showed a blocking effect in NTFSCC89-CM-treated NTF322 ($p<0.05$) using Student's *t*-test. Data represent the mean of (N=3, n=3). Error bars= SD.

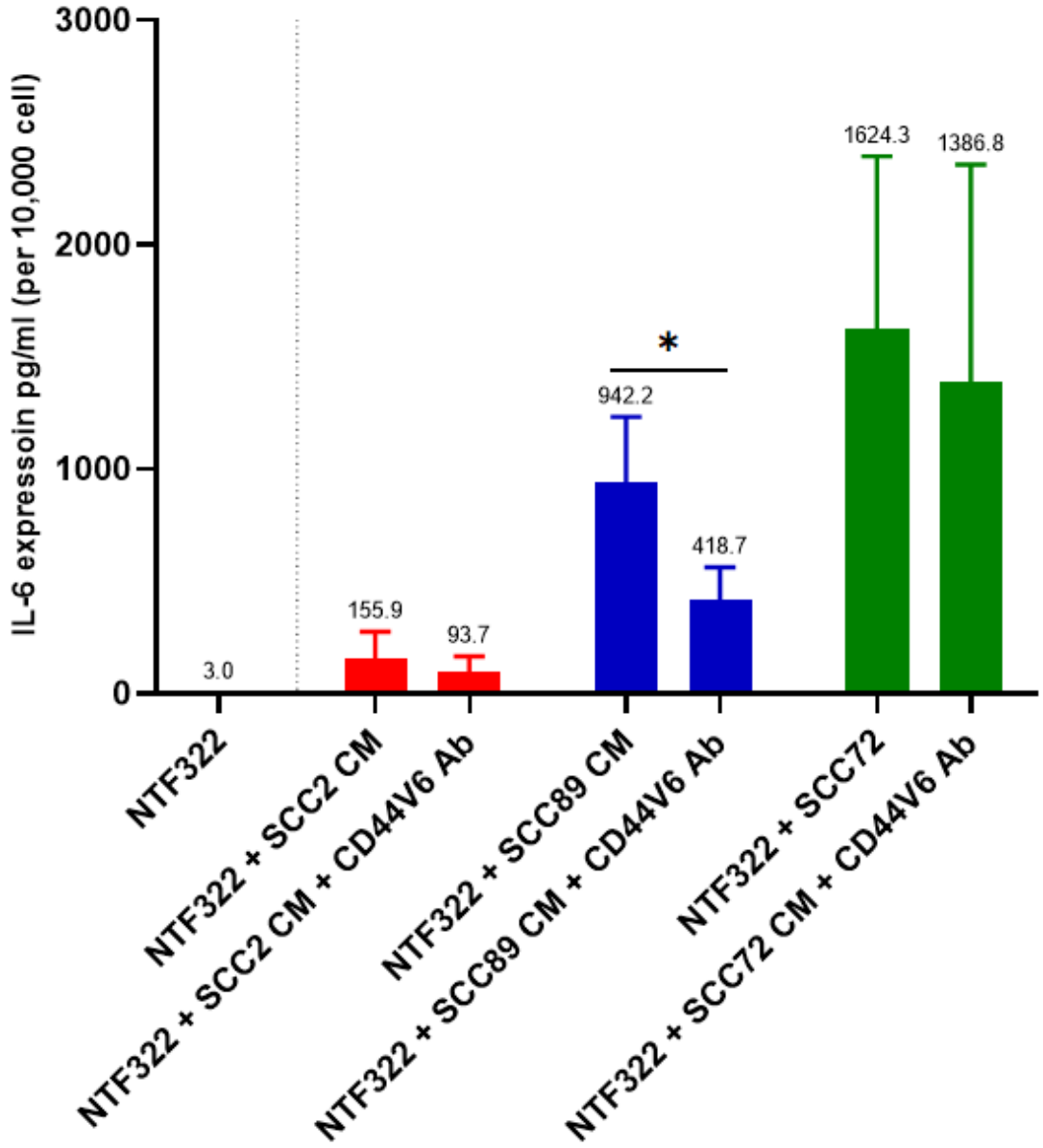

Figure 6.10: Variation in IL-6 protein secretion following CD44v6 blocking in cell line treated NTFs. NTF 322 and NTF 10 were cultured up to 70% confluence in T75 flasks. Cells were incubated with 5 µl/ml of anti-CD44v6 AB for 1h, followed by incubation with SCC2, SCC89 or SCC72 CM for 24h. Untreated counterparts were incubated with serum-free media only without blocking antibody. The media was collected and subjected to IL6 ELISA analysis. Y-axis denotes standardised IL-6 concentration in pg/ml. IL-6 concentrations were optimised according to a fibroblast density of 10,000 cells. Statistical analysis was performed using Student's *t*-test, and statistical significance is shown on the figure by *p<0.05. Error bars = SD for (N=3, n=3).

6.4.7 OPN effects on OPSCCs

In the previous sections, we investigated the functional effects of OPN on OPSCC fibroblasts and observed that OPN was sufficient to establish a myofibroblastic CAF-like phenotype in a subset of NTFs. Here, we aimed to identify the effects of OPN production on OPSCC cancer cells by exploring the activated downstream pathways mediated by OPN binding. We assessed the activation of CD44 and p38 MAPK pathway upon rOPN induction. Mitogen-activated protein kinase (MAPKs) are known to be involved in the regulation of OPN mediated signalling via CD44 and integrins, in different tumour types. p38 is a member of the MAPK family reported to be involved in the regulation of many cellular functions, including cell stress response, proliferation, differentiation and cell migration, among other molecules (Shinohara *et al.*, 2008; Chen *et al.*, 2009). It contributes to the epithelial-mesenchymal transition of the tumour cells which in turn facilitates the acquisition of invasion and migration capabilities (Bhowmick *et al.*, 2001). Activation of the p38 MAPK signalling cascade is triggered by many environmental stresses and inflammatory cytokines including OPN (New and Han, 1998). In OPSCC, the relevance of the p38 MAPK pathway in the context of tumour formation has yet to be investigated.

Cytokine profiling of OPSCC cell lines revealed an exclusive expression of OPN in the HPV-negative OPSCC cell line (SCC89). In this experiment, SCC72 was included for further validation, whereas SCC2 (HPV-positive) was included for comparison as a negative control. MCF7 (Breast cancer cell line) was included as a positive control (Hiscox *et al.*, 2012). The MCF7 cell line was provided kindly by Dr Simon Whawell. Cells were incubated with 180ng/ml rOPN for 48h, then CD44 expression was assessed using immunofluorescent staining using unconjugated CD44 antibody (Proteintech. UK) and by detection of protein abundance using western blot.

At the basal level, immunofluorescent staining showed a remarkable difference in CD44 expression. SCC89 and SCC72 cells showed a faint expression of cell surface CD44 expression, while that was completely lacking in SCC2 (Figure 6.11). Upon rOPN induction, all the tested cancer cells, including SCC2, showed a characteristic glowing aura representing the surface CD44 expression.

This pattern of expression was not observed exactly in the CD44 antibody-blotted membrane. At the basal level, only MCF7, the positive control, showed a faint band of CD44 protein expression, while there were no detectable bands in HPV-negative OPSCC lanes. Optimising the technical protocol with a longer exposure time might reveal a consistent result. However, rOPN-induced SCC72 and SCC89 displayed evident variable CD44 protein abundance, while SCC2 showed a relatively weak band. However, the result of this blot is required validation by normalising with the internal control expression (Figure 6.12).

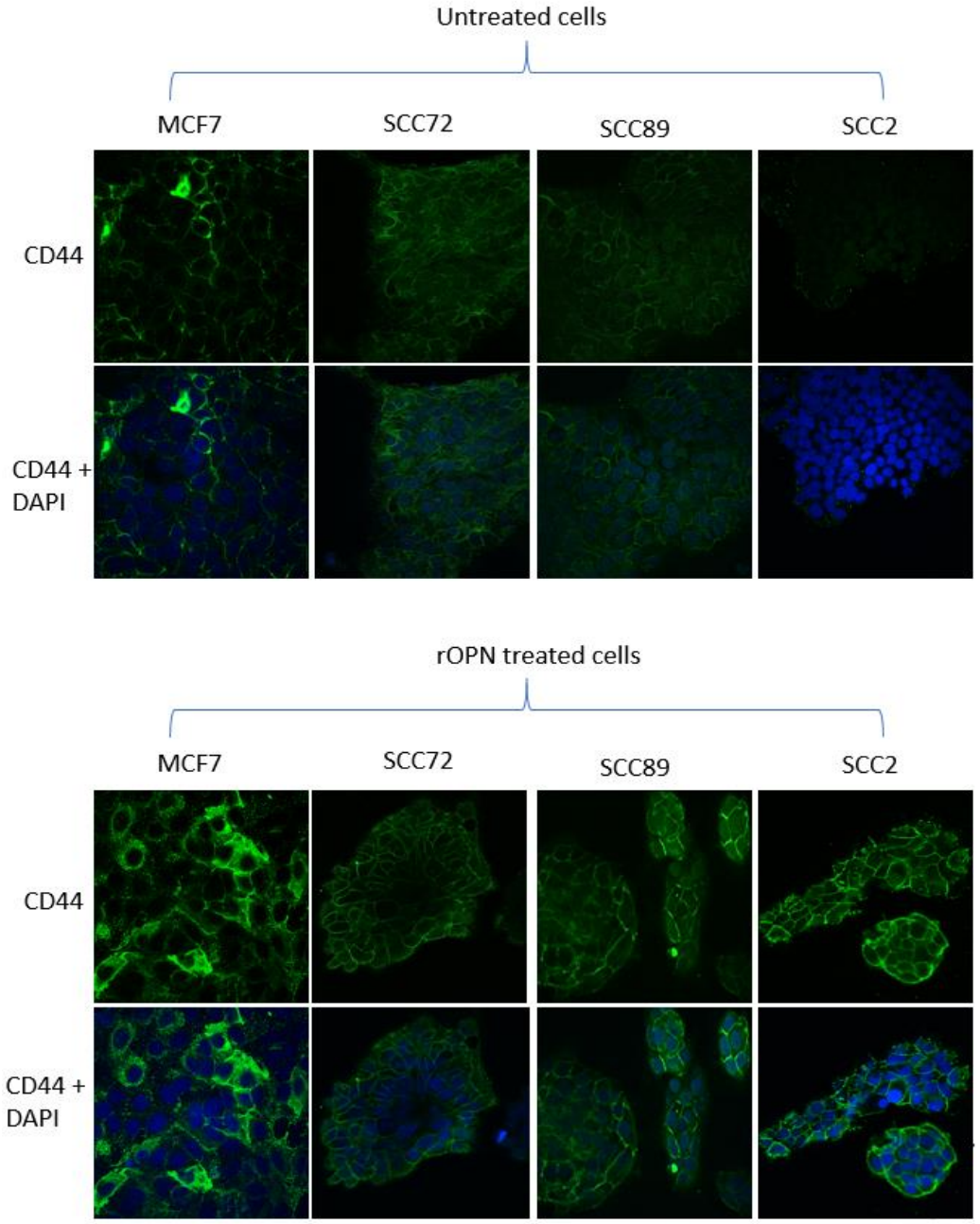

(A)

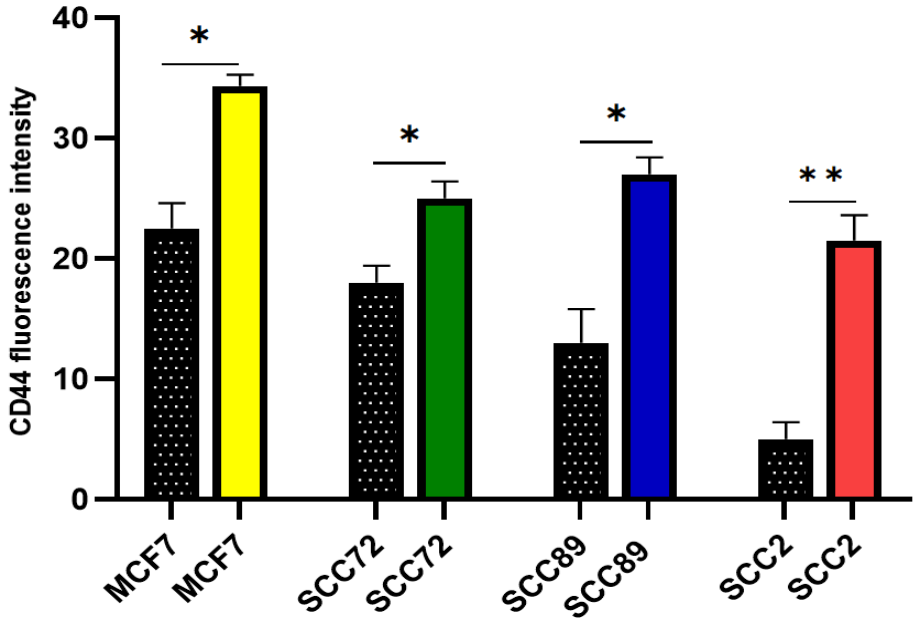

(B)

Figure 6.11: CD44 expression in OPSCC upon rOPN induction. **(A)** Representative photomicrographs demonstrating CD44 basal and induced expression in SCC72, SCC89 and SCC2 cells. MCF7 was included as a positive control. Cells were stimulated with 180ng/ml OPN for 48h then stained with anti CD44 antibody (1:200, 1567-1-AP, Proteintech, UK)). The slide was then mounted on a microscope coverslip using a DAPI-containing mounting medium. CD44 faint expression was observed in HPV-negative cell lines, but not in SCC2. Following OPN induction, an increase in CD44 expression was observed in all OPSCC cell lines. Fluorescent images were taken using a Zeiss 880 Airy-Scan confocal microscope (Carl Zeiss) at 40x magnification. **(B)** Quantification for detected CD44 by image quantification was performed using Fiji-ImageJ. The negative control for each cell line was processed and denoted by the black bar. Statistical analysis was performed using Student's *t*-test, and statistical significance is shown on the figure by *p<0.05, **p<0.01. Error bars = SD for (N=2).

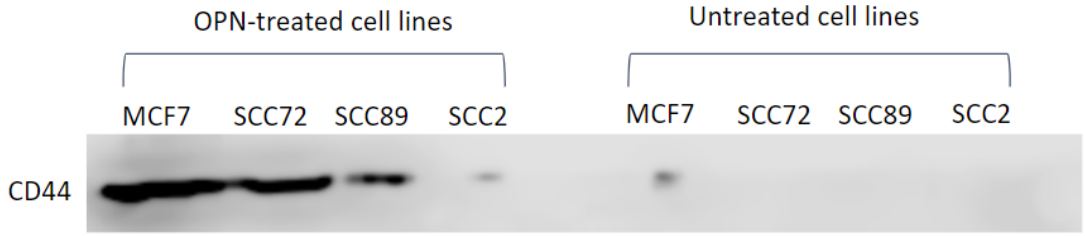

Figure 6.12: Western blot analysis of CD44 in OPSCC following rOPN induction. SCC72, SCC89 and SCC2 were incubated with 180ng/ml rOPN for 48h. The experiment controls were incubated with serum-free media only. MCF7 was included as a positive control. Lysate protein (30 µg) of whole cell were subject CD44 antibody (Proteintech, UK).

6.4.8 IL-6 effect on tumour-derived OPN production in OPSCC

To test the ability of IL-6 to induce OPN production in OPSCC cells, the OPSCC cell lines were incubated with rIL-6 (Peprotech, UK). A dose of 15ng/ml rIL-6 was chosen, as this has been shown to be sufficient for induction in previously reported optimising work on the tumour cells (Chen *et al*., 2018). Thp-1 monocytes were included as a positive control (Uchibori *et al.*, 2017). Thp1 was provided kindly by Dr Emilia Barker. Alterations in OPN expression were assessed using OPN qRT-PCR and ELISA analysis. No significant changes in OPN level were detected following IL-6 treatment at the transcript or secretory levels, even in the positive control. (Figure 6.13 and 6.14). The experiment requires further optimisation including a dose response, as a change would have been expected in Thp-1. A higher dose of 50 ng/ml has been reported in HNSCC (Sun *et al.*, 2014), which would be worth a further trial.

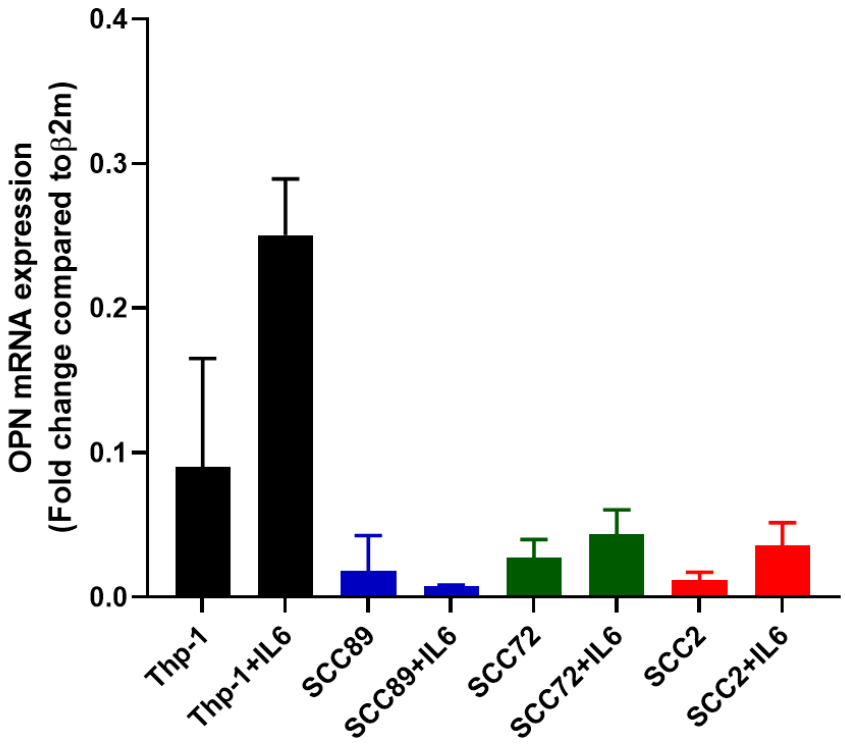

Figure 6.13: No detectable changes in tumour-derived OPN transcript in OPSCC following rIL-6 induction. OPSCC cell lines were cultured in a T75 cm^2 flask in growth media up to 70% confluency then treated with 15ng/ml rIL-6 for 48h. Cell pellets were collected, and cDNA was constructed using 500 ng/ml of total RNA. qRT-PCR was used to analyse OPN expression, normalised to β2m. Thp-1 was included as a positive control. No significant changes in OPN were observed. Error bars = SD for (N=3, n=3).

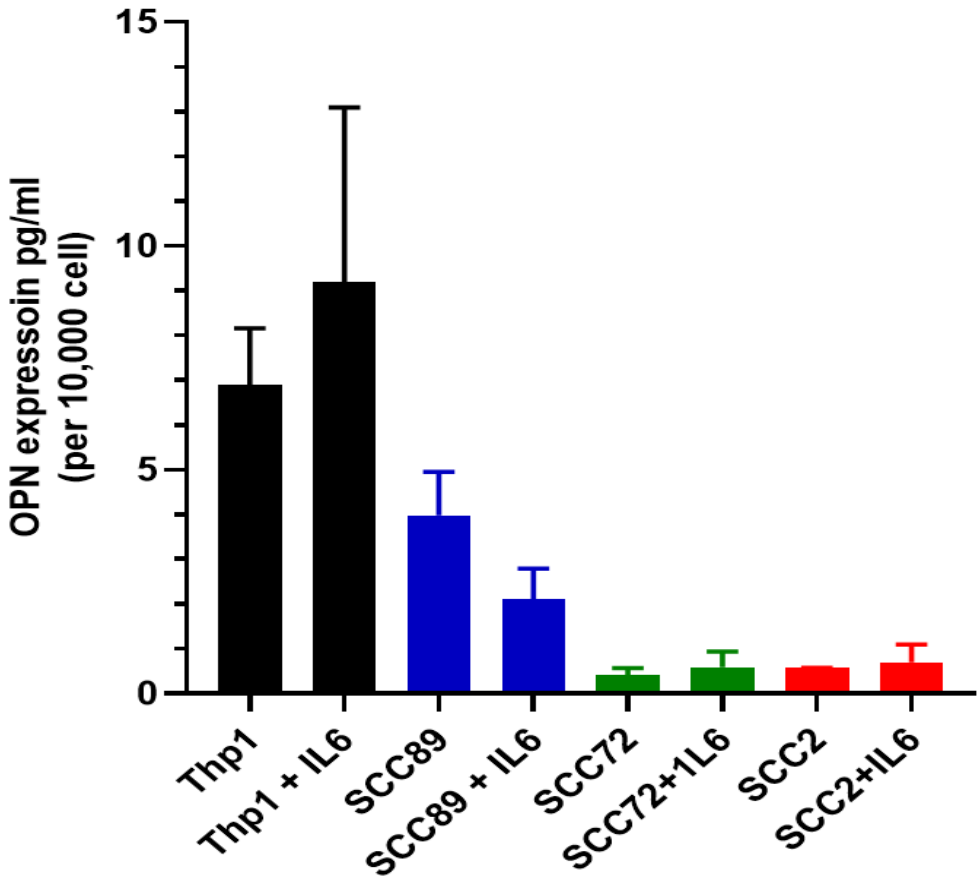

Figure 6.14: No detectable changes in tumour-derived OPN secretory level in OPSCC following rIL-6 induction. SCC89, SCC72 and SCC2 were treated with a single dose of 15ng/ml OPN for 48h. The media was collected and subjected to OPN ELISA analysis. Untreated cells were included for the comparison. Thp-1 was included as a positive control. No evident changes were observed at OPN level. Samples number (n=8), Y-axis denotes standardised OPN concentration in Pg per ml. OPN concentrations were optimised according to fibroblasts density at 10,000 cells. Data represent the mean of (N=3, n=3). Error bars= SD.

6.5 Discussion

In this chapter, we have investigated the effects of OPN on OPSCC fibroblasts. As it has been described, OPN has the ability to reprogram normal fibroblasts into a myofioblastic CAF phenotype (Sharon *et al*.,2015, Prasanna *et al.*, 2021), however, our limited investigation in this chapter showed alteration in NTFs phenotype that warrant further investigation and validation. OPN-induced NTFs showed morphological changes besides enhancement in fibroblasts contractility to some extent, however, these were less marked TGF-β1- induced NTFs described in chapter 4, figure 4.3. We observed a marginal increase in IL-6 production following OPN treatment, but it is neglectable compared to the cell line CM effect on NTF322. However, in Sharon *et al*. (2015) work, IL-6 upregulation was not a feature in evolving CAFs phenotype among other proinflammatory factors. Targeting CD44v6 attenuated the production of IL-6 in rOPN-induced NTF10. However, blocking of CD44v6 on NTF322 before OPSCC CM incubation revealed a variable degree of IL-6 reduction. Preliminary data based on immunofluorescence assay; OPSCC cancer cell lines demonstrated activation of CD44 in response to OPN treatment that was more evident in HPV-negative cell lines.

6.5.1 Osteopontin effects on NTFs

Despite the compelling evidence supporting CAFs' central role in facilitating tumour progression, very little is known regarding the mechanisms of normal resident fibroblast activation. Tumour and immune cell derived molecules have been proposed as factors in fibroblasts activation (Erez *et al.*, 2009; Elkabets *et al.*, 2011; Sahai *et al.*, 2020). Nevertheless, the characterisation of signalling network mediating fibroblast activation is still largely unresolved. TGF-β1 has been identified as one of the most predominant regulators in fibroblast activation. It regulates several pro-fibrotic activities including fibroblast proliferation, and the fibroblast-to-myofibroblast differentiation (Lewis *et al.*, 2004; Hinz *et al.*, 2012; Meng, Nikolic-Paterson and Lan, 2016, Melling et al., 2015). Tumour-derived inflammatory modulators including SDF1, IL-1 α and IL-1β were shown as a promoter in CAF activation. Other factors derived from different cell types also were proposed as candidates that could be involved in fibroblasts activation including PDGF, IL-4, and insulin-like growth factor II (Powell *et al.*, 1999).

The functional role of OPN in stroma activation was described firstly in cardiac and dermal fibroblasts as an essential component in the autocrine activation pathway mediated by TGF-β1. In cardiac and dermal OPN-null fibroblasts, cells showed a significant reduction in response to TGF-β1 stimulation; there was no overexpression of

the activation protein signature including α-SMA and fibronectin. Additionally, they exhibited 50% less proliferation and resistance to detachment by shear force, also they showed a 3-fold reduction in collagen gel contraction compared by wild-type fibroblasts. Furthermore, knockdown of OPN wide-type fibroblasts using small interfering RNA reduced α-SMA expression response to TGF-β1 to levels comparable with OPN-null cells (Lenga *et al.*, 2008). The OPN pro-fibrotic effect has been studied intensively in wound healing and fibrosis-related diseases. OPN-null mice have altered wound healing processes with healing wounds containing smaller collagen fibrils and disorganised ECM (Liaw *et al.*, 1998). Moreover, knockdown of the OPN gene revealed altered healing patterns and significantly reduced scarring (Mori, Shaw and Martin, 2008; Hunter *et al.*, 2012). In lung fibrosis, OPN has shown a critical role in airway remodelling. The functional role of OPN is largely based on pro-fibrogenic myofibroblast stimulation. It initiates the fibroblasts activation, migration, adhesion, and proliferation through a cytokine signalling pathway (Oh *et al.*, 2015).

The impact of OPN in CAF activation was reported by two breast cancer research studies (Sharon *et al.*, 2015, Prasanna *et al.*, 2021). These studies demonstrated that OPN is required, and sufficient, to reprogram normal fibroblasts to myofibroblasts functionally and molecularly. Furthermore, CAF-driven OPN enhanced EMT and angiogenesis via SDF-1 expression. In this study, stimulation of NTFs using rOPN alone induced some phenotypic alterations, including the cell morphology, gene transcription and secretory profile. Under the light microscope, rOPN-induced NTFs displayed changes in cell morphology compared to the untreated cells which retain the spindle-shaped quiescent appearance. As has been discussed in chapter 4, alteration in fibroblast shape is a non-specific feature in fibroblast phenotypic change. To specify the evolving induced phenotype, we performed collagen gel contraction assay and SA-β-gal assay. According to the characterisation work in chapter 4, the active myofibroblastic like phenotype displayed high capability in gel contraction, while premature induced senescent phenotype showed an elevated percentage of SA-β-gal-stained cells. In this chapter, rOPN-induced CAF2 and NTF10 showed a degree in the collagen disc contraction compared with the untreated fibroblasts, while NTF322 showed a neglectable amount of contraction. Assessment of SA-β-gal assay has shown no evident increase in SA-β-gal positive percentage in this chapter.

This ability to shrink a free collagen lattice indicated the increase in fibroblast contractility and phenotype differentiation into myofibroblastic CAFs as we have observed in chapter 4, however, we did observe that much increase in NTFs contractility moreover, we were

not able to assess and compare α-SMA formation in this chapter to confirm the active transition in NTFs phenotype. In a similar experiment on dermal fibroblasts, Hunter *et al.*, (2012) showed a significant increase in contractility, migration, and proliferation of 4 different dermal fibroblasts cultures in response to rOPN induction (50nM). While knockdown of the OPN gene using an OPEN-directed RNA aptamer (OPN-R3) showed significant inhibition of OPN-induced effects on fibroblast cultures (Hunter *et al.*, 2012). The exact mechanism behind fibroblasts activation is still unknown, but it implies an increase in α-SMA or other microfilaments that may be involved in cell contractility (Hunter *et al.*, 2012).

Prasanna *et al*., (2021) study assessed the molecular alteration in CAFs driven by tumour-derived OPN, the evolving CAFs phenotypes showed an overexpression in α-SMA and FAP at gene and protein levels. Their study reported the crosstalk between tumour cells and stromal fibroblasts that leads to tumour progression mediated by tumour-derived OPN and fibroblasts-derived CXCL12. Sharon *et al.*, (2015) work in mammary fibroblasts demonstrated that tumour-derived OPN has the capability to induce normal mammary fibroblasts differentiation into a myofibroblastic CAF active phenotype. The evolving active phenotype showed a high capacity for gel contraction and upregulation in the pro-inflammatory secretory profile, but not including IL-6. Breast cancer is one of the desmoplastic tumour types in the human body. It is characterised by profound myofibroblast infiltration that correlates with tumour progression, invasion and poor survival (Yamashita *et al.*, 2012).

Next, we tested IL-6 upregulation in rOPN-induced fibroblasts to assess the phenotypic changes in OPSCC fibroblasts and investigate the hypothesis of the epithelial-stromal stimulatory loop in OPSCC mediated by OPN and IL-6 expression. We observed a slight increase in IL-6 upregulation at the transcript and secretory profiles, however, the heterogeneity of fibroblast responses was evident. NTF10 showed the highest increase in IL-6 expression, while NTF322 showed the lowest values of IL6 at the basal and induced level. In Qin *et al.*, (2018) study, blocking one of the OPN receptors showed a partial decrease in the effects of OPN, while the combination of more than receptor blocker resulted in a significant effect. We observed a significant reduction in IL-6 production in NTF10, while there was a slight decrease in NTF322 that was statistically insignificant.

6.5.2 Targeting CD44v6 potentially reduces IL-6 production in NTF322 following OPSCC CM stimulation

Incubation of NTF322 with HPV-negative cell line media (from SCC89 and SCC72) resulted in greater upregulation of IL-6 production in NTF322 cultures than in the HPV positive cell line (SCC2) counterparts. This in keeping with our findings in chapter 5 using co-culturing models. The HPV-negative co-cultured model showed a significant upregulation in IL-6 compared to the HPV-positive model. Here, in this chapter, we aimed to test whether the tumour derived OPN in cell line CM will induce an activated fibroblast phenotype. The appropriate methodology to answer this question required targeting of both OPN binding sites (CD44 and integrins), however, our work was limited to CD44v6 blockade.

Blocking of CD44v6 in NTF322 showed a variable degree of IL-6 reduction. In SCC89-induced NTF322, there was a significant decrease in IL6 production with the presence of CD44v6 blocking antibody. SCC2-induced NTF322 cells showed a lower production in IL-6 at a transcript and secretory levels, but that did not reach the statistically significant limit ($p<0.05$). The partial reduction in IL-6 production was expected as we targeted only one ligand-binding site of OPN. The discrepancy in IL-6 reduction in CD44v6-targeted NTF322s suggested the variable capacity of OPSCC cell lines in fibroblasts activation. OPSCC cell line media contain a plethora of factors that might be involved in IL-6 upregulation besides OPN such as HGF (Bolt *et al*., 2018). Interestingly, SCC72-induced NTF322 showed no evident reduction in IL-6 production in response to CD44v6 antibody. This result reminded us of Bolt, (2016) findings on OPSCC cell lines using ORIS™ Assay Cell Migration. In this experiment, the HPV-negative cell lines (SCC89 and SCC72), but not the HPV-positive cell lines, showed a significant migration in response to M2 (induced fibroblast media). However, only SCC72 showed a comparable significant migration when it was incubated M1 media (SCC72 CM and fibroblast media). The result suggested that HPV-negative cell lines were able to induce a fibroblast response capable of promoting additional void closure in the migration assays, nevertheless, the significance of the additional migration in SCC72 M1 may be linked to an inductive pathway unique to SCC72-fibroblast interactions (Bolt, 2016).

6.5.3 Effects of OPN on OPSCC

CD44 expression is regulated through specific signalling networks including epigenetic mechanisms, miRNAs and transcriptional factors (reviewed in Chen *et al.*, 2018). Proinflammatory cytokines such as IL-1β, IL-6, IL-1, IL-4, IL-13, and TGF-β1 were also

reported as inducers that drive CD44 activity (Foster *et al.*, 1998; Ibrahim *et al.*, 2006). OPN/CD44 expression was shown to be correlated positively with cancer progression in different tumour types (Sun *et al.*, 2013; Qiu *et al.*, 2014). The OPN/CD44 interaction was reported to mediate signalling pathways that induce stem cell-like properties, tumour migration and radiation resistance (Desai, Rogers and Chellaiah, 2007; Pietras *et al.*, 2014).

We have seen that the HPV-negative cell line (SCC89) showed a higher basal OPN secretion compared with the HPV-positive cell line (SCC2). Moreover, fibroblast co-cultured SCC89s demonstrated significant upregulation in OPN when compared with SCC2s counterparts (Figure 5.20). Here, in our preliminary findings, we observed that OPN/CD44 association is more evident with HPV-negative cell lines compared to SCC2. This observation could be linked to the p53 degree of integrity in OPSCC subtypes. As HPV-negative tumour carries p53 mutations and HPV-positive counterpart displayed inactivation of p53 due to the expression of HPV E6 oncoprotein. Under normal condition, p53 inhibits the expression of CD44 via the interaction with a non-canonical p53-binding sequence in the CD44 promoter. This binding enables the non-malignant cells to respond to stress-induced p53-dependent cytostatic and pro-apoptotic signals. A lack of p53 function has a de-repressing effect on CD44 expression which appears as an essential factor for tumour cell growth (Godar *et al.*, 2008).

Besides the involvement of CD44 signalling in tumour cells invasion and metastasis, typically, CD44 positive cells demonstrated stem-like properties with increased resistance to chemotherapy and radiotherapy in HNSCC (Chen *et al.*, 2010; Wang and Bourguignon, 2011). These features suggest that CD44 may be useful as a prognostic biomarker (Lin and Ding, 2017; Wang *et al.*, 2019). Indeed, higher CD44 expression in tissue was correlated with advanced stages and poor clinical outcome in HNSCC (Chen *et al.*, 2014). In OPSCC, CD44 IHC expression showed a strong CD44 membrane staining in p16 negative OPSCC while p16 positive OPSCC showed none or light staining in membrane and cytoplasm (Cohen *et al.*, 2017). Assessment of the prognostic value of CD44 IHC expression in HPV-DNA positive OPSCC revealed a superior advantage associated with disease-specific survival compared with p16 IHC expression that showed a correlation with overall survival only (Näsman *et al.*, 2013).

In this chapter, we also planned to investigate the change in p38 MAPK phosphorylation ratio in OPSCC in response to OPN incubation. The specificity of OPN activation cascade also requires further validation targeting OPN and CD44. The clinical

significance of p38 MAPK involvement in OPSCC tumours has yet to be investigated thoroughly. Activation of p38 MAPKs has been shown as a key factor in the production of many cytokines, such as IL-1, TNF-α, and IL-6, which have pro-inflammatory, and angiogenic effects (Kumar, Boehm and Lee, 2003). p38 MAPK was reported to support crucial functions facilitating tumour cell invasion. It induced the expression of the matrix metalloproteinases MMP1, MMP3, and MMP13, which in turn regulate matrix remodelling and degradation (Pourgholami and Morris, 2008), besides its active contribution in epithelial-mesenchymal transition that enhances invasion and migrating capabilities (Bhowmick *et al.*, 2001; Neil A. Bhowmick *et al.*, 2001; Huang *et al.*, 2017). In cervical cancer cells, activation of p38 MAPK has been shown to be driven by OPN/CD44 expression, mediating NF-kB activation. The downstream activation subsequently resulted in NF-kB–dependent expression of furin, which enhanced the tumour growth *in vivo* (Kumar *et al.*, 2010).

6.6 Limitations

We are aware that this chapter has not covered its stated aims. Our assessment on OPN-induced phenotype still requires further confirmation by doing α-SMA and FAP expression assessment. Moreover, including a larger number of NTFs' cultures is crucial before drawing the conclusion.

Targeting of OPN in this chapter was limited to CD44v6 receptor only. A combination of CD44 and integrins blocking is essential to assess thoroughly the effects of OPN on OPSCC fibroblasts. Furthermore, in this chapter, we were not able to analyse OPN signaling pathway mediated by CD44 and p38 MAPK.

6.7 Summary of main findings and clinical implications

To some extent, some findings in this chapter require further validation by future work, as they highlighted new areas for the research in OPSCC:

We investigated for the first time the functional role of OPN on OPSCC fibroblasts and cancer cells. We observed alteration in a subtype of NTF. Moreover, targeting CD44v6 showed a reduction in IL-6 derived on rOPN stimulation NTF10. Although our assessment underpins further investigations, it may provide new molecular insight into the understanding of CAFs development induced by OPN. Targeting the dynamic interaction between tumour cells and CAFs is a much-needed approach to cancer therapy. We have seen that targeting CD44v6 in NTF induced by OPSCC cell line CM

resulted in varying degrees of IL-6 reduction. Targeting integrins in addition to CD44v6 might reveal a potential cancer therapeutic target in OPSCC.

The immunofluorescence assay showed overexpression in CD44 in response to OPN treatment. Further analysis on involvement of CD44 and p38 MAPK pathway activation in OPSCC cell lines is required. Understanding of OPN downstream signaling in OPSCC may suggest further novel therapeutic strategies in OPSCC.

.

Chapter 7: OPN IHC expression in OPSCC

7.1. Introduction

Many researchers are extensively studying novel tumour biomarkers owing to important potential applications in early diagnosis, and therapy modulation. In the clinical setting, the diagnosis and evaluation of cancer are mainly based on the clinical and histo-morphologic assessment. However, molecular biomarkers are more quantifiable and may be more reflective of underlying disease mechanisms. In the *in vitro* sections of this thesis, tumour-derived OPN has shown an exclusive association with one subtype of OPSCC only (HPV-negative). Moreover, it has demonstrated the ability to modulate normal fibroblasts into the more active secretory phenotype. However, our observations were based on an *in vitro* model with the absence of the majority of TME components and associated essential signalling pathways. OPN, as a multifunctional protein, has been known for its functions in promoting tumour cell migration, metastasis and tumour survival. It has been suggested by many authors as a prognostic biomarker (Crawford, Matrisian and Liaw, 1998; Danzaki *et al.*, 2016), however, the prognostic value of OPN expression in OPSCC tissue has not been assessed. Here, in the last chapter, we aimed to examine OPN and IL-6 expression in OPSCC tissue in a validation step of our *in vitro* findings. Moreover, we aimed to determine their prognostic performance in OPSCC using IHC and RNAScope assays.

Unfortunately, our research has been affected by the national lockdown measures against COVID 19 pandemic. Only OPN IHC assay was performed for the whole OPSCC cohort, and we were not able to do OPN ISH. Moreover, IL-6 RNAScope was performed only for cohort 2 TMAs' sections.

7.2. Aims

- Validate the cytokine array findings regarding OPN and IL-6 expression in OPSCC tissue.

- Determine OPN IHC threshold in OPSCC and evaluate its prognostic performance.

7.3. Experimental approach and statistical analysis

- OPN biomarker expression was assessed by performing IHC staining for the study cohort. OPN threshold of expression was assessed using ROC curves. Demographic comparison between OPN groups was performed using Chi-square test.

- The prognostic value of OPN as a biomarker was evaluated and compared in OPSCC subtypes using Kaplan-Meier method, Log-Rank test and Unadjusted Cox regression model (Univariate).

- IL-6 RNAScope was performed only for cohort 2. IL-6 prognostic value was evaluated using Kaplan-Meier method and Log-Rank tests.

- The prognostic strength of the study biomarkers, collectively, was evaluated using multivariate Cox regression model.

- All analysis performed using SPSS (versions 23-26). p-value<0.05 was considered significant. HR>1 indicated a positive correlation with the hazard (Mortality).

7.4. Results

7.4.1. OPN IHC Antibody Titration

To evaluate OPN IHC expression in OPSCC, the study cohort was subjected to OPN IHC staining using OPN antibody (22952, Proteintech, UK). We started by antibody titration following the manufacturer's instructions to select the most appropriate antibody concentration. TMA slides were subjected to both the highest and lowest suggested antibody concentration: 1:50 and 1:200. Under the light microscope, stained slides with (1:50) antibody concentration “OPN1” showed a non-specific high-intensity pattern that covers the majority of cores, without displaying a degree of specificity between tumour and stroma expressions. The demarcation between the tumour islands and stroma was obscured by the deep overlapped staining (Figures 7.1). On other hand, 1:200 antibody concentration “OPN2” showed a clearer background between the stained tumour islands. Also, there was an evident difference in staining intensity within the same core. This dynamic range in OPN stain suggested 1:200 antibody dilution is the most appropriate concentration in OPSCC tissue for this study.

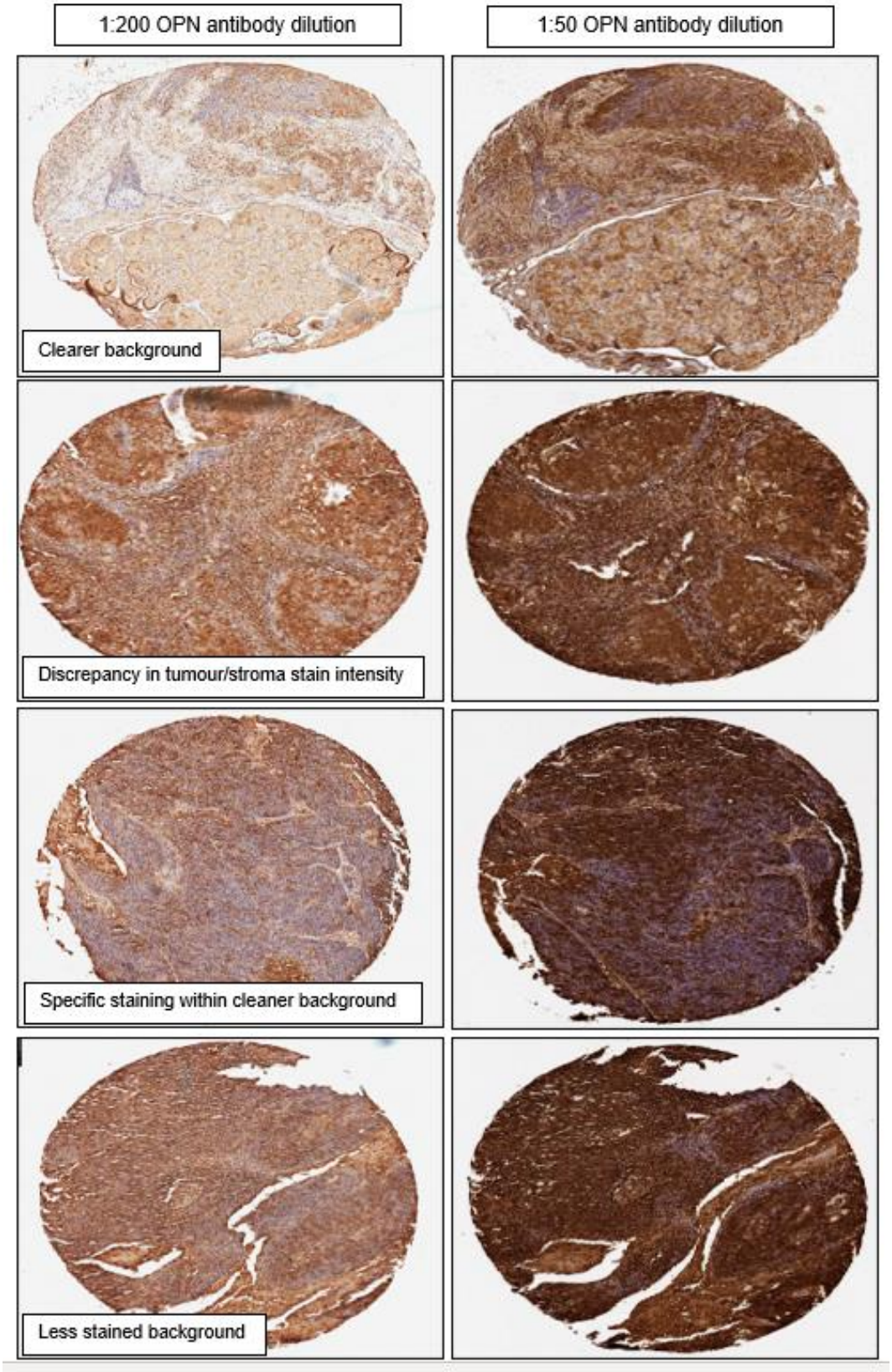

Figure 7.1: Dynamic range in OPN IHC stain using different antibody dilutions. Matched slides were subjected to 1:50 (right panels) and 1:200 (left panels) using OPN antibody (Proteintech, UK).

7.4.2. OPN IHC stain patterns in OPSCC tumour cells

7.4.2.1 OPN IHC assay controls

7.4.2.1.1. Positive control.

A placenta tissue section was provided kindly by Prof. Craig Murdoch to serve as OPN IHC positive control. OPN has been detected in the human uterus during peri-implantation, suggesting a role in implantation and placentation. Also, its function was linked to cell-cell and cell-ECM communication within the uterus and placenta (Johnson *et al.*, 2003). In this study, placenta tissue showed a strong brown immuno-staining of the chorionic villi, which indicated the optimum staining protocol (Figure 7.2).

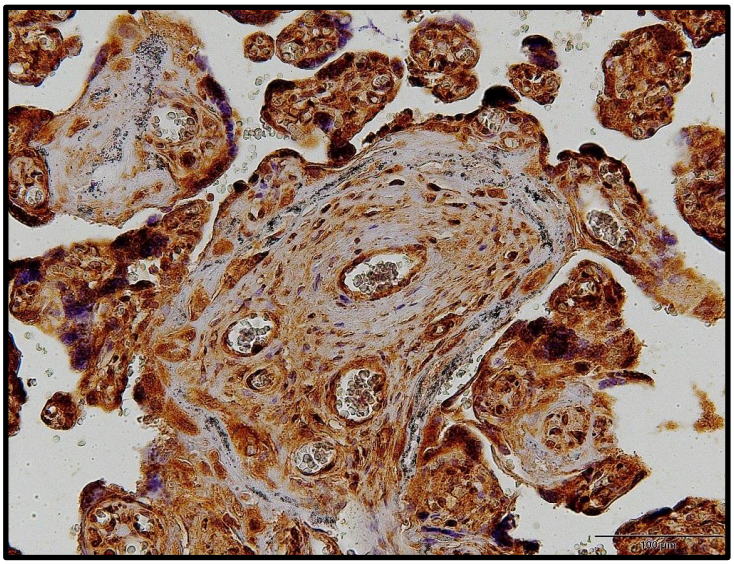

Figure 7.2: IHC staining of OPN expression in the placenta. Example of positive immunostaining for OPN in human tissue (OPN antibody positive control).

7.4.2.1.2. Non-malignant OP tissue.

To assess OPN IHC expression in OPSCC, we had a look at OPN expression in non-malignant OP structures (Figure 7.3). OPN was expressed by the immune cells and lymphoid tissue at different intensities. Macrophages' foci appeared in large deeply stained spots within the stained inflammatory background.

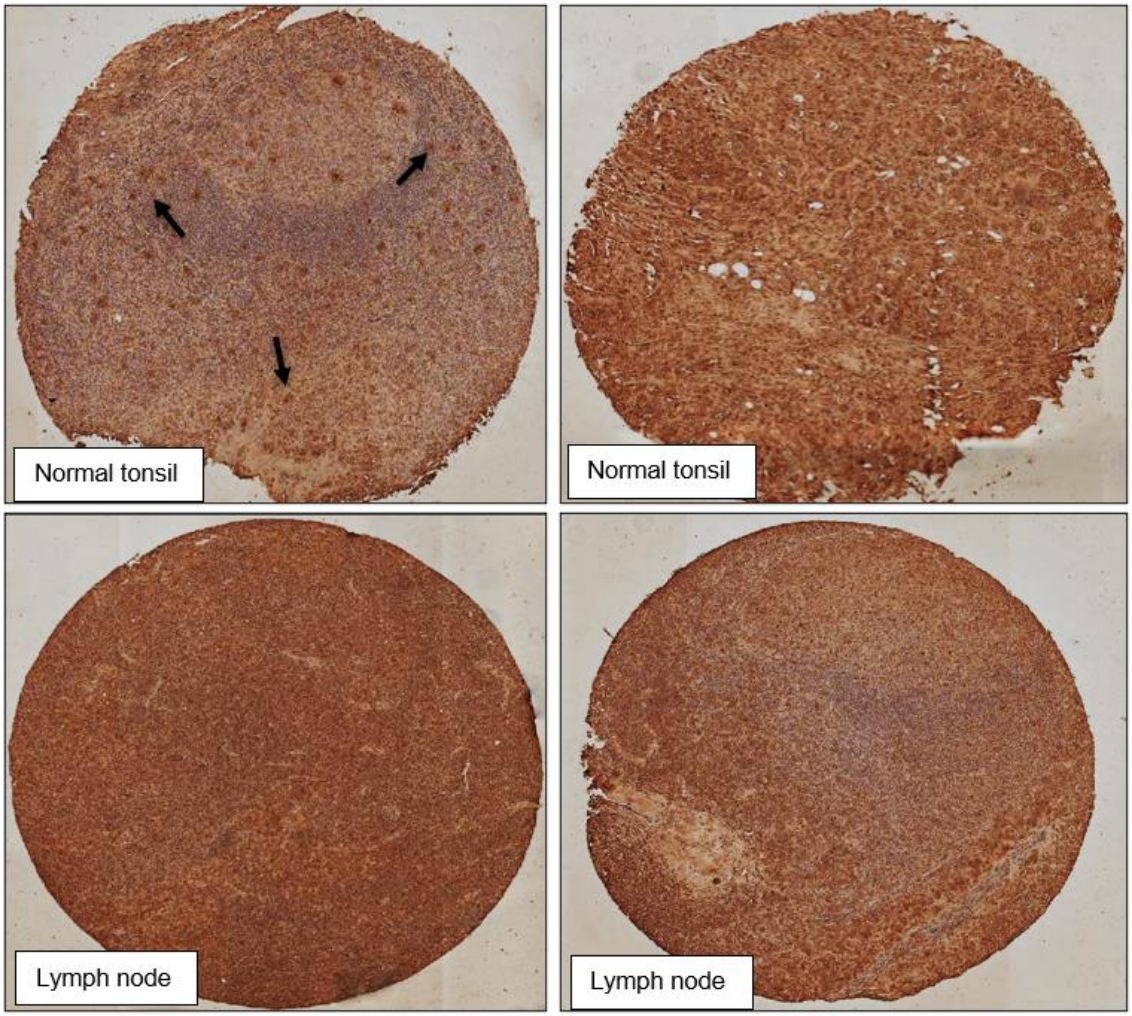

Figure 7.3: OPN expression in normal OP tissue. Sections were subjected to OPN antibody at 1:200 dilution (Proteintech, UK). Arrows pointed to macrophage foci spots.

7.4.2.2 Complete OPN-negative or positive stain pattern in OPSCC.

A complete absence of OPN expression was noticed in a limited number of the tissue cores which further indicated OPN antibody specificity (Figure 7.4). On the contrary, full-thickness OPN positivity with a homogenous intensity was detected in a larger number of tissue cores (Figure 7.5). Notably, the surrounding stroma showed a degree of OPN stain intensity that in some cases was higher than the tumour islands.

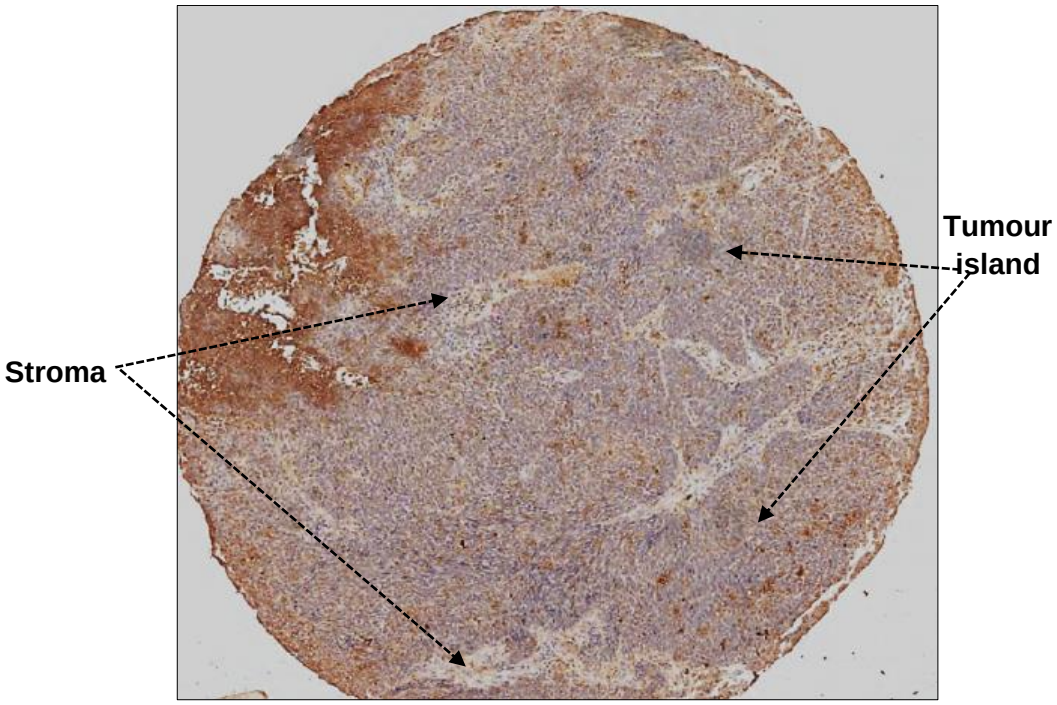

Figure 7.4: Complete OPN-negative OPSCC tissue. The section was subjected to OPN antibody at 1:200 dilution (Proteintech, UK).

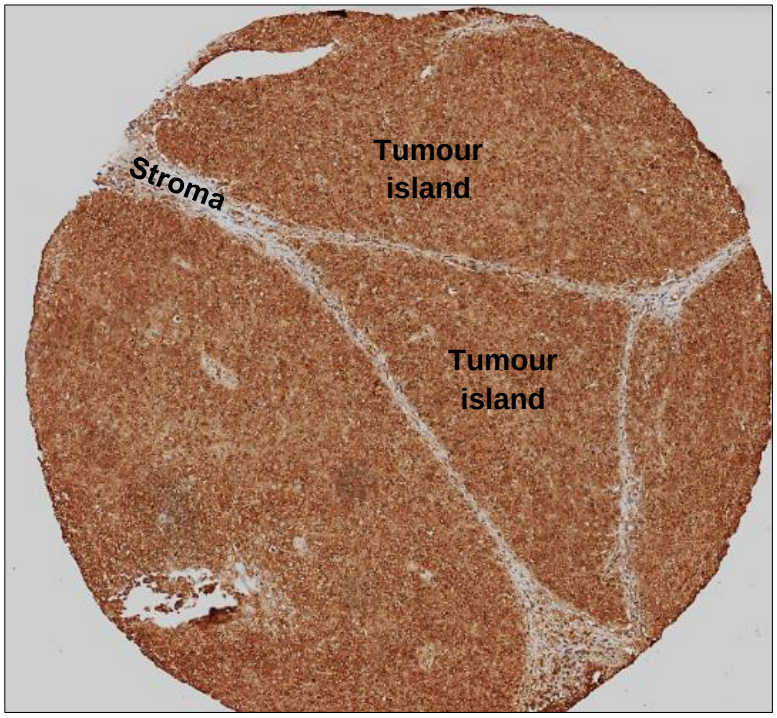

Figure 7.5 A: Full-thickness OPN expression in OPSCC. The section was subjected to OPN antibody at 1:200 dilution (Proteintech, UK). Notice the strong OPN staining in tumour islands while stroma appeared less stained.

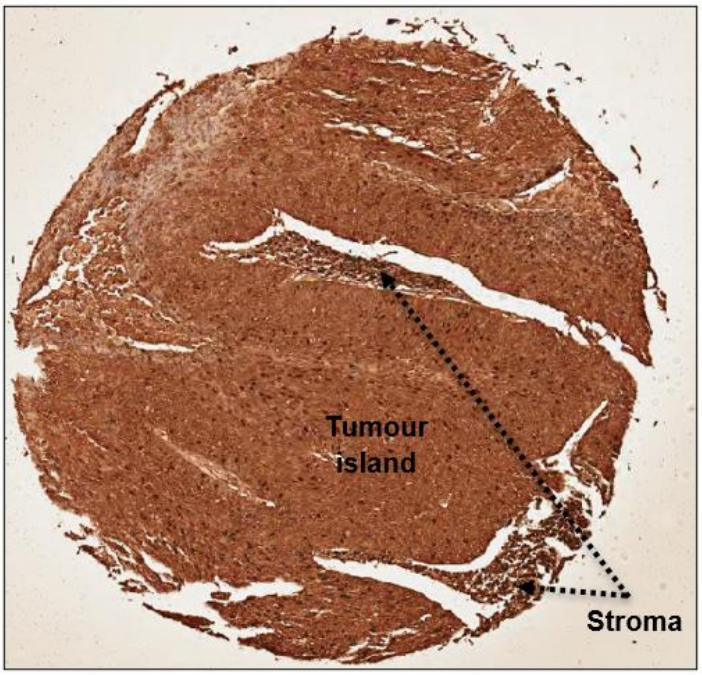

Figure 7.5 B: Full-thickness OPN expression in OPSCC. The section was subjected to OPN antibody at 1:200 dilution (Proteintech, UK). Notice the strong OPN staining in both the tumour islands and the stroma.

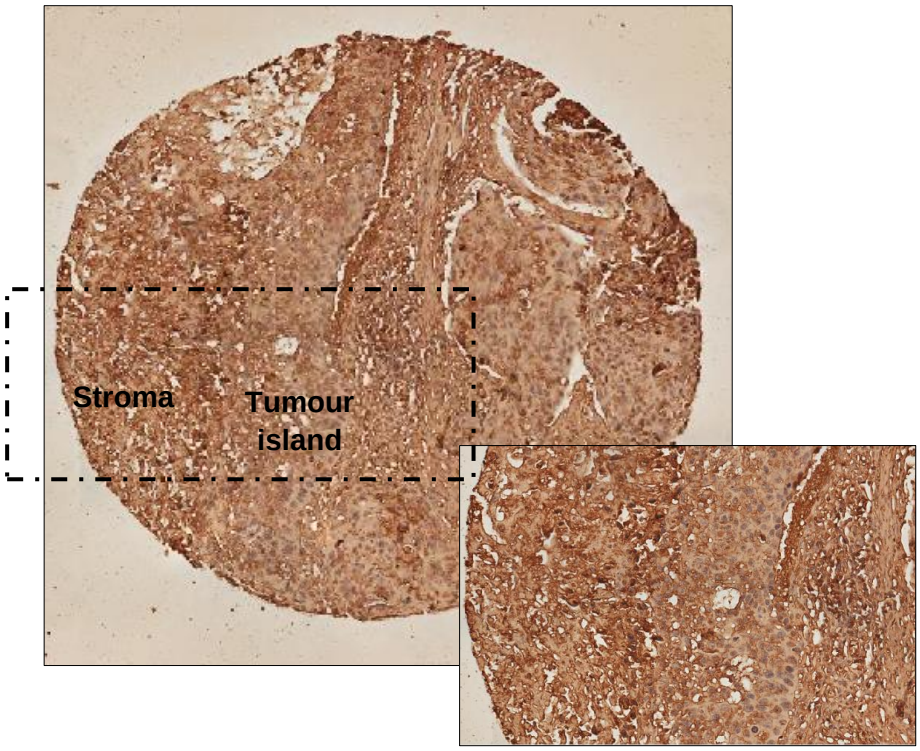

Figure 7.5 C: Full-thickness OPN expression in OPSCC. The section was subjected to OPN antibody at 1:200 dilution (Proteintech, UK). Notice the strong OPN staining in stroma while tumour cells showed less OPN stain intensity.

7.4.2.3 OPN partially stained OPSCC.

Due to the nature of the IHC assay, the immunostaining has a wide dynamic range between two ends of strong immunopositivity and completely negative immuno-stain. The OPN IHC assay in OPSCC showed a wide variety of staining patterns that range between a score of 4 - 8 (Figure 7.6). OPN positive cells showed strong brown staining for part of the epithelium thickness, however, in some tissue sections, OPN positive portion was most prominent toward the top (superficial) part of the epithelium or in the edges of the tumour islands. By the comparison with H&E-stained slides, some OPSCC tissue sections showed a degree of terminal differentiation in the higher epithelium layers which correlated with OPN expression. This observation suggests that OPN overexpression may relate to cell differentiation. However, in other cases, this pattern might be a demonstration of the functional crosstalk between stromal cells and adjacent cancer cells in OPN overexpression. Cancer cells that were located in direct interaction with stroma cells, mainly CAFs, might be induced intensively via CAF paracrine signalling mediated by OPN overexpression.

In some sections, with large tumour islands, OPN expression was toward the centre, which suggested the functional expression of OPN in hypoxic tissue. OPN was identified as a hypoxia regulator among other factors in HNSCC (Byers *et al*., 2011). High OPN levels were correlated with tumour hypoxia and worse outcomes in HNSCC (Courter *et al*., 2010). We also noticed that the stroma was heavily infiltrated by deeply stained stroma cells that were merged and overlapped the tumour islands. These are most likely immune cells, which were not included in the *in vitro* model. It was unclear if the OPN immunopositivity was tumour-derived or stroma-derived.

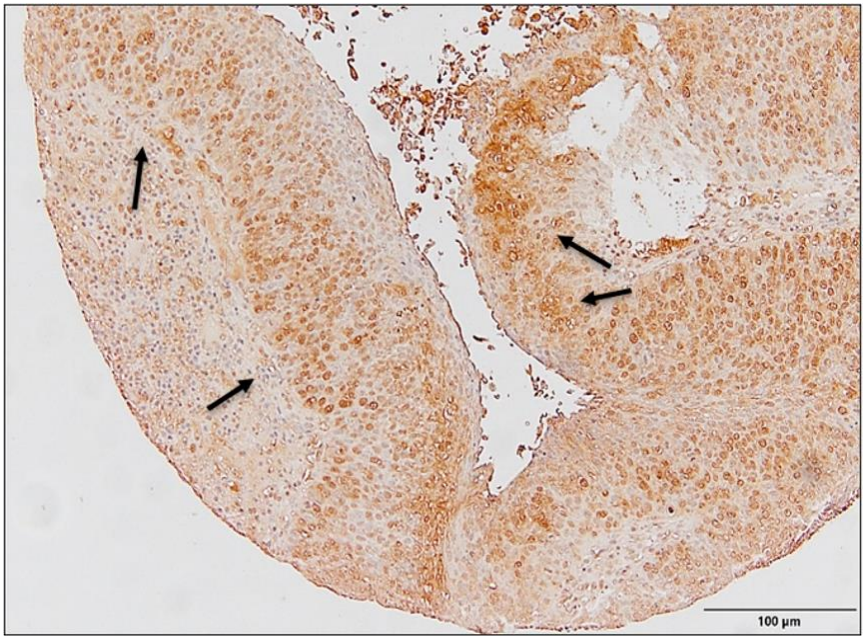

(A)

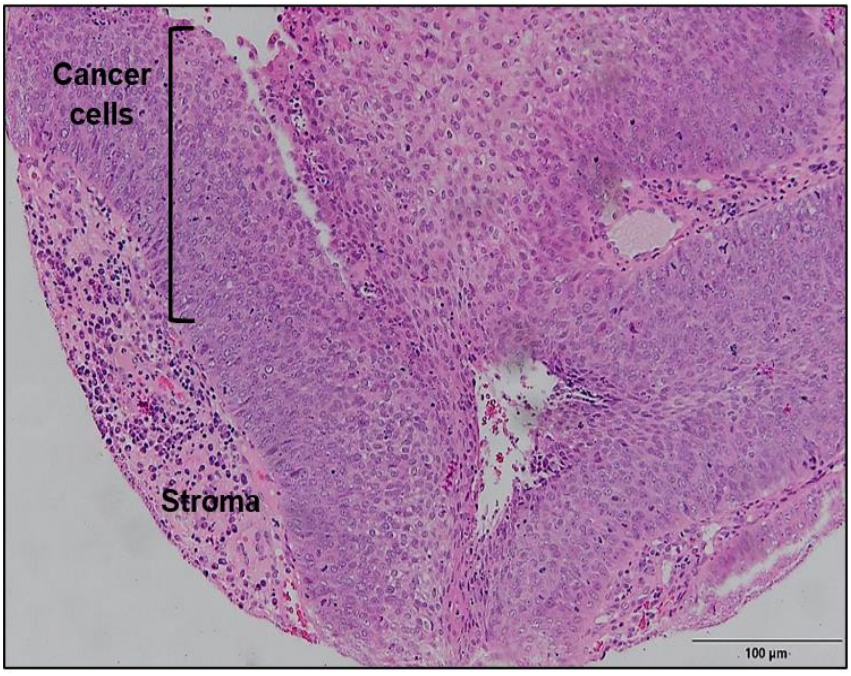

(B)

Figure 7.6 A: OPN partially stained OPSCC. (A) OPN IHC assay using 1:200 antibody dilution (Proteintech, UK). **(B)** Corresponding H/E slide. Notice OPN expression in tumour cells that are in close direct contact with the underlying stroma.

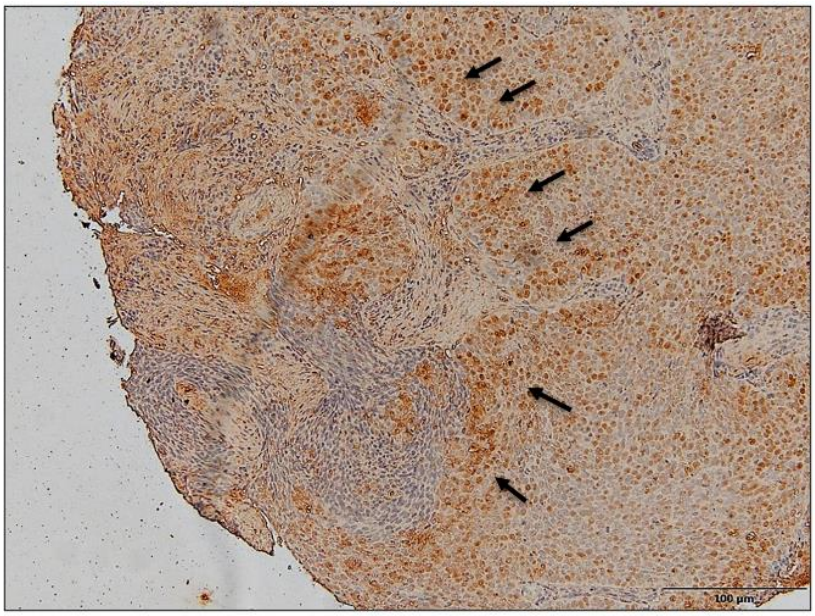

(A)

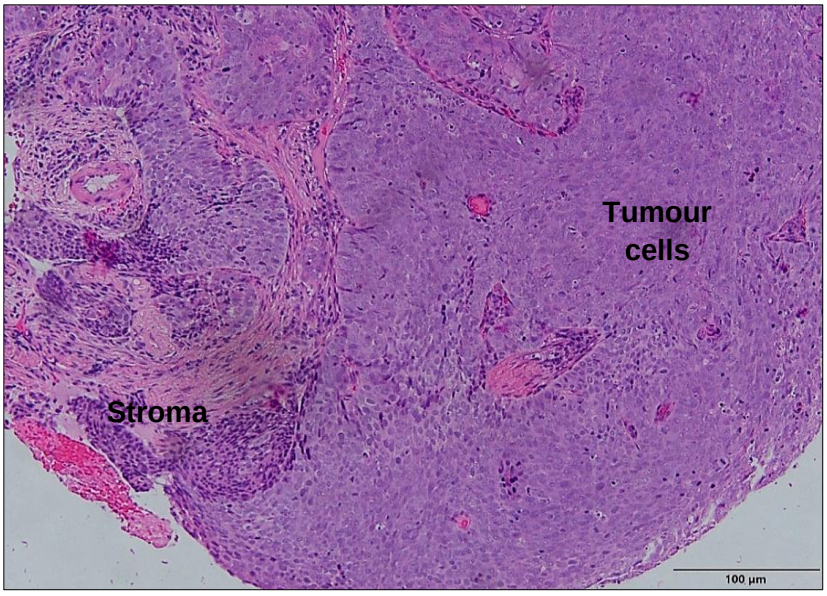

(B)

Figure 7.6 B: Partial OPN staining in OPSCC. (A) OPN IHC assay using 1:200 antibody dilution (Proteintech, UK). **(B)** Corresponding H/E slide. Notice OPN expression in tumour cells which in close direct contact with underlying stroma.

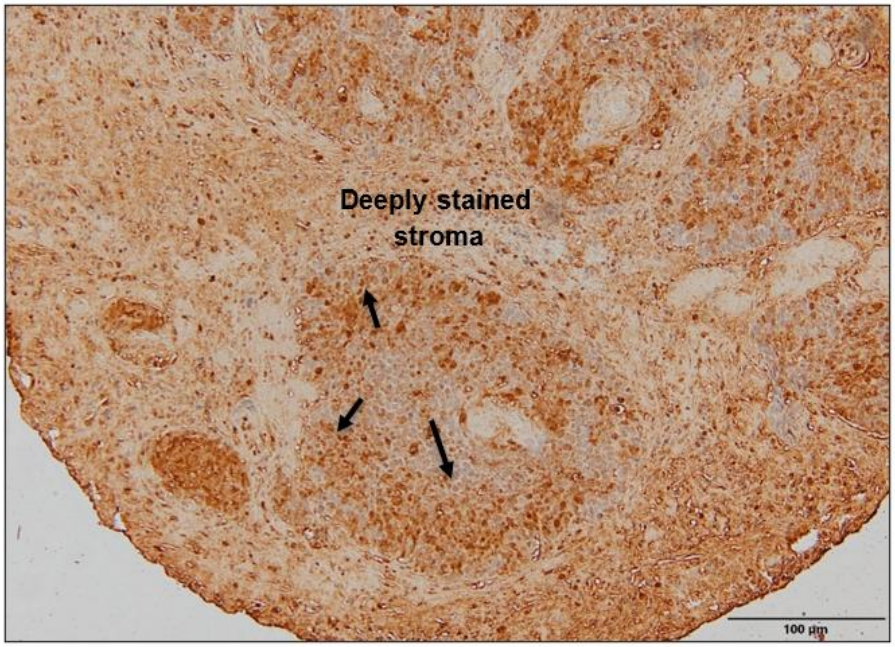

(A)

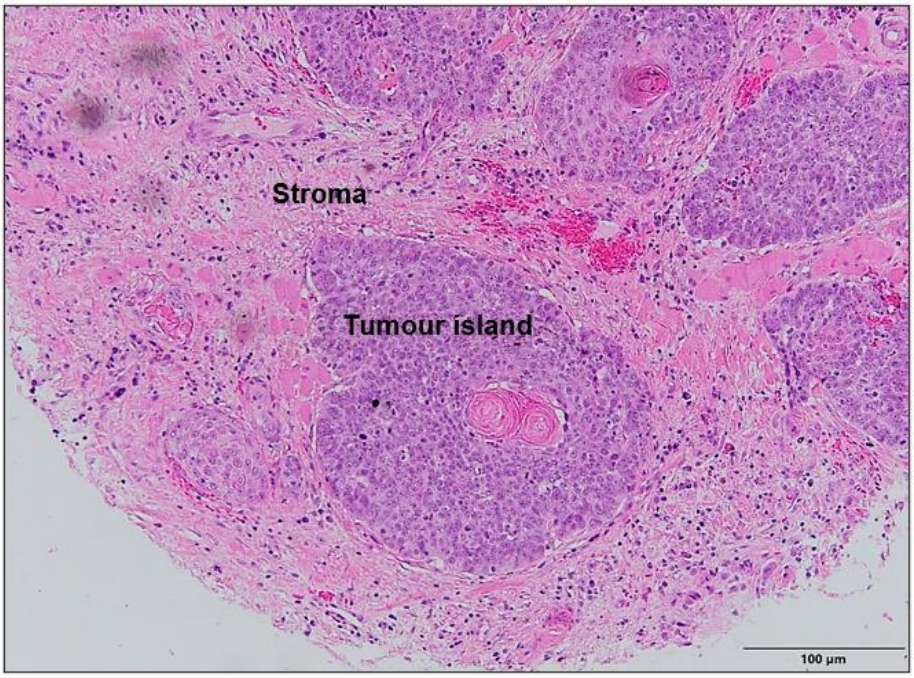

(B)

Figure 7.6 C: OPN partially stained OPSCC. (A) OPN IHC assay using 1:200 antibody dilution (Proteintech, UK). **(B)** Corresponding H/E slide. Notice the outer-layer expression of OPN in tumour island which may relate to tumour cell differentiation. Also noticed the heavily infiltrated stroma with deeply stained cells.

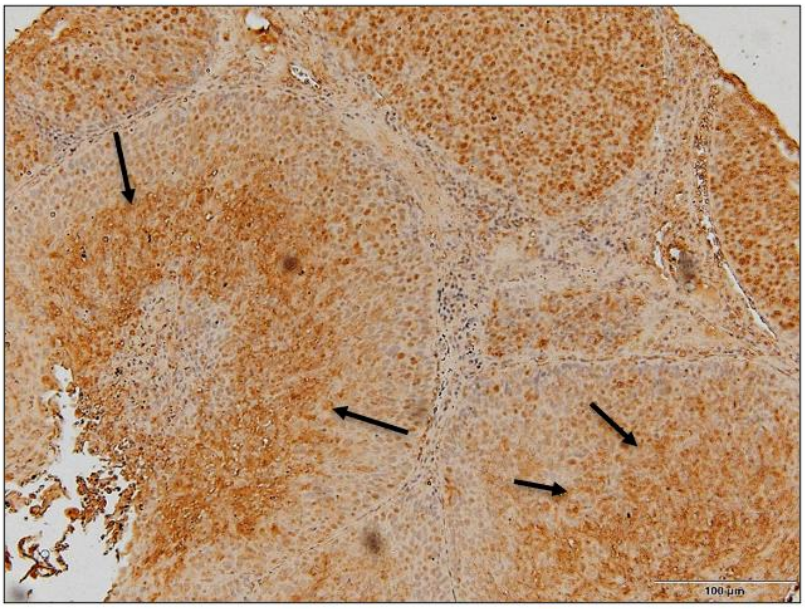

(A)

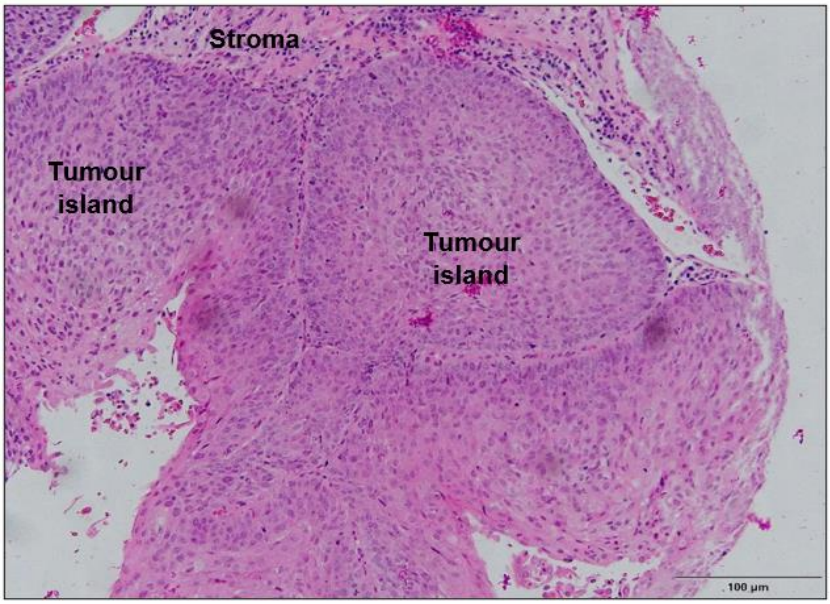

(B)

Figure 7.6 D: OPN partially stained OPSCC. (A) OPN IHC assay using 1:200 antibody dilution (Proteintech, UK). **(B)** Corresponding H/E slide. Notice the outer-layer expression of OPN in tumour island which most likely linked to tumour cells differentiation, however, expression of OPN the centre of tumour islands is most likely related to the hypoxia. A and B imges represent the same tissue core.

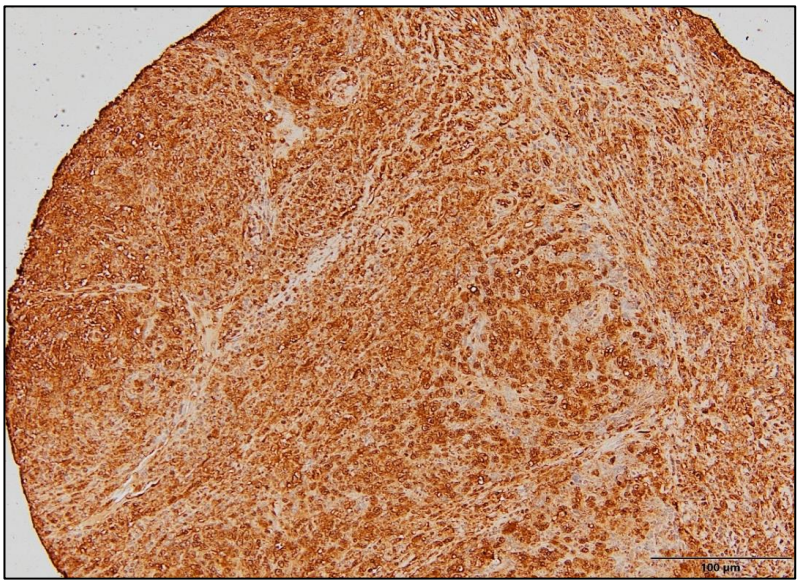

(A)

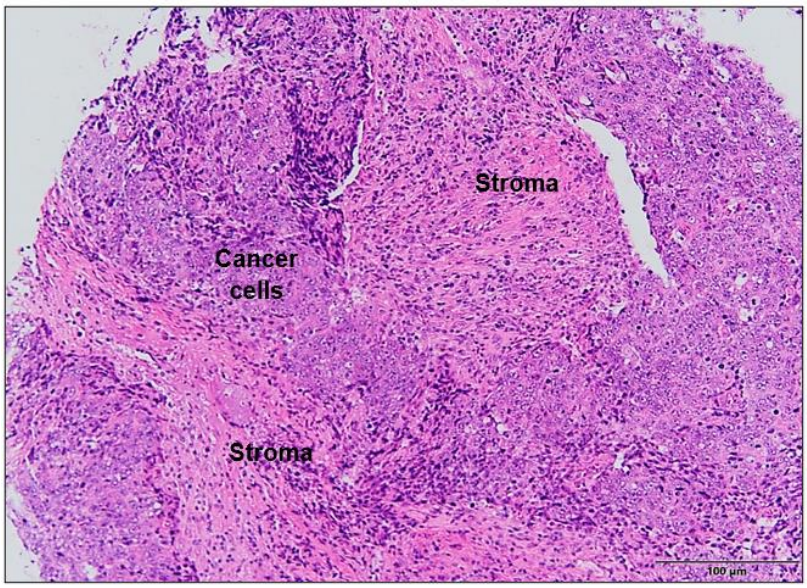

(B)

Figure 7.6 E: OPN partially stained OPSCC. (A) OPN IHC assay using 1:200 antibody dilution (Proteintech, UK). **(B)** Corresponding H/E slide. Notice the heavily stained stroma which overlapped poorly differentiated cancer islands. A and B imges represent the same tissue core.

7.4.3 OPN expression distribution in OPSCC subtypes

OPN IHC score was based on the assessment of OPN stain intensity in the tumour cells (0=absent, 1=weak, 2=moderate, 3=strong) multiply by the score of stained percentage of epithelium thickness (0=<5%, 1=<25%, 2=<50%, 3=<75, 4=75-100%). The scoring scale ranged from 0-12. During the stain scoring, we observed different values of OPN score in TMAs' cores (2,4,6,8,9,12). However, for each case, we selected the highest score among the relative tissue cores. The final OPN score for the cases ranges between (4, 8, and 12). We started the data analysis by assessing OPN expression in OPSCC subtypes and testing if there is a relationship between OPN expression and HPV status (Figure 7.7). Interestingly, OPN scores were distributed in a comparable pattern in both OPSCC groups. In addition to HPV-negative OPSCC, many HPV-positive OPSCC cases also expressed a high amount of OPN. Moreover, a low OPN expression score was observed in some cases of both OPSCC subtypes. Chi-square test (p=0.71).

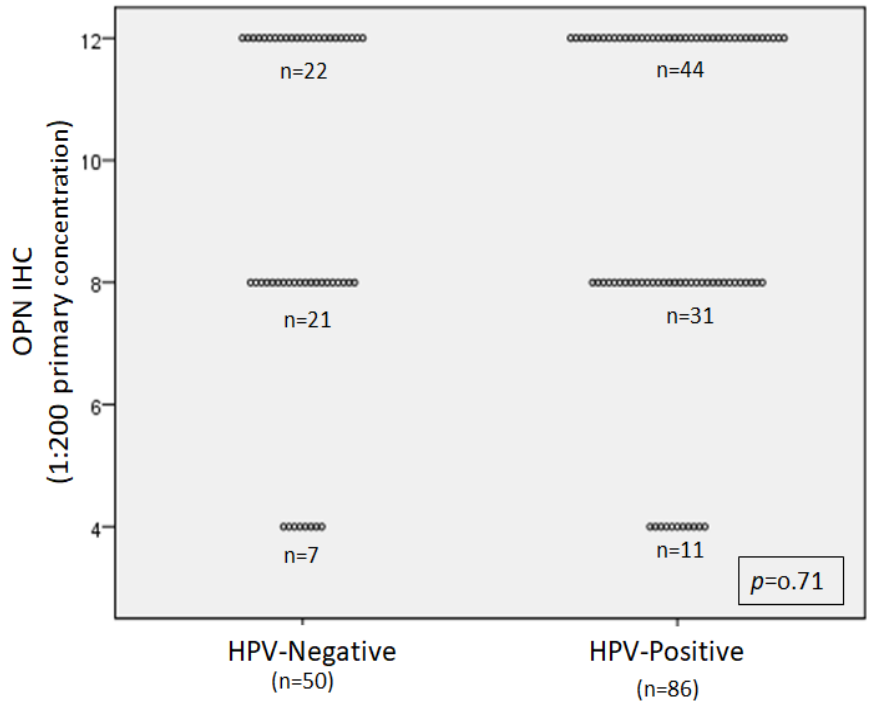

Figure 7.7: OPN IHC expression distribution based on HPV status in OPSCC cohort. Total case number: HPV-positive group (n=86) and HPV-negative group (n=50). IHC was undertaken at 1:200 OPN antibody dilution (Proteintech, UK). No evident difference between the two HPV groups in terms of OPN expression using Chi-square test (p>0.05).

7.4.4 Prognostic threshold determination for OPN IHC

Following OPN IHC scoring, we had to establish the positive cut-off point for OPN IHC in OPSCC, as that has not been done rigorously in the literature. We followed a mathematical approach to determine OPN IHC threshold robustly using ROC curves. Our calculation is based on the clinical correlation between OPN expression and patient prognosis. OPN overexpression was correlated by the majority of authors with diseases severity and poorer clinical outcomes (Coppola *et al.*, 2004; Kita *et al.*, 2006; Chien *et al.*, 2009). ROC curve was plotted in relation to OPN sensitivity and 1-specificity in cohort survival prediction (Figure 7.8).

However, ROC curve analysis indicated a weak correlation between OPN IHC expression and prognosis. The curve was located under the reference number with area under the curve less than 0.5 (AUC= 0.4). Moreover, the test suggested two thresholds of “6” and “10” which displayed poor performance in mortality detection. The threshold of 6 showed relatively high sensitivity (84%) accompanied by low specificity (14%), while threshold 10 showed low sensitivity and specificity (31% and 48%, respectively).

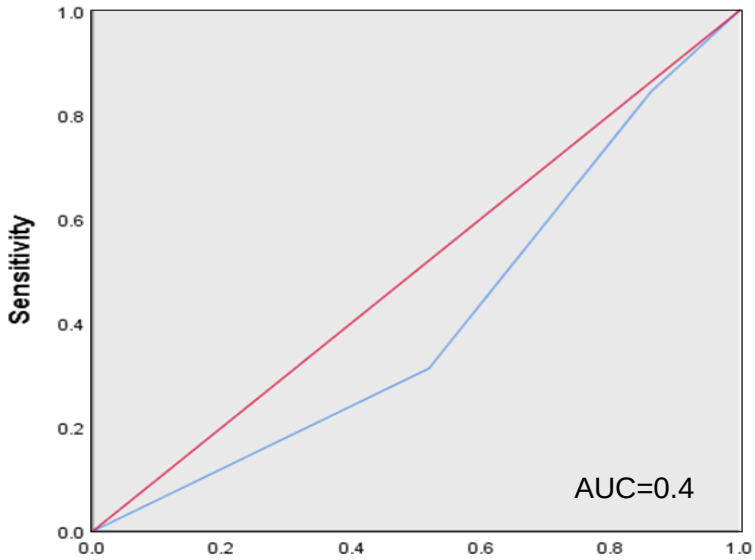

Threshold	6	10
Sensitivity	84%	31%
Specificity	14%	48%

Figure 7.8: Prognostic OPN IHC threshold determination in OPSCC using ROC curve. The curve plotted OPN IHC sensitivity against 1-specificity in survival prediction of the OPSCC cohort. The curve showed a weak association with poor survival (AUC<0.9) and suggested different thresholds depend on varied sensitivity and specificity values.

Based on OPN immunostaining, the study cohort was distributed around 3 groups of OPN IHC score (score 4, score 8, and score12). By utilising this difference in expression, we classified the study cohort into “Low”, “Moderate” and “High” OPN IHC expression, respectively.

7.4.5 OPSCC cohort characterisation based on OPN IHC expression

The study cohort has been categorised into three groups based on the OPN IHC score (Table 7.1). The percentage of HPV positive cases in the low OPN group was 83% (n=18) while it was 61.5% and 60% in the Moderate and High OPN groups, respectively. The distributions of age and gender showed no statistically significant differences between OPN groups ($p>0.05$), however, M:F ratio was relatively higher in the Low OPN group (5:1). Smoking habits also showed comparable data distribution ($p=0.56$). Interestingly, the current smoker percentage among OPN groups was almost the same (around 38%). Moderate and Low OPN groups showed a comparable pattern of T grade status, no evident difference was detected in T1/T2 and T3/T4 distribution (40.3% and 55.5% and 59.6% and 44.4% in Moderate and Low groups, respectively). The high OPN group showed a larger percentage of T1/T2 than T3/T4 (66.1% and 33.8%, respectively). The differences in T stage distribution between OPN groups was statistically significant ($p=0.02$). However, no evident difference was detected in N status nor overall TNM stage ($p>0.05$), although the Low OPN group showed a higher percentage of stage IV (76.4%, n=13/18). On the contrary, the High OPN group showed the largest percentage of non-recurrent disease (93.7%, n=60/64). Moreover, the largest surviving proportion was observed in the High OPN group (84.1%) followed by the Low group (72.2%) (Log-rank $p=0.07$).

Table 7.1: Summary of demographic comparison in OPSCC cohort based on OPN expression. Total number **of** cases (n= 136).

Characterisation	High OPN expression (%)	Moderate OPN expression (%)	Low OPN expression (%)	*P*-value
No. of cases	66 (48.5)	52 (38.2)	18 (13.3)	-
HPV positive HPV negative	40 (60.6) 26 (39.4)	32 (61.5) 20 (38.5)	15 (83) 3 (17)	-
Age at diagnosis: Mean (yrs.) Median (yrs.)	 55.4 55	 56.4 56.6	 58.1 58	0.6
Gender: Men Women M:F	 42 (68.2) 20 (31.7) 2.1:1	 39 (75) 12 (25) 3:1	 15 (83.3) 3 (16.6) 5:1	0.26
Smoking: Never smoke Past smoker Current smoker	 24 (40.6) 12 (20.3) 23 (38.9)	 16 (30.7) 16 (30.7) 14 (38.4)	 6 (33) 5 (27.7) 7 (38.8)	0.56
T grade: T1/T2 T3/T4	 41 (66.1) 21 (33.8)	 21 (40.3) 30 (59.6)	 10 (55.5) 8 (44.4)	0.02
N grade: N0/N2a Nb-N3	 35 (56.4) 27 (43.5)	 27 (51.9) 23 (48.1)	 10 (55.5) 8 (44.4)	0.96
TNM Staging: (7^{th}) III IV	 28 (46) 33 (54)	 23 (44.2) 28 (55.7)	 4 (23.5) 13 (76.4)	0.23
Recurrence Yes No	 4 (6.2) 60 (93.7)	 10 (20) 40 (80)	 2 (11.1) 16 (88.9)	0.08
Clinical outcome: Death A live	 10 (15.8) 53 (84.1)	 17 (32.6) 35 (67.3)	 5 (27.7) 13 (72.2)	0.07

7.4.6 OPN IHC prognostic value in OPSCC

The ROC curve failed to produce an acceptable diagnostic threshold for OPN IHC concerning the cohort's worst prognosis. The result might indicate that OPN has no correlation with OPSCC survival or could provide a protective feature. However, to evaluate this association accurately, we performed the survival analysis comparing the OPN IHC subgroups (High, Moderate and Low). The test was performed for the whole cohort, HPV-negative OPSCC group only and HPV-positive OPSCC group only.

7.4.6.1. Kaplan-Meier method

Kaplan-Meier method demonstrated interesting results by demonstrating that the High OPN group had superior overall survival compared to the Moderate and Low OPN groups. This feature is more evident in HPV-positive group (p=0.06), and the whole cohort in total (p=0.07) than in HPV-negative group (p=0.19). However, p-value did not reach the significance limit (p<0.05) (Figures 7. 9-11). Moderate and Low OPN showed a relationship with low survival to some extent. The low OPN group showed lower survival in HPV-positive group with an estimated mean of 4.1 years (95% CI; 2.7- 5.4), while, in HPV-negative, the moderate group displayed a lower survival estimate of 2.9 years (95% CI; 1.9- 3.8) (Table 7.2).

Table 7.2: Summary of Kaplan-Meier method in OPSCC based on OPN expression

Group	OPN expression	Overall survival Mean (years)	95% Confidence interval	p-value
Whole cohort	High	4.5	(4.3-4.8)	0.07
	Moderate	3.8	(3.3-4.3)	
	Low	4.1	(3.2-4.9)	
HPV-positive group	High	4.8	(4.5-5)	0.06
	Moderate	4.4	(3.9-4.9)	
	Low	4.1	(2.7-5.4)	
HPV-negative group	High	4.2	(3.6-4.7)	0.19
	Moderate	2.9	(1.9-3.8)	
	Low	3.9	(2.8-5.1)	

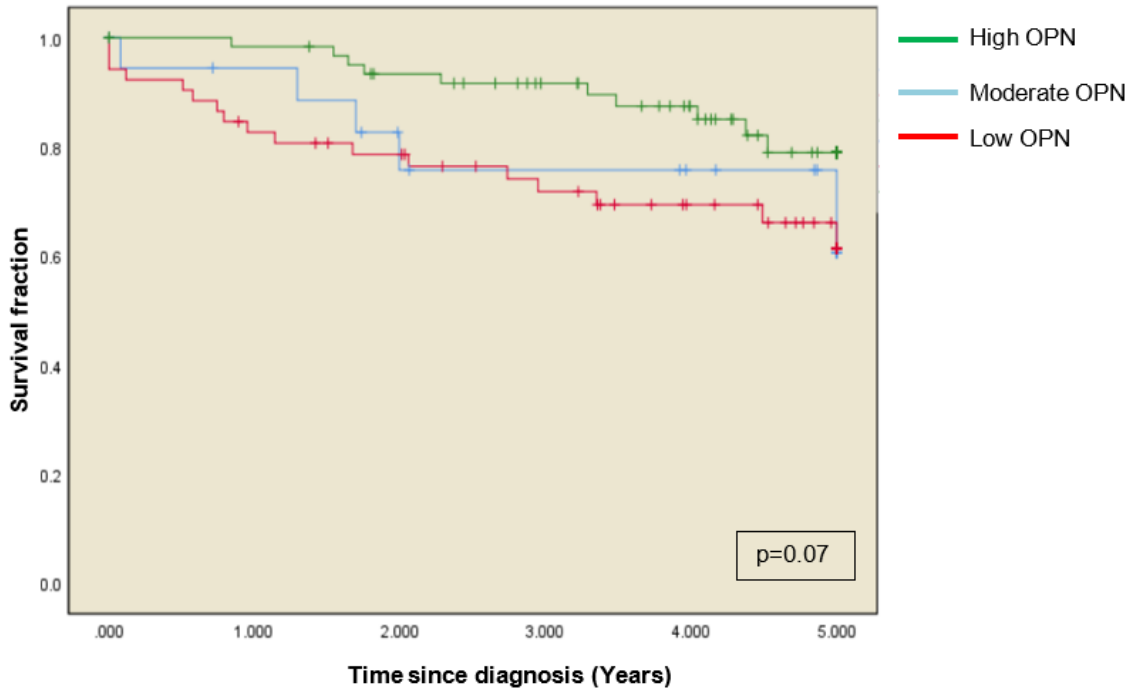

Figure 7.9: Overall survival rates in the whole study cohort based on OPN expression. The survival curve at 5-years follow-up showing overall survival using Kaplan-Meier method. The green curve represents the High OPN group (n=66), the blue curve represents the Moderate OPN group (n=52), and the red curve represents the Low OPN group (n=18). Each drop-step in the curve illustrates a case of death. Each vertical line (Hash lines) on the curve indicates censored data. The High OPN curve demonstrated the best survival fraction. Log-rank p= 0.07.

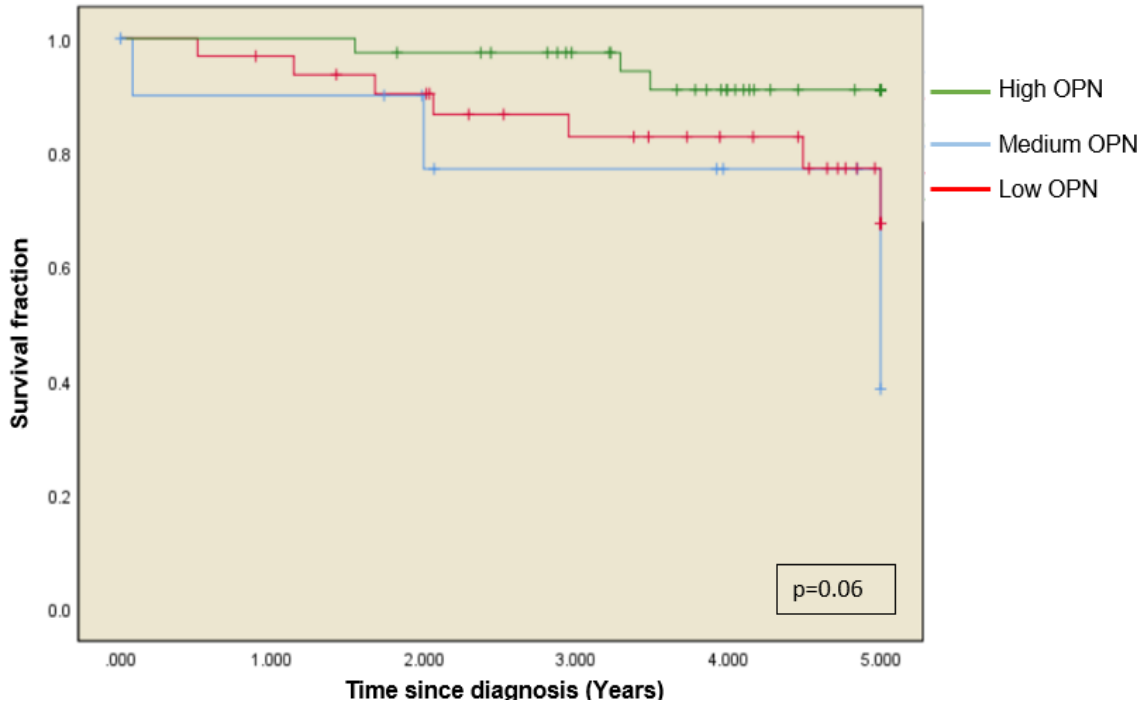

Figure 7.10: Overall survival rates in HPV-positive group based on OPN expression. The survival curve at 5-years follow-up concerning overall survival using Kaplan-Meier method. The green curve represents the High OPN group (n=44), the blue curve represents the Moderate OPN group (n=31), and the red curve represents the Low OPN group (n=11). Each drop-step in the curve illustrates a case of death. Each vertical line (Hash lines) on the curve indicates censored data. The High OPN curve demonstrated the best survival fraction. Log-rank p= 0.06.

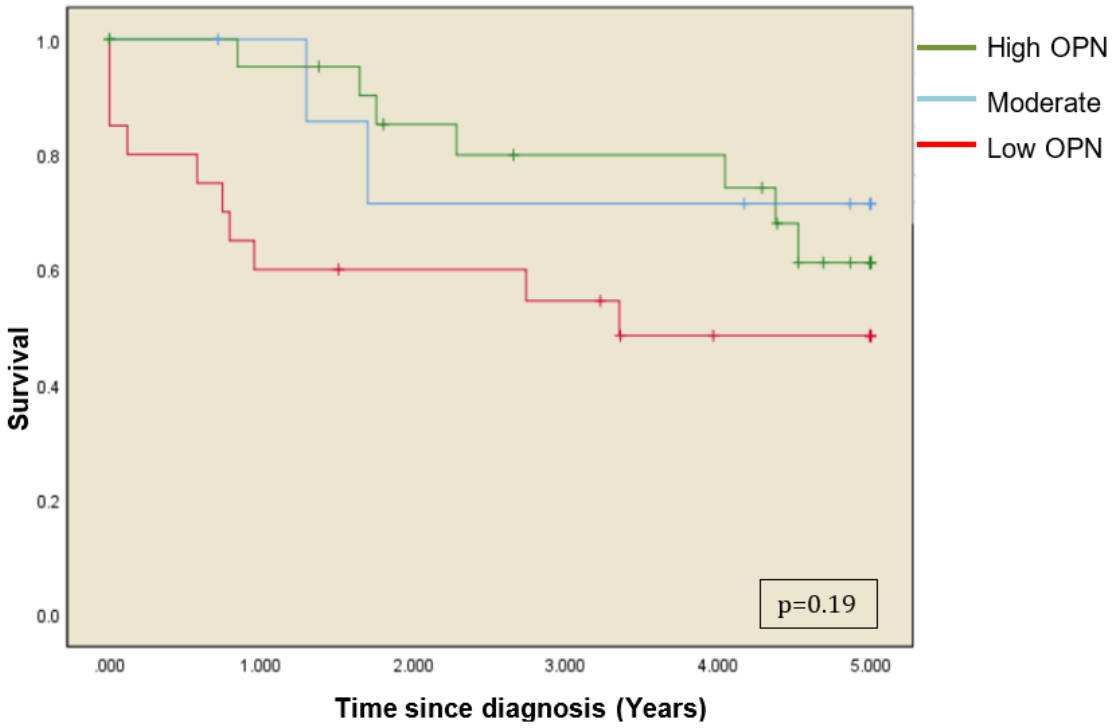

Figure 7.11: Overall survival rates in HPV-negative group based on OPN expression. The survival curve at 5-years follow-up concerning overall survival using Kaplan-Meier method. The green curve represents the High OPN group (n=22), the blue curve represents the Moderate OPN group (n=21), and the red curve represents the Low OPN group (n=7). Each drop-step in the curve illustrates a case of death. Each vertical line (Hash lines) on the curve indicates censored data. Low OPN curve demonstrated the worst survival fraction. Log-rank p= 0.19.

7.4.6.2. Univariate Cox regression Model (Unadjusted)

Based on the Kaplan Meier method, the high OPN group demonstrated the longest survival in all tested cohorts. This observation led to further investigation to assess HR in this group compared to Moderate and Low OPN groups (M/L). Using a univariate regression model, High OPN expression was confirmed as a significant independent prognostic factor in the whole study cohort, regardless of HPV status (p=0.03). High OPN OPSCC group showed a lower hazard ratio compared to the M/L OPN group that demonstrated a higher risk with 2.26-fold (95% CI: 1.07-4.75). However, by evaluating OPN prognostic performance in OPSCC based on HPV positivity, High OPN was identified as a “protective” feature in the HPV-positive group (p=0.05), but not in the HPV-negative (p=0.26) (Table 7.3, Figure 7.12).

Table 7.3: Univariate Cox regression model based on OPN expression

Covariate	Unadjusted Model (Univariate)	
	HR (95%CI)	P-value
Whole cohort		0.03
High	0.44 (0.20-0.93)	
Moderate/ Low	2.26 (1.07-4.75)	
HPV-positive group		0.05
High	0.27 (0.07-1.003)	
Moderate/ Low	3.6 (0.99-13.2)	
HPV-negative group		0.26
High	1.69 (0.66-4.37)	
Moderate/Low	1.79 (0.70-4.58)	

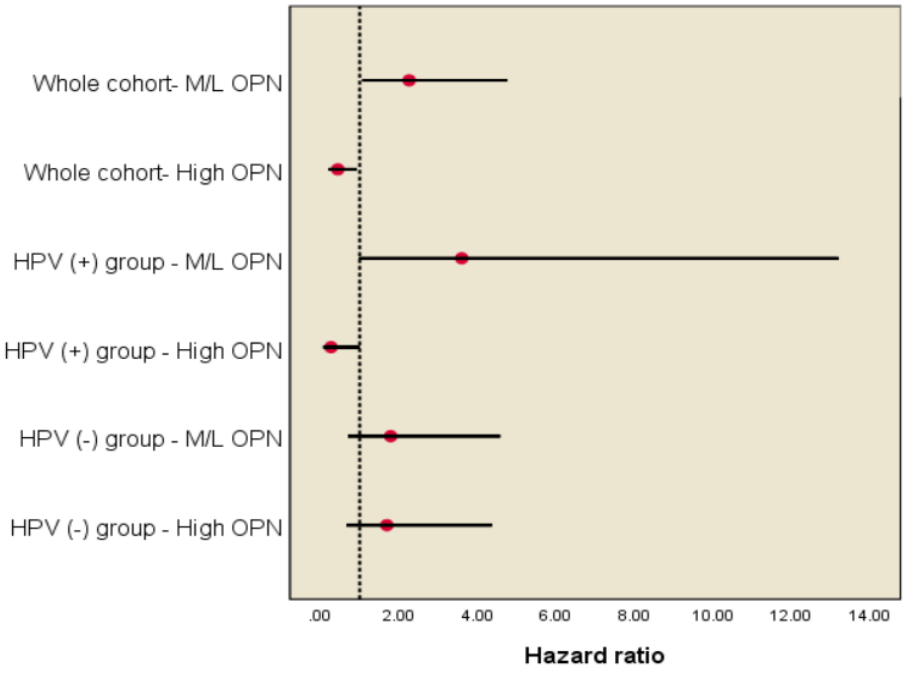

Figure 7.12: Forest plot illustrates OPN hazard ratios according to Univariate regression model. Univariate model was established to obtain the OPN hazard ratio in the whole group, HPV-positive group only and HPV-negative group only. HR (Red dot) presented with 95% CI upper and lower values. The dotted line represents the strength cut-off of HR (1). HR before the line indicates a weak correlation with the hazard (mortality) and *vice versa*. High OPN showed a protective feature in HPV-positive, while it has no impact on HPV-negative group.

7.4.6.3. IL-6 RNAScope analysis in OPSCC

IL-6 mRNA expression assessment in OPSCC was performed on freshly baked slides to ensure RNA integrity using RNAScope RNA ISH. Cohort 1 was provided as already baked tissue sections, and it was not possible to access fresh sections in a timely manner due to the lockdown. In cohort 2, IL-6 transcript signals were observed to a variable extent in cohort 2 sections, however, the normal tonsils cores also showed a high abundance of IL-6 expression (Figure 7.13). Notably, in some OPSCC sections, IL-6 was preferentially located in tumour invasive front sites of the stroma (Figure 7.14).

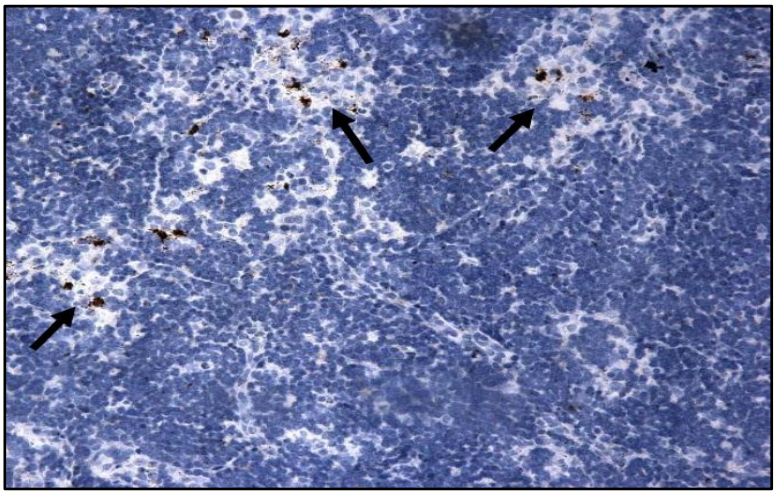

Figure 7.13: IL-6 RNAScope expression in normal tonsillar tissue. Arrows pointed to IL-6 mRNA expression clusters within the lymphoid tissue (magnification 20x).

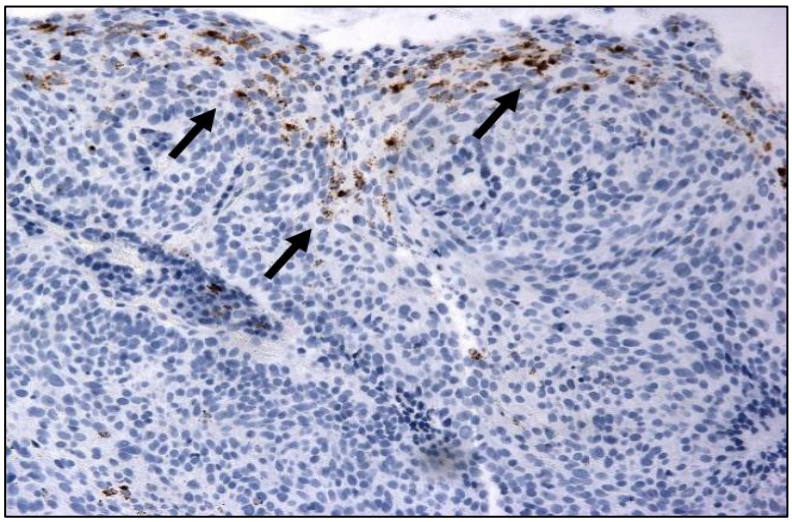

(A)

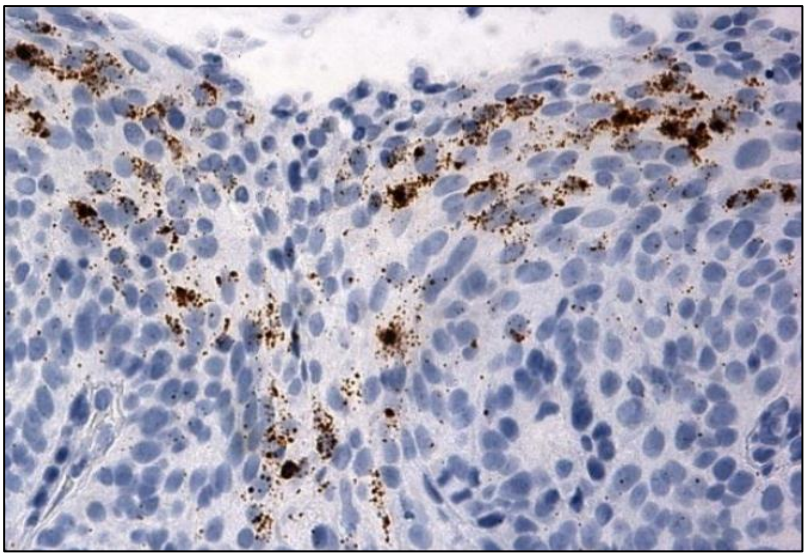

(B)

Figure 7.14: IL-6 RNAScope expression in the stroma in relation to invasive front sites. A and B magnifications 20x and 40x, respectively. Arrows pointed to IL-6 mRNA expression.

7.4.6.4. Distribution of IL-6 RNAScope expression in OPSCC cohort

The expression of IL-6 signals has been evaluated and scored for OPSCC stroma according to a modified scoring scheme from Yu *et al.*, (2015). In their scoring scheme, IL-6 expression was classified into 4 levels according to the number of positive cells: 0, no cells. 1, areas with 5-10 positive cells per 20x field. 2, areas with 11-25 positive cells per 20x field. 3, areas with 26-50 positive cells per 20x. 4, areas of more than 50 positive cells per 20x field.

We grouped those 4 levels into 2 groups: group 1 “Low IL-6” (≥26 positive cells) and group 2 “High IL-6” (≤25 positive cells). By looking at IL-6 RNAScope distribution in OPSCC based on HPV status, there was no significant difference between HPV-positive and negative groups (p=0.77). Both groups showed a high expression of IL-6 transcripts with comparable values. 37.5% in HPV-positive group n=14/39, and 40% in HPV-negative group n=6/15. (Table 7.4).

Table 7.4: Distribution of IL-6 RNAScope expression in OPSCC

	Low IL-6 expression (%)	High IL-6 expression (%)	p-value
HPV-positive group	25 (62.5)	14 (37.5)	0.77
HPV-negative group	9 (60)	6 (40)	

7.4.6.5. Prognostic value of IL-6 in OPSCC

Assessment of the prognostic value of IL-6 mRNA expression in cohort 2 (n=54) based on IL-6 mRNA revealed no statistical significance between HPV-positive and negative OPSCCs (Log-rank p= 0.84) High IL-6 group (n=20) and Low IL-6 group (n=34) showed a similar mean survival time (4.4 years, 95% CI: 3.8-5) and (4.3 years, 95% CI: 3.8-4.7) (Table 7.5, figure 7.15).

Table 7.5: Summary of Kaplan-Meier method for cohort 2 based on IL-6 RNAScope expression.

	Low IL-6 expression	High IL-6 expression	Log-rank p-value
5 years survival (%)	79.4	85	0.84
Estimated survival time. Mean (Yrs) (95% CI)	4.3 (3.8-4.7)	4.4 (3.8-5)	

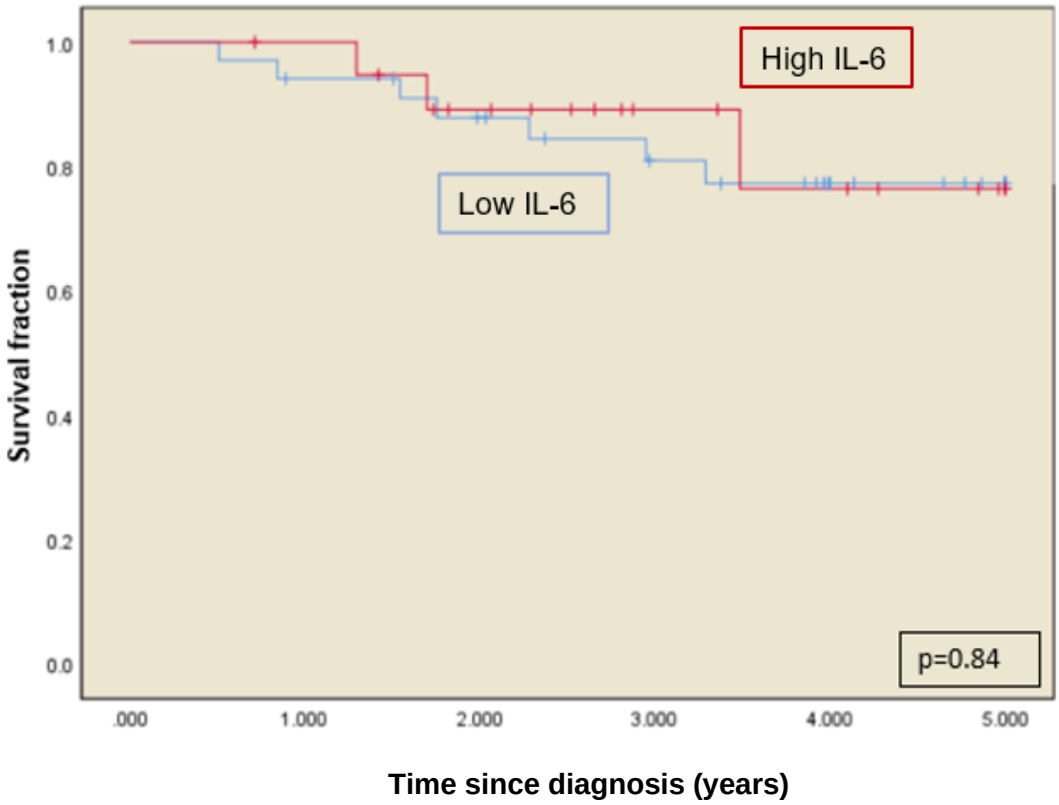

Figure 7.15: Overall survival rate in OPSCC based on IL-6 RNAScope. The overall survival curve at 5-years follow-up using Kaplan-Meier method. The red curve represents the High IL-6 OPSCC group (n=20) and the blue curve represents the Low IL-6 OPSCC group (n=34). Each drop-step in the curve illustrates a case of death. Each vertical line on the curve illustrates the last time seen for a live case. There was no difference in overall survival between the two tested groups. Log-rank p= 0.84.

7.4.7. Multivariate Cox model for the study biomarkers

Multivariate models provide a risk stratification of all of the tested predictors at the same time. HR, here, is adjusted to the other factors in the analysis, not to the control group of the same predictor. p-value here is testing the difference between the HR of positive predictor and negative predictor based on the adjusted model result.

The well-established HPV-related biomarker p16 demonstrated strong independent performance even in the adjusted model. Negative p16 status was strongly associated with mortality with relatively high HR=5.52 (95% CI: 2.6-11.4), while p16 expression was associated with survival (HR= 0.18; 95% CI: 0.08-0.37). The difference between the two HRs is statistically significant ($p<0.001$).

α-SMA biomarker expression in the whole study cohort displayed better performance in multivariate assessment than the univariate. α-SMA HR revealed a significant association with the hazard considering the other covariates. By the comparison with tested positive predictors, High α-SMA expression was associated significantly with the hazard (Mortality) (HR=2.2; 95% CI: 1.06-4.7) (p=0.011). On the other side, Low α-SMA expression provides a favourable indication for the survival compared with other predictors adjusted in the test (HR=0.45; 95% CI: 0.21-0.95). This alteration in the predictive significance in multivariate compared with univariate is a result of including variable (or set of variables) in the regression equation that increases the predictive validity of another, known as “Suppressor effect” (Tzelgov and Henik, 1991). This type of results should be interpreted cautiously considering the clinical implications.

The comparison of OPN biomarker strength in OPSCC with p16 and α-SMA biomarkers revealed a significant independent predictive value of OPN biomarker in OPSCC. High OPN OPSCC population demonstrated low HR (0.37; 95% CI: 0.17-0.79) compared to the Low OPN OPSCC population (HR=2.7; 95% CI: 1.26- 5.7; p=0.01). (Table 7.6 and figure 7.14).

Table 7.6: Multivariate Cox regression model on the whole study cohort based on the study's biomarkers expressions.

Covariate	Adjusted Model (Multivariate)	
	HR (95%CI)	P-value
P16 (IHC expression)		
Negative	5.52 (2.6-11.4)	<0.001
positive	0.18 (0.08-0.37)	
α-SMA (IHC expression)		0.03
Low	0.45 (0.21-0.95)	
High	2.2 (1.06-4.7)	
OPN (IHC expression)		0.01
High	0.37 (0.17-0.79)	
Moderate/Low	2.7 (1.26-5.7)	

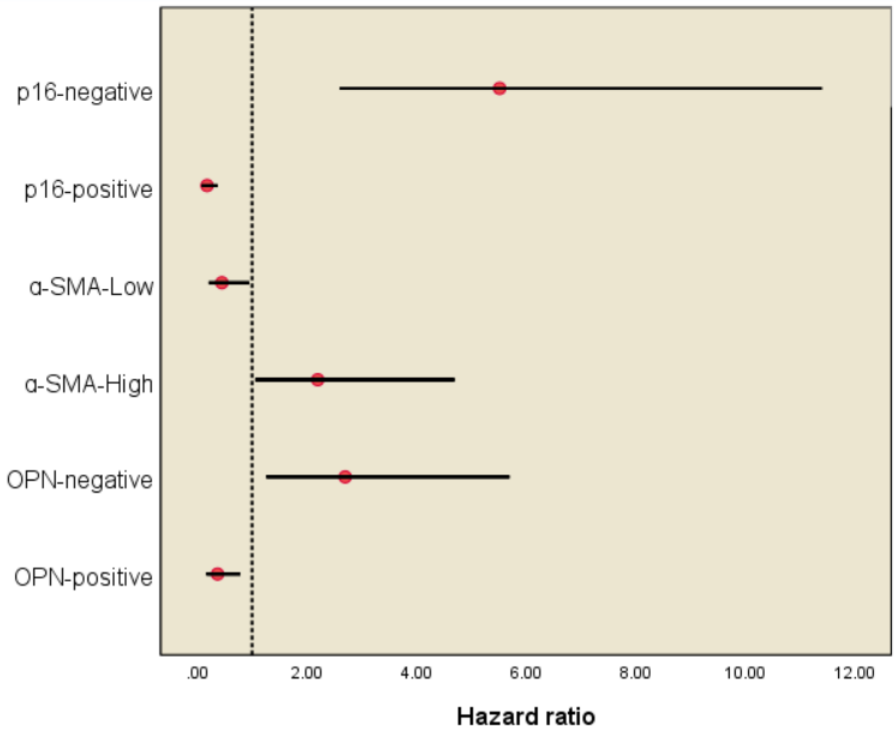

Figure 7.14: Forest plot illustrates the strength of the study's biomarkers expression according to the multivariate regression model. Adjusted model (multivariate) was established to obtain biomarkers hazard ratios in the whole study group. HR (Red dot) presented with 95% CI upper and lower values. The dotted line represents the strength cut-off of HR (1). HR before the line indicates a weak correlation with the hazard (mortality) and *vice versa*.

7.5. Discussion

This is the first study evaluating OPN IHC expression in an established OPSCC cohort. Due to time restrictions, our assessment was limited to IHC assay only that revealed interesting novel findings. Our study reported High OPN IHC expression as an independent predictive biomarker in OPSCC associated positively with overall survival using univariate and multivariate regression models (p-value = 0.03 and 0.01, respectively). We attempted to analyse the available data rigorously and correlate the findings with the available knowledge and our understanding in the field, however, a number of questions have been raised during the results' discussion that requires further investigation. Validation of our novel finding in OPSCC might provide a further feature for OPSCC patient selection for de-intensifying therapy protocols.

7.5.1. OPN expression in OPSCC

OPN expression in normal human tissue has been investigated using a multifaceted approach including in situ hybridisation, immunohistochemistry, and northern blot for frozen tissue. OPN protein deposition in FFPE tissue was identified prominently at the luminal surfaces of the salivary glands, gastrointestinal tract, urinary and reproductive tracts, lung, and breast tissue (Brown *et al.*, 1992). Moreover, OPN IHC expression was observed clearly in the central and peripheral nervous system (Kunii *et al.*, 2009), sweat gland duct (Ogbureke and Fisher, 2007), hair follicles and sebaceous glands (Chang *et al.*, 2008). According to the human protein atlas, normal tonsillar tissue is devoid of OPN protein expression. In normal lymphoid tissue, OPN protein expression is confined to the non-germinal centre cells only (Tissue expression of SPP1 - Summary - The Human Protein Atlas, 2021). However, in this study, we included a number of non-malignant tonsil and lymph node sections that showed a varying degree of OPN staining intensity ranging between weak and moderate. The degree of OPN expression in these sections has raised a concern regarding the OPN immunopositivity threshold in OPSCC. The expression of OPN in non-malignant tonsils might be attributed to an inflammatory mechanism in response to other pathogens that trigger pro-inflammatory cytokines expression including OPN. High OPN expression was reported in non-malignant lymph nodes, and it has been included as an OPN-positive control in some studies (Li *et al.*, 2012). Here, the first question has been raised: should we follow the available suggested thresholds in the literature with OP tissues despite the inflammatory nature of the anatomical site?

OPN expression showed a strong correlation with specific tumours from different body sites. In a study of 350 tissue sections from different body tumours, High OPN expression was observed in all of the tissue from the gastric carcinoma sections (100%). Colorectal carcinomas, transitional cell carcinomas of the renal pelvis, and pancreatic carcinomas all showed a high percentage of OPN overexpression compared to normal counterparts (85%, 82% and 81%, respectively). Renal cell carcinomas, lung and oesophageal carcinomas also demonstrated a relatively high percentage of OPN positivity ranging from 72-70%. Moreover, OPN high expression was detected in 58% of HNSCC sections (n=60, including 5 cases of OPSCC) (Coppola *et al.*, 2004). Notably, the published images in Coppola's paper represented strong OPN stain in OSCC cells within a clear background. The adjacent stroma showed a scant expression of OPN. In contrast, in our OPSCC cohort, we detected High OPN expression in 48.5% (n=66/136) with comparable distribution in both OPSCC subtypes, however, in the majority of OPSCC sections, the associated stroma was extensively stained.

In our study, the cohort showed a wide variation of OPN expression, regardless of HPV status. In both HPV-positive and negative groups, we observed High, Moderate and Low OPN expressions. Interestingly, 83% of the Low OPN group (n=15/18) were HPV-positive. Despite the small number of cases in the Low OPN group, this observation is consistent with our *in vitro* finding in OPSCC cell lines. In an early response to short-term co-culturing with OPSCC fibroblasts, only the HPV-negative cell line (SCC89) demonstrated a significant upregulation in OPN, not the HPV-positive cell line (SCC2), which might suggest a tendency of OPN association with HPV-negative OPSCC. However, High OPN expression was detected also in HPV-positive OPSCC tissue to a great extent in this study.

The challenging dilemma in this chapter was the determination of the OPN IHC staining threshold. Due to the subjective nature of IHC scoring, there is always a possibility of interobserver variability in threshold definition and risk of bias. Since ours was the first study that has investigated OPN IHC in an OPSCC cohort, we tried to establish the OPN cut-off based on a robust mathematical approach using ROC curves. However, the curve analysis revealed an expected result by demonstrating a weak correlation between OPN expression and poor survival. Kita *et al.* (2006) suggested a definition of positive OPN carcinoma tissue based on their observation in oesophageal squamous cell carcinoma. They considered the expression of OPN in more than 10% as the OPN positive cut off. By reviewing Kita's paper images, OPN immune-localisation was confined to carcinoma with intensity ranges between moderate and high, however, there was no detectable

OPN expression in the surrounding stroma. This threshold has been adopted by a large number of studies in OSCC which linked OPN expression with worse outcome parameters including advance T grade and N status. Notably, the OSCC stroma did not show evident OPN expression as we have seen in OPSCC (Chien *et al.*, 2008, 2009; Luo *et al.*, 2015). Again, our previous first question has been highlighted here: is the extensively stained stroma in OPSCC linked to the histological nature of OP tonsil tissue or is it attributable to technical issues related to the antibody concentration and the antigen retrieval method? Can we adopt Kita's threshold in OPSCC? However, we have seen some sections with complete immune-negativity; also, in some High OPN sections, the stroma displayed a weak pattern of staining which suggests that the immune-reactive specificity of the antibody is reasonable. We have seen OPN in the cytoplasm and nuclei of the cancer cells and that was reported before (Junaid *et al.*, 2007; Shinohara *et al.*, 2008). As ours is the first study that detected OPN IHC expression in OPSCC, we preferred to adhere to the manufacturer's instructions in the selection of antibody dilutions to be within the recommended limit.

From our point of view, adoption of the cut off proposed by Kita *et al.* (2006) in OPSCC is dependent, to an extent, on accurate recognition of the cellular source of OPN production in tissue using OPN ISH, especially in partially stained cases. The TME comprises several inflammatory cells and a network of signalling pathways. OPN has been shown to be produced and released by peritumoral inflammatory cells, mainly macrophages, dendritic cells and T cells (Shinohara *et al.*, 2005). There is an assumption by many authors that not all detected OPN protein in cancer cells is tumour-derived. They postulate that secreted stromal-derived OPN could be integrated into cancer cells through cell surface receptors (Brown *et al.*, 1994; Erkvliet *et al.*, 1998). This assumption has been supported by Brown and co-workers. In various types of solid tumours, OPN ISH expression showed an intimate association with macrophages adjacent to cancer cells, while there was no detectable OPN mRNA in related cancer cells (Brown *et al.*, 1994).

However, that does not imply that all the partially stained epithelium is OPN-negative. The localisation of stained cancer cells at the uppermost layers of the epithelium thickness might also suggest the source of OPN secretion in relation to its function in malignant cell transformation and tumour progression. OPN overexpression has been correlated with malignant cell transformation and dedifferentiation (Senger, Wirth and Hynes, 1979). In OSCC and other tumours, the reports have shown that OPN expression has increased from lower to higher histological grades (Korita, Wakai and Shirai, 2008;

Subramani *et al.*, 2015; Aravind *et al.*, 2017). Moreover, the intensity of OPN expression was observed to gradually increase from normal epithelium to dysplastic cells that showed a moderate intensity of expression, while in the invasive front, tumour islands demonstrated strong OPN staining intensity (Chien *et al.*, 2009; Lakshmi *et al.*, 2019). Another possible explanation of partially/low stained superficial epithelial layers and higher expression in the basal compartment is a close approximation with cells in the TME. We have shown in chapter 5 that OPN was significantly upregulated in cancer cells in response to crosstalk with OPSCC fibroblasts. Accumulation of OPN stain at the centre of tumour islands also suggested the functional role of OPN in hypoxic tissue. OPN expression has shown to be strongly modulated by hypoxia *in vitro* (Wohlleben et al., 2015); moreover, its protein expression in tissue has demonstrated a strong correlation with oxygenation parameters in advanced HNC and worse prognosis (Bache et al., 2006). However, this assumption requires further assessment of hypoxia biomarkers in OPSCC cohort.

7.5.2. High OPN OPSCC characteristics

Analysis of the clinical features in the High OPN OPSCC group revealed results inconsistent with the available data in the literature. In the majority of studies, overexpression of OPN was associated with poor differentiation, advanced T and N stage beside the high tendency to develop a recurrent tumour (Chien *et al.*, 2009; Weber, Lett and Haubein, 2010). In our cohort, T stage distribution showed a significant difference among OPN groups (p=0.02). The High OPN group comprised more cases with smaller tumour size (T1/T2 comprised 66.1%) than larger tumours. Moreover, the High OPN group showed the highest percentage of recurrence-free patients (93.7%).

Despite these clinical parameters being distinct and not mutually unrelated, the clinical presentation of the poorly differentiated, high-grade tumour is more likely to be disseminated and consequently develop a high stage tumour. Although the molecular mechanisms behind these events are overlapping, OPN is found to be associated with all of them, which may explain the positive correlation between OPN overexpression and poor clinical outcomes. However, our observation, based on OPN IHC, showed no detectable differences in clinical parameters between Low, Moderate and High; on the contrary, the High OPN group showed smaller tumour size and less recurrence percentage which suggested a different function of OPN IHC expression in OPSCC.

.

7.5.3. OPN IHC prognostic value in OPSCC

The ROC curve analysis indicated a weak correlation between OPN IHC overexpression and poor prognosis. The test was followed by Kaplan-Meier method to investigate thoroughly the prognostic value of OPN staining in OPSCC according to available data. We preferred to assess and compare the survival curve for each OPN IHC group (High, Moderate and Low) to understand the nature of Moderate group expression. Surprisingly, the survival curves revealed expected contradictory results in the OPSCC cohort, as the High OPN group showed a longer survival time compared to other OPN groups. This difference was evident in the HPV-positive group (p=0.06) rather than in the HPV-negative group (p=0.19). This finding is contrary to the known functions of OPN in several tumours where High OPN expression has been correlated with high T stage, N stage and high clinical-stage, suggesting that OPN may be involved in tumour metastasis and progression (Chien *et al.*, 2008; Cho *et al.*, 2008; Chiu *et al.*, 2010; Li *et al.*, 2012).

The survival curve of Moderate OPN group showed better survival than Low OPN in the HPV-positive cohort, while in HPV-negative, it overlapped the High OPN curve, demonstrating a low survival fraction in both groups. In the whole cohort, the survival curves were influenced by the strength of the survival features in HPV groups. High OPN curve demonstrated the best survival time over the other groups, however, that was not statistically significant (p=0.07). Based on Kaplan Meier findings, we postulated that the High OPN group is a distinct population in the OPSCC cohort with better survival features. We assessed our hypothesis by exploring the hazard ratio of High OPN expression against M/L groups. In the whole cohort, High OPN provides a protective feature demonstrated in low HR (HR=0.44; 95% CI; 0.2-0.93) compared to M/L group (HR=2.26; 95% CI; 1.07- 4.75; p= 0.03) at univariate model. Moreover, HPV-positive group showed marginally significant HR differences (p=0.05), while HPV-negative demonstrated no differences statistically (p=0.26). The predictive ability of OPN expression remained evident in the multivariate model, including p16 and α-SMA biomarkers (p=0.01). The evidence above indicated that High OPN IHC expression is a protective feature in OPSCC, regardless of HPV status, but this feature is more prominent in HPV-positive group. This contradictory novel finding has raised the second important question in this chapter: Why did High OPN expression show a distinct role in OPSCC?

At the moment, there is no direct answer to this question. There are many assumptions that might be related to an OPN mediated tumour-suppression effect; however, further investigation is needed to understand this correlation. The first possible explanation is

related to the source of OPN production; in solid tumours, OPN is secreted by cancer cells and cells in the tumour microenvironment (host-derived as described by some authors). Both types interact in a complex process characterised by antagonistic functional roles as was evident *in vivo* using an OPN-null animals' models (Crawford, Matrisian and Liaw, 1998; Hsieh *et al.*, 2012). Absence of stromal-derived OPN accelerated the growth and progression of the tumour cells and developed a greater number of metastases compared with wild-type animals. The difference in tumour growth was inversely correlated with the degree of macrophage infiltration (Crawford, Matrisian and Liaw, 1998). This process was thought to be mediated through the ability of stromal-derived OPN in macrophage chemoattractant via elicitation of an early innate inflammatory response, in addition to its ability in enhancing the survival of inflammatory cells (Hsieh *et al.*, 2012). On the other side, tumour-derived OPN was demonstrated as a potentially destructive and inhibitor factor to the macrophages besides its ability in promoting metastasis growth and survival (Hsieh *et al.*, 2012).

The second possible explanation was related to the distinct functions of OPN form; OPN has two froms that can be generated from the same mRNA transcript. However, the alternation in transduction mechanism resulted in the formation of two different forms with distinct biological roles (Inoue and Shinohara, 2011). OPN was widely known as an extracellular secretory protein that has been described generally in cancer research, with its dark side in promoting and facilitating tumour cell proliferation, migration. In striking contrast, some, but not many, reports have demonstrated that OPN inhibits tumour progression and correlates with favourable survival (Collins *et al.*, 2012; Danzaki *et al.*, 2016; Franklin *et al.*, 2019). This promising side of OPN was linked mostly to the intracellular OPN form (iOPN) rather than the secreted OPN (sOPN) (Inoue and Shinohara, 2011). iOPN is a non-secretory form of OPN that was detected in different cell types, localised into the cytoplasm and cell nuclei. In the tumour microenvironment, iOPN is synthesised mainly by macrophages, T cells and dendritic cells and was linked to several immune mechanisms. It is identified as an adaptor molecule in signalling pathways downstream of innate immune receptors (Shinohara *et al.*, 2012). The innate immune system is the first line of defence against HPV infection which is mediated by a variety of mechanisms' involvement, including macrophages and NK cells recruitment; however, the innate immune response to HPV infection in OPSCC is incompletely understood and we do not know if it is mediated by iOPN.

The integrity of the natural killer (NK) defences is considered a vital innate immune function in host defences against pathogens and cancer development. iOPN has been

identified as a crucial molecular component for the maintenance of functional NK cells, including NK expansion and differentiation. Deficiency in iOPN leads to a significant decrease in NK infiltration in tumour stroma (Danzaki *et al.*, 2016). Moreover, it results in impaired expansion of long-lived NK cells and evolving incomplete responses to viral infection and the tumour cells (Leavenworth *et al.*, 2015). In a transgenic adenocarcinoma of the mouse prostate, deficiency of stromal-derived OPN reduces NK infiltration into the tumour. For further confirmation for the *in vivo* finding, NK derived from OPN-deficient mice demonstrated a decrease in migration ability toward the cancer cells compared to NK cells from wild-type mice *in vitro* (Danzaki *et al.*, 2016). To this point, some questions have been raised. Does the iOPN isoform relate to the stromal-derived OPN in terms of the regulatory and activation processes? Are they both referring to the same molecule under different nomenclatures? Thus far, these questions have not been answered.

The role of OPN in T cell activation was the last possible explanation; in OPSCC, oncogenic HPV-infection presents viral antigens that elicit specific antibody and T cell responses. These reactions are thought to be due to the tight anatomical proximity of infected mucosa and immune tissue in OP (Kreimer *et al.*, 2017; Welters *et al.*, 2018). T cells are believed to contribute to tumour rejection and long-term immune surveillance. Moreover, it has been shown that T-cells are further promoted to mediate anti-tumour immunity upon radiation treatment (Manukian *et al.*, 2019). CD8+ cytotoxic T lymphocytes are the central component of the host adaptive immune system. Extensive CD8+ T cell infiltration was correlated with overall survival in HNSCC, regardless of HPV status (Punt *et al.*, 2016; Welters *et al.*, 2018; Kemnade *et al.*, 2020), which suggested that T cell response is promoted by HPV oncogenic infection and irradiation that might contribute to an enhanced T-cell response in HPV-associated tumours. In graft versus host disease, CD8+ action was facilitated through the host-derived OPN expression. It is involved in the initiation, activation, and survival of CD8+ against the recipient organ (Zhao *et al.*, 2011; Kawakami *et al.*, 2017). However, the role of tumour-derived OPN in CD8+ lymphocytes has been reported with contradictory effects. It acts as an immune checkpoint to suppress T cell activation and has been correlated with decreased patient survival in colon carcinoma (Klement *et al.*, 2018). Molecular analysis of OPN forms in dendritic cells and T cells revealed that dendritic cells can express high levels of iOPN rather than sOPN, whereas the reverse is true of activated T cells (Shinohara *et al.*, 2005). The next question was raised here: Does stroma sOPN provide the same anti-tumour immunity feature as iOPN?

7.5.4. IL-6 RNAScope expression in OPSCC

IL-6 RNAScope analysis was limited to a small number of cases (cohort 2, n=54). High IL-6 mRNA expression was observed in both HPV-positive and negative OPSCC (p=0.7); however, IL-6 expression did not correlate with the survival of the tested population. IL-6 has been reported as an independent prognostic biomarker in several types of tumours including HNSCC, where high IL-6 expression in tissue has been related to tumour recurrence, metastasis and poor survival (Choudhary *et al.*, 2016; Kobawala *et al.*, 2016; Ahmad *et al.*, 2018). Here, in OPSCC, IL-6 transcript expression was detected in non-malignant lymphoid tissues which might be a part of an inflammatory mechanism attributed to recurrent chronic infection (Todorović and Zvrko, 2013), although in some sections, IL-6 expression signals were located intimately with stroma-adjacent cancer cells, suggesting specific reactions in stroma cells to cancer cells paracrine signalling pathways. The histology of the anatomical site could be a reason behind our findings, while the cohort's small size may be another factor. Our separate observation for Cohort 2's performance indicated it is an underpowered cohort. Further validation with a larger cohort is essential.

7.5.5 Concluding remarks

Cytokine profiling data showed that OPN was a factor expressed exclusively by an HPV-negative cell line, not the HPV-positive cell line. However, our data are limited to two OPSCC cell lines and the cytokine assessment was based on the early short response. OPN IHC assessment revealed no differences in OPN expression at different score levels, as even in HPV-negative OPSCC, some cases showed low OPN expression. However, the exact source of detected OPN in IHC assay is obscure, and this reflects a limitation in our co-culture model that is devoid of the presence of the immune cells, the second important component in TME.

Based on IHC evaluation, high OPN expression was correlated positively with the favourable prognosis. Nevertheless, determination of OPN source is a fundamental key to understand the biological function of OPN expression in OPSCC: is the protective function of OPN in OPSCC attributable to tumour-derived OPN or stromal-derived OPN? In situ hybridisation for OPN mRNA would be an optimum method to answer this question by providing the feasibility to score OPN expression in tumour cells and stromal cells independently. Using digital software such as Qupath software may aid in this process effectively. Moreover, assessment of the clinical significance of secreted OPN in OPSCC

patient serum is another important issue that has not been investigated thoroughly. This may expose the other face of OPN (sOPN) that was known widely for its correlation with poor clinical outcome.

7.6. Limitations

We are aware that our method of assessment still needs further investigation by evaluating OPN mRNA expression that might provide the feasibility to identify the amount of stromal-derived OPN in OPSCC and establish a separate scoring of the epithelial and stromal compartments using quantitative staining analysis on the digital images. Moreover, the IHC assay was performed using a single type of polyclonal antibody only. In the Kunii *et al.* (2009) study, OPN polyclonal antibody performance has been assessed against the monoclonal counterpart. Monoclonal OPN antibody was reported with slight advantages over the polyclonal OPN antibody. The use of a combination of both antibodies was recommended.

7.7. Summary of main findings and clinical implications:

This is the first study to assess OPN IHC expression in OPSCC in detail. OPN has shown different patterns of staining that have been seen in both OPSCC entities. Nevertheless, the High OPN expressing OPSCC sub-population demonstrated superior survival. Multivariate regression analysis confirmed High OPN expression as an independent prognostic factor in OPSCC. However, performing OPN ISH is essential to identify the cellular source of OPN in OPSCC and confirm our results. Validation of this finding might introduce OPN as a prognostic biomarker in OPSCC that could be utilised for patient selection for de-intensification protocols.

Because of the general understanding of OPN as a factor facilitating tumour formation and progression, OPN is now considered a target for cancer therapy. However, as there is, in some circumstances an anti-tumorigenic role for OPN, as reported here (and by some other investigators), targeting OPN may also reduce the antitumorigenic features of OPN in this tumour. Thus, further investigation, including characterisation of OPN isoforms in OPSCC, might provide novel candidates for target therapy or avoid the loss of helpful features of OPN action in these tumours.

Chapter 8: General Discussion and Conclusion

8.1 General discussion

Squamous cell carcinoma is the most common tumour type in HNC, a group of cancers characterised by aggressive behaviour and high morbidity and mortality rates within the first five years from diagnosis (Johnson *et al.*, 2020). In 2018, more than 890,000 new cases were diagnosed with 450,000 deaths (Bray, Ferlay and Soerjomataram, 2018). Based on Global Cancer Observatory (GLOBOCAN) estimation, HNSCC incidence is projected to rise further by a third in the next decade to reach 1.08 million new cases in 2030 (Ferlay *et al.*, 2019). However, the risk factors attributed to the HNSCC burden vary worldwide. Whereas the consumption of alcohol and tobacco in different forms are the common risk factors in Southeast Asia, high prevalence in HNSCC in western countries is attributed to HPV-associated OPSCC (Hashibe *et al.*, 2007; Mehanna *et al.*, 2013). The prevalence of HPV-positive OPSCC in epidemic regions was reported to be more than two-thirds of all OPSCC (70%). In our cohort, the prevalence of the HPV16/18 genotypes were 60.8% of all included cases (87/143).

Clinically, HPV-associated OPSCC patients demonstrate different clinical presentation and clinical outcomes from the non-HPV related counterparts. HPV-patients tend to be non-smoker males within the middle age group and from a high socioeconomic background. Most importantly, they demonstrated better prognosis regardless of therapy strategy protocols (Ang *et al*., 2010). HR-HPV status in OPSCC is well documented as a reliable prognostic factor for tumour progression, and we observed a longer estimated overall survival time (p= 0.002) in the HPV-positive group compared to HPV-negative OPSCC indicated by a high hazard ratio in the univariate regression model (HR: 2.68; 95%CI: 1.35-5.31, p=0.005). Comparing smoking habit data between OPSCC entities emphasises the etiological role of HPV in OPSCC development; HPV-positive group contained significantly fewer smokers than the HPV-negative counterpart (p<0.001). The status of smoking habit at diagnosis (Never, Former and Current) provided a further clinical feature for outcome prediction of HPV-negative (p<0.001).

Several techniques have been utilised for HPV detection in tissue materials that demonstrated varying diagnostic values. However, besides the diagnostic performance, researchers were also considering the prognostic value of these techniques, to be utilised effectively in clinical trials. According to recent AJCC guidelines, identification of HPV status in OPSCC has become a fundamental requirement in the clinical setting and that based on p16 IHC positivity. In comparison with different HPV detection methods,

p16 has many advantages given the simplicity, feasibility and low cost, besides high prognostic value. However, due to the evident shortcomings in p16 IHC specificity, other HPV specific tests based on nucleic acid detection were recommended in step-wise algorithms, particularly, in non-epidemic regions. Our assessment for p16 IHC performance against RNAScope assay revealed acceptable sensitivity of 97.6%, and relatively low specificity (72%), nevertheless, it revealed better prognostic value than RNAscope assay. It is worth mentioning here that p16 positivity was based on H-score threshold 144.5 that was selected mathematically using ROC curve. 144.5 H-score threshold is most likely to be consistent with >50% positivity threshold. Since the low specificity of p16 IHC has been improved by the combination with an HPV specific test, further validation is warranted to assess the prognostic performance of >50% p16 positivity threshold, which may provide a more accurate prediction of OPSCC survival than >70% positivity threshold.

The reasons behind better HPV-positive OPSCC outcomes still are not fully clear. Different explanations have been proposed by many authors which include, the patient's general condition: patients with HPV-positive tumours usually present younger in age, with good performance status, and fewer comorbidities (Ang and Sturgis, 2012). Higher radio-sensitivity is another factor for the improved outcome that might be the result of an intact apoptotic response to radiation (Fakhry *et al.*, 2017). Moreover, the difference in genetic alterations is another possible factor. HR-HPV-associated SCC is considered a genetically stable tumour, harbouring less genetic mutations and loss of heterozygosity on chromosome 3p and retaining active p53 and pRb pathways (GS-OSCC) (Braakhuis *et al.*, 2004; Parkinson, James and Prime, 2016), while non-HPV OSCC is characterised by several genetic mutations and gross deletions of whole or large parts of chromosomal arms including loss of heterozygosity TP53 and CDKN2A which indicates it considered as a genetically unstable subtype of OSCC (GU-OSCC) (Braakhuis *et al.*, 2004). The genetic landscape of tumour cells has its evident reflection in the underlying TME. In response to tumour-derived oncogenic signals, the TME continually changes to support tumour cell progression (Lim *et al.*, 2011; Quail and Joyce, 2013). In OSCC, fibroblasts derived from GU-OSCC showed high senescence percentage and distinct inflammatory profiles from GS-OSCC-derived fibroblasts (Lim *et al.*, 2011; Hassona *et al.*, 2013, 2014). Moreover, studies from our lab demonstrated differences in normal fibroblasts early responses to OPSCC cell lines conditioned media. HPV-negative cell lines conditioned media showed a larger amount of secretome (Bolt, 2016) that demonstrated a high ability to modulate the secretory profile of fibroblasts to a more inflammatory profile (Bolt *et al.*,

2018; Peacock *et al.*, 2018; Al-Sahaf *et al.*, 2019). This concept promoted us to investigate in-depth the early crosstalk between OPSCC tumour cells and fibroblast. This aspect may provide additional therapeutic options to treat malignant carcinomas.

CAFs are the major component of the cellular part of the ECM that plays a crucial role in tumour progression and chemoresistance in OSCC among other tumour types (Fiori *et al.*, 2019; Sun *et al.*, 2019; Mughees *et al.*, 2021). Conversely, in some reports from pancreatic ductal adenocarcinoma and breast cancer, CAFs were reported to exert tumour-suppressive effects in the TME (Rhim *et al.*, 2014; Brechbuhl *et al.*, 2017). Upregulation of α-SMA has been reported in GU-OSCC-derived CAFs (Lim et al., 2011), and was linked with poor prognosis in OSCC tissue material (Dourado *et al.*, 2018). In OPSCC, we have observed a comparable distribution of α-SMA expression in HPV-positive OPSCC and HPV-negative OPSCC, although the latter is considered GU-OPSCC. However, expression of α-SMA biomarker is not specific for myofibroblastic CAFs phenotype, it was also upregulated in senescent fibroblasts via TGF-β/Smad signalling provoked by reactive oxygen species (Oh, Lee and Wagers, 2014).

Traditional CAFs molecular biomarker and scRNA-seq analysis demonstrated that the term" CAF" represent a wide heterogeneous family with subtypes of distinct biomarker expression and functionality phenotype which are believed to be attributed to diversity in CAF origin (Kidd *et al.*, 2012; Prime *et al.*, 2017). scRNA-seq analysis revealed also intra-tumour heterogeneity in CAFs subtypes within the same tumour type (Galbo, Zang and Zheng, 2021). We observed this heterogeneity using molecular biomarkers expression during CAFs cultures characterisation. Although CAF1 and CAF2 were extracted from the same tumour type (HPV-positive OPSCC), the latter displayed myofibroblastic CAF-like phenotype by overexpressing α-SMA, while the former showed a high percentage of SA-β-gal stain and a larger number of inflammatory profile upregulation following cell line media incubation (Table 5.4 & 5.5). This provided us with both major phenotypes in our CAF established models (myofibroblastic CAF model and a senescent CAF model) a better understanding of OPSCC CAFs phenotypes.

In a recent scRNA-seq study that profiled CAFs from HNSCC, lung cancer and melanoma, six pan-CAF subtypes were detected, each with a distinct genetic profile and functional role (Galbo, Zang and Zheng, 2021). myCAF subtype was reported with activated fibroblast biomarker and upregulation in smooth muscle-related contractive genes. The high ability of the myCAF subtype in ECM remodelling and activation of underlying pathways associated with smooth muscle cell contraction is thought the main

factors behind the worse clinical outcomes. iCAF subtype showed upregulation of gene sets related to interleukin signalling pathways, moreover, the iCAF-2 subtype showed expression of IL-6 gene exclusively (Galbo, Zang and Zheng, 2021). These observations suggested that iCAF subtypes are most likely to be associated with an inflammatory TME, implicated in cancer cell stemness and cancer therapy resistance (Su *et al.*, 2018). A better understanding of CAFs molecular heterogeneity provides a potential explanation of CAFs functional role in TME. In this study, evaluating the clinical significance of CAFs based on α-SMA expression revealed a potential prognostic value in HPV-positive group only (p=0.02). Low α-SMA subgroup demonstrated better overall survival than High α-SMA counterpart in HPV-positive group. This observation may suggest a different functional role of CAF subtypes in OPSCC driven by the diversity in OPSCC signalling pathways.

Cytokine profiling introduced novel candidates that were particularly expressed by the HPV-negative cell line (M1), but not by the HPV-positive counterpart, that includes OPN, KLK6 and GM-CSF. These factors were associated with senescence, ageing and tumour metastasis (Borgoño and Diamandis, 2004; Coppé *et al.*, 2008; Zhao *et al.*, 2018). We also observed modulation in the secretory profile of OPSCC fibroblasts with IL-6 and IL-8 upregulation following co-culturing with HPV-negative OPSCC conditioned media (M2). We chose to focus on OPN and IL-6 as they were previously described as candidates in a dynamic communication loop between the tumour cells and CAFs in OSCC (Qin *et al.*, 2018). Targeting the reciprocal interaction between tumour cells and CAFs is a much-needed approach to cancer therapy. Our initial investigations determined that the HPV-negative tumour cell was the main source of OPN in the interactive co-culture models, and IL-6 was upregulated in fibroblast in response to the HPV-negative cell line only. This novel finding indicates the presence of early reciprocal crosstalk between HPV-negative cell line and fibroblast mediated by OPN and IL-6.

As a multifunctional molecule, OPN is known as a pro-fibrotic factor that has been implicated in various fibrosis-related diseases in the lung and cardiac muscle. It has been described as an essential factor in dermal fibroblast activation through the TGF-β1 pathway. In breast cancer, tumour-derived OPN showed the ability to reprogram normal fibroblasts into myofibroblastic CAFs phenotypes with evident contractility, α-SMA upregulation and proinflammatory secretory profile, however, IL-6 was not a prominent feature in the secretome of these OPN-induced CAFs. Our preliminary investigation showed a degree of phenotypic modulation in one NTF culture following rOPN induction, with enhanced contractility and slight upregulation of IL-6. These observations warrant

further validation using a larger number of cultures, moreover, fibroblast activation status should be confirmed by assessing the expression of fibroblasts activation biomarker, such as α-SMA.

The reciprocal relationship hypothesis between OPN and IL-6 was tested in one direction: we assessed the effect of OPN on IL-6 upregulation. Due to time restriction, only one NTF culture (NTF322) was tested and that by targeting the CD44v6 receptor alone. OPN has a number of binding sites, including the CD44 receptor and integrins. Blocking one of the OPN receptors showed a partial decrease in the effects of OPN in OSCC, while the combination of more than receptor blocker resulted in a significant reduction in OPN effects (Qin *et al*., 2018). We observed a degree of IL-6 reduction in rOPN-induced NTF, where that was variable in NTF322-induced with cell line conditioned media.

Overexpression of OPN in tissue has been linked with disease progression in poor prognosis in HNSCC, however, in other a handful of reports demonstrated a favourable prognosis value for OPN in pancreas cancer (Collins *et al.*, 2012; Danzaki *et al.*, 2016; Franklin *et al.*, 2019). In OPSCC, we observed a strong correlation between high OPN IHC expression and a better prognosis. This finding highlights the heterogeneous functions of OPN forms and isoforms concerning tumour development and progression. OPN functions reported as pro-tumorigenic or anti-tumorigenic according to cell type and tumour microenvironment (Lamort *et al*., 2019). Therefore, further investigation on OPN source in OPSCC is needed, which may provide new insights to depict the difference in the functional role of OPN variants.

8.2 Conclusion

This study was conducted in a new complex research area concerning the role of CAFs in OPSCC subtypes. All the presented data here are original and novel. Although not all study's aims were covered due to the time restrictions imposed due to the COVID-19 pandemic, the available findings established a strong framework of understanding. The isolation and characterisation of OPSCC fibroblasts described here provide a novel insight into the role of CAFs in OPSCC mediated by OPSCC cancer cell and CAF crosstalk that was evident in HPV-negative cell line. Moreover, it is proposed that α-SMA has the potential as a prognostic biomarker for HPV-positive OPSCC stratification. Our analysis of OPN in OPSCC demonstrated a positive correlation between OPN overexpression and survival that warrants further investigations.

8.2.1 Summary of each chapters' main findings and clinical implications

Chapter 3: A p16 H-score cut off of 144.5 is a promising diagnostic and prognostic tool that demonstrated high sensitivity and acceptable low specificity compared to HPV 16/18 mRNA, in addition to the predictive performance. This finding underpins the requirement of clinical validation of H-score performance that might be adopted as a tool addressing the partial stain dilemma between >70% and >50% positivity thresholds.

Our findings propose α-SMA expression for further study and clinical validation to assess its predictive strength in HPV-positive OPSCC. The findings might provide a stratification tool within HPV-positive OPSCC cohorts for the best benefit of de-intensifying protocols. Moreover, the proposed crucial influences of CAFs in HPV-OPSCC tumour microenvironment suggest introducing HPV-positive OPSCC as an option of the emerging potential targeting strategies in cancer therapy.

Chapter 4: The establishment of OPSCC-CAF co-cultures provides the opportunity for further investigations *in vitro* to aid our understanding of OPSCC tumour cells and CAF crosstalk. Recognition of CAF characteristics in different phenotypes provides a

framework for better understating of CAFs' varied role in OPSCC. Moreover, it highlights the need to consider multiple parameters for the analysis of CAF activation.

Chapter 5: We have reported, for the first time a number of cytokines secreted particularly by HPV-negative OPSCC cell line namely, OPN, KLK6 and GM-CSF, in addition to other cytokines produced under all conditions. Molecular analysis of interactive co-culture models identified the source of OPN and IL6 production. At the basal level, more OPN was produced by HPV-negative cell lines than HPV-positive cell lines. Upon 48h of interactive co-culturing, only HPV-negative cell lines demonstrated significantly higher levels IL-6 overexpression indicated active crosstalk between cancer cells and fibroblasts. These findings underpin the need for better understating the role of TME in OPSCC development and progression.

Chapter 7: This is the first study to assess OPN expression in OPSCC in detail. OPN has shown different patterns of staining that have been seen in both OPSCC entities. Nevertheless, the High OPN expressing OPSCC sub-population demonstrated superior survival. Multivariate regression analysis confirmed High OPN expression as an independent predictive in OPSCC. However, performing OPN ISH is essential to identify the cellular source of OPN in OPSCC and confirm our results. Validation of this finding may allow for the development of OPN as a predictive biomarker in OPSCC that could be utilised for patient selection in de-intensification protocols. Given the general understanding of OPN as a factor facilitating tumour formation and progression, OPN is now considered a target for cancer therapy. However, as there is, in some circumstances an anti-tumorigenic role for OPN, as reported here (and by some other investigators), targeting OPN may also reduce the antitumorigenic features of OPN in this tumour. Further investigation, including characterisation of OPN isoforms in OPSCC, might provide novel candidates for targeted therapy or avoid the loss of helpful features of OPN action in these tumours.

Chapter 9: Future work

Chapter 3:

- Validataion α-SMA biomarker prognostic value of in a larger OPSCC cohort. Determination of HPV status here should be performed using a higher number of RNAScope probes.

Chapter 4:

- Perform scRNA-seq analysis for CAF1 and CAF2 in addition to CAFs cultures extracted from HPV-negative OPSCC. Genetic characterisation of OPSCC CAFs may expose the heterogeneity of genetic signature for both subtypes. Identification of the genetic landscape CAFs may explain different functional role in OPSCC stroma and that by referring to The Cancer Genome Atlas (TCGA). This work may provide new insights into how OPSCC entities may benefit from CAF subtype targeted therapy.

Chapter 5:

- In the validation process to cytokines arrays findings, CCL2 refractory level was assessed using ELISA assay. We noticed higher upregulation in CCL2 level in SCC89-fibroblast co-cultured model than SCC2 counterpart. This difference was evident with NTFs more than CAFs (Figure 9.1). CCL2 has been reported to exert its effect in the recruitment of circulating monocytes *in vivo* and in a 3D *ex-vivo* model from breast cancer (Jia *et al*., 2015) Recruitment of macrophages into TME mediated by CAFs was reported with different molecular pathways such as stromal cell-derived factor 1 (SDF1)/CXCL12 in prostate cancer (Comito *et al*., 2014). Investigation of the functional role of CCL2 in OPSCC macrophage recruitment may provide a therapeutic target in HPV-negative OPSCC.

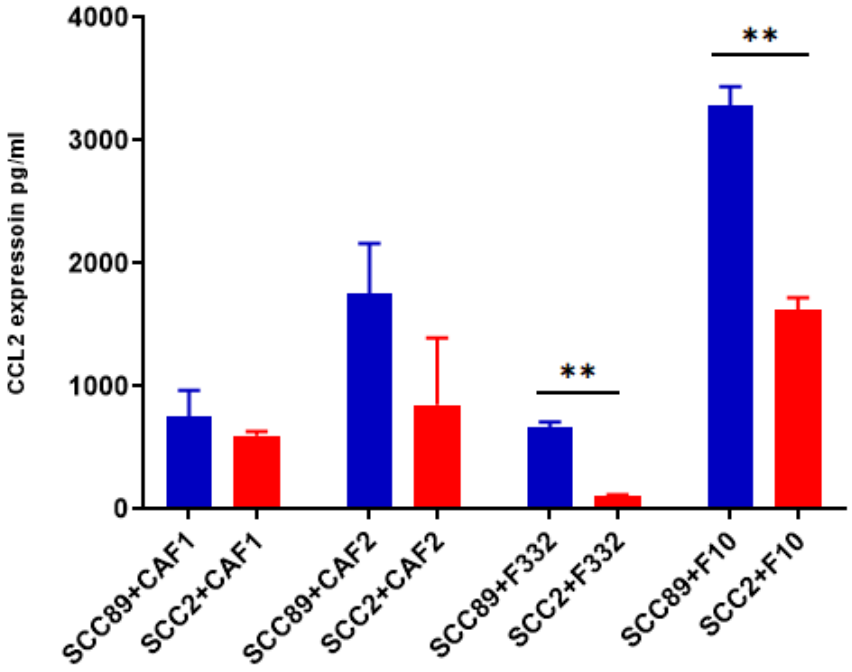

Figure 9.1: Higher levels of CCL2 protein secretion in SCC89-fibroblast co-cultures than in SCC2-fibroblast co-cultures. SCC89 or SCC2 ($3x10^5$ cells) were co-cultured with OPSCC fibroblasts (CAF1, CAF2, NTF322, NTF10) (50,000 cells) using transwell insert (0.45 µm) for 48h. The collected media was subjected to CCL2 ELISA analysis. Samples number (n=8), Y-axis denotes standardised CCL2 concentration in Pg per ml. Blue bars denote SCC89 co-cultures. Red bars denote SCC2 co-cultures. Only SCC89 co-cultures showed apparent OPN expression. Error bars= SD. Data represent the mean of (N=3, n=3). Statistical analysis was determined using two-tailed Student *t*-test with $^{**}p < 0.01$.

- Further investigation of candidates identified by cytokines profiling (KLK6, GM-CSF) including identification of their production source, the effect on OPSCC tumour cells and fibroblasts.

- Investigate OPSCC-CAFs crosstalk at the direct contact approach using a 3-dimensional organoid model and analysis the sorting cells. The addition of the immune cells (macrophage or T-cell) to the 3D-model may reveal the significance of the presence of stroma derived OPN in both OPSCC subtypes.

Chapter 6:

- In this chapter, the effects of OPN on NTFs activation still require further investigation and validation by assessing fibroblasts activation biomarkers in larger NTFs cultures numbers.

- In addition to CD44v6 targeting, integrin blocking needs to be assessed to understand the correlation between OPN/IL-6 production loop.

- Investigate the effect of IL-6 on OPN derived OPSCC cell lines using a higher IL-6 dose (50 ng/ml).

- Investigate OPN/CD44/p38 signalling pathway in OPSCC and assess the functional role ofp38 expression in OPSCC using functional assays.

Chapter 7:

- Investigate the possibility of the construction of customised *in situ* hybridisation probes for different OPN mRNA isoforms and types (sOPN and iOPN). Identification of OPN source of production may clarify the correlation between OPN forms and survival.

- Conducting CD44 IHC assay for the TMA study cohort may reveal further insights into the functional roles of OPN in OPSCC.

Appendix

A.1 HPV profiling for OPSCC cell lines

Name	Dilution	Other	G16	G18
SCC2	1 in 4156	N	P	N
SCC2	1 in 20781	N	P	N
SCC2	1 in 33	N	P	N
SCC2	1 in 7.5	N	P	N
SCC2	1 in 166	N	P	N

Name	Dilution	Other	G16	G18
SCC90	1 in 831	N	P	N
SCC90	1 in 7.5	N	P	N
SCC90	1 in 4156	N	P	N
SCC90	1 in 33	N	P	N
SCC90	1 in 20781	N	P	N
SCC90	1 in 166	N	P	N

Name	Dilution	Other	G16	G18
SCC72	1 in 4156	N	N	N
SCC72	1 in 831	N	N	N
SCC72	1 in 166	N	N	N
SCC72	1 in 20781	N	N	N
SCC72	1 in 7.5	N	N	N

Name	Dilution	Other	G16	G18
SCC89	1 in 33	N	N	N
SCC89	1 in 20781	N	N	N
SCC89	1 in 831	N	N	N
SCC89	1 in 7.5	N	N	N
SCC89	1 in 166	N	N	N

Table A.1: Cell lines screening using Roche 6800 instrument for HPV16 (G16) and HPV18 (G18). (A) SCC2 cell line. (B) OPSCC 90. (C) OPSCC 72. (D) OPSCC 89.

A.2 : The cytokine arrays (Number ARY026) - Full details.

The full name of cytokines presented in the proteome profiler Human XL Oncology Array kit (Catalogue number ARY026, R&D Systems, Inc., Minneapolis, US) that have been used in this study.

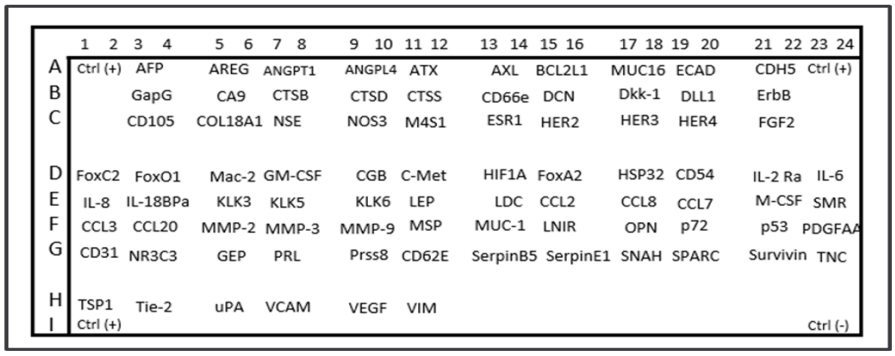

Coordinate	Analyte/Control	Entrez Gene ID	Alternate Nomenclature
A1, A2	Reference Spots	N/A	———
A3, A4	α-Fetoprotein	174	AFP, DSCAM2
A5, A6	Amphiregulin	374	AREG
A7, A8	Angiopoietin-1	284	ANGPT1
A9, A10	Angiopoietin-like 4	51129	ANGPTL4
A11, A12	ENPP-2/Autotaxin	5168	ATX, Lysophosphatidic Acid, NPP2, PDNP2
A13, A14	Axl	558	Ark, Ufo
A15, A16	BCL-x	598	BCL2L1
A17, A18	CA125/MUC16	94025	MUC16
A19, A20	E-Cadherin	999	Arc-1, CAD1, Cadherin-1, CD324, CDH1, Cell-CAM120/80, ECAD, L-CAM
A21, A22	VE-Cadherin	1003	Cadherin-5, CD144, CDH5
A23, A24	Reference Spots	N/A	———
B3, B4	CapG	822	AFCP
B5, B6	Carbonic Anhydrase IX	768	CA9, G250, MN, RCC
B7, B8	Cathepsin B	1508	CTSB
B9, B10	Cathepsin D	1509	CTSD
B11, B12	Cathepsin S	1520	CTSS
B13, B14	CEACAM-5	1048	CD66e, CEA
B15, B16	Decorin	1634	DCN, DSPG2, PG-II, PSG2, SLRR1B
B17, B18	Dkk-1	22943	Dickkopf-1
B19, B20	DLL1	28514	Delta 1
B21, B22	EGF R/ErbB1	1956	ErbB, ErbB1, HER-1
C3, C4	Endoglin/CD105	2022	CD105, ENG
C5, C6	Endostatin	80781	COL18A1
C7, C8	Enolase 2	2026	ENO2; γ-Enolase; NSE
C9, C10	eNOS	4846	NOS3
C11, C12	EpCAM/TROP1	4072	17-1A, CD326, GA733-2, gp40, KS1/4, M4S1, TACSTD1
C13, C14	ERα/NR3A1	2099	ESR1, NR3A1
C15, C16	ErbB2	2064	CD340, HER2, Neu Oncogene, NGL, TKR1
C17, C18	ErbB3/Her3	2065	HER3
C19, C20	ErbB4	2066	HER4
C21, C22	FGF basic	2247	FGF2, FGF-2, FGF2AS, GFG1, HBGH-2, NUDT6, Prostatropin
D1, D2	FoxC2	2303	Fkh14, LD, MFH1
D3, D4	FoxO1/FKHR	2308	FKH1, FKHR
D5, D6	Galectin-3	3958	AGE-R3, CBP35, GAL3, L29, LGALS3, Mac-2
D7, D8	GM-CSF	1437	CSF2
D9, D10	CG α/β (HCG)	1081 (α)/1082 (β)	CGB, CGB3, Choriogonadotropin
D11, D12	HGF R/c-Met	4233	MET

Coordinate	Analyte/Control	Entrez Gene ID	Alternate Nomenclature
D13, D14	HIF-1α	3091	HIF1A
D15, D16	HNF-3β	3170	FoxA2
D17, D18	HO-1/HMOX1	3162	HSP32
D19, D20	ICAM-1/CD54	3383	———
D21, D22	IL-2 Rα	3559	CD25, IL2RA
D23, D24	IL-6	3569	BSF-2, IFN-β2, MGI-2A
E1, E2	CXCL8/IL-8	3576	GCP1, IL8, LAI, MDNCF, NAP1, NCF, TCF, TSG1
E3, E4	IL-18 BPa	10068	IL18BP
E5, E6	Kallikrein 3/PSA	354	KLK3
E7, E8	Kallikrein 5	25818	KLK5, KLK-L2, SCTE
E9, E10	Kallikrien 6	5653	KLK6, Neurosin, Protease M, PRSS18, PRSS9, SP59, Zyme
E11, E12	Leptin	3952	LEP, OB
E13, E14	Lumican	4060	LDC, LUM, SLRR2D
E15, E16	CCL2/MCP-1	6347	MCAF
E17, E18	CCL8/MCP-2	6355	———
E19, E20	CCL7/MCP-3	6354	MARC
E21, E22	M-CSF	1435	CSF1, CSF-1
E23, E24	Mesothelin	10232	CAK1, MPF, MSLN, SMR
F1, F2	CCL3/MIP-1α	6348/6351	LD78a; MIP-1 alpha
F3, F4	CCL20/MIP-3α	6364	exodus-1; LARC; MIP-3 alpha
F5, F6	MMP-2	4313	Gelatinase A
F7, F8	MMP-3	4314	Stromelysin-1
F9, F10	MMP-9	4318	CLG4B, Gelatinase B, GELB
F11, F12	MSP/MST1	4485	HGFL, MST1, SF2
F13, F14	MUC-1	4582	CD227, Episialin, H23AG, KL-6, Mucin-1, PEM, PEMT
F15, F16	Nectin-4	81607	LNIR, PRR4, PVRL4
F17, F18	Osteopontin (OPN)	6696	Eta-1, Spp1
F19, F20	p27/Kip1	1027	CDKN1B
F21, F22	p53	7157	BCC7, LFS1, TP53, TRP53
F23, F24	PDGF-AA	5154	———
G1, G2	CD31/PECAM-1	5175	PECAM1
G3, G4	Progesterone R/NR3C3	5241	———
G5, G6	Progranulin	2896	Acrogranin, GEP, GP88, GRN, PCDGF, PEPI, PGRN, Proepithelin
G7, G8	Prolactin	5617	PRL
G9, G10	Prostasin/Prss8	5652	———
G11, G12	E-Selectin/CD62E	6401	ELAM1, LECAM2, SELE
G13, G14	Serpin B5/Maspin	5268	PI5
G15, G16	Serpin E1/PAI-1	5054	Nexin, PLANH1

Coordinate	Analyte/Control	Entrez Gene ID	Alternate Nomenclature
G17, G18	Snail	6615	SLUGH2, SNAH, SNAI1
G19, G20	SPARC	6678	BM-40, Osteonectin
G21, G22	Survivin	332	API4, BIRC5
G23, G24	Tenascin C	3371	Cytotactin, HXB, Tenascin J1, TNC
H1, H2	Thrombospondin-1	7057	THBS1, TSP-1
H3, H4	Tie-2	7010	———
H5, H6	u-Plasminogen Activator/Urokinase	5328	PLAU, uPA
H7, H8	VCAM-1/CD106	7412	———
H9, H10	VEGF	7422	VAS, Vasculotropin, VEGFA, VPF
H11, H12	Vimentin	7431	VIM
I1, I2	Reference Spots	N/A	———
I23, I24	Negative Control	N/A	———

A.3 Raybiotech cytokine arrays map

Maps of Cytokine arrays Raybiotech C2000 Human Cytokine Arrays (Raybiotechnology, Norcross, USA, cat number: AAH-CYT-2000) that have been used by Bolt *et al*., (2016) for profiling OPSCC cell line conditioned media.

	A	B	C	D	E	F	G	H	I	J	K	L	M	N
1	POS	POS	NEG	NEG	BLANK	ANG	BDNF	BLC	BMP 4	BMP 6	CCL23	CNTF	EGF	Eotaxin 1
2	POS	POS	NEG	NEG	BLANK	ANG	BDNF	BLC	BMP 4	BMP 6	CCL23	CNTF	EGF	Eotaxin 1
3	Eotaxin 2	Eotaxin 3	FGF-6	FGF-7	Flt-3 Ligand	Fractalkine	GCP-2	GDNF	GM CSF	I-309	IFN gamma	IGFBP 1	IGFBP 2	IGFBP 4
4	Eotaxin 2	Eotaxin 3	FGF-6	FGF-7	Flt-3 Ligand	Fractalkine	GCP-2	GDNF	GM CSF	I-309	IFN gamma	IGFBP 1	IGFBP 2	IGFBP 4
5	IGF-1	IL-10	IL-13	IL-15	IL-16	IL-1 alpha	IL-1 beta	IL-1ra	IL-2	IL-3	IL-4	IL-5	IL-6	IL-7
6	IGF-1	IL-10	IL-13	IL-15	IL-16	IL-1 alpha	IL-1 beta	IL-1ra	IL-2	IL-3	IL-4	IL-5	IL-6	IL-7
7	Leptin	LIGHT	MCP-1	MCP-2	MCP-3	MCP-4	M-CSF	MDC	MIG	MIP-1 delta	MIP-3 alpha	NAP-2	NT-3	PARC
8	Leptin	LIGHT	MCP-1	MCP-2	MCP-3	MCP-4	M-CSF	MDC	MIG	MIP-1 delta	MIP-3 alpha	NAP-2	NT-3	PARC
9	PDGF BB	RANTES	SCF	SDF-1 alpha	TARC	TGF beta 1	TGF beta 3	TNF alpha	TNF beta	BLANK	BLANK	BLANK	BLANK	POS
10	PDGF BB	RANTES	SCF	SDF-1 alpha	TARC	TGF beta 1	TGF beta 3	TNF alpha	TNF beta	BLANK	BLANK	BLANK	BLANK	POS

(C6)

	A	B	C	D	E	F	G	H	I	J	K	L	M	N
1	POS	POS	NEG	NEG	BLANK	Acrp30	AgRP	ANGPT2	AREG	Axl	bFGF	b-NGF	BTC	CCL28
2	POS	POS	NEG	NEG	BLANK	Acrp30	AgRP	ANGPT2	AREG	Axl	bFGF	b-NGF	BTC	CCL28
3	CTACK	Dtk	EGFR	ENA-78	Fas	FGF-4	FGF-9	G-CSF	GITR Ligand	GITR	GRO	GRO alpha	HCC-4	HGF
4	CTACK	Dtk	EGFR	ENA-78	Fas	FGF-4	FGF-9	G-CSF	GITR Ligand	GITR	GRO	GRO alpha	HCC-4	HGF
5	ICAM-1	ICAM-3	IGFBP 3	IGFBP 6	IGF-1 sR	IL-1 R4	IL-1 R1	IL-11	IL-12 p40	IL-12 p70	IL-17	IL-2 R alpha	IL-6 R	IL-8
6	ICAM-1	ICAM-3	IGFBP 3	IGFBP 6	IGF-1 sR	IL-1 R4	IL-1 R1	IL-11	IL-12 p40	IL-12 p70	IL-17	IL-2 R alpha	IL-6 R	IL-8
7	I-TAC	XCL1	MIF	MIP-1 alpha	MIP-1 beta	MIP-3 beta	MSP alpha	NT-4	OPG	OSM	PLGF	sgp130	sTNFRII	sTNFRI
8	I-TAC	XCL1	MIF	MIP-1 alpha	MIP-1 beta	MIP-3 beta	MSP alpha	NT-4	OPG	OSM	PLGF	sgp130	sTNFRII	sTNFRI
9	TECK	TIMP-1	TIMP-2	THPO	TRAIL R3	TRAIL R4	uPAR	VEGF	VEGF-D	BLANK	BLANK	BLANK	BLANK	POS
10	TECK	TIMP-1	TIMP-2	THPO	TRAIL R3	TRAIL R4	uPAR	VEGF	VEGF-D	BLANK	BLANK	BLANK	BLANK	POS

(C7)

	A	B	C	D	E	F	G	H	I	J	K	L	M	N
1	POS	POS	NEG	NEG	BLANK	Activin A	ALCAM	CD80	BMP 5	BMP 7	CT-1	CD14	CXCL16	DR6
2	POS	POS	NEG	NEG	BLANK	Activin A	ALCAM	CD80	BMP 5	BMP 7	CT-1	CD14	CXCL16	DR6
3	Endoglin	ErbB3	E Selectin	Fas Ligand	ICAM 2	IGF-2	IL-1 R 2	IL-10 R beta	IL-13 R alpha 2	IL-18 BP alpha	IL-18 R beta	MMP 3	IL-2 R beta	IL-2 R gamma
4	Endoglin	ErbB3	E Selectin	Fas Ligand	ICAM 2	IGF-2	IL-1 R 2	IL-10 R beta	IL-13 R alpha 2	IL-18 BP alpha	IL-18 R beta	MMP 3	IL-2 R beta	IL-2 R gamma
5	IL-21 R	IL-5 R alpha	IL-9	IP-10	LAP	Leptin R	LIF	L Selectin	M-CSF R	MMP 1	MMP 13	MMP 9	MPIF-1	NGF R
6	IL-21 R	IL-5 R alpha	IL-9	IP-10	LAP	Leptin R	LIF	L Selectin	M-CSF R	MMP 1	MMP 13	MMP 9	MPIF-1	NGF R
7	PDGF AA	PDGF AB	PDGF R alpha	PDGF R beta	PECAM 1	PRL	SCF R	SDF-1 beta	Siglec 5	TGF alpha	TGF beta 2	TIE-1	TIE-2	TIMP-4
8	PDGF AA	PDGF AB	PDGF R alpha	PDGF R beta	PECAM 1	PRL	SCF R	SDF-1 beta	Siglec 5	TGF alpha	TGF beta 2	TIE-1	TIE-2	TIMP-4
9	VE Cadherin	VEGF R2	VEGF R3	BLANK	BLANK	BLANK	BLANK	BLANK	BLANK	BLANK	BLANK	BLANK	BLANK	POS
10	VE Cadherin	VEGF R2	VEGF R3	BLANK	BLANK	BLANK	BLANK	BLANK	BLANK	BLANK	BLANK	BLANK	BLANK	POS

(C8)

A.4 Tissue microarrays map

Maps of tissue microarrays that was constructed to include cohort 2 cases.

	A	B	C	D	E	F	G
	Guide Block: Prostate	Guide Block: Prostate	Guide Block: Prostate				
1	SMA + Block: Sub.SG	Case:1 Block: OPSCC	Case:1 Block: OPSCC	Case:1 Block: OPSCC	Case: 2 Block: OPSCC	Case: 2 Block: OPSCC	SMA + Block: Sub.SG
2	SMA + Block: Sub.SG	Case: 3 Block: OPSCC	Case: 3 Block: OPSCC	Case: 3 Block: OPSCC	Case: 4 Block: OPSCC	Case: 4 Block: OPSCC	SMA + Block: Sub.SG
3	SMA + Block: Sub.SG	Case: 4 Block: OPSCC	Case: 5 Block: OPSCC	Case: 5 Block: OPSCC	Case: 6 Block: OPSCC	Case: 6 Block: OPSCC	SMA + Block: Sub.SG
4	IL-6/8 + Block: LN	Case: 6 Block: OPSCC	Case: 7 Block: OPSCC	Case: 7 Block: OPSCC	Case: 8 Block: OPSCC	Case: 8 Block: OPSCC	IL-6/8 + Block: LN
5	IL-6/8 + Block: LN	Case: 8 Block: OPSCC	Case: 9 Block: OPSCC	Case: 9 Block: OPSCC	Case: 10 Block: OPSCC	Case: 10 Block: OPSCC	IL-6/8 + Block: LN
6	IL-6/8 + Block: LN	Case: 10 Block: OPSCC	Case: 11 Block: OPSCC	Case: 11 Block: OPSCC	Case: 12 Block: OPSCC	Case: 12 Block: OPSCC	IL-6/8 + Block: LN
7	Block: Tonsil	Case: 13 Block: OPSCC	Case: 13 Block: OPSCC	Case: 13 Block: OPSCC	Case: 14 Block: OPSCC	Case: 14 Block: OPSCC	Block: Tonsil
8	Block: Tonsil	Case: 14 Block: OPSCC	Case: 16 Block: OPSCC	Case: 16 Block: OPSCC	Case: 17 Block: OPSCC	Case: 17 Block: OPSCC	Block: Tonsil
9	Block: Tonsil	Case: 17 Block: OPSCC	Case: 20 Block: OPSCC	Case: 20 Block: OPSCC	Case: 21 Block: OPSCC	Case: 22 Block: OPSCC	Block: Tonsil
10	Block: N.mucosa	Case: 24 Block: OPSCC	Case: 24 Block: OPSCC	Case: 24 Block: OPSCC	Case: 26 Block: OPSCC	Case: 26 Block: OPSCC	Block: Granulation T
11	Block: N.mucosa	Case: 27 Block: OPSCC	Case: 27 Block: OPSCC	Case: 27 Block: OPSCC	Case: 29 Block: OPSCC	Case: 45 Block: OPSCC	Block: Granulation T

TMA map
(n =60)
B1
Page 1/3

	A	B	C	D	E	F	G
	Guide Block: Prostate	Guide Block: Prostate	Guide Block: Prostate				
1	SMA + Block: Sub.SG	Case: 30 Block: OPSCC	Case: 30 Block: OPSCC	Case: 30 Block: OPSCC	Case: 31 Block: OPSCC	Case: 31 Block: OPSCC	SMA + Block: Sub.SG
2	SMA + Block: Sub.SG	Case: 32 Block: OPSCC	Case: 32 Block: OPSCC	Case: 32 Block: OPSCC	Case: 33 Block: OPSCC	Case: 33 Block: OPSCC	SMA + Block: Sub.SG
3	SMA + Block: Sub.SG	Case: 34 Block: OPSCC	Case: 34 Block: OPSCC	Case: 35 Block: OPSCC	Case: 35 Block: OPSCC	Case: 35 Block: OPSCC	SMA + Block: Sub.SG
4	IL-6/8 + Block: LN	Case: 37 Block: OPSCC	Case: 37 Block: OPSCC	Case: 37 Block: OPSCC	Case: 38 Block: OPSCC	Case: 38 Block: OPSCC	IL-6/8 + Block: LN
5	IL-6/8 + Block: LN	Case: 38 Block: OPSCC	Case: 39 Block: OPSCC	Case: 39 Block: OPSCC	Case: 39 Block: OPSCC	Case: 41 Block: OPSCC	IL-6/8 + Block: LN
6	IL-6/8 + Block: LN	Case: 41 Block: OPSCC	Case: 41 Block: OPSCC	Case: 44 Block: OPSCC	Case: 44 Block: OPSCC	Case: 44 Block: OPSCC	IL-6/8 + Block: LN
7	Block: Tonsil	Case: 46 Block: OPSCC	Case: 46 Block: OPSCC	Case: 46 Block: OPSCC	Case: 47 Block: OPSCC	Case: 47 Block: OPSCC	Block: Tonsil
8	Block: Tonsil	Case: 47 Block: OPSCC	Case: 48 Block: OPSCC	Case: 49 Block: OPSCC	Case: 49 Block: OPSCC	Case: 49 Block: OPSCC	Block: Tonsil
9	Block: Tonsil	Case: 50 Block: OPSCC	Case: 50 Block: OPSCC	Case: 50 Block: OPSCC	Case: 51 Block: OPSCC	Case: 51 Block: OPSCC	Block: Tonsil
10	Block: N.mucosa	Case: 51 Block: OPSCC	Case: 52 Block: OPSCC	Case: 52 Block: OPSCC	Case: 52 Block: OPSCC	Case: 53 Block: OPSCC	Block: Granulation T
11	Block: N.mucosa	Case: 53 Block: OPSCC	Case: 65 Block: OPSCC	Case: 65 Block: OPSCC	Case: 66 Block: OPSCC	Case: 66 Block: OPSCC	Block: Granulation T

TMA map
(n =60)
B2
Page 2/3

	A	B	C	D	E	F	G
	Guide Block: Prostate	Guide Block: Prostate	Guide Block: Prostate				
1	SMA + Block: Sub.SG	Case: 54 Block: OPSCC	Case: 54 Block: OPSCC	Case: 54 Block: OPSCC	Case: 57 Block: OPSCC	Case: 57 Block: OPSCC	Block: Tonsil
2	SMA + Block: Sub.SG	Case: 57 Block: OPSCC	Case: 58 Block: OPSCC	Case: 58 Block: OPSCC	Case: 58 Block: OPSCC	Case: 59 Block: OPSCC	Block: Tonsil
3	SMA + Block: Sub.SG	Case: 59 Block: OPSCC	Case: 59 Block: OPSCC	Case:61 Block: OPSCC	Case:61 Block: OPSCC	Case:61 Block: OPSCC	Block: Tonsil
4	SMA + Block: Sub.SG	Case: 62 Block: OPSCC	Case: 62 Block: OPSCC	Case: 62 Block: OPSCC	Case: 63 Block: OPSCC	Case: 63 Block: OPSCC	Block: Tonsil
5	IL-6/8 + Block: LN	Case: 63 Block: OPSCC	Case: 67 Block: OPSCC	Case: 67 Block: OPSCC	Case: 68 Block: OPSCC	Case: 68 Block: OPSCC	Block: Granulation T
6	IL-6/8 + Block: LN	Case: 68 Block: OPSCC	Case: 69 Block: OPSCC	Case: 69 Block: OPSCC	Case: 69 Block: OPSCC	Case: 70 Block: OPSCC	Block: Granulation T
7	IL-6/8 + Block: LN	Case: 70 Block: OPSCC	Case: 70 Block: OPSCC	Case: 71 Block: OPSCC	Case: 71 Block: OPSCC	Case: 72 Block: OPSCC	Block: N.mucosa
8	IL-6/8 + Block: LN	Case: 72 Block: OPSCC	Case: 72 Block: OPSCC	Case: 25 Block: OPSCC	Case: 43 Block: OPSCC	Case: 43 Block: OPSCC	Case: 43 Block: OPSCC

TMA map
(n =60)
B3
Page 3/3

A.5 List of H-score thresholds suggested by ROC curve analysis.

Coordinates of the Curve

Test Result Variable(s): H_score_p16

Positive if Greater Than or Equal To[a]	Sensitivity	1 - Specificity
-1.00	1.000	1.000
8.30	1.000	.400
19.14	1.000	.380
38.34	1.000	.360
57.50	1.000	.340
69.16	1.000	.320
89.17	1.000	.300
113.34	.988	.300
132.84	.977	.300
144.50	.977	.280
151.50	.953	.280
154.00	.942	.280
166.50	.930	.280
180.67	.919	.280
185.42	.907	.280
189.75	.895	.280
193.50	.884	.280
195.83	.872	.280
198.33	.860	.280
204.06	.779	.260
211.56	.767	.260
215.83	.767	.220
216.77	.767	.200
217.82	.756	.200

221.88	.756	.180
227.50	.744	.180
230.83	.721	.180
232.71	.709	.180
234.38	.698	.180
236.56	.686	.180
239.06	.674	.180
244.17	.640	.180
248.54	.628	.180
249.38	.616	.180
250.63	.605	.160
252.29	.593	.160
254.17	.581	.160
256.88	.570	.160
259.38	.558	.160
261.25	.535	.120
263.75	.523	.100
267.50	.512	.100
271.66	.465	.080
274.16	.453	.080
275.50	.442	.060
277.38	.430	.060
279.38	.419	.060
282.09	.349	.060
284.59	.337	.060
285.31	.314	.060
285.73	.302	.060
286.25	.291	.060
287.09	.267	.060
288.75	.256	.060

293.13	.244	.040
296.46	.233	.020
298.34	.221	.020
301.00	.000	.000

The test result variable(s): H_score_p16 has at least one tie between the positive actual state group and the negative actual state group.

References

Abdel-Hafiz, S. M., Hamdy, H. E. M., Khorshed, F. M., Aboushousha, T. S., Safwat, G., Saber, M. A., Seleem, M. and Soliman, A. H. (2018) 'Evaluation of osteopontin as a biomarker in Hepatocellular carcinomas in Egyptian patients with chronic HCV cirrhosis', *Asian Pacific Journal of Cancer Prevention*, 19(4), pp. 1021–1027. doi: 10.22034/APJCP.2018.19.4.1021.

Abidin, A. (2017) Role of microRNAs in Determining the Cancer-associated Fibroblast Phenotype. Ph.D. Univrsity of Sheffield.

Acosta, J. C., O'Loghlen, A., Banito, A., Guijarro, M. V., Augert, A., Raguz, S., Fumagalli, M., Da Costa, M., Brown, C., Popov, N., Takatsu, Y., Melamed, J., d'Adda di Fagagna, F., Bernard, D., Hernando, E. and Gil, J. (2008) 'Chemokine Signaling via the CXCR2 Receptor Reinforces Senescence', *Cell*, 133(6), pp. 1006–1018. doi: 10.1016/j.cell.2008.03.038.

Afify, A., Purnell, P. and Nguyen, L. (2009) 'Role of CD44s and CD44v6 on human breast cancer cell adhesion, migration, and invasion', *Experimental and Molecular Pathology*, 86(2), pp. 95–100. doi: 10.1016/j.yexmp.2008.12.003.

Agorku, D. J., Langhammer, A., Heider, U., Wild, S., Bosio, A. and Hardt, O. (2019) 'CD49b, CD87, and CD95 Are Markers for Activated Cancer-Associated Fibroblasts Whereas CD39 Marks Quiescent Normal Fibroblasts in Murine Tumor Models', *Frontiers in Oncology*, 9(8), pp. 1–13. doi: 10.3389/fonc.2019.00716.

Agrawal, N., Frederick, M. J., Pickering, C. R., Bettegowda, C., Chang, K., Li, R. J., Fakhry, C., Xie, T. X., Zhang, J., Wang, J., Zhang, N., El-Naggar, A. K., Jasser, S. A., Weinstein, J. N., Treviño, L., Drummond, J. A., Muzny, D. M., Wu, Y., Wood, L. D., Hruban, R. H., Myers, J. N. (2011). Exome sequencing of head and neck squamous cell carcinoma reveals inactivating mutations in NOTCH1. *Science*, *333*(6046), pp. 1154–1157. https://doi.org/10.1126/science.1206923.

Ahmad, N., Ammar, A., Storr, S. J., Green, A. R., Rakha, E., Ellis, I. O. and Martin, S. G. (2018) 'IL-6 and IL-10 are associated with good prognosis in early stage invasive breast cancer patients', *Cancer Immunology, Immunotherapy*. Springer Berlin Heidelberg, 67(4), pp. 537–549. doi: 10.1007/s00262-017-2106-8.

Aiuti, A., Cicchini, C., Bernardini, S., Fedele, G., Amicone, L., Fantoni, A. and Tripodi, M. (1998) 'Hematopoietic support and cytokine expression of murine-stable hepatocyte cell lines (MMH)', *Hepatology*, 28(6), pp. 1645–1654. doi: 10.1002/hep.510280626.

Akrish, S. J., Rachmiel, A., Sabo, E., Vered, M. and Ben-Izhak, O. (2017) 'Cancer-associated fibroblasts are an infrequent finding in the microenvironment of proliferative verrucous leukoplakia-associated squamous cell carcinoma', *Journal of Oral Pathology and Medicine*, 46(5), pp. 353–358. doi: 10.1111/jop.12503.

Al-Sahaf, S., Hunter, K. D., Bolt, R., Ottewell, P. D. and Murdoch, C. (2019) 'The IL-1/IL-1R axis induces greater fibroblast-derived chemokine release in human papillomavirus-negative compared to positive oropharyngeal cancer', *International Journal of Cancer*, 144(2), pp. 334–344. doi: 10.1002/ijc.31852.

Alarcon-Martinez, L., Yilmaz-Ozcan, S., Yemisci, M., Schallek, J., Kılıç, K., Can, A., Di Polo, A., & Dalkara, T. (2018). Capillary pericytes express α-smooth muscle actin, which requires prevention of filamentous-actin depolymerization for detection. *eLife*, *7*, e34861. https://doi.org/10.7554/eLife.34861.

Albers, A. E., Qian, X., Kaufmann, A. M. and Coordes, A. (2017) 'Meta analysis: HPV and p16 pattern determines survival in patients with HNSCC and identifies potential new biologic subtype', *Scientific Reports*, 7(1), pp. 1–14. doi: 10.1038/s41598-017-16918-w.

Alphonso, A. and Alahari, S. K. (2009) 'Stromal cells and integrins: Conforming to the needs of the tumor microenvironment', *Neoplasia*, 11(12), pp. 1264–1271. doi: 10.1593/neo.91302.

Alt, E., Welte, G., Li, J., Hennessy, B. T., Devarajan, E., Krishnappa, S., Pinilla, S., Droll, L. and Jotzu, C. (2010) 'Adipose tissue-derived stem cells differentiate into carcinoma-associated fibroblast-like cells under the influence of tumor-derived factors', *Analytical Cellular Pathology*, 33(2), pp. 61–79. doi: 10.3233/ACP-CLO-2010-0535.

Amin, M. B., Greene, F. L., Edge, S. B., Compton, C. C., Gershenwald, J. E., Brookland, R. K., Meyer, L., Gress, D. M., Byrd, D. R. and Winchester, D. P. (2017) 'The Eighth Edition AJCC Cancer Staging Manual: Continuing to build a bridge from a population-based to a more "personalized" approach to cancer staging', *CA: A Cancer Journal for Clinicians*, 67(2), pp. 93–99. doi: 10.3322/caac.21388.

Anderson, C. M., Zhang, B., Miller, M., Butko, E., Wu, X., Laver, T., Kernag, C., Kim, J., Luo, Y., Lamparski, H., Park, E., Su, N. and Ma, X. J. (2016) 'Fully Automated RNAscope In Situ Hybridization Assays for Formalin-Fixed Paraffin-Embedded Cells and Tissues', *Journal of Cellular Biochemistry*, 2208(5), pp. 2201–2208. doi: 10.1002/jcb.25606.

Ang, K. K., Harris, J., Wheeler, R., Weber, R., Rosenthal, D. I., Nguyen-Tân, P. F., Westra, W. H., Chung, C. H., Jordan, R. C., Lu, C., Kim, H., Axelrod, R., Silverman, C. C., Redmond, K. P. and Gillison, M. L. (2010) 'Human Papillomavirus and Survival of Patients with Oropharyngeal Cancer', *New England Journal of Medicine*, 363(1), pp. 24–35. doi: 10.1056/NEJMoa0912217.

Aravind, T., Janardhanan, M., Rakesh, S., Savithri, V., & Unnikrishnan, U. G. (2017). Immunolocalization of osteopontin in dysplasias and squamous cell carcinomas arising from oral epithelium. *Journal of oral and maxillofacial pathology : JOMFP*, *21*(1), pp. 18–23. https://doi.org/10.4103/0973-029X.203764.

Arina, A., Idel, C., Hyjek, E. M., Alegre, M. L., Wang, Y., Bindokas, V. P., Weichselbaum, R. R. and Schreiber, H. (2016) 'Tumor-associated fibroblasts predominantly come from local and not circulating precursors', *Proceedings of the National Academy of Sciences of the United States of America*, 113(27), pp. 7551–7556. doi: 10.1073/pnas.1600363113.

Assidi, M., Gomaa, W., Jafri, M., Hanbazazh, M., Al-Ahwal, M., Pushparaj, P., Al-Harbi, A., Al-Qahtani, M., Buhmeida, A. and Al-Maghrabi, J. (2019) 'Prognostic value of Osteopontin (SPP1) in colorectal carcinoma requires a personalized molecular approach', *Tumor Biology*, 41(9), pp. 1–11. doi: 10.1177/1010428319863627.

Attieh, Y. and Vignjevic, D. M. (2016) 'The hallmarks of CAFs in cancer invasion', *European Journal of Cell Biology*. Elsevier GmbH., 95(11), pp. 493–502. doi: 10.1016/j.ejcb.2016.07.004.

Augsten M. (2014). Cancer-associated fibroblasts as another polarized cell type of the tumor microenvironment. *Frontiers in oncology*, 4(62). https://doi.org/10.3389/fonc.2014.00062.

Avery, D., Govindaraju, P., Jacob, M., Todd, L., Monslow, J. and Puré, E. (2018) 'Extracellular matrix directs phenotypic heterogeneity of activated fibroblasts', *Matrix Biology*. Elsevier B.V., 67, pp. 90–106. doi: 10.1016/j.matbio.2017.12.003.

Avirović, M., Matušan-Ilijaš, K., Damante, G., Fabrro, D., Cerović, R., Juretić, M., Grahovac, B., Jonjić, N. and Lučin, K. (2013) 'Osteopontin expression is an independent factor for poor survival in oral

squamous cell carcinoma: A computer-assisted analysis on TMA sections', *Journal of Oral Pathology and Medicine*, 42(8), pp. 620–626. doi: 10.1111/jop.12055.

Baker, S. J., Fearon, E. R., Nigro, J. M., Hamilton, S. R., Preisinger, A. C., Jessup, J. M., vanTuinen, P., Ledbetter, D. H., Barker, D. F., Nakamura, Y., White, R., & Vogelstein, B. (1989). Chromosome 17 deletions and p53 gene mutations in colorectal carcinomas. *Science. 244*(4901), pp. 217–221. https://doi.org/10.1126/science.2649981.

Bayani, J., & Diamandis, E. P. (2011). The physiology and pathobiology of human kallikrein-related peptidase 6 (KLK6). *Clinical chemistry and laboratory medicine*, *50*(2), pp. 211–233. https://doi.org/10.1515/CCLM.2011.750

Bartoschek, M., Oskolkov, N., Bocci, M., Lövrot, J., Larsson, C., Sommarin, M., Madsen, C. D., Lindgren, D., Pekar, G., Karlsson, G., Ringnér, M., Bergh, J., Björklund, Å. and Pietras, K. (2018) 'Spatially and functionally distinct subclasses of breast cancer-associated fibroblasts revealed by single cell RNA sequencing', *Nature Communications*. Springer US, 9(1). doi: 10.1038/s41467-018-07582-3.

Beaty, B. T., Moon, D. H., Shen, C. J., Amdur, R. J., Weiss, J., Grilley-Olson, J., Patel, S., Zanation, A., Hackman, T. G., Thorp, B., Blumberg, J. M., Patel, S. N., Weissler, M. C., Yarbrough, W. G., Sheets, N. C., Parker, J. S., Hayes, D. N., Weck, K. E., Ramkissoon, L. A., Mendenhall, W. M., Dagan, R., Tan, X., Gupta, G. P. and Chera, B. S. (2020) 'PIK3CA mutation in HPV-associated OPSCC patients receiving deintensified chemoradiation', *Journal of the National Cancer Institute*, 112(8), pp. 855–858. doi: 10.1093/jnci/djz224.

Beausejour, C. M., Krtolica, A., Galimi, F., Narita, M., Lowe, S. W., Yaswen, P. and Campisi, J. (2003) 'Reversal of human cellular senescence: roles of the p53 and p16 pathways', *The EMBO Journal*, 22(16), pp. 4212–4222. doi: 10.1093/emboj/cdg417.

Behera, R., Kumar, V., Lohite, K., Karnik, S. and Kundu, G. C. (2010) 'Activation of JAK2/STAT3 signaling by osteopontin promotes tumor growth in human breast cancer cells', *Carcinogenesis*, 31(2), pp. 192–200. doi: 10.1093/carcin/bgp289.

Benzerdjeb, N., Tantot, J., Blanchet, C., Philouze, P., Mekki, Y., Lopez, J., & Devouassoux-Shisheboran, M. (2021). Oropharyngeal squamous cell carcinoma: p16/p53 immunohistochemistry as a strong predictor of HPV tumor status. *Histopathology*, 10.1111/his.14350. Advance online publication. https://doi.org/10.1111/his.14350.

Berdiel-Acer, M., Sanz-Pamplona, R., Calon, A., Cuadras, D., Berenguer, A., Sanjuan, X., Paules, M. J., Salazar, R., Moreno, V., Batlle, E., Villanueva, A. and Molleví, D. G. (2014) 'Differences between CAFs and their paired NCF from adjacent colonic mucosa reveal functional heterogeneity of CAFs, providing prognostic information', *Molecular Oncology*, 8(7), pp. 1290–1305. doi: 10.1016/j.molonc.2014.04.006.

Berg, T. and Archambault, A. (2010) 'Small-molecule inhibitors of protein–protein interactions', *Protein-Protein Complexes: Analysis, Modeling and Drug Design*, 514, pp. 318–339. doi: 10.1142/9781848163409_0012.

Bernard, H.U., Burk, R. D., Chen, Z., van Doorslaer, K., Hausen, H. zur and de Villiers, E.M. (2010) 'Classification of papillomaviruses (PVs) based on 189 PV types and proposal of taxonomic amendments', *Virology*. Academic Press, 401(1), pp. 70–79. doi: 10.1016/J.VIROL.2010.02.002.

Bhaumik, D., Scott, G. K., Schokrpur, S., Patil, C. K., Orjalo, A. V., Rodier, F., Lithgow, G. J. and Campisi, J. (2009) 'MicroRNAs miR-146a/b negatively modulate the senescence-associated

inflammatory mediators IL-6 and IL-8', *Aging*, 1(4), pp. 402–411. doi: 10.18632/aging.100042.

Bhowmick, N. A., Ghiassi, M., Bakin, A., Aakre, M., Lundquist, C. A., Engel, M. E., Arteaga, C. L. and Moses, H. L. (2001) 'Transforming growth factor-β1 mediates epithelial to mesenchymal transdifferentiation through a RhoA-dependent mechanism', *Molecular Biology of the Cell*, 12(1), pp. 27–36. doi: 10.1091/mbc.12.1.27.

Bhowmick, N.A., Zent, R., Ghiassi, M., McDonnell, M. and Moses, H. L. (2001) 'Integrin β1 Signaling is Necessary for Transforming Growtn Factor-β Activation of p38MAPK and Epithelial Plasticity', *Journal of Biological Chemistry*. 2001 ASBMB. Currently published by Elsevier Inc; originally published by American Society for Biochemistry and Molecular Biology., 276(50), pp. 46707–46713. doi: 10.1074/jbc.M106176200.

Biffi, G., Oni, T. E., Spielman, B., Hao, Y., Elyada, E., Park, Y., Preall, J. and Tuveson, D. A. (2019) 'Il1-induced Jak/STAT signaling is antagonized by TGFβ to shape CAF heterogeneity in pancreatic ductal adenocarcinoma', *Cancer Discovery*, 9(2), pp. 282–301. doi: 10.1158/2159-8290.CD-18-0710.

Biffi, G. and Tuveson, D. A. (2021) 'Diversity and Biology of Cancer-Associated Fibroblasts', *Physiological reviews*, 101(1), pp. 147–176. doi: 10.1152/physrev.00048.2019.

Bishop, J. A. (2015) 'Histopathology of human papillomavirus-related oropharyngeal carcinoma: a review of classic and variant forms', *Diagnostic Histopathology*, 21, pp. 70–76. doi: 10.1016/j.mpdhp.2015.02.001.

Bishop, J. A., Ma, X. J., Wang, H., Luo, Y., Illei, P. B., Begum, S., Taube, J. M., Koch, W. M. and Westra, W. H. (2012) 'Detection of transcriptionally active high-risk HPV in patients with head and neck squamous cell carcinoma as visualized by a novel E6/E7 mRNA in situ hybridization method', *American Journal of Surgical Pathology*, 36(12), pp. 1874–1882. doi: 10.1097/PAS.0b013e318265fb2b.

Blagosklonny, M. V. (2012) 'Cell cycle arrest is not yet senescence, which is not just cell cycle arrest: Terminology for TOR-driven aging', *Aging*, 4(3), pp. 159–165. doi: 10.18632/aging.100443.

Bolt, R. (2016) *Novel Biomarkers in the Management of HPV-Positive & -Negative Oropharyngeal Carcinoma*. Ph.D, University of Sheffield.

Bolt, R., Foran, B., Murdoch, C., Lambert, D. W., Thomas, S. and Hunter, K. D. (2018) 'HPV-negative, but not HPV-positive, oropharyngeal carcinomas induce fibroblasts to support tumour invasion through micro-environmental release of HGF and IL-6', *Carcinogenesis*, 39(2), pp. 170–179. doi: 10.1093/carcin/bgx130.

Borgoño, C. A. and Diamandis, E. P. (2004) 'The emerging roles of human tissue kallikreins in cancer', *Nature Reviews Cancer*, 4(11), pp. 876–890. doi: 10.1038/nrc1474.

Bourassa, B., Monaghan, S., & Rittling, S. R. (2004). Impaired anti-tumor cytotoxicity of macrophages from osteopontin-deficient mice. *Cellular immunology*, *227*(1), pp. 1–11. https://doi.org/10.1016/j.cellimm.2004.01.001.

Bouvard, V., Baan, R., Straif, K., Grosse, Y., Secretan, B., El Ghissassi, F., Benbrahim-Tallaa, L., Guha, N., Freeman, C., Galichet, L. and Cogliano, V. (2009) 'A review of human carcinogens--Part B: biological agents.', *The lancet oncology*, 10(4), pp. 321–322. doi: 10.1016/s1470-2045(09)70096-8.

Bova, R. J., Quinn, D. I., Nankervis, J. S., Cole, I. E., Sheridan, B. F., Jensen, M. J., Morgan, G. J. and Hughes, C. J. (2001) 'Cyclin D1 expression predicts reduced survival in early stage carcinoma of the

anterior tongue', *Australian Journal of Otolaryngology*, 4(1), pp. 41–46.

Bozõky, B., Savchenko, A., Csermely, P., Korcsmáros, T., Dúl, Z., Pontén, F., Székely, L. and Klein, G. (2013) 'Novel signatures of cancer-associated fibroblasts', *International Journal of Cancer*, 133(2), pp. 286–293. doi: 10.1002/ijc.28035.

Braakhuis, B. J., Snijders, P. J., Keune, W. J., Meijer, C. J., Ruijter-Schippers, H. J., Leemans, C. R. and Brakenhoff, R. H. (2004) 'Genetic patterns in head and neck cancers that contain or lack transcriptionally active human papillomavirus', *Journal of the National Cancer Institute*, 96(13), pp. 998–1006. doi: 10.1093/jnci/djh183.

Bramwell, V. H, Doig, G. S., Tuck, A. B., Wilson, S. M., Tonkin, K. S., Tomiak, A., Perera, F., Vandenberg, T. A. and Chambers, A. F. (2006) 'Serial plasma osteopontin levels have prognostic value in metastatic breast cancer', *Clinical Cancer Research*, 12(11 I), pp. 3337–3343. doi: 10.1158/1078-0432.CCR-05-2354.

Bray, F., Ferlay, J. and Soerjomataram, I. (2018) 'Global Cancer Statistics 2018 : GLOBOCAN Estimates of Incidence and Mortality Worldwide for 36 Cancers in 185 Countries', pp. 394–424. doi: 10.3322/caac.21492.

Brechbuhl, H. M., Finlay-Schultz, J., Yamamoto, T. M., Gillen, A. E., Cittelly, D. M., Tan, A. C., Sams, S. B., Pillai, M. M., Elias, A. D., Robinson, W. A., Sartorius, C. A. and Kabos, P. (2017) 'Fibroblast subtypes regulate responsiveness of luminal breast cancer to estrogen', *Clinical Cancer Research*, 23(7), pp. 1710–1721. doi: 10.1158/1078-0432.CCR-15-2851.

Brown, L. F., Berse, B., Water, L. Van De, Papadopoulos-sergiou, A., Perruzzi, C. A., Manseau, E. J., Dvorak, H. F. and Senger, D. R. (1992) 'Expression and Distribution of Osteopontin in Human Tissues : Widespread Association with Luminal Epithelial Surfaces', 3(10), pp. 1169–1180.

Brown, L. F., Papadopoulos-Sergiou, A., Berse, B., Manseau, E. J., Tognazzi, K., Perruzzi, C. A., Dvorak, H. F., & Senger, D. R. (1994). Osteopontin expression and distribution in human carcinomas. *The American journal of pathology*, 145(3), pp. 610–623.

Budu, V. A., Decuseară, T., Balica, N. C., Mogoantă, C. A., Rădulescu, L. M., Chirilă, M., Maniu, A. A., Mistra, D. M., Muşat, G. C., Oprişcan, I. C. and Georgescu, M. G. (2019) 'The role of hpv infection in oropharyngeal cancer', *Romanian Journal of Morphology and Embryology*, 60(3), pp. 769–773.

Burd, E. M. (2003) 'Human papillomavirus and cervical cancer', *Clinical Microbiology Reviews*, 16(1), pp. 1–17. doi: 10.1128/CMR.16.1.1-17.2003.

Burk, R. D., Chen, Z., Harari, A., Smith, B. C., Kocjan, B. J., Maver, P. J. and Poljak, M. (2011) 'Classification and nomenclature system for Human Alphapapillomavirus variants: general features, nucleotide landmarks and assignment of HPV6 and HPV11 isolates to variant lineages', *Acta Dermatovenrol Alip Panonica Adriat*, 20(3), pp. 113–123.

Byers, L. A., Holsinger, F. C., Kies, M. S., William, W. N., El-naggar, A. K., Lee, J. J., Hu, J., Lopez, A., Tran, H. T., Du, Z., Ang, K. K., Glisson, B. S., Raso, M. G., Ignacio, I., Myers, J. N., Hong, W., Papadimitrakopoulou, V., Scott, M. and Heymach, J. V (2011) 'Serum signature of hypoxia-regulated factors is associated with progression after induction therapy in head and neck squamous cell cancer', 9(6), pp. 1755–1763. doi: 10.1158/1535-7163.MCT-09-1047.Serum.

Bzhalava, D., Eklund, C., & Dillner, J. (2015). International standardization and classification of human papillomavirus types. *Virology*, *476*, pp. 341–344. https://doi.org/10.1016/j.virol.2014.12.028.

Caja, L., Dituri, F., Mancarella, S., Caballero-Diaz, D., Moustakas, A., Giannelli, G. and Fabregat, I. (2018) 'TGF-β and the tissue microenvironment: Relevance in fibrosis and cancer', *International Journal of Molecular Sciences*, 19(5). doi: 10.3390/ijms19051294.

Cajone, F. and Sherbet, G. V. (1999) 'Stathmin is involved in S100A4-mediated regulation of cell cycle progression', *Clinical and Experimental Metastasis*, 17(10), pp. 865–871. doi: 10.1023/A:1006778804532.

Camussi, G., Deregibus, M. C., Bruno, S., Cantaluppi, V. and Biancone, L. (2010) 'Exosomes / microvesicles as a mechanism of cell-to-cell communication', *Kidney International*. Elsevier Masson SAS, 78(9), pp. 838–848. doi: 10.1038/ki.2010.278.

Cantor, H. and Shinohara, M. L. (2009) 'Regulation of T-helper-cell lineage development by osteopontin: The inside story', *Nature Reviews Immunology*, 9(2), pp. 137–141. doi: 10.1038/nri2460.

Carpén, T., Saarilahti, K., Haglund, C., Markkola, A., Tarkkanen, J., Hagström, J., Mattila, P., & Mäkitie, A. (2018). Tumor volume as a prognostic marker in p16-positive and p16-negative oropharyngeal cancer patients treated with definitive intensity-modulated radiotherapy. *Comparative Study*. *194*(8), pp. 759–770. https://doi.org/10.1007/s00066-018-1309-z.

Castello, L. M., Raineri, D., Salmi, L., Clemente, N., Vaschetto, R., Quaglia, M., Garzaro, M., Gentilli, S., Navalesi, P., Cantaluppi, V., Dianzani, U., Aspesi, A., & Chiocchetti, A. (2017). Osteopontin at the Crossroads of Inflammation and Tumor Progression. *Mediators of inflammation*, *2017*, 4049098. https://doi.org/10.1155/2017/4049098

Celetti, A., Testa, D., Staibano, S., Merolla, F., Guarino, V., Castellone, M. D., Iovine, R., Mansueto, G., Somma, P., De Rosa, G., Galli, V., Melillo, R. M. and Santoro, M. (2005) 'Overexpression of the cytokine osteopontin identifies aggressive laryngeal squamous cell carcinomas and enhances carcinoma cell proliferation and invasiveness', *Clinical Cancer Research*, 11(22), pp. 8019–8027. doi: 10.1158/1078-0432.CCR-05-0641.

Chakraborty, D., Viveka, T. S., Arvind, K., Shyamsundar, V., Kanchan, M., Alex, S. A., Chandrasekaran, N., Vijayalakshmi, R., & Mukherjee, A. (2018). A facile gold nanoparticle-based ELISA system for detection of osteopontin in saliva: Towards oral cancer diagnostics. *Clinica chimica acta; international journal of clinical chemistry*, 477, pp. 166–172. https://doi.org/10.1016/j.cca.2017.09.009.

Chan, P. K., Luk, A. C., Park, J. S., Smith-McCune, K. K., Palefsky, J. M., Konno, R., Giovannelli, L., Coutlée, F., Hibbitts, S., Chu, T. Y., Settheetham-Ishida, W., Picconi, M. A., Ferrera, A., De Marco, F., Woo, Y. L., Raiol, T., Piña-Sánchez, P., Cheung, J. L., Bae, J. H., Chirenje, M. Z., Banks, L. (2011). Identification of human papillomavirus type 58 lineages and the distribution worldwide. *The Journal of infectious diseases*, 203(11), pp.1565–1573. https://doi.org/10.1093/infdis/jir157.

Chandrasekhar, S., Sorrentino, J. A. and Millis, A. J. (1983) 'Interaction of fibronectin with collagen: age-specific defect in the biological activity of human fibroblast fibronectin.', *Proceedings of the National Academy of Sciences of the United States of America*, 80(15), pp. 4747–4751. doi: 10.1073/pnas.80.15.4747.

Chang, P., Harkins, L., Hsieh, Y., Hicks, P., Sappayatosok, K., Yodsanga, S., Swasdison, S., Chambers, A. F., Elmets, C. A. and Ho, K. (2008) 'Osteopontin Expression in Normal Skin and Non-melanoma Skin Tumors The Journal of Histochemistry & Cytochemistry', 56(1), pp. 57–66. doi: 10.1369/jhc.7A7325.2007.

Chaudhri, V. K., Salzler, G. G., Dick, S. A., Buckman, M. S., Sordella, R., Karoly, E. D., Mohney, R.,

Stiles, B. M., Elemento, O., Altorki, N. K., & McGraw, T. E. (2013). Metabolic alterations in lung cancer-associated fibroblasts correlated with increased glycolytic metabolism of the tumor. *Molecular cancer research : MCR*, *11*(6), 579–592. https://doi.org/10.1158/1541-7786.MCR-12-0437-T.

Che, C., Liu, J., Yang, J., Ma, L., Bai, N. and Zhang, Q. (2018) 'Osteopontin is essential for IL-1β production and apoptosis in peri-implantitis', *Clinical Implant Dentistry and Related Research*, 20(3), pp. 384–392. doi: 10.1111/cid.12592.

Chen, C., Zhao, S., Karnad, A. and Freeman, J. W. (2018) 'The biology and role of CD44 in cancer progression: Therapeutic implications', *Journal of Hematology and Oncology*. Journal of Hematology & Oncology, 11(1), pp. 1–23. doi: 10.1186/s13045-018-0605-5.

Chen, J., Yang, P., Xiao, Y., Zhang, Y., Liu, J., Xie, D., Cai, M. and Zhang, X. (2017) 'Overexpression of α-sma-positive fibroblasts (CAFs) in nasopharyngeal Carcinoma predicts poor prognosis', *Journal of Cancer*, 8(18), pp. 3897–3902. doi: 10.7150/jca.20324.

Chen, J., Zhou, J., Lu, J., Xiong, H., Shi, X. and Gong, L. (2014) 'Significance of CD44 expression in head and neck cancer: A systemic review and meta-analysis', *BMC Cancer*, 14(1), pp. 1–9. doi: 10.1186/1471-2407-14-15.

Chen, L., Mayer, J. A., Krisko, T. I., Speers, C. W., Wang, T., Hilsenbeck, S. G. and Brown, P. H. (2009) 'Inhibition of the p38 kinase suppresses the proliferation of human ER-negative breast cancer cells', *Cancer Research*, 69(23), pp. 8853–8861. doi: 10.1158/0008-5472.CAN-09-1636.

Chen, S. Y., Massa, S., Mazul, A. L., Kallogjeri, D., Yaeger, L., Jackson, R. S., Zevallos, J. and Pipkorn, P. (2020) 'The association of smoking and outcomes in HPV-positive oropharyngeal cancer: A systematic review', *American Journal of Otolaryngology - Head and Neck Medicine and Surgery*. Elsevier, 41(5), p. 102592. doi: 10.1016/j.amjoto.2020.102592.

Chen, W, J., Li, C., Pierson, C. R., Finlay, J. L. and Lin, J. (2018) 'Blocking interleukin-6 signaling inhibits cell viability/proliferation, glycolysis, and colony forming activity of human medulloblastoma cells', *International Journal of Oncology*, 52(2), pp. 571–578. doi: 10.3892/ijo.2017.4211.

Chen, X., Luther, G., Zhang, W., Nan, G., Wagner, E. R., Liao, Z., Wu, N., Zhang, H., Wang, N., Wen, S., He, Y., Deng, F., Zhang, J., Wu, D., Zhang, B., Haydon, R. C., Zhou, L., Luu, H. H. and He, T. C. (2013) 'The E-F hand calcium-binding protein s100a4 regulates the proliferation, survival and differentiation potential of human osteosarcoma cells', *Cellular Physiology and Biochemistry*, 32(4), pp. 1083–1096. doi: 10.1159/000354508.

Chen, X. and Thibeault, S. (2012a) 'Cell–cell interaction between vocal fold fibroblasts and bone marrow mesenchymal stromal cells in three-dimensional hyaluronan hydrogel', *Physiology & behavior*, 176(1), pp. 100–106. doi: 10.1002/term.1757.Cell.

Chen, X and Thibeault, S. L. (2012b) 'Response of fibroblasts to transforming growth factor-β1 on two-dimensional and in three-dimensional hyaluronan hydrogels', *Tissue Engineering - Part A*, 18(23–24), pp. 2528–2538. doi: 10.1089/ten.tea.2012.0094.

Chen, Y. W., Chen, K. H., Huang, P. I., Chen, Y. C., Chiou, G. Y., Lo, W. L., Tseng, L. M., Hsu, H. S., Chang, K. W. and Chiou, S. H. (2010) 'Cucurbitacin I suppressed stem-like property and enhanced radiation-induced apoptosis in head and neck squamous carcinoma-derived CD44 +ALDH1+ cells', *Molecular Cancer Therapeutics*, 9(11), pp. 2879–2892. doi: 10.1158/1535-7163.MCT-10-0504.

Chien, C. Y., Su, C. Y., Chuang, H. C., Fang, F. M., Huang, H. Y., Chen, C. M., Chen, C. H., & Huang, C. C. (2008). Clinical significance of osteopontin expression in T1 and T2 tongue cancers. *Head & neck*, 30(6), pp. 776–781.https://doi.org/10.1002/hed.20783.

Chien, C., Su, C., Chuang, H., Fang, F. and Huang, H. (2009) 'Comprehensive study on the prognostic role of osteopontin expression in oral squamous cell carcinoma', *Oral Oncology*. Elsevier Ltd, 45(9), pp. 798–802. doi: 10.1016/j.oraloncology.2008.12.006.

Chien, Y., Scuoppo, C., Wang, X., Fang, X., Balgley, B., Bolden, J. E., Premsrirut, P., Luo, W., Chicas, A., Lee, C. S., Kogan, S. C. and Lowe, S. W. (2011) 'Control of the senescence-associated secretory phenotype by NF-κB promotes senescence and enhances chemosensitivity', *Genes and Development*, 25(20), pp. 2125–2136. doi: 10.1101/gad.17276711.

Chiu, Y., Tu, H., Wang, I., Wu, C., Chang, K. and Liu, T. (2010) 'The implication of osteopontin (OPN) expression and genetic polymorphisms of OPN promoter in oral carcinogenesis', *Oral Oncology*. Elsevier Ltd, 46(4), pp. 302–306. doi: 10.1016/j.oraloncology.2010.01.018.

Cho, H., Hong, S. W., Oh, Y. J., Kim, M. A., Kang, E. S., Lee, J. M., Kim, S. W., Kim, S. H., Kim, J. H., Kim, Y. T., & Lee, K. (2008). Clinical significance of osteopontin expression in cervical cancer. *Journal of cancer research and clinical oncology*, 134(8), pp. 909–917. https://doi.org/10.1007/s00432-007-0351-5.

Choudhary, M. M., France, T. J., Teknos, T. N. and Kumar, P. (2016) 'Interleukin-6 role in head and neck squamous cell carcinoma progression Production and Hosting by Elsevier on behalf of KeAi', *World Journal of Otorhinolaryngology-Head and Neck Surgery*, 2, pp. 90–97. doi: 10.1016/j.wjorl.2016.05.002.

Christensen, B., Petersen, T. E. and Sørensen, E. S. (2008) 'Post-translational modification and proteolytic processing of urinary osteopontin', *Biochemical Journal*, 411(1), pp. 53–61. doi: 10.1042/BJ20071021.

Chu, A., Genden, E., Posner, M. and Sikora, A. (2013) 'A patient-centered approach to counseling patients with head and neck cancer undergoing human papillomavirus testing: a clinician's guide.', *The oncologist*. AlphaMed Press, 18(2), pp. 180–9. doi: 10.1634/theoncologist.2012-0200.

Cirri, P., & Chiarugi, P. (2011). Cancer associated fibroblasts: the dark side of the coin. *American journal of cancer research*, *1*(4), pp. 482–497.

Cirri, P. and Chiarugi, P. (2012) 'Cancer-associated-fibroblasts and tumour cells: A diabolic liaison driving cancer progression', *Cancer and Metastasis Reviews*, 31(1–2), pp. 195–208. doi: 10.1007/s10555-011-9340-x.

Clemente, N., Raineri, D., Cappellano, G., Boggio, E., Favero, F., Soluri, M., Dianzani, C., Comi, C., Dianzani, U. and Chiocchetti, A., 2016. Osteopontin Bridging Innate and Adaptive Immunity in Autoimmune Diseases. *Journal of Immunology Research*, 2016, pp.1-15.

Cohen, E. R., Reis, I. M., Gomez, C., Pereira, L., Freiser, M. E., Hoosien, G. and Franzmann, E. J. (2017) 'Immunohistochemistry Analysis of CD44, EGFR, and p16 in Oral Cavity and Oropharyngeal Squamous Cell Carcinoma', *Otolaryngology - Head and Neck Surgery (United States)*, 157(2), pp. 239–251. doi: 10.1177/0194599817700371.

Collins, A. L., Rock, J., Malhotra, L., Frankel, W. L. and Bloomston, M. (2012) 'Osteopontin Expression is Associated with Improved Survival in Patients with Pancreatic Adenocarcinoma', *Bone*, 23(1), pp. 1–7. doi: 10.1245/s10434-012-2337-z.Osteopontin.

Comito, G., Giannoni, E., Segura, C. P., Barcellos-De-Souza, P., Raspollini, M. R., Baroni, G., Lanciotti, M., Serni, S. and Chiarugi, P. (2014) 'Cancer-associated fibroblasts and M2-polarized macrophages synergize during prostate carcinoma progression', *Oncogene*. Nature Publishing Group, 33(19), pp. 2423–2431. doi: 10.1038/onc.2013.191.

Coppé, J.P., Desprez, P.Y., Krtolica, A. and Campisi, J. (2010) 'The Senescence-Associated Secretory Phenotype: The Dark Side of Tumor Suppression', *Annual Review of Pathology: Mechanisms of Disease*, 5(1), pp. 99–118. doi: 10.1146/annurev-pathol-121808-102144.

Coppé, J.P., Patil, C. K., Rodier, F., Sun, Y., Muñoz, D. P., Goldstein, J., Nelson, P. S., Desprez, P.-Y. and Campisi, J. (2008) 'Senescence-Associated Secretory Phenotypes Reveal Cell-Nonautonomous Functions of Oncogenic RAS and the p53 Tumor Suppressor', *PLoS Biology*. Edited by J. Downward. Public Library of Science, 6(12), p. e301. doi: 10.1371/journal.pbio.0060301.

Coppola, D., Szabo, M., Boulware, D., Muraca, P., Alsarraj, M., Chambers, A. F., & Yeatman, T. J. (2004). Correlation of osteopontin protein expression and pathological stage across a wide variety of tumor histologies. *Clinical cancer research: an official journal of the American Association for Cancer Research*, 10(11), pp. 184–190. https://doi.org/10.1158/1078-0432.ccr-1405-2.

Corey, A. S. and Hudgins, P. A. (2012) 'Radiographic Imaging of Human Papillomavirus Related Carcinomas of the Oropharynx', *Head and Neck Pathology*, 6(S1), pp. 25–40. doi: 10.1007/s12105-012-0374-3.

Costa, A., Kieffer, Y., Scholer-Dahirel, A., Pelon, F., Bourachot, B., Cardon, M., Sirven, P., Magagna, I., Fuhrmann, L., Bernard, C., Bonneau, C., Kondratova, M., Kuperstein, I., Zinovyev, A., Givel, A. M., Parrini, M. C., Soumelis, V., Vincent-Salomon, A. and Mechta-Grigoriou, F. (2018) 'Fibroblast Heterogeneity and Immunosuppressive Environment in Human Breast Cancer', *Cancer Cell*. Elsevier, 33(3), pp. 463-479.e10. doi: 10.1016/j.ccell.2018.01.011.

Costa, A., Scholer-Dahirel, A. and Mechta-Grigoriou, F. (2014) 'The role of reactive oxygen species and metabolism on cancer cells and their microenvironment', *Seminars in Cancer Biology*. Elsevier Ltd, 25, pp. 23–32. doi: 10.1016/j.semcancer.2013.12.007.

Costea, D. E., Hills, A., Osman, A. H., Thurlow, J., Kalna, G., Huang, X., Murillo, C. P., Parajuli, H., Suliman, S., Kulasekara, K. K., Johannessen, A. C. and Partridge, M. (2013) 'Identification of two distinct carcinoma-associated fibroblast subtypes with differential tumor-promoting abilities in oral squamous cell carcinoma', *Cancer Research*, 73(13), pp. 3888–3901. doi: 10.1158/0008-5472.CAN-12-4150.

Courter, D., Cao, H., Kwok, S., Kong, C., Banh, A., Kuo, P., Bouley, D. M., Vice, C., Brustugun, O. T., Denko, N. C., Koong, A. C., Giaccia, A. and Le, Q. T. (2010) 'The RGD domain of human osteopontin promotes tumor growth and metastasis through activation of survival pathways', *PLoS ONE*, 5(3). doi: 10.1371/journal.pone.0009633.

Craig, S. G., Anderson, L. A., Moran, M., Graham, L., Currie, K., Rooney, K., Robinson, M., Bingham, V., Cuschieri, K. S., McQuaid, S., Schache, A. G., Jones, T. M., McCance, D., Salto-Tellez, M., McDade, S. S. and James, J. A. (2020) 'Comparison of molecular assays for HPV testing in oropharyngeal squamous cell carcinomas: A population-based study in Northern Ireland', *Cancer Epidemiology Biomarkers and Prevention*, 29, pp. 31–38. doi: 10.1158/1055-9965.EPI-19-0538.

Craig, S. G., Anderson, L. A., Schache, A. G., Moran, M., Graham, L., Currie, K., Rooney, K., Robinson, M., Upile, N. S., Brooker, R., Mesri, M., Bingham, V., McQuaid, S., Jones, T., McCance, D. J., Salto-Tellez, M., McDade, S. S. and James, J. A. (2019) 'Recommendations for determining HPV status in patients with oropharyngeal cancers under TNM8 guidelines: a two-tier approach', *British Journal of*

Cancer. Springer US, 120(8), pp. 827–833. doi: 10.1038/s41416-019-0414-9.

Crawford, H. C., Matrisian, L. M., & Liaw, L. (1998). Distinct roles of osteopontin in host defense activity and tumor survival during squamous cell carcinoma progression in vivo. *Cancer research*, *58*(22), 5206–5215.

Custódio, M., Biddle, A. and Tavassoli, M. (2020) 'Portrait of a CAF: The story of cancer-associated fibroblasts in head and neck cancer', *Oral Oncology*. Elsevier, 110(8), pp. 104972. doi: 10.1016/j.oraloncology.2020.104972.

Cuthbert, A. P., Bond, J., Trott, D. A., Gill, S., Broni, J., Marriott, A., Khoudoli, G., Parkinson, E. K., Cooper, C. S. and Newbold, R. F. (1999) 'Telomerase repressor sequences on chromosome 3 and induction of permanent growth arrest in human breast cancer cells', *Journal of the National Cancer Institute*, 91(1), pp. 37–45. doi: 10.1093/jnci/91.1.37.

D'Souza, G., Kreimer, A. R., Viscidi, R., Pawlita, M., Fakhry, C., Koch, W. M., Westra, W. H. and Gillison, M. L. (2007) 'Case–Control Study of Human Papillomavirus and Oropharyngeal Cancer', *New England Journal of Medicine*, 356(19), pp. 1944–1956. doi: 10.1056/NEJMoa065497.

Dai, J., Peng, L., Fan, K., Wang, H., Wei, R., Ji, G., Cai, J., Lu, B., Li, B., Zhang, D., Kang, Y., Tan, M., Qian, W. and Guo, Y. (2009) 'Osteopontin induces angiogenesis through activation of PI3K/AKT and ERK1/2 in endothelial cells', *Oncogene*, 28(38), pp. 3412–3422. doi: 10.1038/onc.2009.189.

Dangi-Garimella, S., Krantz, S. B., Barron, M. R., Shields, M. A., Heiferman, M. J., Grippo, P. J., Bentrem, D. J. and Munshi, H. G. (2011) 'Three-dimensional collagen I promotes gemcitabine resistance in pancreatic cancer through MT1-MMP-mediated expression of HMGA2', *Cancer Research*, 71(3), pp. 1019–1028. doi: 10.1158/0008-5472.CAN-10-1855.

Dangi-Garimella, S., Sahai, V., Ebine, K., Kumar, K. and Munshi, H. G. (2013) 'Three-Dimensional Collagen I Promotes Gemcitabine Resistance In Vitro in Pancreatic Cancer Cells through HMGA2-Dependent Histone Acetyltransferase Expression', *PLoS ONE*, 8(5), pp. 1–9. doi: 10.1371/journal.pone.0064566.

Danos, O., Katinka, M., & Yaniv, M. (1982). Human papillomavirus 1a complete DNA sequence: a novel type of genome organization among papovaviridae. *The EMBO journal*, *1*(2), pp.231–236.

Danzaki, K., Kanayama, M., Alcazar, O. and Shinohara, M., 2016. Osteopontin has a protective role in prostate tumor development in mice. *European Journal of Immunology*, 46(11), pp.2669-2678.

Darling, M. R., Jackson-Boeters, L., Daley, T. D. and Diamandis, E. P. (2006) 'Human kallikrein 6 expression in salivary gland tumors', *Journal of Histochemistry and Cytochemistry*, 54(3), pp. 337–342. doi: 10.1369/jhc.5A6803.2005.

Davidson, S., Efremova, M., Riedel, A., Mahata, B., Pramanik, J., Huuhtanen, J., Kar, G., Vento-Tormo, R., Hagai, T., Chen, X., Haniffa, M. A., Shields, J. D. and Teichmann, S. A. (2020) 'Single-Cell RNA Sequencing Reveals a Dynamic Stromal Niche That Supports Tumor Growth', *Cell Reports*. ElsevierCompany., 31(7), pp. 107628. doi: 10.1016/j.celrep.2020.107628.

Demaria, M., O'Leary, M. N., Chang, J., Shao, L., Liu, S., Alimirah, F., Koenig, K., Le, C., Mitin, N., Deal, A. M., Alston, S., Academia, E. C., Kilmarx, S., Valdovinos, A., Wang, B., De Bruin, A., Kennedy, B. K., Melov, S., Zhou, D., Sharpless, N. E., Muss, H. and Campisi, J. (2017) 'Cellular senescence promotes adverse effects of chemotherapy and cancer relapse', *Cancer Discovery*, 7(2), pp. 165–176.

doi: 10.1158/2159-8290.CD-16-0241.

Denhardt, D. T., Noda, M., O'Regan, A. W., Pavlin, D. and Berman, J. S. (2001) 'Osteopontin as a means to cope with environmental insults: Regulation of inflammation, tissue remodeling, and cell survival', *Journal of Clinical Investigation*, 107(9), pp. 1055–1061. doi: 10.1172/JCI12980.

Desai, B., Rogers, M. J. and Chellaiah, M. A. (2007) 'Mechanisms of osteopontin and CD44 as metastatic principles in prostate cancer cells', *Molecular Cancer*, 6, pp. 1–16. doi: 10.1186/1476-4598-6-18.

Desai, V. D., Hsia, H. C. and Schwarzbauer, J. E. (2014) 'Reversible modulation of myofibroblast differentiation in adipose-derived mesenchymal stem cells', *PLoS ONE*, 9(1), pp. 1–12. doi: 10.1371/journal.pone.0086865.

Desmouliere, A., Geinoz, A., Gabbiani, F. and Gabbiani, G. (1993) 'Transforming growth factor-β1 induces α-smooth muscle actin expression in granulation tissue myofibroblasts and in quiescent and growing cultured fibroblasts', *Journal of Cell Biology*, 122(1), pp. 103–111. doi: 10.1083/jcb.122.1.103.

Desmouliere, A., Redard, M., Darby, I. and Gabbiani, G. (1995) 'Apoptosis mediates the decrease in cellularity during the transition between granulation tissue and scar', *American Journal of Pathology*, 146(1), pp. 56–66.

Dickstein, D. R., Egerman, M. A., Bui, A. H., Doucette, J. T., Sharma, S., Liu, J., Gupta, V., Miles, B. A., Genden, E., Westra, W. H., Misiukiewicz, K., Posner, M. R., & Bakst, R. L. (2020). A new face of the HPV epidemic: Oropharyngeal cancer in the elderly. *Oral oncology*, *109*, 104687. Advance online publication. https://doi.org/10.1016/j.oraloncology.2020.104687.

Dimri, G., Lee, X., Basile, G., Acosta, M., Scott, G., Roskelley, C., Medrano, E., Linskens, M., Rubelj, I. and Pereira-Smith, O., 1995. A biomarker that identifies senescent human cells in culture and in aging skin in vivo. *Proceedings of the National Academy of Sciences*, 92(20), pp.9363-9367.

Dionísio de Sousa, I. J., Marques, D. S., Príncipe, C., Portugal, R. V., Canberk, S., Prazeres, H., Lopes, J. M., Gimba, E., Lima, R. T., & Soares, P. (2020). Predictive Biomarkers and Patient Outcome in Platinum-Resistant (PLD-Treated) Ovarian Cancer. *Diagnostics (Basel, Switzerland)*, 10(8), 525. https://doi.org/10.3390/diagnostics10080525.

Dourado, M. R., Guerra, E. N. S., Salo, T., Lambert, D. W. and Coletta, R. D. (2018) 'Prognostic value of the immunohistochemical detection of cancer-associated fibroblasts in oral cancer: A systematic review and meta-analysis', *Journal of Oral Pathology and Medicine*, 47(5), pp. 443–453. doi: 10.1111/jop.12623.

Driver, J., Weber, C., Callaci, J., Kothari, A., Zapf, M., Roper, P., Borys, D., Franzen, C., Gupta, G., Wai, P., Zhang, J., Denning, M., Kuo, P. and Mi, Z., 2015. Alcohol Inhibits Osteopontin-dependent Transforming Growth Factor-β1 Expression in Human Mesenchymal Stem Cells. *Journal of Biological Chemistry*, 290(16), pp.9959-9973.

Druelle, C., Drullion, C., Deslé, J., Martin, N., Saas, L., Cormenier, J., Malaquin, N., Huot, L., Slomianny, C., Bouali, F., Vercamer, C., Hot, D., Pourtier, A., Chevet, E., Abbadie, C. and Pluquet, O. (2016) 'ATF6a regulates morphological changes associated with senescence in human fibroblasts', *Oncotarget*, 7(42), pp. 67699–67715. doi: 10.18632/oncotarget.11505.

Dulauroy, S., Di Carlo, S. E., Langa, F., Eberl, G. and Peduto, L. (2012) 'Lineage tracing and genetic

ablation of ADAM12 + perivascular cells identify a major source of profibrotic cells during acute tissue injury', *Nature Medicine*, 18(8), pp. 1262–1270. doi: 10.1038/nm.2848.

Ecis.jrc.ec.europa.eu. 2021. *European Cancer Information System*. [online] Available at: <https://ecis.jrc.ec.europa.eu/explorer.php?$0-0$1-All$2-All$4-1,2$3-66$6-0,85$5-2008,2008$7-7$CEstByCountry$X0_8-3$X0_19-AE27$X0_20-No$CEstBySexByCountry$X1_8-3$X1_19-AE27$X1_-1-1$CEstByIndiByCountry$X2_8-3$X2_19-AE27$X2_20-No$CEstRelative$X3_8-3$X3_9-AE27$X3_19-AE27$CEstByCountryTable$X4_19-AE27> [Accessed 20 March 2021].

Elkabets, M., Gifford, A. M., Scheel, C., Nilsson, B., Reinhardt, F., Bray, M. A., Carpenter, A. E., Jirström, K., Magnusson, K., Ebert, B. L., Pontén, F., Weinberg, R. A. and McAllister, S. S. (2011) 'Human tumors instigate granulin-expressing hematopoietic cells that promote malignancy by activating stromal fibroblasts in mice', *Journal of Clinical Investigation*, 121(2), pp. 784–799. doi: 10.1172/JCI43757.

Elmusrati, A., 2020. *The Role of Cancer Associated Fibroblasts in Bone Invasive Oral Squamous Cell Carcinoma*. Ph.D. University of Sheffield.

Elmusrati, A. A., Pilborough, A. E., Khurram, S. A. and Lambert, D. W. (2017) 'Cancer-associated fibroblasts promote bone invasion in oral squamous cell carcinoma', *British Journal of Cancer*. Nature Publishing Group, 117(6), pp. 867–875. doi: 10.1038/bjc.2017.239.

El-Naggar AK, Chan JKC, Grandis JR, Slootweg PJ. WHO Classification of Head and Neck Tumours. (2017) ISBN: 9789283224389.

Erez, N., Truitt, M., Olson, P. and Hanahan, D. (2009) 'Cancer-Associated Fibroblasts Are Activated in Incipient Neoplasia to Orchestrate Tumor-Promoting Inflammation in an NF-κB-Dependent Manner', *Cancer Cell*, 17, pp. 135–147. doi: 10.1016/j.ccr.2009.12.041.

Erkvliet, N. K., Aad, Z. S., Oig, G. S. D. and Hambers, A. F. C. (1998) 'Osteopnotin in expression in a group of lymph node negative breast cancer patients', *Human Cancer.* 79(5), pp. 502–508. doi:10.1002/(SICI)1097-0215(19981023)79.

Evans, M., Newcombe, R., Fiander, A., Powell, J., Rolles, M., Thavaraj, S., Robinson, M., & Powell, N. (2013). Human Papillomavirus-associated oropharyngeal cancer: an observational study of diagnosis, prevalence and prognosis in a UK population. *BMC cancer*, *13*, 220. https://doi.org/10.1186/1471-2407-13-220.

Eyden, B., Banerjee, S. S., Shenjere, P. and Fisher, C. (2009) 'The myofibroblast and its tumours', *Journal of Clinical Pathology*, 62(3), pp. 236–249. doi: 10.1136/jcp.2008.061630.

Fafián-Labora, J. A. and O'Loghlen, A. (2020) 'Classical and Nonclassical Intercellular Communication in Senescence and Ageing', *Trends in Cell Biology*, 30(8), pp. 628–639. doi: 10.1016/j.tcb.2020.05.003.

Fakhry, C., Lacchetti, C., Rooper, L. M., Jordan, R. C., Rischin, D., Sturgis, E. M., Bell, D., Lingen, M. W., Harichand-Herdt, S., Thibo, J., Zevallos, J. and Perez-Ordonez, B. (2018) 'Human papillomavirus testing in head and neck carcinomas: ASCO clinical practice guideline endorsement of the college of American pathologists guideline', *Journal of Clinical Oncology*, 36(31), pp. 3152–3161. doi: 10.1200/JCO.18.00684.

Ferreira, L. B., Tavares, C., Pestana, A., Pereira, C. L., Eloy, C., Pinto, M. T., Castro, P., Batista, R., Rios, E., Sobrinho-Simões, M., Pereira Gimba, E. R. and Soares, P. (2016) 'Osteopontin-a splice

variant is overexpressed in papillary thyroid carcinoma and modulates invasive behavior', *Oncotarget*, 7(32), pp. 52003–52016. doi: 10.18632/oncotarget.10468.

Ferris, R. L., Martinez, I., Sirianni, N., Wang, J., Gollin, S. M., Johnson, J. T. and Khan, S. (2005) 'Human papillomavirus-16 associated squamous cell carcinoma of the head and neck (SCCHN): A natural disease model provides insights into viral carcinogenesis', *Euorpean Journal of Cancer.* 41, pp. 807–815. doi: 10.1016/j.ejca.2004.11.023.

Fiori, M. E., Di Franco, S., Villanova, L., Bianca, P., Stassi, G. and De Maria, R. (2019) 'Cancer-associated fibroblasts as abettors of tumor progression at the crossroads of EMT and therapy resistance', *Molecular Cancer*. Molecular Cancer, 18(1), pp. 1–16. doi: 10.1186/s12943-019-0994-2.

Fischer, K. R., Durrans, A., Lee, S., Sheng, J., Li, F., Wong, S. T. C., Choi, H., El Rayes, T., Ryu, S., Troeger, J., Schwabe, R. F., Vahdat, L. T., Altorki, N. K., Mittal, V. and Gao, D. (2015) 'Epithelial-to-mesenchymal transition is not required for lung metastasis but contributes to chemoresistance', *Nature*. Nature Publishing Group, 527(7579), pp. 472–476. doi: 10.1038/nature15748.

Fisher, L. W. and Ogbureke, K. U. E. (2007) 'SIBLING Expression Patterns in Duct Epithelia Reflect the Degree of Metabolic Activity', 55(4), pp. 403–409. doi: 10.1369/jhc.6A7075.2007.

Fisher, L. W., Torchia, D. A., Fohr, B., Young, M. F. and Fedarko, N. S. (2001) 'Flexible structures of SIBLING proteins, bone sialoprotein, and osteopontin', *Biochemical and Biophysical Research Communications*, 280(2), pp. 460–465. doi: 10.1006/bbrc.2000.4146.

Flajollet, S., Tian, T. V., Flourens, A., Tomavo, N., Villers, A., Bonnelye, E., Aubert, S., Leroy, X. and Duterque-Coquillaud, M. (2011) 'Abnormal expression of the ERG transcription factor in prostate cancer cells activates osteopontin', *Molecular Cancer Research*, 9(7), pp. 914–924. doi: 10.1158/1541-7786.MCR-10-0537.

Fordyce, C. A., Patten, K. T., Fessenden, T. B., DeFilippis, R. A., Hwang, E. S., Zhao, J. and Tlsty, T. D. (2012) 'Cell-extrinsic consequences of epithelial stress: Activation of protumorigenic tissue phenotypes', *Breast Cancer Research*, 14(6). doi: 10.1186/bcr3368.

Foster, C. T., Gualdrini, F. and Treisman, R. (2017) 'Mutual dependence of the MRTF-SRF and YAP-TEAD pathways in cancer-associated fibroblasts is indirect and mediated by cytoskeletal dynamics', *Genes and Development*, 31(23–24), pp. 2361–2375. doi: 10.1101/gad.304501.117.

Foster, D. S., Jones, R. E., Ransom, R. C., Longaker, M. T. and Norton, J. A. (2018) 'The evolving relationship of wound healing and tumor stroma', *JCI insight*, 3(18). doi: 10.1172/jci.insight.99911.

Foster, L., Arkonac, B., Sibinga, N., Shi, C., Perrella, M. and Haber, E., 1998. Regulation of CD44 Gene Expression by the Proinflammatory Cytokine Interleukin-1β in Vascular Smooth Muscle Cells. *Journal of Biological Chemistry*, 273(32), pp.20341-20346.

Frangogiannis, N. G., Michael, L. H. and Entman, M. L. (2000) 'Myofibroblasts in reperfused myocardial infarcts express the embryonic form of smooth muscle myosin heavy chain (SMemb)', *Cardiovascular Research*, 48(1), pp. 89–100. doi: 10.1016/S0008-6363(00)00158-9.

Franklin, O., Billing, O., Öhlund, D., Berglund, A., Herdenberg, C., Wang, W., Hellman, U. and Sund, M. (2019) 'Novel prognostic markers within the CD44-stromal ligand network in pancreatic cancer', *Journal of Pathology: Clinical Research*, 5(2), pp. 130–141. doi: 10.1002/cjp2.122.

Franzen, A. and Heinegard, D. (1985) 'Isolation and characterization of two sialoproteins present only in bone calcified matrix', *Biochemical Journal*, 232(3), pp. 715–724. doi: 10.1042/bj2320715.

Frippiat, C., Chen, Q. M., Zdanov, S., Magalhaes, J. P., Remacle, J. and Toussaint, O. (2001) 'Subcytotoxic H2O2 Stress Triggers a Release of Transforming Growth Factor-β1, Which Induces Biomarkers of Cellular Senescence of Human Diploid Fibroblasts', *Journal of Biological Chemistry*, 276(4), pp. 2531–2537. doi: 10.1074/jbc.M006809200.

Frippiat, C., Dewelle, J., Remacle, J. and Toussaint, O. (2002) 'Signal transduction in H2O2-induced senescence-like phenotype in human diploid fibroblasts', *Free Radical Biology and Medicine*, 33(10), pp. 1334–1346. doi: 10.1016/S0891-5849(02)01044-4.

Gabbiani, G., Ryan, G. and Majno, G., 1971. Presence of modified fibroblasts in granulation tissue and their possible role in wound contraction. *Experientia*, 27(5), pp.549-550.

Galbo, P. M., Jr, Zang, X., & Zheng, D. (2021). Molecular Features of Cancer-associated Fibroblast Subtypes and their Implication on Cancer Pathogenesis, Prognosis, and Immunotherapy Resistance. *Clinical cancer research : an official journal of the American Association for Cancer Research*, 10.1158/1078-0432.CCR-20-4226. Advance online publication. https://doi.org/10.1158/1078-0432.CCR-20-4226.

Galván, J. A., García-Martínez, J., Vázquez-Villa, F., García-Ocaña, M., García-Pravia, C., Menéndez-Rodríguez, P., González-del Rey, C., Barneo-Serra, L. and de los Toyos, J. R. (2014) 'Validation of COL11A1/procollagen 11A1 expression in TGF-β1-activated immortalised human mesenchymal cells and in stromal cells of human colon adenocarcinoma', *BMC Cancer*, 14(1), pp. 1–12. doi: 10.1186/1471-2407-14-867.

Gao, G., Chernock, R. D., Gay, H. A., Thorstad, W. L., Zhang, T. R., Wang, H., Ma, X. J., Luo, Y., Lewis, J. S. and Wang, X. (2012) 'A novel RT-PCR method for quantification of human papillomavirus transcripts in archived tissues and its application in oropharyngeal cancer prognosis', *International Journal of Cancer*, 132(4), pp. 882–890. doi: 10.1002/ijc.27739.

Gao, G., Johnson, S. H., Kasperbauer, J. L., Eckloff, B. W., Tombers, N. M., Vasmatzis, G. and Smith, D. I. (2014) 'Mate pair sequencing of oropharyngeal squamous cell carcinomas reveals that HPV integration occurs much less frequently than in cervical cancer', *Journal of Clinical Virology*. Elsevier B.V., 59(3), pp. 195–200. doi: 10.1016/j.jcv.2013.12.006.

Gascard, P. and Tlsty, T. D. (2016) 'Carcinoma-associated fibroblasts: Orchestrating the composition of malignancy', *Genes and Development*, 30(9), pp. 1002–1019. doi: 10.1101/gad.279737.116.

Ghosh, M. C., Grass, L., Soosaipillai, A., Sotiropoulou, G. and Diamandis, E. P. (2004) 'Human kallikrein 6 degrades extracellular matrix proteins and may enhance the metastatic potential of tumour cells', *Tumor Biology*, 25(4), pp. 193–199. doi: 10.1159/000081102.

Gillison, M. L., Chaturvedi, A. K., Anderson, W. F. and Fakhry, C. (2015) 'Epidemiology of human papillomavirus-positive head and neck squamous cell carcinoma', *Journal of Clinical Oncology*, 33(29), pp. 3235–3242. doi: 10.1200/JCO.2015.61.6995.

Gillison, M. L., D'Souza, G., Westra, W., Sugar, E., Xiao, W., Begum, S. and Viscidi, R. (2008) 'Distinct Risk Factor Profiles for Human Papillomavirus Type 16–Positive and Human Papillomavirus Type 16–Negative Head and Neck Cancers', *JNCI: Journal of the National Cancer Institute*, 100(6), pp. 407–420. doi: 10.1093/jnci/djn025.

Gillison, M. L., Koch, W. M., Capone, R. B., Spafford, M., Westra, W. H., Wu, L., Zahurak, M. L., Daniel, R. W., Viglione, M., Symer, D. E., Shah, K. V. and Sidransky, D. (2000) 'Evidence for a Causal Association Between Human Papillomavirus and a Subset of Head and Neck Cancers', *Journal of the National Cancer Institute*. Oxford University Press, 92(9), pp. 709–720. doi: 10.1093/jnci/92.9.709.

Givel, A. M., Kieffer, Y., Scholer-Dahirel, A., Sirven, P., Cardon, M., Pelon, F., Magagna, I., Gentric, G., Costa, A., Bonneau, C., Mieulet, V., Vincent-Salomon, A. and Mechta-Grigoriou, F. (2018) 'MiR200-regulated CXCL12β promotes fibroblast heterogeneity and immunosuppression in ovarian cancers', *Nature Communications*. Springer US, 9(1). doi: 10.1038/s41467-018-03348-z.

Gkretsi, V., Stylianou, A., Papageorgis, P., Polydorou, C. and Stylianopoulos, T. (2015) 'Remodeling components of the tumor microenvironment to enhance cancer therapy', *Frontiers in Oncology*, 5(10). doi: 10.3389/fonc.2015.00214.

Godar, S., Ince, T. A., Bell, G. W., Feldser, D., Donaher, J. L., Bergh, J., Liu, A., Miu, K., Watnick, R. S., Reinhardt, F., McAllister, S. S., Jacks, T. and Weinberg, R. A. (2008) 'Growth-Inhibitory and Tumor-Suppressive Functions of p53 Depend on Its Repression of CD44 Expression', *Cell*, 134(1), pp. 62–73. doi: 10.1016/j.cell.2008.06.006.

Gotlib, J. and Cools, J. (2008) 'Five years since the discovery of FIP1L1-PDGFRA: What we have learned about the fusion and other molecularly defined eosinophilias', *Leukemia*, 22(11), pp. 1999–2010. doi: 10.1038/leu.2008.287.

Greaney-Davies, F., Risk, J., Robinson, M., Liloglou, T., Shaw, R. and Schache, A., 2020. Essential characterisation of human papillomavirus positive head and neck cancer cell lines. *Oral Oncology*, 103, p.104613.

Griffin, H., Soneji, Y., Van Baars, R., Arora, R., Jenkins, D., Van De Sandt, M., Wu, Z., Quint, W., Jach, R., Okon, K., Huras, H., Singer, A. and Doorbar, J. (2015) 'Stratification of HPV-induced cervical pathology using the virally encoded molecular marker E4 in combination with p16 or MCM', *Modern Pathology*, 28(7), pp. 977–993. doi: 10.1038/modpathol.2015.52.

Grum-Schwensen, B., Klingelhofer, J., Berg, C. H., El-Naaman, C., Grigorian, M., Lukanidin, E. and Ambartsumian, N. (2005) 'Suppression of tumor development and metastasis formation in mice lacking the S100A4(mts1) gene', *Cancer Research*, 65(9), pp. 3772–3780. doi: 10.1158/0008-5472.CAN-04-4510.

Guertin, D. A. and Sabatini, D. M. (2007) 'Defining the Role of mTOR in Cancer', *Cancer Cell*, 12(1), pp. 9–22. doi: 10.1016/j.ccr.2007.05.008.

Gutjahr, J. C., Szenes, E., Tschech, L., Asslaber, D., Schlederer, M., Roos, S., Yu, X., Girbl, T., Sternberg, C., Egle, A., Aberger, F., Alon, R., Kenner, L., Greil, R., Orian-Rousseau, V. and Hartmann, T. N. (2018) 'Microenvironment-induced CD44v6 promotes early disease progression in chronic lymphocytic leukemia', *Blood*, 131(12), pp. 1337–1349. doi: 10.1182/blood-2017-08-802462.

Hafkamp, H. C., Manni, J. J., Haesevoets, A., Voogd, A. C., Schepers, M., Bot, F. J., Hopman, A. H. N., Ramaekers, F. C. S. and Speel, E. J. M. (2008) 'Marked differences in survival rate between smokers and nonsmokers with HPV 16-associated tonsillar carcinomas', *International Journal of Cancer*, 122(12), pp. 2656–2664. doi: 10.1002/ijc.23458.

Han, C., Liu, T. and Yin, R. (2020) 'Biomarkers for cancer-associated fibroblasts', *Biomarker Research*. Biomarker Research, 8(1), pp. 1–8. doi: 10.1186/s40364-020-00245-w.

Hanahan, D. and Weinberg, R. A. (2011) 'Hallmarks of cancer: The next generation', *Cell*. Elsevier Inc., 144(5), pp. 646–674. doi: 10.1016/j.cell.2011.02.013.

Hao, C., Cui, Y., Hu, M., Zhi, X., Zhang, L., Li, W., Wu, W., Cheng, S. and Jiang, W. G. (2017) 'OPN-a splicing variant expression in non-small cell lung cancer and its effects on the bone Metastatic abilities of lung cancer cells in vitro', *Anticancer Research*, 37(5), pp. 2245–2254. doi:

10.21873/anticanres.11561.

Hassona, Y., Cirillo, N., Heesom, K., Parkinson, E. K. and Prime, S. S. (2014) 'Senescent cancer-associated fibroblasts secrete active MMP-2 that promotes keratinocyte dis-cohesion and invasion', *British Journal of Cancer*. doi: 10.1038/bjc.2014.438.

Hassona, Y., Cirillo, N., Lim, K. P., Herman, A., Mellone, M., Thomas, G. J., Pitiyage, G. N., Parkinson, E. K. and Prime, S. S. (2013) 'Progression of genotype-specific oral cancer leads to senescence of cancer-associated fibroblasts and is mediated by oxidative stress and TGF-β', *Carcinogenesis*, 34(6), pp. 1286–1295. doi: 10.1093/carcin/bgt035.

Hawkins, P. G., Mierzwa, M. L., Bellile, E., Jackson, W. C., Malloy, K. M., Chinn, S. B., Spector, M. E., Shuman, A. G., Stucken, C. L., McLean, S. A., Bradford, C. R., Prince, M. E., Carey, T. E., Worden, F. P., Swiecicki, P. L., Taylor, J., Wolf, G. T., Eisbruch, A., & Casper, K. A. (2019). Impact of American Joint Committee on Cancer Eighth Edition clinical stage and smoking history on oncologic outcomes in human papillomavirus-associated oropharyngeal squamous cell carcinoma. *Head & neck*, *41*(4), pp. 857–864. https://doi.org/10.1002/hed.25336.

Heck, J. E., Berthiller, J., Vaccarella, S., Winn, D. M., Smith, E. M., Shan'gina, O., Schwartz, S. M., Purdue, M. P., Pilarska, A., Eluf-Neto, J., Menezes, A., McClean, M. D., Matos, E., Koifman, S., Kelsey, K. T., Herrero, R., Hayes, R. B., Franceschi, S., Wünsch-Filho, V., Fernández, L., Daudt, A. W., Curado, M. P., Chen, C., Castellsagué, X., Ferro, G., Brennan, P., Boffetta, P. and Hashibe, M. (2010) 'Sexual behaviours and the risk of head and neck cancers: a pooled analysis in the International Head and Neck Cancer Epidemiology (INHANCE) consortium.', *International journal of epidemiology*. Oxford University Press, 39(1), pp. 166–81. doi: 10.1093/ije/dyp350.

Heider, K. H., Kuthan, H., Stehle, G. and Munzert, G. (2004) 'CD44v6: A target for antibody-based cancer therapy', *Cancer Immunology, Immunotherapy*, 53(7), pp. 567–579. doi: 10.1007/s00262-003-0494-4.

Hendawi, N., Niklander, S., Allsobrook, O., Khurram, S. A., Bolt, R., Doorbar, J., Speight, P. M. and Hunter, K. D. (2020) 'Human papillomavirus (HPV) can establish productive infection in dysplastic oral mucosa, but HPV status is poorly predicted by histological features and p16 expression', *Histopathology*, 76(4), pp. 592–602. doi: 10.1111/his.14019.

Herfs, M., Yamamoto, Y., Laury, A., Wang, X., Nucci, M. R. and Mclaughlin-drubin, M. E. (2012) 'A discrete population of squamocolumnar junction cells implicated in the pathogenesis of cervical cancer', 109(26). doi: 10.1073/pnas.1202684109.

Hinz, B., Mastrangelo, D., Iselin, C. E., Chaponnier, C., & Gabbiani, G. (2001). Mechanical tension controls granulation tissue contractile activity and myofibroblast differentiation. *The American journal of pathology*, 159(3), pp.1009–1020. https://doi.org/10.1016/S0002-9440(10)61776-2.

Hinz, B., Phan, S. H., Thannickal, V. J., Galli, A., Bochaton-Piallat, M.-L. and Gabbiani, G. (2007) 'The Myofibroblast: One Function, Multiple Origins', *The American Journal of Pathology*. Elsevier, 170(6), pp. 1807–1816. doi: 10.2353/AJPATH.2007.070112.

Hinz, B., Phan, S. H., Thannickal, V. J., Prunotto, M., Desmoulire, A., Varga, J., De Wever, O., Mareel, M. and Gabbiani, G. (2012) 'Recent developments in myofibroblast biology: Paradigms for connective tissue remodeling', *American Journal of Pathology*. Elsevier Inc., 180(4), pp. 1340–1355. doi: 10.1016/j.ajpath.2012.02.004.

Hirsch, F. R., Varella-Garcia, M., Bunn, P. A., Di Maria, M. V, Veve, R., Bremmes, R. M., Barón, A. E., Zeng, C. and Franklin, W. A. (2003) 'Epidermal growth factor receptor in non-small-cell lung

carcinomas: correlation between gene copy number and protein expression and impact on prognosis.', *Journal of clinical oncology : official journal of the American Society of Clinical Oncology*, 21(20), pp. 3798–807. doi: 10.1200/JCO.2003.11.069.

Hiscox, S., Baruha, B., Smith, C., Bellerby, R., Goddard, L., Jordan, N., Poghosyan, Z., Nicholson, R. I., Barrett-Lee, P. and Gee, J. (2012) 'Overexpression of CD44 accompanies acquired tamoxifen resistance in MCF7 cells and augments their sensitivity to the stromal factors, heregulin and hyaluronan', *BMC Cancer*. BMC Cancer, 12(1), p. 1. doi: 10.1186/1471-2407-12-458.

Hoare, M., Ito, Y., Kang, T. W., Weekes, M. P., Matheson, N. J., Patten, D. A., Shetty, S., Parry, A. J., Menon, S., Salama, R., Antrobus, R., Tomimatsu, K., Howat, W., Lehner, P. J., Zender, L. and Narita, M. (2016) 'NOTCH1 mediates a switch between two distinct secretomes during senescence', *Nature Cell Biology*, 18(9), pp. 979–992. doi: 10.1038/ncb3397.

Hong, A. M., Martin, A., Chatfield, M., Jones, D., Zhang, M., Armstrong, B., Lee, C. S., Harnett, G., Milross, C., Clark, J., Elliott, M., Smee, R., Corry, J., Liu, C., Porceddu, S., Rees, G. and Rose, B. (2013) 'Human papillomavirus, smoking status and outcomes in tonsillar squamous cell carcinoma', *International Journal of Cancer*, 132(12), pp. 2748–2754. doi: 10.1002/ijc.27956.

Hoos, A. and Cordon-Cardo, C. (2001) 'Tissue microarray profiling of cancer specimens and cell lines: opportunities and limitations.', *Laboratory Investigation*, 81(10), pp. 1331–8. doi: 10.1038/labinvest.3780347.

Howard, J., Dwivedi, R. C., Masterson, L., Kothari, P., Quon, H., & Holsinger, F. C. (2018). De-intensified adjuvant (chemo)radiotherapy versus standard adjuvant chemoradiotherapy post transoral minimally invasive surgery for resectable HPV-positive oropharyngeal carcinoma. *The Cochrane database of systematic reviews*, *12*(12), CD012939. https://doi.org/10.1002/14651858.CD012939.pub2.

Hsieh, Y.-H., Margaret Juliana, M., Ho, K. J., Kuo, H. C., Van Der Heyde, H., Elmets, C. and Chang, P. L. (2012) 'Host-derived osteopontin maintains an acute inflammatory response to suppress early progression of extrinsic cancer cells', *International Journal of Cancer*, 131(2), pp. 322–333. doi: 10.1002/ijc.26359.

Huang, C. C., Qiu, J. T., Kashima, M. L., Kurman, R. J., & Wu, T. C. (1998). Generation of type-specific probes for the detection of single-copy human papillomavirus by a novel in situ hybridization method. *Modern pathology : an official journal of the United States and Canadian Academy of Pathology, Inc*, 11(10), pp. 971–977.

Huang, R. H., Quan, Y. J., Chen, J. H., Wang, T. F., Xu, M., Ye, M., Yuan, H., Zhang, C. J., Liu, X. J. and Min, Z. J. (2017) 'Osteopontin promotes cell migration and invasion, and inhibits apoptosis and autophagy in colorectal cancer by activating the p38 MAPK signaling pathway', *Cellular Physiology and Biochemistry*, 41(5), pp. 1851–1864. doi: 10.1159/000471933.

Hui, E. P., Sung, F. L., Yu, B. K. H., Wong, C. S. C., Ma, B. B. Y., Lin, X., Chan, A., Wong, W. L. and Chan, A. T. C. (2008) 'Plasma osteopontin, hypoxia, and response to radiotherapy in nasopharyngeal cancer', *Clinical Cancer Research*, 14(21), pp. 7080–7087. doi: 10.1158/1078-0432.CCR-08-0364.

Huibregtse, J. M., Scheffner, M. and Howley, P. M. (1991) 'A cellular protein mediates association of p53 with the E6 oncoprotein of human papillomavirus types 16 or 18', *EMBO Journal*, 10(13), pp. 4129–4135. doi: 10.1002/j.1460-2075.1991.tb04990.x.

Hunter, C., Bond, J., Kuo, P. C., Selim, M. A. and Levinson, H. (2012) 'The role of osteopontin and osteopontin aptamer (OPN-R3) in fibroblast activity', *Journal of Surgical Research*. Elsevier Inc,

176(1), pp. 348–358. doi: 10.1016/j.jss.2011.07.054.

Hunter, K. D., Parkinson, E. K. and Harrison, P. R. (2005) 'Profiling early head and neck cancer', *Nature Reviews Cancer*, 5(2), pp. 127–135. doi: 10.1038/nrc1549.

Ibrahim, E. M., Stewart, R. L., Corke, K., Blackett, A. D., Tidy, J. A. and Wells, M. (2006) 'Upregulation of CD44 expression by interleukins 1, 4, and 13, transforming growth factor-β1, estrogen, and progestogen in human cervical adenocarcinoma cell lines', *International Journal of Gynecological Cancer*, 16(4), pp. 1631–1642. doi: 10.1111/j.1525-1438.2006.00637.x.

Inoue, M. and Shinohara, M. L. (2011) 'Intracellular osteopontin (iOPN) and immunity', *Immunologic Research*, 49(1–3), pp. 160–172. doi: 10.1007/s12026-010-8179-5.

Inoue, Y., Yokobori, T., Yokoe, T., Toiyama, Y., Miki, C., Mimori, K., Mori, M. and Kusunoki, M. (2010) 'Clinical significance of human Kallikrein7 gene expression in colorectal cancer', *Annals of Surgical Oncology*, 17(11), pp. 3037–3042. doi: 10.1245/s10434-010-1132-y.

Ishii, G., Ochiai, A. and Neri, S. (2016) 'Phenotypic and functional heterogeneity of cancer-associated fibroblast within the tumor microenvironment', *Advanced Drug Delivery Reviews*. Elsevier B.V., 99, pp. 186–196. doi: 10.1016/j.addr.2015.07.007.

Jackson, H. W., Fischer, J. R., Zanotelli, V. R. T., Ali, H. R., Mechera, R., Soysal, S. D., Moch, H., Muenst, S., Varga, Z., Weber, W. P. and Bodenmiller, B. (2020) 'The single-cell pathology landscape of breast cancer', *Nature*. Springer US, 578(7796), pp. 615–620. doi: 10.1038/s41586-019-1876-x.

Jain, R. K., Martin, J. D. and Stylianopoulos, T. (2014) 'The role of mechanical forces in tumor growth and therapy', *Annual Review of Biomedical Engineering*, 16, pp. 321–346. doi: 10.1146/annurev-bioeng-071813-105259.

James, E. L., Michalek, R. D., Pitiyage, G. N., De Castro, A. M., Vignola, K. S., Jones, J., Mohney, R. P., Karoly, E. D., Prime, S. S. and Parkinson, E. K. (2015) 'Senescent human fibroblasts show increased glycolysis and redox homeostasis with extracellular metabolomes that overlap with those of irreparable DNA damage, aging, and disease', *Journal of Proteome Research*, 14(4), pp. 1854–1871. doi: 10.1021/pr501221g.

Jia, R., Liang, Y., Chen, R., Liu, G., Wang, H., Tang, M., Zhou, X., Wang, H., Yang, Y., Wei, H., Li, B., Song, Y., & Zhao, J. (2016). Osteopontin facilitates tumor metastasis by regulating epithelial-mesenchymal plasticity. *Cell death & disease*, *7*(12), e2564. https://doi.org/10.1038/cddis.2016.422.

Jia, X. H., Du, Y., Mao, D., Wang, Z. L., He, Z. Q., Qiu, J. D., Ma, X. B., Shang, W. T., Ding, D. and Tian, J. (2015) 'Zoledronic acid prevents the tumor-promoting effects of mesenchymal stem cells via MCP-1 dependent recruitment of macrophages', *Oncotarget*, 6(28), pp. 26018–26028. doi: 10.18632/oncotarget.4658.

Jiang, E., Xu, Z., Wang, M., Yan, T., Huang, C., Zhou, X., Liu, Q., Wang, L., Chen, Y., Wang, H., Liu, K., Shao, Z. and Shang, Z. (2019) 'Tumoral microvesicle–activated glycometabolic reprogramming in fibroblasts promotes the progression of oral squamous cell carcinoma', *FASEB Journal*, 33(4), pp. 5690–5703. doi: 10.1096/fj.201802226R.

Johansson, A. C., Ansell, A., Jerhammar, F., Lindh, M. B., Grénman, R., Munck-Wikland, E., Östman, A. and Roberg, K. (2012) 'Cancer-associated fibroblasts induce matrix metalloproteinase-mediated cetuximab resistance in head and neck squamous cell carcinoma cells', *Molecular Cancer Research*, 10(9), pp. 1158–1168. doi: 10.1158/1541-7786.MCR-12-0030.

John, T., Liu, G. and Tsao, M.-S. (2009) 'Overview of molecular testing in non-small-cell lung cancer: mutational analysis, gene copy number, protein expression and other biomarkers of EGFR for the prediction of response to tyrosine kinase inhibitors', *Oncogene*, 28, pp. S14–S23. doi: 10.1038/onc.2009.197.

Johnson, G. A., Burghardt, R. C., Bazer, F. W. and Spencer, T. E. (2003) 'Osteopontin : Roles in Implantation and Placentation 1', 1471(7), pp. 1458–1471. doi: 10.1095/biolreprod.103.020651.

Jones, D. A., Mistry, P., Dalby, M., Fulton-Lieuw, T., Kong, A. H., Dunn, J., Mehanna, H. M. and Gray, A. M. (2020) 'Concurrent cisplatin or cetuximab with radiotherapy for HPV-positive oropharyngeal cancer: Medical resource use, costs, and quality-adjusted survival from the De-ESCALaTE HPV trial', *European Journal of Cancer*. Elsevier Ltd, 124, pp. 178–185. doi: 10.1016/j.ejca.2019.10.025.

Jones, D. L. and Münger, K. (1996) 'Interactions of the human papillomavirus E7 protein with cell cycle regulators', *Seminars in Cancer Biology*, 7(6), pp. 327–337. doi: 10.1006/scbi.1996.0042.

Jordan, R. C., Lingen, M. W., Perez-ordonez, B., He, X., Pickard, R., Koluder, M., Jiang, B., Wakely, P., Xiao, W., Gillison, M. L., Francisco, S. and Francisco, S. (2019) 'HHS Public Access', 36(7), pp. 945–954. doi: 10.1097/PAS.0b013e318253a2d1.Validation.

Junaid, A., Moon, M. C., Harding, G. E. J. and Zahradka, P. (2007) 'Osteopontin localizes to the nucleus of 293 cells and associates with polo-like kinase-1', *American Journal of Physiology - Cell Physiology*, 292(2), pp. 919–926. doi: 10.1152/ajpcell.00477.2006.

Jung, Y., Kim, J. K., Shiozawa, Y., Wang, J., Mishra, A., Joseph, J., Berry, J. E., McGee, S., Lee, E., Sun, H., Wang, J., Jin, T., Zhang, H., Dai, J., Krebsbach, P. H., Keller, E. T., Pienta, K. J., & Taichman, R. S. (2013). Recruitment of mesenchymal stem cells into prostate tumours promotes metastasis. *Nature communications*, 4, p. 1795. https://doi.org/10.1038/ncomms2766

Kabir, T. D., Leigh, R. J., Tasena, H., Mellone, M., Coletta, R. D., Parkinson, E. K., Prime, S. S., Thomas, G. J., Paterson, I. C., Zhou, D., McCall, J., Speight, P. M. and Lambert, D. W. (2016) 'A miR-335/COX-2/PTEN axis regulates the secretory phenotype of senescent cancer-associated fibroblasts', *Aging*, 8(8), pp. 1608–1635. doi: 10.18632/aging.100987.

Kagawa, S., Natsuizaka, M., Whelan, K. A., Facompre, N., Naganuma, S., Ohashi, S., Kinugasa, H., Egloff, A. M., Basu, D., Gimotty, P. A., Klein-Szanto, A. J., Bass, A. J., Wong, K. K., Diehl, J. A., Rustgi, A. K. and Nakagawa, H. (2015) 'Cellular senescence checkpoint function determines differential Notch1-dependent oncogenic and tumor-suppressor activities', *Oncogene*. Nature Publishing Group, 34(18), pp. 2347–2359. doi: 10.1038/onc.2014.169.

Kallioniemi, O.-P., Wagner, U., Kononen, J. and Sauter, G. (2001) 'Tissue microarray technology for high-throughput molecular profiling of cancer', *Human Molecular Genetics*. Oxford University Press, 10(7), pp. 657–662. doi: 10.1093/hmg/10.7.657.

Kalluri, R. (2016) 'The biology and function of fibroblasts in cancer', *Nature Reviews Cancer*. Nature Publishing Group, 16(9), pp. 582–598. doi: 10.1038/nrc.2016.73.

Kalluri, R. and Zeisberg, M. (2006) 'Fibroblasts in cancer', *Nature Reviews Cancer*, 6(5), pp. 392–401. doi: 10.1038/nrc1877.

Kanzaki, R. and Pietras, K. (2020) 'Heterogeneity of cancer-associated fibroblasts: Opportunities for precision medicine', *Cancer Science*, 111(8), pp. 2708–2717. doi: 10.1111/cas.14537.

Katabi, N. and Lewis, J. S. (2017) 'Update from the 4th Edition of the World Health Organization

Classification of Head and Neck Tumours: What Is New in the 2017 WHO Blue Book for Tumors and Tumor-Like Lesions of the Neck and Lymph Nodes', *Head and Neck Pathology*. Springer US, 11(1), pp. 48–54. doi: 10.1007/s12105-017-0796-z.

Kaukonen, R., Mai, A., Georgiadou, M., Saari, M., De Franceschi, N., Betz, T., Sihto, H., Ventelä, S., Elo, L., Jokitalo, E., Westermarck, J., Kellokumpu-Lehtinen, P. L., Joensuu, H., Grenman, R. and Ivaska, J. (2016) 'Normal stroma suppresses cancer cell proliferation via mechanosensitive regulation of JMJD1a-mediated transcription', *Nature Communications*, 7. doi: 10.1038/ncomms12237.

Kavsak, P., Rasmussen, R. K., Causing, C. G., Bonni, S., Zhu, H., Thomsen, G. H., & Wrana, J. L. (2000). Smad7 binds to Smurf2 to form an E3 ubiquitin ligase that targets the TGF beta receptor for degradation. *Molecular cell*, *6*(6), pp. 1365–1375. https://doi.org/10.1016/s1097-2765(00)00134-9

Kawakami, K., Minami, N., Matsuura, M., Iida, T., Toyonaga, T., Nagaishi, K., Arimura, Y., Fujimiya, M., Uede, T. and Nakase, H. (2017) 'Osteopontin attenuates acute gastrointestinal graft-versus-host disease by preventing apoptosis of intestinal epithelial cells', *Biochemical and Biophysical Research Communications*. Elsevier Ltd, 485(2), pp. 468–475. doi: 10.1016/j.bbrc.2017.02.047.

Kellermann, M. G., Sobral, L. M., da Silva, S. D., Zecchin, K. G., Graner, E., Lopes, M. A., Kowalski, L. P. and Coletta, R. D. (2008) 'Mutual paracrine effects of oral squamous cell carcinoma cells and normal oral fibroblasts: Induction of fibroblast to myofibroblast transdifferentiation and modulation of tumor cell proliferation', *Oral Oncology*, 44(5), pp. 509–517. doi: 10.1016/j.oraloncology.2007.07.001.

Kellermann, M G, Sobral, L. M., Silva, S. D. da, Zecchin, K. G., Graner, E., Lopes, M. A., Nishimoto, I., Kowalski, L. P. and Coletta, R. D. (2007) 'Myofibroblasts in the stroma of oral squamous cell carcinoma are associated with poor prognosis', *Histopathology*, 51(6), pp. 849–853. doi: 10.1111/j.1365-2559.2007.02873.x.

Kemnade, J. O., Elhalawani, H., Castro, P., Yu, J., Lai, S., Ittmann, M., Mohamed, A. S. R., Lai, S. Y., Fuller, C. D., Sikora, A. G. and Sandulache, V. C. (2020) 'CD8 infiltration is associated with disease control and tobacco exposure in intermediate-risk oropharyngeal cancer', *Scientific Reports*, 10(1), pp. 1–10. doi: 10.1038/s41598-019-57111-5.

Khan, F., Gurung, S., Gunassekaran, G. R., Vadevoo, S. M. P., Chi, L., Permpoon, U., Haque, M. E., Lee, Y. K., Lee, S. W., Kim, S. and Lee, B. (2021) 'Identification of novel CD44v6-binding peptides that block CD44v6 and deliver a pro-apoptotic peptide to tumors to inhibit tumor growth and metastasis in mice', *Theranostics*, 11(3), pp. 1326–1344. doi: 10.7150/thno.50564.

Khan, Z. and Marshall, J. F. (2016) 'The role of integrins in TGFβ activation in the tumour stroma', *Cell and Tissue Research*, 365, pp. 657–673. doi: 10.1007/s00441-016-2474-y.

Khuri, F. R., Lee, J. J., Lippman, S. M., Kim, E. S., Cooper, J. S., Benner, S. E., Winn, R., Pajak, T. F., Williams, B., Shenouda, G., Hodson, I., Fu, K., Shin, D. M., Vokes, E. E., Feng, L., Goepfert, H. and Hong, W. K. (2006) 'Randomized phase III trial of low-dose isotretinoin for prevention of second primary tumors in stage I and II head and neck cancer patients', *Journal of the National Cancer Institute*, 98(7), pp. 441–450. doi: 10.1093/jnci/djj091.

Kidd, S., Spaeth, E., Watson, K., Burks, J., Lu, H., Klopp, A., Andreeff, M. and Marini, F. C. (2012) 'Origins of the tumor microenvironment: Quantitative assessment of adipose-derived and bone marrow-derived stroma', *PLoS ONE*, 7(2). doi: 10.1371/journal.pone.0030563.

Kikuchi, N., Horiuchi, A., Osada, R., Imai, T., Wang, C., Chen, X. and Konishi, I. (2006) 'Nuclear expression of S100A4 is associated with aggressive behavior of epithelial ovarian carcinoma: An important autocrine/paracrine factor in tumor progression', *Cancer Science*, 97(10), pp. 1061–1069.

doi: 10.1111/j.1349-7006.2006.00295.x.

Kilvaer, T. K., Khanehkenari, M. R., Hellevik, T., Al-Saad, S., Paulsen, E. E., Bremnes, R. M., Busund, L. T., Donnem, T. and Martinez, I. Z. (2015) 'Cancer associated fibroblasts in stage I-IIIA NSCLC: Prognostic impact and their correlations with tumor molecular markers', *PLoS ONE*, 10(8), pp. 1–15. doi: 10.1371/journal.pone.0134965.

Kim, D. K., Kim, E. K., Jung, D. W. and Kim, J. (2019) 'Cytoskeletal alteration modulates cancer cell invasion through RhoA-YAP signaling in stromal fibroblasts', *PLoS ONE*, 14(3), pp. 1–21. doi: 10.1371/journal.pone.0214553.

Kim, E. K., Moon, S., Kim, D. K., Zhang, X. and Kim, J. (2018) 'CXCL1 induces senescence of cancer-associated fibroblasts via autocrine loops in oral squamous cell carcinoma', *PLoS ONE*, 13(1), pp. 1–17. doi: 10.1371/journal.pone.0188847.

Kim, M. M. and Califano, J. A. (2004) 'Molecular pathology of head-and-neck cancer', *International Journal of Cancer*, 112(4), pp. 545–553. doi: 10.1002/ijc.20379.

Kinugasa, Y., Matsui, T. and Takakura, N. (2014) 'CD44 expressed on cancer-associated fibroblasts is a functional molecule supporting the stemness and drug resistance of malignant cancer cells in the tumor microenvironment', *Stem Cells*, 32(1), pp. 145–156. doi: 10.1002/stem.1556.

Kita, Y., Natsugoe, S., Okumura, H., Matsumoto, M., Uchikado, Y., Setoyama, T., Owaki, T., Ishigami, S. and Aikou, T. (2006) 'Expression of Osteopontin in oesophageal squamous cell carcinoma', *British Journal of Cancer*, 95(5), pp. 634–638. doi: 10.1038/sj.bjc.6603296.

Klein, S., Quaas, A., Quantius, J., Löser, H., Meinel, J., Peifer, M., Wagner, S., Gattenlöhner, S., Wittekindt, C., von Knebel Doeberitz, M., Prigge, E. S., Langer, C., Noh, K. W., Maltseva, M., Reinhardt, H. C., Büttner, R., Klussmann, J. P., & Wuerdemann, N. (2021). Deep Learning Predicts HPV Association in Oropharyngeal Squamous Cell Carcinomas and Identifies Patients with a Favorable Prognosis Using Regular H&E Stains. *Clinical cancer research : an official journal of the American Association for Cancer Research*, *27*(4), pp. 1131–1138. https://doi.org/10.1158/1078-0432.CCR-20-3596.

Klement, J. D., Paschall, A. V., Redd, P. S., Ibrahim, M. L., Lu, C., Yang, D., Celis, E., Abrams, S. I., Ozato, K. and Liu, K. (2018) 'An osteopontin/CD44 immune checkpoint controls CD8+ T cell activation and tumor immune evasion', *Journal of Clinical Investigation*, 128(12), pp. 5549–5560. doi: 10.1172/JCI123360.

Klussmann, J. P., Gültekin, E., Weissenborn, S. J., Wieland, U., Dries, V., Dienes, H. P., Eckel, H. E., Pfister, H. J., & Fuchs, P. G. (2003). Expression of p16 protein identifies a distinct entity of tonsillar carcinomas associated with human papillomavirus. *The American journal of pathology*, 162(3), pp. 747–753. https://doi.org/10.1016/S0002-9440(10)63871-0.

Kobawala, T. P., Trivedi, T. I., Gajjar, K. K., Patel, D. H., Patel, G. H. and Ghosh, N. R. (2016) 'Significance of Interleukin-6 in Papillary Thyroid Carcinoma', *Journal of Thyroid Research*, 2016. doi: 10.1155/2016/6178921.

Kojima, Y., Acar, A., Eaton, E. N., Mellody, K. T., Scheel, C., Ben-Porath, I., Onder, T. T., Wang, Z. C., Richardson, A. L., Weinberg, R. A. and Orimo, A. (2010) 'Autocrine TGF-β and stromal cell-derived factor-1 (SDF-1) signaling drives the evolution of tumor-promoting mammary stromal myofibroblasts', *Proceedings of the National Academy of Sciences of the United States of America*, 107(46), pp. 20009–20014. doi: 10.1073/pnas.1013805107.

Kónya, J., Veress, G., Hernádi, Z., Soós, G., Czeglédy, J. and Gergely, L. (1995) 'Correlation of human papillomavirus 16 and 18 with prognostic factors in invasive cervical neoplasias', *Journal of Medical Virology*. Wiley Subscription Services, Inc., A Wiley Company, 46(1), pp. 1–6. doi: 10.1002/jmv.1890460102.

Korita, P. V, Wakai, T. and Shirai, Y. (2008) 'Overexpression of osteopontin independently correlates with vascular invasion and poor prognosis in patients with hepatocellular carcinoma', *Human Pathology*. Elsevier Inc., 39(12), pp. 1777–1783. doi: 10.1016/j.humpath.2008.05.006.

Kreimer, A. R., Clifford, G. M., Boyle, P. and Franceschi, S. (2005) 'Human papillomavirus types in head and neck squamous cell carcinomas worldwide: A systemic review', *Cancer Epidemiology Biomarkers and Prevention*, 14(2), pp. 467–475. doi: 10.1158/1055-9965.EPI-04-0551.

Kreimer, A. R., Johansson, M., Yanik, E. L., Katki, H. A., Check, D. P., Kuhs, K. A. L., Willhauck-Fleckenstein, M., Holzinger, D., Hildesheim, A., Pfeiffer, R., Williams, C., Freedman, N. D., Huang, W. Y., Purdue, M. P., Michel, A., Pawlita, M., Brennan, P. and Waterboer, T. (2017) 'Kinetics of the Human Papillomavirus Type 16 E6 Antibody Response Prior to Oropharyngeal Cancer', *Journal of the National Cancer Institute*, 109(8), pp. 1–9. doi: 10.1093/jnci/djx005.

Krishnamurthy, J., Torrice, C., Ramsey, M. R., Kovalev, G. I., Al-Regaiey, K., Su, L. and Sharpless, N. E. (2004) 'Ink4a/Arf expression is a biomarker of aging', *Journal of Clinical Investigation*, 114(9), pp. 1299–1307. doi: 10.1172/JCI22475.

Kristensen, S. R. and Petersen, P. H. (1988) 'Quiescent fibroblasts in a cellular model system', *Scandinavian Journal of Clinical and Laboratory Investigation*, 48(5), pp. 413–417. doi: 10.1080/00365518809085750.

Krtolica, A. and Campisi, J. (2002) 'Cancer and aging : a model for the cancer promoting effects of the aging stroma', 34, pp. 1401–1414.

Krtolica, A., Parrinello, S., Lockett, S., Desprez, P.-Y. and Campisi, J. (2001) 'Senescent fibroblasts promote epithelial cell growth and tumorigenesis: A link between cancer and aging', *Proceedings of the National Academy of Sciences*, 98(21), pp. 12072–12077. doi: 10.1073/pnas.211053698.

Krtolica, A., Parrinello, S., Lockett, S., Desprez, P. Y., & Campisi, J. (2001). Senescent fibroblasts promote epithelial cell growth and tumorigenesis: a link between cancer and aging. *Proceedings of the National Academy of Sciences of the United States of America*, 98(21), pp. 12072–12077. https://doi.org/10.1073/pnas.211053698.

Kuilman, T., Michaloglou, C., Vredeveld, L. C. W., Douma, S., van Doorn, R., Desmet, C. J., Aarden, L. A., Mooi, W. J. and Peeper, D. S. (2008) 'Oncogene-Induced Senescence Relayed by an Interleukin-Dependent Inflammatory Network', *Cell*. Cell Press, 133(6), pp. 1019–1031. doi: 10.1016/J.CELL.2008.03.039.

Kumar, B., Cordell, K. G., Lee, J. S., Prince, M. E., Tran, H. H., Wolf, G. T., Urba, S. G., Worden, F. P., Chepeha, D. B., Teknos, T. N., Eisbruch, A., Tsien, C. I., Taylor, J. M. G., Silva, N. J. D., Yang, K., Kurnit, D. M., Bradford, C. R. and Carey, T. E. (2008) 'Response to Therapy and Outcome in Oropharyngeal Cancer are Associated with Biomarkers Including HPV, EGFR, Gender and Smoking', *International Journal of Radiation Oncology, Biology, Physics*, 69(19), pp. 1–6. doi: 10.1200/JCO.2007.12.7662.EGFR.

Kumar, S., Boehm, J. and Lee, J. C. (2003) 'P38 MAP kinases: Key signalling molecules as therapeutic targets for inflammatory diseases', *Nature Reviews Drug Discovery*, 2(9), pp. 717–726. doi: 10.1038/nrd1177.

Kumar, V., Behera, R., Lohite, K., Karnik, S. and Kundu, G. C. (2010) 'P38 Kinase Is Crucial for Osteopontin-Induced Furin Expression That Supports Cervical Cancer Progression', *Cancer Research*, 70(24), pp. 10381–10391. doi: 10.1158/0008-5472.CAN-10-1470.

Kunii, Y., Yoshiaki, H., Shin-ichi, N., Masahiro, M. and Seitoh, T. (2009) 'The immunohistochemical expression profile of osteopontin in normal human tissues using two site-specifi c antibodies reveals a wide distribution of positive cells and extensive expression in the central and peripheral nervous systems', pp. 155–161. doi: 10.1007/s00795-009-0459-6.

Laberge, R.-M., Sun, Y., Orjalo, A. V., Patil, C. K., Freund, A., Zhou, L., Curran, S. C., Davalos, A. R., Wilson-Edell, K. A., Liu, S., Limbad, C., Demaria, M., Li, P., Hubbard, G. B., Ikeno, Y., Javors, M., Desprez, P.-Y., Benz, C. C., Kapahi, P., Nelson, P. S. and Campisi, J. (2015) 'MTOR regulates the pro-tumorigenic senescence-associated secretory phenotype by promoting IL1A translation', *Nature Cell Biology*, 17(8), pp. 1049–1061. doi: 10.1038/ncb3195.

Lai, R. W., Lu, R., Danthi, P. S., Bravo, J. I., Goumba, A., Sampathkumar, N. K. and Benayoun, B. A. (2019) 'Multi-level remodeling of transcriptional landscapes in aging and longevity', *BMB Reports*, 52(1), pp. 86–108. doi: 10.5483/BMBRep.2019.52.1.296.

Jeyasivanesan, D. L., Mohamed, S. P., Pandiar, D., & Basheer, S. (2019). Immunohistochemical analysis of osteopontin expression in oral squamous cell carcinoma. *Indian journal of dental research : official publication of Indian Society for Dental Research*, 30(4), 539–543. https://doi.org/10.4103/ijdr.IJDR_474_17.

Lambrechts, D., Wauters, E., Boeckx, B., Aibar, S., Nittner, D., Burton, O., Bassez, A., Decaluwé, H., Pircher, A., Van den Eynde, K., Weynand, B., Verbeken, E., De Leyn, P., Liston, A., Vansteenkiste, J., Carmeliet, P., Aerts, S. and Thienpont, B. (2018) 'Phenotype molding of stromal cells in the lung tumor microenvironment', *Nature Medicine*. Springer US, 24(8), pp. 1277–1289. doi: 10.1038/s41591-018-0096-5.

Lamort, A. S., Giopanou, I., Psallidas, I. and Stathopoulos, G. T. (2019) 'Osteopontin as a Link between Inflammation and Cancer: The Thorax in the Spotlight', *Cells*, 8(8), pp. 1–20. doi: 10.3390/cells8080815.

Langer, E. M., Allen-Petersen, B. L., King, S. M., Kendsersky, N. D., Turnidge, M. A., Kuziel, G. M., Riggers, R., Samatham, R., Amery, T. S., Jacques, S. L., Sheppard, B. C., Korkola, J. E., Muschler, J. L., Thibault, G., Chang, Y. H., Gray, J. W., Presnell, S. C., Nguyen, D. G., & Sears, R. C. (2019). Modeling Tumor Phenotypes In Vitro with Three-Dimensional Bioprinting. *Cell reports*, *26*(3), pp. 608–623.e6. https://doi.org/10.1016/j.celrep.2018.12.090.

Lassen, P., Eriksen, J. G., Hamilton-Dutoit, S., Tramm, T., Alsner, J. and Overgaard, J. (2009) 'Effect of HPV-associated p16INK4A expression on response to radiotherapy and survival in squamous cell carcinoma of the head and neck', *Journal of Clinical Oncology*, 27(12), pp. 1992–1998. doi: 10.1200/JCO.2008.20.2853.

Lawless, C., Jurk, D., Gillespie, C. S., Shanley, D., Saretzki, G., von Zglinicki, T. and Passos, J. F. (2012) 'A stochastic step model of replicative senescence explains ROS production rate in ageing cell populations', *PLoS ONE*, 7(2), pp. 1–7. doi: 10.1371/journal.pone.0032117.

Lawrence, M. S., Sougnez, C., Lichtenstein, L., Cibulskis, K., Lander, E., Gabriel, S. B., Getz, G., Ally, A., Balasundaram, M., Birol, I., Bowlby, R., Brooks, D., Butterfield, Y. S. N., Carlsen, R., Cheng, D., Chu, A., Dhalla, N., Guin, R., Holt, R. A., Jones, S. J. M., Lee, D., Li, H. I., Marra, M. A., Mayo, M., Moore, R. A., Mungall, A. J., Robertson, A. G., Schein, J. E., Sipahimalani, P., Tam, A., Thiessen, N., Wong, T., Protopopov, A., Santoso, N., Lee, S., Parfenov, M., Zhang, Jianhua, Mahadeshwar, H. S.,

Tang, J., Ren, X., Seth, S., Haseley, P., Zeng, D., Yang, Lixing, Xu, A. W., Song, X., Pantazi, A., Bristow, C. A., Hadjipanayis, A., Seidman, J., Chin, L., Park, P. J., Kucherlapati, R., Akbani, R., Casasent, T., Liu, W., Lu, Y., Mills, G., Motter, T., Weinstein, J., Diao, L., Wang, J., Hong Fan, Y., Liu, J., Wang, K., Auman, J. T., Balu, S., Bodenheimer, T., Buda, E., Hayes, D. N., Hoadley, K. A., Hoyle, A. P., Jefferys, S. R., Jones, C. D., Kimes, P. K., Liu, Yufeng, Marron, J. S., Meng, S., Mieczkowski, P. A., Mose, L. E., Parker, J. S., Perou, C. M., Prins, J. F., Roach, J., Shi, Y., Simons, J. V., Singh, D., Soloway, M. G., Tan, D., Veluvolu, U., Walter, V., Waring, S., Wilkerson, M. D., Wu, J., Zhao, N., Cherniack, A. D., Hammerman, P. S., Tward, A. D., Pedamallu, C. S., Saksena, G., Jung, J., Ojesina, A. I., Carter, S. L., Zack, T. I., Schumacher, S. E., Beroukhim, R., Freeman, S. S., Meyerson, M., Cho, J., Noble, M. S., DiCara, D., Zhang, H., Heiman, D. I., Gehlenborg, N., Voet, D., Lin, P., Frazer, S., Stojanov, P., Liu, Yingchun, Zou, L., Kim, J., Muzny, D., Doddapaneni, H. V., Kovar, C., Reid, J., Morton, D., Han, Y., Hale, W., Chao, H., Chang, K., Drummond, J. A., Gibbs, R. A., Kakkar, N., Wheeler, D., Xi, L., Ciriello, G., Ladanyi, M., Lee, W., Ramirez, R., Sander, C., Shen, R., Sinha, R., Weinhold, N., Taylor, B. S., Aksoy, B. A., Dresdner, G., Gao, J., Gross, B., Jacobsen, A., Reva, B., Schultz, N., Sumer, S. O., Sun, Y., Chan, T. A., Morris, L. G., Stuart, J., Benz, S., Ng, S., Benz, C., Yau, C., Baylin, S. B., Cope, L., Danilova, L., Herman, J. G., Bootwalla, M., Maglinte, D. T., Laird, P. W., Triche, T., Weisenberger, D. J., Van Den Berg, D. J., Agrawal, N., Bishop, J., Boutros, P. C., Bruce, J. P., Byers, L. A., Califano, J., Carey, T. E., Chen, Z., Cheng, H., Chiosea, S. I., Cohen, E., Diergaarde, B., Egloff, A. M., El-Naggar, A. K., Ferris, R. L., Frederick, M. J., Grandis, J. R., Guo, Y., Haddad, R. I., Harris, T., Hui, A. B. Y., Lee, J. J., Lippman, S. M., Liu, F. F., McHugh, J. B., Myers, J., Ng, P. K. S., Perez-Ordonez, B., Pickering, C. R., Prystowsky, M., Romkes, M., Saleh, A. D., Sartor, M. A., Seethala, R., Seiwert, T. Y., Si, H., Van Waes, C., Waggott, D. M., Wiznerowicz, M., Yarbrough, W. G., Zhang, Jiexin, Zuo, Z., Burnett, K., Crain, D., Gardner, J., Lau, K., Mallery, D., Morris, S., Paulauskis, J., Penny, R., Shelton, C., Shelton, T., Sherman, M., Yena, P., Black, A. D., Bowen, J., Frick, J., Gastier-Foster, J. M., Harper, H. A., Leraas, K., Lichtenberg, T. M., Ramirez, N. C., Wise, L., Zmuda, E., Baboud, J., Jensen, M. A., Kahn, A. B., Pihl, T. D., Pot, D. A., Srinivasan, D., Walton, J. S., Wan, Y., Burton, R. A., Davidsen, T., Demchok, J. A., Eley, G., Ferguson, M. L., Mills Shaw, K. R., Ozenberger, B. A., Sheth, M., Sofia, H. J., Tarnuzzer, R., Wang, Z., Yang, Liming, Zenklusen, J. C., Saller, C., Tarvin, K., Chen, C., Bollag, R., Weinberger, P., Golusiński, W., Golusiński, P., Ibbs, M., Korski, K., Mackiewicz, A., Suchorska, W., Szybiak, B., Curley, E., Beard, C., Mitchell, C., Sandusky, G., Ahn, J., Khan, Z., Irish, J., Waldron, J., William, W. N., Egea, S., Gomez-Fernandez, C., Herbert, L., Bradford, C. R., Chepeha, D. B., Haddad, A. S., Jones, T. R., Komarck, C. M., Malakh, M., Moyer, J. S., Nguyen, A., Peterson, L. A., Prince, M. E., Rozek, L. S., Taylor, E. G., Walline, H. M., Wolf, G. T., Boice, L., Chera, B. S., Funkhouser, W. K., Gulley, M. L., Hackman, T. G., Hayward, M. C., Huang, M., Rathmell, W. K., Salazar, A. H., Shockley, W. W., Shores, C. G., Thorne, L., Weissler, M. C., Wrenn, S., Zanation, A. M., Brown, B. T. and Pham, M. (2015) 'Comprehensive genomic characterization of head and neck squamous cell carcinomas', *Nature*, 517(7536), pp. 576–582. doi: 10.1038/nature14129.

Leavenworth, J. W., Verbinnen, B., Wang, Q., Shen, E. and Cantor, H. (2015) 'Intracellular osteopontin regulates homeostasis and function of natural killer cells', *Proceedings of the National Academy of Sciences of the United States of America*, 112(2), pp. 494–499. doi: 10.1073/pnas.1423011112.

LeBleu, V. S. and Kalluri, R. (2018) 'A peek into cancer-associated fibroblasts: Origins, functions and translational impact', *DMM Disease Models and Mechanisms*, 11(4), pp. 1–9. doi: 10.1242/dmm.029447.

Lee, B. Y., Han, J. A., Im, J. S., Morrone, A., Johung, K., Goodwin, E. C., Kleijer, W. J., DiMaio, D. and Hwang, E. S. (2006) 'Senescence-associated β-galactosidase is lysosomal β-galactosidase', *Aging Cell*, 5(2), pp. 187–195. doi: 10.1111/j.1474-9726.2006.00199.x.

Leemans, C. R., Braakhuis, B. J., & Brakenhoff, R. H. (2011). The molecular biology of head and neck cancer. *Nature reviews. Cancer*, 11(1), 9–22. https://doi.org/10.1038/nrc2982.

Lenga, Y., Koh, A., Perera, A. S., McCulloch, C. A., Sodek, J. and Zohar, R. (2008) 'Osteopontin expression is required for myofibroblast differentiation', *Circulation Research*, 102(3), pp. 319–327.

doi: 10.1161/CIRCRESAHA.107.160408.

Levental, K. Yu, H. (2010) 'Matrix Crosslinking Forces Tumor Progression by Enhancing Integrin signaling', *Bone*, 23(1), pp. 1–20. doi: 10.1016/j.cell.2009.10.027.Matrix.

Lewis, J. S. (2020) 'Human Papillomavirus Testing in Head and Neck Squamous Cell Carcinoma in 2020: Where Are We Now and Where Are We Going?', *Head and Neck Pathology*. Springer US, 14(2), pp. 321–329. doi: 10.1007/s12105-019-01117-y.

Lewis, J. S., Chernock, R. D. and Chernock, R. D. (2014) 'Human papillomavirus and Epstein Barr virus in head and neck carcinomas: suggestions for the new WHO classification.', *Head and neck pathology*. Springer, 8(1), pp. 50–8. doi: 10.1007/s12105-014-0528-6.

Lewis, M. P., Lygoe, K. A., Nystrom, M. L., Anderson, W. P., Speight, P. M., Marshall, J. F. and Thomas, G. J. (2004) 'Tumour-derived TGF-β1 modulates myofibroblast differentiation and promotes HGF/SF-dependent invasion of squamous carcinoma cells', *British Journal of Cancer*. Nature Publishing Group, 90(4), pp. 822–832. doi: 10.1038/sj.bjc.6601611.

Li, H., Courtois, E. T., Sengupta, D., Tan, Y., Chen, K. H., Goh, J. J. L., Kong, S. L., Chua, C., Hon, L. K., Tan, W. S., Wong, M., Choi, P. J., Wee, L. J. K., Hillmer, A. M., Tan, I. B., Robson, P. and Prabhakar, S. (2017) 'Reference component analysis of single-cell transcriptomes elucidates cellular heterogeneity in human colorectal tumors', *Nature Genetics*. Nature Publishing Group, 49(5), pp. 708–718. doi: 10.1038/ng.3818.

Li, J., Yang, G. Z., Zhu, Z. M., Zhou, Z. Y., & Li, L. (2012). Osteopontin is overexpressed in colorectal carcinoma and is correlated with P53 by immunohistochemistry. *Experimental and therapeutic medicine*, 3(4), 621–624. https://doi.org/10.3892/etm.2012.465.

Li, X., Xu, Q., Wu, Y., Li, J., Tang, D., Han, L. and Fan, Q. (2014) 'A CCL2/ROS autoregulation loop is critical for cancer-associated fibroblasts-enhanced tumor growth of oral squamous cell carcinoma', *Carcinogenesis*, 35(6), pp. 1362–1370. doi: 10.1093/carcin/bgu046.

Li, Y. yin, Zhou, C. X. and Gao, Y. (2018) 'Interaction between oral squamous cell carcinoma cells and fibroblasts through TGF-β1 mediated by podoplanin', *Experimental Cell Research*. Elsevier Inc., 369(1), pp. 43–53. doi: 10.1016/j.yexcr.2018.04.029.

Liaw, L., Birk, D. E., Ballas, C. B., Whitsitt, J. S., Davidson, J. M. and Hogan, B. L. (1998) 'Altered wound healing in mice lacking a functional osteopontin gene (spp1).', *Journal of Clinical Investigation*, 101(7), pp. 1468–1478. doi: 10.1172/jci2131.

Liguori, M., Solinas, G., Germano, G., Mantovani, A. and Allavena, P. (2011) 'Tumor-associated macrophages as incessant builders and destroyers of the cancer stroma', *Cancers*, 3(4), pp. 3740–3761. doi: 10.3390/cancers3043740.

Lim, K. P., Cirillo, N., Hassona, Y., Wei, W., Thurlow, Johanna K., Cheong, S. C., Pitiyage, G., Parkinson, E. K. and Prime, S. S. (2011) 'Fibroblast gene expression profile reflects the stage of tumour progression in oral squamous cell carcinoma', *Journal of Pathology*, 223(4), pp. 459–469. doi: 10.1002/path.2841.

Lim, K. P., Cirillo, N., Hassona, Y., Wei, W., Thurlow, Johanna K, Cheong, S. C., Pitiyage, G., Parkinson, E. K. and Prime, S. S. (2011) 'Fibroblast gene expression profile reflects the stage of tumour progression in oral squamous cell carcinoma', *The Journal of Pathology*, 223(4), pp. 459–469. doi: 10.1002/path.2841.

Lin, J. and Ding, D. (2017) 'The prognostic role of the cancer stem cell marker CD44 in ovarian cancer: A meta-analysis', *Cancer Cell International*. BioMed Central, 17(1), pp. 1–11. doi: 10.1186/s12935-016-0376-4.

Lindquist, D., Romanitan, M., Hammarstedt, L., Näsman, A., Dahlstrand, H., Lindholm, J., Onelöv, L., Ramqvist, T., Ye, W., Munck-Wikland, E. and Dalianis, T. (2007) 'Human papillomavirus is a favourable prognostic factor in tonsillar cancer and its oncogenic role is supported by the expression of E6 and E7', *Molecular Oncology*, 1(3), pp. 350–355. doi: 10.1016/j.molonc.2007.08.005.

Liu, F., Lagares, D., Choi, K. M., Stopfer, L., Marinković, A., Vrbanac, V., Probst, C. K., Hiemer, S. E., Sisson, T. H., Horowitz, J. C., Rosas, I. O., Fredenburgh, L. E., Feghali-Bostwick, C., Varelas, X., Tager, A. M. and Tschumperlin, D. J. (2015) 'Mechanosignaling through YAP and TAZ drives fibroblast activation and fibrosis', *American Journal of Physiology - Lung Cellular and Molecular Physiology*, 308(4), pp. L344–L357. doi: 10.1152/ajplung.00300.2014.

Liu, K., Hu, H., Jiang, H., Liu, C., Zhang, H., Gong, S., Wei, D. and Yu, Z. (2020) 'Upregulation of secreted phosphoprotein 1 affects malignant progression, prognosis, and resistance to cetuximab via the KRAS/MEK pathway in head and neck cancer', *Molecular Carcinogenesis*, 59(10), pp. 1147–1158. doi: 10.1002/mc.23245.

Liu, T., Han, C., Wang, S., Fang, P., Ma, Z., Xu, L. and Yin, R. (2019) 'Cancer-associated fibroblasts: An emerging target of anti-cancer immunotherapy', *Journal of Hematology and Oncology*. Journal of Hematology & Oncology, 12(1), pp. 1–15. doi: 10.1186/s13045-019-0770-1.

Liu, W. L., Zhang, H., Zheng, Y., Wang, H. T., Chen, F. H., Xu, L., Wei, Y., Sun, Y. Q., Shi, J. B. and Li, H. B. (2015) 'Expression and regulation of osteopontin in chronic rhinosinusitis with nasal polyps', *Clinical and Experimental Allergy*, 45(2), pp. 414–422. doi: 10.1111/cea.12320.

Liu, Y., Hu, T., Shen, J., Li, S. F., Lin, J. W., Zheng, X. H., Gao, Q. H. and Zhou, H. M. (2006) 'Separation, cultivation and biological characteristics of oral carcinoma-associated fibroblasts', *Oral Diseases*, 12(4), pp. 375–380. doi: 10.1111/j.1601-0825.2005.01207.x.

Lloyd, A. C. (2013) 'XThe regulation of cell size', *Cell*. Elsevier Inc., 154(6), p. 1194. doi: 10.1016/j.cell.2013.08.053.

Loffredo, F. S., Steinhauser, M. L., Jay, S. M., Gannon, J., Pancoast, J. R., Yalamanchi, P., Sinha, M., Dall'Osso, C., Khong, D., Shadrach, J. L., Miller, C. M., Singer, B. S., Stewart, A., Psychogios, N., Gerszten, R. E., Hartigan, A. J., Kim, M. J., Serwold, T., Wagers, A. J. and Lee, R. T. (2013) 'Growth differentiation factor 11 is a circulating factor that reverses age-related cardiac hypertrophy', *Cell*, 153(4), pp. 828–839. doi: 10.1016/j.cell.2013.04.015.

Logan, B., 2016. McMinn's color atlas of head and neck anatomy. 5th ed. Elsevier Limited, p.397.

Löhr, M., Schmidt, C., Ringel, J., Kluth, M., Müller, P., Nizze, H. and Jesnowski, R. (2001) 'Transforming growth factor-β1 induces desmoplasia in an experimental model of human pancreatic carcinoma', *Cancer Research*, 61(2), pp. 550–555.

Longworth, M. S. and Laimins, L. a (2004) 'Pathogenesis of Human Papillomaviruses in Differentiating Epithelia Pathogenesis of Human Papillomaviruses in Differentiating Epithelia', *Microbiology and molecular biology reviews*, 68(2), pp. 362–372. doi: 10.1128/MMBR.68.2.362.

Lotfi, N., Thome, R., Rezaei, N., Zhang, G. X., Rezaei, A., Rostami, A. and Esmaeil, N. (2019) 'Roles

of GM-CSF in the pathogenesis of autoimmune diseases: An update', *Frontiers in Immunology*, 10(6), pp. 1–14. doi: 10.3389/fimmu.2019.01265.

Loughran, O., Clark, L. J., Bond, J., Baker, A., Berry, I. J., Edington, K. G., Ly, I. S., Simmons, R., Haw, R., Black, D. M., Newbold, R. F. and Parkinson, E. K. (1997) 'Evidence for the inactivation of multiple replicative lifespan genes in immortal human squamous cell carcinoma keratinocytes', *Oncogene*, 14(16), pp. 1955–1964. doi: 10.1038/sj.onc.1201028.

Louie, K. S., Mehanna, H. and Sasieni, P. (2015) 'Trends in head and neck cancers in England from 1995 to 2011 and projections up to 2025', *Oral Oncology*. Elsevier Ltd, 51(4), pp. 341–348. doi: 10.1016/j.oraloncology.2015.01.002.

Lu, P., Weaver, V. M. and Werb, Z. (2012) 'The extracellular matrix: a dynamic niche in cancer progression.', *The Journal of cell biology*. The Rockefeller University Press, 196(4), pp. 395–406. doi: 10.1083/jcb.201102147.

Ludwig, N., Szczepanski, M. J., Gluszko, A., Szafarowski, T., Azambuja, J. H., Dolg, L., Gellrich, N. C., Kampmann, A., Whiteside, T. L. and Zimmerer, R. M. (2019) 'CD44(+) tumor cells promote early angiogenesis in head and neck squamous cell carcinoma', *Cancer Letters*. Elsevier, 467(9), pp. 85–95. doi: 10.1016/j.canlet.2019.10.010.

Luo, S. D., Chen, Y. J., Liu, C. T., Rau, K. M., Chen, Y. C., Tsai, H. T., Chen, C. H. and Chiu, T. J. (2015) 'Osteopontin Involves Cisplatin Resistance and Poor Prognosis in Oral Squamous Cell Carcinoma', *BioMed Research International*. Hindawi Publishing Corporation, 2015. doi: 10.1155/2015/508587.

Ma, C. and Lewis, J. (2012) 'Small Biopsy Specimens Reliably Indicate p16 Expression Status of Oropharyngeal Squamous Cell Carcinoma', *Head and Neck Pathology*, 6(2), pp. 208–215. doi: 10.1007/s12105-011-0322-7.

Mac, M. and Moody, C. A. (2020) 'Epigenetic regulation of the human papillomavirus life cycle', *Pathogens*. Seminars in Immunopathology, 9(6), pp. 1–18. doi: 10.3390/pathogens9060483.

Madar, S., Goldstein, I. and Rotter, V. (2013) '"Cancer associated fibroblasts" – more than meets the eye', *Trends in Molecular Medicine*, 19(8), pp. 447–453. doi: 10.1016/j.molmed.2013.05.004.

Madsen, C. D., Pedersen, J. T., Venning, F. A., Singh, L. B., Moeendarbary, E., Charras, G., Cox, T. R., Sahai, E. and Erler, J. T. (2015) ' Hypoxia and loss of PHD 2 inactivate stromal fibroblasts to decrease tumour stiffness and metastasis ', *EMBO reports*, 16(10), pp. 1394–1408. doi: 10.15252/embr.201540107.

Maleš, J., Mihalj, H., Šestak, A., Kralik, K. and Smolić, M., 2021. Osteopontin Levels in Patients with Squamous Metastatic Head and Neck Cancer. *Medicina*, 57(2), p.185.

Malyankar, U. M., Almeida, M., Johnson, R. J., Pichler, R. H. and Giachelli, C. M. (1997) 'Osteopontin regulation in cultured rat renal epithelial cells', *Kidney International*. Elsevier Masson SAS, 51(6), pp. 1766–1773. doi: 10.1038/ki.1997.243.

Manukian, G., Bar-Ad, V., Lu, B., Argiris, A. and Johnson, J. M. (2019) 'Combining radiation and immune checkpoint blockade in the treatment of head and neck squamous cell carcinoma', *Frontiers in Oncology*, 9(3), pp. 1–14. doi: 10.3389/fonc.2019.00122.

Maris, P., Blomme, A., Palacios, A. P., Costanza, B., Bellahcène, A., Bianchi, E., Gofflot, S., Drion, P., Trombino, G. E., Di Valentin, E., Cusumano, P. G., Maweja, S., Jerusalem, G., Delvenne, P., Lifrange,

E., Castronovo, V. and Turtoi, A. (2015) 'Asporin Is a Fibroblast-Derived TGF-β1 Inhibitor and a Tumor Suppressor Associated with Good Prognosis in Breast Cancer', *PLoS Medicine*, 12(9), pp. 1–29. doi: 10.1371/journal.pmed.1001871.

Marques, C., Priscila, S., Abreu, M. De, Ventorin, S., Laís, V. Z. and Jesus, M. De (2021) 'Human Papillomavirus DNA Detection by Droplet Digital PCR in Formalin - Fixed Paraffin - Embedded Tumor Tissue from Oropharyngeal Squamous Cell Carcinoma Patients', *Molecular Diagnosis & Therapy*. Springer International Publishing, 25(1), pp. 59–70. doi: 10.1007/s40291-020-00502-6.

Marsh, D., Suchak, K., Moutasim, Karwan A, Vallath, S., Hopper, C., Jerjes, W., Upile, T., Kalavrezos, N., Violette, S. M., Weinreb, P. H., Chester, K. A., Chana, J. S., Marshall, J. F., Hart, I. R., Hackshaw, A. K., Piper, K. and Thomas, G. J. (2011) 'Stromal features are predictive of disease mortality in oral cancer patients', *The Journal of Pathology*, 223(4), pp. 470–481. doi: 10.1002/path.2830.

Martel, C. De, Georges, D., Bray, F., Ferlay, J. and Clifford, G. M. (2020) 'Global burden of cancer attributable to infections in 2018 : a worldwide incidence analysis', *The Lancet Global Health*. International Agency for Research on Cancer, 8(2), pp. e180–e190. doi: 10.1016/S2214-109X(19)30488-7.

Martel, C., Plummer, M., Vignat, J. and Franceschi, S. (2017) 'Worldwide burden of cancer attributable to HPV by site, country and HPV type', *International Journal of Cancer*, 141(4), pp. 664–670. doi: 10.1002/ijc.30716.

Massagué, J. (2012) 'TGFβ signalling in context', *Nature Reviews Molecular Cell Biology*. Nature Publishing Group, 13(10), pp. 616–630. doi: 10.1038/nrm3434.

Maxwell, J., Kumar, B., Feng, F., Worden, F., Lee, J., Eisbruch, A., Wolf, G., Prince, M., Moyer, J., Teknos, T., Chepeha, D., McHugh, J., Urba, S., Stoerker, J., Walline, H., Kurnit, D., Cordell, K., Davis, S., Ward, P., Bradford, C. and Carey, T., 2010. Tobacco Use in Human Papillomavirus-Positive Advanced Oropharynx Cancer Patients Related to Increased Risk of Distant Metastases and Tumor Recurrence. *Clinical Cancer Research*, 16(4), pp.1226-1235.

Mazul, A., Rodriguez-Ormaza, Nidia. Taylor, J., Dipan D Desai2, F. and Paul Brennan, C. (2016) 'Prognostic significance of non-HPV16 genotypes in oropharyngeal squamous cell carcinoma', *Physiology & behavior*, 176(10), pp. 139–148. doi: 10.1016/j.oraloncology.2016.08.019.Prognostic.

McAllister, S. S., Gifford, A. M., Greiner, A. L., Kelleher, S. P., Saelzler, M. P., Ince, T. A., Reinhardt, F., Harris, L. N., Hylander, B. L., Repasky, E. A. and Weinberg, R. A. (2008) 'Systemic Endocrine Instigation of Indolent Tumor Growth Requires Osteopontin', *Cell*, 133(6), pp. 994–1005. doi: 10.1016/j.cell.2008.04.045.

McAnulty, R. J. (2007) 'Fibroblasts and myofibroblasts: Their source, function and role in disease', *The International Journal of Biochemistry & Cell Biology*. Pergamon, 39(4), pp. 666–671. doi: 10.1016/J.BIOCEL.2006.11.005.

McLaughlin-Drubin, M. E., Crum, C. P. and Münger, K. (2011) 'Human papillomavirus E7 oncoprotein induces KDM6A and KDM6B histone demethylase expression and causes epigenetic reprogramming', *Proceedings of the National Academy of Sciences of the United States of America*, 108(5), pp. 2130–2135. doi: 10.1073/pnas.1009933108.

Mehanna, H., Robinson, M., Hartley, A., Kong, A., Foran, Bernadette, Fulton-Lieuw, T., Dalby, M., Mistry, P., Sen, M., O'Toole, L., Al Booz, H., Dyker, K., Moleron, R., Whitaker, S., Brennan, Sinead, Cook, A., Griffin, M., Aynsley, E., Rolles, M., De Winton, E., Chan, A., Srinivasan, D., Nixon, I., Grumett, J., Leemans, C. R., Buter, J., Henderson, J., Harrington, K., McConkey, C.,

Gray, A., Dunn, J., McArdle, O., Husband, D., Loo, V., Soe, W., Sridhar, T., Jankowska, P., Joseph, M., Geropantas, K., Vaidya, D., Vijayan, R., Hwang, D., Pettit, L., Brennan, Sinéad, Mendes, R., Forster, M., Evans, M., Foran, Bernie, Nankivell, P., Bryant, J., Sharma, N., Spruce, R., Brooks, J., Batis, N., Roques, T., Bidmead, M., Yang, H., Nutting, C., Tyler, J., Baines, H., Gasnier, A., Miles, E. and Clark, C. (2019) 'Radiotherapy plus cisplatin or cetuximab in low-risk human papillomavirus-positive oropharyngeal cancer (De-ESCALaTE HPV): an open-label randomised controlled phase 3 trial', *The Lancet*, 393(10166), pp. 51–60. doi: 10.1016/S0140-6736(18)32752-1.

Melling, G. E. (2015) *The Role of microRNA-145 in the Tumour Microenvironment* . Ph.D, University of Sheffield.

Melling, G. E., Flannery, S. E., Abidin, S. A., Clemmens, H., Prajapati, P., Hinsley, E. E., Hunt, S., Catto, J. W. F., Coletta, R. Della, Mellone, M., Thomas, G. J., Parkinson, E. K., Prime, S. S., Paterson, I. C., Buttle, D. J. and Lambert, D. W. (2018) 'A miRNA-145/TGF-β1 negative feedback loop regulates the cancer-associated fibroblast phenotype', *Carcinogenesis*. doi: 10.1093/carcin/bgy032.

Mellone, M., Hanley, C. J., Thirdborough, S., Mellows, T., Garcia, E., Woo, J., Tod, J., Frampton, S., Jenei, V., Moutasim, K. A., Kabir, T. D., Brennan, P. A., Venturi, G., Ford, K., Herranz, N., Lim, K. P., Clarke, J., Lambert, D. W., Prime, S. S., Underwood, T. J., Vijayanand, P., Eliceiri, K. W., Woelk, C., King, E. V., Gil, J., Ottensmeier, C. H. and Thomas, G. J. (2016) 'Induction of fibroblast senescence generates a non-fibrogenic myofibroblast phenotype that differentially impacts on cancer prognosis', *Aging*, 9(1), pp. 114–132. doi: 10.18632/aging.101127.

Mena, M., Taberna, M., Tous, S., Marquez, S., Clavero, O., Quiros, B., Lloveras, B., Alejo, M., Leon, X., Quer, M., Bagué, S., Mesia, R., Nogués, J., Gomà, M., Aguila, A., Bonfill, T., Blazquez, C., Guix, M., Hijano, R., Torres, M., Holzinger, D., Pawlita, M., Pavon, M. A., Bravo, I. G., de Sanjosé, S., Bosch, F. X. and Alemany, L. (2018) 'Double positivity for HPV-DNA/p16ink4a is the biomarker with strongest diagnostic accuracy and prognostic value for human papillomavirus related oropharyngeal cancer patients', *Oral Oncology*, 78(2), pp. 137–144. doi: 10.1016/j.oraloncology.2018.01.010.

Mendez-Pena, J. E., Sadow, P. M., Nose, V. and Hoang, M. P. (2017) 'RNA chromogenic in situ hybridization assay with clinical automated platform is a sensitive method in detecting high-risk human papillomavirus in squamous cell carcinoma', *Human Pathology*. Elsevier Inc., 63, pp. 184–189. doi: 10.1016/j.humpath.2017.02.021.

Meng, W., Xia, Q., Wu, L., Chen, S., He, X., Zhang, L., Gao, Q. and Zhou, H. (2011) 'Downregulation of TGF-beta receptor types II and III in oral squamous cell carcinoma and oral carcinoma-associated fibroblasts', *BMC Cancer*. BioMed Central Ltd, 11(1), p. 88. doi: 10.1186/1471-2407-11-88.

Meng, X. M., Nikolic-Paterson, D. J. and Lan, H. Y. (2016) 'TGF-β: The master regulator of fibrosis', *Nature Reviews Nephrology*. Nature Publishing Group, 12(6), pp. 325–338. doi: 10.1038/nrneph.2016.48.

Mirghani, H., Amen, F., Blanchard, P., Moreau, F., Guigay, J., Hartl, D. M. and Lacau St Guily, J. (2015) 'Treatment de-escalation in HPV-positive oropharyngeal carcinoma: Ongoing trials, critical issues and perspectives', *International Journal of Cancer*, 136(7), pp. 1494–1503. doi: 10.1002/ijc.28847.

Mirghani, H., Amen, F., Moreau, F., Guigay, J., Ferchiou, M., Melkane, A. E., Hartl, D. M. and Lacau St Guily, J. (2014) 'Human papilloma virus testing in oropharyngeal squamous cell carcinoma: What the clinician should know', *Oral Oncology*, 50(1), pp. 1–9. doi: 10.1016/j.oraloncology.2013.10.008.

Mirghani, H., Casiraghi, O., Guerlain, J., Amen, F., He, M., Ma, X., Luo, Y., Mourareau, C., Drusch, F., Ben, A., Melkane, A., St, L., Badoual, C., Yves, J., Borget, I., Aupérin, A., Dalstein, V. and Vielh, P.

(2016) ‘Diagnosis of HPV driven oropharyngeal cancers : Comparing p16 based algorithms with the RNAscope HPV-test’, 62, pp. 101–108. doi: 10.1016/j.oraloncology.2016.10.009.

Mirza, M., Shaughnessy, E., Hurley, J. K., Vanpatten, K. A., Pestano, G. A., He, B. and Weber, G. F. (2008) ‘Osteopontin-c is a selective marker of breast cancer’, *International Journal of Cancer*, 122(4), pp. 889–897. doi: 10.1002/ijc.23204.

Moorman, H. R., Poschel, D., Klement, J. D., Lu, C., Redd, P. S. and Liu, K. (2020) ‘Osteopontin: A key regulator of tumor progression and immunomodulation’, *Cancers*, 12(11), pp. 1–31. doi: 10.3390/cancers12113379.

Morgan, I. M., DiNardo, L. J., & Windle, B. (2017). Integration of Human Papillomavirus Genomes in Head and Neck Cancer: Is It Time to Consider a Paradigm Shift?. *Viruses*, *9*(8), 208. https://doi.org/10.3390/v9080208

Mori, R., Shaw, T. J. and Martin, P. (2008) ‘Molecular mechanisms linking wound inflammation and fibrosis: Knockdown of osteopontin leads to rapid repair and reduced scarring’, *Journal of Experimental Medicine*, 205(1), pp. 43–51. doi: 10.1084/jem.20071412.

Mourik, J. A., Leeksma, O. C., Reinders, J. H., de Groot, P. G. and Zandbergen-Spaargaren, J. (1985) ‘Vascular endothelial cells synthesize a plasma membrane protein indistinguishable from the platelet membrane glycoprotein IIa’, *Journal of Biological Chemistry*, 260(20), pp. 11300–11306. doi: 10.1016/S0021-9258(17)39180-9.

Moutasim, K. A., Robinson, M. and Thavaraj, S. (2015) ‘Human papillomavirus testing in diagnostic head and neck histopathology’, *Diagnostic Histopathology*. Elsevier BV, 21(2), pp. 77–84. doi: 10.1016/j.mpdhp.2015.02.002.

Müller, S., Khuri, F. R., Kono, S. A., Beitler, J. J., Shin, D. M., & Saba, N. F. (2012). HPV positive squamous cell carcinoma of the oropharynx. Are we observing an unusual pattern of metastases?. *Head and neck pathology*, *6*(3), pp. 336–344. https://doi.org/10.1007/s12105-012-0355-6.

Mughees, M., Sengupta, A., Khowal, S. and Wajid, S. (2021) ‘Mechanism of tumour microenvironment in the progression and development of oral cancer’, *Molecular Biology Reports*. Springer Netherlands, 48(2), pp. 1773–1786. doi: 10.1007/s11033-020-06054-6.

Mukaratirwa, S., Koninkx, J. F., Gruys, E. and Nederbragt, H. (2005) ‘Mutual paracrine effects of colorectal tumour cells and stromal cells: Modulation of tumour and stromal cell differentiation and extracellular matrix component production in culture’, *International Journal of Experimental Pathology*, 86(4), pp. 219–229. doi: 10.1111/j.0959-9673.2005.00425.x.

Näsman, A., Nordfors, C., Grün, N., Munck-Wikland, E., Ramqvist, T., Marklund, L., Lindquist, D. and Dalianis, T. (2013) ‘Absent/weak CD44 intensity and positive human papillomavirus (HPV) status in oropharyngeal squamous cell carcinoma indicates a very high survival’, *Cancer Medicine*, 2(4), pp. 507–518. doi: 10.1002/cam4.90.

Naugler, W. E. and Karin, M. (2008) ‘The wolf in sheep’s clothing: the role of interleukin-6 in immunity, inflammation and cancer’, *Trends in Molecular Medicine*, 14(3), pp. 109–119. doi: 10.1016/j.molmed.2007.12.007.

Neal, J. T., Li, X., Zhu, J., Giangarra, V., Caitlin, L., Ju, J., Liu, I. H., Chiou, S., Salahudeen, A. A., Smith, R., Deutsch, B. C., Liao, L., Zemek, A. J., Zhao, F., Schultz, L. M., Metzner, T. J., Nadauld, L. D., Tseng, Y., Alkhairy, S., Oh, C., Keskula, P., Mendoza-villanueva, D. and De, F. M. (2019) ‘Organoid

modeling of the tumor immune microenvironment James', 175(7), pp. 1972–1988. doi: 10.1016/j.cell.2018.11.021.Organoid.

New, L. and Han, J. (1998) 'The p38 MAP kinase pathway and its biological function', *Trends in Cardiovascular Medicine*, 8(5), pp. 220–228. doi: 10.1016/S1050-1738(98)00012-7.

Nice.org.uk. 2021. *Overview | Cancer of the upper aerodigestive tract: assessment and management in people aged 16 and over | Guidance | NICE*. [online] Available at: <https://www.nice.org.uk/guidance/ng36> [Accessed 14 March 2021].

Ninck, S., Reisser, C., Dyckhoff, G., Helmke, B., Bauer, H. and Herold-Mende, C. (2003) 'Expression profiles of angiogenic growth factors in squamous cell carcinomas of the head and neck', *International Journal of Cancer*, 106(1), pp. 34–44. doi: 10.1002/ijc.11188.

O'Brien, E. R., Garvin, M. R., Stewart, D. K., Hinohara, T., Simpson, J. B., Schwartz, S. M. and Giachelli, C. M. (1994) 'Osteopontin is synthesized by macrophage, smooth muscle, and endothelial cells in primary and restenotic human coronary atherosclerotic plaques', *Arteriosclerosis and Thrombosis*, 14(10), pp. 1648–1656. doi: 10.1161/01.atv.14.10.1648.

O'Sullivan, B., Huang, S. H., Perez-Ordonez, B., Massey, C., Siu, L. L., Weinreb, I., Hope, A., Kim, J., Bayley, A. J., Cummings, B., Ringash, J., Dawson, L. A., Cho, B. C. J., Chen, E., Irish, J., Gilbert, R. W., Hui, A., Liu, F.-F., Zhao, H., Waldron, J. N. and Xu, W. (2012) 'Outcomes of HPV-related oropharyngeal cancer patients treated by radiotherapy alone using altered fractionation', *Radiotherapy and Oncology*, 103(1), pp. 49–56. doi: 10.1016/j.radonc.2012.02.009.

O'Sullivan, B., Huang, S. H., Siu, L. L., Waldron, J., Zhao, H., Perez-Ordonez, B., Weinreb, I., Kim, J., Ringash, J., Bayley, A., Dawson, L. A., Hope, A., Cho, J., Irish, J., Gilbert, R., Gullane, P., Hui, A., Liu, F.-F., Chen, E. and Xu, W. (2013) 'Deintensification Candidate Subgroups in Human Papillomavirus–Related Oropharyngeal Cancer According to Minimal Risk of Distant Metastasis', *Journal of Clinical Oncology*, 31(5), pp. 543–550. doi: 10.1200/JCO.2012.44.0164.

Ogbureke, K. U., Nikitakis, N. G., Warburton, G., Ord, R. A., Sauk, J. J., Waller, J. L. and Fisher, L. W. (2007) 'Up-regulation of SIBLING proteins and correlation with cognate MMP expression in oral cancer', *Oral Oncology*, 43(9), pp. 920–932. doi: 10.1016/j.oraloncology.2006.11.011.

Ogbureke, K. U., Weinberger, P. M., Looney, S. W., Li, L. and Fisher, L. W. (2012) 'Expressions of matrix metalloproteinase-9 (MMP-9), dentin sialophosphoprotein (DSPP), and osteopontin (OPN) at histologically negative surgical margins may predict recurrence of oral squamous cell carcinoma', *Oncotarget*, 3(3), pp. 286–298. doi: 10.18632/oncotarget.373.

Oguejiofor, k., 2016. *Prognostic markers in oropharyngeal cancers*. Ph.D. University of Manchester.

Oh, J., Lee, Y. D. and Wagers, A. J. (2014) 'Stem cell aging: Mechanisms, regulators and therapeutic opportunities', *Nature Medicine*. Nature Publishing Group, 20(8), pp. 870–880. doi: 10.1038/nm.3651.

Oh, K., Seo, M. W., Kim, Y. W. and Lee, D.-S. (2015) 'Osteopontin Potentiates Pulmonary Inflammation and Fibrosis by Modulating IL-17/IFN-γ-secreting T-cell Ratios in Bleomycin-treated Mice', *Immune Network*, 15(3), p. 142. doi: 10.4110/in.2015.15.3.142.

Öhlund, D., Elyada, E. and Tuveson, D. (2014) 'Fibroblast heterogeneity in the cancer wound', *Journal of Experimental Medicine*, 211(8), pp. 1503–1523. doi: 10.1084/jem.20140692.

Öhlund, D., Handly-Santana, A., Biffi, G., Elyada, E., Almeida, A. S., Ponz-Sarvise, M., Corbo, V., Oni, T. E., Hearn, S. A., Lee, E. J., Chio, I. I. C., Hwang, C. Il, Tiriac, H., Baker, L. A., Engle, D. D., Feig, C., Kultti, A., Egeblad, M., Fearon, D. T., Crawford, J. M., Clevers, H., Park, Y. and Tuveson, D. A. (2017) 'Distinct populations of inflammatory fibroblasts and myofibroblasts in pancreatic cancer', *The Journal of experimental medicine*, 214(3), pp. 579–596. doi: 10.1084/jem.20162024.

Olsen, C. L., Gardie, B., Yaswen, P. and Stampfer, M. R. (2002) 'Raf-1-induced growth arrest in human mammary epithelial cells is p16-independent and is overcome in immortal cells during conversion', *Oncogene*, 21(41), pp. 6328–6339. doi: 10.1038/sj.onc.1205780.

Olthof, N. C., Speel, E. M., Kolligs, J., Haesevoets, A., Henfling, M., Ramaekers, F. C. S., Preuss, S. F., Drebber, U., Wieland, U., Silling, S., Lam, W. L., Vucic, E. A., Kremer, B., Klussmann, J. and Huebbers, C. U. (2014) 'Comprehensive Analysis of HPV16 Integration in OSCC Reveals No Significant Impact of Physical Status on Viral Oncogene and Virally Disrupted Human Gene Expression', 9(2), pp. 1–8. doi: 10.1371/journal.pone.0088718.

Orimo, A. and Weinberg, R. A. (2006) 'Stromal fibroblasts in cancer: A novel tumor-promoting cell type', *Cell Cycle*, 5(15), pp. 1597–1601. doi: 10.4161/cc.5.15.3112.

Orimo, A. and Weinberg, R. A. (2007) 'Heterogeneity of stromal fibroblasts in tumors', *Cancer Biology and Therapy*, 6(4), pp. 618–619. doi: 10.4161/cbt.6.4.4255.

Oropharynx: Introduction. Radiology Key. 2021. [online] Available at: <https://radiologykey.com/oropharynx-introduction/> [Accessed 9 March 2021].

Osei-Sarfo, K., Tang, X.-H., Urvalek, A. M., Scognamiglio, T. and Gudas, L. J. (2013) 'The molecular features of tongue epithelium treated with the carcinogen 4-nitroquinoline-1-oxide and alcohol as a model for HNSCC', *Carcinogenesis*, 34(11), pp. 2673–2681. doi: 10.1093/carcin/bgt223.

Österreicher, C. H., Penz-Österreicher, M., Grivennikov, S. I., Guma, M., Koltsova, E. K., Datz, C., Sasik, R., Hardiman, G., Karin, M. and Brenner, D. A. (2011) 'Fibroblast-specific protein 1 identifies an inflammatory subpopulation of macrophages in the liver', *Proceedings of the National Academy of Sciences of the United States of America*, 108(1), pp. 308–313. doi: 10.1073/pnas.1017547108.

Östman, A. and Augsten, M. (2009) 'Cancer-associated fibroblasts and tumor growth - bystanders turning into key players', *Current Opinion in Genetics and Development*, 19(1), pp. 67–73. doi: 10.1016/j.gde.2009.01.003.

Overgaard, J., Eriksen, J. G., Nordsmark, M., Alsner, J. and Horsman, M. R. (2005) 'Plasma osteopontin, hypoxia, and response to the hypoxia sensitiser nimorazole in radiotherapy of head and neck cancer: Results from the DAHANCA 5 randomised double-blind placebo-controlled trial', *Lancet Oncology*. Elsevier Ltd, 6(10), pp. 757–764. doi: 10.1016/S1470-2045(05)70292-8.

Özdemir, B. C., Pentcheva-Hoang, T., Carstens, J. L., Zheng, X., Wu, C. C., Simpson, T. R., Laklai, H., Sugimoto, H., Kahlert, C., Novitskiy, S. V., DeJesus-Acosta, A., Sharma, P., Heidari, P., Mahmood, U., Chin, L., Moses, H. L., Weaver, V. M., Maitra, A., Allison, J. P., LeBleu, V. S. and Kalluri, R. (2014) 'Depletion of carcinoma-associated fibroblasts and fibrosis induces immunosuppression and accelerates pancreas cancer with reduced survival', *Cancer Cell*, 25(6), pp. 719–734. doi: 10.1016/j.ccr.2014.04.005.

Park, C. K., Jung, W. H. and Koo, J. S. (2016) 'Expression of cancer-associated fibroblast-related proteins differs between invasive lobular carcinoma and invasive ductal carcinoma', *Breast Cancer Research and Treatment*. Springer US, 159(1), pp. 55–69. doi: 10.1007/s10549-016-3929-2.

Park, J. E., Lenter, M. C., Zimmermann, R. N., Garin-Chesa, P., Old, L. J. and Rettig, W. J. (1999) 'Fibroblast activation protein, a dual specificity serine protease expressed in reactive human tumor stromal fibroblasts', *Journal of Biological Chemistry*, 274(51), pp. 36505–36512. doi: 10.1074/jbc.274.51.36505.

Parkinson, E. K., James, E. L. and Prime, S. S. (2016) 'Senescence-Derived Extracellular Molecules as Modulators of Oral Cancer Development: A Mini-Review', *Gerontology*, 62(4), pp. 417–424. doi: 10.1159/000440954.

Parrinello, S., Coppe, J. P., Krtolica, A. and Campisi, J. (2005) 'Stromal-epithelial interactions in aging and cancer: Senescent fibroblasts alter epithelial cell differentiation', *Journal of Cell Science*, 118(3), pp. 485–496. doi: 10.1242/jcs.01635.

Parsons, M. and Grabsch, H. (2009) 'How to make tissue microarrays', *Diagnostic Histopathology*. Elsevier Ltd., 15(3), pp. 142–150. doi: 10.1016/j.mpdhp.2009.01.010.

Parts of the throat (pharynx). Mayo Clinic. 2021. [online] Available at: <https://www.mayoclinic.org/parts-of-the-throat-pharynx/img-20005644> [Accessed 9 March 2021].

Patel, A. K., Vipparthi, K., Thatikonda, V., Arun, I., Bhattacharjee, S., Sharan, R., Arun, P. and Singh, S. (2018) 'A subtype of cancer-associated fibroblasts with lower expression of alpha-smooth muscle actin suppresses stemness through BMP4 in oral carcinoma', *Oncogenesis*. Springer US, 7(10). doi: 10.1038/s41389-018-0087-x.

Pazolli, E., Luo, X., Brehm, S., Carbery, K., Chung, J. J., Prior, J. L., Doherty, J., Demehri, S., Salavaggione, L., Piwnica-Worms, D. and Stewart, S. A. (2009) 'Senescent stromal-derived osteopontin promotes preneoplastic cell growth', *Cancer Research*, 69(3), pp. 1230–1239. doi: 10.1158/0008-5472.CAN-08-2970.

Peacock, B. (2018) Characterisation of extracellular vesicles released by HPV+ and HPV- oropharyngeal carcinoma cells *in vitro*. Ph.D. University of Sheffield.

Peacock, B., Rigby, A., Bradford, J., Pink, R., Hunter, K., Lambert, D. and Hunt, S. (2018) 'Extracellular vesicle microRNA cargo is correlated with HPV status in oropharyngeal carcinoma', *Journal of Oral Pathology and Medicine*, 47(10), pp. 954–963. doi: 10.1111/jop.12781.

Petraki, C. D., Gregorakis, A. K., Vaslamatzis, M. M., Papanastasiou, P. A., Yousef, G. M., Levesque, M. A. and Diamandis, E. P. (2005) 'Prognostic implications of the immunohistochemical expression of human kallikreins 5, 6, 10 and 11 in renal cell carcinoma', *Tumor Biology*, 27(1), pp. 1–7. doi: 10.1159/000090150.

Pett, M. R., Alazawi, W. O. F., Roberts, I., Dowen, S., Smith, D. I., Stanley, M. A. and Coleman, N. (2004) 'Acquisition of High-Level Chromosomal Instability Is Associated with Integration of Human Papillomavirus Type 16 in Cervical Keratinocytes', 9, pp. 1359–1368.

Pickard, R. K. L., Xiao, W., Broutian, T. R., He, X. and Gillison, M. L. (2012) 'The Prevalence and Incidence of Oral Human Papillomavirus Infection Among Young Men and Women, Aged 18–30 Years', *Sexually Transmitted Diseases*, 39(7), pp. 559–566. doi: 10.1097/OLQ.0b013e31824f1c65.

Pickering, C. R., Zhang, J., Yoo, S. Y., Bengtsson, L., Cortez, E., Xie, T., Zhang, D., Chung, W., Zweidler-mckay, P. A., Wu, X., El-naggar, A. K., Weinstein, J. N. and Frederick, M. J. (2014) 'Integrative genomic characterization of oral squamous cell carcinoma identifies frequent somatic drivers', 3(7), pp. 1–21. doi: 10.1158/2159-8290.CD-12-0537.Integrative.

Pietras, A., Katz, A. M., Ekström, E. J., Wee, B., Halliday, J. J., Pitter, K. L., Werbeck, J. L., Amankulor, N. M., Huse, J. T. and Holland, E. C. (2014) 'Osteopontin-CD44 signaling in the glioma perivascular niche enhances cancer stem cell phenotypes and promotes aggressive tumor growth', *Cell Stem Cell*, 14(3), pp. 357–369. doi: 10.1016/j.stem.2014.01.005.

Plebani, M., Al, S., Verderio, P., Locati, L., Perrone, F., Quattrone, P., Carbone, A., Pilotti, S. and Gloghini, A. (2018) 'In situ hybridization detection methods for HPV16 E6 / E7 mRNA in identifying transcriptionally active HPV infection of oropharyngeal carcinoma ':, pp. 32–42. doi: 10.1016/j.humpath.2017.09.011.

Postlethwaite, A. E., Keski-Oja, J., Moses, H. L. and Kang, A. H. (1987) 'Stimulation of the chemotactic migration of human fibroblasts by transforming growth factor β', *Journal of Experimental Medicine*, 165(1), pp. 251–256. doi: 10.1084/jem.165.1.251.

Potdar, P. D. and Chaudhary, S. (2017) 'Molecular characterization of cancer-associated fibroblasts isolated from human colorectal cancer as a major stromal cell component promoting metastasis', *Journal of Unexplored Medical Data*, 2(1), pp. 1–8. doi: 10.20517/2572-8180.2016.10.

Pourgholami, M. and Morris, D. (2008) 'Inhibitors of Vascular Endothelial Growth Factor in Cancer', *Cardiovascular & Hematological Agents in Medicinal Chemistry*, 6(4), pp. 343–347. doi: 10.2174/187152508785909528.

Powell, D. W., Adegboyega, P. A., Mari, J. F. Di and Mifflin, R. C. (2005) 'Epithelial Cells and Their Neighbors I . Role of intestinal myofibroblasts in development , repair , and cancer', pp. 2–7. doi: 10.1152/ajpgi.00075.2005.

Powell, D. W., Mifflin, R. C., Valentich, J. D., Crowe, S. E., Saada, J. I., & West, A. B. (1999). Myofibroblasts. I. Paracrine cells important in health and disease. *The American journal of physiology*, *277*(1), pp.1–9. https://doi.org/10.1152/ajpcell.1999.277.1.C1

Prasanna, V., Deepti, G., Dhiraj, T., Mane, A., Gill, S. S., Patil, T., Weber, G. F. and Kundu, G. C. (2021) 'Tumor-derived osteopontin drives the resident fi broblast to myo fi broblast differentiation through Twist1 to promote breast cancer progression', *Oncogene*. Springer US. doi: 10.1038/s41388-021-01663-2.

Prieto, L. I., Graves, S. I. and Baker, D. J. (2020) 'Insights from In Vivo Studies of Cellular Senescence', *Cells*, 9(4), pp. 1–13.

Prime, S. S., Cirillo, N., Hassona, Y., Lambert, D. W., Paterson, I. C., Mellone, M., Thomas, G. J., James, E. N. L. and Parkinson, E. K. (2017) 'Fibroblast activation and senescence in oral cancer', *Journal of Oral Pathology and Medicine*, 46(2), pp. 82–88. doi: 10.1111/jop.12456.

Proteinatlas.org. 2021. Tissue expression of SPP1 - Summary - The Human Protein Atlas. [online] Available at: <https://www.proteinatlas.org/ENSG00000118785-SPP1/tissue> [Accessed 7 February 2021].

Punt, S., Dronkers, E. A. C., Welters, M. J. P., Goedemans, R., Koljenović, S., Bloemena, E., Snijders, P. J. F., Gorter, A., van der Burg, S. H., de Jong, R. J. B. and Jordanova, E. S. (2016) 'A beneficial tumor microenvironment in oropharyngeal squamous cell carcinoma is characterized by a high T cell and low IL-17+ cell frequency', *Cancer Immunology, Immunotherapy*, 65(4), pp. 393–403. doi: 10.1007/s00262-016-1805-x.

Puram, S. V, Bober, S. L., Daly, M. B., Program, C., Chase, F., Sciences, B., Care, P., Chase, F., Behavior, S. and Neoplasms, B. (2018) 'Single-cell transcriptomic analysis of primary and metastatic

tumor ecosystems in head and neck cancer', *Cell*, 123(24), pp. 4757–4763. doi: 10.1016/j.cell.2017.10.044.Single-cell.

Qian, B. Z. and Pollard, J. W. (2010) 'Macrophage Diversity Enhances Tumor Progression and Metastasis', *Cell*, 141(1), pp. 39–51. doi: 10.1016/j.cell.2010.03.014.

Qin, C., Baba, O. and Butler, W., 2004. Post-translational Modifications of SIBLING Proteins and Their Roles in Osteogenesis and Dentinogenesis. *Critical Reviews in Oral Biology & Medicine*, 15(3), pp.126-136.

Qin, X., Yan, M., Wang, Xu, Xu, Q., Wang, Xiaoning, Zhu, X., Shi, J., Li, Z., Zhang, J. and Chen, W. (2018) 'Cancer-associated Fibroblast-derived IL-6 promotes head and neck cancer progression via the osteopontin-NF-kappa B signaling pathway', *Theranostics*, 8(4), pp. 921–940. doi: 10.7150/thno.22182.

Qiu, Y., Hu, Y., Zhang, Z. Y., Ye, L., Xu, F. H., Schneider, M. E., Ma, X. L., Du, Y. X., Zuo, X. B., Zhou, F. S., Chen, G., Xie, X. S., Zhang, Y., Xia, H. Z., Wu, J. F. and Du, W. D. (2014) 'Genetic association of osteopontin (OPN) and its receptor CD44 genes with susceptibility to Chinese gastric cancer patients', *Journal of Cancer Research and Clinical Oncology*, 140(12), pp. 2143–2156. doi: 10.1007/s00432-014-1761-9.

Quail, D. F. and Joyce, J. A. (2013) 'Microenvironmental regulation of tumor progression and metastasis', *Nature Medicine*, 19(11), pp. 1423–1437. doi: 10.1038/nm.3394.

Ragin, C. C., & Taioli, E. (2007). Survival of squamous cell carcinoma of the head and neck in relation to human papillomavirus infection: review and meta-analysis. *International journal of cancer*, 121(8), pp. 1813–1820. https://doi.org/10.1002/ijc.22851.

Ragin C. C, Reshmi SC, Gollin SM. (2004) Mapping and analysis of HPV16 integration sites in a head and neck cancer cell line. *Int J Cancer*. 10;110(5): pp. 701-9. doi: 10.1002/ijc.20193. PMID: 15146560.

Rahrotaban, S., Mahdavi, N., Abdollahi, A., Yazdani, F., Kaghazloo, A. and Derakhshan, S. (2019) 'Carcinoma-associated Fibroblasts are a Common Finding in the Microenvironment of HPV-positive Oropharyngeal Squamous Cell Carcinoma', *Applied Immunohistochemistry and Molecular Morphology*, 27(9), pp. 683–688. doi: 10.1097/PAI.0000000000000687.

Rail, C. J. N. and Rustgi, A. K. (1995) 'CD44 Isoform Expression in Primary and Metastatic Pancreatic Adenocarcinoma', *Cancer Research*, 55(9), pp. 1831–1835.

Randén-Brady, R., Carpén, T., Jouhi, L., Syrjänen, S., Haglund, C., Tarkkanen, J., Remes, S., Mäkitie, A., Mattila, P. S., Silén, S. and Hagström, J. (2019) 'In situ hybridization for high-risk HPV E6/E7 mRNA is a superior method for detecting transcriptionally active HPV in oropharyngeal cancer', *Human Pathology*, 90, pp. 97–105. doi: 10.1016/j.humpath.2019.05.006.

Rangaswami, H., Bulbule, A. and Kundu, G. C. (2006) 'Osteopontin: Role in cell signaling and cancer progression', *Trends in Cell Biology*, 16(2), pp. 79–87. doi: 10.1016/j.tcb.2005.12.005.

Rettig, E., Kiess, A. P. and Fakhry, C. (2014) 'The role of sexual behavior in head and neck cancer: Implications for prevention and therapy', *Expert Review of Anticancer Therapy*, 15(1), pp. 35–49. doi: 10.1586/14737140.2015.957189.

Rettig, E. M., Fakhry, C., Khararjian, A. and Westra, W. H. (2018a) 'Age profile of patients with oropharyngeal squamous cell carcinoma', *JAMA Otolaryngology - Head and Neck Surgery*, 144(6), pp. 538–539. doi: 10.1001/jamaoto.2018.0310.

Rettig, E. M., Zaidi, M., Faraji, F., Eisele, D. W., El Asmar, M., Fung, N., D'Souza, G. and Fakhry, C. (2018b) 'Oropharyngeal cancer is no longer a disease of younger patients and the prognostic advantage of Human Papillomavirus is attenuated among older patients: Analysis of the National Cancer Database', *Oral Oncology*. Elsevier, 83(June), pp. 147–153. doi: 10.1016/j.oraloncology.2018.06.013.

Rhim, A. D., Oberstein, P. E., Thomas, D. H., Mirek, E. T., Palermo, C. F., Sastra, S. A., Dekleva, E. N., Saunders, T., Becerra, C. P., Tattersall, I. W., Westphalen, C. B., Kitajewski, J., Fernandez-Barrena, M. G., Fernandez-Zapico, M. E., Iacobuzio-Donahue, C., Olive, K. P. and Stanger, B. Z. (2014) 'Stromal elements act to restrain, rather than support, pancreatic ductal adenocarcinoma', *Cancer Cell*. Elsevier Inc., 25(6), pp. 735–747. doi: 10.1016/j.ccr.2014.04.021.

Riechelmann, H., Sauter, A., Golze, W., Hanft, G., Schroen, C., Hoermann, K., Erhardt, T. and Gronau, S. (2008) 'Phase I trial with the CD44v6-targeting immunoconjugate bivatuzumab mertansine in head and neck squamous cell carcinoma', *Oral Oncology*, 44(9), pp. 823–829. doi: 10.1016/j.oraloncology.2007.10.009.

Rinn, J. L., Bondre, C., Gladstone, H. B., Brown, P. O. and Chang, H. Y. (2006) 'Anatomic demarcation by positional variation in fibroblast gene expression programs', *PLoS Genetics*, 2(7), pp. 1084–1096. doi: 10.1371/journal.pgen.0020119.

Robinson, M., Schache, A., Sloan, P. and Thavaraj, S. (2012) 'HPV Specific Testing: A Requirement for Oropharyngeal Squamous Cell Carcinoma Patients', *Head and Neck Pathology*, 6(SUPPL. 1), pp. 83–90. doi: 10.1007/s12105-012-0370-7.

Roden, D. F., Hobelmann, K., Vimawala, S., Richa, T., Fundakowski, C. E., Goldman, R., Luginbuhl, A., Curry, J. M. and Cognetti, D. M. (2020) 'Evaluating the impact of smoking on disease-specific survival outcomes in patients with human papillomavirus–associated oropharyngeal cancer treated with transoral robotic surgery', *Cancer*, 126(9), pp. 1873–1887. doi: 10.1002/cncr.32739.

Rooper, L. M., Gandhi, M., Bishop, J. A. and Westra, W. H. (2016) 'RNA in-situ hybridization is a practical and effective method for determining HPV status of oropharyngeal squamous cell carcinoma including discordant cases that are p16 positive by immunohistochemistry but HPV negative by DNA in-situ hybridization', *Oral Oncology*. Elsevier Ltd, 55, pp. 11–16. doi: 10.1016/j.oraloncology.2016.02.008.

Routray, S., Kheur, S. M. and Kheur, M. (2013) 'Osteopontin: A marker for invasive oral squamous cell carcinoma but not for potentially malignant epithelial dysplasias', *Annals of Diagnostic Pathology*. Elsevier Inc., 17(5), pp. 421–424. doi: 10.1016/j.anndiagpath.2013.03.005.

Safran, J. B., Butler, W. T., & Farach-Carson, M. C. (1998). Modulation of osteopontin post-translational state by 1, 25-(OH)2-vitamin D3. Dependence on Ca2+ influx. *The Journal of biological chemistry*, 273(45), pp. 29935–29941. https://doi.org/10.1074/jbc.273.45.29935.

Sahai, E., Astsaturov, I., Cukierman, E., DeNardo, D. G., Egeblad, M., Evans, R. M., Fearon, D., Greten, F. R., Hingorani, S. R., Hunter, T., Hynes, R. O., Jain, R. K., Janowitz, T., Jorgensen, C., Kimmelman, A. C., Kolonin, M. G., Maki, R. G., Powers, R. S., Puré, E., Ramirez, D. C., Scherz-Shouval, R., Sherman, M. H., Stewart, S., Tlsty, T. D., Tuveson, D. A., Watt, F. M., Weaver, V., Weeraratna, A. T. and Werb, Z. (2020) 'A framework for advancing our understanding of cancer-associated fibroblasts', *Nature Reviews Cancer*. Springer US, 20(3), pp. 174–186. doi: 10.1038/s41568-019-0238-1.

Salem, A. F., Sotgia, F. and Lisanti, M. P. (2013) 'Smoke Cancer', *Cell Cycle*, 12(5), pp. 818–825.

Salgueiredo-Giudice, F., Fornias-Sperandio, F., Martins-Pereira, É., da Costa dal Vechio, A. M., de Sousa, S. C. O. M. and dos Santos-Pinto-Junior, D. (2011) 'The immunohistochemical profile of oral inflammatory myofibroblastic tumors', *Oral Surgery, Oral Medicine, Oral Pathology, Oral Radiology, and Endodontology*, 111(6), pp. 749–756. doi: 10.1016/j.tripleo.2010.12.023.

Sanjose, S. De, Quint, W. G. V, Alemany, L., Geraets, D. T., Klaustermeier, J. E., Lloveras, B., Tous, S., Felix, A., Garland, S. M., Sasagawa, T., Ferrera, A., Hammouda, D., Mariani, L., Pelayo, A., Steiner, I., Oliva, E. and Valle, U. (2010) 'Human papillomavirus genotype attribution in invasive cervical cancer : a retrospective cross-sectional worldwide study', 11(11), pp. 7–11. doi: 10.1016/S1470-2045(10)70230-8.

Schache, A. G., Liloglou, T., Risk, J. M., Filia, A., Jones, T. M., Sheard, J., Woolgar, J. A., Helliwell, T. R., Triantafyllou, A., Robinson, M., Sloan, P., Harvey-Woodworth, C., Sisson, D. and Shaw, R. J. (2011) 'Evaluation of human papilloma virus diagnostic testing in oropharyngeal squamous cell carcinoma: Sensitivity, specificity, and prognostic discrimination', *Clinical Cancer Research*, 17(19), pp. 6262–6271. doi: 10.1158/1078-0432.CCR-11-0388.

Schache, A. G., Liloglou, T., Risk, J. M., Jones, T. M., Ma, X.-J., Wang, H., Bui, S., Luo, Y., Sloan, P., Shaw, R. J. and Robinson, M. (2013) 'Validation of a novel diagnostic standard in HPV-positive oropharyngeal squamous cell carcinoma.', *British journal of cancer*. Nature Publishing Group, 108(6), pp. 1332–9. doi: 10.1038/bjc.2013.63.

Schache, A. G., Powell, N. G., Cuschieri, K. S., Robinson, M., Leary, S., Mehanna, H., Rapozo, D., Long, A., Cubie, H., Junor, E., Monaghan, H., Harrington, K. J., Nutting, C. M., Schick, U., Lau, A. S., Upile, N., Sheard, J., Brougham, K., West, C. M. L., Oguejiofor, K., Thomas, S., Ness, A. R., Pring, M., Thomas, G. J., King, E. V., McCance, D. J., James, J. A., Moran, M., Sloan, P., Shaw, R. J., Evans, M. and Jones, T. M. (2016) 'HPV-related oropharynx cancer in the United Kingdom: An evolution in the understanding of disease etiology', *Cancer Research*, 76(22), pp. 6598–6606. doi: 10.1158/0008-5472.CAN-16-0633.

Schiffman, M., Clifford, G., & Buonaguro, F. M. (2009). Classification of weakly carcinogenic human papillomavirus types: addressing the limits of epidemiology at the borderline. *Infectious agents and cancer*, 4, p. 8. https://doi.org/10.1186/1750-9378-4-8.

Schimizu, Y., Van Seventer, G. A., Siraganian, R., Wahl, L. and Shaw, S. (1989) 'Dual role of the CD44 molecule in T cell adhesion and activation', *The Journal of Immunology*, 143(8), pp. 2457–2463.

Schlotzhauer, W. S. and Chortyk, O. T. (1987) 'Recent advances in studies on the pyrosynthesis of cigarette smoke constituents', *Journal of Analytical and Applied Pyrolysis*, 12(3–4), pp. 193–222. doi: 10.1016/0165-2370(87)85002-7.

Schrank, T. P., Han, Y., Weiss, H., & Resto, V. A. (2011). Case-matching analysis of head and neck squamous cell carcinoma in racial and ethnic minorities in the United States--possible role for human papillomavirus in survival disparities. *Head & neck*, 33(1), 45–53. https://doi.org/10.1002/hed.21398.

Schultz, J., Lorenz, P., Ibrahim, S. M., Kundt, G., Gross, G. and Kunz, M. (2009) 'The functional -443T/C osteopontin promoter polymorphism influences osteopontin gene expression in melanoma cells via binding of c-Myb transcription factor', *Molecular Carcinogenesis*, 48(1), pp. 14–23. doi: 10.1002/mc.20452.

Screaton, G. R., Bell, M. V., Jackson, D. G., Cornelis, F. B., Gerth, U. and Bell, J. I. (1992) 'Genomic structure of DNA encoding the lymphocyte homing receptor CD44 reveals at least 12 alternatively spliced exons', *Proceedings of the National Academy of Sciences of the United States of America*, 89(24), pp. 12160–12164. doi: 10.1073/pnas.89.24.12160.

Sedghizadeh, P. P., Billington, W. D., Paxton, D., Ebeed, R., Mahabady, S., Clark, G. T. and Enciso, R. (2016) 'Is p16-positive oropharyngeal squamous cell carcinoma associated with favorable prognosis? A systematic review and meta-analysis', *Oral Oncology*. Pergamon, 54, pp. 15–27. doi: 10.1016/J.ORALONCOLOGY.2016.01.002.

Selcuk, O., 2016. Human papillomavirus positive oropharyngeal cancer: The general information. *Egyptian Journal of Ear, Nose, Throat and Allied Sciences*, 17(3), pp.127-132.

Semenza, G., 2000. Hypoxia, Clonal Selection, and the Role of HIF-1 in Tumor Progression. *Critical Reviews in Biochemistry and Molecular Biology*, 35(2), pp.71-103.

Senbanjo, L. T. and Chellaiah, M. A. (2017) 'CD44: A multifunctional cell surface adhesion receptor is a regulator of progression and metastasis of cancer cells', *Frontiers in Cell and Developmental Biology*, 5(3). doi: 10.3389/fcell.2017.00018.

Senger, D. R., Wirth, D. F., & Hynes, R. O. (1979). Transformed mammalian cells secrete specific proteins and phosphoproteins. *Cell*, *16*(4), pp. 885–893. https://doi.org/10.1016/0092-8674(79)90103-x.

Serini, G. and Gabbiani, G. (1999) 'Mechanisms of myofibroblast activity and phenotypic modulation', *Experimental Cell Research*, 250(2), pp. 273–283. doi: 10.1006/excr.1999.4543.

Servais, C. and Erez, N. (2013) 'From sentinel cells to inflammatory culprits: Cancer-associated fibroblasts in tumour-related inflammation', *Journal of Pathology*, 229(2), pp. 198–207. doi: 10.1002/path.4103.

Shan, S. J. C., Scorilas, A., Katsaros, D. and Diamandis, E. P. (2007) 'Transcriptional upregulation of human tissue kallikrein 6 in ovarian cancer: Clinical and mechanistic aspects', *British Journal of Cancer*, 96(2), pp. 362–372. doi: 10.1038/sj.bjc.6603556.

Sharon, Y., Raz, Y., Cohen, N., Ben-Shmuel, A., Schwartz, H., Geiger, T. and Erez, N. (2015) 'Tumor-derived osteopontin reprograms normal mammary fibroblasts to promote inflammation and tumor growth in breast cancer', *Cancer Research*, 75(6), pp. 963–973. doi: 10.1158/0008-5472.CAN-14-1990.

Chin, L., Pomerantz, J., & DePinho, R. A. (1998). The INK4a/ARF tumor suppressor: one gene--two products--two pathways. *Trends in biochemical sciences*, 23(8), pp. 291–296. https://doi.org/10.1016/s0968-0004(98)01236-5.

Sharpless, N. E. and Sherr, C. J. (2015) 'Forging a signature of in vivo senescence', *Nature Reviews Cancer*, 15(7), pp. 397–408. doi: 10.1038/nrc3960.

Shelton, D. N., Chang, E., Whittier, P. S., Choi, D., & Funk, W. D. (1999). Microarray analysis of replicative senescence. *Current biology : CB*, 9(17), pp. 939–945. https://doi.org/10.1016/s0960-9822(99)80420-5.

Shelton, J., Purgina, B. M., Cipriani, N. A., Dupont, W. D., Plummer, D. and Lewis, J. S. (2017) 'p16 immunohistochemistry in oropharyngeal squamous cell carcinoma: a comparison of antibody clones using patient outcomes and high-risk human papillomavirus RNA status', *Nature Publishing Group*, 30, pp. 1194–1203. doi: 10.1038/modpathol.2017.31.

Shen, Z., Qin, X., Yan, M., Li, R., Chen, G., Zhang, J. and Chen, W. (2017) 'Cancer-associated fibroblasts promote cancer cell growth through a miR-7-RASSF2-PAR-4 axis in the tumor microenvironment', *Oncotarget*, 8(1), pp. 1290–1303. doi: 10.18632/oncotarget.13609.

Sheth, S., Farquhar, D. R., Lenze, N. R., Mazul, A., Brennan, P., Anantharaman, D., Abedi-Ardekani, B., Zevallos, J. P., Hayes, D. N. and Olshan, F. (2021) 'Decreased overall survival in black patients with HPV-associated oropharyngeal cancer', *American Journal of Otolaryngology - Head and Neck Medicine and Surgery*. Elsevier Inc., 42(1), p. 102780. doi: 10.1016/j.amjoto.2020.102780.

Shiga, K., Hara, M., Nagasaki, T., Sato, T., Takahashi, H. and Takeyama, H., 2015. Cancer-Associated Fibroblasts: Their Characteristics and Their Roles in Tumor Growth. *Cancers*, 7(4), pp.2443-2458..

Salmaninejad, A., Valilou, S. F., Soltani, A., Ahmadi, S., Abarghan, Y. J., Rosengren, R. J., & Sahebkar, A. (2019). Tumor-associated macrophages: role in cancer development and therapeutic implications. *Cellular oncology (Dordrecht)*, 42(5), pp. 591–608. https://doi.org/10.1007/s13402-019-00453-z.

Shinohara, M. L., Jansson, M., Hwang, E. S., Werneck, M. B. F., Glimcher, L. H. and Cantor, H. (2005) 'T-bet-dependent expression of osteopontin contributes to T cell polarization', *Proceedings of the National Academy of Sciences of the United States of America*, 102(47), pp. 17101–17106. doi: 10.1073/pnas.0508666102.

Shinohara, M. L., Kim, H. J., Kim, J. H., Garcia, V. A. and Cantor, H. (2008) 'Alternative translation of osteopontin generates intracellular and secreted isoforms that mediate distinct biological activities in dendritic cells', *Proceedings of the National Academy of Sciences of the United States of America*, 105(20), pp. 7235–7239. doi: 10.1073/pnas.0802301105.

Shinohara, M. L., Linrong Lu, J. B., Werneck, iriam B. F., Kobayashi, K. S., Glimcher, L. H. and Cantor, H. (2012) 'Osteopontin expression is essential for interferon-α production by plasmacytoid dendritic cells', *Bone*, 23(1), pp. 1–7. doi: 10.1038/ni1327.Osteopontin.

Singhi, A. D., & Westra, W. H. (2010). Comparison of human papillomavirus in situ hybridization and p16 immunohistochemistry in the detection of human papillomavirus-associated head and neck cancer based on a prospective clinical experience. *Cancer*, 116(9), pp. 2166–2173. https://doi.org/10.1002/cncr.25033.

Smeets, S. J., Hesselink, A. T., Speel, E.-J. M., Haesevoets, A., Snijders, P. J. F., Pawlita, M., Meijer, C. J. L. M., Braakhuis, B. J. M., Leemans, C. R. and Brakenhoff, R. H. (2007) 'A novel algorithm for reliable detection of human papillomavirus in paraffin embedded head and neck cancer specimen', *International Journal of Cancer*. Wiley Subscription Services, Inc., A Wiley Company, 121(11), pp. 2465–2472. doi: 10.1002/ijc.22980.

Son, H. K., Park, I., Kim, J. Y., Kim, D. K., Illeperuma, R. P., Bae, J. Y., Lee, D. Y., Oh, E. S., Jung, D. W., Williams, D. R. and Kim, J. (2015) 'A Distinct Role for Interleukin-6 as a Major Mediator of Cellular Adjustment to an Altered Culture Condition', *Journal of Cellular Biochemistry*, 116(11), pp. 2552–2562. doi: 10.1002/jcb.25200.

Stein, A. P., Saha, S., Kraninger, J. L., Swick, A. D., Yu, M., Lambert, P. F., & Kimple, R. J. (2015). Prevalence of Human Papillomavirus in Oropharyngeal Cancer: A Systematic Review. *Cancer journal (Sudbury, Mass.)*, 21(3), pp. 138–146. https://doi.org/10.1097/PPO.0000000000000115.

Stjernstrøm, K. D., Jensen, J. S., Kronberg, K., Grønhøj, C. and Buchwald, C. Von (2019) 'Current status of human papillomavirus positivity in oropharyn geal squamous cell carcinoma in Europe : a systematic review', *Acta Oto-Laryngologica*. Taylor & Francis, 139(12), pp. 1112–1116. doi: 10.1080/00016489.2019.1669820.

Stransky, N., Egloff, A. M., Tward, A. D., Kostic, A. D., Cibulskis, K., Sivachenko, A., Kryukov, G. V.,

Lawrence, M. S., Sougnez, C., McKenna, A., Shefler, E., Ramos, A. H., Stojanov, P., Carter, S. L., Voet, D., Cortés, M. L., Auclair, D., Berger, M. F., Saksena, G., Guiducci, C., Onofrio, R. C., Parkin, M., Romkes, M., Weissfeld, J. L., Seethala, R. R., Wang, L., Rangel-Escareño, C., Fernandez-Lopez, J. C., Hidalgo-Miranda, A., Melendez-Zajgla, J., Winckler, W., Ardlie, K., Gabriel, S. B., Meyerson, M., Lander, E. S., Getz, G., Golub, T. R., Garraway, L. A. and Grandis, J. R. (2011) 'The mutational landscape of head and neck squamous cell carcinoma', *Science*, 333(6046), pp. 1157–1160. doi: 10.1126/science.1208130.

Strutz, F., Okada, H., Lo, C. W., Danoff, T., Carone, R. L., Tomaszewski, J. E. and Neilson, E. G. (1995) 'Identification and characterization of a fibroblast marker: FSP1', *Journal of Cell Biology*, 130(2), pp. 393–405. doi: 10.1083/jcb.130.2.393.

Sturgis, E. M., & Ang, K. K. (2011). The epidemic of HPV-associated oropharyngeal cancer is here: is it time to change our treatment paradigms?. *Journal of the National Comprehensive Cancer Network : JNCCN*, 9(6), pp. 665–673. https://doi.org/10.6004/jnccn.2011.0055.

Subramani, V. N., Narashman, M., Thiyagarajan, M., Davidmunuswamy, B. and Jayamani, L. (2015) 'Expression of osteopontin in oral squamous cell carcinoma and its surgical margins-an immunohistochemical study', *Journal of Clinical and Diagnostic Research*, 9(11), pp. ZC66–ZC69. doi: 10.7860/JCDR/2015/12777.6836.

Sugimoto, H., Mundel, T. M., Kieran, M. W., & Kalluri, R. (2006). Identification of fibroblast heterogeneity in the tumor microenvironment. *Cancer biology & therapy*, 5(12), pp. 1640–1646. https://doi.org/10.4161/cbt.5.12.3354.

Sun, B. S., Li, Y., Zhang, Z. F., You, J. and Wang, C. L. (2013) 'Osteopontin combined with CD44v6, a novel prognostic biomarker in non-small cell lung cancer undergoing curative resection', *Annals of Thoracic Surgery*. Elsevier Inc, 96(6), pp. 1943–1951. doi: 10.1016/j.athoracsur.2013.07.089.

Sun, W., Liu, D. B., Li, W. W., Zhang, L. L., Long, G. X., Wang, J. F., Mei, Q. and Hu, G. Q. (2014) 'Interleukin-6 promotes the migration and invasion of nasopharyngeal carcinoma cell lines and upregulates the expression of MMP-2 and MMP-9', *International Journal of Oncology*, 44(5), pp. 1551–1560. doi: 10.3892/ijo.2014.2323.

Suresh, K., Shah, P. V., Coates, S., Alexiev, B. A. and Samant, S. (2021) 'In situ hybridization for high risk HPV E6/E7 mRNA in oropharyngeal squamous cell carcinoma', *American Journal of Otolaryngology - Head and Neck Medicine and Surgery*. Elsevier Inc., 42(1), p. 102782. doi: 10.1016/j.amjoto.2020.102782.

Tang et al., 2005 (2008) 'Sp1 Regulates Osteopontin Expression in SW480 Human Colon Adenocarcinoma Cells', *Bone*, 23(1), pp. 1–7.

Tchou, J., Zhang, P. J., Bi, Y., Satija, C., Marjumdar, R., Stephen, T. L., Lo, A., Chen, H., Mies, C., June, C. H., Conejo-Garcia, J. and Puré, E. (2013) 'Fibroblast activation protein expression by stromal cells and tumor-associated macrophages in human breast cancer', *Human Pathology*. Elsevier Inc., 44(11), pp. 2549–2557. doi: 10.1016/j.humpath.2013.06.016.

Terabe, M., & Berzofsky, J. A. (2007). NKT cells in immunoregulation of tumor immunity: a new immunoregulatory axis. *Trends in immunology*, *28*(11), pp. 491–496. https://doi.org/10.1016/j.it.2007.05.008.

Thavasu, P. W., Longhurst, S., Joel, S. P., Slevin, M. L. and Balkwill, F. R. (1992) 'Measuring cytokine levels in blood. Importance of anticoagulants, processing, and storage conditions', *Journal of Immunological Methods*, 153(1–2), pp. 115–124. doi: 10.1016/0022-1759(92)90313-I.

Thibaudeau, E., Fortin, B., Coutlée, F., Nguyen-Tan, P., Weng, X., Audet, M.-L., Abboud, O., Guertin, L., Christopoulos, A., Tabet, J. and Soulières, D. (2013) 'HPV Prevalence and Prognostic Value in a Prospective Cohort of 255 Patients with Locally Advanced HNSCC: A Single-Centre Experience.', *International journal of otolaryngology*. Hindawi, 2013, p. 437815. doi: 10.1155/2013/437815.

Thiery J. P. (2002). Epithelial-mesenchymal transitions in tumour progression. *Nature reviews. Cancer*, *2*(6), 442–454. https://doi.org/10.1038/nrc822.

Thiery, J. P., Acloque, H., Huang, R. Y. J. and Nieto, M. A. (2009) 'Epithelial-Mesenchymal Transitions in Development and Disease', pp. 871–890. doi: 10.1016/j.cell.2009.11.007.

Tilli, T. M., Thuler, L. C., Matos, A. R., Coutinho-Camillo, C. M., Soares, F. A., da Silva, E. A., Neves, A. F., Goulart, L. R. and Gimba, E. R. (2012) 'Expression analysis of osteopontin mRNA splice variants in prostate cancer and benign prostatic hyperplasia', *Experimental and Molecular Pathology*. Elsevier Inc., 92(1), pp. 13–19. doi: 10.1016/j.yexmp.2011.09.014.

Tlsty, T. D. (2001) 'Stromal cells can contribute oncogenic signals', *Seminars in Cancer Biology*, 11(2), pp. 97–104. doi: 10.1006/scbi.2000.0361.

Todorović, M. M. and Zvrko, E. Z. (2013) 'Immunoregulatory cytokines and chronic tonsillitis', *Bosnian Journal of Basic Medical Sciences*, 13(4), pp. 230–236. doi: 10.17305/bjbms.2013.2330.

Tomasek, J. J., Gabbiani, G., Hinz, B., Chaponnier, C. and Brown, R. A. (2002) 'Myofibroblasts and mechano-regulation of connective tissue remodelling', *Nature Reviews Molecular Cell Biology*, 3(5), pp. 349–363. doi: 10.1038/nrm809.

Tschumperlin, D. J. (2013) 'Fibroblasts and the ground they walk on', *Physiology*, 28(6), pp. 380–390. doi: 10.1152/physiol.00024.2013.

Tzelgov, J. and Henik, A., 1991. Suppression situations in psychological research: Definitions, implications, and applications. *Psychological Bulletin*, 109(3), pp.524-536.

Uchibori, T., Matsuda, K., Shimodaira, T., Sugano, M., Uehara, T. and Honda, T. (2017) 'IL-6 trans-signaling is another pathway to upregulate Osteopontin', *Cytokine*. Elsevier Ltd, 90, pp. 88–95. doi: 10.1016/j.cyto.2016.11.006.

Ukpo, O. C., Flanagan, J. J., Ma, X. J., Luo, Y., Thorstad, W. L. and Lewis, J. S. (2011) 'High-risk human papillomavirus E6/E7 mRNA detection by a novel in situ hybridization assay strongly correlates with p16 expression and patient outcomes in oropharyngeal squamous cell carcinoma', *American Journal of Surgical Pathology*, 35(9), pp. 1343–1350. doi: 10.1097/PAS.0b013e318220e59d.

Valach, J., Fík, Z., Strnad, H., Chovanec, M., Plzák, J., Cada, Z., Szabo, P., Sáchová, J., Hroudová, M., Urbanová, M., Steffl, M., Pačes, J., Mazánek, J., Vlček, C., Betka, J., Kaltner, H., André, S., Gabius, H. J., Kodet, R., Smetana, K., Jr, … Kolář, M. (2012). Smooth muscle actin-expressing stromal fibroblasts in head and neck squamous cell carcinoma: increased expression of galectin-1 and induction of poor prognosis factors. *International journal of cancer*, 131(11), pp. 2499–2508. https://doi.org/10.1002/ijc.27550.

.Vaughan, M. B., Howard, E. W. and Tomasek, J. J. (2000) 'Transforming growth factor-β1 promotes the morphological and functional differentiation of the myofibroblast', *Experimental Cell Research*, 257(1), pp. 180–189. doi: 10.1006/excr.2000.4869.

Vaupel, P., Mayer, A., Briest, S. and Höckel, M. (2003) 'Oxygenation Gain Factor: A Novel Parameter

Characterizing the Association between Hemoglobin Level and the Oxygenation Status of Breast Cancers', *Cancer Research*, 63(22), pp. 7634–7637.

Vered, M., Allon, I., Buchner, A. and Dayan, D. (2007) 'Stromal myofibroblasts and malignant transformation in a 4NQO rat tongue carcinogenesis model', *Oral Oncology*, 43(10), pp. 999–1006. doi: 10.1016/j.oraloncology.2006.11.007.

Viallard, J. F., Bloch-Michel, C., Neau-Cransac, M., Taupin, J. L., Garrigue, S., Miossec, V., Mercie, P., Pellegrin, J. L. and Moreau, J. F. (2001) 'HLA-DR expression on lymphocyte subsets as a marker of disease activity in patients with systemic lupus erythematosus', *Clinical and Experimental Immunology*, 125(3), pp. 485–491. doi: 10.1046/j.1365-2249.2001.01623.x.

Virgilio, L., Shuster, M., Gollin, S. M., Veronese, M. L., Ohta, M., Huebner, K., & Croce, C. M. (1996). FHIT gene alterations in head and neck squamous cell carcinomas. *Proceedings of the National Academy of Sciences of the United States of America*, 93(18), pp. 9770–9775. https://doi.org/10.1073/pnas.93.18.9770.

Wai, P. Y., & Kuo, P. C. (2004). The role of Osteopontin in tumor metastasis. *The Journal of surgical research*, *121*(2), 228–241. https://doi.org/10.1016/j.jss.2004.03.028.

Wain, S. L., Kier, R., Vollmer, R. T., & Bossen, E. H. (1986). Basaloid-squamous carcinoma of the tongue, hypopharynx, and larynx: report of 10 cases. *Human pathology*, 17(11), pp. 1158–1166. https://doi.org/10.1016/s0046-8177(86)80422-1.

Wald, A. I., Hoskins, E. E., Wells, S. I., Ferris, R. L. and Khan, S. A. (2011) 'Alteration of microRNA profiles in squamous cell carcinoma of the head and neck cell lines by human papillomavirus', *Head & Neck*, 33(4), pp. 504–512. doi: 10.1002/hed.21475.

Wang, M., Su, Z. and Amoah, P. (2020) 'Crosstalk among colon cancer-derived exosomes , fi broblast-derived exosomes , and macrophage phenotypes in colon cancer metastasis', *International Immunopharmacology*. Elsevier, 81(11), p. 106298. doi: 10.1016/j.intimp.2020.106298.

Wang, S. J. and Bourguignon, L. Y. W. (2011) 'Role of hyaluronan-mediated CD44 signaling in head and neck squamous cell carcinoma progression and chemoresistance', *American Journal of Pathology*. Elsevier Inc., 178(3), pp. 956–963. doi: 10.1016/j.ajpath.2010.11.077.

Wang, Z., Tang, Y., Xie, L., Huang, A., Xue, C., Gu, Z., Wang, K. and Zong, S. (2019) 'The prognostic and clinical value of CD44 in colorectal cancer: A meta-analysis', *Frontiers in Oncology*, 9(4), pp. 1–11. doi: 10.3389/fonc.2019.00309.

Weber, C. E., Kothari, A. N., Wai, P. Y., Li, N. Y., Driver, J., Zapf, M. A. C., Franzen, C. A., Gupta, G. N., Osipo, C., Zlobin, A., Syn, W. K., Zhang, J., Kuo, P. C. and Mi, Z. (2015) 'Osteopontin mediates an MZF1-TGF-β1-dependent transformation of mesenchymal stem cells into cancer-associated fibroblasts in breast cancer', *Oncogene*, 34(37), pp. 4821–4833. doi: 10.1038/onc.2014.410.

Weber, G. F., Ashkar, S., Glimcher, M. J., & Cantor, H. (1996). Receptor-ligand interaction between CD44 and osteopontin (Eta-1). *Science (New York, N.Y.)*, *271*(5248), pp. 509–512. https://doi.org/10.1126/science.271.5248.509.

Weber, G., Lett, G. and Haubein, N., 2010. Osteopontin is a marker for cancer aggressiveness and patient survival. *British Journal of Cancer*, 103(6), pp.861-869. doi: 10.1038/sj.bjc.6605834.

Weber, R. G., Scheer, M., Born, I. A., Joos, S., Cobbers, J. M. J. L., Hofele, C., Reifenberger, G., Zöller, J. E. and Lichter, P. (1998) 'Recurrent chromosomal imbalances detected in biopsy material

from oral premalignant and malignant lesions by combined tissue microdissection, universal DNA amplification, and comparative genomic hybridization', *American Journal of Pathology*, 153(1), pp. 295–303. doi: 10.1016/S0002-9440(10)65571-X.

Wei, L. Y., Lee, J. J., Yeh, C. Y., Yang, C. J., Kok, S. H., Ko, J. Y., Tsai, F. C., & Chia, J. S. (2019). Reciprocal activation of cancer-associated fibroblasts and oral squamous carcinoma cells through CXCL1. *Oral oncology*, 88, pp.115–123. https://doi.org/10.1016/j.oraloncology.2018.11.002.

Weinberger, P. M., Yu, Z., Haffty, B. G., Kowalski, D., Harigopal, M., Brandsma, J., Sasaki, C., Joe, J., Camp, R. L., Rimm, D. L. and Psyrri, A. (2006) 'Molecular classification identifies a subset of human papillomavirus- associated oropharyngeal cancers with favorable prognosis', *Journal of Clinical Oncology*, 24(5), pp. 736–747. doi: 10.1200/JCO.2004.00.3335.

Welters, M. J., Ma, W., Santegoets, S. J., Goedemans, R., Ehsan, I., Jordanova, E. S., Van Ham, V. J., Van Unen, V., Koning, F., Van Egmond, S. I., Charoentong, P., Trajanoski, Z., Van Der Velden, L. A. and Van Der Burg, S. H. (2018) 'Intratumoral HPV16-specific T cells constitute a type I–oriented tumor microenvironment to improve survival in HPV16-driven oropharyngeal cancer', *Clinical Cancer Research*, 24(3), pp. 634–647. doi: 10.1158/1078-0432.CCR-17-2140.

Westra, W. H. (2012) 'The morphologic profile of HPV-related head and neck squamous carcinoma: implications for diagnosis, prognosis, and clinical management.', *Head and neck pathology*. Springer, 6 Suppl 1(Suppl 1), pp. S48-54. doi: 10.1007/s12105-012-0371-6.

Westra, W. H. (2014) 'Detection of human papillomavirus (HPV) in clinical samples: Evolving methods and strategies for the accurate determination of HPV status of head and neck carcinomas', *Oral Oncology*. Elsevier Ltd, 50(9), pp. 771–779. doi: 10.1016/j.oraloncology.2014.05.004.

White, J. S., Weissfeld, J. L., Ragin, C. C. R., Rossie, K. M., Martin, C. L., Shuster, M., Ishwad, C. S., Law, J. C., Myers, E. N., Johnson, J. T. and Gollin, S. M. (2007) 'The influence of clinical and demographic risk factors on the establishment of head and neck squamous cell carcinoma cell lines', *Oral Oncology*, 43(7), pp. 701–712. doi: 10.1016/j.oraloncology.2006.09.001.

Wiest, T., Schwarz, E., Enders, C., Flechtenmacher, C. and Bosch, F. X. (2002) 'Involvement of intact HPV16 E6/E7 gene expression in head and neck cancers with unaltered p53 status and perturbed pRB cell cycle control', *Oncogene*, 21(10), pp. 1510–1517. doi: 10.1038/sj.onc.1205214.

Windon, M. J., D'Souza, G., Rettig, E. M., Westra, W. H., van Zante, A., Wang, S. J., Ryan, W. R., Mydlarz, W. K., Ha, P. K., Miles, B. A., Koch, W., Gourin, C., Eisele, D. W. and Fakhry, C. (2018) 'Increasing prevalence of human papillomavirus–positive oropharyngeal cancers among older adults', *Cancer*, 124(14), pp. 2993–2999. doi: 10.1002/cncr.31385.

Wipff, P.-J., Rifkin, D. B., Meister, J.-J. and Hinz, B. (2007) 'Myofibroblast contraction activates latent TGF-β1 from the extracellular matrix', *The Journal of Cell Biology*, 179(6), pp. 1311–1323. doi: 10.1083/jcb.200704042.

Witkiewicz, A. K., Knudsen, K. E., Dicker, A. P. and Knudsen, E. S. (2011) 'The meaning of p16ink4a expression in tumors: Functional significance, clinical associations and future developments', *Cell Cycle*, 10(15), pp. 2497–2503. doi: 10.4161/cc.10.15.16776.

Wong, T. S., Kwong, D. L. W., Sham, J., Wei, W. I., Kwong, Y. L. and Yuen, A. P. W. (2005) 'Elevation of plasma osteopontin level in patients with undifferentiated nasopharyngeal carcinoma', *European Journal of Surgical Oncology*, 31(5), pp. 555–558. doi: 10.1016/j.ejso.2005.01.005.

Wu, T., Hong, Y., Jia, L., Wu, J., Xia, J., Wang, J., Hu, Q. and Cheng, B. (2016) 'Modulation of IL-1β

reprogrammes the tumor microenvironment to interrupt oral carcinogenesis', *Scientific Reports*. Nature Publishing Group, 6(February), pp. 1–10. doi: 10.1038/srep20208.

Würdemann, N., Wagner, S., Sharma, S. J., Prigge, E. S., Reuschenbach, M., Gattenlöhner, S., Klussmann, J. P., & Wittekindt, C. (2017). Prognostic Impact of AJCC/UICC 8th Edition New Staging Rules in Oropharyngeal Squamous Cell Carcinoma. *Frontiers in oncology*, 7, p.129. https://doi.org/10.3389/fonc.2017.00129.

Xi, L. F., Schiffman, M., Koutsky, L. A., Hughes, J. P., Winer, R. L., Mao, C., Hulbert, A., Lee, S. K., Shen, Z., & Kiviat, N. B. (2014). Lineages of oncogenic human papillomavirus types other than type 16 and 18 and risk for cervical intraepithelial neoplasia. *Journal of the National Cancer Institute*, 106(10), dju270. https://doi.org/10.1093/jnci/dju270.

Xing, F., Saidou, J., & Watabe, K. (2010). Cancer associated fibroblasts (CAFs) in tumor microenvironment. *Frontiers in bioscience (Landmark edition)*, 15, pp.166–179. https://doi.org/10.2741/3613.

Yamashita, M., Ogawa, T., Zhang, X., Hanamura, N., Kashikura, Y., Takamura, M., Yoneda, M. and Shiraishi, T. (2012) 'Role of stromal myofibroblasts in invasive breast cancer: Stromal expression of alpha-smooth muscle actin correlates with worse clinical outcome', *Breast Cancer*, 19(2), pp. 170–176. doi: 10.1007/s12282-010-0234-5.

Yim, E.K. and Park, J.S. (2005) 'The Role of HPV E6 and E7 Oncoproteins in HPV-associated Cervical Carcinogenesis', *Cancer Research and Treatment*, 37(6), p. 319. doi: 10.4143/crt.2005.37.6.319.

Yin, L. X., D'Souza, G., Westra, W. H., Wang, S. J., van Zante, A., Zhang, Y., Rettig, E. M., Ryan, W. R., Ha, P. K., Wentz, A., Koch, W., Eisele, D. W. and Fakhry, C. (2018) 'Prognostic factors for human papillomavirus–positive and negative oropharyngeal carcinomas', *Laryngoscope*, 128(8), pp. E287–E295. doi: 10.1002/lary.27130.

Young, M. F., Kerr, J. M., Termine, J. D., Wewer, U. M., Wang, M. G., McBride, O. W. and Fisher, L. W. (1990) 'cDNA cloning, mRNA distribution and heterogeneity, chromosomal location, and RFLP analysis of human osteopontin (OPN)', *Genomics*, 7(4), pp. 491–502. doi: 10.1016/0888-7543(90)90191-V.

Yu, S.-H., Zheng, Q., Esopi, D., Macgregor-Das, A., Luo, J., Antonarakis, E. S., Drake, C. G., Vessella, R., Morrissey, C., De Marzo, A. M. and Sfanos, K. S. (2015) 'A Paracrine Role for IL6 in Prostate Cancer Patients: Lack of Production by Primary or Metastatic Tumor Cells', *Cancer Immunology Research*, 3(10), pp. 1175–1184. doi: 10.1158/2326-6066.CIR-15-0013.

Yuan, G. C., Cai, L., Elowitz, M., Enver, T., Fan, G., Guo, G., Irizarry, R., Kharchenko, P., Kim, J., Orkin, S., Quackenbush, J., Saadatpour, A., Schroeder, T., Shivdasani, R. and Tirosh, I. (2017) 'Challenges and emerging directions in single-cell analysis', *Genome Biology*. Genome Biology, 18(1), pp. 1–8. doi: 10.1186/s13059-017-1218-y.

Zamani, M., Grønhøj, C., Jensen, D. H., Carlander, A. F., Agander, T., Kiss, K., Olsen, C., Baandrup, L., Nielsen, F. C., Andersen, E., Friborg, J. and von Buchwald, C. (2020) 'The current epidemic of HPV-associated oropharyngeal cancer: An 18-year Danish population-based study with 2,169 patients', *European Journal of Cancer*. Elsevier Ltd, 134, pp. 52–59. doi: 10.1016/j.ejca.2020.04.027.

Zaravinos, A. (2014) 'An updated overview of HPV-associated head and neck carcinomas', *Oncotarget*, 5(12), pp. 3956–69. doi: 10.18632/oncotarget.1934.

Zhan, S., Liu, Z., Zhang, M., Guo, T., Quan, Q., Huang, L., Guo, L., Cao, L. and Zhang, X. (2020)

‘Overexpression of B7-H3 in α-SMA-Positive Fibroblasts Is Associated With Cancer Progression and Survival in Gastric Adenocarcinomas’, *Frontiers in Oncology*, 9(1), pp. 1–13. doi: 10.3389/fonc.2019.01466.

Zhang, H., Guo, M., Chen, J. H., Wang, Z., Du, X. F., Liu, P. X. and Li, W. H. (2014) ‘Osteopontin knockdown inhibits α v ,β 3 integrin-induced cell migration and invasion and promotes apoptosis of breast cancer cells by inducing autophagy and inactivating the PI3K/Akt/mTOR Pathway’, *Cellular Physiology and Biochemistry*, 33(4), pp. 991–1002. doi: 10.1159/000358670.

Zhang, H., Liu, F. Y., Liu, Y. H., Peng, Y. M., Liao, Q., & Zhang, K. (2005). Effect of TGF-β1 Stimulation on the Smad Signal Transduction Pathway of Human Peritoneal Mesothelial Cells. *International journal of biomedical science : IJBS*, 1(1), pp.8–15.

Zhang, L., Sharma, S., Zhu, L. X., Kogai, T., Hershman, J. M., Brent, G. A., Dubinett, S. M. and Huang, M. (2003) ‘Nonradioactive iodide effectively induces apoptosis in genetically modified lung cancer cells’, *Cancer Research*, 63(16), pp. 5065–5072.

Zhao, F., Zhang, Yi, Wang, H., Jin, M., He, S., Shi, Y., Guo, Y. and Zhang, Yanyun (2011) ‘Blockade of osteopontin reduces alloreactive CD8+ T cell-mediated graft-versus-host disease’, *Blood*, 117(5), pp. 1723–1733. doi: 10.1182/blood-2010-04-281659.

Zhao, H., Chen, Q., Alam, A., Cui, J., Suen, K. C., Soo, A. P., Eguchi, S., Gu, J., & Ma, D. (2018). The role of osteopontin in the progression of solid organ tumour. *Cell death & disease*, 9(3), 356. https://doi.org/10.1038/s41419-018-0391-6.

Zheng, Z. M., & Baker, C. C. (2006). Papillomavirus genome structure, expression, and post-transcriptional regulation. *Frontiers in bioscience : a journal and virtual library*, 11, pp. 2286–2302. https://doi.org/10.2741/1971.

Zhu, B., Suzuki, K., Goldberg, H. A., Rittling, S. R., Denhardt, D. T., McCulloch, C. A. G. and Sodek, J. (2004) ‘Osteopontin Modulates CD44-Dependent Chemotaxis of Peritoneal Macrophages Through G-Protein-Coupled Receptors: Evidence of a Role for an Intracellular Form of Osteopontin’, *Journal of Cellular Physiology*, 198(1), pp. 155–167. doi: 10.1002/jcp.10394.

Zhu, Q., Zhang, X., Zhang, L., Li, W., Wu, H., Yuan, X., Mao, F., Wang, M., Zhu, W., Qian, H. and Xu, W. (2014) ‘The IL-6-STAT3 axis mediates a reciprocal crosstalk between cancer-derived mesenchymal stem cells and neutrophils to synergistically prompt gastric cancer progression’, *Cell Death and Disease*, 5(6), pp. 1–11. doi: 10.1038/cddis.2014.263.

Zohar, R., Lee, W., Arora, P., Cheifetz, S., McCulloch, C. and Sodek, J. (1997) ‘Single cell analysis of intracellular osteopontin in osteogenic cultures of fetal rat calvarial cells’, *Journal of Cellular Physiology*, 170(1), pp. 88–100. doi: 10.1002/(SICI)1097-4652(199701)170:1<88::AID-JCP10>3.0.CO;2-K.

Zohar, R., Suzuki, N., Suzuki, K., Arora, P., Glogauer, M., McCulloch, C. A., & Sodek, J. (2000). Intracellular osteopontin is an integral component of the CD44-ERM complex involved in cell migration. *Journal of cellular physiology*, 184(1), 118–130. https://doi.org/10.1002/(SICI)1097-4652(200007)184:1<118::AID-JCP13>3.0.CO;2-Y.

Zou, C., Luo, Q., Qin, J., Shi, Y., Yang, L., Ju, B. and Song, G. (2013) ‘Osteopontin Promotes Mesenchymal Stem Cell Migration and Lessens Cell Stiffness via Integrin β1, FAK, and ERK Pathways’, *Cell Biochemistry and Biophysics*, 65(3), pp. 455–462. doi: 10.1007/s12013-012-9449-8.

Zumsteg, Z. S., Cook-Wiens, G., Yoshida, E., Shiao, S. L., Lee, N. Y., Mita, A., Jeon, C., Goodman,

M. T. and Ho, A. S. (2016) ‘Incidence of oropharyngeal cancer among elderly patients in the United States’, *JAMA Oncology*, 2(12), pp. 1617–1623. doi: 10.1001/jamaoncol.2016.1804.